The Lubrication of Aluminium-Silicon Surfaces with a Novel Antiwear Additive

Michael Stephen Burkinshaw

Submitted in accordance with the requirements for the degree of

Doctor of Philosophy

The University of Leeds

School of Mechanical Engineering

September 2010

Intellectual Property and Publication Statements

The candidate confirms that the work submitted is his/her own, except where work which has formed part of jointly-authored publications has been included. The contribution of the candidate and the other authors to this work has been explicitly indicated below. The candidate confirms that appropriate credit has been given within the thesis where reference has been made to the work of others.

Chapters 4 - 7 are based on work from jointly-authored publications

Burkinshaw, M., Neville, A., Morina, A. and Sutton, M. Calcium Sulfonate and its Interactions with ZDDP on both Aluminium-Silicon and Model Silicon Surfaces. Submitted for Publication, 2010.

Burkinshaw, M., Neville, A., Morina, A. and Sutton, M. Calcium Sulfonate and its Interactions with an Organic Antiwear Additive on both Aluminium-Silicon and Model Silicon Surfaces. Submitted for Publication, 2010.

Lead Author: Michael Burkinshaw

Supervisors: Professor Anne Neville, Dr Ardian Morina

Industrial Supervisors: Dr Mike Sutton

Acknowledgements

I would like to thank my two supervisors, Professor Anne Neville and Dr Ardian Morina, for their help throughout this Ph.D., as I would not have been able to complete this work was it not for their input. They were always available when I needed assistance and were enthusiastic throughout this Ph.D. study.

I am grateful to Lubrizol UK Limited who funded this work. I would like to thank Dr Mike Sutton, Dr Oliver Smith and John Durham for their assistance with regards to information about the lubricant additives used throughout this project. Dr Steve Cook helped a great deal with regards to understanding the chemistry of worn substrates.

I am indebted to the technicians within the department of Mechanical Engineering at the University of Leeds, specifically Ron Cellier and Graham Jakeman. Their assistance with regards to designing and manufacturing test equipment was invaluable. I would like to pay special thanks to my friends Andy and John who supported me throughout my Ph.D. study.

I would like to dedicate this work to Paula Burkinshaw, Stephen Burkinshaw and Von Woodward, for without whom, I would not have attempted this Ph.D. study. I would like to thank my brother Julian and sister Helen for their encouragement and support throughout my Ph.D. study.

Abstract

Even though research into aluminium-silicon alloys is becoming increasingly fashionable, very little is known regarding the tribochemistry of these substrates when lubricated with conventional engine oil additives, especially when compared against ferrous surfaces. In this thesis, many advancements and thus contributions have been made in the field of aluminium-silicon lubrication.

Firstly, using a Cameron Plint TE77 tribometer, the tribological performance of overbased calcium sulfonate, zinc dialkyldithiophosphate and an organic antiwear additive on aluminium-silicon surfaces were evaluated. Secondly, contact conditions on silicon grains within the Al-Si alloy were replicated using a silicon crystal substrate, as the silicon regions were vital in the effective lubrication of the aluminium-silicon alloy. Simulation was validated through tribological testing. Thirdly, the role of the aluminium matrix under boundary lubricated wear was evaluated using a replicate aluminium alloy.

Tribofilm formation and morphology on the three substrates was analysed using scanning electron microscopy (SEM) and atomic force microscopy (AFM). Tribofilms were generated on silicon surfaces more effectively than on the aluminium alloy. Wear levels were lower on the non-conductive substrate compared to the aluminium substrate. The mechanical properties of tribofilms on silicon crystal surfaces were analysed using AFM and nanoindentation, and related to observed wear levels. Fourier transform infrared (FTIR) and secondary ion mass spectrometry (SIMS) determined the tribochemistry of generated tribofilms on all three tribosystems to be very similar to those on ferrous substrates.

The addition of the organic antiwear additive to lubricants containing detergent, ZDDP or a combination of the two, consistently improved film formation and wear levels in the three tribosystems. The mechanisms by which this occurred were identified using labelling techniques. This research has provided great insight into the effective lubrication of aluminium-silicon substrates, with the results compiled to provide a definitive mechanism by which the boundary lubrication of aluminium-silicon alloys occurs.

Table of Contents

Table of Figures

List of Tables

List of Equations

Abbreviations and Nomenclature

F^T	Tangential applied force
F_s	Static friction force
F_k	Kinetic friction force
W	Normal load
F	Frictional force
μ	Coefficient of friction
λ	Lambda ratio
h_{min}	Minimum film thickness
R_q	Root-mean-square surface roughness
SEM	Scanning electron microscope
ESEM	Environmental scanning electron microscope
SE	Secondary electron
BSE	Backscattered electron
AFM	Atomic force microscope
SPM	Scanning probe microscope
H	Hardness
A	Area of contact
E_s	Elastic modulus of substrate
E_i	Elastic modulus of indenter
υ	Poisson's ratio
EDS	Energy dispersive X-Ray spectrometer
FTIR	Fourier transform infrared

SIMS	Secondary ion mass spectrometry
ToF-SIMS	Time-of-Flight secondary ion mass spectrometry
kV	Kilovolt
ACEA	European automobile manufacturers' association
ILSAC	International lubricant standardization and approval committee
m / m	Molecular mass
F_x	Axial friction force on piston ring
F_p	Radial friction force at pivot
g	Acceleration due to gravity
m	Mass of piston ring
P_A	Axial applied gas pressure force on piston ring
P_L	Radial gas pressure relief on piston ring lower edge
P_R	Radial gas pressure force on piston ring
P_U	Radial gas pressure relief on piston ring upper edge
R_H	Axial component of hydrodynamic force on piston ring
R_P	Axial reaction force at pivot
T_R	Radial force due to ring elastic tension
W_C	Radial force due to asperity contact
W_H	Radial component of hydrodynamic force
p_1	Gas pressure above piston ring
p_2	Gas pressure below piston ring
x_r	Axial coordinate relative to centre of mass of piston ring
z_r	Radial coordinate relative to centre of mass of piston ring

α_r	Angle of twist of piston ring about centre of mass
Al-Si	Aluminium-silicon alloy
Wt. %	Weight percentage
ZDDP	Zinc dialkyldithiophosphate
OBCS	Overbased calcium sulfonate
NOCH	Nitrogen, Oxygen, Carbon & Hydrogen (Novel antiwear additive)
NMR	Nuclear magnetic resonance
HSAB	Hard and soft acid and base theory
XANES	X-ray absorption near edge structure
AES	Auger electron spectroscopy
TEM	Transmission electron microscopy
X-PEEM	X-ray photoemission electron microscopy
PAO	Poly alpha olefin
EDM	Electrical discharge machining
R_a	Average of absolute surface roughness
T	Transmittance
η_0	Viscosity of lubricant at ambient pressure
α	Pressure-viscosity coefficient of lubricant
E	Elastic modulus
E^*	Equivalent elastic modulus
E_s	Elastic modulus of substrate
R	Reduced radius of curvature

P_0	Maximum Hertzian contact pressure
L	Contact length
P_m	Mean Hertzian contact pressure
U	Entrainment speed
ECR	Electrical contact resistance
ECV	Electrical contact voltage
PDMS	Polydimethylsiloxane
R^*	Radius of curvature of steel pin
EDTA	Ethylenediaminetetraacetic acid
E^r	Reduced elastic modulus
E^r_f	Reduced elastic modulus of tribofilm
E^r_{app}	Reduced elastic modulus at each indentation point for tribofilm and substrate
E^r_s	Reduced elastic modulus of silicon crystal substrate
a	Radius of *Berkovich* type indenter
t	Tribofilm average thickness
WSW	Wear scar width
V	Volume loss
d	Average diameter of wear scar
K	Dimensional wear coefficient
s	Sliding distance

1. Introduction

Ever increasingly stringent legislation on emissions produced by passenger motor vehicles are affecting both engine oil and automotive manufacturers. Indeed, to solve these problems, the former are looking at novel solutions to reduce phosphorus and ash content of engine oils, for example. Passenger vehicle manufacturers are finding ways in which the mass of a means of transport can be reduced in order to improve the fuel consumption, yet minimise the emissions of the engine. Substitution of conventional ferrous-based cylinder liners with hypereutectic aluminium-silicon variants is one such example. Novel solutions such as the organic antiwear additive used in this work are the result of work conducted by large oil companies in order to meet emissions regulations.

The lubrication of an aluminium-silicon alloy has only been investigated by a relatively small group of authors to date. Indeed, compared to ferrous surfaces, the research conducted into this area in terms of tribology and tribochemistry is somewhat limited. Since some researchers focus on the tribochemistry of the aluminium alloys, yet others on the complicated methods by which the alloys are thought to undergo low levels of boundary lubricated wear, comparison of results between the two groups is not always simple.

1.1. Rationale and Objectives of this Study

The purpose of this research was to determine how a novel antiwear additive works in a tribosystem between an aluminium-silicon alloy and steel substrate. In addition, a thorough investigation into the tribochemistry and wear methods of aluminium-silicon alloys in lubricated tribosystems was conducted.

In research to date, aluminium-silicon alloys have only been lubricated with ZDDP, a lubricant containing a number of additives or a fully formulated engine oil. Therefore, in order to advance the research within this area, the lubricating abilities of a detergent additive were investigated. Furthermore, conclusive evidence with regards to the location of tribofilm formation on aluminium-silicon alloys would benefit the research community. Thus, the objectives of this research were as follows:

- To understand the methods by which aluminium-silicon alloys undergo low levels of wear

- To identify and analyse the tribochemistry of worn surfaces
- To observe tribofilm formation on aluminium-silicon alloys using a range of additives and quantify the rates and mechanisms of film formation
- To propose mechanisms by which tribofilms are generated on these aluminium alloys
- To determine the film formation mechanisms of a novel NOCH antiwear additive

1.2. Thesis Outline

This thesis is arranged into ten separate chapters, of which this introduction is the first. Chapter two provides an overview to the theory behind friction, wear and tribology. In addition, the experimental techniques employed within this research are introduced and the theory behind the way in which these techniques operate are described. The third chapter is the literature review, in which numerous areas of research have been analysed and discussed in reference to the current research topic, with a view to understanding such topics as ZDDP film formation and the wear of aluminium-silicon alloys, for example.

The fourth chapter presents the materials and experimental methods employed in order to study the lubrication of aluminium-silicon surfaces. Results obtained using the physical and chemical surface analysis techniques described in chapter two are presented in chapter five and subsequently discussed. Model surfaces were computer generated in order to provide an overview to the results. It was obvious from the results obtained that in order to fully understand tribofilm formation onto, and lubrication methods of, these aluminium alloys, research into the lubrication of silicon and aluminium surfaces, respectively, would have to be performed. A hypothesis as to the way in which aluminium-silicon surfaces undergo wear was devised, in relation to the literature.

In chapter six, replication of the contact conditions generated on silicon grains within the aluminium-silicon substrate studied in chapter 4 is conducted using a silicon crystal substrate. The materials and method by which this replication was completed are stated, with the results presented and subsequently discussed in chapter seven. Schematic diagrams were devised which described tribofilm structure and chemical composition on these semi-conductive substrates. Chapter eight investigates what would happen if the counterpart substrate were to interact with the aluminium matrix within an

aluminium-silicon alloy, with the materials and experimental method described in this chapter. Subsequent results are presented and discussed in chapter nine.

The final chapter concludes the results obtained and discussed within this thesis, with future work proposed. The data obtained throughout this work is also used to generate an advanced lubrication hypothesis of aluminium-silicon substrates.

2. Theory and General Techniques

2.1. Theory

2.1.1. Friction

When a solid substrate is placed in direct contact with another rigid surface and a force applied in order to move the former across the latter, the opposition to movement encountered is termed *Friction* [1-3].

Two different forms of frictional force are experienced when one object moves in relation to another, initiated by a tangential force F^T (Figure 1) [2, 3]. The first is the force necessary to commence motion, which is defined as the *static friction force*, F_s [2, 3]. Once movement of the solid body has begun, the force required to sustain motion is termed the *kinetic friction force,* F_k [2, 3]. The static frictional force is usually greater than the kinetic frictional force [2].

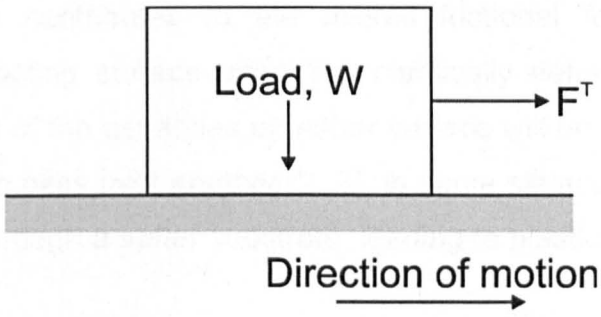

Figure 1: Solid object with load W on a horizontal surface

The three basic laws which govern friction are stated as follows:

- "The frictional force, F, is proportional to the normal load, W" [4]
- "The frictional force is independent of the apparent area of contact" [5]
- "The frictional force is independent of the sliding velocity, v" [5]

The first law can be written in the format shown in Equation 1, where μ = coefficient of friction. The coefficient of friction varies between substrate material and the experimental conditions employed [2].

$$F = \mu W$$

Equation 1: Frictional force [2, 3]

The friction measured in a contact originates from two main sources; *adhesive* friction and *deformation* [2, 3]. On a micro scale, the asperities present on the surfaces of the two interacting solid objects will look similar to that shown in Figure 2, where surface number 1 is moving relative to surface number 2 [2, 3]. Therefore, the load placed upon the contact will be supported by the

interacting, and subsequently deforming, surface asperities on the two substrates [3].

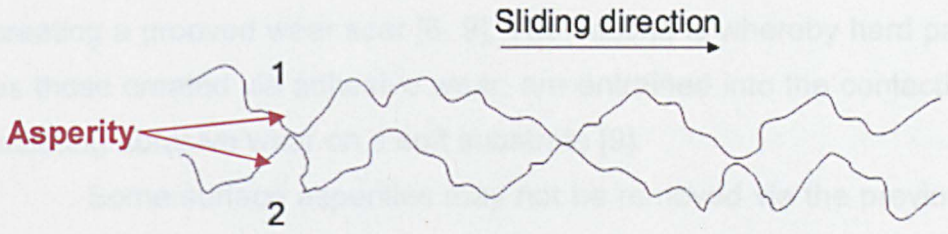

Figure 2: Surface asperity interaction

Surface asperities will adhere to one another because of chemical or physical interactions [3]. In order to overcome these bonds, via shear, a force in the sliding direction is required [3]. This force is referred to as the *adhesive frictional force* and in some circumstances can result in surface asperities being removed from a substrate [3].

Deformation contributes to the overall frictional force in a contact because the interacting surface asperities plastically deform under load [3]. Also, displacement of the asperities on either surface will be necessary in order for one substrate to pass over another [2, 3]. In some situations, a hard surface may also plough through a softer substrate, leading to plastic deformation of the latter [3].

2.1.2. Wear

When material is removed from a solid substrate, due to mechanical processes, *wear* is said to be occurring [6]. Wear will occur predominantly at interacting asperities, such as those shown in Figure 2 [7].

Some types of wear can be advantageous to a tribological system, such as "running-in" wear [8]. This is where the two contacting surfaces become more conformal, through the removal of unwanted surface asperities during the initial stages of running, ultimately reducing friction and wear in the system [8]. There are four main types of wear which occur on contacting surfaces [6, 9]:

1. Adhesive wear
2. Abrasive wear
3. Fatigue wear
4. Corrosive wear

The first type of wear transpires when a surface asperity removes material from the opposing contacting substrate via the *adhesion* of one

asperity to another [6]. *Abrasive wear* occurs in two different forms. The first is when a physically hard, rough substrate ploughs through a softer material, creating a grooved wear scar [6, 9]. The second is whereby hard particles, such as those created via adhesive wear, are entrained into the contacting interface, initiating abrasive wear on a soft substrate [9].

Some surface asperities may not be removed via the previous two types of wear [9]. If this is the case, repeated loading can provoke *Fatigue wear* and the asperity will be removed from the substrate [9]. The final main type of wear experienced in a tribosystem is *corrosive wear*. Chemical reactions between a corrosive liquid, for example, and a metal substrate produce compounds which bind to the metal surface [6]. Through sliding, these reaction products are removed and the process of chemical reaction occurs once more, each time increasing the wear volume from the metal substrate [6].

2.1.3. Tribology

Tribology is defined by the Oxford English Dictionary as "The branch of science and technology concerned with interacting surfaces in relative motion and with associated matters" [10].

The topic encapsulates the friction and wear of materials, with the objective to understand and explain the behaviour witnessed between two contacting surfaces. Due to the fact that the interactions on a micro scale between the two substrates will be influencing both the frictional response and wear observed, surface analysis of the test samples using multifaceted analytical techniques also falls under the topic of *Tribology* [11].

By analysing interacting asperities on contacting surfaces, using equipment designed to determine, for example, the topography and chemical nature of a substrate, an engineer has the tools required to comprehend the micro-scale workings of an engineering interface [11]. This can lead to improvements in design of a tribosystem and increase the performance of the interface.

2.1.4. Lubrication Regimes

In lubricated contacts undergoing relative motion, four main lubrication regimes exist, namely *Hydrodynamic*, *Elastohydrodynamic*, *Mixed* and *Boundary* [12]. In the former, a fluid film separates interacting surfaces [12]. High contact pressures result in elastohydrodynamic lubrication, in which a thin fluid film

procured through elastic deformation and variations in lubricant viscosity affords separation; surface interaction may additionally occur [12]. During boundary lubrication, in which contact conditions are severe, surface asperities on either substrate, such as those in Figure 2, are in direct contact [12]. Separation is afforded through the generation of adsorbed *tribofilms* on the substrates [13]. Mixed lubrication is whereby a combination of boundary and hydrodynamic lubrication regimes prevail in the interface[12].

The lubrication regime experienced by the interacting substrates is determined using the lambda ratio (Equation 2) [14].

$$\lambda = \frac{h_{min}}{\sqrt{(R_{q1})^2 + (R_{q2})^2}}$$

Equation 2: Lambda ratio [14]

This equation relates the minimum calculated film thickness (h_{min}) to the root mean square roughness (R_q) of the two interacting substrates. If the lambda ratio were greater than 5, hydrodynamic lubrication dominates; boundary lubrication will prevail if λ is less than one [14].

2.2. General Techniques

2.2.1. Topographical

2.2.1.1. Scanning Electron Microscopy (SEM)

Scanning electron microscopy was conducted using a Philips XL30 environmental scanning electron microscope (ESEM). In SEM, a cathode provides a source of electrons, which are passed through a voltage difference of varying electron volt intensity dictated by the user [15]. The electrons are focussed onto a substrate and interact with the surface to release two types of electron, namely; secondary (SE) and backscattered (BS) [15].

The former are accumulated after emission and typically possess a low electron voltage [15]. Analysis using a photomultiplier, via a process of acceleration, ultimately leads to the generation of an image of the sample under examination [15]. The topographical contrast of the substrate is generated by the SE mode of operation due to a number of different contrast methods [16].

Different types of detector to those employed for SE mode are used by an SEM to collect backscattered electrons (BSE) [15]. Backscattered electrons afford the user a visual representation of the various chemical phases within the

substrate in question [15]. This is because BSE are dependent on the atomic number in the region of electron incidence [15]. Contrast is typically generated between these different phases in the sample [16]; however topographical information regarding the substrate is also generated [16].

2.2.1.2. Atomic Force Microscopy (AFM)

The principle function of an atomic force microscope is to determine the topography of a surface to a high resolution [17]. The way by which the microscope obtains this data is by evaluating and recording the forces of attraction and or repulsion between a scanning tip and a surface of interest [18]. An atomic force microscope has three main modes of operation: contact, non-contact and tapping [17].

A Veeco Explorer scanning probe microscope (SPM), onto which Veeco MLCT-EXMT-A1 non-conductive cantilever type silicon nitride tips were fitted, was used to obtain the surface topography of test substrates in this work. The apparatus was of a tripod type arrangement, with a 100 μm x 100 μm range in the XY axis and 10.6 μm maximum range in the Z axis. The maximum and nominal radii of the tips were 60 nm and 20 nm, respectively. A SPM has a resolution of 0.05 nm vertically and 2 nm - 10 nm within the XY axis [19]. Operation of the atomic force microscope and subsequent data analysis was performed using SPMLab NT version 6.0.2 software.

For all data acquisition within this project, the apparatus was operated in contact mode. A constant force is applied to the silicon nitride tip, which is in direct contact with the substrate of interest [17]. When the tip is scanning across the surface, forces of repulsion between the two result in a vertical deflection of the tip from the substrate [17]. Using a laser, which is focussed onto the tip, this deflection is measured and consequently processed to provide topographical information regarding the substrate [17].

2.2.1.3. Stylus Profilometry

Stylus profilometry is whereby a stylus is repeatedly passed over a substrate, with which the tip of the stylus is in direct contact [20]. The vertical deflection, as with atomic force microscopy, is recorded and once analysed, provides representative information regarding the roughness and topography of the substrate [20].

A Taylor Hobson Form Talysurf 120L surface profilometer was used to obtain surface roughness values for substrates throughout this work. Data was obtained from a contacting conical diamond tip with a 2.5 μm radius, on to which a 0.85 mN load was applied. The apparatus was capable of resolving 10 nm in the vertical axis. The speed of the traverse was 0.5 mm / s, with 4000 data points obtained in one 7 mm traverse of the substrate.

2.2.1.4. White Light Interferometry

Substrate topography can be determined using white light interferometry by measuring the differences in the interference pattern of visible light produced when analysing a surface [21].

White light interferometry was conducted using a Veeco WYKO® NT3300S profiling system in VSI mode. All data was acquired and analysed using Vison32® software. Measurements were taken using optical phase-shifting and white light vertical scanning interferometry modes. The light source wavelength was between 400 – 700 nm. The apparatus had a vertical measuring range and resolution of 2 mm and 3 nm, respectively.

2.2.1.5. Nanoindentation

As with conventional indentation methods, nanoindentation can be used to determine the mechanical properties of substrates of interest [22]. In order to do this, an indenter, of known hardness, elastic modulus and geometry, is pressed into a test sample using an applied load [22]. As the name suggests, nanoindentation is concerned with measuring the depth penetration of the indenter into the substrate on the nanoscale [22]. Many different types of indenters can be used to determine the mechanical properties of substrates, for example, *Vickers, Berkovich, and conical* [23].

In this work, nanoscale indentation was completed using a Micro Materials Ltd NanoTest™ Platform One device. The equipment was fitted with a low load head, capable of applying 0.01 mN - 500 mN. The resolution in terms of applied load and depth penetration were < 100 nN and < 0.1 nm, respectively. The apparatus was housed within a closed temperature controlled cabinet. The substrate under examination was loaded into a moveable stage inside the machine whereby a microscope was used to identify the area of interest on the test sample. The stage was then positioned so that a *Berkovich* type indenter was in direct contact with the substrate.

Loading and unloading cycles were entered into the software supplied with the device, whereby the maximum load and depth penetration were stated. The apparatus was setup so that it would stop applying a load if either of these variables were reached. The device would then hold at this point for 5 seconds, in order to measure drift, before gradually reducing the applied load. The load and depth penetration were measured in real time, so that a loading-unloading curve for the substrate could be constructed. The NanoTest™ platform then proceeded to move the stage by a set increment, in order to permit for repeat measurements to be taken.

Once all scheduled indentations had been conducted, reduced elastic modulus and hardness data was deduced from individual loading and unloading plots obtained from the test substrate. In order to determine the hardness of the test substrate, the geometry of the *Berkovich* type indenter and maximum recorded depth were utilised [23]. Indeed, from this combination, an area of contact could be determined [23]. Since hardness, H, is equal to the mean contact pressure [24], a value for the former could be acquired using Equation 3, where W_{Max} is maximum applied load and A is contact area.

$$H = \frac{W_{Max}}{A}$$

Equation 3: Hardness of substrate [24]

Calculation of the reduced elastic modulus, E^r, from the unloading section of the aforementioned plot is more difficult, however. A process devised by Oliver and Pharr was used by the NanoTest™ platform software for this task, using a polynomial of order 2 for the power law equation [24]. In this, the gradient of the top 80 % of the unloading curve is entered into a series of equations, in order to determine the reduced elastic modulus of the substrate in question [24].

Conversion into elastic modulus from reduced form requires the mechanical properties of the *Berkovich* type indenter (Table 1).

Mechanical Property	Value
Poisson's Ratio	0.07
Elastic Modulus	1141 GPa

Table 1: Mechanical properties of Berkovich indenter [24]

Equation 4 is used to determine the elastic modulus of the substrate, E_s, from the reduced elastic modulus recorded by the nanoindenter. Where E_i and υ_i are the elastic modulus and Poisson's ratio of the indenter, and υ_s the Poisson's ratio of the substrate.

$$E_s = \left[\frac{1}{E^r} - \frac{(1-\upsilon_i^2)}{E_i}\right]^{-1} \times (1-\upsilon_s^2)$$

Equation 4: Determining elastic modulus of substrate using reduced elastic modulus [25]

The elastic modulus of the substrate is determined from each indentation completed. Both the hardness and elastic modulus for each substrate are averaged and a standard deviation calculated using Microsoft® Excel®.

2.2.2. Chemical Analysis

2.2.2.1. Energy Dispersive X-Ray Spectrometer (EDS)

EDS analysis of certain substrates was performed using the Philips XL30 environmental scanning electron microscope (ESEM) when scanning electron microscopy was conducted. Data was obtained and analysed using the INCA microanalysis system attached to the SEM. The energy dispersive x-ray technique affords the user an indication as to the chemical composition of a region of interest on a substrate [26]. The energy of emitted x-rays, which are generated through interaction between the electron source and substrate, are recorded; these provide elemental information regarding the surface under examination [26].

2.2.2.2. Fourier Transform Infrared (FTIR)

Infrared analysis provides detailed information regarding the molecular structure of a substance of interest [27]. This is obtained by subjecting the substance to an electromagnetic field [28] generated by an FTIR instrument. Energy transfer from field to multiatomic molecule is absorbed by the various atoms and subsequently leads to an excited state [28]. As an atom returns to its original non-excited state, emission of radiation ensues [28, 29]. This radiation is collected and analysed [30] by the FTIR apparatus. Information regarding the vibrational and rotational translations of a molecule lies within the infrared spectrum of the radiation [27]. Many different forms of both vibrational and rotational motion can occur [29]; different wavelengths of radiation are emitted for a given translation of a particular molecule [29]. A typical FTIR will employ a

interferometer to generate data from a molecule; a *Fourier Transform* performs mathematical processes on the resultant data to afford spectral wavelengths [30], thereby minimising the complexity of the results [31].

The FTIR apparatus used to perform infrared analysis on test substrates within this work was a PerkinElmer® Spotlight 400 Imaging system. The equipment contained a mercury cadmium telluride (MCT) infrared detector and was capable of analysing wavenumbers between 7800 cm^{-1} - 600 cm^{-1}. The equipment was calibrated using a gold reference slide prior to analysis. FTIR analysis of oils prior to experimentation was conducted using a PerkinElmer® Spectrum™ 100. The apparatus could measure wavenumbers between 8300 cm^{-1} - 250 cm^{-1}. The resolution used on both pieces of equipment was set at 4 cm^{-1}; data obtained was analysed using the *Spectrum*® software provided with the Spotlight 400 Imaging system.

2.2.2.3. Secondary Ion Mass Spectrometry (SIMS)

Secondary ion mass spectrometry provides chemical information about a surface by bombarding the substrate with a source of focused primary ions [32, 33]. When the ion source impacts the substrate, the emission of numerous *secondary* particles, of both positive and negative charge, ensues [32, 34]. This process is destructive to the sample [33]. The chemical nature of the surface is determined by evaluating the secondary particles using a form of mass analysis technique, such as a quadrupole mass spectrometer or a time-of-flight (ToF) analyser [32]. The latter possesses a much superior mass resolution and range [32, 33].

High magnification chemical analysis of test substrates was performed using a Millbrook Mini SIMS MC 300 MKII device. This apparatus had an operating pressure of 1 x 10^{-3} mbar. Samples were analysed using a 6 kV gallium liquid metal used as an ion source with a 10 µm beam size. The detector employed was a channel electron multiplier, and a quadrupole mass spectrometer determined the atomic mass of emitted secondary particles. Both static and depth profiling SIMS analysis were performed using this device. When operating in the latter mode, a much greater primary ion current density is employed [33].

ToF-SIMS was employed in order to attain very high mass and spatial resolution data from substrates of interest. The apparatus used was a ToF-

SIMS IV device, which was manufactured by ION-TOF GmBH. The spatial resolution was less than 100 nm, and the mass resolution greater than 10,000 atomic mass units. The source employed for static analysis was of liquid bismuth type, maintained at 1 kV, whilst depth profiling was conducted using a liquid caesium source operating at 5 kV.

3. Literature Review

The literature review section of this thesis encompasses a number of topics and research areas in order to attain information with regards to the subject matter of this thesis. Indeed, this chapter begins with addressing emissions regulations and then investigates the piston ring and cylinder liner interface. From here, a complete review of aluminium-silicon alloys is undertaken. After this, engine oils are discussed, with two additives reviewed in detail. Subsequently, the lubrication of aluminium alloys with organic additives is comprehensively reviewed, with the final section of this chapter researching the novel antiwear additive used throughout this work. The structure of the review is as follows:

- Emissions Regulations
- The Piston Ring / Cylinder Liner Tribological System
- Aluminium-Silicon Alloys
    - Types of Aluminium-Silicon Alloy
    - Structure and Mechanical Properties
    - Applications
    - Wear
- Engine Oil
    - ZDDP
    - Overbased Calcium Sulfonate
- Aluminium Alloys Lubricated by Organic Additives
    - Aluminium Alloys
    - Aluminium-Silicon Alloy / Aluminium-Silicon Alloy
    - Aluminium-Silicon Alloy / Steel
- Novel Antiwear Additive

3.1. Emissions Regulations

Regulations governing the emissions produced as a by-product of the internal combustion engines found in passenger motor vehicles, along with many other types of automotive-based transport, are becoming more restrictive [35-37]. Due to the fact that exhaust emissions can be damaging both health-wise and also environmentally, the need to maintain low levels of certain chemical products from internal combustion is paramount [38].

Modern automotive vehicles are tested thoroughly and various chemicals found within the exhaust emissions are monitored [36]. The European Union is the main body responsible for producing guidelines for all types of modern vehicles with respect to the composition of exhaust gases. The Euro 5

emissions standards [36] are the current set of laws which stipulate the maximum limits for particular chemicals within the exhaust of the aforementioned motor vehicles [36]. These chemicals, along with their upper values in petrol and diesel engined passenger transport, are listed in Table 2.

Chemical	Maximum Values (mg / km)	
	Petrol Engine	Diesel Engine
Carbon Monoxide (CO)	1000.0	500.0
Nitrogen Oxide (NO_x)	60.0	180.0
Hydrocarbons	100.0	-
Particulate Matter	4.5	4.5

Table 2: Euro 5 emissions standards for passenger motor vehicles

The Euro 5 governing rules will remain up-to-date until 2015, where the standards will be replaced with the Euro 6 regulations [39]. This document will see fit to significantly reduce the permissible mass of nitrogen oxide in diesel exhaust emissions from 180 mg / km (Euro 5) to 80 mg / km (Euro 6).

Engine lubricating oils also have to conform to standards which dictate the maximum quantities of certain constituents within the lubricant [35, 37]. Both the European Automobile Manufacturers' Association (ACEA) and the International Lubricant Standardization and Approval Committee (ILSAC) regulate the mass of both sulphur and phosphorus within an engine oil [35, 37]. The ACEA also place a restraint on the total percentage of molar mass of sulphated ash found within the fluid [35]. It is important to note that between these two regulatory bodies, a total of seventeen major vehicle manufacturers are represented [40, 41]. The maximum limits for phosphorus, sulphur and sulphated ash, as stated by ACEA and ILSAC, are shown in Table 3. These three components are regulated because if not employed in correct quantities, can lead to irreversible damage of the catalyst found in motor vehicles [42].

Chemical	Regulatory Board and Maximum Values	
	ACEA C1-08 (% m / m)	ILSAC GF5 (% Mass)
Phosphorus	0.05	0.08
Sulphur	0.2	0.5
Sulphated Ash	0.5	-

Table 3: Phosphorus, sulphur and sulphated ash maximum limits within passenger vehicle engine oils

As increasingly stringent guidelines are developed, and the permissible mass of phosphorus is potentially reduced, the quantity of ZDDP blended into a lubricating fluid will be heavily affected [42]. This is because within an engine oil, the main supply of phosphorus is the popular antiwear additive [42]. The zinc-based molecule will therefore either have to be completely removed from engine oil chemistry and substituted with a similarly effective yet more regulatory-conformal additive, or be utilised in decreased quantities within the lubricating fluid [42]. The problem with the former of these two points is that discovering a worthy successor to ZDDP is a challenging process, due to the zinc dialkyldithiophosphate's extremely effective capabilities [42]. The more feasible option is to reduce the level of ZDDP used and enhance its performance with an additional additive, such as that found in section 3.6.

Therefore, various constituents of exhaust emissions have to be regulated to ensure a passenger motor vehicle meets and exceeds various worldwide guidelines. An increasing number of restrictions placed upon these emissions will encourage both oil and automotive manufacturers to seek novel ways to ensure their products achieve the necessary standards.

3.2. The Piston Ring / Cylinder Liner Tribological System

A decrease in fuel consumption, and thus emissions, from a passenger motor vehicle can be induced by minimising energy loss within an engine, which is derived from four main sources, namely *exhaust*, *cylinder cooling*, *mechanical* and *brake power* [43]. As shown in Figure 3, the main contributor to mechanical, predominantly friction-related, energy loss is the piston ring and cylinder liner interface [43, 44], which is dependent on engine speed and load [45].

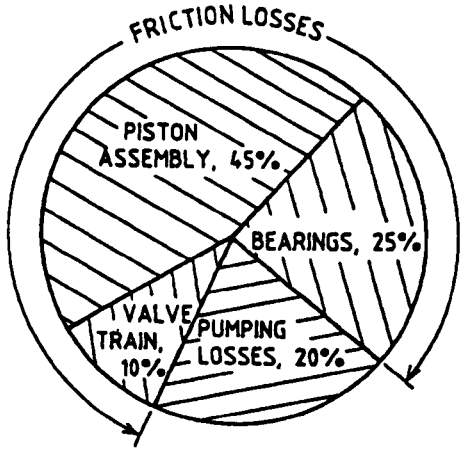

Figure 3: Mechanical energy loss within an engine [43]

These mechanical energy losses are relevant to this work since a piston ring and cylinder liner tribosystem is tribologically tested in this thesis. Hence, a complete review of the tribocouple is necessary in order to fully understand the interface. Therefore, the materials from which piston rings and cylinder liners are manufactured have been researched, together with their function and application. The lubrication regimes experienced within the tribosystem have also been comprehensively reviewed.

3.2.1. Piston Rings

Piston rings have numerous functions within an engine, such as heat transfer to the cylinder liner, which is cooled by the water jacket or air cooling fins, and away from the piston. In addition, they act as a seal to restrict blow-by gases from the crankcase and also ensure a standard amount of oil is available to the piston ring and cylinder liner interface [46, 47]. According to a number of authors, [48, 49], the piston ring pack, and of those piston rings from which it consists, is regarded as not only one of the most intricate tribological parts in the modern day engine, but also one of the most vital components to the system [48, 49].

Piston rings are located within grooves contained on piston crowns, and there are three types available, namely top compression, scraper (2^{nd} compression) and oil control (Figure 4A) [45]. This is the order in which the piston rings are located away from the top of the piston and as such, the former endures the greatest temperatures and pressures due to its proximity to the combustion chamber [45]. Compression rings provide sealing against the combustion gas pressures; in addition, the scraper ring minimises oil flow up the piston [45]. The oil control ring has a sole responsibility insofar as it regulates the oil volume transferred to the combustion chamber from the crankcase of the engine; for this reason, it has two operating surfaces (lands) and contains a spring to increase the radial force placed on the cylinder liner [45]. The flanks are the top and bottom inner edges of a piston ring groove [50]. To perform efficiently, the piston rings have to conform closely with the cylinder liner and the piston ring groove over the speed range of the engine [45]. The section beneath the piston rings on the piston is termed the skirt (Figure 4A) [45].

Depending on the engine and its application, different numbers of piston rings can be utilised on one piston [49]. In most modern engines, three rings per

piston are utilised, comprising of one of each of the aforementioned ring type [49]. In engines which have been designed specifically to minimise friction losses and therefore increase engine efficiency, only a top compression and oil control ring are utilised [46].

As it can be seen in Figure 4B, a number of forces act upon a piston ring when in operation [51]. The various forces enable it to be highly proficient in maintaining the contact between the cylinder wall and itself. Two important forces are the axial and radial cylinder gas pressures, P_A and P_R, respectively, which improve the piston ring's effectiveness (Figure 4B) [46, 51].

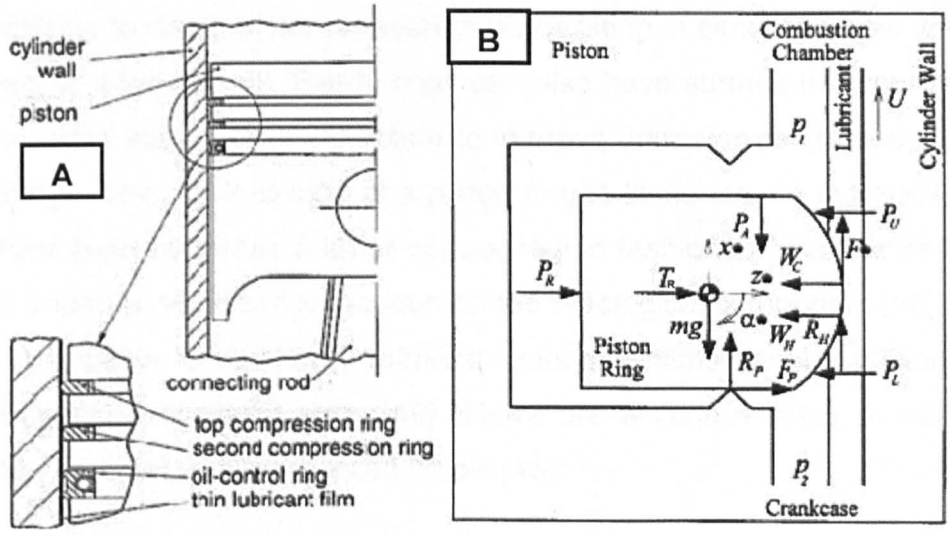

Figure 4: The piston assembly (A) [45] and forces acting on a piston ring [52] (B)

There are various designs of both compression and oil control rings [46], but it is important to note that the former acts as a seal to decrease the amount of blow-by gas while the latter is used to maintain a suitable engine oil thickness between the piston ring and cylinder liner contact in a functioning engine [46]. A large number of variants of compression ring can be acquired by a manufacturer when designing a new engine [46]. The various designs of the compression ring impart differing properties to the cylinder liner and piston ring contact, such as an increase in sealing efficiency and a decrease in the time duration required to undertake run-in [46]. Oil control rings can also be manufactured from an array of designs, depending on the application of the engine. Some oil control ring designs impart a small level of oil expenditure onto the engine, whilst an enhancement in the ability of the oil control ring to remove excess oil from the contact surface is also achievable [46].

The two forms of materials from which piston rings can be manufactured are cast iron or steel [46, 47, 49]. Flaked graphite cast iron of both alloyed

hardened and unhardened forms are not used as the material from which top compression rings are produced, but do find application as the base material for the remaining two piston rings [49]. An alloyed hardened form of spheroidal graphite cast iron and also steel can be used for the material from which top compression rings are fashioned, because of the enhancement in the opposition to bending which the two materials provide [46].

The substrate from which piston rings are manufactured is important because the material has to provide consistent mechanical and thermal properties to the piston ring over the entire speed range of the engine, and must also continue to do so when the system is operating in circumstances which are regarded as adverse [46]. Piston rings can also have surface treatments added after the initial stages of manufacture to improve corrosion resistance, amongst other things. The run-in period of a piston ring is lessened via the addition of a phosphate layer, whereas a tin or copper region fashioned to a finalised piston ring will impart a degree of lubrication on the tribological component [46].

In addition to surface treatment, defensive films can be affixed to the contacting edge of piston rings [49]. There are a various array of treatments available, some of which are listed below [46]:

- High velocity oxy-fuel Layers
- Chrome-ceramic Layer
- Molybdenum coating
- Physical vapour deposition
- Plasma spatter layers
- Chrome plating
- Nitriding / Nitrocarburising

These films impart properties to the base and surface treated material, such as a reduction in wear, along with a greater exterior hardness of the final product [46].

3.2.2. Cylinder Liners

Cylinder liners are available in two clearly distinct forms; dry liner or wet liner. The differences in engine block design dictate the type of liner required for a given application [53]. A dry liner differs to a wet liner because the former is not in contact with the water jacket, whereas a wet liner is an integral part of the

engine; it creates the coolant reservoir between itself and the engine block [53]. Dry cylinder liners are installed via either shrinking, pressing or casting in place techniques, whilst wet liners are slid into their final location [53].

Cylinder liners can be produced from either cast iron or aluminium-silicon materials [15]. Dry liners are generally manufactured from hypereutectic aluminium-silicon or cast iron [15]. Depending on the application, cylinder liners of a wet design can be produced from both hypoeutectic and hypereutectic aluminium-silicon materials; also, cast iron can be used to create the final product [53].

In order to provide a surface topography which is suitable for the given application, cast iron cylinder liners are machined in order to produce the desired topography of the surface [53]. Dry and wet production cylinder liners are etched, if produced from a hypereutectic aluminium-silicon material, or coated with a nickel dispersion film if fashioned from a hypoeutectic form of aluminium-silicon [53]. The final surface finish of a cylinder liner is of upmost priority, in order to ensure the contact between liner and piston ring are as accurate as possible, and this is conducted via honing procedures; the most efficient seal between the two engine components will then be formed [53].

The advantages and disadvantages of both dry and wet cylinder liners are shown below in Table 4 [53].

Dry Liner	Wet Liner
Advantages	
Sealing is not necessary	Uncomplicated system of replacement
Large pool of production materials	
Unite liner and block when both are manufactured from varying types of aluminium	
Disadvantages	
Unsatisfactory levels of heat transmission	
Large per unit costing[1]	

Table 4: Advantages and disadvantages of dry and wet cylinder liners [53] ([1] Compared to an engine block which has cylinder liners cast in place during the production of the block)

3.2.3. Piston Ring / Cylinder Liner Interface

The greatest contact pressure endured by the piston ring and cylinder liner interface in a conventional petrol engine operating under the Otto cycle is approximately 70 MPa, at the top compression ring [49]. The highest temperature expected in the contact between ring and liner in such an engine would be approximately 120°C at the liner and 200°C at the piston land above the top compression ring [49]. Film thickness for the tribosystem is reported to be less than 0.2 µm [49]. It must be noted, however, that this data was published in 2000 and as such, due to engine downsizing and increases in power outputs of engines over the past decade, contact pressures between ring and liner will have increased. Furthermore, this will have also increased the operating temperatures of the piston ring and cylinder liner interface.

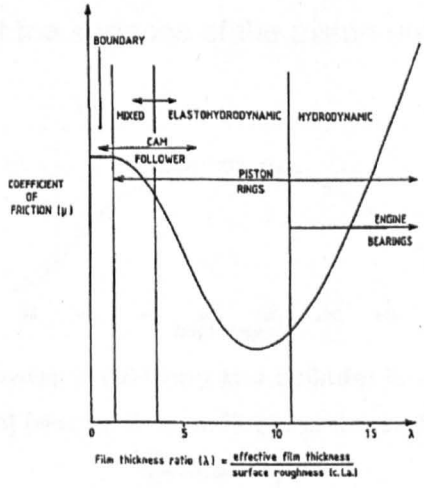

Figure 5: Stribeck diagram [49]

During one stroke of the crank in an engine, and thus moving the piston from top dead centre (0 degrees) to bottom dead centre (180 degrees) during the expansion stroke, four lubrication regimes (boundary, mixed, elastohydrodynamic and hydrodynamic) are said to influence the friction and wear in the contact between piston ring and cylinder liner; as shown in Figure 5 [50, 51, 54-57]. As the crank rotates around its axis and begins to move the piston away from the top dead centre position in the combustion chamber, it is clear to see that the coefficient of friction, as shown in Figure 6, begins to increase to the maximum value obtained in the entire 180° stroke of the crank [54]. Squeeze-film lubrication imparts an advantageous effect on the piston ring and cylinder liner interface following top dead centre in an engine, ensuring the greatest value of µ is not obtained until around 10° crank angle [50].

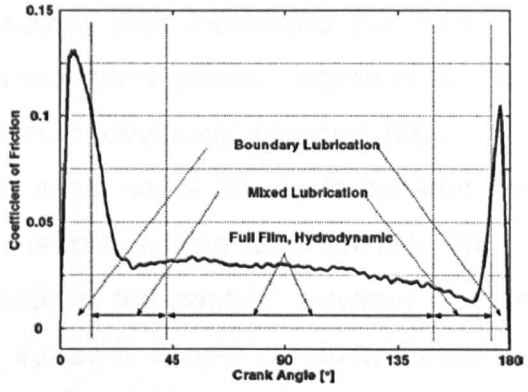

Figure 6: Friction coefficient throughout the expansion stroke in an engine [54]

When the friction coefficient is at its greatest, and the film thickness at its lowest value (Figure 7) just after top dead centre, it can be said that the main lubrication regime in the contact between liner and ring is boundary lubrication [51, 54, 56]. Therefore, at this location in the engine, a great amount of wear will occur, due to the fact that the surfaces of the piston ring and cylinder liner are in contact [50].

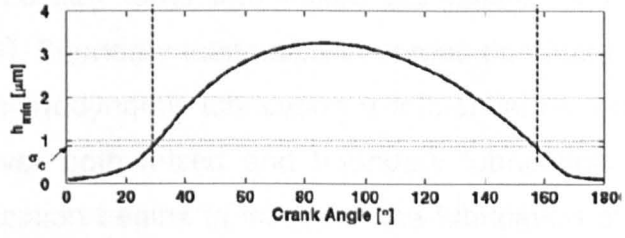

Figure 7: Film thickness between piston ring and cylinder liner throughout the expansion stroke in an engine [54] (dotted lines indicate onset and end of hydrodynamic lubrication)

As the crank angle increases towards 15° - 20°, and the entrainment velocity amplifies, the film thickness in the contact between the top compression ring and the cylinder begins to decrease and the friction coefficient also reduces (Figure 6 and Figure 7) [53, 54]. Mixed lubrication is seen to be the governing system in the contact at this point; thus a degree of full fluid film lubrication, along with surface interaction, is occurring in the interface [51, 54].

Dowson et al. [50] demonstrated that the contact between top compression rings and cylinder liners in engines endure a degree of elastohydrodynamic lubrication where previous authors had only predicted boundary and mixed lubrication [50]. It was stated that the presence of the elastohydrodynamic lubrication regime in the contact meant that not only would the cylinder liner and piston ring deform slightly under the immense loads placed upon the contact during operation, but also the engine lubricating oil

would increase its viscosity with increasing pressure [50]. Consequently, the two would combine to provide a greater degree of film thickness in the contact between ring and liner than previously expected [50].

When the crank angle nears 30°, hydrodynamic lubrication becomes the dominant system in the piston ring and cylinder liner interface; this is the primary lubrication mode in the contact between ring and liner [54, 55]. The lubrication of the two surfaces is now conducted entirely through full fluid film lubrication and thus the film thickness reaches its maximum value at around mid-stroke (Figure 7). Consequently, the coefficient of friction achieves its minimum value (Figure 6) and the energy expenditure endured by the viscous shear of the engine oil is the solitary contributor to the frictional force in the contact [54].

When the crank angle nears the end of its expansion stroke, toward bottom dead centre, the converse series of lubrication regimes takes place; hydrodynamic lubrication turns into mixed lubrication as the velocity of the piston reduces [54]. Boundary lubrication becomes dominant near bottom dead centre and elastohydrodynamic lubrication is influential on the friction and wear in the interface over both mixed and boundary lubrication regimes [50, 54]. Squeeze-film lubrication begins to influence the lubrication of the contact when the entrainment velocity of the engine oil reaches its minimum value at bottom dead centre [50, 54].

3.2.4. Tribochemistry of the Piston Ring / Cylinder Liner Interface

Although the tribochemistry of worn cylinder liners from fired engines can be evaluated [58, 59], it is common practice to simulate the piston ring and cylinder liner tribocouple [25, 59, 60] and subsequently chemically analyse the interface. This permits the chemical evaluation of tribofilms generated on either substrate using various operating conditions. A comprehensive review of the tribochemistry of ferrous and aluminium-silicon substrates lubricated with antiwear and detergent engine oil additives is presented in section 3.4.

3.3. Aluminium-Silicon Alloys

3.3.1. The Three Forms of Aluminium-Silicon Alloy

If two substances coalesce at respective particular fractions and impart the ensuing product with a melting temperature which, when compared to other

percentage blends of the two substances, is of the lowest possible value, the aforementioned combination is known as the *eutectic* mixture [61]. To generate a *eutectic* form of an aluminium-silicon alloy, a proportion of 12.6 wt. % silicon should be added to the material during the stages of manufacture, as shown in the phase diagram in Figure 8; the resulting melting temperature is 577 °C (Figure 8) [62, 63].

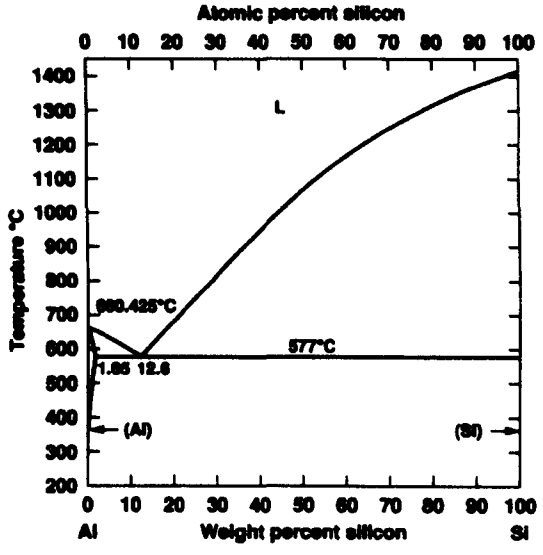

Figure 8: Aluminium-silicon binary phase diagram [62]

A mixture of aluminium and silicon can be classed as *hypoeutectic* if the proportion of aluminium in the mixture is greater than that found in the eutectic composition [61, 64]. Dissimilarly, if the wt. % of silicon in the alloy is larger than that fashioned in the eutectic composition, the final product is recognised as *hypereutectic* aluminium-silicon [61, 64].

3.3.2. Chemical Additions to Aluminium-Silicon Alloys

Aluminium-silicon (Al-Si) alloys are, as mentioned previously, available in three guises; *hypoeutectic*, *eutectic* and *hypereutectic*. Silicon is added to an aluminium substrate to bestow the resulting alloy with an increase in the material's resistance to wear, in both physical and chemical forms [65-67], and also decrease the thermal expansion coefficient, compared to pure aluminium [68-70].

Various other elements can be introduced into an aluminium-silicon alloy during manufacture, to impart the alloy with the mechanical and thermal properties suitable for a given application [63]. Such chemicals are listed below:

- Copper

- Iron
- Manganese
- Magnesium

The aluminium-silicon matrix is reinforced through the addition of copper to the alloy during the production processes used to create aluminium-silicon alloys; replacement of previously brittle and inductile stages within the material take place, or alternatively, a degree of precipitation-hardening may occur [63, 71]. The resulting material may have a greater strength [63, 71] but a reduction in both the original material's resistance to corrosive wear [63, 71] and its ductile nature [71] will ultimately transpire. Aluminium-iron-silicon and aluminium-iron phases can be introduced to an Al-Si material via the addition of iron prior to manufacture [71]. The former of the two stages is replaced by the addition of copper to the alloy [63].

The high temperature characteristics of an aluminium-silicon material are enhanced through the addition of manganese, which also decreases the solubility of both silicon and iron in the alloy, and further modifies the aluminium-iron-silicon phase [63]. The final main metallic addition to aluminium-silicon alloys is magnesium. As with copper, magnesium reinforces the aluminium-silicon matrix, however now does so via precipitation of magnesium-silicon molecules into the aluminium substrate [71, 72]. Other chemicals, such as tin, chromium, zinc and nickel, can be added to an aluminium-silicon alloy [68]. This effectively dilutes the aluminium substrate, meaning that the properties which silicon bestows upon an aluminium alloy are more pronounced [63]. The proceeding sections in this review focus on the structure, mechanical properties and applications of aluminium-silicon alloys.

3.3.3. The Structure of Hypoeutectic, Eutectic and Hypereutectic Aluminium-Silicon Alloys

When the wt. % of silicon in an aluminium-silicon alloy is lower than 12.6, and the resulting substrate referred to as hypoeutectic, α-Aluminium is seen to be the main phase in the material [63, 73, 74]; this is believed to be of a ductile and weak nature [63]. As can be seen in Figure 9, the main phase in this alloy, exhibits a branching layout to its configuration [73-75]; it is of a dendrite nature [73-75]. There is also a degree of silicon in a eutectic form within the material [63, 75]; this of a diamond cubic structure [63, 76], revealing itself as a flat and

non-uniform object (Figure 9) [73, 75]. The mechanical properties of this region are opposite to those of which the aluminium phase exhibits; silicon is brittle and hard [63]. As described previously in this thesis, metallic additions to the aluminium-silicon material form various phases within the material during the manufacturing process [63, 74, 75]; these are located within the α-Aluminium phase [63, 75] (Figure 9).

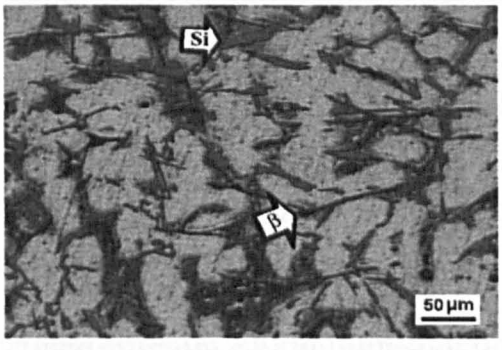

Figure 9: Optical micrograph of an Al - 9 wt. % Si alloy [75]

A eutectic form of an aluminium-silicon alloy is shown in Figure 10 [77]. The substrate comprises a random orientation of eutectic needle-shaped aluminium-silicon [63, 78]. Silicon can be observed within the alloy by its long, needle-shaped and non-uniform format [75, 77]. Figure 10 also highlights a phase which is composed of a mixture between the numerous chemicals added to the aluminium-silicon material during production [77].

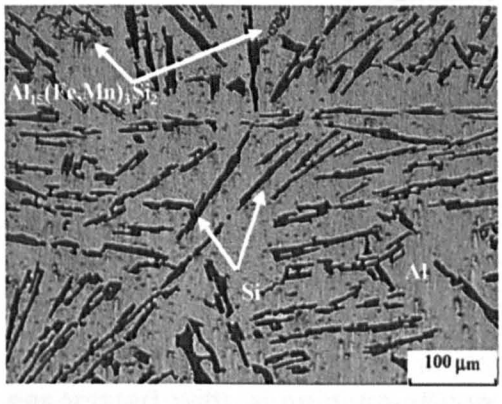

Figure 10: Optical micrograph of an Al - 12 wt. % Si alloy [77]

Hypereutectic aluminium-silicon alloys resemble that of which is shown in Figure 11 [79]. The main phase in the substrate is now silicon [63, 79, 80], which is of a rough and randomly orientated nature [63, 79, 80], and diamond cubic in its structure [63, 76]. The size of the silicon particles has increased, compared to low percentage silicon Al-Si alloys (Figure 9, Figure 10 and Figure 11 [75, 77, 79]). A degree of the eutectic form of silicon is also present in the

alloy [63, 80], along with an amount of α-Aluminium [80], which was observed in hypoeutectic forms of the alloy (Figure 9 [75]). Once again, the aluminium-silicon material comprised a composite between various additives and the base materials [63, 79] (Figure 11).

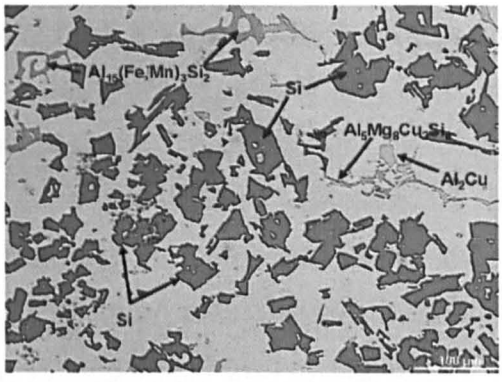

Figure 11: Optical micrograph of an Al - 18.5 wt. % Si alloy [79]

3.3.4. Properties of Hypereutectic Aluminium-Silicon Alloys

A hypereutectic aluminium-silicon alloy displays a number of good mechanical and thermal properties which enables it to be used in various applications (section 3.3.6) [81]. Some of these characteristics for a hypereutectic aluminium-silicon alloy, namely, A390, which has been manufactured using the processes of permanent mould casting and T5 heat treatment, are highlighted in Table 5.

Tensile Strength (MPa)	Hardness (HV)	Thermal Conductivity (W / m K)	Thermal Expansion Coefficient (20 - 100 °C) (µm / m K)	Density (Kg / m^3)
200	125	134	18	2730

Table 5: Mechanical and thermal properties of T5 permanent mould cast A390 aluminium-silicon [81]

The low mass associated with aluminium-silicon alloys is derived from the aluminium base material [82]; pure aluminium has a density of 2700 Kg / m^3 [82]. When aluminium is combined with the various alloying elements which in due course produces the A390 material, the resulting density increases slightly to 2730 Kg / m^3 [81] (Table 5). The thermal expansion coefficient of the permanent mould cast alloy in Table 5 is believed to be approximately 18 µm / m K [81], which is lower than that of pure aluminium; 23.6 µm / m K [82]. This 24 % reduction in the coefficient of thermal expansion is accredited to the

addition of silicon to the substrate (Table 6) [68-70]. Thermal conductivity of the A390 substrate highlighted in Table 5 is 134 W / m K [81], enabling the hypereutectic aluminium-silicon material to be utilised in applications which require effective heat transmission either to, or from, a heat source [83].

The tensile strength of a typical A390 alloy, which has undergone T5 tempering, is said to be 200 MPa (Table 5) [81]. This strength, along with the hardness of the material, can be increased by using different production methods [81]. However, as mentioned in section 3.3, the strength which the A390 material does possess is bestowed upon the substrate by various chemical additions. The maximum extent to which elements are permitted to be added to A390 during production is shown in Table 6.

Maximum Wt. % of Various Elements in A390											
Si	**Fe**	**Cu**	**Mn**	**Mg**	**Cr**	**Ni**	**Zn**	**Sn**	**Ti**	**Others; Each**	**Others; Total**
16.0 - 18.0	0.5	4.0 - 5.0	0.1	0.45 - 0.65	N/A	N/A	0.10	N/A	0.20	0.10	0.20

Table 6: Maximum wt. % of various elements in an A390 Al-Si alloy [84]

As Table 5 highlights, the Vickers hardness of a permanent mould cast A390 alloy which has undergone T5 heat treatment is approximately 125 HV [81]. The silicon present within hypereutectic Al-Si alloys, which is regarded as the main phase in the material [63, 79, 80], is reported to possess a hardness in the region of 715 - 1450 Kgf / mm^2 [76]. The resistance to wear which a hypereutectic aluminium-silicon alloy displays is provided by the aforementioned hardness of silicon [58, 65, 81]. Overall, therefore, it is possible to say that hypereutectic aluminium-silicon alloys exhibit a number of key properties, namely:

- Low mass [81]
- Good thermal properties [81]
- Effective resistance to wear [58, 65, 81]
- Low coefficient of thermal expansion [81]

3.3.5. Comparison between a Hypereutectic Al-Si Alloy and Cast Iron

The mechanical and thermal properties of a form of grey cast iron, class BS EN 1561-GJL-200, are shown in Table 7 [85-88]. Grey cast irons, such as that shown in Table 7 and similar versions to it, are typically utilised within engines [83, 89, 90]. Due to a marked reduction in density and increase in thermal conductivity, cast iron is most susceptible to being exchanged for an alternative material such as hypereutectic aluminium-silicon [83, 89-91].

Tensile Strength (MPa)	Hardness (HV)	Thermal Conductivity (W / m K)	Thermal Expansion Coefficient (20 - 100 °C) (µm / m K)	Density (Kg / m^3)
230 [88]	150 [87]	49 [85]	10.6 [86]	7150 [88]

Table 7: Mechanical and thermal properties of EN 1561-GJL-200 (BS1452) grey cast iron

Comparing Table 7 with Table 5, it is clear that the two engineering materials have differing mechanical and physical properties. The density of the EN 1561-GJL-200 cast iron shown in Table 5, 7150 Kg/m^3, is 2.6 x greater than that of which the A390 material enjoys [81, 88]. Subsequently, automotive applications which utilise a hypereutectic aluminium-silicon alloy, will benefit in terms of mass reduction, compared to its cast iron counterpart [83, 89-91]. A decrease in the mass of a vehicle, imparted by the usage of aluminium-silicon alloys, will ultimately lead to a reduction in the fuel consumption of that means of transport [89, 90], and also a possible decline in total engine vibration [89], compared to when using a cast iron component.

The thermal expansion coefficient exhibited by cast iron in Table 7 is 59 % of that displayed by A390 (Table 5) [81, 86]. Thus, in situations which involve heat addition, aluminium-silicon alloys are less advantageous compared to cast iron, due to the unsatisfactory levels of expansion under heat addition [83, 91]. Conversely, aluminium-silicon alloys may find employment within an internal combustion engine due to its excellent thermal conductivity, which, at 134 W / m K is 2.7 x greater compared to cast iron (Table 7, Table 5) [81, 85]. This property of a hypereutectic aluminium-silicon alloy allows it to dissipate heat away much more effectively than cast iron, thus avoiding regions which may suffer excessive heat build-up [81, 83, 85, 91].

The hardness, on a macro scale, of EN 1561-GJL-200 cast iron is 20 % greater than that of A390 (Table 7, Table 5) [81, 87], and the tensile strengths of the two materials are also comparable [81, 88]. The ability of aluminium alloys to be manufactured without difficulty means that this becomes the primary choice for manufacturers wishing to produce parts of an engine, such as a cylinder, which require tight tolerances [83, 91].

Therefore, overall, it can be said that the slight reduction in both strength and hardness, on a macro scale, of a hypereutectic Al-Si material does not dramatically hinder the ability of the alloy from being utilised in circumstances where cast iron would typically find employment [83, 89, 90]. The thermal conductivity [83, 91], along with both the density [83, 89-91] and the relative simplicity of manufacture [83, 91] of the aluminium alloy are suffice to guarantee its position as an automotive engineering material [83, 91].

3.3.6. Applications

Aluminium-Silicon alloys find application in a varied array of appliances and circumstances [6-16]. Due to the different mechanical and thermal properties of hypoeutectic, eutectic and hypereutectic Al-Si alloys (section 3.3.4), the three forms of alloy are utilised in numerous areas of modern day engineering [6-16]. Generally, aluminium-silicon materials find usage in three core subject matters [53, 58, 68, 69, 84, 92-97]:

- The automotive industry [53, 58, 68, 69, 84, 94-96]
- Electronics [84, 93]
- Refrigeration / air compressors [84, 92, 93, 97]

Hypoeutectic forms of aluminium-silicon alloys are used in both motor vehicles and also compressors designated for employment in the refrigeration and air compression markets [53, 69, 97]. In terms of automotive applications, engine blocks of a monolithic nature can be manufactured from hypoeutectic Al-Si [53], along with pistons [69, 84], cylinder heads [84] and the housing unit for turbochargers [84]. The low percentage silicon form of aluminium is used as a material from which compressor innards for the refrigeration market are produced [97]. The main reasons why the aforementioned products are manufactured from hypoeutectic aluminium-silicon are because of its inherent

low mass, reasonable strength and relative ease with which the material can be cast, to name but a few [68, 84].

Eutectic aluminium-silicon alloys are generally utilised as the material from which pistons and some potentially problematic castings are fashioned [84]. This is mainly due to the increase in silicon in the matrix of the alloy, in contrast to the lower percentage variety of Al-Si, which enhance the thermal properties of the material, along with improving the resistance to wear [66, 68].

Finally, a high percentage silicon aluminium alloy finds employment in the automotive sector as the material from which engine blocks of a monolithic nature are produced [53, 58, 95, 96], as well as being used as a piston substrate [68, 95] and the substance from which various ancillary pumps are produced [84]. Both dry and wet cylinder liners can be fashioned from a high silicon content aluminium alloy [53]. As with hypoeutectic Al-Si, hypereutectic alloys can be the basis of compressors and their workings which are used in the air conditioning and refrigeration sectors [84, 97]. The very good wear and thermal properties exhibited by hypereutectic aluminium-silicon alloys are the main reason for application in the aforementioned areas [66, 68, 84].

3.3.7. Lubricated Wear of Aluminium-Silicon Alloys

Under lubricated conditions, an aluminium-silicon substrate is thought to experience wear according to two different theories; one suggested by Nicholls et al. [66, 98] and the other by Dienwiebel et al. [58]; the two models are shown below. Also discussed in this section is the low wear of Al-Si alloys.

3.3.7.1. Conventional Theory of Al-Si Wear in Lubricated Contacts

A theory which is postulated predominantly by Nicholls et al. [66, 79, 98] states that under lubricated conditions, the material which is incident upon an aluminium-silicon substrate will be directly supported by the particles of silicon present in the matrix of the alloy (Figure 12) [66, 98].

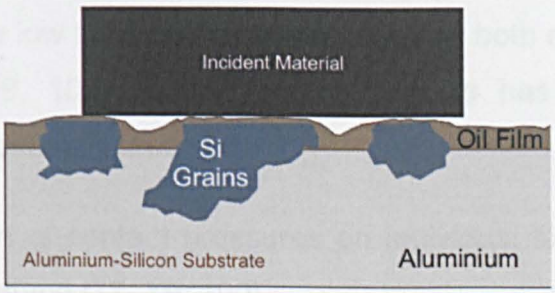

Figure 12: Conventional theory of aluminium-silicon wear (adapted from [58])

Subsequently, the silicon grains will endure the majority of the wear in the contact and prevent the aluminium substrate from encountering excessive amounts of wear [79].

3.3.7.2. New Theory of Al-Si Wear in Lubricated Contacts

The other theory on how aluminium-silicon surfaces prevent excessive wear under moderate loads is that of which has been described by Dienwiebel et al. [58] and less recently by Reddy et al. [67]. As shown in Figure 13, silicon particles, along with various other materials found on the surface of the alloy, are worn during the initial wear-in period of the aluminium alloy [58]. The ensuing small particles are then forced back into the surface of the aluminium substrate [58, 67]; this is said to bestow the alloy with its resistance to wear [58]. After this process, silicon particles do not extend beyond the surface of the aluminium substrate [58].

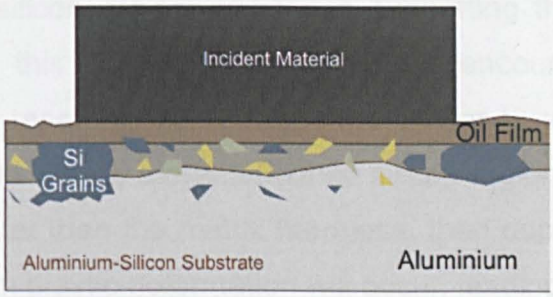

Figure 13: New theory of aluminium-silicon wear (adapted from [58])

3.3.7.3. Lubricated Low Levels of Wear on Al-Si Alloys

Recently, the methods by which aluminium-silicon alloys wear whilst experiencing low applied loads within a lubricated tribosystem, have become increasingly attractive to researchers. The reason for this is because Al-Si cylinder liners operating within engines encounter minimal levels of wear, resulting in something called *ultra-mild wear* [99]. In this situation, wear on the aluminium substrate will be less than 10^{-4} mm^3 / m [99].

Studying these low levels of lubricated wear on both eutectic [77, 79] and hypereutectic [79, 99, 100] aluminium-silicon alloys has lead to two main progressions in this research area:

- The calculation of contact pressures on individual silicon grains located on the alloy surface [77, 79, 100]

- Hypotheses as to how Al-Si alloys wear when experiencing low loads [77, 79, 99, 100]

Indeed, using a number of equations [77, 79, 100-102] it has been possible to determine contact pressures applied to the protruding silicon grains on the surface of aluminium-silicon alloys. This is reported to lie anywhere between ~ 650 MPa for a eutectic alloy with dendrite-like silicon regions [77], to 715 MPa [79] and 1500 MPa [100] on square shaped silicon areas found within a hypereutectic form of the alloy [79, 100].

The contact pressure can subsequently be used to estimate the extent of wear within the contact. If the applied contact pressure is deduced to be less than the known hardness of the aluminium matrix which supports the exposed silicon grains, ultra-mild wear will dominate in the contact [79]. Within the ultra-mild wear regime, the majority of the wear on the substrate is believed to occur solely on exposed silicon grains, which are supporting the applied load [79]. When operating in this condition, the alloy will encounter little change in topography and will resemble something very similar to an unworn substrate, except for wear marks on the aforementioned silicon regions [79]. Conversely, if the pressure is greater than the matrix hardness, then depression of the silicon grains and aluminium plastic deformation will occur, leading to a greater amount of wear recorded in the contact [79]. This new wear regime typically endures wear levels from 10^{-4} to 10^{-3} mm^3 / m, and is termed *mild-wear* [103].

The way in which an aluminium-silicon alloy will endure lubricated low wear levels, has been proposed by many authors [77, 79, 99, 100, 104]. Accumulating this data results in the following series of steps:

1. Some silicon grains fracture, reducing their size [99, 100]. If silicon grain size can be preserved, wear levels will not increase [99]

2. Fragments of silicon are created via wear and lead to abrasive wear of matrix and also silicon grains [99, 104]

3. Load carrying silicon grains depress into matrix [77, 79, 99, 100]

4. Aluminium matrix plastically deforms under applied load and becomes amassed around depressed silicon grains [77, 79, 100].

5. **With extended sliding distances** silicon becomes level with aluminium base material [77, 79] and wear of now exposed aluminium regions occurs [77, 99, 100]

Therefore, it can be stated that aluminium-silicon alloys are extremely complex in the ways in which they wear. As this section has highlighted, the alloy will experience wear depending on the applied contact pressure and the hardness of the matrix within the alloy under investigation.

3.4. Engine Oil

An engine oil is comprised of hydrocarbons when in the form of a mineral oil [105, 106]. The fluid can also be produced synthetically, which improves on the properties revealed by mineral oils [106]; these are generally derived from hydrocarbons also [106]. To these base oils, whether mineral, synthetic or a combination of the two, a number of additives can be added [106]. These enhance certain characteristics of the lubricant, along with providing the fluid with a reduction in those qualities of the oil which are unfavourable [106]. Additives are found in quantities of up to 20 % of the total molecular mass of the lubricating fluid [106]; such additives are listed below [106-108].

- Antiwear Additives [106-108]
- Detergents [106-108]
- Friction Modifiers [107]
- Dispersants [106-108]
- Foam Inhibitors [106]

An engine oil has to be able to protect an engine from excessive wear and decrease the friction loss endured within the system [106]. Also, for example, an engine oil must possess good viscosity with varying temperature characteristics, along with an ability to not degrade seals which exist within an internal combustion engine [106]. Therefore, depending on the oil utilised, a system such as an internal combustion engine will notice a reduction in wear, decrease in fuel consumption and an increase in the time duration before the oil will need replacing [106].

3.4.1. Antiwear Additives

The level of wear between two fairly high loaded interfaces can be reduced by the action of an antiwear (AW) additive [106, 109]. These additives are generally fashioned from chemistry which contains a degree of ash [109] and provide a resistance to wear via the formation of a boundary lubrication tribofilm upon the two contacting tribological surfaces [106].

3.4.1.1. Zinc Dialkyl Dithiophosphate

The conception of zinc dialkyldithiophosphate (ZDDP) in the early 1940's was to generate a chemical additive which could impart a system, in which the metal dithiophosphate found employment, with a reduction in both the degree of oxidation and corrosion previously witnessed [107, 110-114]. The most renowned characteristic of ZDDP is its ability to reduce the amount of wear in an automotive interface such as the piston ring and cylinder liner contact [107, 111]; this was not realised until the following decade from its inception [115]. In addition to this, ZDDP also exhibits good extreme-pressure characteristics [116]. The general chemical structure of zinc dialkyldithiophosphate is shown in Figure 14 [42, 107]. In order to permit the additive to possess oil solubility, a number of groupings have to be added to the chemical [107]; these are either aryl or alkyl in nature [107, 110]. Therefore, there are vast arrays of zinc dialkyldithiophosphates available [117].

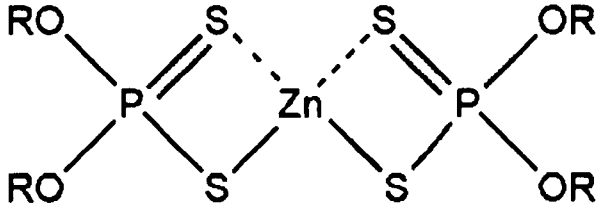

Figure 14: The structure of ZDDP [42, 107]

ZDDP is conventionally used to limit the wear between two ferrous-based surfaces undergoing boundary lubrication [118, 119]. However, as the need to reduce mass of vehicles intensifies, modern versions of these tribosystems are being invented. This leads to the incorporation of aluminium-silicon alloys as, for example, cylinder liners in passenger cars. Therefore, the ways in which ZDDP lubricates Al-Si surfaces is becoming increasingly important. A review into the film formation, structure and antiwear properties of ZDDP on ferrous-based and Al-Si alloys is now presented.

3.4.1.1.1. ZDDP Film Formation on Ferrous Surfaces

It is well known ZDDP minimises wear upon incident ferrous surfaces by generating a tribofilm on the substrates [120] [119-123]. In order to impart a tribological contact with a reduction in wear, the ZDDP molecule in the lubricating base oil has to decompose [121, 124-131]. Even though the way in which ZDDP forms on contacting surfaces in a tribosystem has been studied for a considerable period of time, the method of ZDDP film formation is widely disputed. A number of authors have investigated and hypothesised as to how the ZDDP molecule breaks down to initiate the formation of the aforementioned tribofilm, but as yet, it is still not clear which route(s) the ZDDP structure takes.

It is believed that the addition of either heat [121, 124, 126, 127, 129-131] and or the effect of rubbing [120, 126, 132, 133] initiates the degradation of ZDDP. The main disagreement in this area is whether the ZDDP molecule initially adsorbs onto the surface of the ferrous substrate and then decomposes [128-130, 132] or whether the metal dithiophosphate only chemically adsorbs to the iron/steel surface after degradation [124, 125, 127]. There are generally five key areas into which the breakdown of ZDDP and adsorption onto the ferrous surface can be classified:

- Thermal Degradation
- Acid and Base Hardness Principle
- Thermo-Oxidation
- Hydrolysis
- Linkage Isomer

Thermal degradation

The degradation of zinc dialkyldithiophosphate under the addition of heat (125 °C - 180 °C) was studied in the 1960s [134-136]. The resultant products from these decomposition experiments were deemed to be mercaptans, hydrogen sulphide, olefins, sulphides and zinc phosphates [134-137]. Ashford at al. [136] investigated the effect aeration has on the thermal degradation of ZDDP; It was concluded that the degradation of the metal dithiophosphate does not initiate nor advance due to the presence of oxygen [136].

Coy and Jones [116, 138] used NMR to study the products created from the heating of three types of ZDDP at 180°C for between 1 and 16 hours. It was

found that ZDDP does decompose under the addition of heat to form zinc phosphates, alkyl sulphides and a mercaptan [138]. It was determined that the aforementioned products of decomposition must play an important role in the extreme pressure characteristics of ZDDP [116]. This was demonstrated by conducting tribological experiments using a four-ball test rig; investigating the extreme-pressure properties of the oils which had been heated and analysed previously versus that of synthesised products of degradation [116]. The tribological studies revealed that the synthesised compounds had comparable abilities to that of both fresh ZDDP and also pre-heated solutions [116]. A conclusive process by which zinc dialkyldithiophosphate decomposes via the addition of heat was described in the second of the two papers by Coy and Jones [138].

Acid and Base Hardness Principle

Martin *et al.* [126, 139] described a way in which the ZDDP molecule reacts with the iron-based contacting surfaces, incorporating the theory of hard and soft Lewis acids and bases (HSAB) into the functionality of ZDDP. Key to this was the earlier work of Pearson [140]. XANES and AES were used to chemically identify ZDDP tribofilms created on ferrous-only tribocouples using reciprocating tribometers [126, 139]. A TEM was also used in one article to study both the physical nature and the chemistry of wear particles obtained from the aforementioned contact [126].

The authors stipulate that in order for this proposed model to work, the zinc-based polyphosphate molecule will react with iron oxide [126, 139]; operating in this manner, the physically hard Fe_2O_3 is consumed by ZDDP, reducing wear [126, 139]. The by-product of this reaction was deemed to be zinc oxide [126, 139]. Through a series of reactions given in literature [126] both zinc and iron sulphides are said to be created when the theory of hard acids and bases is incorporated into the workings of the ZDDP molecule [126].

Thermo-Oxidation

Willermet et al. [141] studied the effect of an air or a nitrogen atmosphere on the wear of ferrous surfaces using a four-ball test setup. It was found that the degree of wear on the test specimens lubricated with ZDDP was considerably reduced when the experiment was run in air. It was concluded that oxygen must

therefore play a key role in ZDDP film formation on ferrous surfaces; the decomposition of the metal dithiophosphate was deemed to be thermo-oxidative [141].

Further work by Willermet et al. [127] examined the products of both thermal and thermo-oxidative degradation of ZDDP; the former of the two was produced by passing argon through ZDDP in base oil prior to heating. FTIR was used to analyse the two resulting solutions versus that of a generated ZDDP tribofilm; it was observed that the spectra for the thermo-oxidative compound was comparable to that of the tribofilm. The authors concluded that oxygen is therefore an important component in the degradation of the metal dithiophosphate molecule [127]. Mechanisms by which the thermo-oxidation of ZDDP occurs have been described [128, 132, 142]. Thermo-oxidative degradation leads to the production of zinc and iron phosphates [132] and zinc sulphides [128, 132].

Hydrolysis

Spedding and Watkins [124] used various analysis methods, such as FTIR and NMR, to study the resultant products obtained from thermal decomposition tests carried out on zinc dialkyldithiophosphate at temperatures between 160 °C and 200 °C [124]. The authors found that when the heating process of the ZDDP molecule was starved of water using boiling solvent, the degradation of the metal dithiophosphate was practically halted [124].

Hydrolysis was deemed to be the main manner by which ZDDP will degrade under the addition of heat [124]. The mechanism devised by Spedding and Watkins is described in literature [124]; it is proposed that water is created, acts as a catalyst and then is consumed in the processes which will result in the decomposition of ZDDP [124]. The final components obtained after degradation were determined to be a combination of alkyl sulphides and a zinc polyphosphate [124, 125]. Integrating this method within a typical internal combustion engine would not be difficult, state the authors, as the water volume and operating temperatures within the engine are suffice to promote the onset of hydrolysis [124].

Linkage Isomer

Fuller et al. studied the chemical characteristics of both antiwear and also thermal films which had been fashioned from ZDDP on ferrous surfaces using a reciprocating tribometer and oil bath, respectively [131]. The two forms of ZDDP-derived film were analysed using XANES and NMR techniques [131]. Comparing the results, it was deemed that the thermally-derived films were analogous to the antiwear films under study [131]. The authors thought that zinc dialkyldithiophosphate film formation onto ferrous surfaces involved a number of steps [131], which encompassed not only both thermo-oxidative degradation of the ZDDP molecule, but also hydrolysis; ultimately leading to both short and long chain zinc polyphosphate formation [131].

However, key to the author's procedure of ZDDP film formation [131] was the existence of a linkage isomer. This molecule was determined chemically to be a modified form of ZDDP, which possessed a relocation of the alkyl groupings on the antiwear additive [131]. The isomer was said to be created in solution and would then adsorb, in conjunction with unmodified ZDDP, onto the ferrous substrate. Both would decompose in a similar manner via thermo-oxidation and hydrolysis [131].

3.4.1.1.2. ZDDP Film Structure and Properties

Once the initial decomposition of the ZDDP molecule has occurred, the process of antiwear film formation can begin. Tribofilm formation will occur exclusively in the contacting regions of rubbing [133, 139, 143]. The reported chemical composition of these ZDDP-based tribofilms on ferrous substrates varies between author and publication, yet most highlight a common structure as described in the following paragraphs.

A ZDDP tribofilm is considered to have three key sections to its structure, namely; substrate-additive layer, bulk, and tribofilm surface [42, 120, 129, 132, 139]. Physically, it is widely acknowledged that tribofilms generated from the zinc-based additive distribute themselves into configurations which resemble a "pad-like" [144] nature, and are of no consistent dimension [42, 120, 145-147]. A computer generated image of a traditional ZDDP tribofilm on a ferrous surface is shown in Figure 15, whilst Figure 16 shows the morphology of a ZDDP tribofilm on 52100 steel. The reported thicknesses of these tribofilms on iron-based surfaces are documented in Table 8.

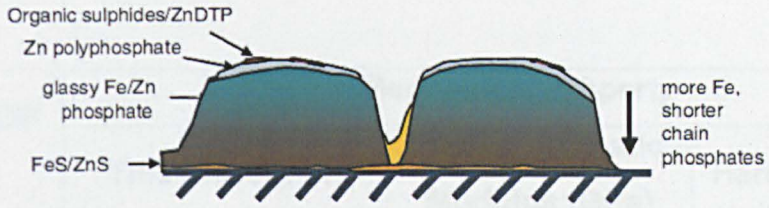

Figure 15: The traditional ZDDP tribofilm on a ferrous surface [42]

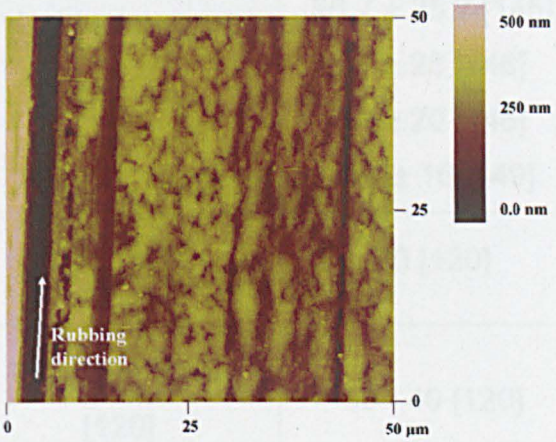

Figure 16: AFM Image of a ZDDP tribofilm on 52100 steel [123]

It is thought that the base layer of a ZDDP tribofilm (the part of the tribofilm adsorbed onto the substrate) is an iron or zinc sulphide [120, 125, 132]. Articles by Martin et al. [118, 126, 139] have alluded to the fact that the authors suspect the principle of acids and bases shows the production of iron polyphosphates (and zinc oxide (ZnO)) [118, 126, 139]. The bulk section of the metal dithiophosphate antiwear film is widely thought to be constructed from zinc and iron-based short chain polyphosphates [60, 118, 121, 127, 129, 131, 132, 139]. It is thought that contained within this section are also zinc and iron sulphides [118, 126, 139]. The final, outer tribofilm surface is believed to consist of long chain zinc polyphosphate [121, 129, 132, 139]. Work carried out by Bec *et al.* [120] has shown that prior to rinsing with solvent, there is also an alkyl phosphate region generated by the aforementioned decomposition of ZDDP observed on the very top part of the antiwear structure.

The generation of a thermally-induced layer present on non-wear regions of test substrates has been observed [121, 126, 139]. This is believed to be chemically similar to a ZDDP mechanically-generated tribofilm [121, 129, 131] and is suggested to only form at temperatures > 110 °C [129, 133]. However, the thermal film is seen to not possess the mechanical properties exhibited by a ZDDP tribofilm [145]. Table 8 highlights various physical and mechanical

properties of both ZDDP thermal films and tribofilms generated on ferrous substrates.

Type of ZDDP Film	Mechanical Property		
	Thickness (nm)	Reduced Elastic Modulus (GPa)	Hardness (GPa)
Tribofilm	150 [120, 148] 120 [143]	82 ± 18 [122] 96.7 ± 25.7 [145] 87 ± 23 [146] 74 ± 20 [146] 117 ± 16 [149]	3.9 ± 1.0 [145]
Substrate-Additive Layer	≤ 50 [120]	90 [120]	4.7 [120]
Bulk (Short Chain Polyphosphate)	100 [139] 50-90 [120]	30 - 40 [120]	2 [120]
Surface (Long Chain Polyphosphate)	10 [139]		
Thermal Film	11 [150]	34.8 ± 9.7 [145]	1.5 ± 0.2 [145]

Table 8: Mechanical properties of ZDDP films on ferrous surfaces

3.4.1.1.3. ZDDP Tribofilms on Al-Si surfaces

Investigations into the lubrication of aluminium-silicon surfaces with ZDDP has only recently become topical; this is probably due to the alloys' relatively recent inception into the automotive world. Initial work carried out by Fuller et al. [151] found that polyphosphate tribofilms can be generated on aluminium-silicon surfaces using all Al-Si tribocouples; indeed, the authors reported that these films were in fact chemically identical to those found on steel substrates [151].

Nicholls et al. [98] studied the chemical nature of the resulting tribofilms formed on eutectic aluminium-silicon substrates using the XANES technique. It was reported that zinc polyphosphate tribofilms could be formed on test Al-Si surfaces when a set of four conditions were fulfilled; these included the ability to withstand adverse pressure in the contact and also the lack of abrasive particles in the tribosystem [98]. It is the former of these two which identifies the physically hard silicon grains within the aluminium matrix as favourable areas

onto which ZDDP film formation can occur [98]. Film formation was then postulated to arise on the Al-Si surfaces using an altered version of the chemical reactions proposed by Fuller et al. [131], incorporating a linkage isomer as per [131]. It was stipulated that when the level of wear on the aluminium alloy was high, it was possible for aluminium phosphide to be created [98].

The chemistry of 52100 steel pins incident against hypereutectic aluminium-silicon alloy plates using XANES and X-PEEM was the study of the Nicholls' group in 2005 [66]. It was observed that a ZDDP antiwear tribofilm was generated on silicon grains under relatively high contact pressures (~ 240 M Pa); these were believed to be identical to those films formed on ferrous substrates [66]. An observed ZDDP-based tribofilm on a silicon grain is shown in Figure 17. Indeed, the authors reported that the films on the silicon surfaces consisted of short chain zinc polyphosphates in the main section of the tribofilm and long chain at the very outermost region of the protective layer [66]. It was found that this zinc polyphosphate structure was witnessed also on the aluminium regions of the alloy; this, however, was thought to have been transferred from the considerably harder silicon areas [66].

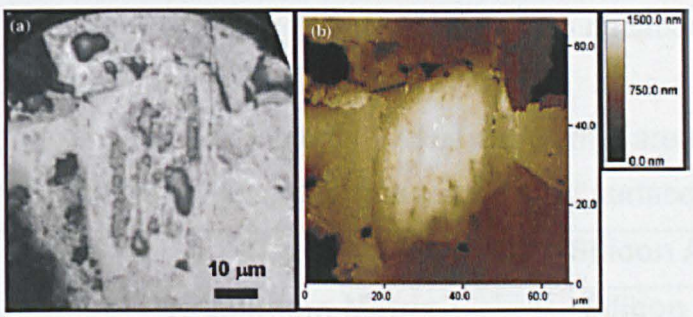

Figure 17: X-PEEM (a) and AFM (b) of ZDDP tribofilm on a silicon grain [66]

Pereira et al. [25] studied the chemistry of 25 wt. % Si aluminium-silicon surfaces which had been in a tribocouple with 52100 steel pins lubricated with ZDDP under various temperatures, using XANES and X-PEEM. Once again, the tribofilms formed on the Al-Si surfaces were said to be created on protruding silicon grains and were chemically comparable to those found on ferrous surfaces [25]. The authors found long chain polyphosphates formed on silicon grains after long test durations, whereas a high oil temperature reduced this chain length [25]. It was reported that ZDDP in its un-reacted state was observed, along with short chain polyphosphates, on the aluminium section of the alloy [25]. The tribofilm was only found on the aluminium matrix because of

transfer from protruding silicon grains and thermal decomposition of ZDDP [25]. As with ferrous surfaces, it was noticed that ZnS was created under tribological conditions; FeS was said to be created via heavy wear [25]. The authors also amended the four point system proposed by Nicholls et. al [98], adding the ease at which the ZDDP tribofilm can bind to contacting surfaces [25].

XANES was used once again to analyse the tribochemistry of the surfaces in a eutectic Al-Si / 52100 steel pin contact [152]. Low contact pressures were employed (< 45 MPa) and the variation in tribofilm with varying oil temperature was observed [152]. The linkage isomer documented earlier [98, 131] was reported to only form at high oil temperatures [152]. Short chain polyphosphates were identified on the aluminium regions of the alloy [152]. The length of the chain on the silicon grains was dictated by temperature; high oil temperature equalled shorter chains, whilst the chain length increased with reduced temperatures [152].

Jiménez et al. [153] found that the tribocouple between a hypereutectic Al-Si alloy and 52100 steel pin lubricated with oil containing ZDDP and employing a contact pressure of 150 MPa, generated tribofilms on protruding silicon grains [153]. The authors stipulated that any tribofilm species observed on the aluminium regions of the alloy were present only because of transfer from the aforementioned silicon crystals [153].

As observed in Table 9, the majority of authors in this area of research agree on a number of aspects of tribofilm formation on Al-Si surfaces.

ZDDP Tribofilm Key Points	**Region of Aluminium-Silicon Alloy**	
	Aluminium Matrix	**Silicon Crystal**
Tribofilm Observed?	Yes [25, 66, 152, 153]	Yes [25, 66, 98, 152, 153]
Similar to that Found on Ferrous Surface?	Yes [25, 66, 151]	
Chemical Nature of Tribofilm	Zinc polyphosphate [25, 66, 152]	Zinc polyphosphate [25, 66, 98, 152, 154] ZnS [25]
Method of Formation	Transfer [25, 66, 153] Thermal decomposition [25]	Linkage Isomer [98, 152] Adsorption [98, 152]

Table 9: ZDDP tribofilms on Al-Si alloys

3.4.1.1.4. Mechanical Properties of ZDDP Tribofilms on Al-Si Alloys

The mechanical properties of tribofilms created using ZDDP to lubricate aluminium-silicon alloys have been documented; these values, along with the thickness of the films on Al-Si substrates, are given in Table 10.

Mechanical Property of Tribofilm	Region of Aluminium-Silicon Alloy	
	Aluminium Matrix	Silicon Crystal
Reduced Elastic Modulus (GPa)	56 ± 12 [152]	30.3 ± 7.8 [153] 84 ± 10 [152] 77 ± 11 [25]
Hardness (GPa)		1.4 ± 0.4 [153]
Thickness (nm)	42 ± 4 [152]	42 ± 4 [152] 40 - 225 [25] 150 - 250 [66]

Table 10: Mechanical properties of ZDDP tribofilms on Al-Si alloys

Comparing the values in Table 10 with those shown in Table 8 for ZDDP tribofilms on ferrous surfaces, it is clear that the protective films formed on the silicon section of the aluminium alloy possess similar reduced elastic modulus values to those found on iron-based substrates. However, the reported thicknesses of the zinc-based films on silicon regions within an aluminium-silicon material can be greatly reduced, compared to the protective layer found on ferrous substrates.

In terms of the aluminium matrix, the reduced elastic modulus of films found here appear to have decreased in value, compared to the ferrous-based substrates and also the silicon regions within the aluminium alloy. The documented thickness of ZDDP-derived tribofilms on the aluminium matrix seems at the lower end of film thickness observed on silicon grains.

3.4.1.1.5. Antiwear Characteristics of ZDDP tribofilms on both Ferrous and Al-Si Substrates

The way in which ZDDP imparts wear reduction on a tribosystem is believed to fall into five categories:

- By protecting the surfaces from corrosion
- Utilising the mechanical properties of the tribofilm
- Supporting load

- Preferential shearing
- Removal of hard Fe_2O_3 particles

The former of the five relate to ZDDP's ability to react with hydroperoxides in solution, minimising the degree of wear achieved via corrosion on the contacting surfaces [155, 156]. Obviously, this would be more suited to a ferrous-based material as these surfaces are more susceptible to corrosive wear than the more modern Al-Si substrates.

The majority of authors believe that the mechanical properties of the aforementioned ZDDP tribofilms play the key role in providing low wear levels in the tribosystem. The ability of the phosphate-based film to support the applied load in the contact is thought to limit wear [120, 146], as this would stop the interaction between peaks on either surface [120, 123]. The other main point related to the film's mechanical property is that of shear strength. The ZDDP antiwear film is thought to possess a rate of shear which is significant enough to permit the ZDDP film to grow, yet at such a level which will mean the tribofilm will encounter shear preferentially to that of the surface onto which it is forming [120, 145]. This means that the surface will remain undamaged and the film can continue replenishing itself prior to acting in a sacrificial manner [145, 157].

The final suggested method of antiwear protection imparted by ZDDP is that devised by Martin and co-workers [118, 126, 139, 158]. This method encompasses the hard acid and bases theory previously suggested as a process by which ZDDP film generation occurs [126] (section 3.4.1.1.1). Physically hard Fe_2O_3, created during tribological rubbing of surfaces, is thought to be consumed via a reaction between zinc polyphosphate and iron oxide (Equation 5) [126].

$$5Zn(PO_3)_2 + Fe_2O_3 \rightarrow Fe_2Zn_3P_{10}O_{31} + 2ZnO$$

Equation 5: Iron oxide consumption via zinc polyphosphate [126]

Acting in this manner, the potentially damaging oxide is removed from the tribosystem and abrasive wear is reduced [126].

3.4.2. Detergents

Detergent additives have two principal areas to address when being employed in a lubricating oil within a tribological system [34, 159, 160]. The first is to hinder the formation of unwanted residue on contacting surfaces; the second, to

neutralise acidic compounds, which, for example, are produced during combustion, and would lead to deterioration of the lubricating fluid and the onset of corrosion in the tribosystem [34, 159, 160].

3.4.2.1. Overbased Calcium Sulfonate

Overbased calcium sulfonate (OBCS) is the most prominent of the overbased-type detergent additives blended within modern engine lubricating oils [34] and is shown in Figure 18. The detergent is created in overbased form in order to enhance the additive's ability to neutralise acidic compounds [160, 161]. Overbased means that the metallic base at the heart of the additive is extremely alkaline-rich due to the vast amounts of the metal, such as calcium carbonate, present in that region [160, 161].

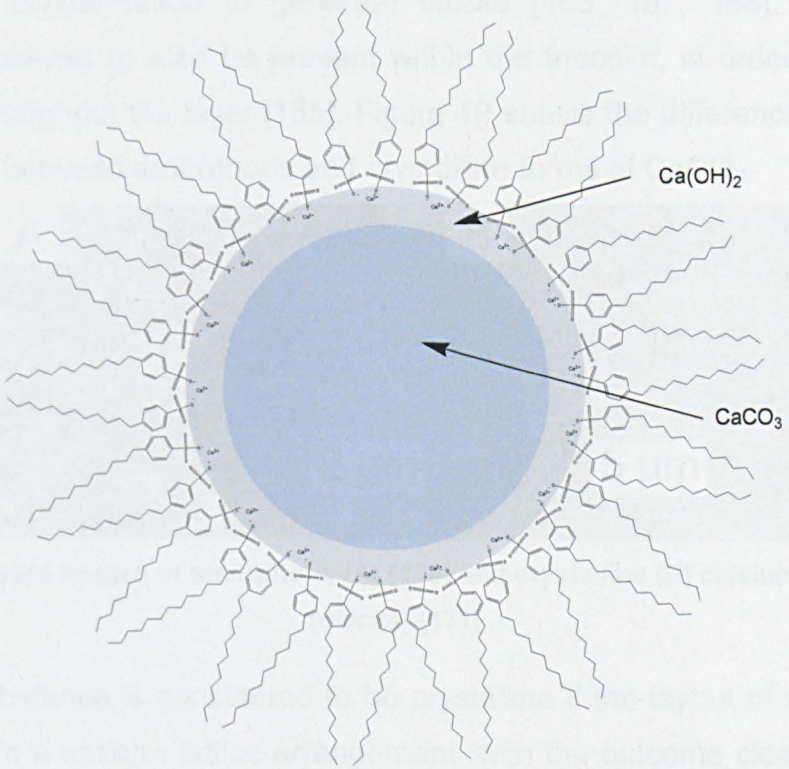

Figure 18: Overbased calcium sulfonate molecule (adapted from [34])

As it can be seen in Figure 18, the OBCS molecule comprises a calcium carbonate core, onto which sulfonate surfactant polar groups are coupled [34]. The core is thought to possess a diameter of no greater than 10 nm [34, 162] and is of an amorphous type [163]. Stabilisation of the detergent is imparted by hydrophobic alkyl chains, making the additive soluble in oil [34]. This format can be termed micellar [164]. Work done by Cizaire et al. using ToF-SIMS has alluded to the presence of calcium hydroxide around the carbonate core of the molecule [34].

3.4.2.1.1. Film Formation by Overbased Calcium Sulfonate

Under tribological conditions, calcium sulfonate is believed to adsorb onto the contacting surfaces [165, 166] via entrainment of the detergent into the tribocouple [160]. This initial stage of film formation occurs via the rubbing action of the tribosystem, promoting the removal of the surfactant chains from the additive's core [165, 167, 168] via the breaking of various ionic bonds [168]. Adsorption can also occur without frictional stimulus, where the calcium-based molecules position themselves on the substrates such that attached sulfonate chains are directed vertically upwards toward the counterface surface [167].

Calcium carbonate is thought to then build up on the surfaces of the two substrates [165, 167, 169]. The amorphous calcium carbonate film is believed to undergo crystallisation to generate calcite [165, 167, 168]. Amorphous $CaCO_3$ is believed to also be present within the tribofilm, in order to facilitate cohesion throughout the layer [165]. Figure 19 shows the difference in physical appearance between amorphous and crystalline forms of $CaCO_3$.

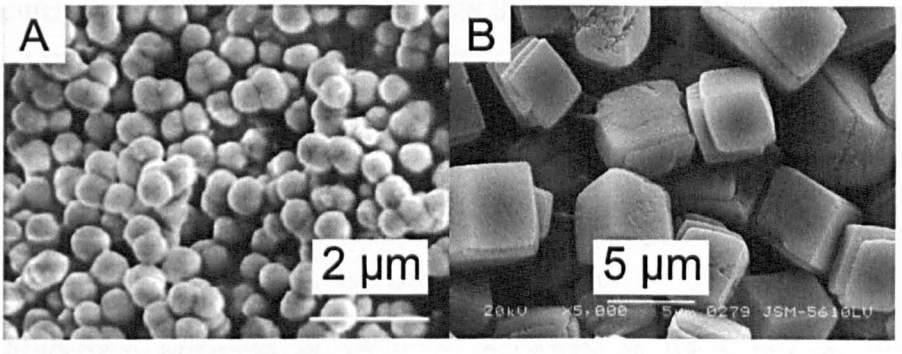

Figure 19: SEM images of amorphous (A) [170] and crystalline (B) calcium carbonate (calcite) [171]

A substance is considered to be crystalline if the layout of its molecular structure is in a uniform lattice arrangement, with the outcome clearly exhibited in its physical appearance [172]. Crystallisation is a multi-faceted process which incorporates *supersaturation, nucleation and growth, interfacial phenomena, breakage and agglomeration* [173]. The temperature of the substance and its concentration within a solvent play two very important roles in determining the crystallisation of a material [173].

Calcium carbonate will transform from an amorphous type to calcite due to heating of the substance, which dehydrates the molecule [170, 174]. Varying the volume of water added to amorphous $CaCO_3$ prior to the addition of heat will lead to different forms of crystals being created [170]. However, one

tribologically-based author reports that crystallisation is hindered by water [167]. In any case, it can be said that the conversion from amorphous to crystalline calcium carbonate is a complicated and varied process, which is still not understood fully.

An OBCS tribofilm is reported to be a "solid-like" [175], strongly adhered [165] and rapidly forming layer [160, 176]. Lubricating a 52100 steel ball-on-disc setup with various OBCS detergents using an MTM-SLIM tribometer, Miklozic et al. [177] determined tribofilm thicknesses to range from 100 nm - 150 nm [177].

Recent work conducted on the tribochemistry of the film generated from calcium sulfonate reveals that calcium carbonate is not the only product to be formed on contacting surfaces. Indeed, Cizaire et al. [168] observed, using auger electron spectroscopy, the creation of calcium oxide from $CaCO_3$ due to the evaporation of carbon dioxide. Calcium oxide was also witnessed, beneath the upmost tribofilm layers of both $CaCO_3^-$ and SO_3^-, using ToF-SIMS by Kubo et al. [178]. The creation of calcium oxide was thought to permeate through the pyrolysis of calcium carbonate, combined with the action of rubbing between the two surfaces [178]. Finally, Minami et al. showed the existence of $Ca(OH)_2$ on the very top of the tribofilm using XPS; this was generated via a reaction between CaO and water [166]. It is postulated that water enables an enhancement in the concentration of calcium sulfonate molecules within a region of the tribosystem, boosting film formation [179].

One important property of calcium sulfonate is its ability to form a tribofilm on non-ferrous surfaces [165]. Kubo et al. [180] also gave a detailed account of how overbased calcium sulfonate forms on DLC coated samples, using ToF-SIMS. This initially occurred via transfer of a CaO layer from the steel surface to DLC substrate [180]. Subsequent build up of calcium carbonate ensued, and both surfaces housed a tribofilm comprising of both calcium carbonate and calcium oxide [180].

3.4.2.1.2. Antiwear Characteristics of Overbased Calcium Sulfonate

The antiwear characteristics of calcium sulfonate have become an increasingly attractive topic to researchers of late. Indeed, it has been reported that calcium sulfonate has very good antiwear properties on ferrous-based surfaces [160, 165, 166, 168, 169, 176, 178] and in some circumstances instilling the tribosystem with wear levels lower than those obtained with ZDDP alone [165,

166, 169, 176]. It is also shown that overbased calcium sulfonate reduces the wear in a contact, compared to the neutral form of the molecule [160, 169, 178]. This latter point is explained by the colloidal disposition of this overbased additive and its subsequent ability to generate a thick layer on the contacting surfaces [160].

Deposited calcium carbonate-based tribofilms serve to protect the substrates from wear [165, 169]. However, it has been reported that the calcium oxide layer formed on rubbing surfaces has a positive effect on the wear and friction in the tribosystem, improving both, compared to ZDDP [166]. The relative hardness of calcium oxide, calcium carbonate and calcium hydroxide is: CaO [181] > $CaCO_3$ [182] > $Ca(OH)_2$ [183]. Therefore, the composition of the calcium-based tribofilm present on contacting substrates will influence the wear and friction in the tribosystem.

The antiwear characteristics of the calcium-based tribofilm generated from overbased calcium sulfonate additives are believed to originate from the film minimising the degree of interaction between contacting surfaces [160] via preferential removal and shear of the aforementioned tribofilm [165]. This, as one author correctly identified, is similar in nature to the antiwear function of ZDDP [160].

3.4.2.1.3. Interactions between Calcium Sulfonate and ZDDP on Ferrous Substrates

Understanding the effects detergents and antiwear additives such as calcium sulfonate and ZDDP have on tribofilm formation, friction and wear in a tribosystem is very important. This is because modern engine oils contain varying amounts of such chemicals, along with other additives, and being able to predict the synergistic / antagonistic behaviour between numerous molecules would be very useful to formulators.

The antiwear performance of a combination of ZDDP and overbased calcium sulfonate has been observed by a number of authors in various different ferrous-based tribosystems [166, 169, 176, 184, 185]. It was found that when the tribocouple was lubricated with a combination of overbased calcium sulfonate and ZDDP, wear measured on test specimens was greater than with both ZDDP [166, 176, 184, 185] and calcium sulfonate [166, 176, 185] alone; indicating competition between additives on the test surfaces. However, it must

be noted, that one author did report a slight reduction in wear, using a four-ball setup [169], when lubricating the contact with overbased calcium sulfonate and ZDDP, compared to single usage of both detergent and antiwear additives, respectively [169]. The frictional response of a tribological interface is also influenced by the combination of overbased calcium sulfonate and ZDDP [166, 176]. Indeed, it was observed that the combination of additives increased the friction in the contact, compared to the overbased detergent alone [176] and also to a higher value than solitary ZDDP [166].

Therefore, it is clear to see that there is certainly a degree of antagonistic behaviour occurring between the two additives. Thus, there must be chemical differences in the tribofilms formed on the surfaces of substrates when a combination of additives are employed.

Indeed, it has been shown that when lubricating ferrous surfaces with overbased calcium sulfonate and ZDDP, the amount of calcium found on the surface has decreased compared to detergent alone [166, 176]. This is highlighting a reduction in calcium carbonate / calcium oxide on the interacting surfaces [166, 176]. Sulphur is believed to exist in three separate forms within the tribofilm created from ZDDP and calcium sulfonate [186, 187]. Sulphate and sulphite are witnessed within the protective layer as the calcium-based detergent undergoes disproportionate reactions [187]. In addition to this, ZDDP donates sulphide to the tribofilm [186] and is thought to be the main form of sulphur within the protective layer [187]. Zinc sulphide has been observed in tribofilms generated from a combination of ZDDP and calcium sulfonate additives [187]. Therefore, this constituent of the ZDDP protective layer (section 3.4.1.1.2) is still forming under competition from calcium sulfonate [187]. Indeed, HSAB has been used to explain the formation of ZnS in the presence of other additives; the soft Zn^{2+} acid would favourably bond with S^{2-}, because the latter is a soft base [188].

The addition of overbased calcium sulfonate to ZDDP results in a reduced amount of phosphorus in the tribofilm [176], along with the entire removal, from the protective layer, of long chain polyphosphates [185, 187]. This latter point is explained by the presence of the calcium cations (Ca^{2+}), which act to reduce the length of the phosphate chains [186, 189]. The most significant observation, perhaps, is the existence of calcium phosphate within the tribofilm [184, 185, 187]. Reduced amounts of phosphorus and the previous

comment also hold true for competition between overbased calcium phenates and salicylates with ZDDP [186]; showing that it is the calcium carbonate core of the additive which plays an important role in film formation [184].

Calcium phosphate [190] is known to possess a greater mechanical hardness than calcium carbonate [182]. Therefore, if calcium phosphate is indeed present within the tribofilm on contacting surfaces, abrasion of the carbonate-based protective layer will most probably occur [185, 187]; leading to increased wear in the tribosystem. The formation of calcium phosphate has been postulated to occur by exchange of zinc from ZDDP with calcium from the overbased detergent [185, 186, 189]. A two way mechanism by which this process may occur has been proposed [185]. Firstly, it is suggested that ZDDP decomposes via hydrolysis and oxidation, leading to the generation of a phosphate anion, which then reacts with calcium in solution [185]. In combination with, or alternatively, polyphosphates are created from ZDDP; subsequent hydrolysis and then reaction with calcium leads to calcium phosphate [185]. Due to the inherent stability of calcium phosphate, generation of this molecule is ideal [185].

The chemical hardness model devised by Pearson [140] has also been used to explain how calcium phosphate may be generated on the surfaces of the substrates [188]. Due to the fact that Ca^{2+} has a greater acidic hardness than Zn^{2+}, the favoured reaction product using the HSAB theory would be calcium phosphate [188]. The formation of both calcium phosphate and also ZnS using the HSAB theory is shown in Equation 6.

$$3CaS + Zn_3P_4O_{13} \rightarrow 3ZnS + Ca_3P_4O_{13}$$

Equation 6: Formation of ZnS and calcium phosphate using the HSAB theory [188]

Therefore, the documented increase in wear levels noticed when combinations of overbased calcium sulfonate and ZDDP are used to lubricate contacts, compared to the sole use of either additive, can be accredited to a number of key points. These are:

- Decrease in the quantity of calcium-based tribofilm species on contacting surfaces [166, 176]
- Significant reduction in / removal of the amount of long chain phosphate in tribofilm [185]

- Calcium phosphate formation - abrasive to tribofilm [185, 187, 190]

Overall, it can be said that the effectiveness of both ZDDP and overbased calcium sulfonate in their frictional and wear characteristics are reduced when the two additives are combined within a functioning lubricating oil. However, since both additives have their own unique characteristics such as anti-oxidation and removal of corrosive products, it is important formulators find effective working concentrations for the two molecules.

3.4.2.1.4. Calcium Sulfonate Lubricating Al-Si Surfaces

There has been very little work conducted on the lubrication of aluminium-silicon substrates with calcium sulfonate. Indeed, the research that has been completed has focussed on fully formulated oils lubricating these aluminium alloys. However, since there were many similarities between ferrous and Al-Si surfaces in terms of ZDDP film formation (section 3.4.1.1.3), perhaps the same is true regarding calcium sulfonate.

The chemistry of a worn Al-Si cylinder liner which had been under test in a fired dynamometer and lubricated with commercially available oil was studied by Dienwiebel et al. using auger electron spectroscopy [58]. Calcium, along with zinc, sulphur and phosphorus were witnessed on the silicon grains within the alloy after test [58]. However, the latter three chemicals were reported to be of very low intensities [58]. The author noted the far greater intensities and depths of calcium and phosphorus on the aluminium regions of the alloy, compared to silicon [58]. This was attributed to the mechanical working of the aluminium matrix during test, which lead to the accumulation of various chemicals within the worn surface [58]. Evidence of a physical tribofilm was not documented by the authors, suggesting the protective layer is difficult to identify on these aluminium alloys [58].

Using XPS, Tomastik et al. [59] identified the presence of zinc, phosphorus, sulphur and calcium on worn aluminium-silicon cylinder liners evaluated in engine tests using a commercial engine oil [59]. These chemicals were thought to originate from a film of residual lubricant, soot and wear debris [59]. Cylinder liners were also tested using a tribometer and lubricated by commercial engine oil and diesel; ZDDP tribofilm generation was observed [59].

On both engine and tribometer samples, Zinc and phosphorus content decreased during depth profiling [59].

Generation of low wear levels on aluminium-silicon surfaces using incident 52100 steel balls and lubricated with fully formulated oil, has been conducted by a number of authors [77, 79, 99, 100]. Whilst all articles discuss the ways in which these aluminium alloys wear [77, 79, 99, 100], the chemical nature of a film generated by one test oil on the aluminium substrate was analysed using XPS and FIB-SEM by Chen et al. [100].

Indeed, this tribofilm (Figure 20) was comprised of calcium, zinc and sulphur [100]. It was reported, using an electron energy loss spectrometer, that amorphous carbon was present within the tribofilm; therefore, referring to section 3.4.2.1.1, this could originate from the carbonate in a calcium carbonate protective layer [100]. Unfortunately, no further embellishment was provided; however, it can be said that the film seemed to have been present on the aluminium base material, and was also located on the exposed silicon grains [100].

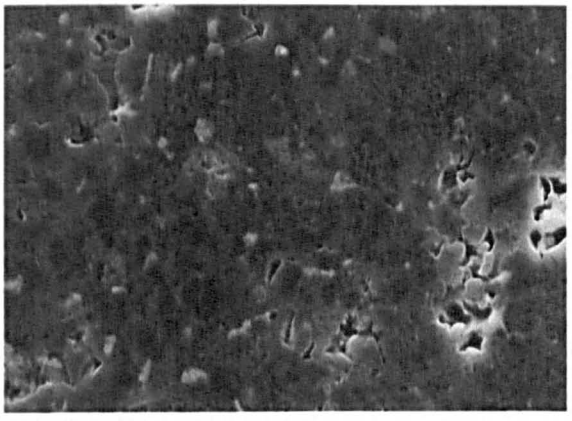

Figure 20: Tribofilm on an Al-Si Alloy [100]

Pereira et al. used a Cameron Plint reciprocating tribometer to generate tribofilms on hypoeutectic (10.5 wt. % Si) A383 aluminium-silicon alloy plates [191]. A 52100 steel pin was incident to the alloy and the tribocouple lubricated with commercially available engine oil at various temperatures [191]. Chemical analysis was performed on the aluminium alloy using synchrotron radiation and XANES techniques [191]. Calcium phosphate was the primary type of phosphate formed within the tribofilms formed on the aluminium alloy [191] and calcium carbonate was also witnessed within the protective layer on the substrates [191]. Zinc sulphide was believed to be the main form of the metal within the tribofilm formed on the alloy. Small amounts of zinc phosphate and

un-reacted ZDDP were present; zinc oxide was not observed [191]. ZnS was present in smaller amounts throughout the tribofilm when similar experiments were conducted on all-ferrous tribosystems [188, 191].

As with work carried out on ZDDP lubricating Al-Si surfaces [25], the length of the phosphate chains were short on the aluminium matrix of the alloy, whilst the chain length was found to be long on the silicon grains [191]. The general structure of the tribofilm formed using the fully formulated oil was determined to be similar to that found with ZDDP tribofilms on Al-Si alloys (section 3.4.1.1.3); long chain phosphates at the top of the film, with shorter chain length phosphates in the main section of the protective layer [191].

Film phosphate concentration and thickness were reported to be less than their equivalents obtained from similar tests carried out on 52100 steel [188, 191]. However, in direct opposition to data obtained using ferrous substrates [188], the fully formulated lubricant facilitated a reduction in wear in the tribosystem, compared to solitary use of ZDDP [191].

One final article [192] has studied the lubrication of the previous tribosystem [191] with ZDDP and calcium phenate, using 150 and 250 total base number versions of the detergent, respectively. Even though this research has not been conducted using calcium sulfonate as a lubricant additive, it is relevant to this current research as there is so little work carried out using detergents on Al-Si alloys. Using the XANES technique to analyse Al-Si samples, which had been lubricated with a combination of ZDDP and calcium phenate, zinc phosphates were witnessed within the generated tribofilm on the aluminium alloy [192]. In addition, low quantities of calcium phosphate were identified in the uppermost region of the tribofilm [192]. Compared to ZDDP alone, detergent and ZDDP increased the amount of generated polyphosphate; these chains ranged from short to medium in length [192].

At each operating temperature studied (60 °C, 100 °C & 150 °C), the combination of detergent and ZDDP provided better wear results than the use of solitary ZDDP [192] (Figure 21). In addition, the higher TBN detergent reduced the wear in the contact by a further amount [192]. A similar benefit was witnessed in terms of the friction coefficient; the addition of detergent to ZDDP reduced the frictional response in the tribosystem, compared to ZDDP alone [192]. The wear protection imparted by both detergents was seen to originate from an increase in film thickness and the reduction in homogeneity of the

tribofilm, when compared to solitary ZDDP [192]. Indeed, film thickness was significantly enhanced when detergent and ZDDP were employed as lubricant, compared to ZDDP alone; this was further improved by the 250 TBN detergent [192].

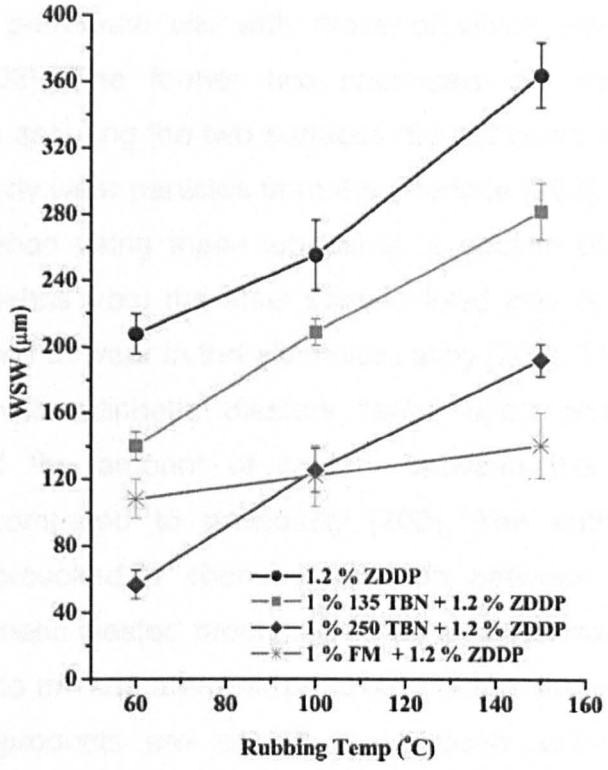

Figure 21: Wear scar width on steel pin in contact with an Al-Si alloy [192]

Therefore, it can be said that even though there has been little research carried out into the lubrication of Al-Si substrates with calcium sulfonate, it seems as if certain observations such as calcium phosphate and ZnS formation on steel surfaces hold true for these modern alloyed substrates.

3.5. Aluminium and Aluminium Alloys Lubricated by Organic Chemicals

The lubrication of aluminium and its alloys using organic chemicals has been studied previously [92, 93, 97, 193-208]; however, the degree of research into this area is still at a relatively low level. The majority of the articles available are based upon the lubrication of an aluminium alloy and steel contact, and it is these articles which are reviewed first.

3.5.1. Aluminium and its Alloys Lubricated by Organic Chemicals

Early work on the subject was conducted by Montgomery [201-205], where the author studied the effects on a lubricated 750 aluminium alloy pin-against 1045

carbon steel cylinder contact using different ethers [201, 204], esters [202, 203, 205] and alcohols [201], amongst other chemicals [201, 202], to lubricate the interface between the two samples.

The first paper in the series compared the lubricating properties of alkanes and neutral petroleum oils with those of which were exhibited by aliphatic diesters [202]. The former two chemicals did not aid in wear resistance, apart from ensuring the two surfaces did not come into contact and also removing third body wear particles from the interface [202]. It was reported by the author that, when using these lubricants, a section of the aluminium substrate had wear debris from the steel sample fixed into its surface, which lead to a greater degree of wear in the aluminium alloy [202]. The lubrication of the sliding contact with aliphatic diesters relied upon adsorption, which considerably reduced the amount of contact between the steel pin and aluminium cylinder compared to previously [202]. The author states that asperity interaction provoked a chemical reaction between the aluminium substrate and the aliphatic diester, producing metal soaps or salts [202]. These in turn were believed to provide antiwear protection to the aluminium substrate; the aforementioned products are said to have been embedded into the crevasses on the surface of the steel sample [202].

As with the lubrication of the pin-on-cylinder contact with aliphatic diesters, when using aliphatic ethers or alcohols as a lubricant for the interface, the wear is said to be mainly that of a chemical nature [201, 202]. Unlike the aliphatic diesters [202], however, the author reported the tribofilms formed on the surface of the aluminium substrate to be weakly adhered and the wear results obtained comparable to those found for the lubrication of the contact with an alkane observed in [201, 202]. Montgomery [201] found that an ether had lower amounts of chemical wear, compared to its corresponding alcohol; ethers need to be divided before subsequent reaction with the aluminium alloy, whereas alcohols do not [201].

Using phthalic acid esters to lubricate the interface between aluminium pin on steel cylinder, as above, was researched by Montgomery in 1966 [203]. Once again, the author commented that the acid esters imparted primarily a degree of chemical wear on the aluminium substrate [203]. As with the tribofilms formed in the previous study [201], the steel substrate was not witnessed to have the by-products of chemical reaction imbedded in its surface [201, 203].

Montgomery stated that an increase in wear recorded in the experiments in this current journal article [203], compared to that of which is seen in an earlier paper [202] can be accredited to a slight variation in chemical structure of the respective by-products of chemical reaction [203].

The penultimate paper in the five-part series by Montgomery saw the lubrication of the aforementioned pin-on-cylinder contact by polypropylene and polyethylene glycols [205]. The chemicals under study were found to react with the aluminium alloy at a swift rate, thus increasing wear by a large amount, compared to an alkane, which was used in an earlier paper [202, 205].

The final journal paper by Montgomery investigated the effects of lubricating the aluminium and steel interface using polyphenyl ethers [204]. Montgomery identified that the organic chemicals studied in this article were more prone to producing large volumes of wear, compared to the aliphatic diesters used as a lubricant [202, 204]. Overall, the results obtained by Montgomery in this sequence of articles [201-205] established the aliphatic diester researched in 1965 as the most effective antiwear agent on aluminium-steel contacts [201-205].

St. Pierre, et al. [206] used a flat on flat setup, with both components being manufactured from 1100 aluminium alloy, to study the lubricating abilities of cetane, l-cetene and a number of other chemicals, on the interface [206]. Those fluids under test which were of a polar nature were found to express successful lubricating characteristics [206]. The authors commented that in order to facilitate favourable lubrication of aluminium when the film thickness lies within the boundary regime, the number of carbons in a chain in the lubricant should be large [206], and reaction between fluid and substrate in a chemical manner should also take place [206].

Hotten [194] conducted a series of experiments using a "standard Falex machine" [209] to record wear and load-carrying ability; the components under test were a 5083 aluminium alloy v-block and a 52100 steel bar. Scuffing and friction characteristics of test samples were elucidated using an all aluminium pin-on-disc setup [194]. Both contacts were lubricated with a number of mixtures which comprised 90 % water, and a further addition of base oil and emulsifier; test complexes, such as unidentate and difunctional molecules, were added to this solution at 2 % concentration [194]. A selection of diol and phenol molecules were blended into a base oil at varying percentages for further

testing [194]. Lubricants which contained an alcohol and found application in the contact were identified by the author as being able to create an alkoxide tribofilm on the surface of the aluminium material; the majority of layers witnessed were not effective in terms of supporting an applied load [194]. Bidentate bonding (Figure 22) was observed on aluminium substrates by using lubricants which contained ketol and diol compounds [194]; this method of bonding enhances the wear characteristics of an alloy [194], along with providing the contact with a decrease in the value of friction coefficient [194].

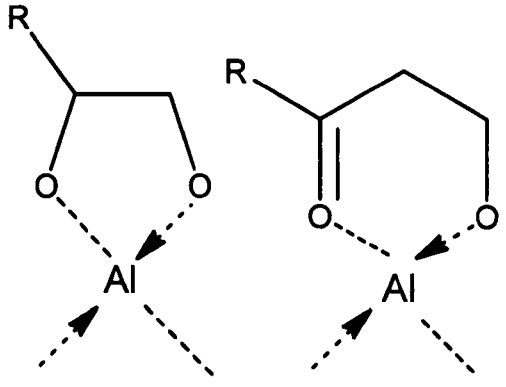

Figure 22: Diol and ketol complexes (adapted from [194])

Hironaka and Sakurai [193] studied the friction and wear of aluminium using a pin-on-disc tribometer. The setup incorporated an S55C steel disc and a practically-pure aluminium incident pin; the contact was lubricated with both a partial and a full, pentaerythritol ester, along with kerosene [193]. The author observed the creation of a salt or a metal compound when aluminium was lubricated with a partial ester [193]. The tribofilm formed was seen to be successful at reducing the wear in the contact [193], compared to when the interface was lubricated with either of the other two lubricants under study [193]. As with Montgomery [201-205], Hironaka and Sakurai [193] commented on the significant and central role which wear of a chemical nature plays on the overall wear of a lubricated aluminium alloy [193].

A method by which alcohols are thought to lubricate an aluminium-on-steel contact was proposed by Kajdas [198]. The author [198] proposed that after adsorption of alcohol structures onto a metallic face, via ionisation, radical anions and anions are created; these are subsequently chemisorbed onto peaks on a metal substrate [198]. It was reported that there is a high chance that complexes which are organo-metallic in nature will desorb from an

aluminium material [198]. Through an increase in temperature of the lubricated surfaces, an alcohol can produce a number of alkenes or alkynes [198].

Wan et al. [207] conducted friction and wear tests using an AISI 52100 steel ball on Al 2024 alloy flat setup; the interface was lubricated by various diol compounds, which found application either undiluted or in the form of an additive in distilled water at 10 % concentration [207]. The authors witnessed that, when employed in both undiluted and additive guises, the chemical which not only produced the smallest value of the coefficient of friction for the contact, but also minimised wear to the greatest degree, was 1,3 butanediol [207]. As with those conclusions arrived at by Hotten [194], it was suggested by Wan, et al. that the beneficial properties shown by 1,3 butanediol is accredited to the aforementioned molecule creating bonds of a bidentate nature with the aluminium substrate [207] (Figure 23). The type of diol compound used as a lubricant for an interface determines the antiwear and frictional characteristics of the chemical [207].

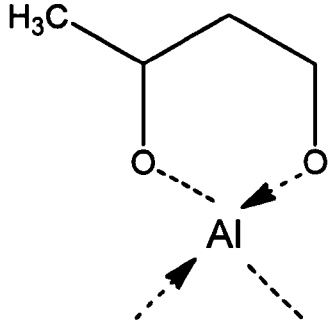

Figure 23: 1,3 butanediol complex (adapted from [207])

Wan and Xue [208], used the same format as with the previous paper [207], but instead increased the testing time by a factor of two, to 30 minutes and the load to 50N [208]. The lubricants used in the study were created by diluting liquid paraffin with various amine salts, a borate, an olefin or ZDDP, respectively, to a wt. % of 1.0 [208]. The amine salt was seen to provide the best antiwear properties in the aluminium and steel interface [208].

Hu and Liu [195], researched the effects liquid paraffin, containing 3 wt. % of various alcohols, including 1,3 butanediol and n-butanol, had on the wear of an Al 2024 aluminium block incident on a 52100 steel ring [195]. The extent to which a test lubricant provided resistance to wear for the interface between block and ring was accredited to the creation of a tribofilm, friction polymer or possibly a metal complex on the aluminium surface [195]; the authors stated

that it is possible to successfully lubricate aluminium alloys using an alcohol [195].

The same experimental setup as that of which shown previously [195] was used by Hu and Liu [196] once more, to study the lubrication of aluminium surfaces with different chlorides contained within liquid paraffin at various concentrations up to 5.0 wt. % [196]. The authors found that chlorides of an unsaturated guise were the chemical group which imparted good wear characteristics to the interface; the existence of a tribofilm and friction polymer were witnessed [196].

Igari et al. [197] utilised a FALEX apparatus to measure the friction and wear in the contact of a JIS H 4040 alloy against an AISI 1137 steel v-block, lubricated with a wide range of diols and polyalkylene glycol, to name but a couple [197]. In contrast to that proposed by Hu and Liu [195], Igari et al. [197] state that the creation of an alkoxide tribofilm on an aluminium substrate intensifies the degree of wear observed in the interface; this is due to a subsequent increase in the vulnerability of the beneficial aluminium oxide film [197]. It was mentioned by the authors [197] that the alkoxide tribofilm is also thought to impart the ability of a wear reducing film to be fashioned on the surface of the substrate [197].

Therefore, in terms of the lubrication of aluminium and its alloys using organic chemicals, a number of conclusions can be drawn:

- It was observed that both ester [193, 202], diol [194, 207] and amine [208] compounds, respectively, were beneficial in terms of their employment in lubricating plain aluminium alloys [193, 202, 208]
- Bidentate bonding was witnessed on aluminium alloys when a lubricating fluid incorporating diols was used in conjunction with the aforementioned substrate [194, 207]
- Kajdas [198] suggested a way in which an alcohol bestowed an aluminium and steel interface with beneficial lubricating effects [198]
- Protective structures, such as a polymer created via friction [195, 196], a compound fashioned between the aluminium substrate and lubricating chemical [193, 195], and or tribofilm [195-197] were witnessed on the surface of a test sample

- Three authors noted the existence of an alkoxide tribofilm on top of the surface of an aluminium substrate [194, 195, 197]; one researcher suggested this lessened wear loss [195], however another author states the aforementioned tribofilm tends to enhance the degree of wear on the substrate [197]

3.5.2. The Lubrication of a Contact between two Aluminium-Silicon Alloys Using Organic Chemicals

The lubrication of aluminium-silicon surfaces with organic chemicals has been the research topic of only a small number of authors and thus very little work has been conducted on the matter [92, 93, 97, 199, 200, 210]; however, a review of the literature has none the less been conducted, as is shown below.

The lubrication of an aluminium-silicon alloy with any nature of fluid is arduous [92]; however tests carried out by Hu et al. [92], Konishi and Perez [200], Konishi et al. [93] and Kawamura and Fujita [199] have studied the lubrication of an interface between two forms of the aforementioned aluminium-silicon alloys using a range organic chemicals, such as amines [92], esters [93, 200] and organo-phosphorus chemicals [199].

The former of the four papers listed above utilised a cylinder-on-block tribometer which incorporated two 12.0 wt. % silicon, Al-Si substrates [92]; the authors used 0.5 ml of three amine and one glycol compounds to lubricate the interface [92]. Triethylenetetramine was seen to generate both the smallest volume of wear (Figure 24) and coefficients of friction for the contact between the two aluminium-silicon alloys [92]. Via XPS analysis, Hu et al. hypothesised that the beneficial effects of triethylenetetramine could be accredited to the creation of a friction polymer and or amine-aluminium composites [92].

Konishi and Perez [200], conducted tribological tests on a number of esters which were used as lubricants in a pin-on-disc tribotester; this housed two hypereutectic A390 Al-Si alloys [200]. The extent to which a chemical would provide an opposition to both scuffing and wear in the tribological contact, was identified by the authors to be greatest in those lubricants which were comprised of long chain acids, which in turn were linear in nature [200]. Konishi and Perez [200] also stated that the more willing a chemical under test was to react with an aluminium substrate, the greater was the quantity of wear witnessed in the tribological interface [200].

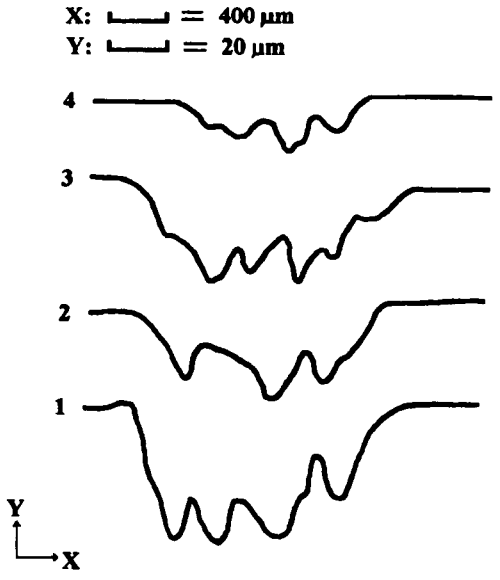

Figure 24: Wear profiles extracted from a worn Al-Si alloy lubricated with (1) ethyleneglycol (2) ethylenediamine (3) ethanolamine and (4) triethylenetetramine [92]

Konishi et al. [93], used a pin-on-disc tribometer, within which a number of oils were used, respectively, in order to lubricate the interface between the two chemically-identical A390 Al-Si samples [93]. The authors state, in deviation with that mentioned by Konishi and Perez [200], the more the lubricant was prepared to interact with the substrate, the more advantageous were the characteristics of lubrication shown by the fluid when a low mass was placed upon the contact; esters and glycols were seen to create a tribofilm on the aluminium test sample [93]. When a wt. % of tricresyl phosphate, which equalled two, was added to the test oils, the wear in the contact altered diminutively, compared against plain oils as tribological fluids [93].

The latter of the four authors mentioned above conducted a study on the lubricating characteristics of an oil which contained five percent concentration of various organic-phosphorus chemicals, when used as the lubricating fluid for an interface between two pins manufactured from an A390 Al-Si alloy [199]. The researchers stated that the chemicals under study which were more beneficial in terms of minimising the degree of wear in the contact were those which possessed chains of alkyl groupings in a straight form [199]; the lowest wear was witnessed when the interface was lubricated with a fluid containing tri-n-amyl phosphate [199].

3.5.3. The Lubrication of a Contact between an Aluminium-Silicon Alloy and Steel Using Organic Chemicals

The lubrication of an aluminium-silicon substrate against a steel test sample using organic additives has been studied by a small number of researchers [97, 210].

A range of aluminium alloys, which included two hypereutectic A390 Al-Si alloys, were tribologically tested by Yoon et al. [97] using a 1018 carburised steel pin-on-aluminium disc arrangement [97]. As the research was directed towards the air conditioning industry, refrigerants were added to such base chemicals as esters and polyalkylene glycol, and subsequently used to lubricate the aforementioned tribological interface [97]. Yoon et al. [97] found that a hypereutectic A390 Al-Si alloy expressed the greatest opposition to wear during tribological tests [97]. When an ester was used as base lubricant for the setup mentioned previously, the authors noticed that the wear in the contact was at its lowest value [97]; this was accredited to bidentate bonding, previously seen by Hotten [194] [97, 194].

Liu et al. [210] performed block-on-52100 steel ring tribological tests; a 12 wt. % Al-Si material was used as the substance from which the blocks would be manufactured [210]. The interface was lubricated using various amine and glycol chemicals, which were contained at a wt. % of three within liquid paraffin [210]. N,N-dibutylethanolamine proved to be the most effective lubricating agent for the above block-on-ring setup [210]; the authors hypothesised that the chemical's excellent behaviour can be accredited to its extensive chain length of alkyl groupings [210]. Liu et al. [210] identified, as with previous papers [97, 194], that a bond of a bidentate nature may be fashioned [210]; a metal-amine compound may be created [210].

Therefore, after reviewing the articles which have undertaken studies on organic lubricants on the contact of an aluminium-silicon alloy against either another Al-Si alloy or a steel component, the following can be concluded:

- Both amines [92, 210] and esters [93, 97, 200] were shown by a number of authors to impart advantageous lubricating qualities on an aluminium-silicon couple [92, 93, 200] and also to an aluminium-silicon and steel interface [97, 210]

- One researcher stated that wear in an aluminium-silicon / aluminium-silicon contact would enlarge if the lubricating liquid had a great willingness to react with the aluminium substrate [200]. Whereas another paper [93] contradicted this comment; the researchers believed wear in the interface would diminish (at low applied mass) as the more reactive a fluid became [93]
- The form [199] and chain length [210] of the groupings of alkyl structures within a liquid was seen to be key to the ability of a chemical to provide good lubricating qualities [199, 210]
- Both bonding of a bidentate nature [210] and metal-amine composites [92, 210] were thought to occur during lubrication of aluminium-silicon substrates [92, 210]

3.6. Novel Antiwear Additive

The novel additive discussed within this thesis is triethyl citrate. Throughout this thesis, it is referred to as NOCH; this is the name used by Lubrizol® UK Ltd to describe their novel organic compounds. The structure of triethyl citrate is shown in Figure 25. As it can be seen, the molecule is comprised of oxygen, hydrogen and carbon; the chemical formula of the molecule is $C_{12}H_{20}O_7$.

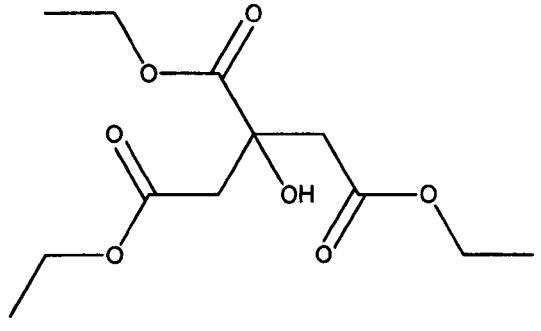

Figure 25: Novel antiwear additive - triethyl citrate

Triethyl citrate is an ester of citric acid [211], and enjoys manifold uses in many different applications, as exemplified by its extensive use in the food industry as an antioxidant [212] and flavouring agent [211, 213], to give just two examples. The compound's versatility is reflected in the fact that it can also be used to form products for the cosmetic and medical industries [211], along with the material from which food packaging is created [211]. However, the areas in which the citric acid ester finds employment may soon increase dramatically. This is because of the increasingly difficult ability to satisfy ever more stringent worldwide emissions regulations (section 3.1).

As one way to meet these regulations, engine oil manufacturers are seeking ways to boost the performance of traditional phosphorus containing additives, such as ZDDP, whilst at the same time reducing the volume of phosphorus contained within the lubricating oil. Indeed, this is the function which Lubrizol® has envisaged for the citric acid derivative; this would result in the successful compliance of the resulting engine oil with emissions standards.

However, this view on the subject matter is not exclusive [214]. This is highlighted by the existence of a patent which describes the antiwear performance of test oils; these contained ZDDP in combination with numerous esters, including triethyl citrate [214]. Using a Cameron Plint TE77, it was observed that the combination of triethyl citrate and ZDDP provided an improvement in wear performance on test ferrous substrates at operating temperatures up to 150 °C [214]. This was determined by comparing against results obtained when the contact was lubricated with ZDDP only in base oil [214]. Interestingly, the potential use of the citric acid ester with other modern engine oil additives has also been documented in the patent, suggesting the benefits of the molecule within a modern automotive lubricating fluid could be diverse [214].

The effects which a NOCH additive has on the tribological properties of a ferrous only contact were reported previously using a Cameron Plint TE77 [215]. Compared to ZDDP alone, ZDDP + NOCH improved the friction and wear characteristics of a ball on plate arrangement [215]. Using Auger spectroscopy, the enhanced tribological properties were accredited to a marked increase in phosphorus concentration in the top 500 angstroms of the tribofilm, along with a significant reduction in both sulphur and zinc within the same region of the protective layer [215]. Even though oxygen content in the tribofilm decreased with the addition of the NOCH additive, the improved wear performance was ascribed to an increase in the amount of zinc polyphosphate within the generated film [215].

The combination of NOCH and calcium sulfonate detergent also reduced the friction in the contact, compared to the solitary use of the calcium-based detergent, ZDDP and also ZDDP + NOCH, respectively [215]. Measured wear in the contact was lowest of all lubricants, and this was found to be due to an increase in calcium carbonate throughout the generated tribofilm [215]. As with

ZDDP + NOCH, a reduction in the amount of oxygen within the protective layer was observed [215].

It is the intention of this research to observe the effects of the NOCH additive on the tribological performance in combination with various additives and relate the results to the chemical nature of fashioned tribofilms. It would be very interesting to witness similar effects to those described within this review and, of course, very important to understand the mechanisms by which the novel antiwear additive operates.

3.7. Summary

This literature review has focussed on a number of key aspects with regards to attaining information in the context of the lubrication of an aluminium-silicon alloy using various additives. Regulations are becoming increasingly stringent worldwide on emissions such as carbon monoxide, along with the sulphated ash and phosphorus content of engine oils. The piston ring and cylinder liner interface is an important tribological component within a modern engine.

As reported, aluminium-silicon alloys are extremely complex and comprise various chemicals which afford them certain thermal and mechanical properties. These alloys are employed in a wide variety of applications in a wide variety of markets and undergo low levels of wear through a complicated process.

Additives such as ZDDP and overbased calcium sulfonate conventionally find usage with ferrous substrates and thus little research has been completed on aluminium-silicon alloys with such engine oil additives. The way in which the two additives are thought to generate tribofilms on ferrous surfaces are vastly different and evidence for antagonistic behaviour has been observed when the two are used in conjunction with one another.

A wide array of aluminium alloys, including aluminium-silicon types, have been lubricated with organic chemicals. Film formation by these additives was diverse, but bidentate bonding was regularly reported. The novel antiwear additive used throughout this project finds conventional usage in many applications but has been effective in reducing wear on ferrous substrates when used in conjunction with ZDDP or calcium sulfonate. Ferrous surfaces were not the subject of this review, nor were other engine oil additives since these were not part of this research project.

4. The Lubrication of an Aluminium-Silicon Alloy with a Novel Antiwear Additive

4.1. Introduction

One way in which automotive manufacturers are reducing the fuel consumption of modern vehicles is by minimising the mass of the petrol or diesel engine used to power the automotive product [58, 79]. A fashionable way to achieve this reduction is by replacing conventional ferrous-based parts with lighter aluminium alloys [99]. One such example is the development of the piston ring-cylinder liner interface, whereby aluminium-silicon alloys are finding employment as substitutes for conventional grey cast iron cylinder liners [99].

As worldwide emission legislation becomes increasingly stringent, with tighter limits being placed on sulphated ash and phosphorus content within engine oils [35, 37], for example, oil formulators are seeking ways in which to boost the performance of oils whilst reducing the concentration of additives such as ZDDP in the engine oil [42]. One such way is the usage of novel antiwear additives such as the NOCH molecule in this research.

Studies into the lubrication of aluminium-silicon substrates have focussed primarily on ZDDP hitherto [25, 66, 93, 98, 151-154, 199], although a blend of additives and fully formulated oils have been investigated by a small group of authors [58, 77, 79, 100, 153, 154, 191, 192]. Tribofilms were identified to form primarily on silicon grains within aluminium-silicon alloys due to the fact that these physically hard regions support the load placed upon the contact [25, 66, 98] and provide a stable surface onto which film formation can occur [98]. Tribofilms were generated on the aluminium matrix due to film transfer [25, 66, 153] or ZDDP thermal decomposition [25].

The tribochemistry of aluminium-silicon surfaces lubricated with ZDDP is thought to be very similar to that observed on ferrous substrates, comprising polyphosphate-based tribofilms [25, 66, 98, 151, 152]. The formation of calcium phosphate has also been witnessed using fully formulated oils [191]. However, as yet, the lubrication of aluminium-silicon alloys solely with a detergent has not been investigated. These important engine oil additives, which are primarily employed for their cleaning ability [34], are known to impart low frictional response onto a tribosystem [176], whilst possessing good antiwear properties [160, 165, 166, 168, 169, 176, 178]. Evaluation of the lubricating abilities of a

detergent against that of ZDDP on Al-Si surfaces will allow for comparisons with results obtained from ferrous surfaces.

Recently, the low wear of aluminium-silicon alloys has become an increasingly popular research topic. Indeed, a number of authors have formulated processes by which these complicated aluminium alloys endure low levels of wear [77, 79, 99, 100, 104]. However, an understanding of tribofilm formation onto silicon grains within these seemingly important methods has as yet been neglected.

In this chapter and the next, an interface between ferrous piston ring and aluminium-silicon alloy has been investigated using a number of test oils, which contained ZDDP, overbased calcium sulfonate and NOCH, respectively. The frictional response and wear in the interface has been evaluated and related to the morphology, tribochemistry and film formation of the various additives on both the ferrous and aluminium-silicon substrates under examination. Computer generated model surfaces have been devised in order to depict tribofilm topography imparted by each lubricant. An hypothesis as to the lubrication of aluminium-silicon alloys encountering three different levels of wear, respectively, has also been developed.

4.2. Aims and Objectives

4.2.1. Aims

- Present the rationale for and methodology behind the evaluation of an interface between a hypereutectic aluminium-silicon cylinder liner and a ferrous piston ring
- Tribologically investigate the lubrication of a hypereutectic aluminium-silicon cylinder liner which is in contact with a ferrous piston ring

4.2.2. Objectives

- To evaluate the performance of test lubricants in terms of friction, electrical contact voltage and wear
- To investigate the tribochemistry of aluminium-silicon and ferrous surfaces and relate the results to those observed in literature
- To identify differences between test oils in terms of wear performance and categorise results into a clearly defined grading system

- To observe tribofilm formation on aluminium-silicon substrates
- To associate tribological performance with the morphology and tribochemistry of worn substrates
- To conceive detailed models by which aluminium-silicon alloys endure different severities of wear

4.3. Tribology of Aluminium-Silicon Alloys

4.3.1. Materials

4.3.1.1. AluSil®

The aluminium-silicon alloy used within this project is AluSil®. This hypereutectic material was based on A390 [58] and was produced using low pressure die casting methods [216]. The aluminium alloy was designed for usage as a cylinder liner and, therefore, various processes, such as honing, were applied to the raw material to transform the surface of the alloy into a functioning running face for piston rings. The alloy was supplied by Elring Parts Ltd in cylinder liner form with final machining completed on the internal bore of the substrate. The surface roughness (Table 11) of the aluminium alloy surface was determined using a Taylor Hobson Form Talysurf 120L surface profilometer.

Parameter	Value
R_a	0.324 µm
R_q	0.431 µm

Table 11: Surface roughness of AluSil® substrates

The substrate had an internal diameter of 83.0 mm ± 0.1 mm and was subsequently cut into 7.0mm x 7.0mm x 3.5 mm (wxlxh) samples using a wire EDM machine, taking care not to damage the running surface. The chemical composition of the alloy is shown in Table 12.

	Chemical Composition (Wt. %)									
Substrate	**Si**	**Fe**	**Cu**	**Mn**	**Mg**	**Cr**	**Ni**	**Zn**	**Ti**	**Al**
A390 / AluSil®	16.0-18.0	0.5	4.0-5.0	0.1	0.45-0.65	0.0	0.0	0.1	0.2	Balance

Table 12: Chemical composition of A390 / AluSil®

AluSil® contained a large amount of silicon and also copper. Iron and magnesium were present in comparable weight percentages. There was also manganese, zinc and titanium within the aluminium alloy. All these chemicals modified the alloy in different manners; section 3.3.2 explains this in detail.

4.3.1.1.1. Surface Topography and Morphology

Honing processes are completed on ferrous cylinder liners to minimise both the amount of oil consumed within an engine as well as the amount of wear that occurs during initial use of the cylinder liner [217]; in the case of the aluminium alloy, the main aim of honing is to expose the silicon grains within the aluminium matrix [218]. The mechanical honing processes employed for the aluminium alloy leave the protruding silicon grains with round edges, thereby reducing wear on the contacting surface [218].

As Figure 26 reveals, it is possible to show both the random distribution and similar size of the exposed silicon grains (red areas in Figure 26) in the AluSil® substrates used in this work. Figure 26 also shows that honing marks are evident on the aluminium matrix and a number of valleys are present within the honed alloy (Figure 26).

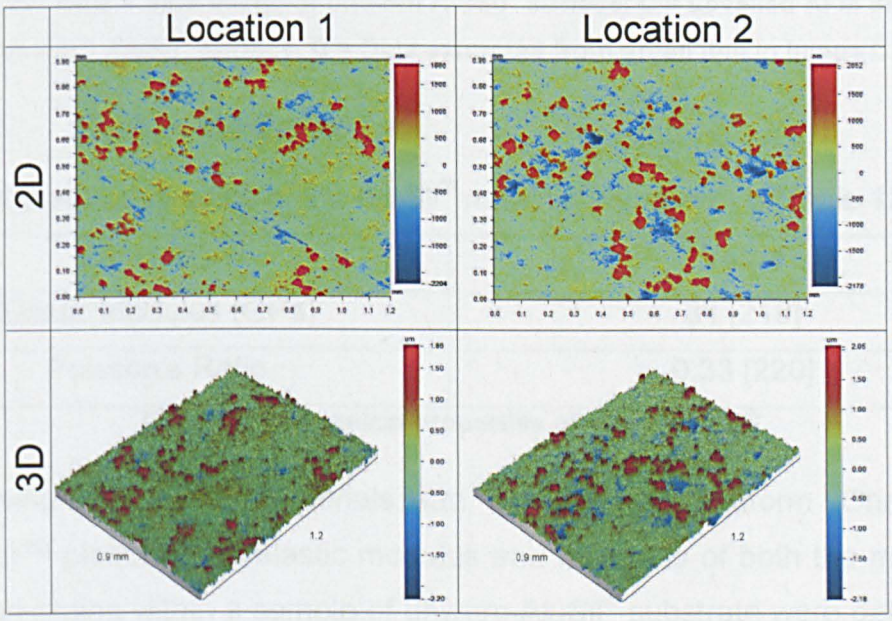

Figure 26: 2D and 3D Interferometry images of unworn AluSil®

Increased magnification of the unworn AluSil® surface is shown in Figure 27. SEM images of the alloy surface (Figure 27A) reveal the non-uniform shape of the silicon grains within the substrate. Honing marks are clearly evident on the silicon grain shown in Figure 27B, with a typical height exposure of the white silicon constituents from the matrix highlighted in Figure 27C. The difference in

height between silicon and aluminium regions in the AluSil® substrate over the length of the green line in Figure 27C is shown in Figure 27D. The average extension possessed by silicon grains from the surface of the aluminium matrix was determined using software supplied with the AFM. Thirty measurements were taken and averaged, from which, the protrusion was found to be 928 nm ± 210 nm.

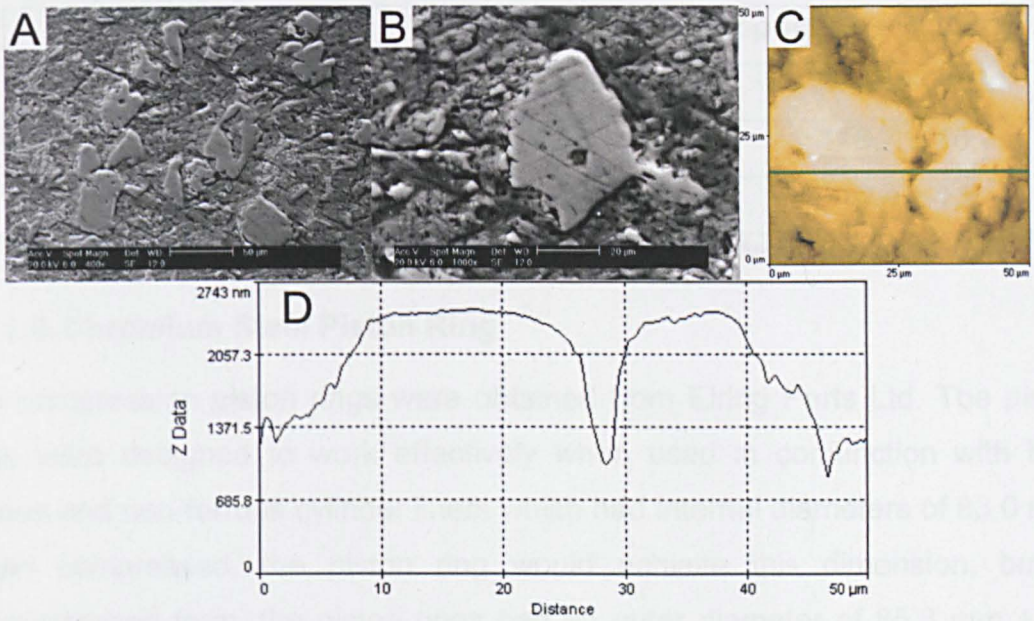

Figure 27: A&B = SEM image of unworn AluSil® surface. C = Levelled AFM image of unworn AluSil® surface. D = Data extracted from green line in image C.

4.3.1.1.2. Mechanical Properties

The mechanical properties of the AluSil® material are shown in Table 13.

Parameter	Value
Elastic Modulus (GPa)	81 [219]
Poisson's Ratio	0.33 [220]

Table 13: Mechanical properties of A390 / AluSil®

Using the Micro Materials Ltd NanoTest™ Platform One device NanoTest™ platform, the elastic modulus and hardness of both the matrix and the silicon grains within a sample of unworn AluSil® substrate were determined. The device would stop applying a load to the indenter if the maximum depth was 1850 nm or the applied load reached 100 mN. The loading / unloading rate was 0.50 mN / s. A total number of 55 indentations, arranged in three columns, were completed on the unworn substrate, fifteen of which obtained data from silicon grains and the remaining forty indentations gathered information from the aluminium matrix. The indentation spacing was 40 µm and 50 µm in the Y and Z

directions, respectively. The retraction distance was 15 μm. Data from each indentation was analysed using the method described in section 2.2.1.5 of this thesis, with the hardness and elastic modulus for the substrate determined for each indentation point. This data was averaged and a standard deviation produced; the results are shown in Table 14 and are very similar to those in literature [25, 152].

	AluSil® Component	
Parameter	**Aluminium Matrix**	**Silicon Grain**
Elastic Modulus (GPa)	90.7 ± 15.0	146.7 ± 10.7
Hardness (GPa)	1.4 ± 0.3	10.4 ± 1.9

Table 14: Experimentally determined mechanical properties of unworn AluSil®

4.3.1.2. Chromium Steel Piston Ring

Top compression piston rings were obtained from Elring Parts Ltd. The piston rings were designed to work effectively when used in conjunction with both ferrous and non-ferrous cylinder liners which had internal diameters of 83.0 mm. When compressed, the piston ring would achieve this dimension, but in uncompressed form, the piston rings had an outer diameter of 85.3 mm ± 0.1 mm. The thickness of the piston ring was 1.2 mm ± 0.0 mm, with the depth of the substrate being 3.2 mm ± 0.0 mm. Analysis of the piston rings by Sheffield Testing Laboratories Ltd. determined the piston ring material to be X105CrMo17 (EN 1.4125) [221] martensitic chromium stainless steel. The surface of the piston rings possessed a 0.07 mm thick surface layer, employed to increase the hardness of the running surface from that of the base material. The hardness of both the bulk and the surface layer of the piston ring were obtained using a Vickers micro hardness tester under an applied load of 0.5 kg (Table 15).

Region of Piston Ring	Hardness (HV)
Bulk Material	371 ± 0.5
Surface Layer	1051 ± 7.1

Table 15: Hardness of piston ring bulk material and surface layer

The surface roughness values of the piston rings, obtained using a Taylor Hobson Form Talysurf 120L surface profilometer which traversed the entire width and length of the substrate, are shown in Table 16.

Parameter	Value (μm)
R_a	0.134
R_q	0.179

Table 16: Surface roughness of piston ring substrates

4.3.1.2.1. Surface Topography

Figure 28A&B show SEM images of the surface of the test stainless steel piston rings from which it is apparent that there were two clearly identifiable regions to the surface of the piston ring, namely one that was smooth (Figure 28A&C) and one that possessed an increased surface roughness (Figure 28B&D). It was assumed that both sections of the piston ring were in contact with the cylinder liner during experimentation and thus a compound surface roughness is reported in Table 16.

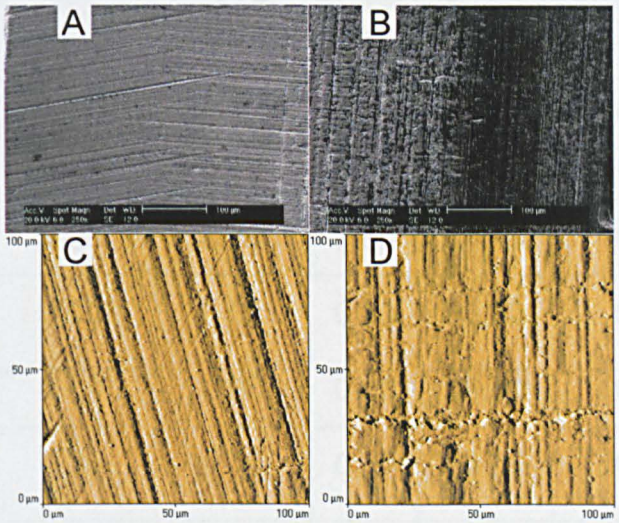

Figure 28: A&B = SEM imagery of an unworn piston ring. C&D = Shaded AFM imagery of those areas shown in A&B

The rough area of the piston ring is used predominantly to assist oil control within a piston ring and cylinder liner interface, whilst the smooth section of the piston ring facilitates tribofilm formation. The machining marks on the smooth portion of the test piston ring surfaces can be seen in Figure 28A&C.

4.3.1.2.2. Mechanical Properties

The mechanical properties of the piston ring substrate are shown in Table 17.

Parameter	Value
Elastic Modulus (GPa)	212 [221]
Poisson's Ratio	0.29 [222]

Table 17: Mechanical properties of chromium steel piston ring

4.3.2. Lubricants

Eight lubricating fluids were evaluated in this work (Table 18), each of which comprised synthetic six centistokes poly alpha olefin (PAO) type base oil, within which various additives were blended. The lubricants that contained either secondary zinc dialkyldithiophosphate and / or 400 TBN overbased calcium sulfonate were designed to conform to international standards governing the percentage of phosphorus and sulphated ash in commercially available engine oil. As discussed in section 3.1, the maximum permissible amounts of sulphated ash and phosphorus within an engine oil, as defined by ACEA C1-08, are 0.5 % m / m and 0.05 % m / m, respectively [35]. Consequently, referring to Table 18, the lubricants evaluated were relevant from an industrial perspective. Triethyl citrate, referred to as NOCH throughout this work, was added at 0.50 mass % to certain lubricating fluids; increasing the mass percentage beyond this level impaired blending.

Lubricant		Mass % of Additive			Mass % of Base Oil	P.P.M. Phosphorus	Mass % Sulphated Ash
Name	Ref.	Secondary ZDDP	Calcium Sulfonate	NOCH			
Base oil	(B)	0.00	0.00	0.00	100.00	0.00	0.00
NOCH in base oil	(N)	0.00	0.00	0.50	99.50	0.00	0.00
ZDDP	(Z)	0.50	0.00	0.00	99.50	500.00	0.08
ZDDP + NOCH	(ZN)	0.50	0.00	0.50	99.00	500.00	0.08
Calcium sulfonate	(C)	0.00	0.94	0.00	99.06	0.00	0.50
Calcium sulfonate + NOCH	(CN)	0.00	0.94	0.50	98.56	0.00	0.50
ZDDP + calcium sulfonate	(ZC)	0.50	0.94	0.00	98.56	500.00	0.50
ZDDP + calcium sulfonate + NOCH	(ZCN)	0.50	0.94	0.50	98.06	500.00	0.50

Table 18: Test lubricants

FTIR was conducted on all lubricants prior to test using a PerkinElmer Spectrum 100 (section 2.2.2.2), with the data obtained using a Specac OMNI

GSO1800 liquid transmission cell with two KBr windows and 0.1 mm Teflon® spacer; samples were scanned over the range 4000 cm^{-1} - 450 cm^{-1} and 50 scans were taken for each sample. Data was obtained in absorbance mode and converted to percentage transmittance by *Spectrum*® software (Equation 7) for comparison with data obtained from worn substrates using the PerkinElmer Spotlight 400 FTIR apparatus (sections 5.5.2&9.5.2). The maximum absorbance on all spectra shown in Figure 29 and Figure 30 did not exceed 1.4, with the vast majority of peaks lying below 0.8.

$$\text{Absorbance} = (-\log T) \times 100$$

Equation 7: Relationship between absorbance and percentage transmittance [223]

The FTIR spectra shown in Figure 29 highlights the four main differences observed for the NOCH in base oil lubricant, compared to PAO6 base oil alone. Indeed, labelled peak #1, at ~ 1030 cm^{-1} is characteristic of C-C stretching within an ethyl group [224], peak #2, at ~ 1190 cm^{-1} is attrubutable to the stretching vibration of C-O [225]. The large peak at 1745 cm^{-1}, number three, was assigned to the stretching vibration of C=O [226]. The final difference, namely peak number four, at ~ 3515 cm^{-1} is assignable to stretching of the O-H group within the molecule [225].

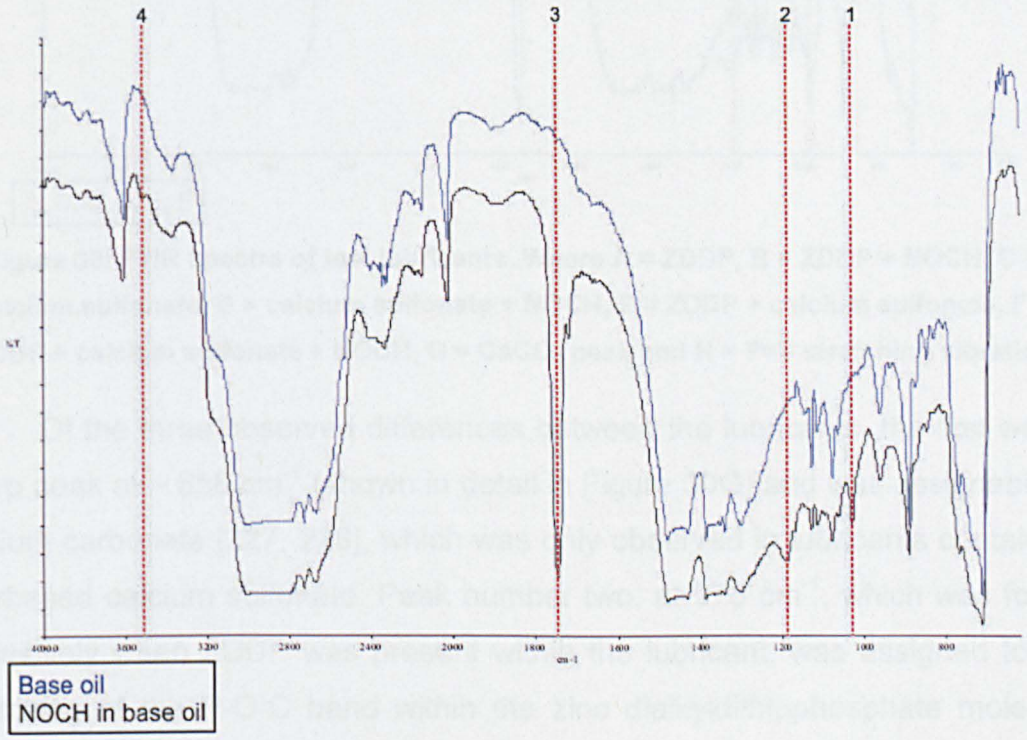

Figure 29: FTIR spectra of base oil and NOCH in base oil lubricants

The spectra shown in Figure 30 highlight the observed variations between the remaining test lubricants listed in Table 18. All three NOCH

containing lubricants (B, D & F) contain the four triethyl citrate related peaks as displayed in Figure 29.

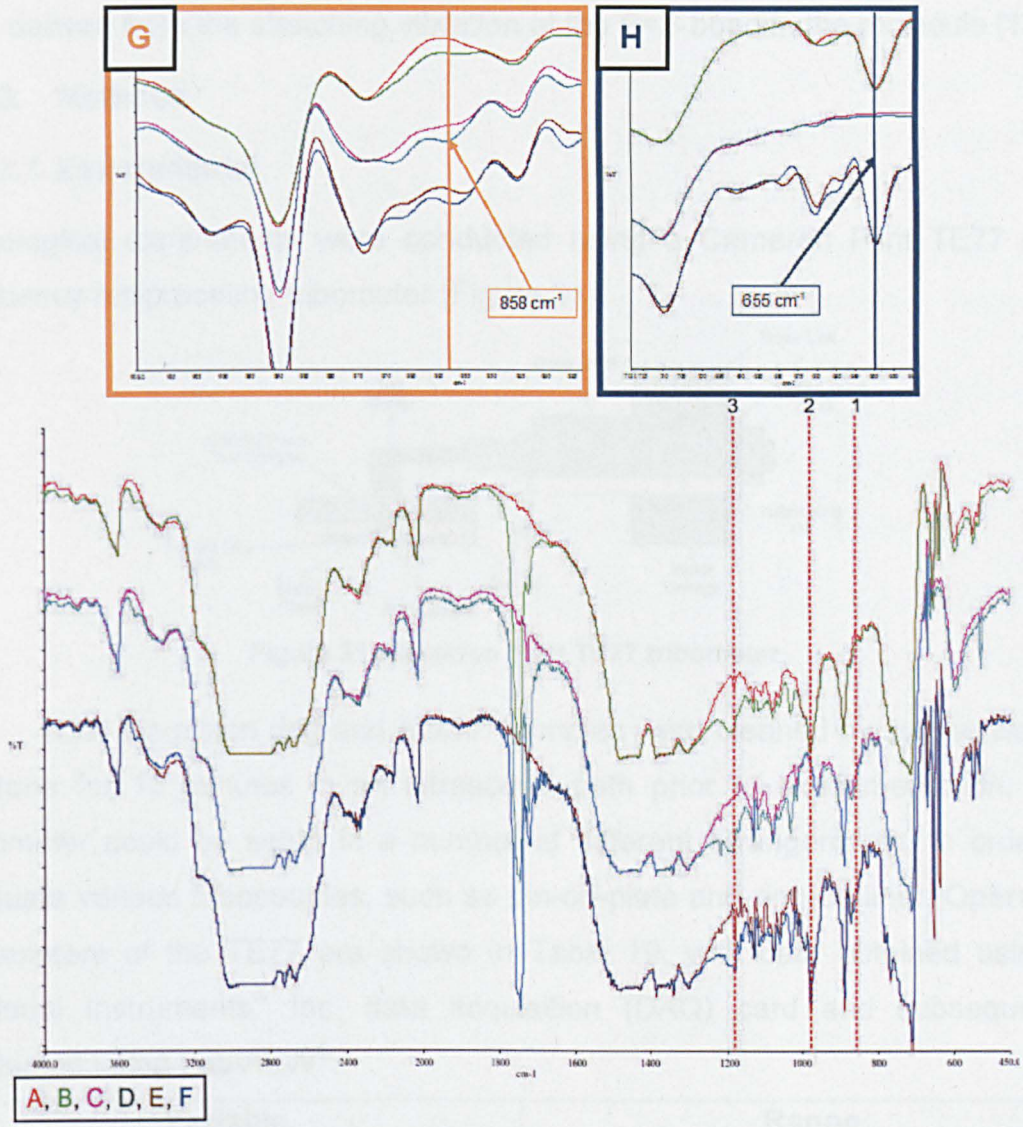

Figure 30: FTIR spectra of test lubricants. Where A = ZDDP, B = ZDDP + NOCH, C = calcium sulfonate, D = calcium sulfonate + NOCH, E = ZDDP + calcium sulfonate, F = ZDDP + calcium sulfonate + NOCH, G = $CaCO_3$ peak and H = P=S stretching vibration

Of the three observed differences between the lubricants, the first was a sharp peak at ~ 858 cm^{-1} (shown in detail in Figure 30G) and was assignable to calcium carbonate [227, 228], which was only observed in lubricants containing overbased calcium sulfonate. Peak number two, at 975 cm^{-1}, which was found exclusively when ZDDP was present within the lubricant, was assigned to the stretching of the P-O-C band within the zinc dialkyldithiophosphate molecule [127, 229, 230]. The peak at 1179 cm^{-1} was again only found in lubricants containing ZDDP and was attributed to the stretching vibration of P=O [231], presumbly derived from partial decompositon of the molecule during blending

as this is not present in the ZDDP structure shown in Figure 14. In addition, a peak was observed at 655 cm^{-1} in lubricants containing ZDDP (Figure 30H); this was derived from the stretching vibration of the P=S bond in the molecule [127].

4.3.3. Methods

4.3.3.1. Experimental

Tribological experiments were conducted using a Cameron Plint TE77 high frequency reciprocating tribometer (Figure 31).

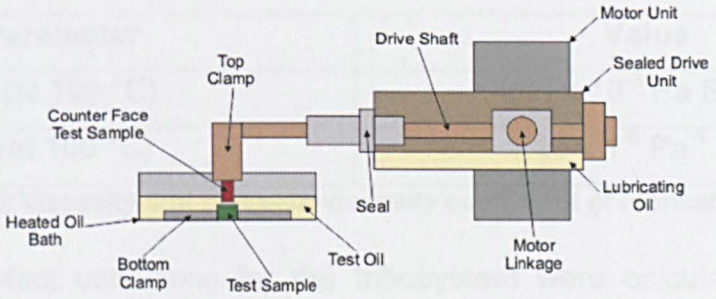

Figure 31: Cameron Plint TE77 tribometer

Both the piston ring and AluSil® samples were cleaned by submersion in acetone for 10 minutes in an ultrasound bath prior to experimentation. The tribometer could be setup in a number of different arrangements, in order to evaluate various tribocouples, such as pin-on-plate and ring-on-liner. Operating parameters of the TE77 are shown in Table 19, with data obtained using a National Instruments® Inc. data acquisition (DAQ) card and subsequently evaluated using LabVIEW®.

Variable	Range
Applied Load	7 N - 98 N
Frequency of Oscillation	1 Hz - 50 Hz
Stroke Length	5 mm - 15 mm
Oil Temperature	0 °C - 120 °C

Table 19: TE77 test variables

The uncompressed piston ring sample was placed in the reciprocating arm of the tribometer, with the AluSil® substrate secured in the fixed oil bath, ensuring that the aluminium alloy could not move under load. Contact was arranged such that the centre points of both the AluSil® and piston ring samples were aligned, thereby guaranteeing the line contact length to be the width of the AluSil® substrate, namely 7.0 mm. A spirit level was used to ensure accurate alignment between ring and liner before the start of each experiment to

enhance repeatability. The height between the ferrous substrate and the AluSil® material was also kept level, so as to ensure that the piston ring did not plough the surface of the aluminium alloy.

The tribosystem was loaded in such a manner to ensure boundary lubrication prevailed in the contact and the contact pressure was maintained at a level that did not overload and damage the physically soft AluSil® surface. The viscosity (η_0) and pressure-viscosity coefficient (α) of the lubricating oils were assumed to be constant in all experiments; these values are shown in Table 20.

Parameter	Value
η_0 (at 100 °C)	4.03×10^{-3} Pa S [232]
α (at 100 °C)	1.10×1^{-8} Pa^{-1} [232]

Table 20: Viscosity and pressure-viscosity coefficient of lubricating oils

The contact conditions for the tribosystem were calculated using the following equations, with the resulting data shown in Table 21. Using Equation 8, the equivalent elastic modulus, E^*, was obtained by inputting the values of elastic modulus, E, and the Poisson's ratio, υ, for both the aluminium-silicon substrate and the steel piston ring, shown in Table 13 and Table 17, respectively.

$$\frac{1}{E^*} = \left(\frac{1-(\upsilon_{Al-Si}{}^2)}{E_{Al-Si}}\right) + \left(\frac{1-(\upsilon_{Steel}{}^2)}{E_{Steel}}\right)$$

Equation 8: Equivalent elastic modulus of AluSil® tribosystem [233]

The reduced radius of curvature, R, for the tribocouple was determined using Equation 9. For simplification purposes, the individual radii of curvature of each substrate, R_1 and R_2, were assumed to be 83.0 mm.

$$\frac{1}{R} = \frac{1}{R_1} + \frac{1}{R_2}$$

Equation 9: Reduced radius of curvature [233]

Once these values were known, the maximum Hertzian line contact pressure, P_0, for the tribosystem could be calculated using Equation 10, where E^* = equivalent elastic modulus, W = applied load, R = reduced radius of curvature and L = contact length. The mean line contact pressure, P_m, was determined using Equation 11, which provided an indication as to the magnitude of the contact pressure in the interface for a large part of the test duration.

$$P_0 = \sqrt{\frac{E^* W}{RL\pi}}$$

Equation 10: Maximum Hertzian line contact pressure [233]

$$P_m = \frac{\pi}{4} \times P_0$$

Equation 11: Mean Hertzian line contact pressure [233]

The minimum film thickness, h_{min}, for the contact between the AluSil® substrate and steel piston ring was calculated using Equation 12 where R = reduced radius of curvature, α = pressure - viscosity coefficient of lubricant, E^* = equivalent elastic modulus, U = entrainment speed, η_0 = viscosity of lubricant at ambient temperature and W = applied load and L = length of contact.

$$\mathbf{h_{min} = 2.65xRx\left[(2\alpha E^*)^{0.54}\left(\frac{U\eta_0}{2E^*R}\right)^{0.7}\left(\frac{W}{2E^*RL}\right)^{-0.13}\right]}$$

Equation 12: Minimum Hertzian line contact film thickness [233]

The lambda ratio, λ, which indicates the lubrication regime in which the contact operates, can be determined using Equation 13 and known values of R_q for the two test substrates, which are given in Table 11 and Table 16, respectively.

$$\lambda = \frac{h_{min}}{\sqrt{\left(\left(R_{q(Al-Si)}\right)^2\right) + \left(\left(R_{q(Piston\ Ring)}\right)^2\right)}}$$

Equation 13: Lambda ratio of AluSil® tribosystem [14]

Variable	Value
Equivalent Elastic Modulus	65 GPa
Reduced Radius of Curvature	2.1×10^{-2} m
Applied Load	10 N
Contact Length	7.0 mm
Maximum Contact Pressure	38 MPa
Mean Contact Pressure	30 MPa
Entrainment Speed	0.2 m / s
Film Thickness	3.11×10^{-2} μm
Lambda Ratio	6.7×10^{-2}

Table 21: Line contact conditions

10 ml of test lubricant was placed in the oil bath and heated to 100 °C. Before the commencement of each experiment, calibration of the tribometer was performed to minimise experimental error. Data was collected using LabVIEW®, which gathered the instantaneous raw data from both the friction force and electrical contact resistance (ECR) channels on the tribological test apparatus. ECR was converted by the TE77 into electrical contact voltage (ECV), with a maximum possible value of 0.45 mV. ECR, and thus ECV, provides an indication as to the degree of contact between the metallic piston ring and AluSil® substrates [234]. Indeed, direct contact between the two substrates would result in a minimum contact voltage [234, 235]. Alternatively, if the maximum value of the ECV was observed, the ferrous and aluminium-silicon substrates would be divided by an insulating tribofilm [234, 235]; an enhancement in the value of the ECV was therefore a indicator of tribofilm generation [176]. The sampling rate was set at 1000 samples per second, with the data recorded every minute for the first five minutes of an experiment and every five minutes thereafter.

Each experiment was conducted for two hours at a frequency of 20 Hz, which was a comparable speed to Al-Si literature [154]. The stroke length was 5 mm because this was the standard setup for the tribometer and was very difficult to modify. The test lubricants were evaluated five times each, using virgin piston ring, AluSil® and lubricant samples in every experiment. Employing the previously obtained calibration values, friction coefficients were calculated from raw frictional force data. Electrical contact voltage and coefficients of friction for each lubricant were determined by averaging the results over all five repeats per test oil using Microsoft® Excel®. The variability in friction and ECV results for all test lubricants over the entire duration of experimentation was, on average, 6 % and 2 %, respectively.

4.3.3.2. Justification of Contact Conditions

This project comprised an investigation of tribofilm formation on AluSil® surfaces using various test oils. If the substrate is subject to large contact pressures, the physically soft material will plastically deform and silicon grains will be removed from the substrate, resulting in a material that does not resemble that of a working cylinder liner. Work conducted by Lubrizol® UK Ltd revealed high wear levels on these aluminium alloys did not generate tribofilms which were

representative of those on worn cylinder liners. To prevent high levels of wear on the AluSil® substrate, all of the contact conditions listed in Table 21 were determined through thorough experimental testing of the tribological interface between piston ring and aluminium alloy.

Experimental testing involved using the standard conditions of duration, temperature of lubricant, frequency of oscillation, stroke length and substrate dimensions described in section 4.3.3. ZDDP + calcium sulfonate was used as lubricant for all evaluations so as to negate the effects of lubricant composition on wear. Isolating all other variables, the two adjustable parameters in the tribosystem were the applied load and usage of uncompressed or compressed piston rings. The applied load was chosen to be 10N, with the rationale behind this choice discussed on page 82.

The ideal form of the piston ring employed was initially evaluated, as contact loading will change depending on the compression of the piston ring used in the contact. A piston ring clamp was designed and manufactured which compressed the piston ring samples into an outer diameter of 83.0 mm. When evaluating the compression of the piston ring in the tribosystem, the load placed on the contact was maintained at 15N and several repeat runs were carried out to determine the repeatability and accuracy of the results. It was found that when using the piston ring compressor, the wear on the test samples was non-uniform in shape and was spread across the width of the substrate, which clearly highlighted differences in both the applied contact pressure and the location of wear on each test sample. This was obviously unacceptable, as any tribofilm formed on the substrates would possibly vary, either physically or chemically, from sample to sample, reducing the accuracy of the results.

When the piston ring was uncompressed, the wear scar location remained constant, with the outer edges of the substrate enduring slightly greater contact pressures than the centre of the alloy, which is termed edge loading. It must be stated that the intention of the experiments conducted in this thesis were not to replicate contact conditions within an engine, instead rather to evaluate tribofilm formation on the aluminium-silicon substrate. Owing to the repeatability of the replication of the wear scar location and the loading on the aluminium-silicon substrate, it was concluded that all experiments were to be undertaken using a piston ring in uncompressed form. It was decided that the outer edges of a test substrate would be the subject of further physical or

chemical analysis of the aluminium-silicon alloy, as the wear levels in this region were repeatable and comparable for all lubricants. As the outer edges of the AluSil® material were deemed to be comparable between test substrates, a map to show the region of analysis on test substrates was produced. This is shown in Figure 32, with the area of surface analysis highlighted as "Region A".

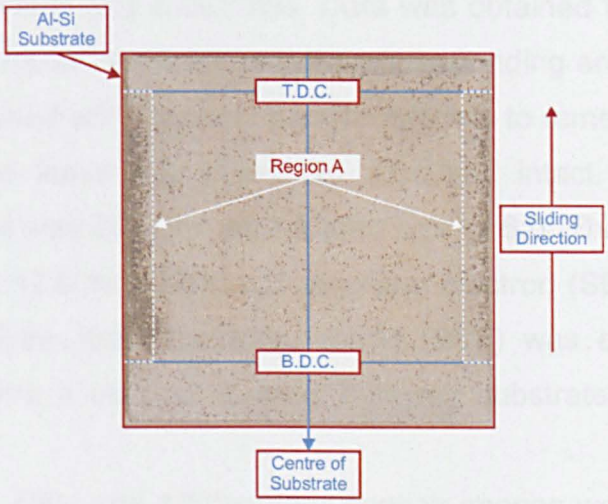

Figure 32: Area of physical and chemical analysis on AluSil® substrates

The most appropriate loading of the contact was determined by applying various loads to the contact, with all other test variables, including the uncompressed piston ring and the lubricating oil ZDDP + calcium sulfonate, being kept constant. Repeats were performed and the wear levels on the outer edges of the test substrates were compared using both optical and scanning electron microscopy. If any test substrate suffered silicon removal and / or large proportions of aluminium smearing, the loading was classed as a fail. Conversely, if the silicon grains were still in place but some had cracked under load, together with the aluminium undergoing small amounts of smearing, the loading on the tribosystem was classed as a pass.

Once the analysis of the samples which had undergone various applied loads was complete, it was clear that the applied load of choice for this particular interface was 10 N. This can be attributed to the samples bearing this loading having consistently endured *ultra mild wear*, which imparted cracking of the silicon regions and smearing of the aluminium areas around the exposed silicon areas. Importantly, the silicon grains contained within the alloy remained in place during the repeat experiments conducted.

4.3.3.3. Surface Analysis

4.3.3.3.1. SEM

Scanning electron microscopy was conducted using a Philips XL30 environmental scanning electron microscope in order to generate images of worn AluSil® and piston ring substrates. Data was obtained from within Region A of Figure 32 on AluSil® samples and the corresponding area on piston rings. Samples were cleaned with Heptane prior to analysis to remove excess oil from the substrates but leave the generated tribofilms intact. The acceleration voltage of the SEM was 20.0 kV, with a spot size of 6.0. The working distance was maintained at 12.0 mm. Although scanning electron (SE) mode was used for all image analysis, back scattered mode (BSE) was employed in some circumstances where a marked contrast between substrate and tribofilm was required.

For AluSil®, 400x and 1000x magnification images were obtained which provided an overview of the silicon grains and surrounding aluminium matrix, together with high magnification images of regions of interest. Piston ring substrates were analysed at 250x and 1000x magnification. Data was therefore comparable to that obtained using atomic force microscopy.

4.3.3.3.2. AFM

Atomic force microscopy was carried out using a Veeco Explorer scanning probe microscope (SPM). Analysis of AluSil® substrates was performed using a 100.16 μm s^{-1} scan rate, employing a 50 μm x 50 μm scan range; the resolution of the AFM was set to 400. Data was obtained from within the wear scar on each sample, Region A in Figure 32. A typical area of analysis included a silicon grain and an area of the aluminium matrix.

AFM analysis of piston ring samples was conducted over a 100 μm x 100 μm scan range at a rate of 400.64 μm s^{-1}, using a resolution of 400. All AFM imagery was obtained from within the wear scar on the piston rings, in the area directly in contact with Region A (Figure 32) on the AluSil® substrates. Data was obtained from the smooth section of piston ring substrates (Figure 28A&C), as data acquisition from the rougher regions of the samples (Figure 28B&D) contained large amounts of noise. Both AluSil® and piston ring samples were cleaned using Heptane before analysis.

Raw data was processed using the SPMLab software supplied with the AFM. Noise was removed from data of interest and the resulting image levelled in order to provide an indication as to the differing heights throughout the dataset. This image was subsequently shaded, which resulted in the generation of a detailed image of the substrate surface. Both levelled and shaded images for all lubricants and substrates are presented in section 5.5.1.

4.3.3.3.3. FTIR

Fourier transform infrared was conducted using a PerkinElmer® Spotlight 400 Imaging system on worn AluSil® samples. Wavenumbers between 4000 cm^{-1} - 600 cm^{-1} were analysed. All data was obtained from Region A (Figure 32) on AluSil® samples. Analysis was conducted using a 100 µm x 100 µm aperture and ten scans were undertaken in each location so as to permit analysis of areas within the AluSil® substrate containing both silicon grains and aluminium matrix.

4.3.3.3.4. Mini SIMS

Mini secondary ion mass spectrometry was carried out on both AluSil® and piston ring samples using a Millbrook Mini SIMS MC 300 MKII instrument. As per the rationale for AFM, substrates were cleaned using Heptane prior to surface analysis.

Positive and negative static ion analysis was performed within Region A in Figure 32 on AluSil® samples, using a region of analysis measuring ~ 130 µm x 130 µm. A typical region of analysis would encompass 2-3 silicon grains and an area of aluminium matrix. The area on the piston rings that was in contact with Region A on the AluSil® substrates was also analysed, using a 180 µm x 180 µm area of analysis. Three scans were performed in both positive and negative modes of analysis to remove noise. A range of 2 m / z - 200 m / z was employed, with a step of 0.2 m / z and a dwell time of 0.01 seconds. Fifteen areas were analysed inside the wear on both substrates, whilst three were performed outside the wear scar.

Positive and negative ion depth profiling was conducted on both AluSil® and ferrous piston ring substrates using the scan areas stated above. A setting of 200 repeats per atomic mass number was used, each with a 2.19 second dwell time. All data was entered into Microsoft® Excel®, where the static analysis scans were averaged and the depth profiles placed in chart form.

Chemical imaging was additionally performed using the mini SIMS technique, whereby atomic masses of interest were analysed in both positive and negative ion modes of operation, with a 300 ms exposure time. The region of analysis measured ~ 130 μm x 130 μm.

4.3.3.4. Wear Measurement

The quantitative measurement of wear of cylinder liners and piston rings when carried out under line contact conditions, is a difficult task [236, 237] owing to the small amount of wear involved, and the very small variations in the surface topography of such substrates [236]. An added complexity in analysing the wear of aluminium-silicon cylinder liners is the protrusion of the silicon grains from the surface of the substrate, because under load, these are depressed into the aluminium matrix [77, 99, 100].

A number of different methods have been used to study the wear of both piston rings [236, 238] and cylinder liners [236-240], when subject to line contact conditions. The most simple method of wear measurement for a piston ring is the mass loss encountered over the course of an experiment [237]. The wear on cylinder liners can be determined from surface images [239-241] and roughness [237, 240] analysis of the worn substrate surface, or replication [237, 239] of the test surface. Wear volumes can be calculated from observed surface roughness data [237, 240]. However, detailed analysis of the wear rates of both cylinder liner and piston ring are seen as important steps in improving current cylinder liner and piston ring interfaces [236, 238]. For this purpose, radiotracer methods have been employed [236, 238], in which both piston ring and cylinder liner running surfaces are irradiated with isotopes which have a known half-life [236, 238]. A spectrometer is then used to measure the decay of the isotopes on the substrate surfaces under test [236, 238]. Removal of the background count rate from the recorded data and the subsequent incorporation of many calibration data sets enables the wear rates on both piston ring and cylinder liner to be evaluated [236].

It was considered important, from an analysis point of view, that an indication of both the nature and extent of wear of the AluSil® substrates used in this work were obtained. Wear volumes were not appropriate because the depression of silicon into the aluminium matrix would be difficult to classify; owing to cost reasons, radiotracer methods were not used. Although roughness

comparisons of the test substrates were performed using a Taylor Hobson Form Talysurf 120L surface profilometer, this data did not produce conclusive results. Consequently, image analysis was considered to constitute the only method of wear measurement analysis of the AluSil® test substrates. Optical analytical techniques for such substrates are very complicated and involve complex algorithms to determine the height and area of the protruding silicon grains [241].

For this work, a simpler, indicative method was sought. Accordingly, digital images of AluSil® samples were obtained using an Olympus® C - 5050 digital camera, arranged at a fixed height from the substrate using an Olympus® SZ-ET camera mount, secured to an Olympus® SZ-ST stand. Each sample was cleaned using acetone and illuminated using a focussed source of white light produced by an Olympus® Highlight 3001 system set to maximum brightness output. Images of the entire aluminium-silicon substrates were obtained, using the 3 x optical zoom of the camera, in addition to a 3 x zoom provided by the Olympus® SZ-ET camera mount. The camera was set to HQ mode and images of 2560 x 1920 pixels were obtained. For every test lubricant, three AluSil® samples were analysed.

Data was normalised using Corel® Photo Paint™, whereby each image was adjusted to the same contrast and brightness settings (Figure 33). After this normalisation process, the images were cropped across the length and width of the wear scar, to isolate the region of interest. Each wear scar image was fed into The MathWorks™ MATLAB® mathematical software, to determine the percentage of white area within the image of the test substrate. This value was subsequently input into Microsoft® Excel® to calculate the average and standard deviations, with the outcome in chart form.

The proportion of white area across the wear scar was sought because this was indicative of the type of wear occurring on the aluminium-silicon substrates. Three main grades of wear using this process were identified, namely, *heavy wear*, which could be identified by a large dark wear scar region on the test substrate, *ultra mild wear*, which imparted little damage to the substrate surface and silicon grains were evident as small dark areas within the wear scar. Lastly, *mild wear*, was ascribed to a wear level which lay in-between the two previously described wear types and was identified by an increase in the amount of darkness, compared to ultra mild wear samples.

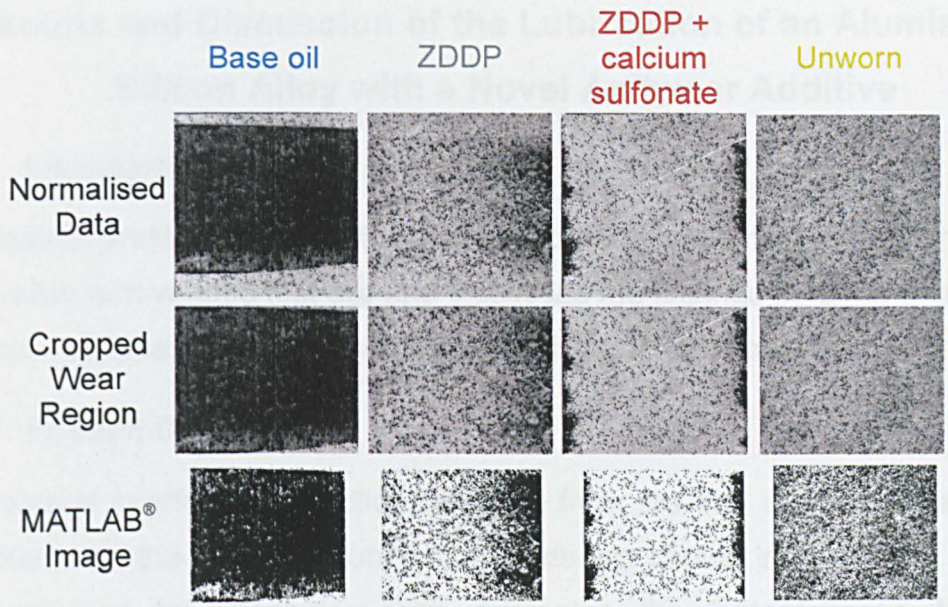

Figure 33: Image analysis process to determine wear grades for AluSil® substrates

The grading of each sample would be an indicator as to the type of wear occurring on the AluSil® substrates. As such, the method of wear analysis was intended to work in conjunction with micro-scale surface topography, in order to provide detailed qualitative analysis of the wear imparted to the test samples.

5. Results and Discussion of the Lubrication of an Aluminium-Silicon Alloy with a Novel Anitwear Additive

5.1. Introduction

This chapter presents the results obtained from the lubrication of an aluminium-silicon alloy with various test oils and discusses the findings in terms of frictional response, surface topography and tribochemistry of the substrates.

5.2. Friction Coefficients

The average coefficient of friction obtained from the line contact experiments lubricated with the eight test lubricating fluids are shown in Figure 34. Values were obtained by absoluting then averaging the instantaneous frictional response of the interface, which resembled that shown in [242], over a second at a given time interval. It is apparent that the greatest frictional force in the contact was obtained using base oil, which increased from a starting value of 0.13 to a maximum of 0.18 after 70 minutes. On average, NOCH in base oil created a maximum value of μ, of 0.16, after one minute of experimentation, this falling to 0.13 after 35 minutes; thereafter, frictional force levelled off.

Oils which contained either ZDDP or calcium sulfonate markedly reduced the friction coefficient in the contact, compared to base oil and NOCH in base oil. In the case of lubricating the tribosystem with ZDDP, the observed trend comprised frictional force falling from an initially high value and thereafter levelling off as evidenced by the friction coefficient obtained after 2 minutes, namely 0.13, gradually decreasing to 0.12 after 120 minutes. The inclusion of NOCH with ZDDP had no effect on either this trend, nor the coefficient of friction obtained for ZDDP alone, insofar as, the maximum friction coefficient of 0.13, which was obtained initially for ZDDP + NOCH, fell to a minimum of 0.12 after 90 minutes of lubricant evaluation, levelling off thereafter.

Lubricating the contact with calcium sulfonate produced the lowest coefficient of friction of any lubricant studied, in that a maximum value of 0.09 was secured at the start of the experiment, with the coefficient of friction reducing by a small amount and levelling off with time. Adding NOCH to calcium sulfonate increased the friction in the contact, but did not alter the trend of the plot, the highest value of μ, 0.11, being obtained after 2 minutes of

experimentation; the frictional response, on average, gradually reduced to 0.10 at the end of the experiment.

The combination of ZDDP and calcium sulfonate created a lower coefficient of friction than that obtained using ZDDP alone. After 1 minute, the highest value of μ, 0.11 was obtained, which reduced to 0.10 after 60 minutes, after which the plot reached a plateau. The addition of NOCH to this lubricant affected the coefficient of friction slightly, with the greatest coefficient of friction (0.11) being achieved just after the start of the experiment, this falling to 0.10 after 95 minutes, after which time, the plot levelled out.

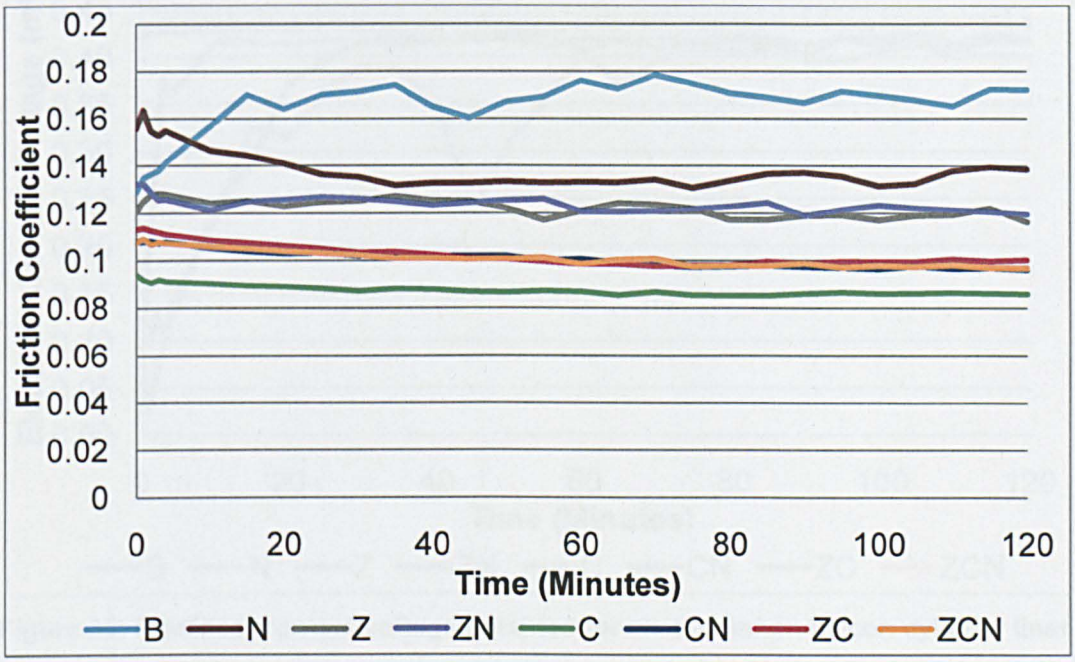

Figure 34: Friction coefficients obtained for an aluminium-silicon cylinder liner / steel piston ring interface lubricated with various oils

5.3. Electrical Contact Voltage

Figure 35 shows the ECV data obtained from averaging the values of the electrical contact voltage, which resembled [242], over a second at a given time period for the tribosystem. All lubricants fully separated the piston ring and aluminium alloy contacting surfaces, achieving a value of approximately 0.43 mV within the first five minutes, with the exception of three oils namely base oil, ZDDP and NOCH in base oil. Of these particular oils, ZDDP was the most efficient at separating the surfaces, creating a maximum electrical contact voltage of 0.42 mV after an average of 35 minutes. However, not only did the addition of NOCH to ZDDP vastly improve the performance of the lubricant in terms of creating a boundary lubricating film, but interestingly, the maximum

ECV was markedly higher than that recorded for ZDDP. Base oil separated the surfaces least efficiently of all lubricating fluids, with a maximum ECV of 0.40 mV obtained after 60 minutes. NOCH in base oil appeared to improve the ability of the lubricant to separate the two contacting surfaces, reaching a maximum electrical contact voltage of 0.42 mV after 30 minutes. In addition, this lubricant provided the interface with a more stable ECV, compared to that generated by base oil alone. Lubricants which contained calcium sulfonate maintained a full film of ~ 0.43 mV throughout the entirety of experimentation.

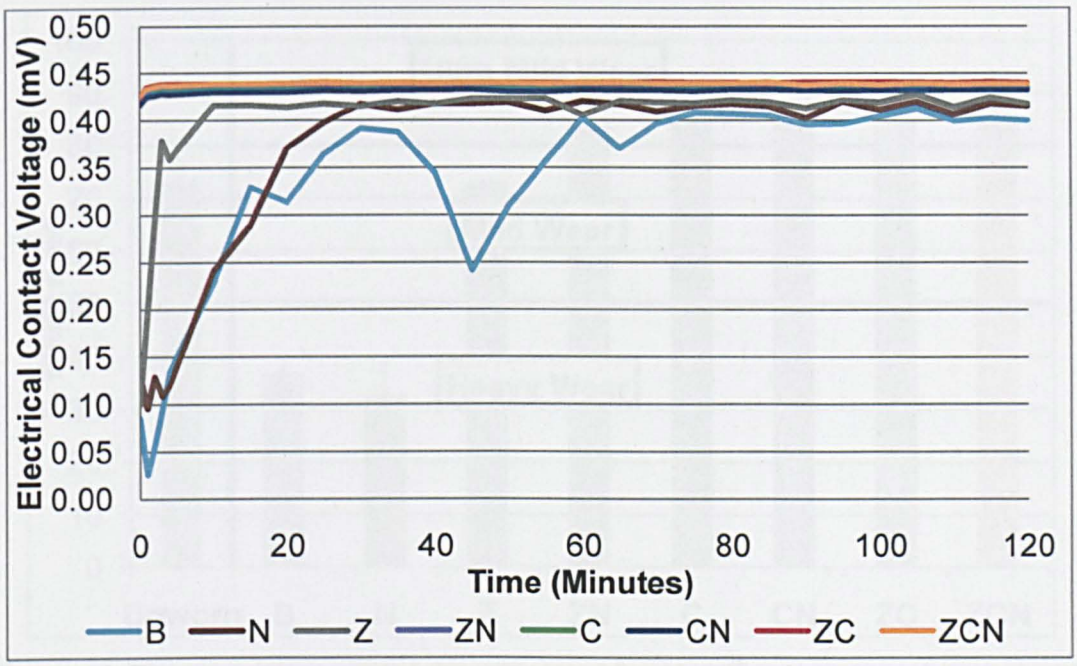

Figure 35: Electrical contact voltage obtained for an aluminium-silicon cylinder liner / steel piston ring interface lubricated with various oils

5.4. Wear Data

Examples of the image analysis process that was used to indicate the type and extent of wear occurring on the AluSil® samples are shown in Figure 33. It is apparent that there was a large difference in appearance between the normalised images obtained using base oil, ZDDP and ZDDP + calcium sulfonate. Indeed, the dark wear scar region obtained for the base oil sample is clearly evident whereas the wear scar region obtained for ZDDP + calcium sulfonate is only identifiable from the darker region at the outer edges of the test sample (Region A in Figure 32). The dark area within the wear scar of the ZDDP sample extended further into the centre of the substrate than in the case of ZDDP + calcium sulfonate. Small, darkly shaded silicon grains can be seen within the wear scar of both ZDDP and ZDDP + calcium sulfonate lubricated

substrates. Once these wear scars had been isolated, the images shown at the bottom of Figure 33 were produced using MATLAB®. The dark areas within each image varied between the three substrates, thus indicating different grades or levels of wear.

The average data obtained from MATLAB® is shown in Figure 36 from which it is evident that most substrates possessed ~ 84 % of white area. However, there were three exceptions to this namely base oil (37 %), NOCH in base oil (32 %) and ZDDP (73 %).

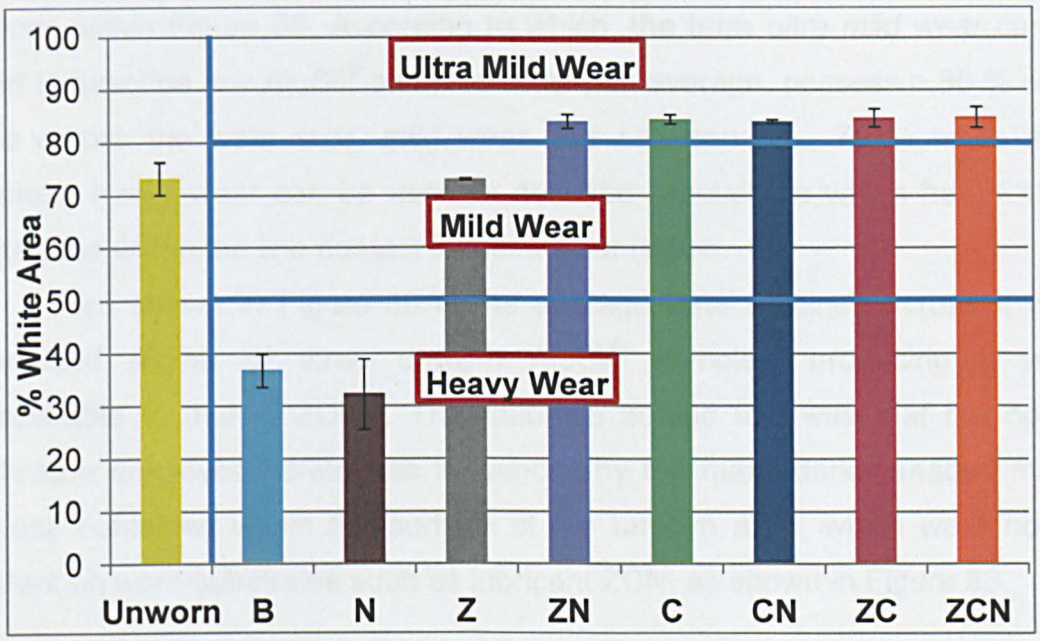

Figure 36: The percentage white area calculated for AluSil® substrates lubricated with various oils

Both base oil and NOCH in base oil were very poor lubricants and the aluminium-silicon alloy was badly damaged after testing (section 5.5.1.1), with the wear scar, shown in Figure 33, being completely black. Therefore, it is possible to classify base oil and NOCH in base oil as lubricants that fall within the *heavy wear* section of the grading system employed.

All other lubricants, except for ZDDP, possessed the same proportion of white area on the AluSil® substrates and thus can be considered as providing similar wear performance on the aluminium surfaces (Figure 36). When analysing the surface of these substrates (section 5.5.1), it is clear that the substrates had not suffered large amounts of wear, and therefore, the grading classification for calcium sulfonate, calcium sulfonate + NOCH, ZDDP + NOCH, ZDDP + calcium sulfonate and ZDDP + calcium sulfonate + NOCH was *ultra mild wear*.

ZDDP was the only lubricant that did not result in either heavy wear or ultra mild wear (Figure 36). Indeed, the lubricant did not meet the ultra mild wear criteria owing to the large amounts of oil residue deposited on the substrate surface by the lubricating fluid (section 5.5.1.2), as observed previously [100]. This undesirable oil-based layer reduced the percentage of white area on the substrate and, as a result, the worn aluminium alloy fell into the *mild wear* category.

Therefore, using these results, three grades of wear were ascribed clear regions within Figure 36. According to which, the term *ultra mild wear* can be used to describe any AluSil® samples which, on average, possess > 80 % white area across the wear scar, *mild wear* falls between 50 - 79 % white area, whereas heavy wear can be used to describe a substrate which has < 49 % white area within the line contact induced wear region.

Also shown in Figure 36 is the average data obtained across a wear scar-sized region of three unworn AluSil® samples, producing a value comparable to that of ZDDP. The rationale behind this was that the optical technique employed herein was influenced by the many darkly shaded matrix regions contained within the surface of the unworn alloy, which were not as evident on worn substrates such as lubricant ZCN, as shown in Figure 33.

5.5. Surface Analysis of Worn Aluminium-Silicon Alloys and Steel Piston Rings

The following subsections to this part of the thesis identify the effects the addition of NOCH has on the four conventional lubricating fluids, namely base oil, ZDDP, calcium sulfonate and ZDDP + calcium sulfonate.

5.5.1. Surface Topography and Morphology

This section highlights the effects of the various lubricating fluids on the topography of the worn AluSil® and piston ring surfaces, detected using both scanning electron and atomic force microscopy within Region A of Figure 32 on AluSil® and the incident area on piston ring substrates. The images shown in this section are representative of tested surfaces. Height measurements between silicon grains and aluminium matrix are stated for AluSil® substrates; ten measurements were taken using AFM and the SPMLab NT software, with an average generated.

With regards to the piston ring samples, both the scanning electron and atomic force microscope images obtained were of the smooth portion of the piston ring (Figure 28A&C), the area of tribofilm formation. In all figures, those images labelled A and B were non-NOCH containing lubricants, whilst those lubricants which contained NOCH were labelled C and D.

5.5.1.1. AluSil® - Base Oil vs NOCH in Base Oil

As can be seen in Figure 37, when the tribosystem under study was lubricated using either base oil or NOCH in base oil, the surface of the test AluSil® substrate was badly damaged.

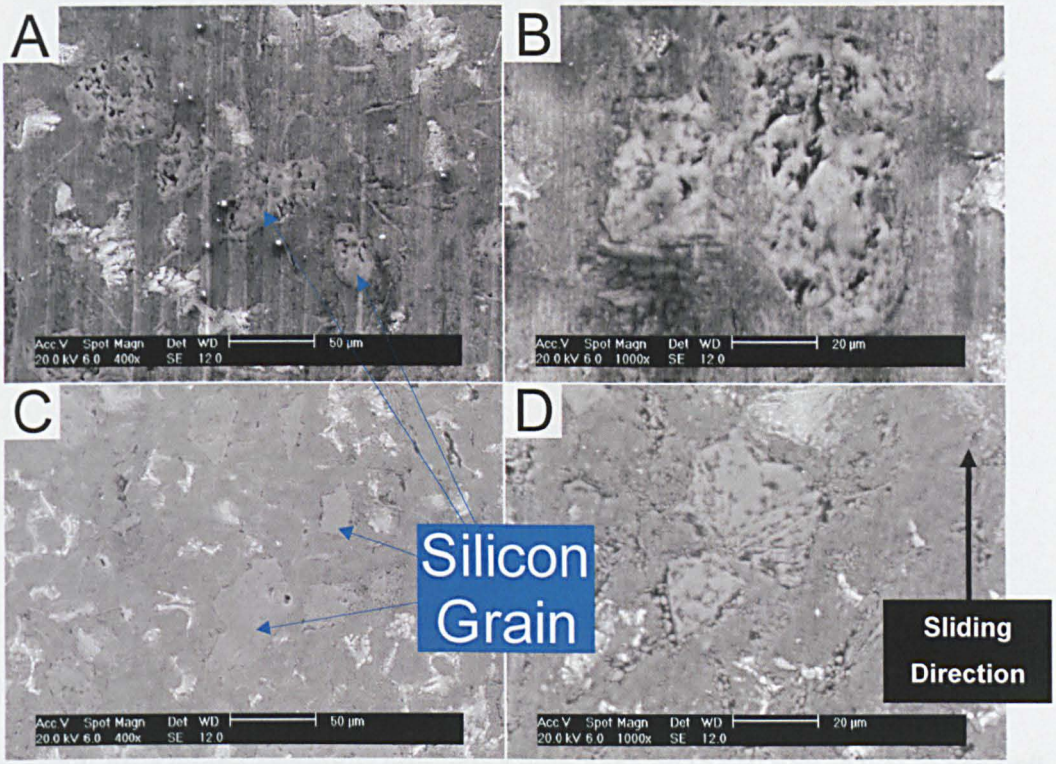

Figure 37: SEM image of AluSil® lubricated with base oil (A&B) and NOCH in base oil (C&D)

Indeed, referring to Figure 37A-D, even though silicon grains were still evident within the substrate surface, the silicon areas differed greatly from their profile prior to test (Figure 27B) as it was evident that the silicon grains were level with the aluminium matrix of the alloy, which itself had encountered vast amounts of wear (Figure 37).

The atomic force microscope images displayed in Figure 38 highlight the extent of the damage to the surface of the aluminium-silicon substrate when lubricated with base oil (Figure 38A&B) and NOCH in base oil (Figure 38C&D). Figure 38A&C show the surface of the AluSil® material after it had been levelled

using the software provided with the atomic force microscope. A number of grooves through the surface of the AluSil® material were evident on both substrates. As seen in the SEM images of the NOCH in base oil sample (Figure 37C&D), silicon grains were present within the badly damaged surface alloy (Figure 38C), but these were depressed into the surface of the substrate; an average measurement of 211 nm ± 26 nm was determined. The shaded versions of these images (Figure 38B&D) revealed that substrate surfaces deteriorated badly, when lubricated with either base oil or NOCH in base oil lubricating fluids.

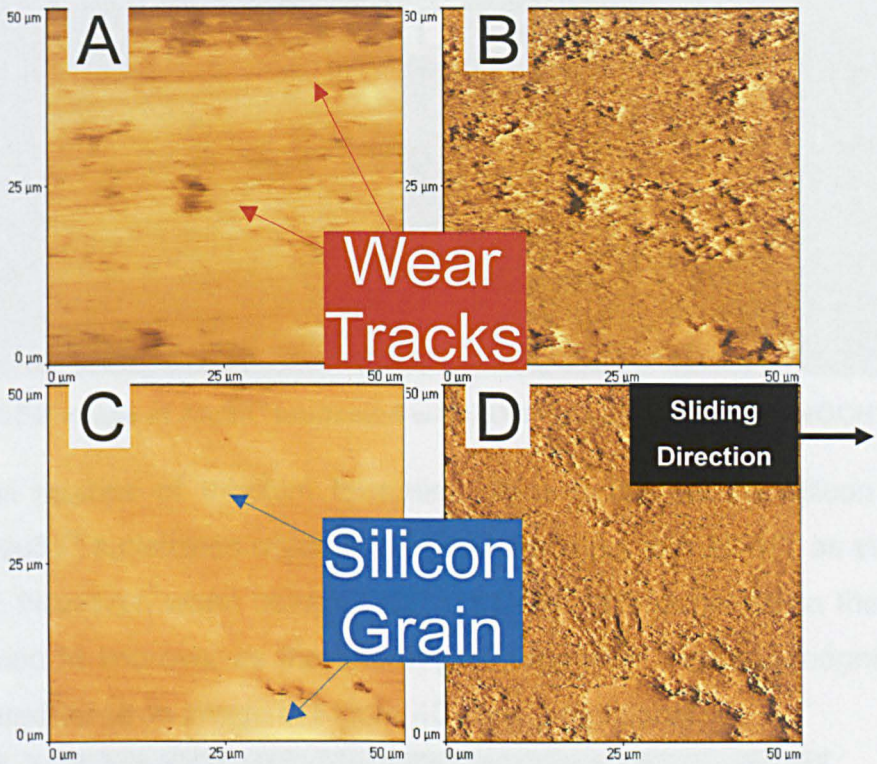

Figure 38: AFM image of AluSil® lubricated with base oil (A&B) and NOCH in base oil (C&D)

5.5.1.2. AluSil® - ZDDP vs ZDDP + NOCH

Lubricating the piston ring and AluSil® contact with ZDDP resulted in the running surface of the AluSil® material identical to that shown in Figure 39A&B. Clearly, honing marks had been removed from the silicon grains on the surface of the substrate and cracking of the protruding silicon within the alloy had occurred (Figure 39B). Also, an oil residue layer was present, which covered the aluminium matrix (Figure 39A&B) and surrounded the silicon grains within the AluSil® material. When the interface was lubricated with ZDDP + NOCH, as shown in Figure 39C&D, the size of the oil layer observed with ZDDP was

reduced considerably. Cracking of some silicon grains within the alloy was observed (Figure 39D).

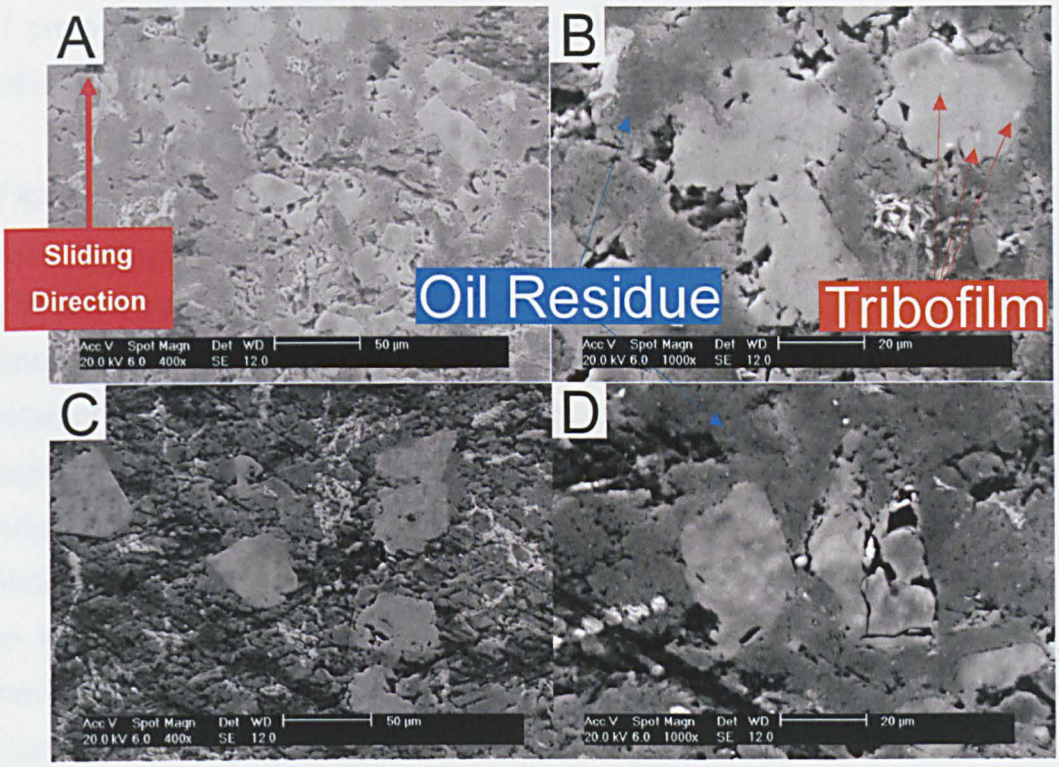

Figure 39: SEM image of AluSil® lubricated with ZDDP (A&B) and ZDDP + NOCH (C&D)

Small regions of tribofilm formation were found on the silicon grains within the AluSil® substrates which had been lubricated with ZDDP, as shown in Figure 39B. However, when using ZDDP + NOCH, film formation on the silicon areas seemed to improve, as the silicon grain shown in the high magnification back scattered electron image in Figure 40 clearly highlights.

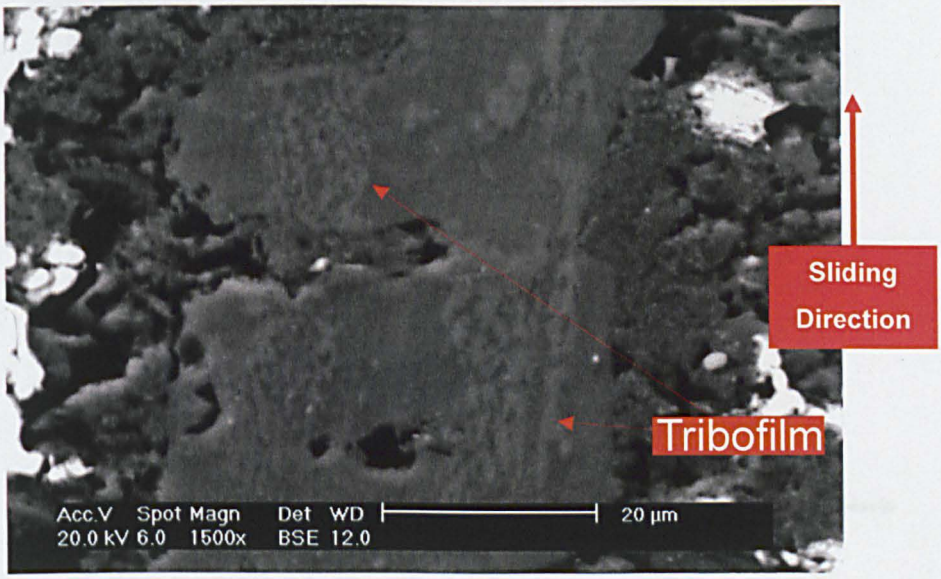

Figure 40: High magnification image of a silicon grain within AluSil® which had been lubricated with ZDDP + NOCH

The observed tribofilm was orientated in the sliding direction of the contact and comprised small pads which were interlinked, forming long lengths of protective film. These pads did not extend onto the aluminium matrix, but rather the oil residue layer was observed silicon grains edges (Figure 40).

The atomic force microscope images of the ZDDP AluSil® substrates (Figure 41A&B) revealed silicon grains were almost level with the oil residue layer that had been observed using SEM (Figure 39B); the mean height difference was 67 nm ± 9 nm. The oil residue regions were identifiable as topographically smooth areas which covered the rough aluminium matrix between silicon grains in the alloy (Figure 41B). Interestingly, the oil residue regions were not removed with Heptane, suggesting they were bound to the substrate, and have been observed previously on Al-Si surfaces [100]. The AluSil® sample which had been lubricated with ZDDP + NOCH did not contain as large a volume of oil residue as was obtained using ZDDP alone and, therefore, the silicon grains still appeared to possess a step height over the aluminium matrix surrounding the hard regions (Figure 39C&D and Figure 41C&D). Indeed, this height difference, on average, was 275 nm ± 36 nm. The lack of any ZDDP-based tribofilm can be attributed to the difficult task of finding a suitable area using the atomic force microscope.

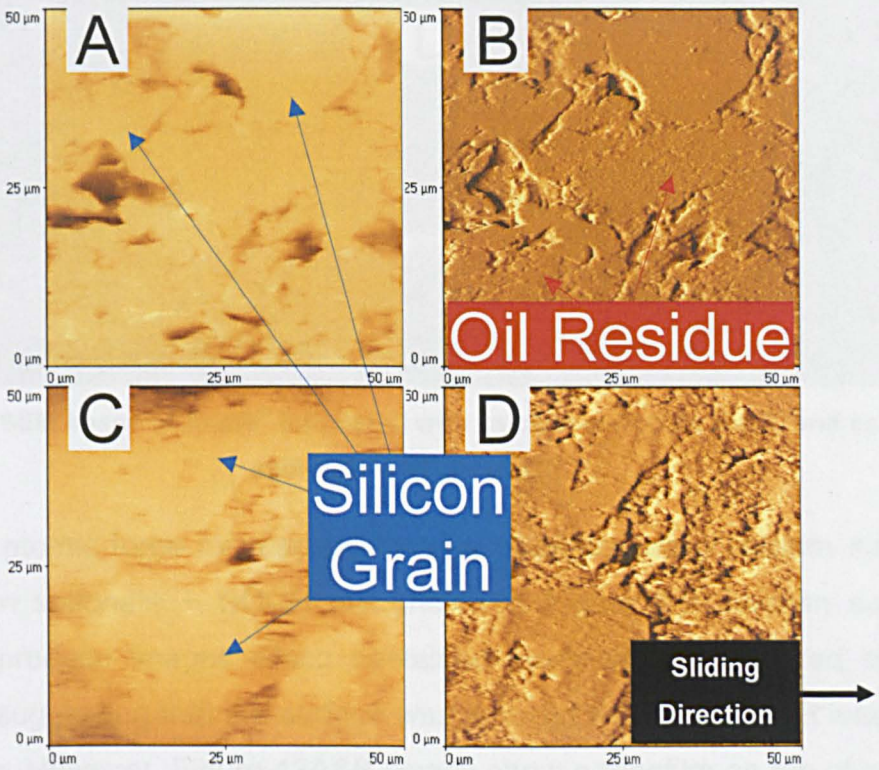

Figure 41: AFM image of AluSil® lubricated with ZDDP (A&B) and ZDDP + NOCH (C&D)

5.5.1.3. AluSil® - Calcium Sulfonate vs Calcium Sulfonate + NOCH

When the tribosystem was lubricated with calcium sulfonate (Figure 42A&B) and calcium sulfonate + NOCH (Figure 42C&D), it was evident that a tribofilm formed on the surface of the silicon grains within the alloy. This tribofilm, which was easy to identify from the darkly shaded area of tribofilm contrasting against the lightly shaded silicon grains, was not orientated in the sliding direction of the contact, but appeared to have covered the exposed silicon grains. Cracking of silicon grains occurred (Figure 42A) and the honing marks had been removed from the regions of silicon not covered by the aforementioned tribofilm. Interestingly, oil residue, as was observed in the cases of ZDDP and ZDDP + NOCH, was not witnessed when the Al-Si alloy had been lubricated with calcium sulfonate or calcium sulfonate + NOCH.

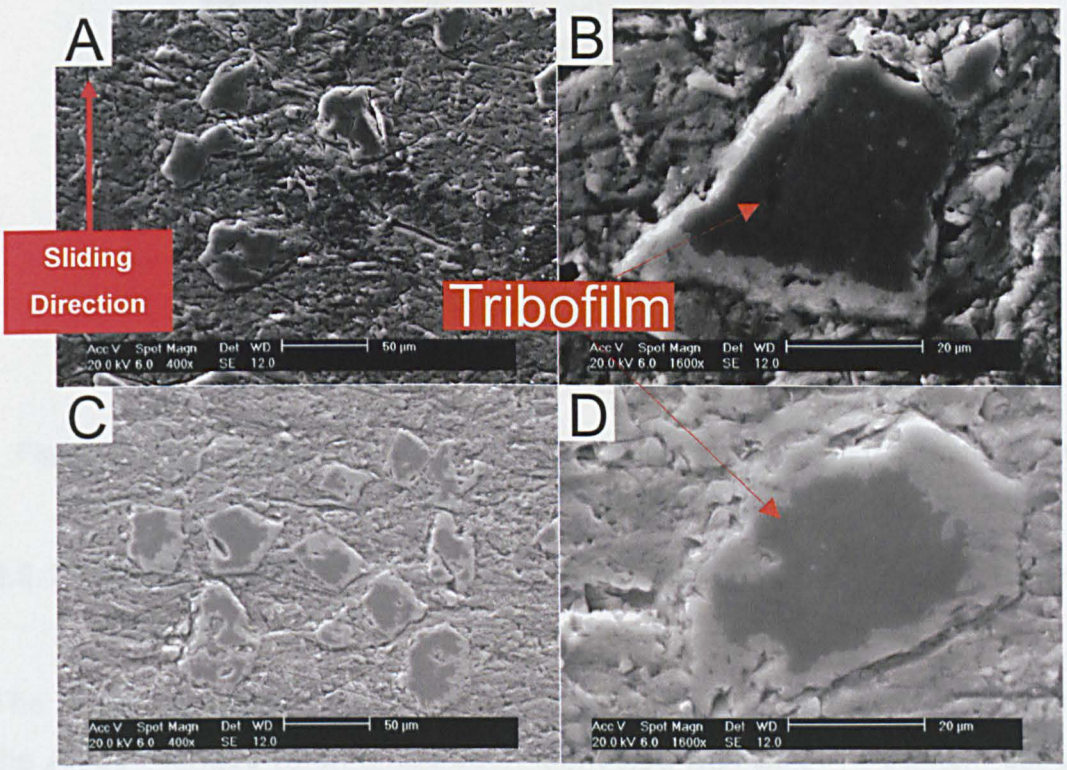

Figure 42: SEM image of AluSil® lubricated with calcium sulfonate (A&B) and calcium sulfonate + NOCH (C&D)

The atomic force microscope images obtained using calcium sulfonate and calcium sulfonate + NOCH are shown in Figure 43. Calcium sulfonate tended to produce images which contained more noise, compared to other lubricants, suggesting that the surface was covered with a layer that was prone to smearing. However, Figure 43A&B clearly show a tribofilm on top of a silicon grain, indicating that the protective layer first displayed in Figure 42B was

neither flat nor uniform and comprised small pad-like structures. The average variation in height between the pad-like film and the adjacent aluminium matrix was 547 nm ± 37 nm. A tribofilm was not observed using AFM for the AluSil® substrate which had been lubricated with calcium sulfonate + NOCH (Figure 43C&D). However, the silicon grain shown in Figure 43C had been depressed into the surface of the substrate; the average step height was 477 nm ± 34 nm.

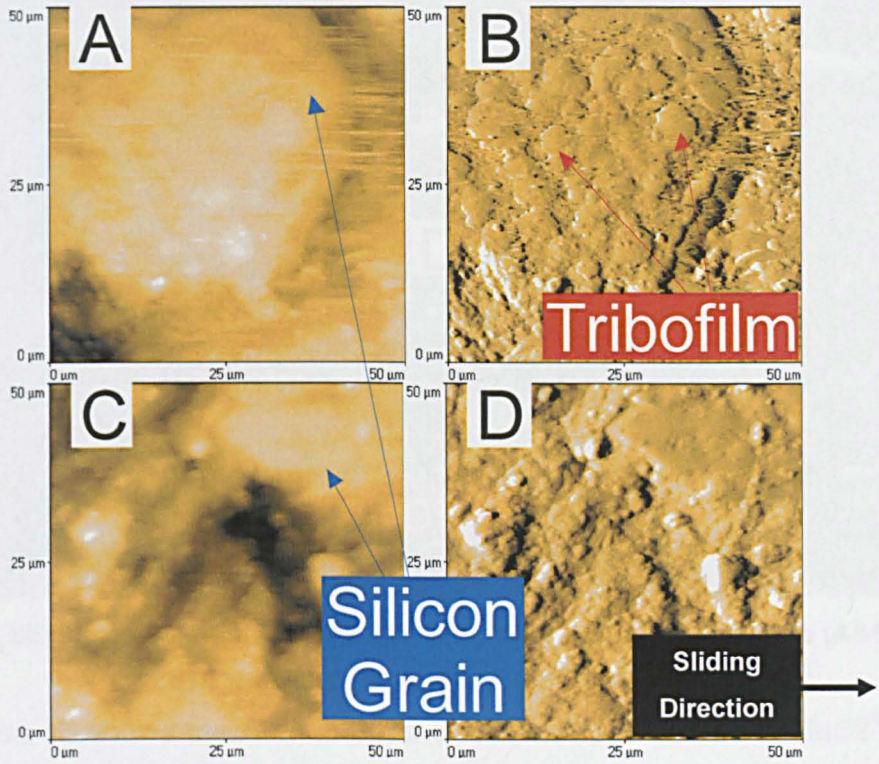

Figure 43: AFM image of AluSil® lubricated with calcium sulfonate (A&B) and calcium sulfonate + NOCH (C&D)

5.5.1.4. AluSil® - ZDDP + Calcium Sulfonate vs ZDDP + Calcium Sulfonate + NOCH

The scanning electron images shown in Figure 44 highlight the topography of the AluSil® surface when it had been lubricated with ZDDP + calcium sulfonate (Figure 44A&B) and ZDDP + calcium sulfonate + NOCH (Figure 44C&D). Cracking of the silicon within the alloy had occurred and, as with the previous lubricants, honing marks were removed from silicon grains. Tribofilms were not evident on the AluSil® substrate which had been lubricated with ZDDP + calcium sulfonate. However, a tribofilm was observed on a silicon grain within Figure 44D when lubricated with ZDDP + calcium sulfonate + NOCH. Interestingly, this film resembled that of the tribofilm previously observed using calcium sulfonate + NOCH as lubricant (Figure 42D), rather than that obtained

using ZDDP + NOCH (Figure 40). An oil residue region was observed adjacent to the silicon grain shown in Figure 44D, but this did not cover a large proportion of the aluminium matrix, as was the case for ZDDP and ZDDP + NOCH.

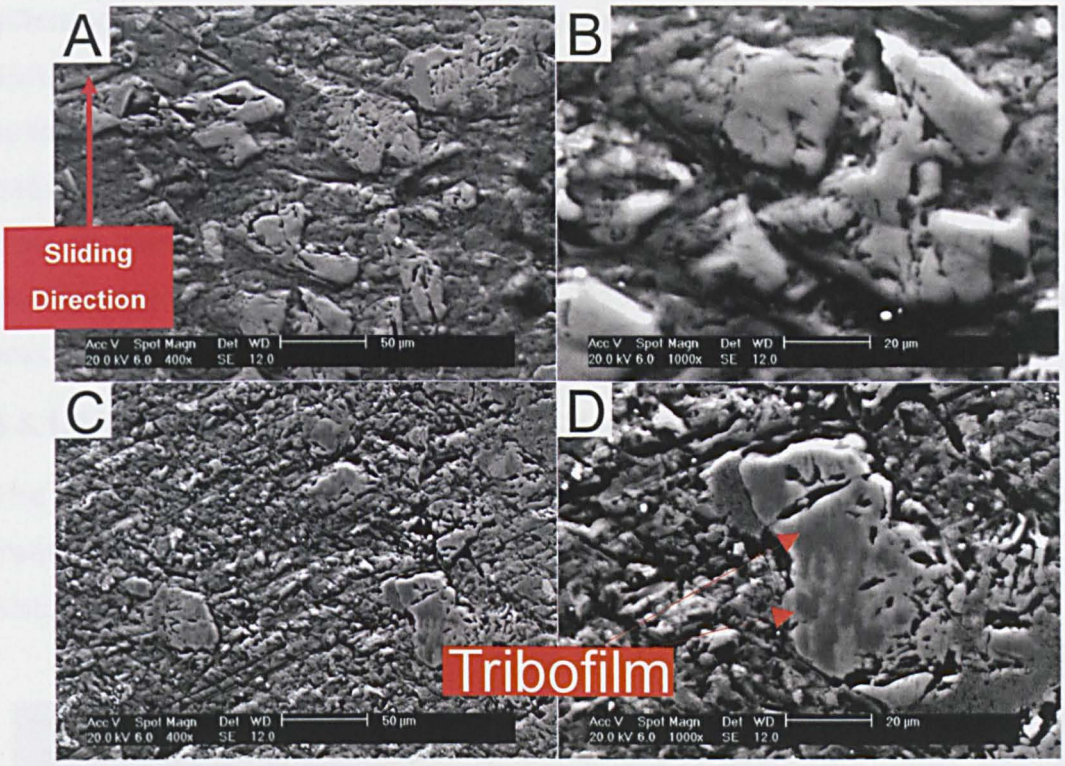

Figure 44: SEM image of AluSil® lubricated with ZDDP + calcium sulfonate (A&B) and ZDDP + calcium sulfonate + NOCH (C&D)

Figure 45 shows the AFM images of lubricant ZC and ZCN AluSil®.

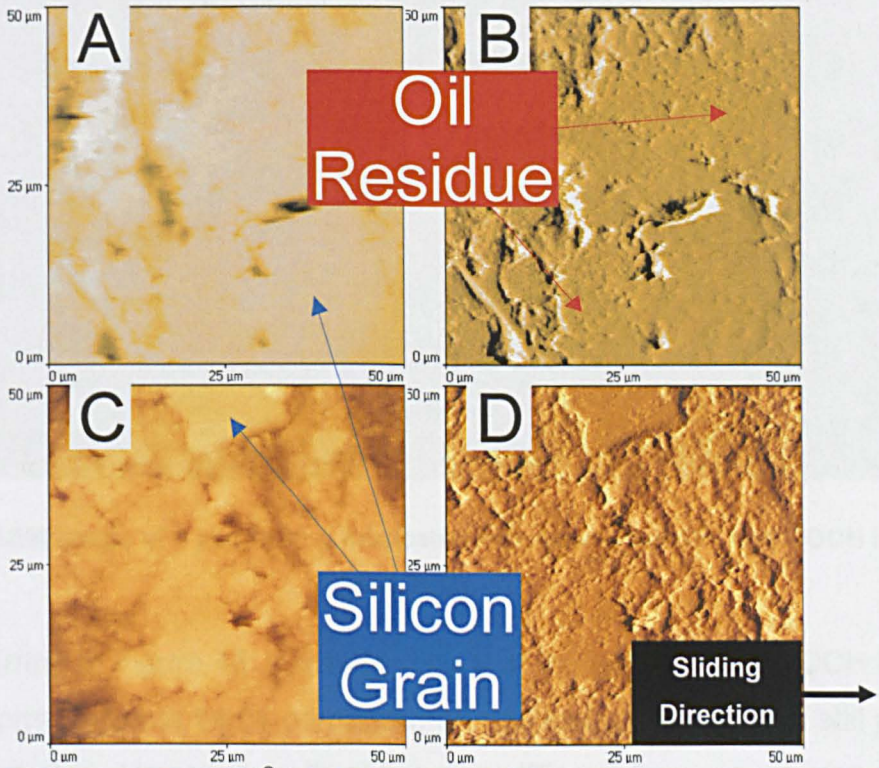

Figure 45: AFM image of AluSil® lubricated with ZDDP + calcium sulfonate (A&B) and ZDDP + calcium sulfonate + NOCH (C&D)

As can be seen in Figure 45A, the surface of the substrate was almost level, with an oil residual layer evident (Figure 45A&B); this was reminiscent of the layer obtained when using ZDDP as lubricant (Figure 39B). The average difference in height between silicon grain and oil residue region in Figure 45A&B was 98 nm ± 8 nm. When lubricating the substrate with ZDDP + calcium sulfonate + NOCH, it was clear that the silicon grain present (Figure 45C&D) had been depressed into the surface of the AluSil® sample and the honing worn from its running surface. The mean extension of the silicon grain from the aluminium matrix in Figure 45C&D was 449 nm ± 46 nm; an oil residue layer was not observed.

5.5.1.5. Piston Ring - Base Oil vs NOCH in Base Oil

The SEM images shown in Figure 46 highlight the amount of wear debris transferred from the heavily damaged AluSil® substrates (Figure 37) to their piston ring counterparts when lubricated with base oil or NOCH in base oil.

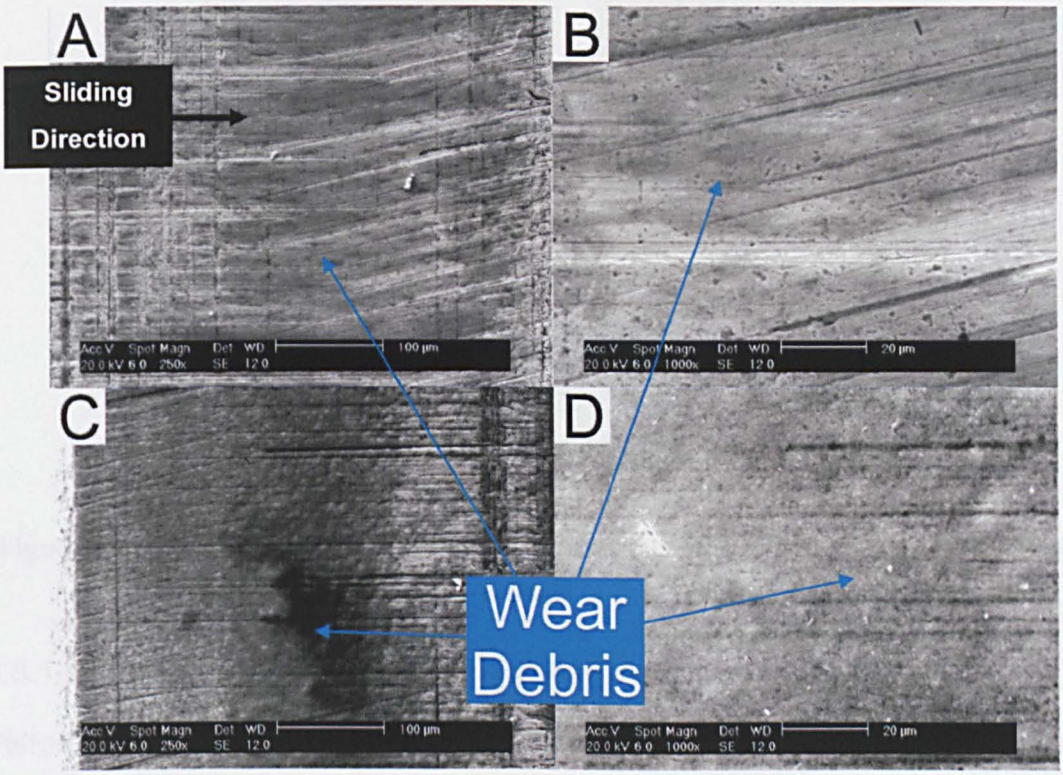

Figure 46: SEM image of a piston ring lubricated with base oil (A&B) and NOCH in base oil (C&D)

Referring to Figure 46, it was evident that the base oil and NOCH in base oil piston rings were not badly damaged, as machining marks were still present on the substrates. However, both substrates differed from an unworn sample

(Figure 28) insofar as physically identifiable areas of material transfer were observed on and arond the machining marks contained within the surface of the piston rings (Figure 46).

AFM images of base oil and NOCH in base oil substrates are shown in Figure 47. These images reiterate what had been observed using SEM (Figure 46), insofar as large amounts of material, which had been transferred from the AluSil® substrate onto the ferrous-based piston ring, covered the surface of the substrate. This material was level across the surface (Figure 47A&C), with the deep grooves produced from machining, as shown in Figure 28, still present on the substrate (Figure 47A&B).

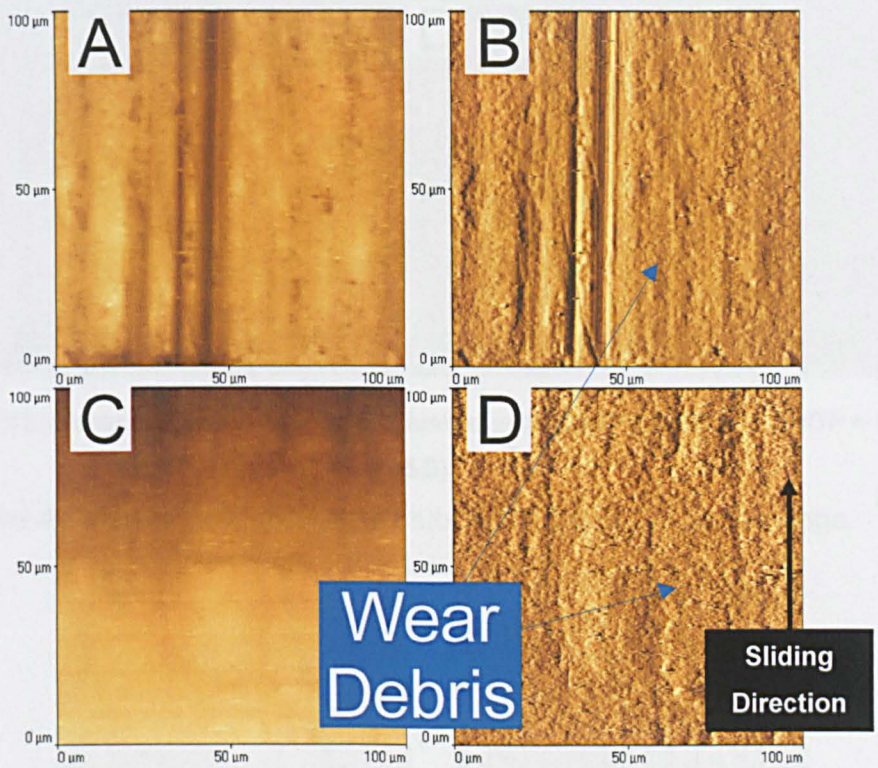

Figure 47: AFM image of a piston ring lubricated with base oil (A&B) and NOCH in base oil (C&D)

5.5.1.6. Piston Ring - ZDDP vs ZDDP + NOCH

Piston rings lubricated with ZDDP and ZDDP + NOCH are shown in Figure 48. There was no material transfer from aluminium substrate to piston ring and the surfaces of the ferrous substrates were intact, with machining marks still evident. However, towards the leading edge of the piston rings, as seen at the right of Figure 48B, was an area in which some machining marks had been removed. A tribofilm originating from ZDDP can be seen in Figure 48B, which did not possess a discernable structure, and which contrasted to that observed

for ZDDP + NOCH, as shown in Figure 48C&D. The ZDDP + NOCH tribofilm appeared to comprise long lengths of patchy areas of protective film, which covered a large proportion of the smooth section of the piston ring (Figure 48C).

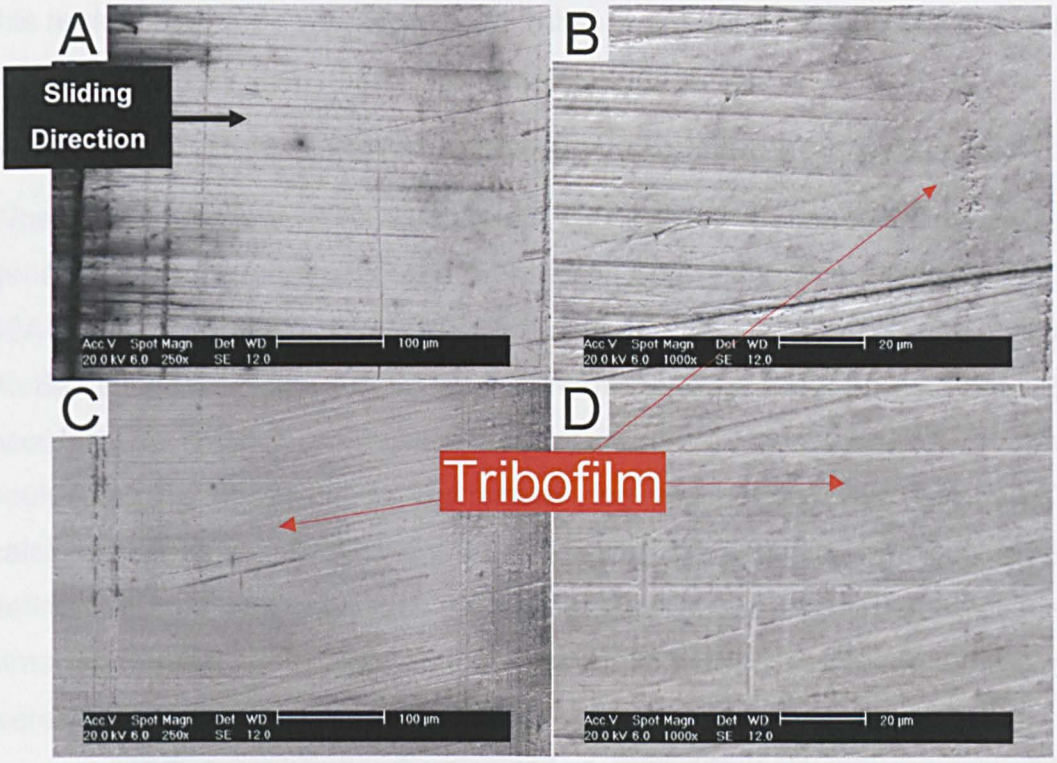

Figure 48: SEM image of a piston ring lubricated with ZDDP (A&B) and ZDDP + NOCH (C&D)

Figure 49 shows AFM images of lubricant Z and ZN piston rings.

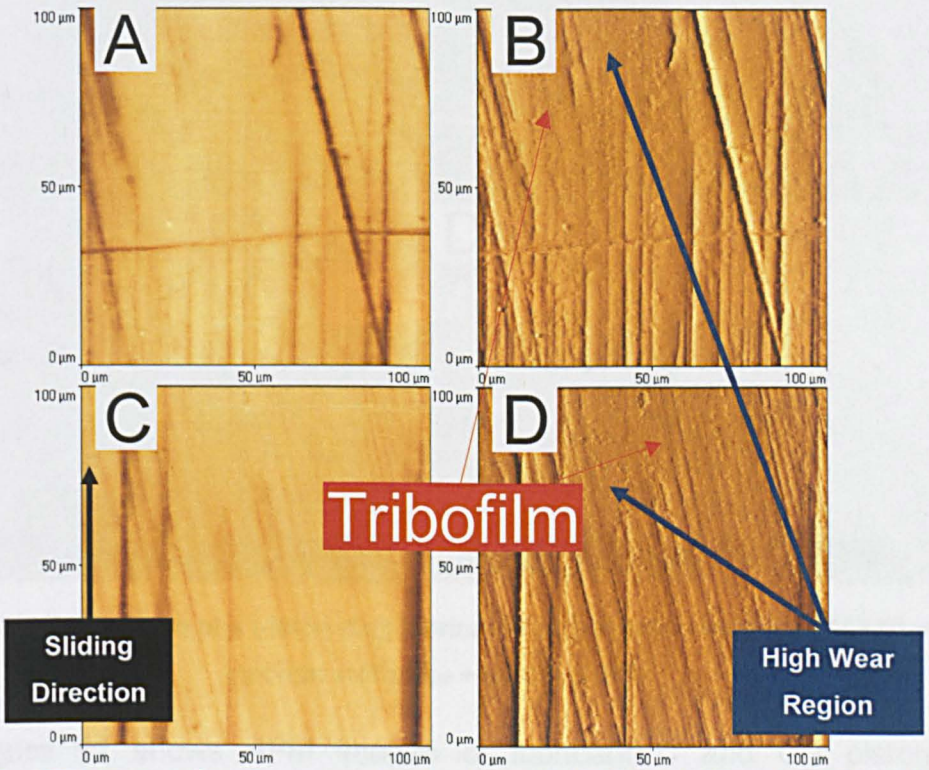

Figure 49: AFM image of a piston ring lubricated with ZDDP (A&B) and ZDDP + NOCH (C&D)

As can be seen, the area located near the top of Figure 49B&D endured more wear than elsewhere on the piston ring, presumbably due to the alignment of the piston ring onto the cylinder liner, which increased the contact pressure in this region. This area was also the location of a tribofilm highlighted in Figure 48 and is labelled as such in the AFM images (Figure 49).

5.5.1.7. Piston Ring - Calcium Sulfonate vs Calcium Sulfonate + NOCH

When the tribosystem was lubricated with calcium sulfonate, a tribofilm was generated on the surface of the smooth portion of the test piston ring (Figure 50A&B). This tribofilm resembled that obtained on the silicon grains within the AluSil® substrate (Figure 42B), as the tribofilm was smooth and did not appear, according to SEM, to possess a pad-like structure (Figure 50A&B). A tribofilm could also be observed on the piston ring which had been lubricated with calcium sulfonate + NOCH (Figure 50C&D). This tribofilm was not as clearly defined as that observed with calcium sulfonate, but the structure of the two films was similar. Both piston rings showed little wear, as the machining marks were still present (Figure 50).

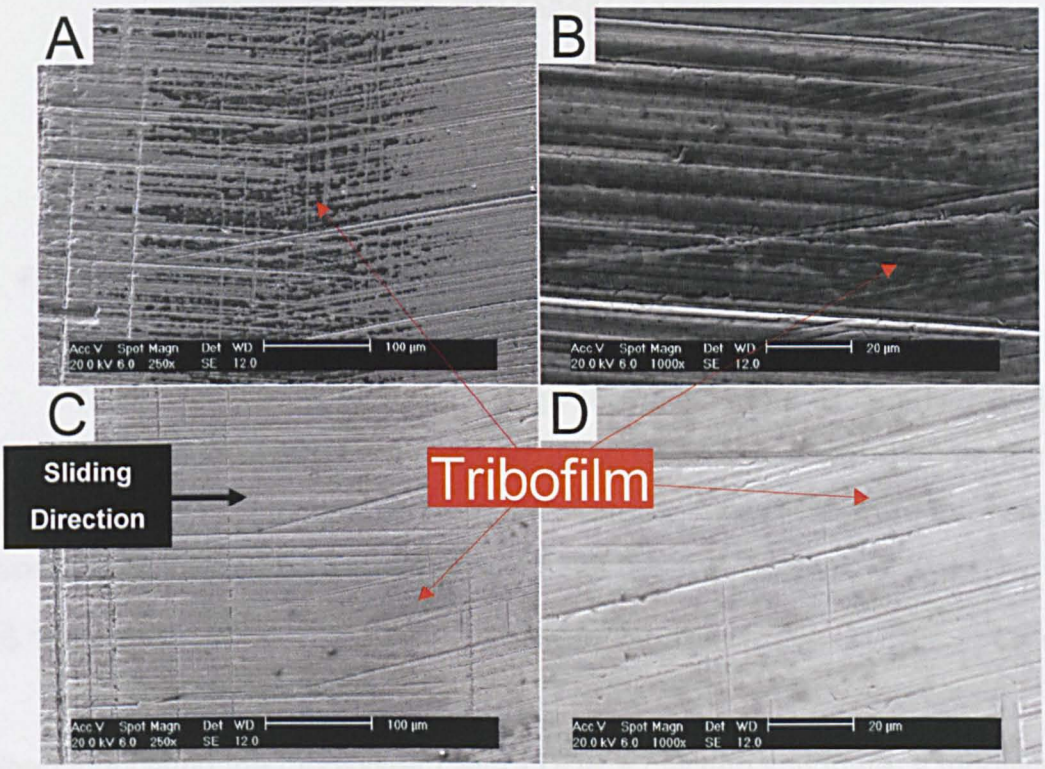

Figure 50: SEM image of a piston ring lubricated with calcium sulfonate (A&B) and calcium sulfonate + NOCH (C&D)

Figure 51 shows AFM images of lubricant C and CN piston ring substrates. Figure 51A&B indicate that the tribofilm generated on the piston ring

substrate using calcium sulfonate as lubricant comprised large pad-like structures that were very similar to those obtained for AluSil® (Figure 43A&B). The tribofilm shown in Figure 51A&B had a thickness of 198 nm ± 11 nm, measured over ten points on five areas of analysis using AFM. The film observed on the piston ring when using calcium sulfonate + NOCH as lubricant (Figure 51C&D) was, as observed using SEM imagery (Figure 50), not as obvious as the protective layer obtained using calcium sulfonate.

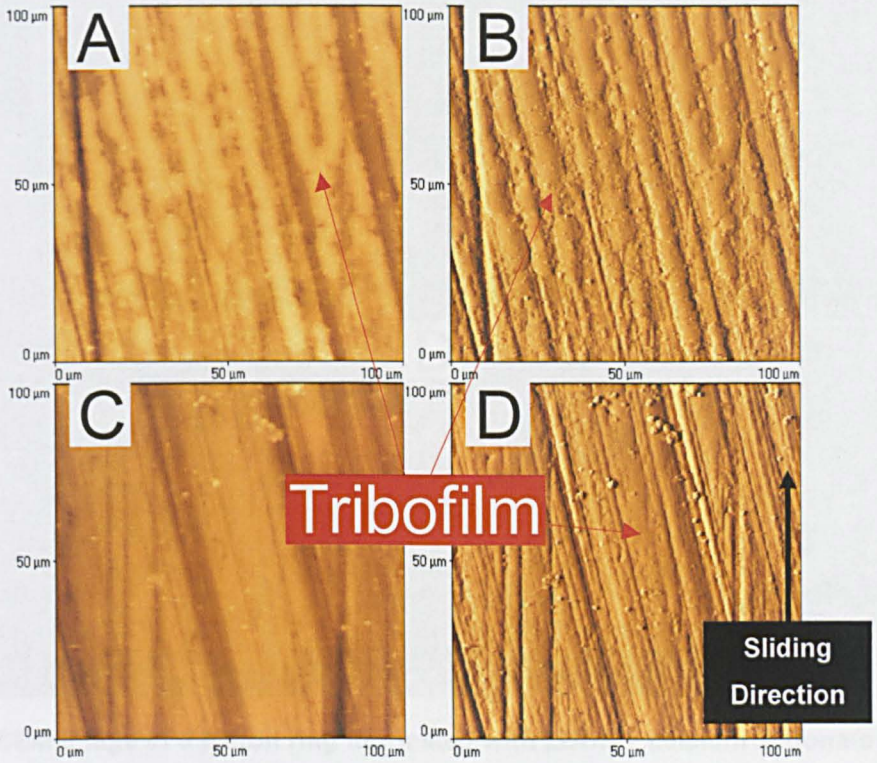

Figure 51: AFM image of a piston ring lubricated with calcium sulfonate (A&B) and calcium sulfonate + NOCH (C&D)

The surface of the two piston rings shown in Figure 51 clearly reveals the minimal amounts of wear that had occurred using these two detergent-based lubricants. All machining marks on the ferrous substrates were present and wear debris from the AluSil® sample was not observed.

5.5.1.8. Piston Ring - ZDDP + Calcium Sulfonate vs ZDDP + Calcium Sulfonate + NOCH

When lubricating the tribosystem with ZDDP + calcium sulfonate, a tribofilm was not observed on the surface of the piston ring (Figure 52A&B). However, the piston ring had not undergone large amounts of wear and there was no material transfer from the aluminium alloy to the ferrous piston ring (Figure 52A&B). Indeed, all machining marks on the surface of the piston ring were intact.

Lubricating the tribosystem with ZDDP + calcium sulfonate + NOCH did not impart adverse wear to the piston ring (Figure 52C&D). Once again, the surface of the ferrous substrate was relatively undamaged (Figure 52C&D), although a tribofilm was obtained in the case of the ZDDP + calcium sulfonate + NOCH piston ring. The protective layer appeared to resemble that observed on a silicon grain within the counterpart AluSil® substrate (Figure 44D).

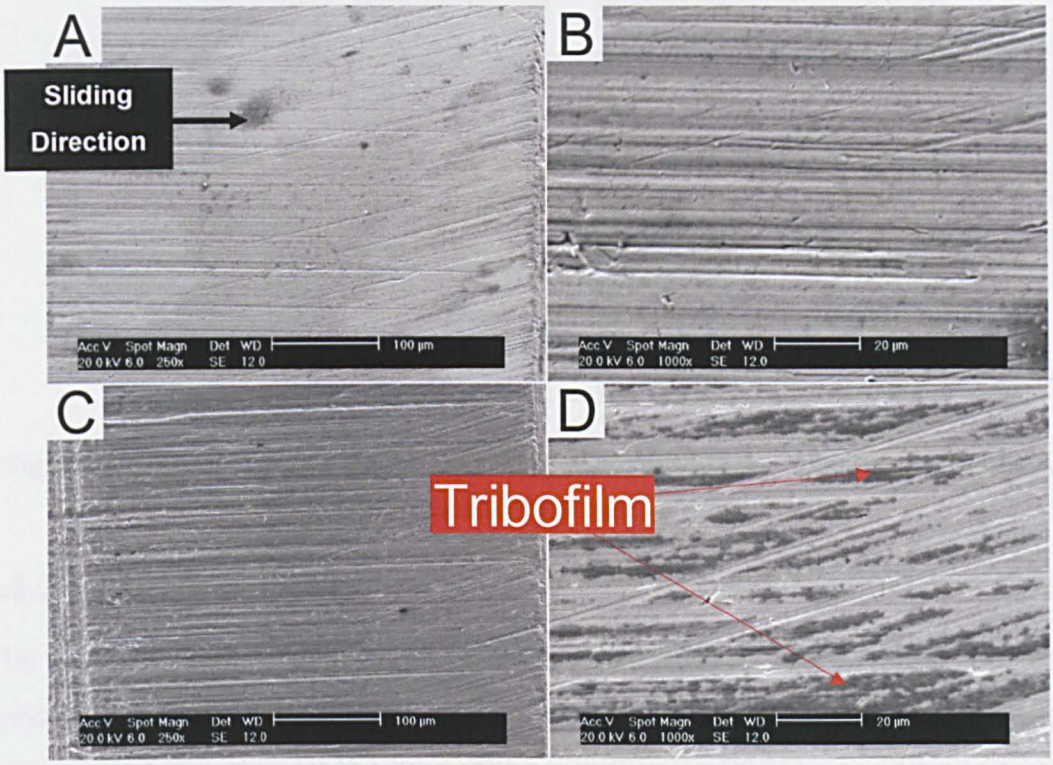

Figure 52: SEM image of a piston ring lubricated with ZDDP + calcium sulfonate (A&B) and ZDDP + calcium sulfonate + NOCH (C&D)

Minimal amounts of wear had occurred on piston ring substrates lubricated with ZDDP + calcium sulfonate and ZDDP + calcium sulfonate + NOCH, as shown in Figure 53. All machining marks on the piston ring were present and the surface resembled that of an unworn substrate (Figure 28C). A tribofilm was not obtained using atomic force microscopy with lubricant ZC or ZCN. This was accredited to the small measuring range of the AFM technique as protective layers were previously identified using scanning electron microscopy on these ferrous surfaces (Figure 52).

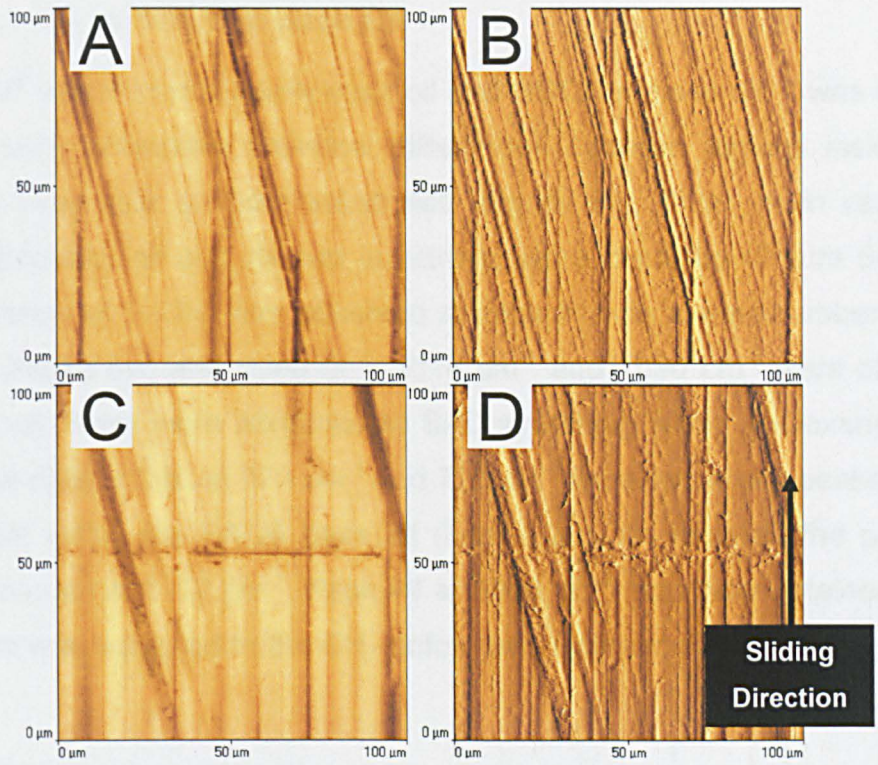

Figure 53: AFM image of a piston ring lubricated with ZDDP + calcium sulfonate (A&B) and ZDDP + calcium sulfonate + NOCH (C&D)

5.5.2. FTIR

The FTIR spectra shown herein are representative of worn AluSil® substrates; axes of transmittance as a function of wavenumber are displayed. Differences were identified between the lubricating oils (Figure 29&Figure 30) and the worn substrates; these were labelled and the peaks identified.

A number of peaks were obtained between 1485 cm^{-1} and 1740 cm^{-1} for the majority of spectra gathered from worn substrates; these were assumed to have derived from the base fluid. The observation of these peaks only on worn surfaces was accredited to the reduced quantity of oil under evaluation. This resulted in a decrease in the influence of the extremely large C-H deformation vibration band of various alkane groups within the hydrocarbon-based oil between ~ 1485 cm^{-1} and ~ 1320 cm^{-1} [224], as seen in Figure 29 & Figure 30. The C-H stretching vibration wavenumbers of the alkane groups within the base oil lay between ~ 3000 cm^{-1} and ~ 2860 cm^{-1} [224].

5.5.2.1. Base Oil vs NOCH in Base Oil

When AluSil® was lubricated with base oil and NOCH in base oil, it was evident that there were noticeable chemical differences between regions inside and outside the wear scar on both substrates (Figure 54). Three main variations between lubricating oil and the two substrates were identified (Figure 54). The rocking vibration of Si-CH_3 was observed at peak #1 with a wavenumber of 790 cm^{-1} [243]. Peaks two and three at ~ 1014 cm^{-1} and 1090 cm^{-1} were obtained using base oil; these were attributed to Si-O stretching within a siloxane chain [243]. To the right of this, at 873 cm^{-1} and 720 cm^{-1} were two sharp peaks; these were present within the PAO6 base oil (Figure 29). As too was the peak on NOCH in base oil at 1112 cm^{-1}. Peak #4 at 1260 cm^{-1} was only obtained using base oil; this was assigned to the CH_3 deformation vibration within Si-CH_3 [243].

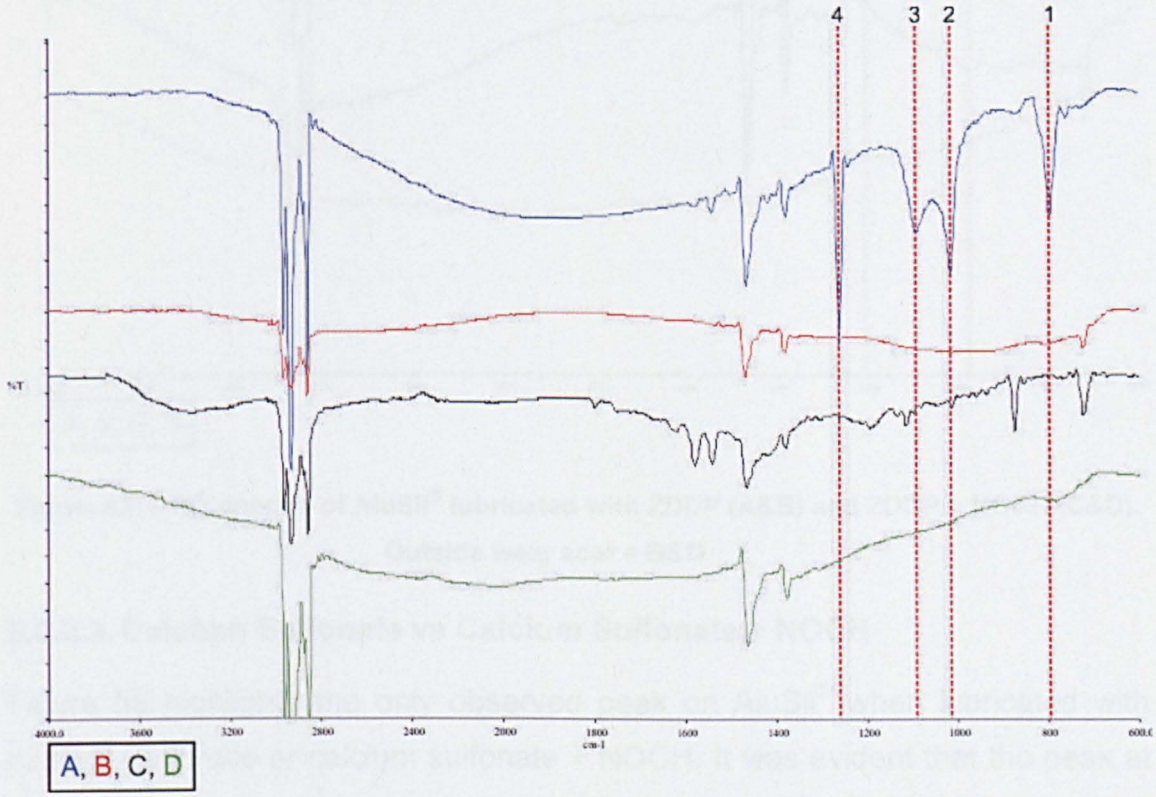

Figure 54: FTIR spectra of AluSil® lubricated with base oil (A&B) and NOCH in base oil (C&D). Outside wear scar = B&D

5.5.2.2. ZDDP vs ZDDP + NOCH

Peak #1 labelled in Figure 55 was obtained on AluSil® lubricated with ZDDP and ZDDP + NOCH; this was observed exclusively within the wear scar of both substrates at 975 cm^{-1} and was identified as stretching of the P-O-C group within the zinc dialkyldithiophosphate molecule [127, 229, 230]. Unlike the P-O-C band, the second peak observed was not found in ZDDP or ZDDP + NOCH

lubricating oils prior to test (Figure 30), nor was it witnessed outside the wear scar (Figure 55B&D). This small, but sharp, peak had a wavenumber of 1205 cm^{-1} and was attributed to either PO_2 stretching [231]. Sharp peaks at 873 cm^{-1} and 1017 cm^{-1} were derived from the base oil (Figure 29). The P-O-P stretching vibration observed between 893 cm^{-1} and 952 cm^{-1} [127] was not identified on either substrate.

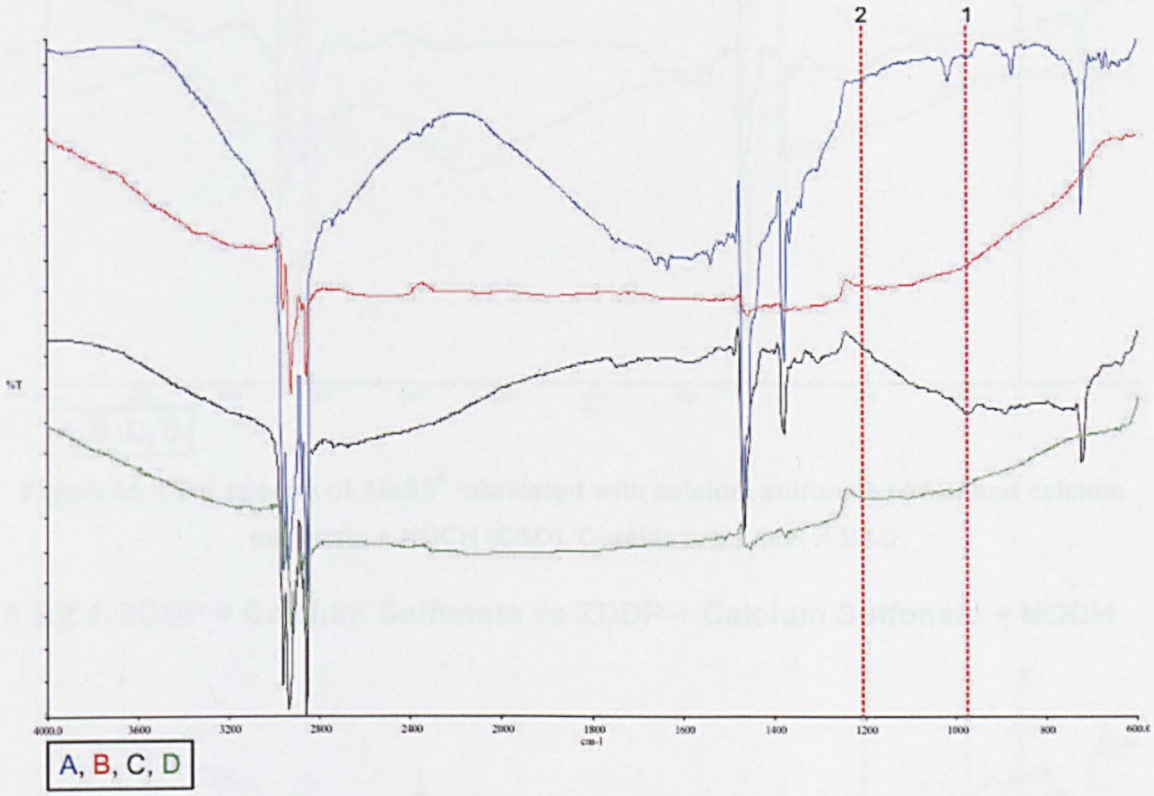

Figure 55: FTIR spectra of AluSil® lubricated with ZDDP (A&B) and ZDDP + NOCH (C&D). Outside wear scar = B&D

5.5.2.3. Calcium Sulfonate vs Calcium Sulfonate + NOCH

Figure 56 highlights the only observed peak on AluSil® when lubricated with calcium sulfonate or calcium sulfonate + NOCH. It was evident that the peak at ~ 858 cm^{-1} was only present within the wear region on the aluminium alloy. This wavenumber was assigned to calcium carbonate [227, 228, 244]. The intensity of the peak implies that the quantity present on the substrate may well be greater on the calcium sulfonate sample, compared to calcium sulfonate + NOCH. The peak at 873 cm^{-1} was derived from PAO6 base oil (Figure 29).

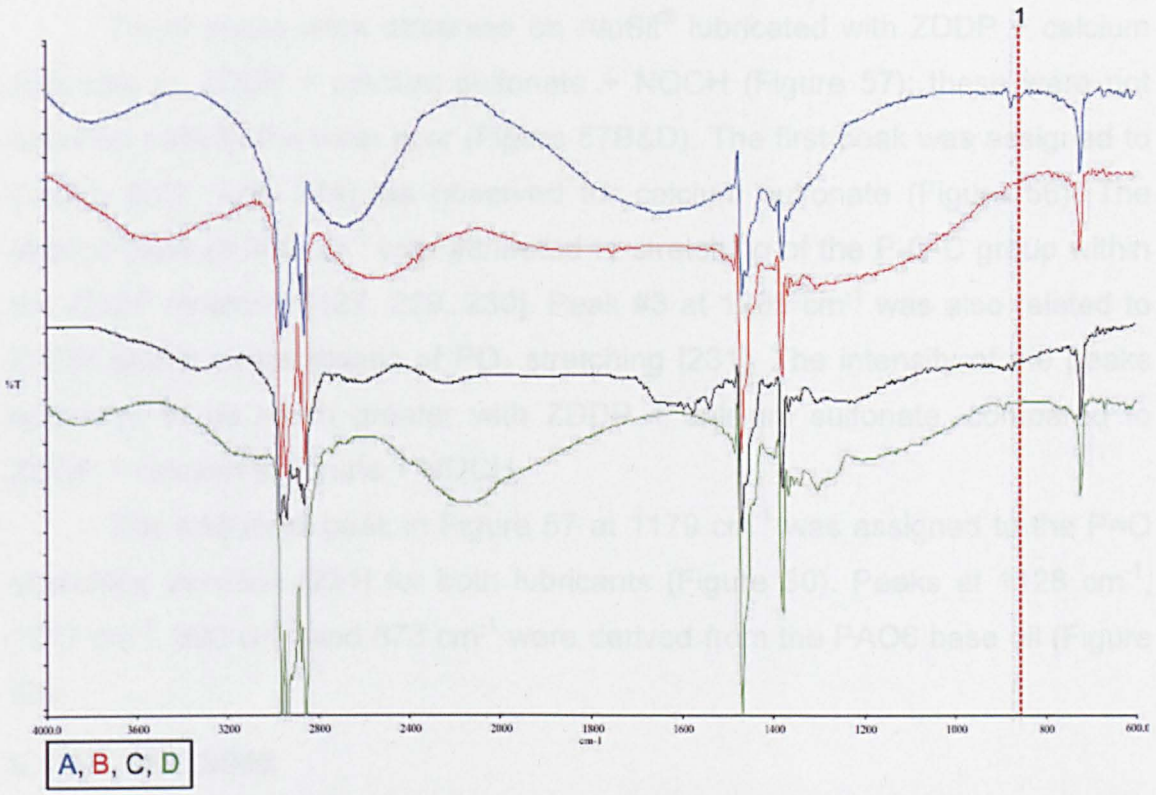

Figure 56: FTIR spectra of AluSil® lubricated with calcium sulfonate (A&B) and calcium sulfonate + NOCH (C&D). Outside wear scar = B&D

5.5.2.4. ZDDP + Calcium Sulfonate vs ZDDP + Calcium Sulfonate + NOCH

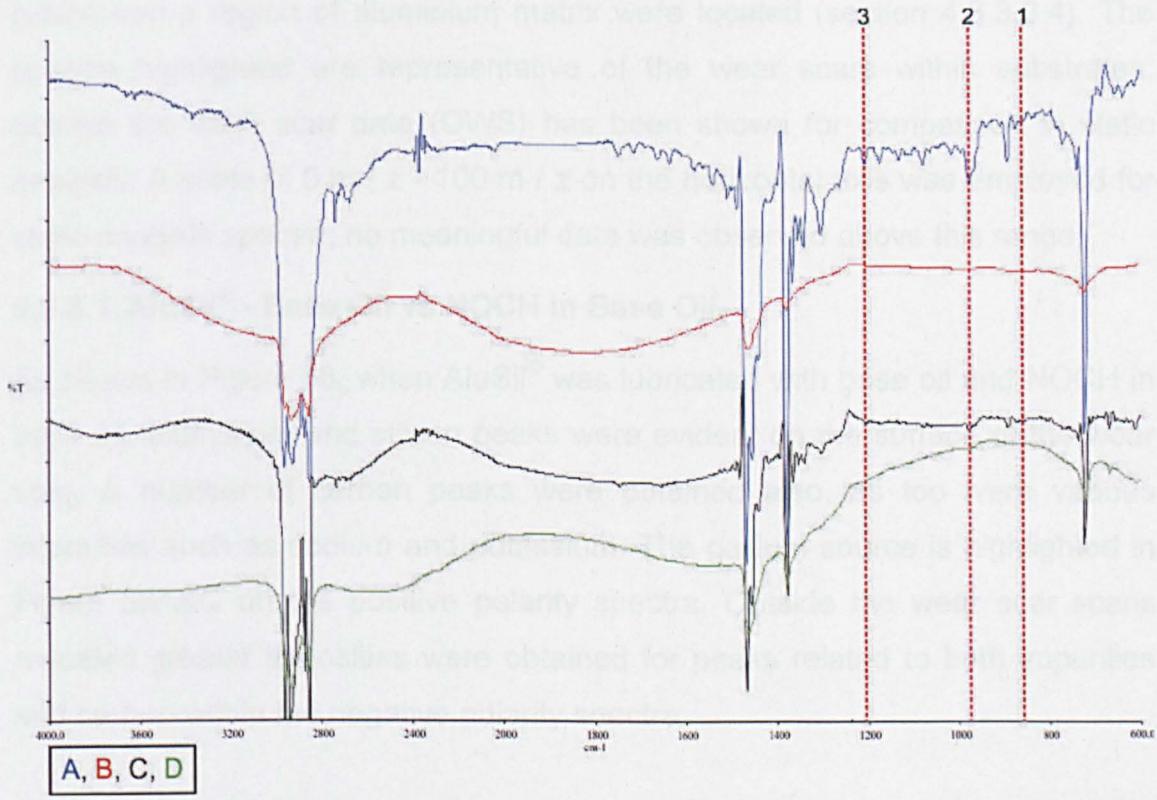

Figure 57: FTIR spectra of AluSil® lubricated with ZDDP + calcium sulfonate (A&B) and ZDDP + calcium sulfonate + NOCH (C&D). Outside wear scar = B&D

Three peaks were observed on AluSil® lubricated with ZDDP + calcium sulfonate or ZDDP + calcium sulfonate + NOCH (Figure 57); these were not obtained outside the wear scar (Figure 57B&D). The first peak was assigned to $CaCO_3$ [227, 228, 244], as observed for calcium sulfonate (Figure 56). The second peak at 975 cm^{-1} was attributed to stretching of the P-O-C group within the ZDDP molecule [127, 229, 230]. Peak #3 at 1205 cm^{-1} was also related to ZDDP and is characteristic of PO_2 stretching [231]. The intensity of the peaks appeared to be much greater with ZDDP + calcium sulfonate, compared to ZDDP + calcium sulfonate + NOCH.

The additional peak in Figure 57 at 1179 cm^{-1} was assigned to the P=O stretching vibration [231] for both lubricants (Figure 30). Peaks at 1128 cm^{-1}, 1077 cm^{-1}, 890 cm^{-1} and 873 cm^{-1} were derived from the PAO6 base oil (Figure 29).

5.5.3. Mini SIMS

In this section, SIMS static and depth profiles of AluSil® and piston ring substrates lubricated with test oils are reported. Data was acquired from within Region A in Figure 32 and was typically obtained from areas in which 2-3 silicon grains and a region of aluminium matrix were located (section 4.3.3.3.4). The spectra highlighted are representative of the wear scars within substrates; outside the wear scar data (OWS) has been shown for comparison in static analysis. A scale of 0 m / z - 100 m / z on the horizontal axis was employed for static analysis spectra; no meaningful data was observed above this range.

5.5.3.1. AluSil® - Base Oil vs NOCH in Base Oil

As shown in Figure 58, when AluSil® was lubricated with base oil and NOCH in base oil, aluminium and silicon peaks were evident on the surface of the wear scar. A number of carbon peaks were obtained also, as too were various impurities such as sodium and potassium. The gallium source is highlighted in Figure 58A&C on the positive polarity spectra. Outside the wear scar scans revealed greater intensities were obtained for peaks related to both impurities and carbon within the negative polarity spectra.

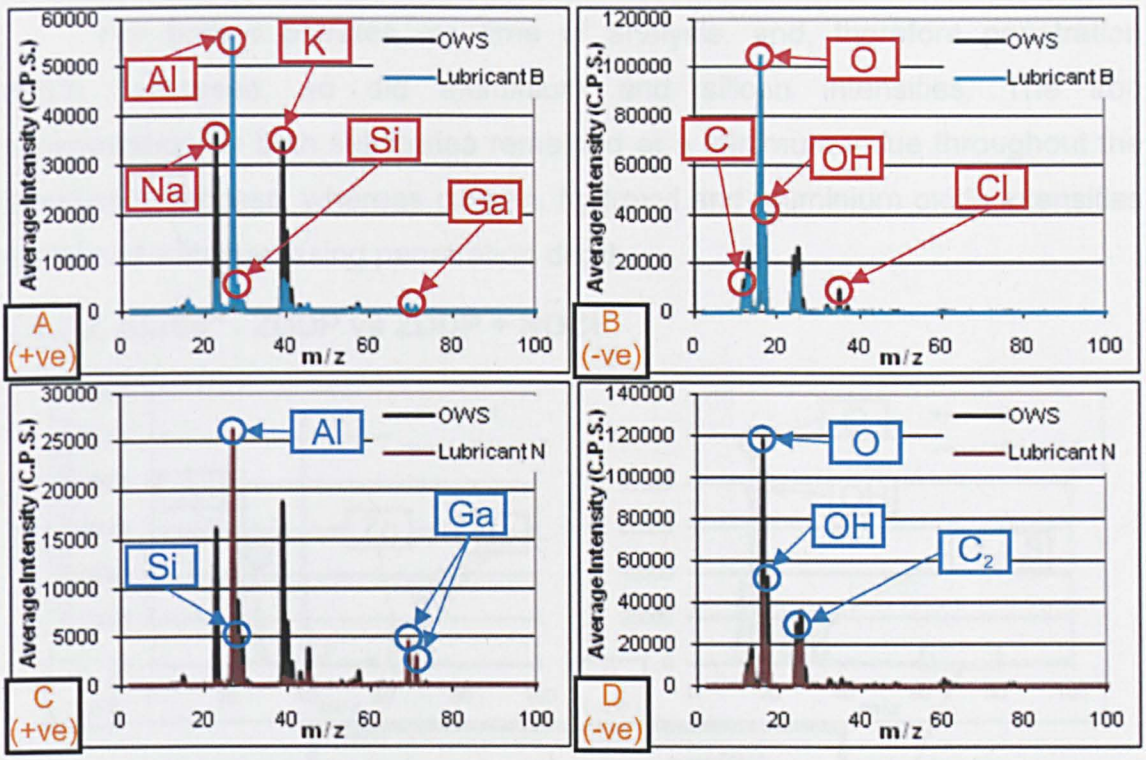

Figure 58: Static mini SIMS spectra of AluSil® lubricated with base oil (A&B) and NOCH in base oil (C&D)

Depth profiles for AluSil® lubricated with base oil and NOCH in base oil are shown in Figure 59.

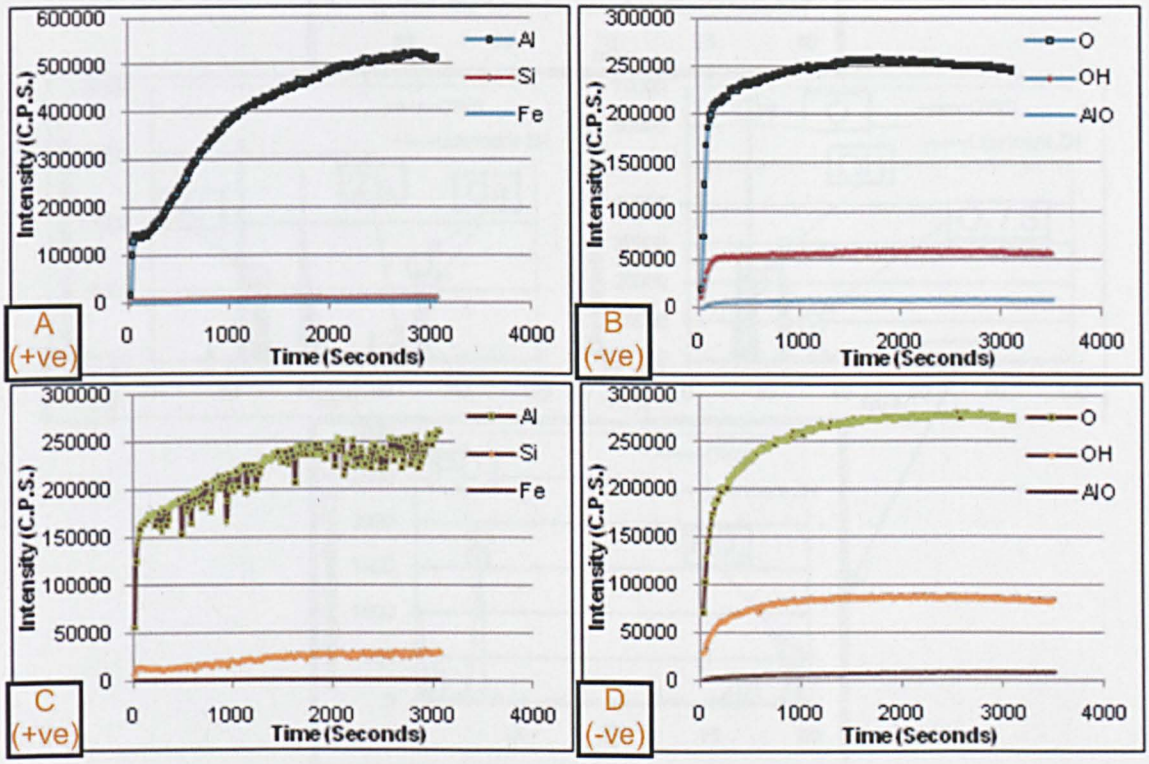

Figure 59: Mini SIMS depth profiles of AluSil® lubricated with base oil (A&B) and NOCH in base oil (C&D)

For both substrates, as time of analysis, and, therefore penetration depth, increased, so did aluminium and silicon intensities. The iron concentration on both substrates remained at a minimum value throughout the destructive process, whereas oxygen, hydroxyl and aluminium oxide intensities enhanced with increasing penetration depth.

5.5.3.2. AluSil® - ZDDP vs ZDDP + NOCH

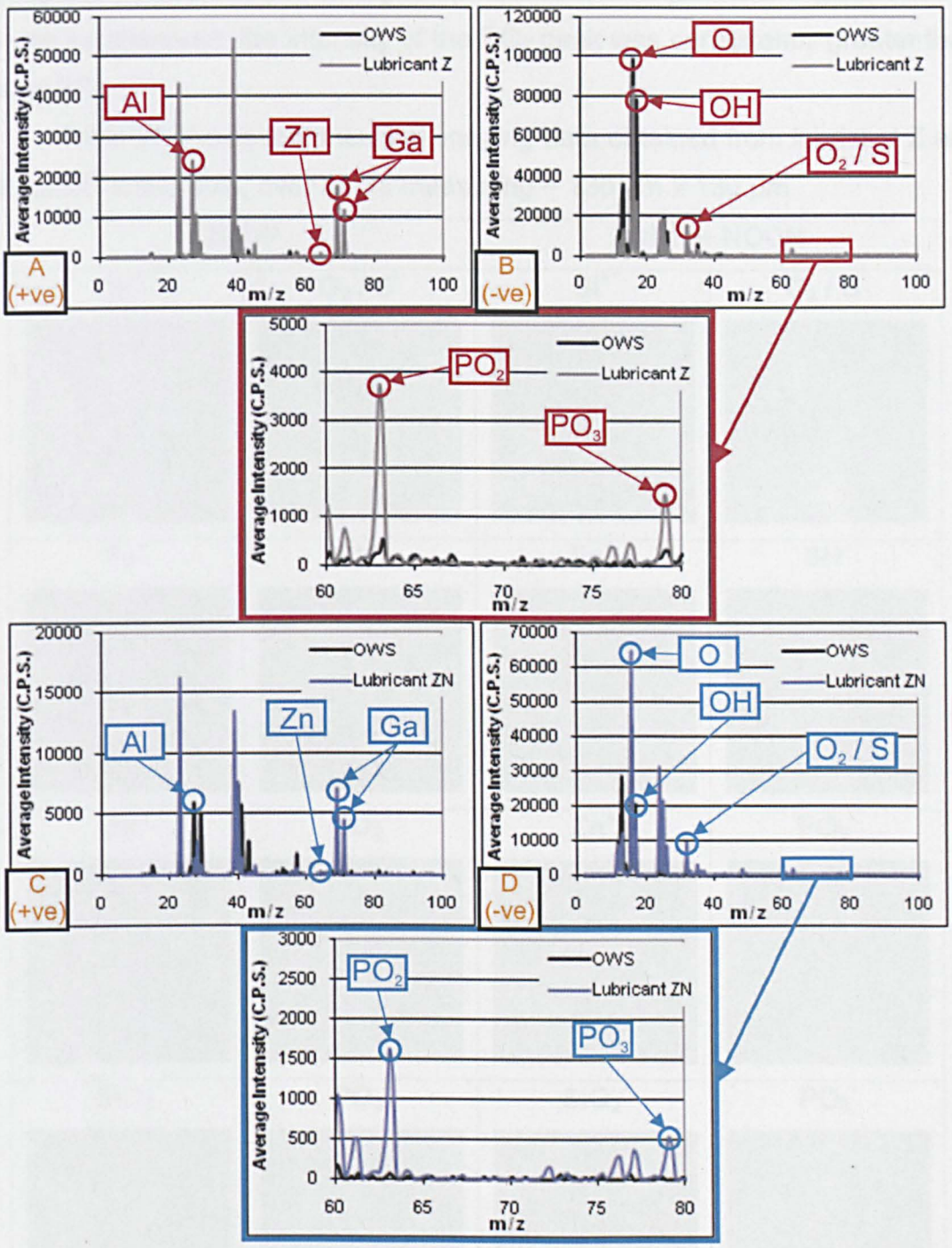

Figure 60: Static mini SIMS spectra of AluSil® lubricated with ZDDP (A&B) and ZDDP + NOCH (C&D)

When AluSil® was lubricated with ZDDP and ZDDP + NOCH, zinc peaks were evident at low intensity on the positive spectra at 64 m / z (Figure 60A&C). For the negative spectra, the O_2 / S peak (32 m / z) enlarged considerably compared to that observed for either base oil or NOCH in base oil (Figure 60B&D). PO_2 and PO_3 were evident on both AluSil® substrates at 63 m / z and 79 m /z. However, these were not observed outside the wear scar and are highlighted in detail in the enlarged spectra shown adjacent to Figure 60B&D. As can be observed, the intensity of the PO_2 peak was consistently greater than that of PO_3.

Table 22 shows the chemical imaging data obtained from lubricant Z and ZN AluSil® substrates, over areas measuring ~ 130 µm x 130 µm.

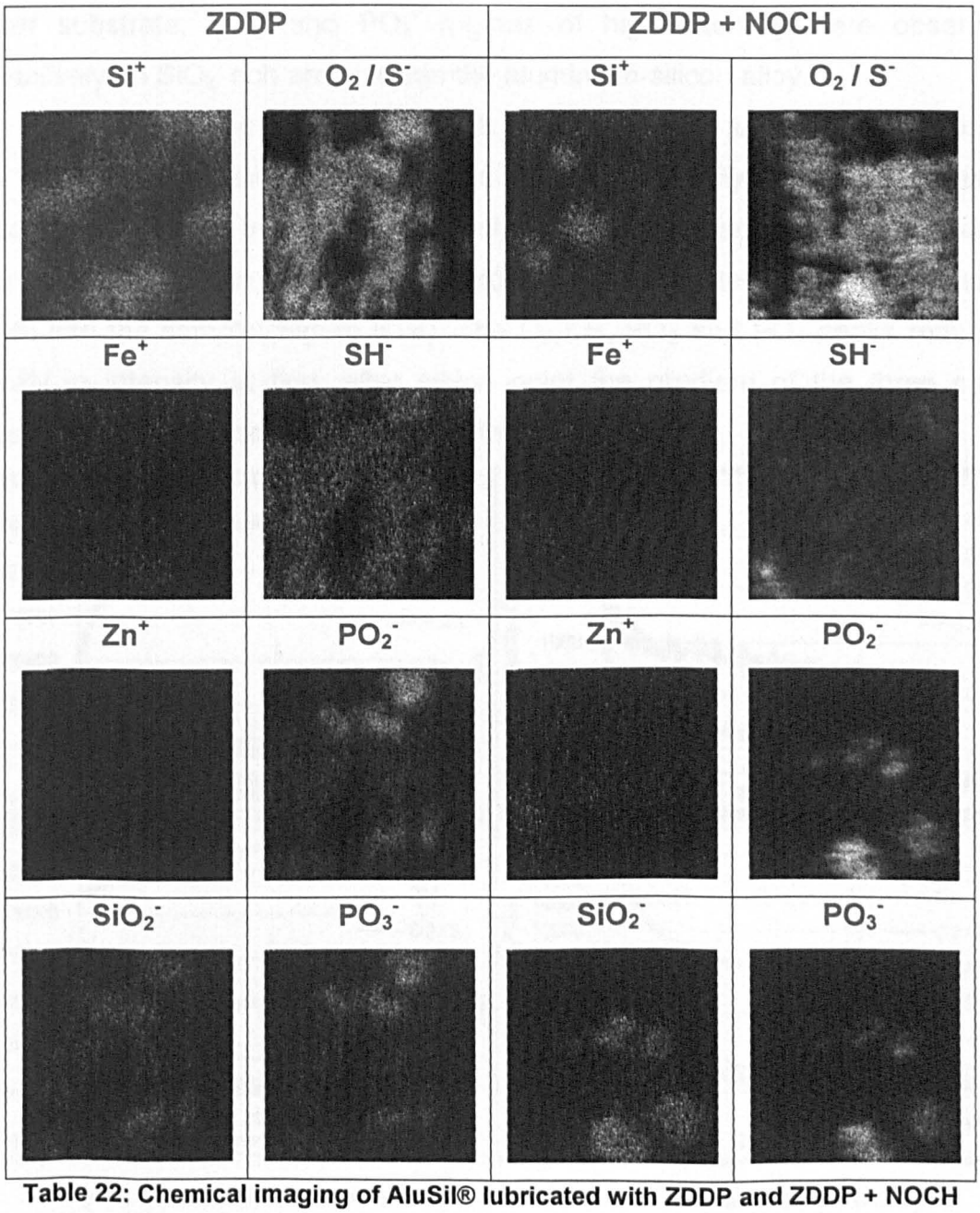

Table 22: Chemical imaging of AluSil® lubricated with ZDDP and ZDDP + NOCH

In this technique, the greater the brightness of an area within an image, the greater the intensity of the stated chemical in that region. The location of these high intensity areas can be compared against other images obtained using the same polarity of secondary ions shown in Table 22.

When AluSil® was lubricated with ZDDP, both Fe^+ and Zn^+ were found on and around Si^+ rich regions; in the case of ZDDP + NOCH, the areas rich in Si^+ matched up very well with the chemical images of Fe^+ and Zn^+. Comparison of SiO_2^-, O_2^- / S^- and SH^- images indicated that these compounds were present over both aluminium and silicon rich regions within the ZDDP lubricated substrate; an enhanced intensity of O_2^- / S^- was observed on a silicon grain using SiO_2^- as a reference when ZDDP + NOCH was the lubricating fluid. On either substrate, PO_2^- and PO_3^- regions of high intensity were observed exclusively on SiO_2^- rich areas within the aluminium-silicon alloy.

With increasing penetration depth on the substrate lubricated with ZDDP, the intensity of the zinc and iron peaks decreased rapidly, whilst those peaks associated with the base material, such as aluminium and silicon, increased (Figure 61A). Oxygen and hydroxyl also increased in intensity with increasing depth into the sample (Figure 61B). The O_2 / S, PO_2 and PO_3 peaks reduced rapidly in intensity at first, after which point the gradient of the three plots reduced and the concentrations began to level off.

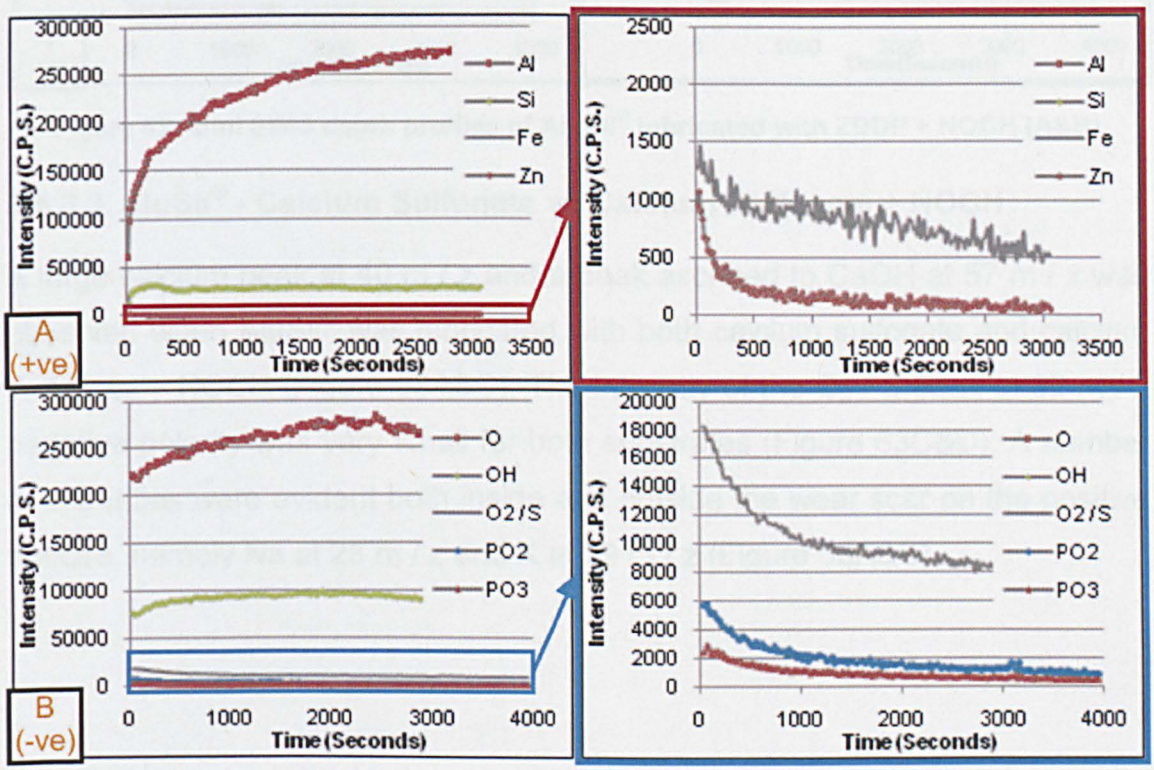

Figure 61: Mini SIMS depth profiles of AluSil® lubricated with ZDDP (A&B)

Depth profiling of AluSil® lubricated with ZDDP + NOCH revealed an abrupt reduction in the intensity of zinc and iron peaks with increasing penetration depth (Figure 62A). Marked enlargement in Al, Si, O and OH concentrations occurred with increasing time duration (Figure 62A&B). PO_2 and PO_3 peaks at first increased to a maximum intensity, then gradually decreased; the former, however, was always of greater concentration. The O_2 / S peak also increased to a maximum intensity, before reducing rapidly with increasing depth of penetration.

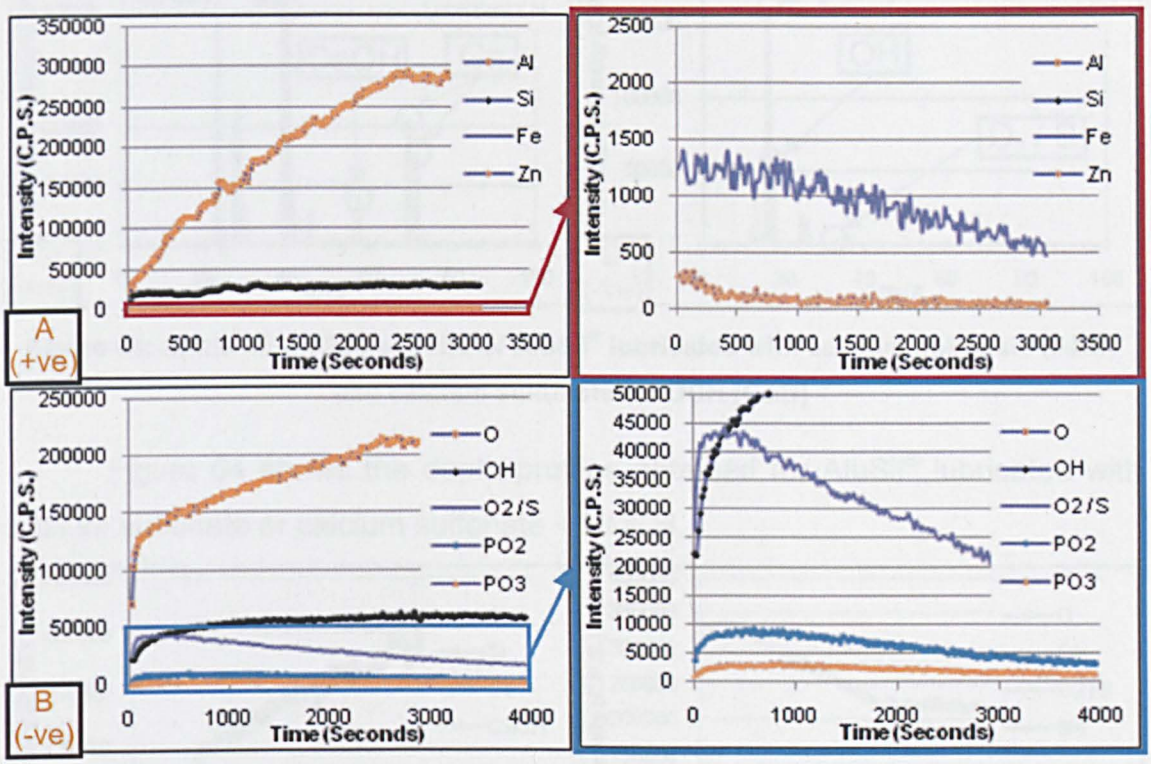

Figure 62: Mini SIMS depth profiles of AluSil® lubricated with ZDDP + NOCH (A&B)

5.5.3.3. AluSil® - Calcium Sulfonate vs Calcium Sulfonate + NOCH

A large calcium peak at 40 m / z and a peak ascribed to CaOH at 57 m / z was observed when AluSil® was lubricated with both calcium sulfonate and calcium sulfonate + NOCH (Figure 63A&C). The intensity of the O_2 / S peak at 32 m / z negative polarity was very small for both substrates (Figure 63C&D). A number of impurities were evident both inside and outside the wear scar on the positive spectra, namely Na at 23 m / z and K at 39 m / z (Figure 63A&C).

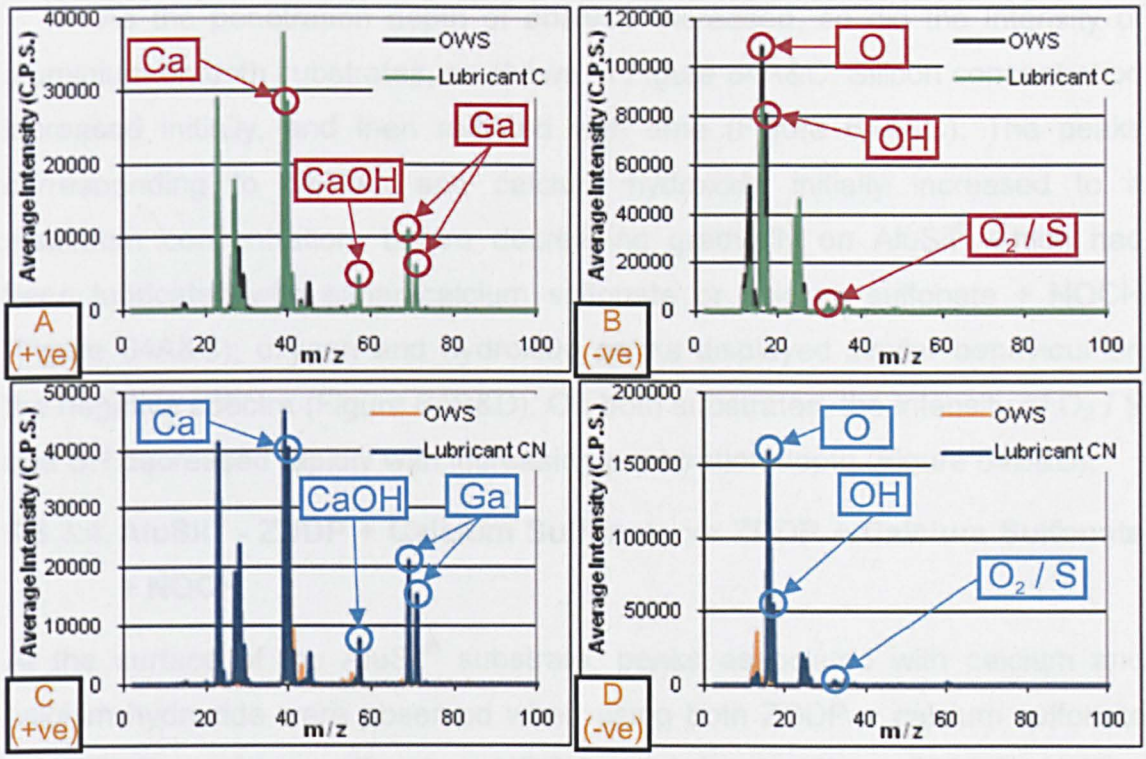

Figure 63: Static mini SIMS spectra of AluSil® lubricated with calcium sulfonate (A&B) and calcium sulfonate + NOCH (C&D)

Figure 64 shows the depth profiles obtained for AluSil® lubricated with calcium sulfonate or calcium sulfonate + NOCH.

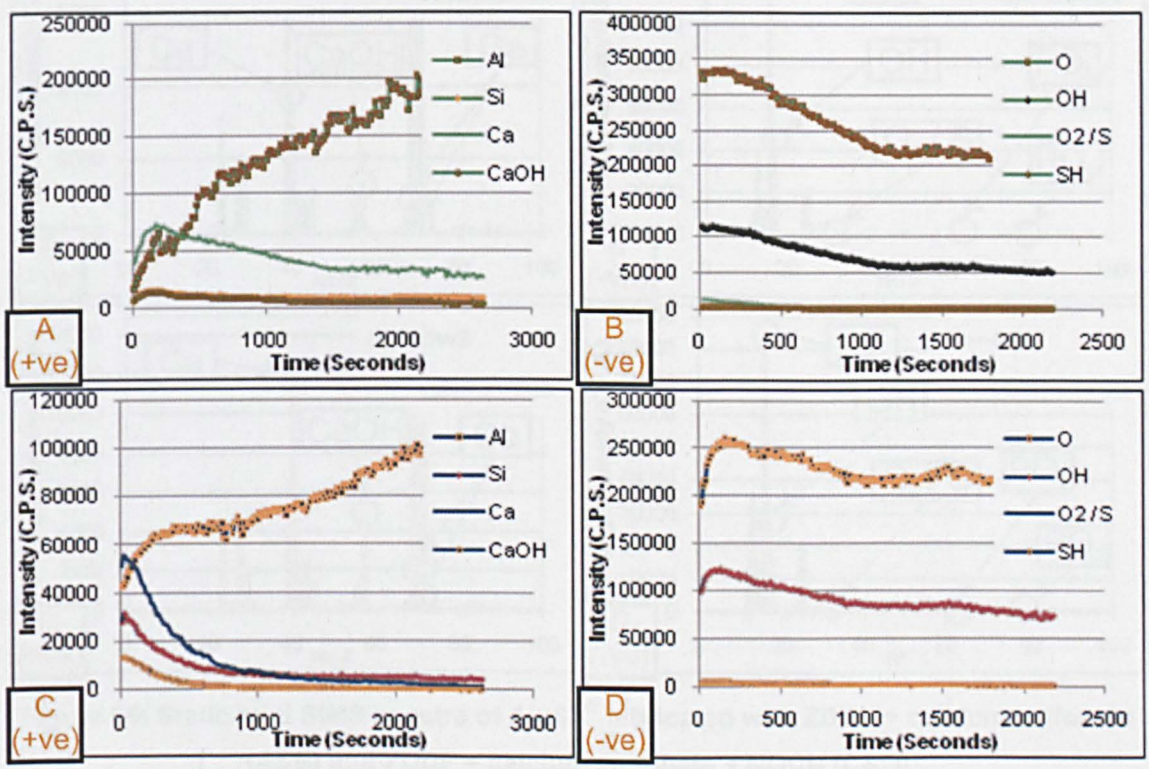

Figure 64: Mini SIMS depth profiles of AluSil® lubricated with calcium sulfonate (A&B) and calcium sulfonate + NOCH (C&D)

As the penetration depth of analysis increased, so did the intensity of aluminium on both substrates, as shown in Figure 64A&C. Silicon concentration increased initially, and then reduced with time (Figure 64A&C). The peaks corresponding to calcium and calcium hydroxide initially increased to a maximum concentration, before decreasing gradually on AluSil® which had been lubricated with either calcium sulfonate or calcium sulfonate + NOCH (Figure 64A&C); oxygen and hydroxide peaks displayed similar behaviour on the negative spectra (Figure 64B&D). On both substrates, the intensity of O_2 / S and SH decreased rapidly with increasing penetration depth (Figure 64B&D).

5.5.3.4. AluSil® - ZDDP + Calcium Sulfonate vs ZDDP + Calcium Sulfonate + NOCH

At the surface of the AluSil® substrate, peaks associated with calcium and calcium hydroxide were observed when using both ZDDP + calcium sulfonate and ZDDP + calcium sulfonate + NOCH as lubricants (Figure 65A&C). Neither zinc, nor phosphate peaks were identified at the surface of the substrate with either lubricant (Figure 65A&C).

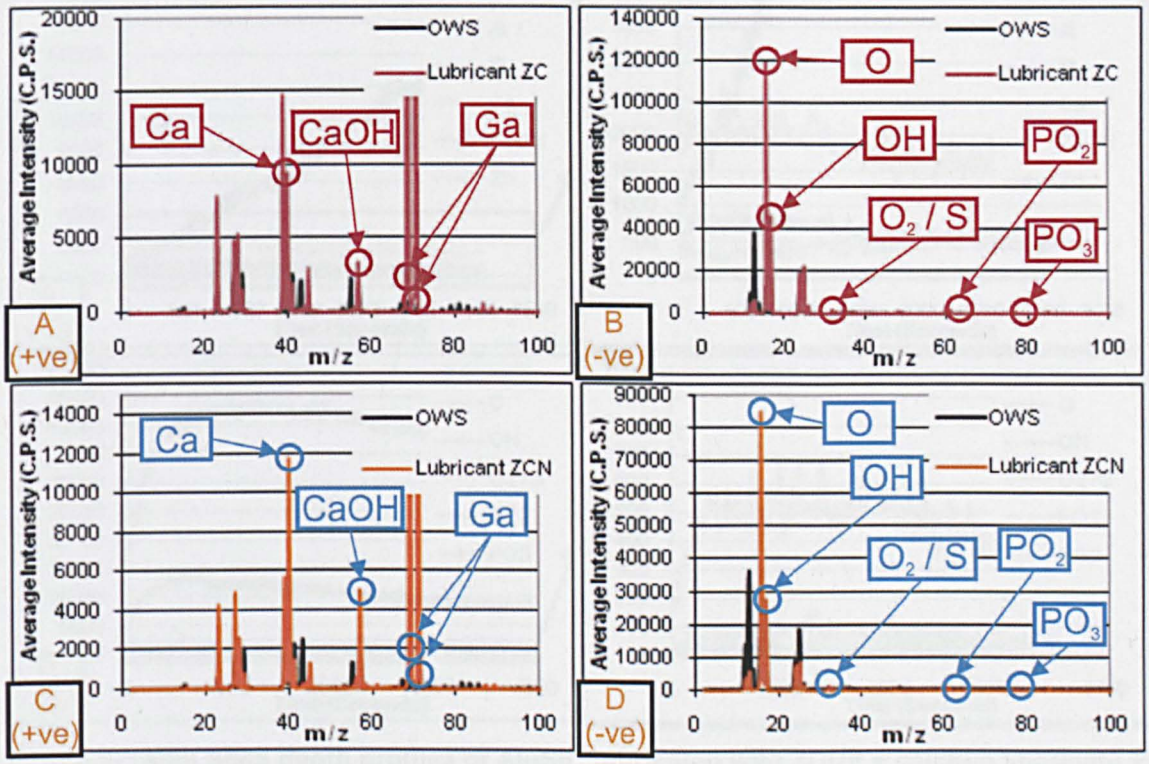

Figure 65: Static mini SIMS spectra of AluSil® lubricated with ZDDP + calcium sulfonate (A&B) and ZDDP + calcium sulfonate + NOCH (C&D)

Figure 66 and Figure 67 show the depth profiles obtained for AluSil® lubricated with ZC and ZCN, respectively.

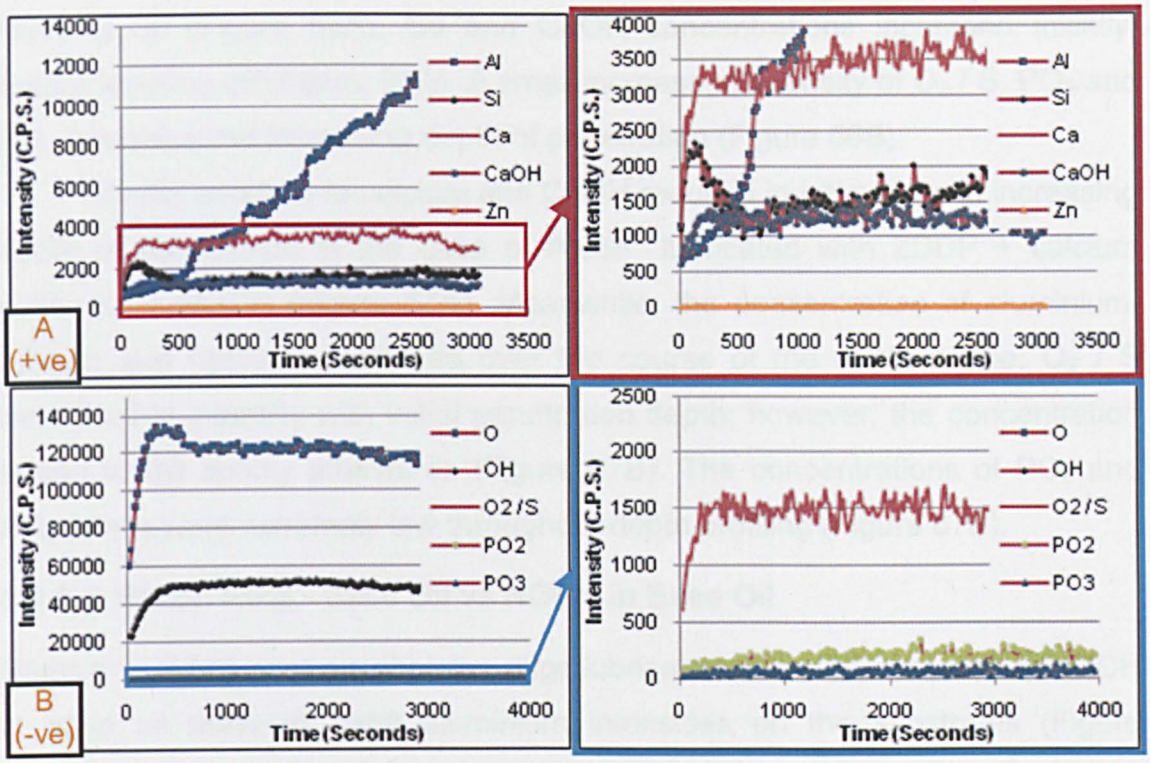

Figure 66: Mini SIMS depth profiles of AluSil® lubricated with ZDDP + calcium sulfonate (A&B)

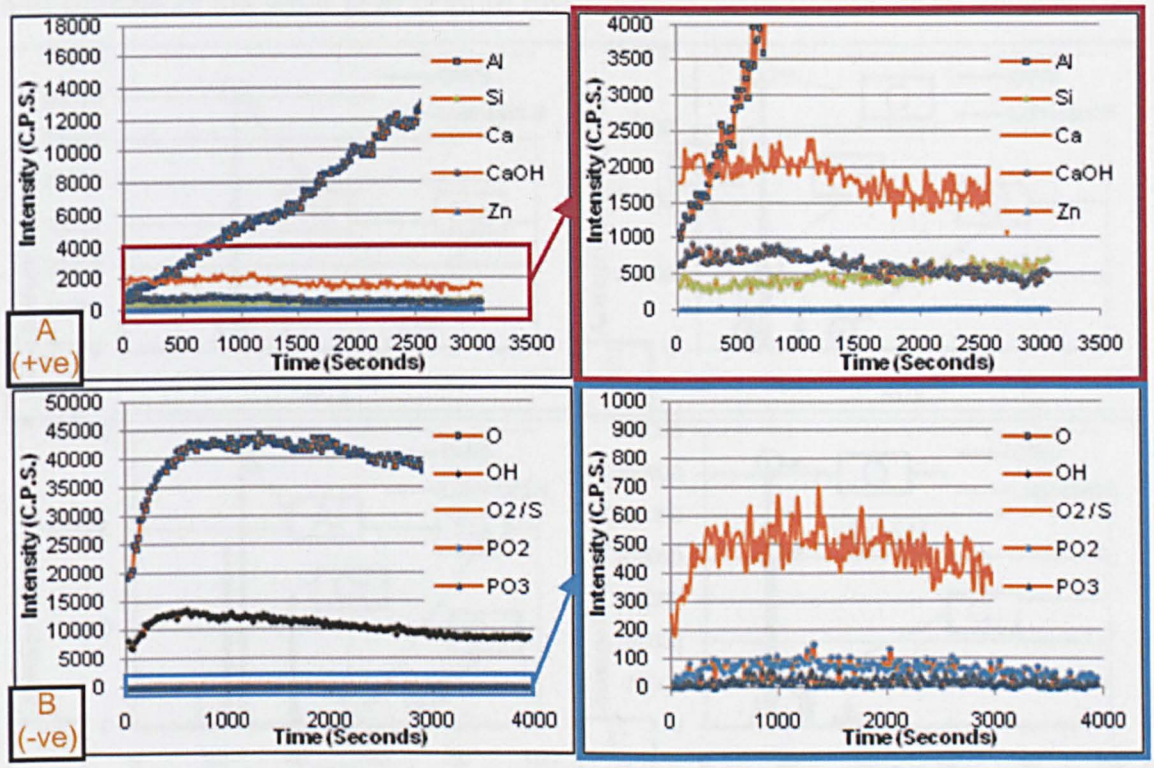

Figure 67: Mini SIMS depth profiles of AluSil® lubricated with ZDDP + calcium sulfonate + NOCH (A&B)

During depth analysis of AluSil® lubricated with ZDDP + calcium sulfonate, the intensities of oxygen, hydroxyl and aluminium increased (Figure 66A&B). The concentration of silicon initially increased, before decreasing and

levelling off (Figure 66A). Ca and CaOH concentrations increased initially, before levelling off (Figure 66A). A small increase in intensity of O_2 / S, PO_2 and PO_3 accompanied increasing depth of penetration (Figure 66B).

Peaks ascribed to calcium and CaOH reduced in intensity with increasing depth of penetration in the case of AluSil® lubricated with ZDDP + calcium sulfonate + NOCH (Figure 67A). Meanwhile, the concentration of aluminium, oxygen and hydroxyl increased over the course of the depth profile. O_2 / S increased in intensity with initial penetration depth; however, the concentration began to fall shortly afterwards (Figure 67B). The concentrations of PO_2 and PO_3 peaks were extremely low throughout depth profiling (Figure 67B).

5.5.3.5. Piston Ring - Base Oil vs NOCH in Base Oil

Static mini SIMS analysis of piston rings lubricated with either base oil or NOCH in base oil revealed large aluminium intensities on the substrates (Figure 68A&C). The chromium and iron base material of the piston ring was evident (Figure 68C), as too were a number of impurities such as chlorine, both inside and outside of the wear scar (Figure 68).

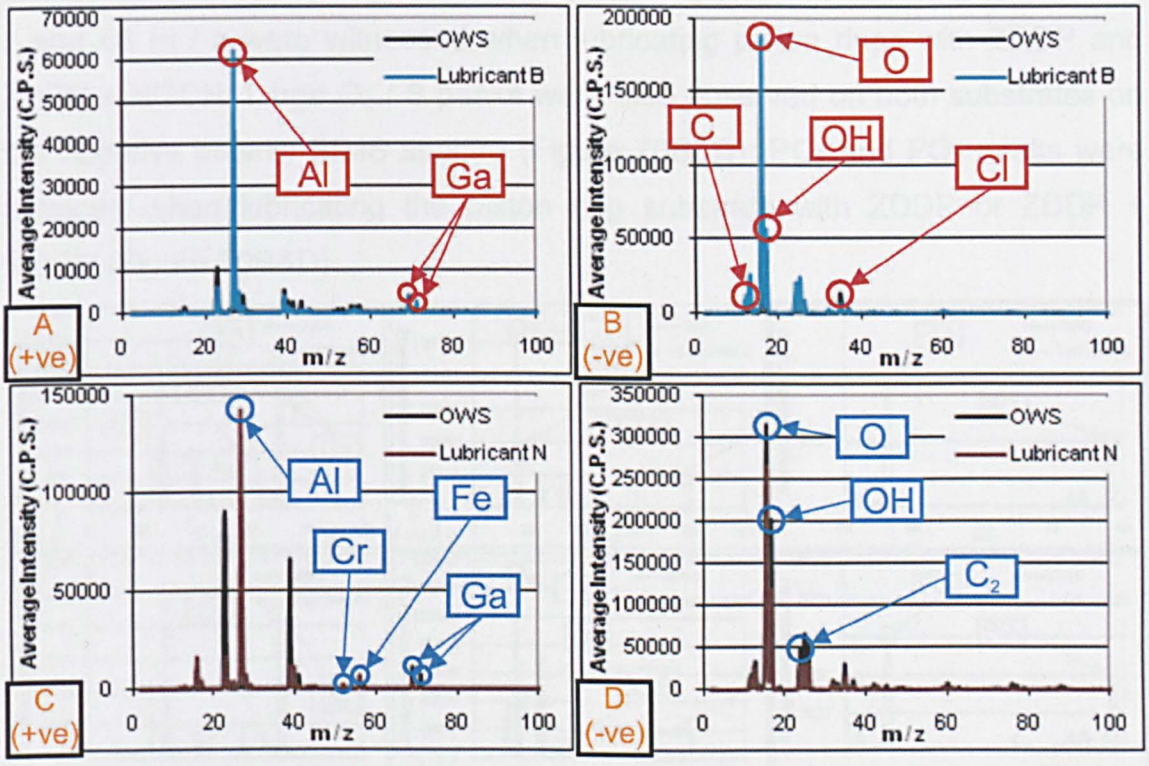

Figure 68: Static mini SIMS spectra of a piston ring lubricated with base oil (A&B) and NOCH in base oil (C&D)

With increasing penetration depth, the intensity of aluminium and silicon on the piston ring substrates decreased markedly (Figure 69A&C). Conversely,

the concentration of Fe and Cr increased as the time duration of dynamic mini SIMS analysis amplified. Oxygen, hydroxyl and AlO decreased with increasing depth of analysis (Figure 69B&D).

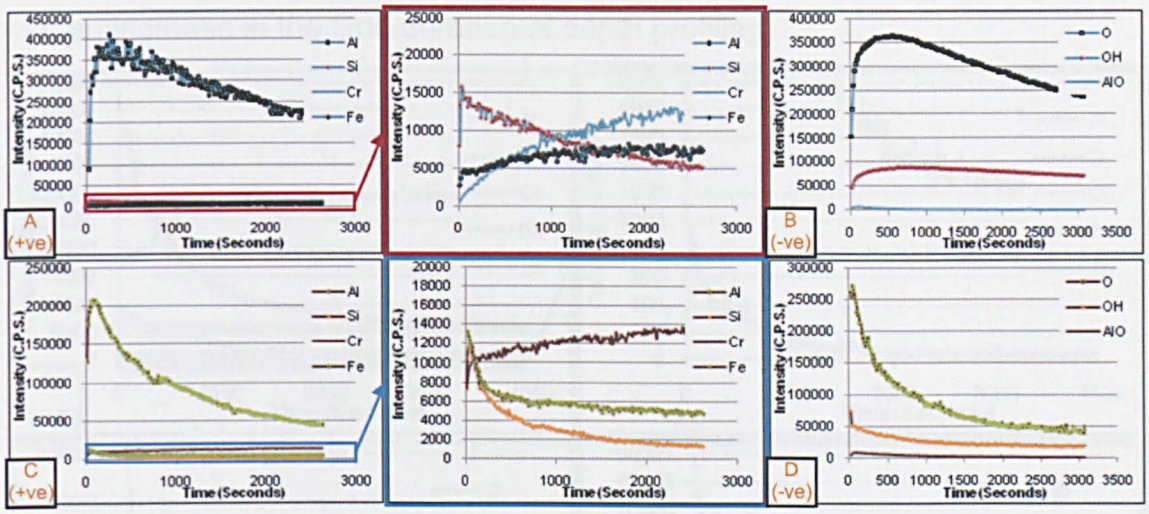

Figure 69: Mini SIMS depth profiles of a piston ring lubricated with base oil (A&B) and NOCH in base oil (C&D)

5.5.3.6. Piston Ring - ZDDP vs ZDDP + NOCH

As can be observed in Figure 70A&C, two strong intensity zinc peaks at 64 m / z and 66 m / z were witnessed when lubricating piston rings with ZDDP and ZDDP + NOCH. Large O_2 / S peaks were also observed on both substrates on the negative polarity SIMS spectra (Figure 70B&D). PO_2 and PO_3 peaks were obtained when lubricating the piston ring substrate with ZDDP or ZDDP + NOCH (Figure 70B&D).

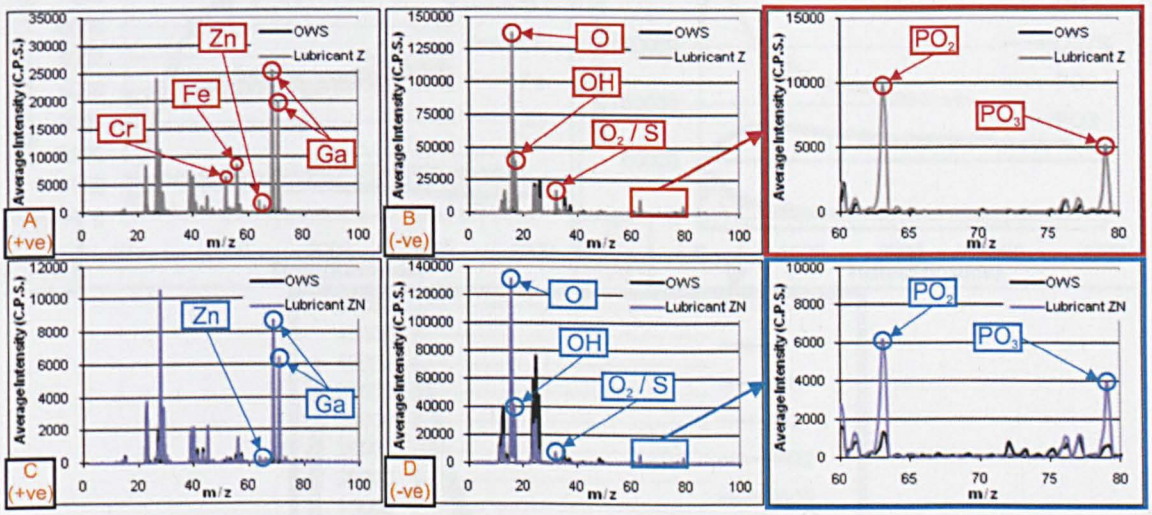

Figure 70: Static mini SIMS spectra of a piston ring lubricated with ZDDP (A&B) and ZDDP + NOCH (C&D)

Depth profiling of the ZDDP sample revealed a sudden decrease in both aluminium and silicon intensities as the distance from the surface of the

substrate increased (Figure 71A). Whilst iron concentration also decreased quite rapidly as penetration depth enlarged, the intensity of chromium increased, however. The concentration of Zn^{64}, O_2 / S, PO_2 and PO_3 reduced with an increase in the time duration of depth profiling.

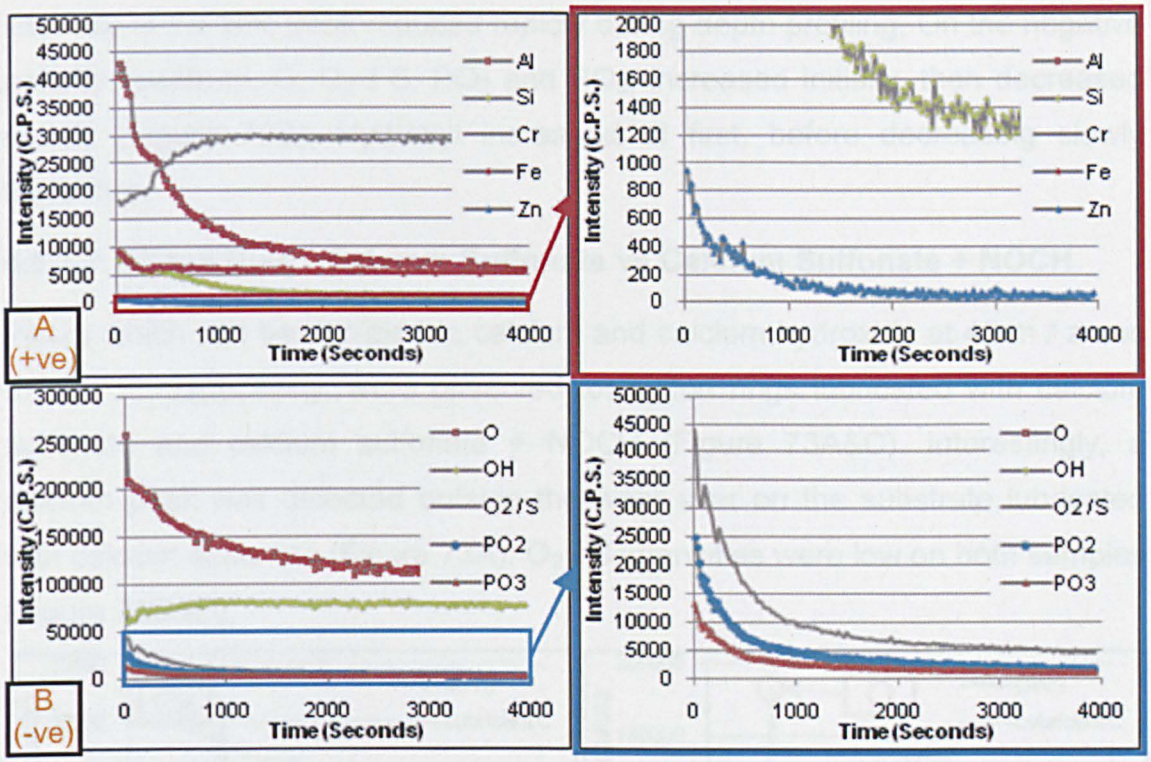

Figure 71: Mini SIMS depth profiles of a piston ring lubricated with ZDDP (A&B)

Figure 72 shows the depth profile for the lubricant ZN piston ring.

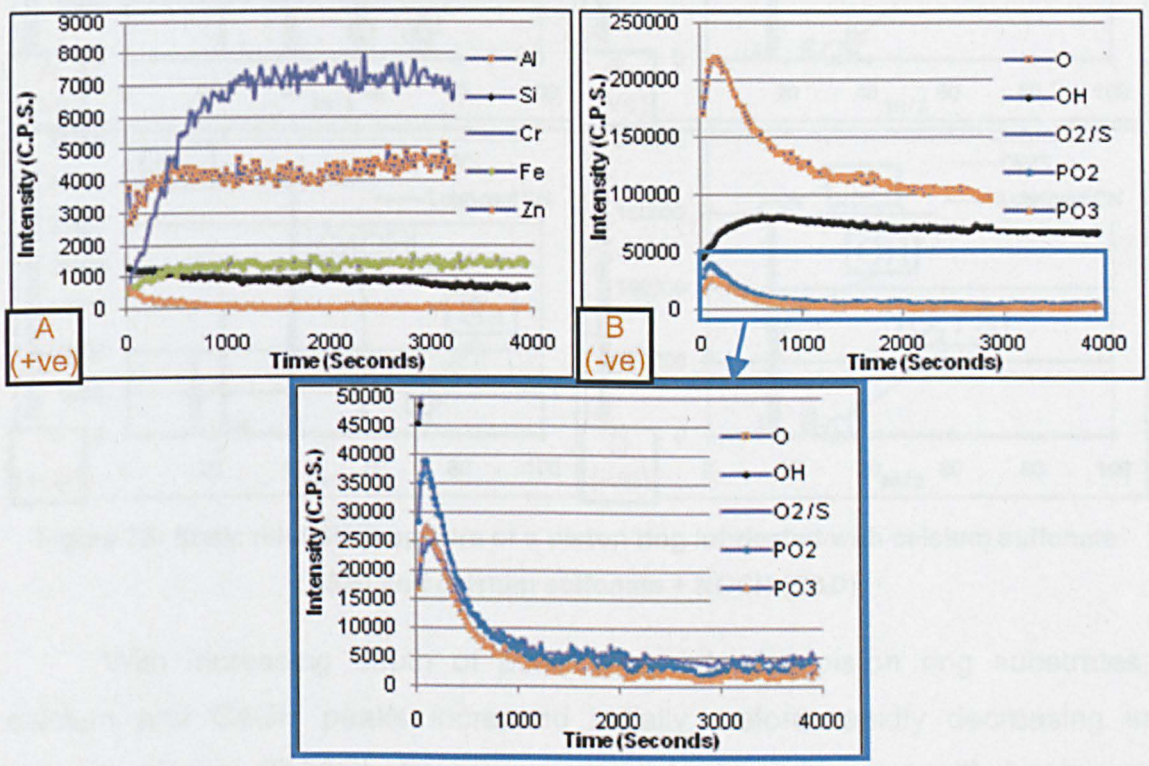

Figure 72: Mini SIMS depth profiles of a piston ring lubricated with ZDDP + NOCH (A&B)

As the depth of penetration into the ZDDP + NOCH substrate increased, a reduction in silicon concentration was observed (Figure 72A). Aluminium, chromium and iron intensities enhanced with increasing depth; the chromium concentration was the greatest recorded in the positive polarity spectrum. The intensity of the zinc peak reduced rapidly during depth profiling. On the negative polarity spectrum, O, O_2 / S, PO_2 and PO_3, increased initially, then decreased rapidly (Figure 72B). Hydroxyl increased at first, before decreasing slowly thereafter.

5.5.3.7. Piston Ring - Calcium Sulfonate vs Calcium Sulfonate + NOCH

Peaks which can be ascribed to calcium and calcium hydroxide at 40 m / z and 57 m / z, respectively, were observed for piston rings lubricated with calcium sulfonate and calcium sulfonate + NOCH (Figure 73A&C). Interestingly, a calcium peak was detected outside the wear scar on the substrate lubricated with calcium sulfonate (Figure 73A). O_2 / S intensities were low on both samples (Figure 73B&D).

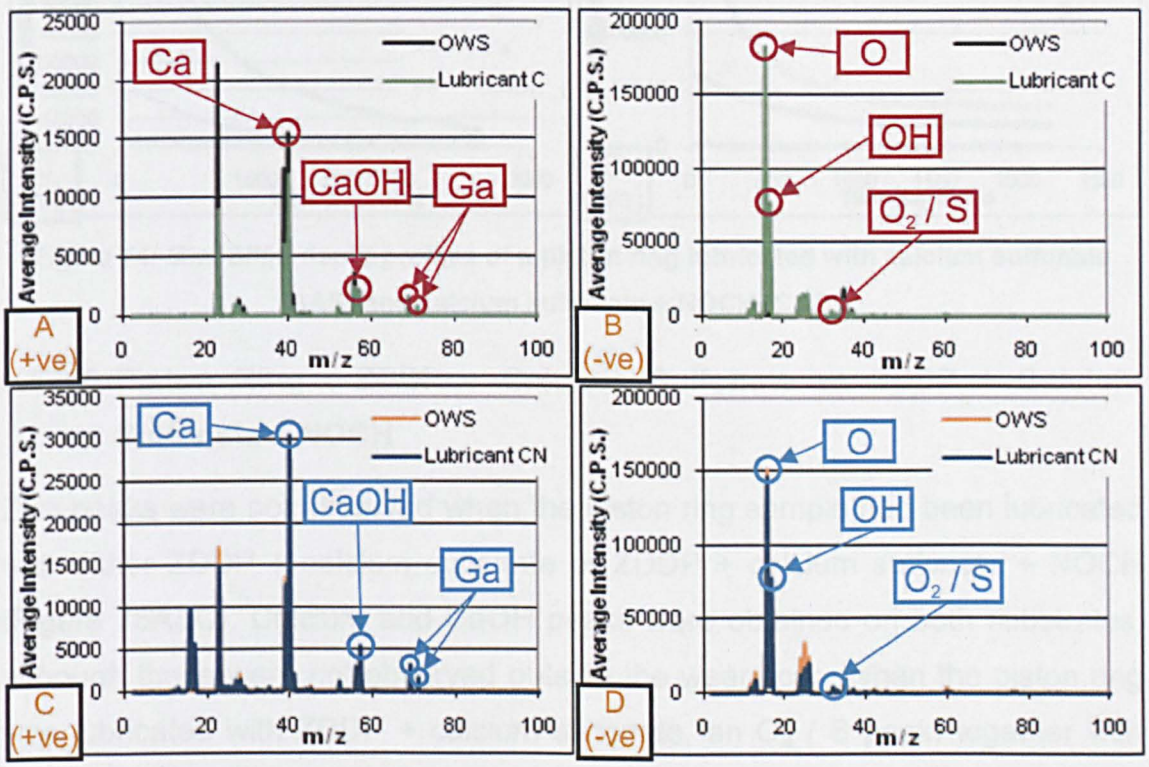

Figure 73: Static mini SIMS spectra of a piston ring lubricated with calcium sulfonate (A&B) and calcium sulfonate + NOCH (C&D)

With increasing depth of penetration into the piston ring substrates, calcium and CaOH peaks increased initially, before rapidly decreasing in intensity (Figure 74A&C). Chromium concentration increased with increasing

depth of analysis on both substrates, whilst iron, aluminium and silicon intensities decreased rapidly for both samples as the time duration of the depth profiling process increased (Figure 74A&C). Oxygen and hydroxyl concentrations, along with O_2 / S and SH, decreased as the penetration depth increased on both the calcium sulfonate and calcium sulfonate + NOCH piston ring substrates (Figure 74B&D).

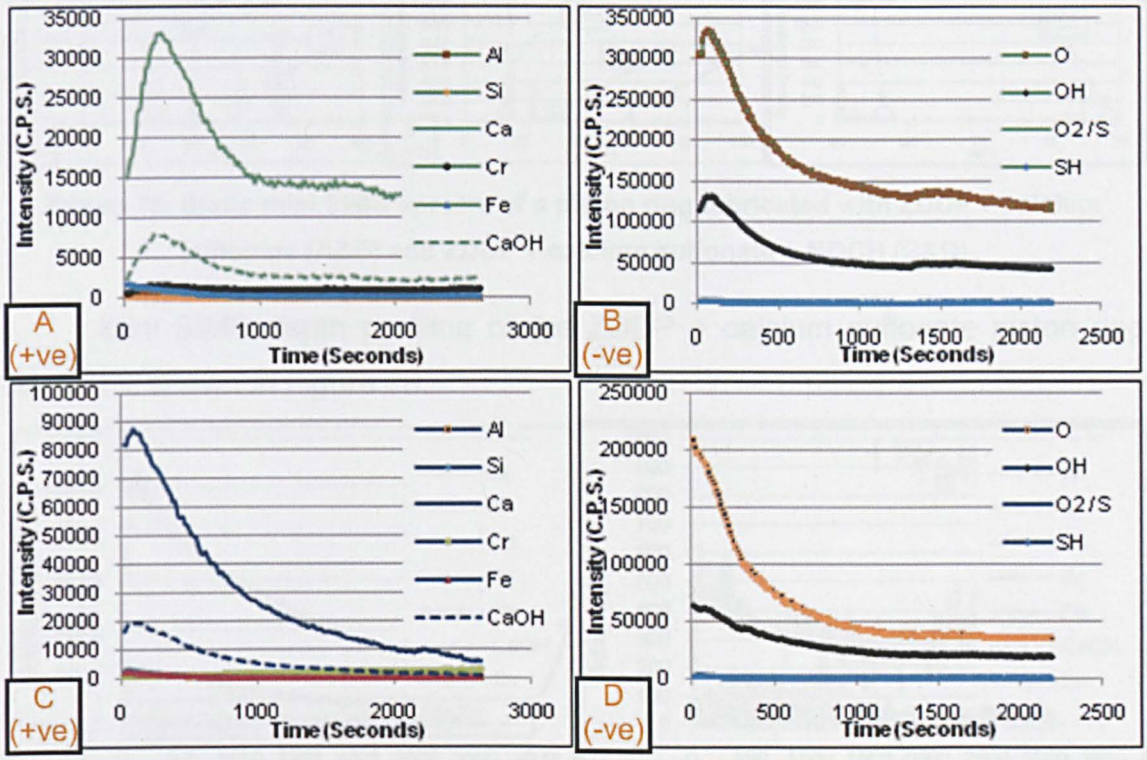

Figure 74: Mini SIMS depth profiles of a piston ring lubricated with calcium sulfonate (A&B) and calcium sulfonate + NOCH (C&D)

5.5.3.8. Piston Ring - ZDDP + Calcium Sulfonate vs ZDDP + Calcium Sulfonate + NOCH

Zinc peaks were not observed when the piston ring sample had been lubricated with either ZDDP + calcium sulfonate or ZDDP + calcium sulfonate + NOCH (Figure 75A&C). Calcium and CaOH peaks were obtained on both substrates, although these were not observed outside the wear scar. When the piston ring was lubricated with ZDDP + calcium sulfonate, an O_2 / S peak, together with two strong intensity PO_2 and PO_3 peaks, were observed inside the wear scar on the substrate (Figure 75B). However, in stark contrast, the piston ring lubricated with ZDDP + calcium sulfonate + NOCH possessed only a small intensity O_2 / S peak; phosphate peaks were not observed (Figure 75D).

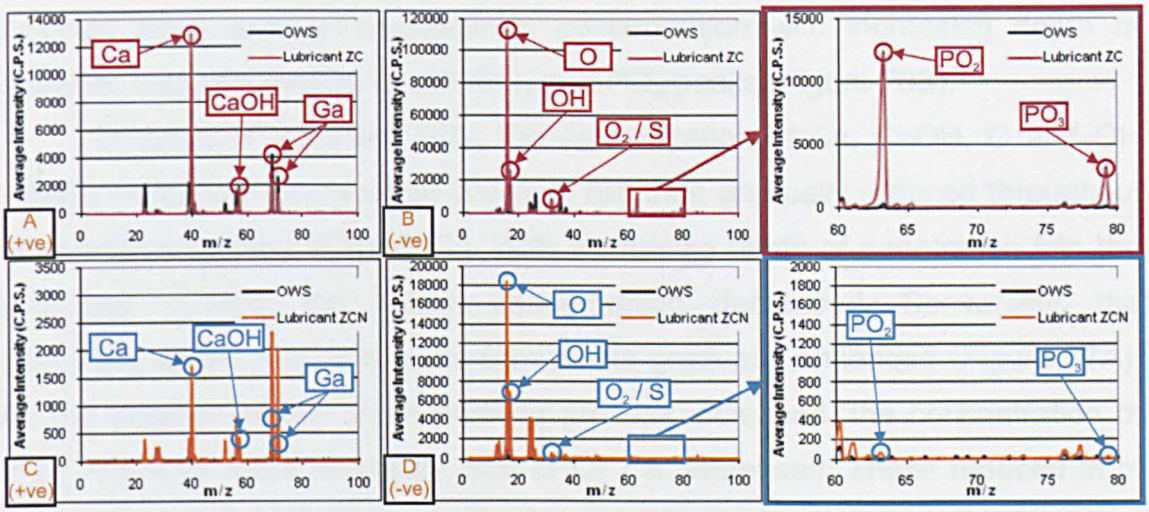

Figure 75: Static mini SIMS spectra of a piston ring lubricated with ZDDP + calcium sulfonate (A&B) and ZDDP + calcium sulfonate + NOCH (C&D)

Mini SIMS depth profiling of the ZDDP + calcium sulfonate piston ring sample is shown in Figure 76.

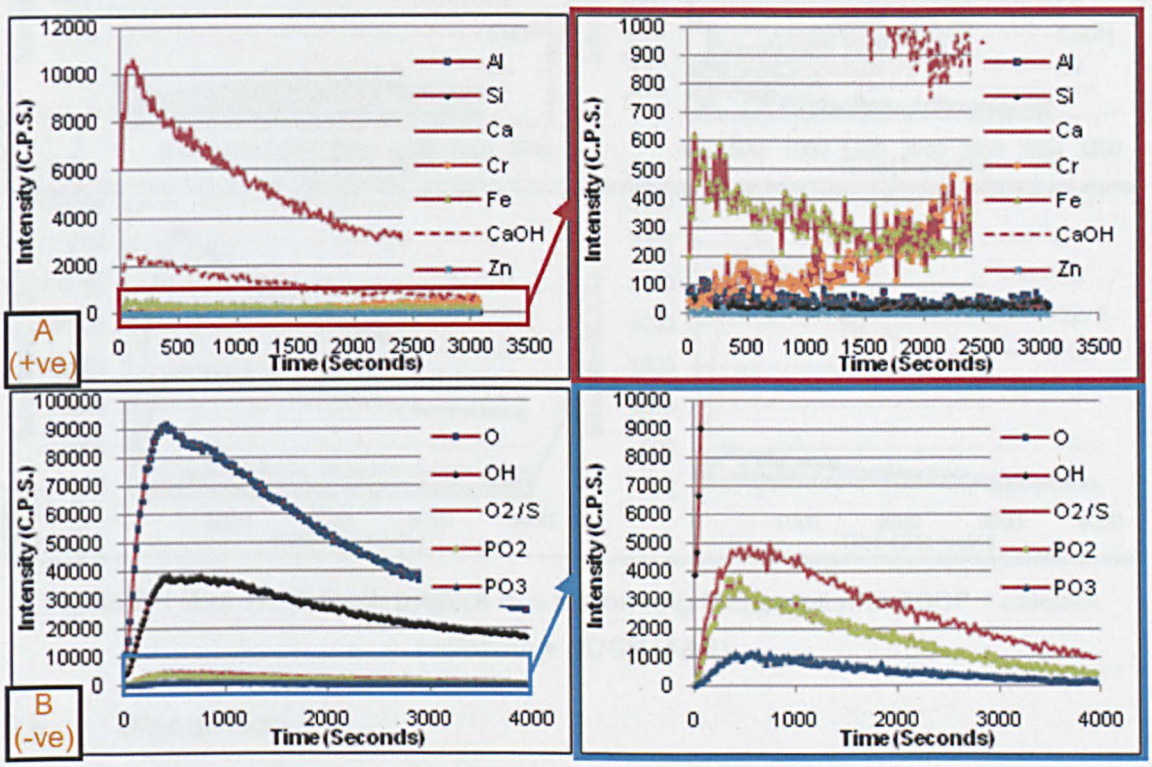

Figure 76: Mini SIMS depth profiles of a piston ring lubricated with ZDDP + calcium sulfonate (A&B)

Calcium and calcium hydroxide intensity initially increased, which subsequently reduced with increasing depth of penetration (Figure 76A). An increase in chromium concentration with duration of analysis was observed. The intensities of iron, aluminium and silicon reduced with increasing penetration depth (Figure 76A). Initial increases in oxygen and hydroxyl,

followed by a gradual decrease in concentration with increasing depth of analysis, was mirrored by O_2 / S, PO_2 and PO_3 peaks (Figure 76B).

In terms of lubricant ZCN, the concentration of Ca, CaOH, O and OH initially increased during depth profiling, but then gradually reduced throughout the analysis process (Figure 77). With increasing depth of penetration into the substrate surface, the silicon concentration decreased. Conversely, the intensities of the iron and aluminium peaks gradually enhanced (Figure 77A). As the duration of the depth profiling process increased, the concentration of PO_2, PO_3 and, more markedly, that of O_2 / S, increased. These reduced from their maximum values as the depth of penetration increased (Figure 77B).

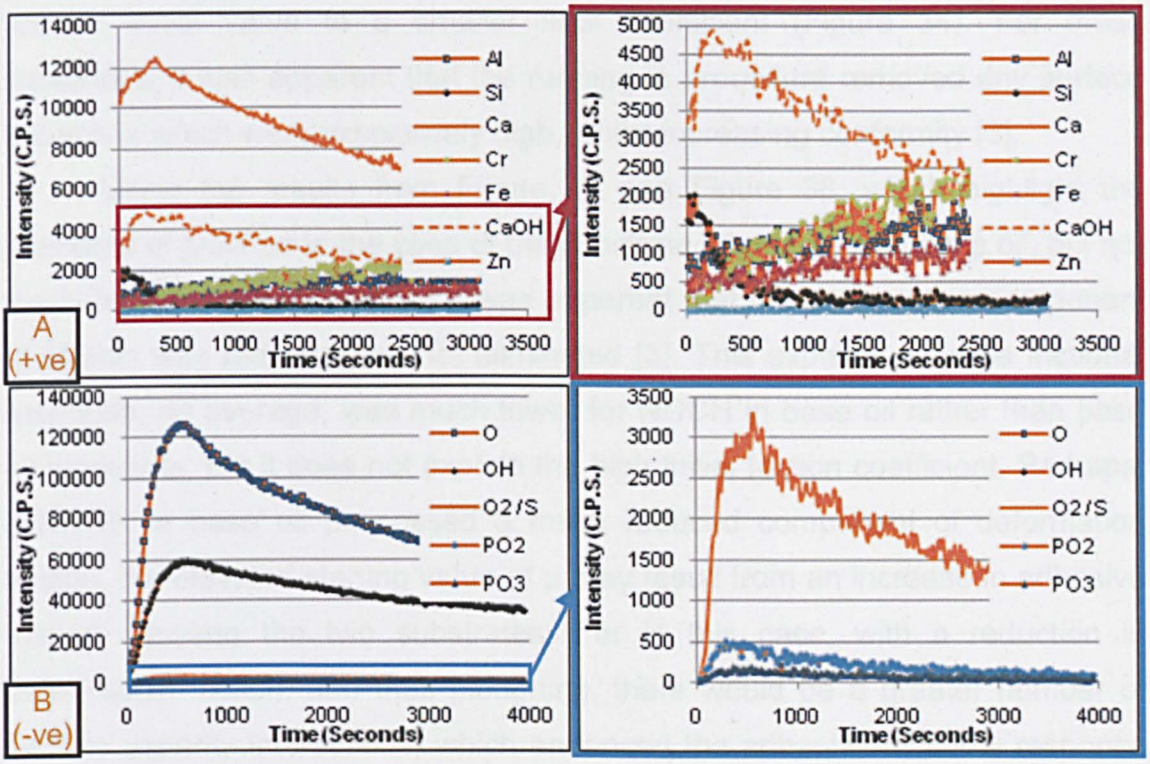

Figure 77: Mini SIMS depth profiles of a piston ring lubricated with ZDDP + calcium sulfonate + NOCH (A&B)

5.6. Discussion

5.6.1. Friction Coefficients and Electrical Contact Voltage

5.6.1.1. Frictional Response

As discussed in section 2.1.1, the frictional response of a tribosystem is influenced by both adhesion and deformation [2, 3]. The frictional response exhibited by base oil, unlike the other test lubricants listed in Table 18, increased initially, before levelling off at a high value of μ. It is most likely, since there is no additive in the base oil to protect the substrates, that the physically

harder piston ring was ploughing the softer aluminium-silicon substrate; thereby increasing the deformation component of friction [3]. This process continued until the two surfaces became conformal and running in of the interface occurred [3] after some 15 minutes. The erratic behaviour exhibited by the friction trace can be accredited to the removal of wear debris from the interface, which reduced the adhesive frictional component [3]. Ensuing formation and entrainment of wear debris into the contact subsequently increased both components of the frictional force [3].

In direct contrast to base oil, the running-in process experienced when using the other seven lubricants had the effect of reducing friction, from a greater initial value to a smaller final coefficient (Figure 34). For these substrates, it was apparent that the running in procedure removed any surface asperities which were excessively high, whilst increasing conformity [3].

Using the results from Figure 37 and Figure 38, which highlight the presence of grooves in the case of the substrate lubricated with base oil, but not the NOCH in base oil sample, it was apparent that the deformation component of friction was reduced, but not eliminated [3]. This explains why the frictional response, on average, was much lower for NOCH in base oil rather than base oil lubricants, but it does not explain the high initial friction coefficient. Perhaps, if NOCH in base oil possessed a much reduced component of deformation friction, the elevated starting value of μ may result from an increase in adhesive friction between the two substrates. For in this case, with a reduction in deformation friction, and thus ploughing, there would be a greater number of surface asperity interactions, which enhanced the adhesive frictional response [3]. As running-in progressed, this reduced, as in Figure 34 [3].

The lower frictional coefficients shown by the remaining six lubricants suggest that tribofilms on both aluminium-silicon and the steel piston ring surfaces were playing a dominant role in the frictional response, as the substrate-substrate interaction observed for base oil and NOCH in base oil was minimised. Indeed, the main sources of deformation friction were consequently the depression of silicon grains [77, 79, 99, 100] and the plastic deformation of aluminium [77, 79, 100], as seen during the low wear of aluminium-silicon alloys [77, 79, 99, 100]. Protection of exposed asperities by generated tribofilms, and thus minimising the adhesion part of friction, reduced the frictional response [13].

As observed on ferrous surfaces [176], OBCS possessed a lower coefficient of friction compared to ZDDP (Figure 34). Since the shear of the generated tribofilm dictated the frictional response in the contact [160], it follows that as the value of μ was the lowest of all lubricants, the shear strength of the calcium sulfonate-based tribofilm was also a minimum. The increase in μ observed when NOCH was added to calcium sulfonate revealed that a degree of antagonistic behaviour occurred between the two additives. The greater frictional response suggests that either the resulting tribofilm possessed a greater shear strength than OBCS alone [160] or, alternatively, an increased number of interactions occurred between the surfaces of the piston ring and cylinder liner, enhancing the adhesive component of friction [3]. This was unlikely, however, since the lubricant C and CN samples altered little (section 5.5.1.3).

However, the analogous results obtained using ZDDP and ZDDP + NOCH imply that NOCH did not influence frictional response here as with calcium sulfonate. The value of μ recorded for either lubricant was similar to that obtained for ZDDP lubricating ferrous [154, 166, 176, 245] and aluminium-silicon surfaces [152]. As witnessed on ferrous surfaces [166, 176], the coefficient of friction was greater than that obtained with OBCS, which was attributed to a high roughness of the tribofilm [143] or shearing of the outer alkyl phosphate section of the ZDDP film [120]; amplification of the adhesion component of friction would therefore ensue. However, when discussed in literature, the roughness of the ZDDP tribofilm was considered not to play the chief role in determining frictional response [148, 246] and a number of alternative mechanisms were evaluated, none of which were confirmed [246].

Interestingly, lubricants ZC and ZCN exhibited friction coefficients that were much reduced compared to ZDDP alone, greater than that of OBCS; this has been previously observed on ferrous substrates [176]. The fact that ZCN exhibited a frictional response very similar to calcium sulfonate + NOCH suggests that ZDDP was no longer playing a principal role in film formation.

5.6.1.2. Electrical Contact Voltage

When the interface between piston ring and aluminium-silicon substrates was lubricated with base oil and NOCH in base oil, full separation of the two surfaces was not obtained (Figure 35). The time required to separate the

contacting surfaces was very high, during which a large amount of substrate-substrate interaction occurred [234]. In the cases of both NOCH in base oil and base oil interfaces, shortly after the maximum ECV value had been obtained, the frictional response reached a steady state (Figure 34), which implies that the two parameters were very much related. Interestingly, on ferrous only interfaces investigated by Yamaguchi et al. [245], ECR output remained at a minimum value when base oil was employed as lubricant. Perhaps the increase in electrical contact voltage observed in this work can be ascribed to wear particles within the interface, which act to separate the two substrates [245].

As observed in ferrous-only interfaces [176, 245, 247, 248], the separation of the two interacting substrates by a ZDDP-based insulating tribofilm was not instantaneous, but, instead, required a period of time to generate a suitable tribofilm. However, the addition of NOCH to ZDDP dramatically reduced this time period, which is indicative of synergistic behaviour. Since NOCH in base oil did not separate the surfaces quickly, it follows that the organic molecule had an effect on the film formation of zinc diakyldithiophosphate. Overbased calcium sulfonate separated the surfaces much more quickly than when the interface was lubricated with ZDDP alone. As this has also been observed in the case of a ferrous tribosystem [176], it can be proffered that there was a marked difference in the film forming mechanism between OBCS and ZDDP [176], as discussed in section 3.4.

The combination of ZDDP + calcium sulfonate exhibited much the same behaviour as calcium sulfonate alone; presumably because the detergent improved film formation (Figure 35). Interestingly, the combination of OBCS and ZDDP is reported [176] to require greater time periods in order to bring about separation, compared to the sole use of either additive. Unlike frictional response, NOCH did not influence film formation in the case of calcium sulfonate + NOCH nor ZDDP + calcium sulfonate + NOCH (Figure 34), since the ECV obtained for both were indistinguishable from lubricant C and ZC, respectively. Therefore, the previously observed differences in frictional response between lubricant C and CN and also ZC and ZCN are not attributable to differences in the separation of the contacting surfaces.

5.6.1.3. Summary

The greatest frictional response in the contact was observed with base oil, which reduced when the interface was lubricated with NOCH in base oil; this was accredited to a reduction in the deformation component of friction due to an improvement in surface separation. Tribofilms generated using the six remaining test lubricants influenced frictional response in the tribosystem.

Lubricants Z and ZN imparted a similar frictional response on the contact, even though film formation was improved with the addition of NOCH. OBCS reduced the friction coefficients compared to ZDDP through a reduction in the shear strength of the fashioned tribofilm and rapid separation of the substrates. The addition of NOCH to OBCS increased tribofilm shear strength, thus increasing the friction coefficient. The frictional response of ZDDP + calcium sulfonate + NOCH was analogous to lubricant CN; suggesting the two possessed similar tribofilm structures. ZDDP + calcium sulfonate increased the friction coefficients in the tribosystem compared to ZCN.

5.6.2. Surface Topography and Wear

5.6.2.1. Base Oil vs NOCH in Base Oil

Of the three main categories of wear observed for aluminium-silicon substrates described in section 5.4, the *heavy wear* type was the most easily identifiable and can be observed on the base oil sample in Figure 78.

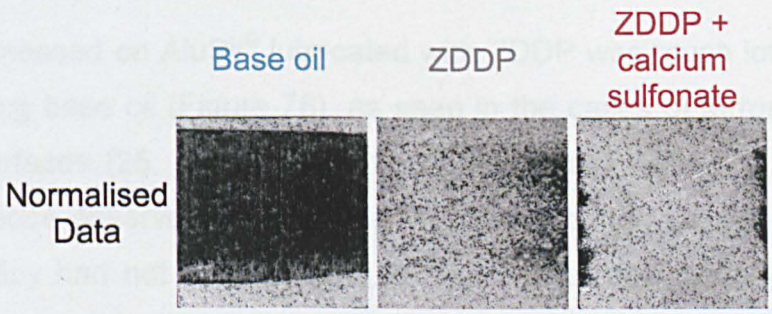

Figure 78: Normalised data obtained from wear analysis

Indeed, *heavy wear* was clearly catastrophic and was observed exclusively on base oil and NOCH in base oil samples. It is evident that the AluSil® substrate had been worn through both adhesion and two body abrasion [7] and, as a consequence, it was likely that particles generated through wear induced third body abrasion of the soft aluminium-silicon substrate [7]. Ploughing of AluSil® is clearly evident; the grooves shown in Figure 37A and Figure 38A indicate that plastic deformation of the alloy occurred [7]. These

severe wear types have been previously identified in studies of the lubricated wear of aluminium-silicon alloys [93, 249, 250].

Since NOCH in base oil is known to reduce wear, compared to base oil alone, on ferrous surfaces [251], the reduction in the severity of the grooves in the aluminium-silicon substrate when lubricated with NOCH in base oil (section 5.5.1.1) can be attributed to potential antiwear properties of the NOCH additive. These could be similar to those observed with ZDDP; preferential wear [145] or load carrying abilities [120, 146].

The minimal extension of silicon grains from the matrix in the cases of both lubricant B and N aluminium substrates can be attributed to abrasion of the aluminium alloy, as well as the depression of these hard areas into the surface of AluSil® [77, 79, 99, 100]. The magnitude of the material transfer to the piston ring substrates shown in section 5.5.1.5 highlights the degree of wear endured. Although piston ring wear was not detected, it cannot be discounted. The prediction made in section 5.6.1 regarding piston ring and AluSil® interaction when lubricated with base oil or NOCH in base oil was completely accurate. As too was the frictional response, which pointed toward excessive wear through elevated friction coefficients. Consequently, the results obtained demonstrate quite clearly, that base oil and NOCH in base oil do not provide effective lubrication of the piston ring and AluSil® tribosystem.

5.6.2.2. ZDDP vs ZDDP + NOCH

The wear witnessed on AluSil® lubricated with ZDDP was much lower than that achieved using base oil (Figure 78), as seen in the cases of ferrous [143, 166] and Al-Si surfaces [25, 93, 199]. Furthermore, wear levels with ZDDP were lower than those observed for NOCH in base oil (section 5.5.1.2). Indeed, the aluminium alloy had not been subject to heavy wear and *mild wear* was now dominant (Figure 36). The extent of the damage to the aluminium-silicon substrate could be assigned to four main areas (Figure 39A&B and Figure 41A&B):

- Removal of honing marks on silicon
- Cracking of silicon grains
- Depression of silicon grains
- Oil residue layer present

Surface honing was removed through abrasion of the hard silicon grains [99, 100, 104], as a consequence of which cracking occurred [99, 100, 104]. Supporting of the applied load [25, 66, 98] resulted in depression of silicon grains [77, 79, 99, 100]. Indeed, this depression was evident on lubricant Z and ZN substrates, since silicon extension was much reduced compared to unworn AluSil® (section 5.5.1.2).

The first three types of wear listed were typical of an aluminium-silicon substrate that had been subject to lubricated low levels of wear [77, 79, 99, 100, 104]. Each of these three wear types indicate the silicon grains within the alloy supported the applied load, as previously reported [66, 98]. The accumulation of the surrounding aluminium matrix discussed in literature [77, 79, 100] as a result of silicon depression, cannot be proved, however.

The presence of a ZDDP tribofilm on silicon grains within the alloy, albeit extremely sporadically, was in accordance with reported observations [25, 66, 152]. An oil residue region has been witnessed previously on an Al-Si alloy when using ZDDP as lubricant [25, 153], this being most likely thermally decomposed ZDDP [25] or tribofilm which had been removed from silicon grains during sliding [25, 66, 153]. As there was no material transfer from aluminium-silicon substrate to the ferrous piston ring, it follows that the ZDDP tribofilm generated on both the piston ring (Figure 48) and silicon grains within the AluSil® substrate (Figure 39&Figure 40) reduced wear in the contact. This was due to the mechanism of preferential wear [145] and load carrying [120, 146] exhibited by conventional ZDDP-based tribofilms on ferrous surfaces. Prevention of substrate-substrate interaction ensued and both abrasive and adhesive wear of the soft aluminium silicon substrate did not occur on a large scale. Corrosion protection [155, 156] and the consumption of iron oxide by ZDDP [126] are not thought to play major roles in this tribosystem.

As shown in Figure 40, triethyl citrate improved the frequency and size of generated tribofilms compared to ZDDP. The aforementioned lubricant ZN film very much resembled that of which is traditionally observed on ferrous substrates [122, 145-147, 149, 252-255] and also on aluminium-silicon alloys [66]. Indeed, it was quite clear that, as the ECV output predicted (section 5.6.1), the film forming properties of the ZDDP + NOCH lubricant were superior to those of ZDDP alone. The other main difference observed between ZDDP and ZDDP + NOCH substrates was a considerable reduction in the oil residue

region, which influenced the wear grade classification used in this work (Figure 36); the lubricant ZN substrate underwent *ultra mild wear*. Therefore, as reported on ferrous surfaces, ZDDP + NOCH imparted lower levels of wear compared to ZDDP [215]. This could be derived from the additional time required to generate a suitable film by ZDDP, compared to ZDDP + NOCH [176] (section 5.6.1.2). A disadvantage of the oil residue layer is that it could contain abrasive particles, which, through interaction with the piston ring, may lead to wear of the aluminium matrix [104].

5.6.2.3. Calcium Sulfonate vs Calcium Sulfonate + NOCH

Referring to section 5.5.1.3, it is apparent that when lubricated with calcium sulfonate or calcium sulfonate + NOCH, the two AluSil® substrates possessed remarkably similar topography. Indeed, both surfaces were relatively undamaged and housed a tribofilm, which formed exclusively on protruding silicon grains and as shown Figure 43A&B, comprised a number of small pads. A matching tribofilm was observed on the accompanying piston rings (section 5.5.1.7), along with minimal levels of wear and no material transfer. Both protective films resembled those typically generated using OBCS on ferrous surfaces [177]. The coverage of the tribofilm on silicon grains, but not the ferrous piston ring surface, was far superior to that obtained with ZDDP or ZDDP + NOCH. Indeed, even on AluSil® lubricated with ZN, the tribofilm covered only ~ 50 % of the silicon grain surface. This was considerably improved using either detergent-based lubricant. Improvements in wear levels may ensue over time, since a greater amount of protection is afforded to silicon grains by employing OBCS.

Unlike ZDDP and ZDDP + NOCH, an oil residue region was not observed, which supports the view that this area must comprise film transfer or thermally decomposed ZDDP. However, as removal of honing, cracking and depression of silicon grains occurred for both detergent-based substrates, it seems this must be a primary step in the very low wear of aluminium-silicon alloys, as discussed by several researchers [77, 79, 99, 100, 104]. The extension of silicon grains observed for the C and CN samples was approximately 500 nm (section 5.5.1.3); this being much greater than that observed using ZDDP or ZDDP + NOCH (section 5.5.1.2). Perhaps the calcium-based tribofilm cushioned the applied load to a greater extent than with ZN,

thereby preventing excessive compression of the important silicon regions. Further research work is required to justify this proposal, however.

Nonetheless, it is likely that calcium sulfonate-based tribofilms impart reduced wear levels to the tribosystem by minimising interaction between substrates [160] and undergoing preferential removal / shearing [165]. OBCS is known to reduce wear compared to ZDDP on ferrous surfaces [165, 166, 169, 176] and this was observed herein insofar as both C and CN lubricants were located in the *ultra mild wear* category (Figure 36). Unfortunately, due to the line contact conditions, and low wear levels employed in this research, it was very difficult to determine whether one detergent-based lubricant provided enhanced wear protection over another. However, It has been reported that the combination of OBCS + NOCH reduces wear on ferrous surfaces, compared to OBCS alone [215]. Therefore, although this work is the first published research on the lubrication of aluminium-silicon alloys using a detergent, let alone OBCS, it is clear that the additive is not only very effective in terms of both friction and wear reduction, but more so than ZDDP or ZDDP + NOCH.

5.6.2.4. ZDDP + Calcium Sulfonate vs ZDDP + Calcium Sulfonate + NOCH

The lack of a physically identifiable tribofilm on both AluSil® and piston ring surfaces when lubricated with ZDDP + calcium sulfonate is indicative of competition for surface interaction between the two additives (section 5.5.1.4&5.5.1.8). The addition of NOCH to lubricant ZC improved film formation, as a tribofilm, albeit patchy and non-uniform in distribution, was evident on both ferrous substrate and silicon grains within AluSil® in the case of ZDDP + calcium sulfonate + NOCH.

The aforementioned lubricant ZCN tribofilm on AluSil® was similar in appearance to a calcium sulfonate-based film (section 5.5.1.3) and bared no resemblance to that generated from ZDDP or ZDDP + NOCH (section 5.5.1.2). The existence of an oil residue layer on the ZCN AluSil® substrate, albeit much reduced in volume compared to ZDDP + NOCH, indicates ZDDP was influencing film formation. It follows, therefore, that even though ZDDP was involved in film generation, the tribofilm formed was calcium sulfonate-based.

Oil residue was also evident in the AFM images of the lubricant ZC AluSil® substrate (Figure 45B), but appeared to be in greater volumes than with ZCN, since the measured step height of 98 nm ± 8 nm was much lower than

that obtained with the addition of NOCH (449 nm ± 46 nm). From which it follows that depression of the silicon components within either AluSil® sample occurred. Furthermore, the removal of honing marks and cracking of silicon regions occurred with ZC and ZCN lubricants, although accumulation of aluminium around depressed silicon grains was not observed (section 5.5.1.4)

Since an *ultra mild wear* classification was ascribed to both ZC and ZCN AluSil® substrates, a tribofilm must have been present on the ZC piston ring and aluminium samples, otherwise, the wear in the contact would have resembled that secured using either base oil or NOCH in base oil. Previous observations that the combination of ZDDP and OBCS on ferrous surfaces imparted greater levels of wear than the sole use of either the antiwear [166, 176, 184, 185] or detergent [166, 176, 185] additive could not be confirmed using the experimental and analytical methods employed in this work, however.

5.6.2.5. Summary

Heavy wear was observed on base oil and NOCH in base oil AluSil® substrates, although NOCH in base oil appeared to possess some antiwear ability. Large amounts of wear debris were evident on both lubricant B and N piston rings. A tribofilm was observed on piston rings lubricated with ZDDP and ZDDP + NOCH. Wear was reduced to a *mild* form on the aluminium-silicon alloy with ZDDP; this was accredited to the known antiwear properties of the additive. ZDDP + NOCH further reduced the wear level in the contact to *ultra mild*, due to a reduction in oil residue regions, through an improvement in tribofilm formation.

Tribofilms were generated on piston rings and exclusively on silicon grains within AluSil® lubricated with calcium sulfonate and calcium sulfonate + NOCH; wear was controlled by minimising interaction between substrates and the films undergoing preferential removal and shearing. Lubricant ZC imparted *ultra mild* levels of wear on the tribosystem, even though oil residue derived from ZDDP film formation was evident on the aluminium matrix of the AluSil® substrate. ZDDP + calcium sulfonate + NOCH generated a clearly identifiable tribofilm on silicon grains within AluSil®, which resembled that obtained using calcium sulfonate + NOCH as lubricant; the wear level was *ultra mild*. A physical tribofilm was only obtained on the ZCN piston ring.

It was evident that ZDDP was not as effective at generating a tribofilm on aluminium-silicon surfaces as it was on ferrous substrates. However, the

remarkable ability of OBCS to generate effective tribofilms on these modern alloys suggests that detergent additives are better suited to the environs of aluminium-silicon lubrication rather than their antiwear counterparts.

An overview of the effect the addition of NOCH has on base oil, ZDDP, calcium sulfonate and ZDDP + calcium sulfonate in terms of tribological performance and surface topography is shown in Table 23.

Lubricant	Effect of the Addition of NOCH
Base oil	Decreased friction coefficient
ZDDP	Improved surface separation and film formation; reduced wear and oil residue
Calcium sulfonate	Increased friction coefficient
ZDDP + calcium sulfonate	Decreased friction coefficient; improved film formation; reduced oil residue

Table 23: Overview of the effect of the addition of NOCH on test oils used to lubricate an Al-Si alloy and steel piston ring tribosystem

5.6.3. Tribochemistry and Film Formation

5.6.3.1. Base Oil vs NOCH in Base Oil

5.6.3.1.1. Tribochemistry

Infrared analysis of base oil and NOCH in base oil AluSil® substrates revealed several differences in the tribochemistry of the two samples. Indeed, when lubricated with base oil, siloxane and silicon-methyl associated compounds were detected on the alloy, which were presumably present due to reactions between the polyalphaolefin base oil and silicon within the alloy under the catastrophic wear conditions experienced. Such compounds have been generated on silicon surfaces previously [256]. In contrast, NOCH in base oil did not contain any of these peaks and importantly, did not display the original NOCH associated peaks assigned in Figure 29. This indicates, therefore, that triethyl citrate was not in the form observed prior to experimentation or that the NOCH molecule was not present in great enough quantities as to be detected.

Mini SIMS analysis of AluSil® revealed a reduction in the level of impurities but no real difference in carbon intensity compared to outside the wear scar, in the case of either sample (section 5.5.3.1). SIMS analysis of the

accompanying piston rings (section 5.5.3.5) showed that, as predicted, the ferrous substrates housed large amounts of material transferred from the aluminium alloy.

5.6.3.1.2. Film Formation

As seen previously during the wear of Al-Si alloys, oxides of aluminium and silicon were generated [66, 93], which prevented interaction between the substrates when low levels of wear occurred [93]. However, oxide layers do not afford sufficient wear protection under high wear situations [257].

As there was a noticeable difference in frictional response, ECR and wear results between base oil and NOCH in base oil, NOCH must have generated a metal complex in the interface. This was achieved via interaction with both the piston ring and aluminium-silicon substrate, and was related to those which arise in the cases of organic compounds used to lubricate steel against both aluminium [193-195, 207] and aluminium-silicon alloys [97, 210]. Such complexes are thought to possess some level of antiwear ability [193-195, 207, 210] and reduce the frictional response of the contact [194, 207, 210]. The possible method of interaction is shown in Figure 79, where M = chromium, iron, aluminium or silicon.

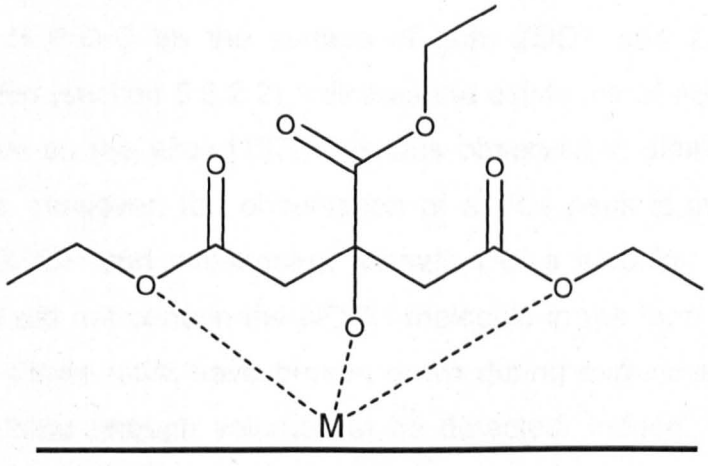

Figure 79: Metal complex formed between triethyl citrate and piston ring or aluminium-silicon alloy

5.6.3.1.3. Summary

Overall, the tribochemistry of base oil and NOCH in base oil substrates varied so far as Si-O and Si-CH_3 compounds were observed on AluSil® lubricated with base oil, but not with NOCH in base oil. Large amounts of material transfer from aluminium alloy to piston rings were evident when the tribosystem was

lubricated with either test oil. A representative model for the surfaces of both AluSil® and steel piston ring after experimentation are shown in Figure 80.

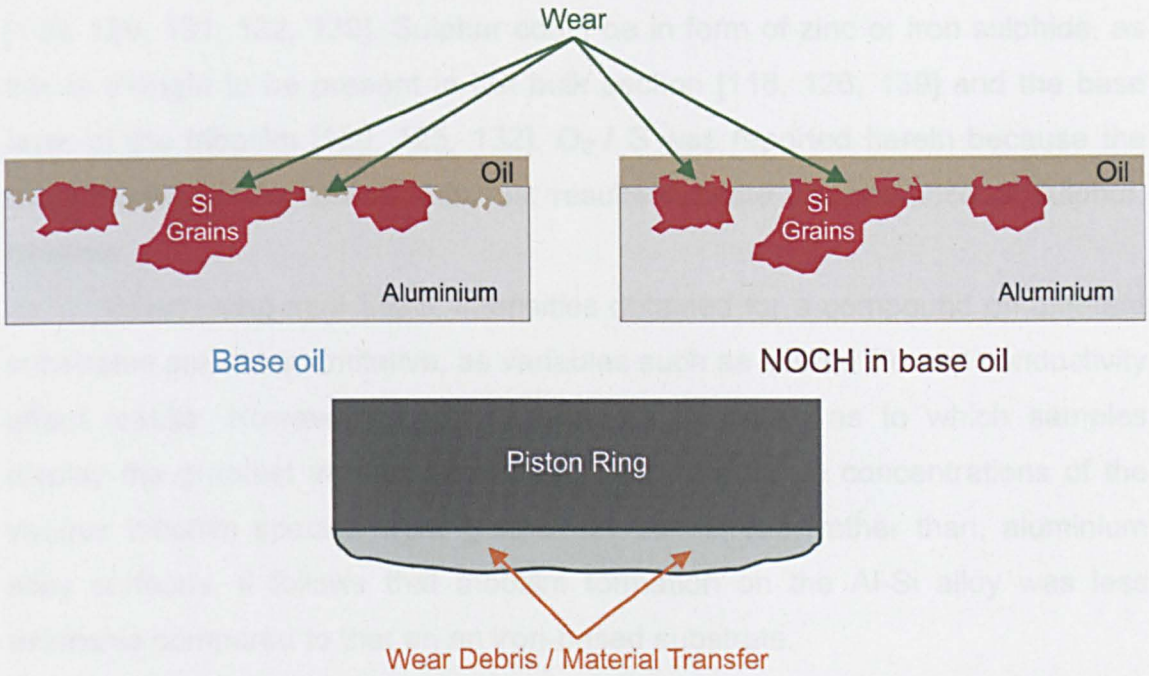

Figure 80: Models of Al-Si alloy and steel piston ring, when lubricated with base oil or NOCH in base oil

5.6.3.2. ZDDP vs ZDDP + NOCH

5.6.3.2.1. Tribochemistry

The presence of P-O-C on the surface of both ZDDP and ZDDP + NOCH AluSil® substrates (section 5.5.2.2) indicates the existence of non-decomposed antiwear additive on the alloy [127]; this was observed in similar amounts on both substrates. However, the observation of a PO_2 peak is indicative of the breakdown of ZDDP and subsequent formation of a tribofilm. FTIR revealed ZDDP + NOCH did not contain the NOCH molecule in the form observed prior to test; triethyl citrate must have broken down during experimentation or was not present in large enough volumes to be detected. Indeed, further work is required to fully understand the nature of the organic additive after experimentation.

As reported in the literature, ZDDP tribofilm composition on the aluminium alloy was analogous to that obtained on a ferrous substrate [25, 66, 151] (section 5.5.3). Indeed, tribofilms fashioned on both substrates using ZDDP or ZDDP + NOCH contained Zn, Fe, PO_2, PO_3 and O_2 / S; these were not obtained OWS. The five compounds listed are thought to be the main peaks observed during SIMS analysis of ZDDP tribofilms on ferrous surfaces and are

indicative of zinc and iron polyphosphate generation [118]. This is widely believed to be the main section of the antiwear tribofilm on ferrous surfaces [118, 129, 131, 132, 139]. Sulphur could be in form of zinc or iron sulphide, as this is thought to be present in the bulk section [118, 126, 139] and the base layer of the tribofilm [120, 125, 132]. O_2 / S was reported herein because the two possess similar atomic masses; results indicate the presence of sulphur, however.

When using mini SIMS, intensities obtained for a compound on different substrates are not quantitative, as variables such as source life and conductivity affect results. However, concentrations are indicative as to which samples display the greatest amount of a particular m / z. Since concentrations of the various tribofilm species were greater on the ferrous, rather than, aluminium alloy surfaces, it follows that tribofilm formation on the Al-Si alloy was less extensive compared to that on an iron-based substrate.

When lubricated with ZDDP alone, the observation that the key tribofilm elements decreased with increasing depth from the top surface of the tribofilm, in the cases of both piston ring and AluSil® substrates, indicates a greater concentration of these components toward the outer layers of the protective film. This trend was also witnessed in the case of zinc concentration for ZDDP + NOCH lubricated substrates. Initial increases in silicon content during the initial stages of depth profiling were accredited to polydimethylsiloxane (PDMS), which is a common contaminant [258]. However, unlike ZDDP, PO_2, PO_3 and O_2 / S concentrations increased initially, before rapidly decreasing; peak values for PO_2 and PO_3 were greater than those obtained for ZDDP alone. This suggests that NOCH enhanced the phosphate concentration within the bulk section of the tribofilm, which agrees with the proposal made from the tribochemical analysis of ferrous surfaces lubricated with ZDDP + NOCH [215].

The finding that the intensity of iron was at a minimum at the outer layer of the tribofilm on the lubricant ZN piston ring suggests that the film had low iron phosphate / sulphide concentration, compared to ZDDP alone; the layer may consist only of zinc polyphosphates and sulphides. Since iron intensities exhibited similar trends for ZDDP and ZDDP + NOCH-lubricated AluSil® substrates, the iron peak witnessed most probably arose from material transfer from piston ring to Al-Si substrate. Material transfer also occurred from AluSil®

to piston ring with both lubricants; the concentration of aluminium decreased throughout depth profiling on the ferrous substrates.

Table 22 shows, quite clearly, that the SiO_2^- areas within AluSil® were the same as those possessing high concentrations of both PO_2 and PO_3. This finding, together with the observed physical tribofilm areas on AluSil® (section 5.6.2.2), unequivocally demonstrates that silicon grains were the sole region on which ZDDP tribofilm formation occurred within the alloy. The silicon regions most likely facilitate film formation through their mechanical strength, as has been previously discussed [25, 98].

5.6.3.2.2. Film Formation

A combinatorial approach to ZDDP film formation is proposed in this work. The method of film formation suggested by Fuller et al. [131] on ferrous surfaces is also applicable to aluminium-silicon substrates, as shown by Nicholls et al. [98]. This particular method proposed that thermo-oxidation and hydrolysis were the processes by which zinc polyphosphate and sulphur compounds are generated [98, 131] and that surface interaction occurs by adsorption of different compounds onto generated oxide layers [98]. An example of which is possible iron oxide transfer onto silicon grains within AluSil®. However, this proposal does not explain iron phosphate formation, which is best described by Martin et al. using the chemical hardness approach [126], according to which, iron phosphate formation would occur on the steel piston ring and regions rich in iron oxide.

If the NOCH molecule formed a metal complex with both substrates in the tribosystem, as described with NOCH in base oil, this may have improved the formation of a ZDDP-based tribofilm on the AluSil® substrate. Indeed, since film formation appeared to be enhanced, both physically and via ECV values (section 5.6.1), and the degree of oil residue layer was markedly reduced compared to ZDDP alone (section 5.6.2), it follows that NOCH enhanced the ability of the tribofilm to adhere to the substrate [176]. NOCH increased the amount of polyphosphate and sulphur species within the tribofilm by providing an increased concentration of oxygen by which thermo-oxidation of the ZDDP molecule can occur [131, 132]; it has been reported that an amplification in oxygen concentration enhances wear results on ferrous surfaces [141]. Thus, a greater amount of decomposed ZDDP on the substrate surfaces results in an

improvement in tribofilm formation, with the films being less patchy and possessing a clearly defined polyphosphate pad-like structure.

5.6.3.2.3. Summary

The tribofilms generated by either lubricant were chemically similar and representative models are shown in Figure 81, which also displays the enhanced film formation and reduced oil residue observed on AluSil® lubricated with ZDDP + NOCH.

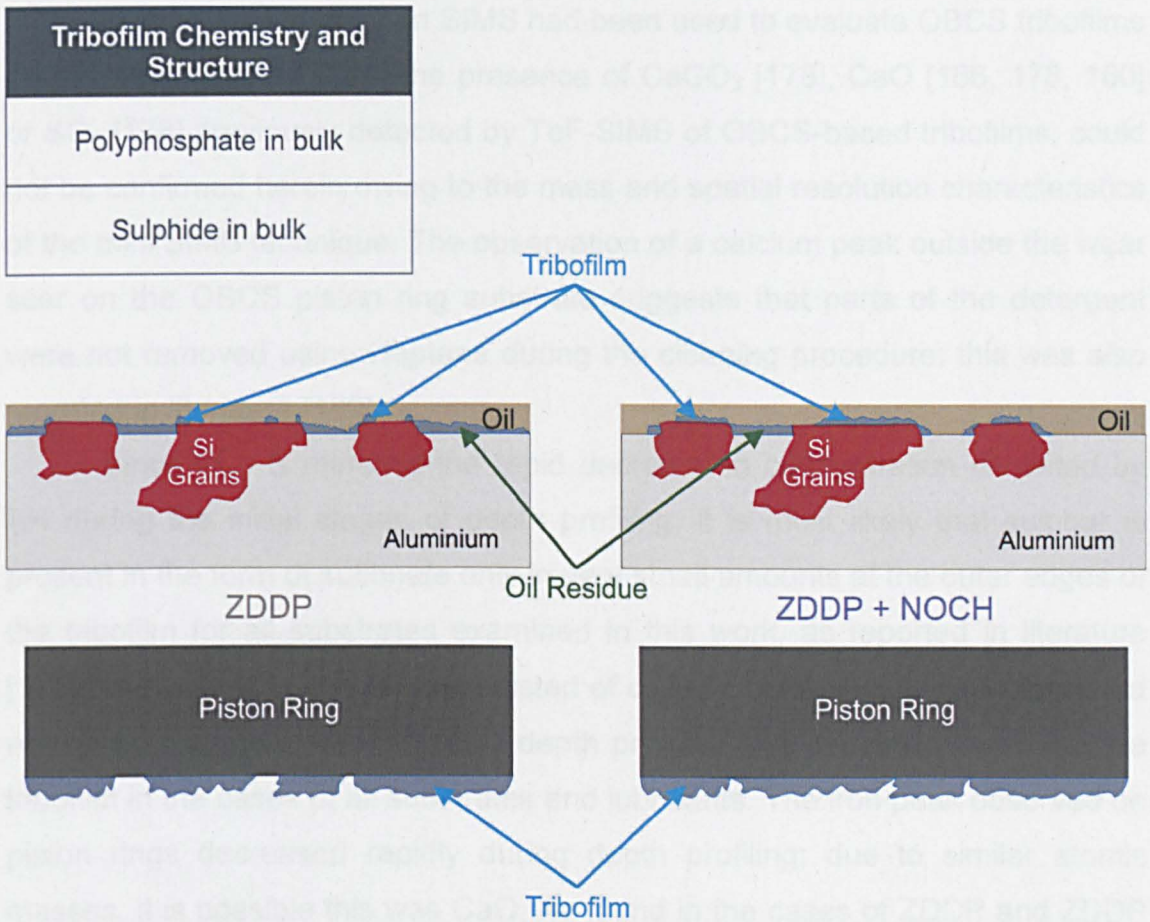

Figure 81: Models of Al-Si alloy and steel piston ring, when lubricated with ZDDP or ZDDP + NOCH

In terms of ZDDP, generation of iron and zinc polyphosphates on the ferrous surface was identified, whereas zinc polyphosphates were only generated on the aluminium alloy. Samples lubricated with ZDDP + NOCH contained only zinc polyphosphates; NOCH boosted the phosphorus concentration within the tribofilm. Together with this bulk polyphosphate content on all samples was zinc sulphide; iron sulphide was additionally present on ZDDP piston ring samples.

5.6.3.3. Calcium Sulfonate vs Calcium Sulfonate + NOCH

5.6.3.3.1. Tribochemistry

As this is the first investigation into the lubrication of aluminium-silicon alloys using overbased calcium sulfonate, it is very interesting to note that tribofilm chemical composition was identical on both aluminium alloy and ferrous substrates, as determined using SIMS (section 5.5.3). Indeed, the main peaks observed were Ca, CaOH and small concentrations of O_2 / S, these being the main constituents found when SIMS had been used to evaluate OBCS tribofilms on ferrous surfaces [178]. The presence of $CaCO_3$ [178], CaO [166, 178, 180] or SO_3 [178] previously detected by ToF-SIMS of OBCS-based tribofilms, could not be confirmed herein owing to the mass and spatial resolution characteristics of the mini SIMS technique. The observation of a calcium peak outside the wear scar on the OBCS piston ring substrate suggests that parts of the detergent were not removed using Heptane during the cleaning procedure; this was also reported in literature [180].

Since O_2 / S mirrored the rapid decrease in concentration exhibited by SH during the initial stages of depth profiling, it is most likely that sulphur is present in the form of sulfonate only in very small amounts at the outer edges of the tribofilm for all substrates examined in this work, as reported in literature [178]. The bulk of the tribofilm consisted of calcium compounds, since these did not obtain maximum intensity until depth profiling had penetrated well into the tribofilm in the cases of all substrates and lubricants. The iron peak observed on piston rings decreased rapidly during depth profiling; due to similar atomic masses, it is possible this was CaO. As found in the cases of ZDDP and ZDDP + NOCH, contamination by PDMS was observed on all substrates, which rapidly decreased in intensity during depth profiling.

Owing to the nature of the SIMS technique, it was not possible to provide a definitive chemical composition of the substrate. FTIR analysis of the aluminium-silicon substrates, however, proved extremely useful in this context. The small, but definite peak observed on both AluSil® samples within the wear scar on the substrates at ~ 860 cm^{-1} was attributable to calcium carbonate [227, 228, 244], probably as amorphous $CaCO_3$ [244, 259]; this being identical to the core of the OBCS micelle [163]. This finding was in contrast to that suggested by other workers [165, 167, 168] who proposed crystalline calcium carbonate

(calcite; ~ 877 cm^{-1} [244]) formed. Hence, the presence of CaOH as detected using SIMS can be explained, since calcium hydroxide is present around the outer edge of the OBCS micelle [34]. The small size of the infrared-deduced peaks were most likely due to the very small quantities of $CaCO_3$ on the aluminium-silicon substrates, since tribofilm formation occurred only on silicon grains within the alloy (section 5.6.2.3). The lack of NOCH associated peaks in the infrared analysis of calcium sulfonate + NOCH once again shows that NOCH has most probably degraded from its original form or is present in small volumes.

5.6.3.3.2. Film Formation

Film formation by OBCS is a far less complicated process than that experienced with ZDDP. Indeed, as described in section 3.4.2.1, micellar adsorption [165, 166] onto the contacting substrates and a mechanistic process to remove sulfonate chains [165, 168] leads to subsequent build up of $CaCO_3$ [165, 167, 169]. Importantly, film formation does not occur via chemical reaction [165], which explains why, as observed in section 5.6.1, ECV indicated film formation was rapid when OBCS was in the lubricating oil, whereas the time required to separate the substrates was much greater when ZDDP was used. As suggested by Mansot et al. [165], film formation by overbased calcium sulfonate is not material dependant; the present work has shown it to readily occur on silicon surfaces.

5.6.3.3.3. Summary

From the work conducted thus far, it was not possible to determine chemical differences between OBCS and OBCS + NOCH tribofilms, apart from a much greater intensity of Ca and CaOH on the piston ring lubricated using OBCS + NOCH. It is believed that NOCH should boost the antiwear performance of OBCS by enhancing the amount of calcium carbonate present on ferrous surfaces [215]. However, owing to the non-quantitative nature of SIMS, enhanced calcium carbonate formation by NOCH cannot be verified. Therefore, if NOCH improved the shear strength of the tribofilm (section 5.6.1) this was not achieved this through a radical change in tribochemistry. Representative models of the tribofilms generated on aluminium-silicon and piston ring substrates lubricated with calcium sulfonate and calcium sulfonate + NOCH are displayed in Figure 82.

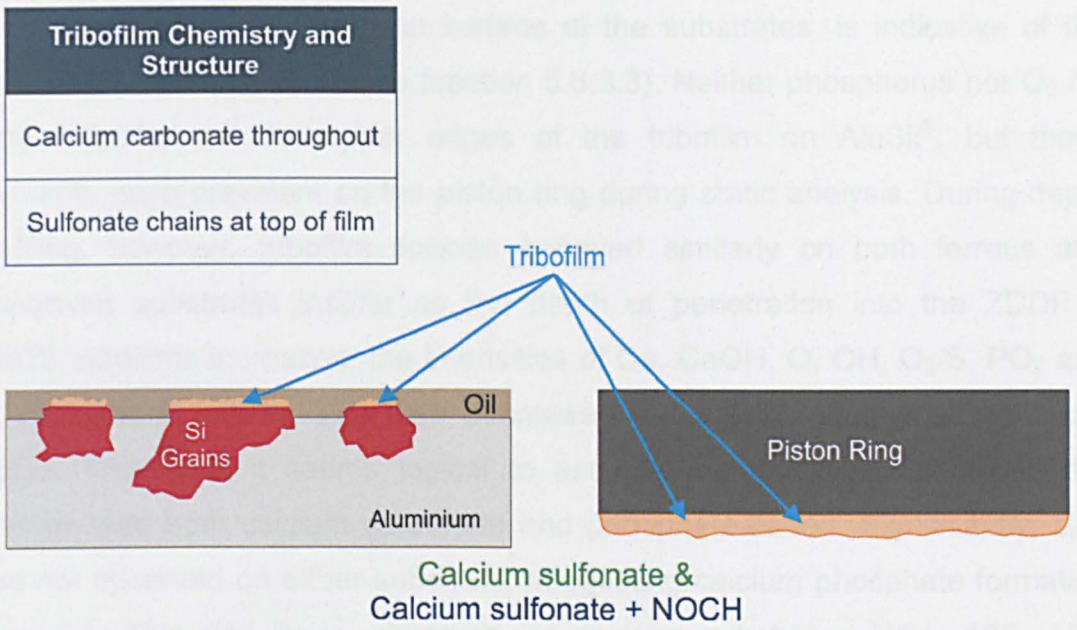

Figure 82: Models of Al-Si alloy and steel piston ring, when lubricated with calcium sulfonate or calcium sulfonate + NOCH

Referring to Figure 82, tribofilms generated from OBCS and OBCS + NOCH were chemically identical on both ferrous and aluminium-silicon substrates. The film structure comprised amorphous $CaCO_3$, which was present throughout the entire depth of the layer. A small number of sulphur species were located toward the outer edges of the tribofilm and were most likely sulfonate chains which been embedded into the tribofilm during frictional processes.

5.6.3.4. ZDDP + Calcium Sulfonate vs ZDDP + Calcium Sulfonate + NOCH

5.6.3.4.1. Tribochemistry

Infrared analysis of AluSil® which had been lubricated with ZC and ZCN showed that the generated tribofilms contained calcium carbonate, non-decomposed ZDDP and PO_2 species. The intensities of the phosphorus species were greatest in the absence of the NOCH additive. As with ZDDP and ZDDP + NOCH, the P-O-C band originated from non-decomposed ZDDP. Both $CaCO_3$ and the PO_2 compound must be present on the silicon regions, as these were observed to possess physically identifiable tribofilms (section 5.6.2). Importantly, as with lubricants N, ZN and CN lubricants, none of the NOCH associated peaks were observed in the FTIR spectra of ZCN lubricated AluSil®.

In the context of the mini SIMS results obtained for the substrates which had been lubricated with ZDDP + C.S. (sections 5.5.3), the observed calcium

peak, along with CaOH on the surface of the substrates, is indicative of the presence of calcium carbonate (section 5.6.3.3). Neither phosphorus nor O_2 / S were detected on the upper edges of the tribofilm on AluSil®, but these elements were prevalent on the piston ring during static analysis. During depth profiling, however, tribofilm species behaved similarly on both ferrous and aluminium substrates insofar as the depth of penetration into the ZDDP + OBCS tribofilms increased, the intensities of Ca, CaOH, O, OH, O_2/S, PO_2 and PO_3 increased initially, and then decreased in the latter stages of the depth profile. Therefore, it seems logical to assume that the bulk section of the tribofilm was both calcium carbonate and phosphate-based. Significantly, zinc was not observed on either substrate, suggesting calcium phosphate formation occurred. This has been observed on ferrous substrates [184, 185, 187] lubricated with ZDDP + OBCS and on Al-Si [191] surfaces lubricated with a fully formulated oil. Sulphur was most probably contained within polyphosphate regions, as sulphide in solid solution [187], since the lack of observed zinc does not favour ZnS generation. Phosphate and calcium intensities were much lower than those obtained when the interface had been lubricated using ZDDP or OBCS, which is indicative of a reduction in polyphosphate and $CaCO_3$ generation. Declines in both calcium [166, 176] and phosphorus content [176] have been observed on ferrous substrates lubricated with ZDDP + OBCS. Additionally, since the iron intensity decreased with increasing penetration depth and mirrored the behaviour of CaOH on the piston ring substrate, it seems likely that CaO, rather than Fe, was being observed.

The piston ring lubricated with ZDDP + calcium sulfonate + NOCH was very different, tribochemically, to that using lubricant ZC. Indeed, a reduction in both phosphorus and sulphur concentration was observed with lubricant ZCN. This appeared to be the case on AluSil® also, but probably due to the resolution of the mini SIMS, was not as obvious. During depth profiling on both aluminium and ferrous substrates, phosphorus and sulphur concentration increased marginally to a maximum shortly after the start of the destructive process. A decline in intensity was then observed, which indicated that the generation of the aforementioned phosphate and sulphur species appeared to be limited to the outer regions of the tribofilms. Therefore, the bulk section of the lubricant ZCN tribofilm appeared to comprise calcium carbonate, with a phosphate and sulphide outer section.

Overall, phosphate formation was far greater on the ferrous, rather than AluSil® surface; probably due to the reduced size of available film formation regions on the latter (silicon grains) and the greater ability of ZDDP to generate a film on a ferrous surface (section 5.6.3.2). The presence of sulfonate chains, as with calcium sulfonate (section 5.6.3.3), at the outer region of all tribofilms cannot be discredited. PDMS contamination [258] was evident on various substrates since silicon content rapidly decreased during the early stages of depth profiling. Given that aluminium content on the piston ring reduced with time, this was indicative of material transfer.

5.6.3.4.2. Film Formation

It was obvious that film formation by ZDDP + OBCS was compromised by a degree of competition for surface active sites on each of the substrates studied. This situation has been reported on ferrous surfaces previously [176]. On ZCN lubricated substrates, where phosphorus concentration was very low but calcium species were evident, it follows the ability of calcium sulfonate and also NOCH to interact with the surface must be greater than that of ZDDP. This indicates that competition for surface interaction transpired between the *three* additives and that ZDDP was out-competed by NOCH due to the complex decomposition steps required by the phosphate-based molecule to form a film.

The rapid film formation observed on these substrates (section 5.6.1), was attributable to initial film generation on the contacting substrates by calcium sulfonate (section 5.6.3.3). Simultaneously, with lubricant ZCN, NOCH generated the metal complex observed previously (Figure 79) with the substrate surfaces and the calcium detergent.

With either lubricant, ZDDP would generate a film through that described for ZDDP alone (section 5.6.3.2); the adsorption of ZDDP and linkage isomer onto ferrous and silicon surfaces, followed by decomposition via the processes proposed by Fuller et al. [131] and Nicholls et al. [98], would yield polyphosphates. This process would be less fruitful with lubricant ZCN on both ferrous and silicon surfaces due to competition with NOCH, however. Calcium phosphate generation was proposed by Kasrai et al. [185] using a multi stage model, which can be incorporated into the scheme proposed by Fuller et al. [131]. However, the mechanisms proposed by Fuller et al. [131] predict ZnS

formation; therefore, this compound must have been present on substrates, but presumably, since it was not detected by SIMS, in very small concentrations.

5.6.3.4.3. Summary

In conclusion, tribofilms fashioned from ZC and ZCN on both ferrous and aluminium-silicon substrates were primarily $CaCO_3$-based, as shown in Figure 83.

Tribofilm Chemistry and Structure
Calcium carbonate in bulk, sulfonate chains at top of film
Ca phosphate and sulphide in bulk with lubricant ZC
Ca phosphate and sulphide at top of film with lubricant ZCN

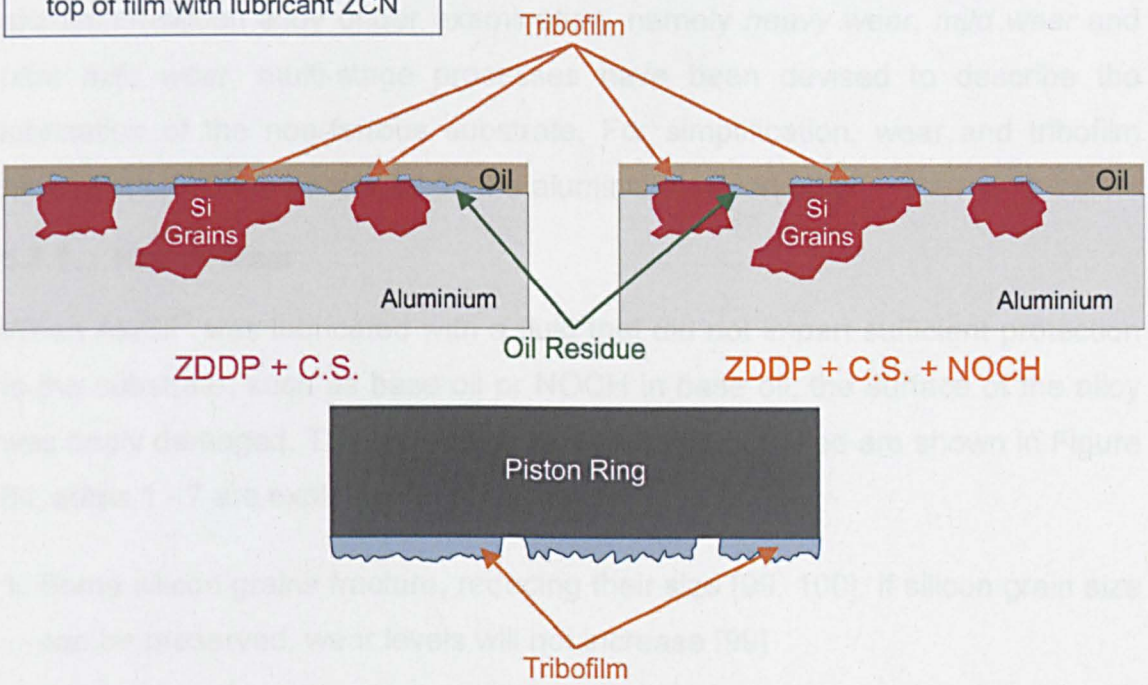

Figure 83: Models of Al-Si alloy and steel piston ring, when lubricated with ZDDP + calcium sulfonate or ZDDP + calcium sulfonate + NOCH

However, calcium phosphate was present in the bulk section of the tribofilm on lubricant ZC substrates, especially the piston ring, as too was sulphide. This phosphorus and sulphur region was restricted to the outer section on lubricant ZCN tribofilms. Sulfonate chains were evident at the outer edge of calcium carbonate-based sections of all tribofilms due to a mixing process. Triethyl citrate competed with ZDDP and thus reduced film formation by the metal antiwear additive. Therefore, it can be stated that NOCH can boost

phosphate formation when used in conjunction with ZDDP, provided ZDDP can adsorb onto the substrate prior to decomposition. The identical frictional response observed previously for OBCS + NOCH and ZDDP + OBCS + NOCH lubricated samples (section 5.6.1) was accredited to a calcium carbonate and NOCH type tribofilm.

5.7. Lubrication Hypotheses of Aluminium-Silicon Alloys

As observed throughout this work, the lubricant employed in the tribosystem between chromium steel piston ring and aluminium-silicon cylinder liner dictates frictional response, ECV and wear in the interface. In this section, the data which has been obtained, accumulated and discussed, is now used to propose an insight into a multi-stage lubrication mechanism for aluminium-silicon alloys.

Under the guise of the three classifications of wear identified on the aluminium-silicon alloy under examination, namely *heavy wear*, *mild wear* and *ultra mild wear*, multi-stage processes have been devised to describe the lubrication of the non-ferrous substrate. For simplification, wear and tribofilm formation has been described on the aluminium-silicon only.

5.7.1. Heavy Wear

When AluSil® was lubricated with a fluid that did not impart sufficient protection to the substrate, such as base oil or NOCH in base oil, the surface of the alloy was badly damaged. The processes by which this occurred are shown in Figure 84; steps 1 - 7 are explained in detail below.

1. Some silicon grains fracture, reducing their size [99, 100]. If silicon grain size can be preserved, wear levels will not increase [99]

2. Fragments of silicon are created via wear and lead to abrasive wear of matrix and also silicon grains [99, 104]

3. Tribofilm with sufficient antiwear characteristics does not form on silicon grains. Silicon regions continue to wear, increasing the amount of third body abrasives in the interface.

4. Load carrying silicon grains depress into matrix [77, 79, 99, 100]

5. Aluminium matrix plastically deforms under applied load and becomes amassed around depressed silicon grains [77, 79, 100]

6. Wear of aluminium ensues; **Heavy wear initiated**

7. Depression plus wear of silicon grains leads to a level surface. Wear levels are very high

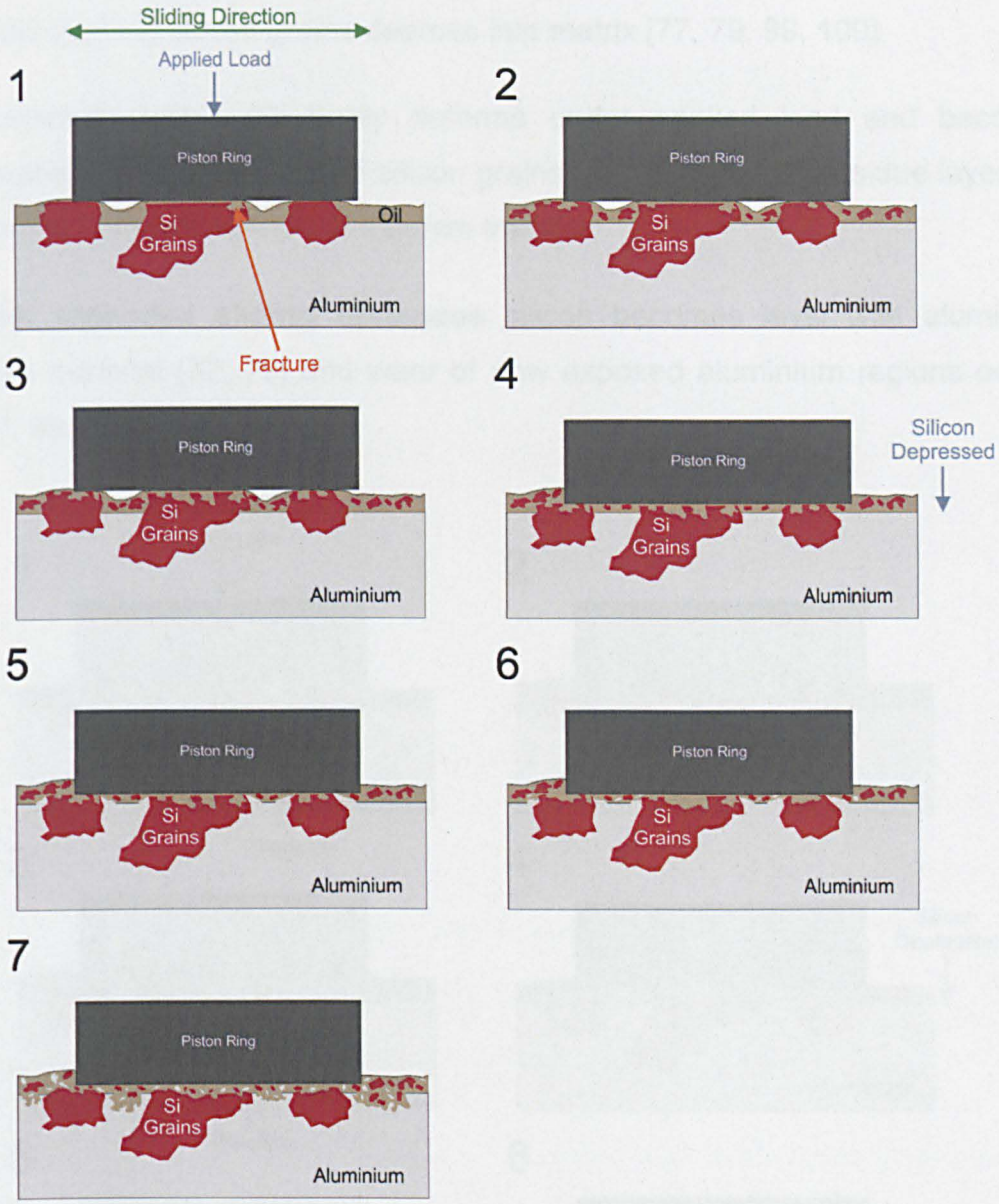

Figure 84: Heavy wear model of an aluminium-silicon substrate

5.7.2. Mild Wear

Mild wear on AluSil® was observed when ZDDP was used as lubricant. Figure 85 highlights the stages involved, and are described in detail below the image.

1. Some silicon grains fracture, reducing their size [99, 100]. If silicon grain size can be preserved, wear levels will not increase [99]

2. Fragments of silicon are created via wear and lead to abrasive wear of matrix and also silicon grains [99, 104]

3. Tribofilm forms on exposed silicon grains; ZDDP-based tribofilm is patchy and does not possess necessary shear strength to remain adhered. Tribofilm is removed and transferred to aluminium matrix as oil residue layer

4. Load carrying silicon grains depress into matrix [77, 79, 99, 100]

5. Aluminium matrix plastically deforms under applied load and becomes amassed around depressed silicon grains [77, 79, 100]. Oil residue layer has increased in volume due to tribofilm transfer

6. **With extended sliding distances** silicon becomes level with aluminium base material [77, 79] and wear of now exposed aluminium regions occurs [77, 99, 100]

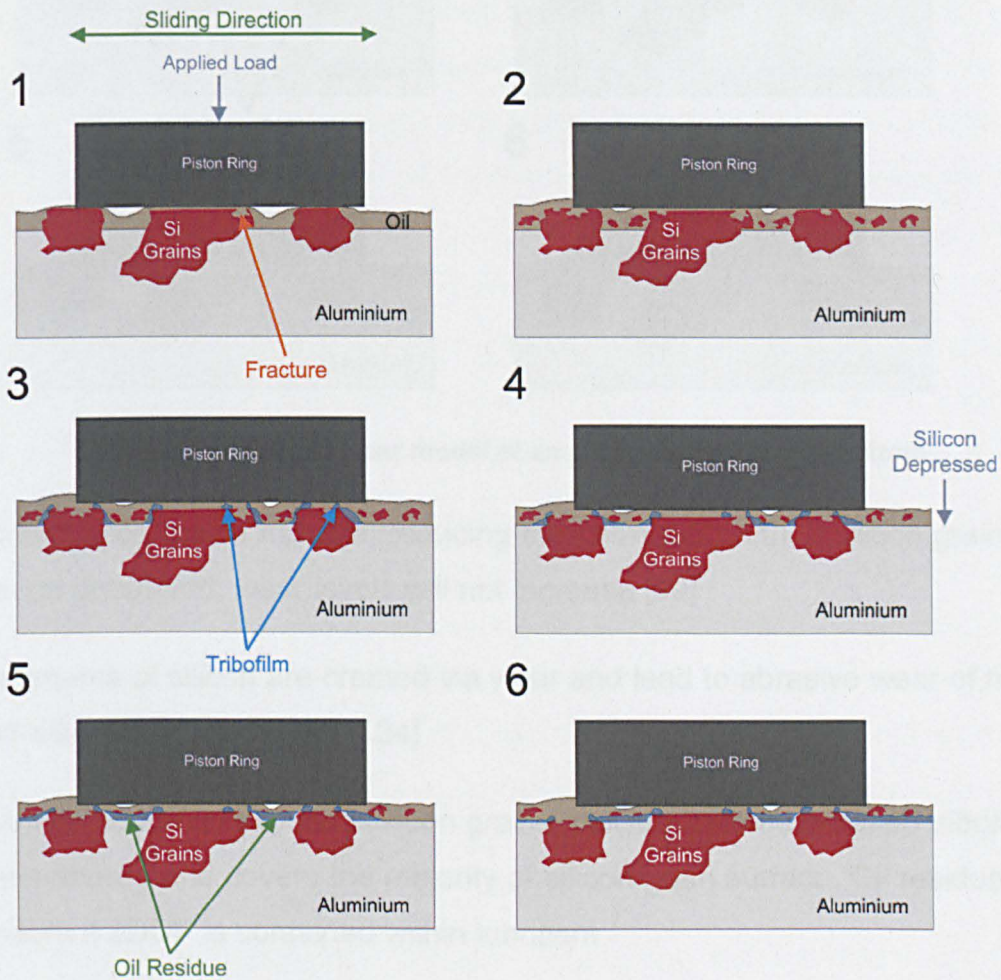

Figure 85: Mild wear model of an aluminium-silicon substrate

5.7.3. Ultra Mild Wear

Ultra mild wear was ascribed to the five remaining lubricants; Figure 86 highlights the different steps involved in this wear classification, with the six

stages described underneath the image. The lubricant used in Figure 86 was overbased calcium sulfonate.

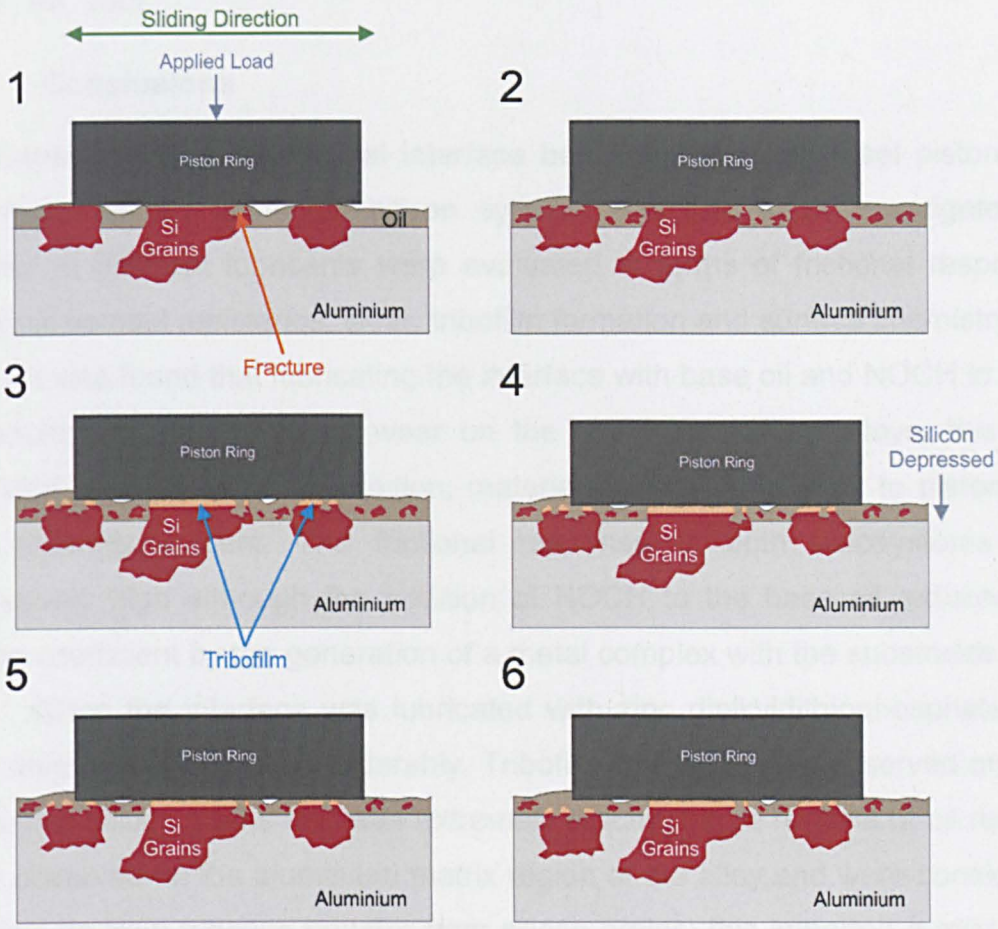

Figure 86: Ultra mild wear model of an aluminium-silicon substrate

1. Some silicon grains fracture, reducing their size [99, 100]. If silicon grain size can be preserved, wear levels will not increase [99]

2. Fragments of silicon are created via wear and lead to abrasive wear of matrix and also silicon grains [99, 104]

3. Tribofilm forms on exposed silicon grains; calcium sulfonate-based tribofilm is well adhered and covers the majority of silicon grain surface. Oil residue only evident if ZDDP is contained within lubricant

4. Load carrying silicon grains depress into matrix [77, 79, 99, 100]

5. Aluminium matrix plastically deforms under applied load and becomes amassed around depressed silicon grains [77, 79, 100].

6. **With extended sliding distances** silicon becomes level with aluminium base material [77, 79] and wear of now exposed aluminium regions occurs [77, 99, 100]

5.8. Conclusions

The lubrication of a tribological interface between chromium steel piston ring and hypereutectic aluminium-silicon cylinder liner has been investigated. A number of different lubricants were evaluated in terms of frictional response, electrical contact resistance, wear, tribofilm formation and surface chemistry.

It was found that lubricating the interface with base oil and NOCH in base oil resulted in high levels of wear on the aluminium-silicon alloys; this was classified as *high wear*. In addition, material transfer from alloy to piston ring was strikingly evident. The frictional response of both tribosystems was excessively high although the addition of NOCH to the base oil reduced the friction coefficient by the generation of a metal complex with the substrates.

When the interface was lubricated with zinc dialkyldithiophosphate, the wear level was reduced considerably. Tribofilm formation was observed only on protruding silicon grains and was extremely patchy. Large regions of oil residue were observed on the aluminium matrix region of the alloy and were considered to originate from tribofilm transfer from silicon grains; this imparted a *mild wear* grade to ZDDP. The lubrication of the tribosystem with ZDDP + NOCH resulted in identical frictional response to that afforded by ZDDP, but a marked improvement in film formation was observed with the addition of triethyl citrate. Indeed, tribofilms were fashioned exclusively on exposed silicon regions and resembled those which were typically obtained using ZDDP on ferrous surfaces. The tribofilms generated from ZDDP and ZDDP + NOCH on silicon grains were chemically identical to those found on ferrous surfaces, including the incident piston ring. The wear classification ascribed to ZDDP + NOCH was *ultra mild wear*, due to a heavy reduction in the oil residue layer on the substrate.

Calcium sulfonate and calcium sulfonate + NOCH displayed similar behaviour, except that the frictional response of the latter was markedly higher, which was accredited to the NOCH molecule competing with or interacting with OBCS. Further work carried out in chapter 6 identifies possible interactions between the two additives using ^{13}C labelled alternatives. Both lubricants generated tribofilms quickly on the surfaces of both piston ring and silicon

grains within the aluminium-silicon alloy. No tribofilm formation was witnessed on the aluminium regions within the alloy. Tribofilms generated on the aluminium-silicon substrate from either lubricant were calcium carbonate-based and possessed small amounts of sulphur towards the outer edges of the protective layers. These films were chemically identical to those fashioned on the piston ring substrate and were comparable to those obtained by other workers for ferrous surfaces. Both lubricants resided within the *ultra mild wear* classification grade.

ZDDP + calcium sulfonate and ZDDP + calcium sulfonate + NOCH behaved slightly differently in terms of their frictional response, the latter producing a plot which very much resembled calcium sulfonate + NOCH. Furthermore, the tribochemistry of both piston ring and aluminium-silicon substrate lubricated with ZDDP + calcium sulfonate + NOCH was very similar to calcium sulfonate + NOCH. The presence of small amounts of calcium phosphate within the depth profiles was the only difference between the two lubricants. Substrates lubricated with ZDDP + calcium sulfonate were calcium carbonate-based, as with OBCS, but also contained large amounts of calcium phosphate, this was most obvious on the ferrous piston ring. Lubricants ZC and ZCN were assigned the *ultra mild wear* classification.

This work has been the first of its kind to study the lubrication of an aluminium-silicon alloy with not only a detergent, but also with detergent + ZDDP. Tribofilm compositions on aluminium alloy and ferrous piston ring were devised and the wear results obtained were analysed in the context of published work in order to identify three wear classifications for the aluminium-silicon alloys, namely *heavy wear*, *mild wear* and *ultra mild wear*.

The next stage of this work will investigate the lubrication of representative forms of both silicon and aluminium regions of an aluminium-silicon alloy. This will be performed using silicon crystal to replicate the contact conditions on silicon grains within AluSil® and an aluminium alloy to simulate the aluminium matrix. Tribological experiments will be conducted using point contact setups, allowing for in-depth knowledge about tribological response, tribofilm formation, mechanical properties and tribochemistry of the interfaces to be deduced. The goal of this work will be to provide conclusive analysis as to the way in which boundary lubrication of a modern aluminium-silicon alloy occurs, by comparing data obtained herein with that observed in literature.

6. Silicon Crystal as a Model to Assess Tribochemistry of a Novel Antiwear Additive

6.1. Introduction

The formation of tribofilms on silicon grains within aluminium-silicon alloys has been documented previously [66] (chapter 5). However, due to the different material phases (section 3.3) and complicated wear mechanisms of Al-Si alloys [77, 79, 99, 100, 104], the frictional and wear performance of the tribofilms generated solely on the silicon regions of the alloy have yet to be fully evaluated. Furthermore, the method of film formation by overbased calcium sulfonate has not been hypothesised as yet.

If the contact conditions generated on the silicon grains in these aluminium alloys can be replicated, a greater range of analysis techniques can be employed in order to fully evaluate the mechanical and chemical properties of the protective layers. This would provide greater insight into the relationship between friction and wear and the mechanical and chemical properties of fashioned films. Therefore, film formation mechanisms by the various lubricant additives can be proposed as a result. Reproduction of silicon grain contact conditions has not been attempted previously and is a powerful tool since results obtained can be directly related to that of which will be observed on the seemingly important silicon grains within the modern aluminium alloy. In addition, through using labelled versions of calcium sulfonate and the NOCH molecule, film formation by the two molecules can be investigated in detail.

In this chapter, replication of silicon grains within the AluSil® alloy discussed in chapter 4 has been conducted using a silicon crystal. Test lubricants were analogous to those used in that tribosystem, except base oil and NOCH in base oil were not investigated due to their reported poor antiwear performance. Tribological results obtained from the silicon crystal tribosystem were related to tribofilm morphology and mechanical properties. These parameters were subsequently correlated to reported tribochemistry, with mechanisms of film formation proposed. Comparisons between aluminium alloy and silicon crystal have been made.

6.2. Aim and Objectives

6.2.1. Aim

- Replicate the contact conditions on silicon grains within the aluminium-silicon alloy previously investigated using a silicon crystal
- Present the experimental methodology for the lubrication of a tribological interface between silicon crystal and chromium steel pin

6.2.2. Objectives

- To evaluate the frictional and antiwear performance of various test oils
- To observe tribofilm formation on silicon crystal and measure the thickness and mechanical properties of these protective layers
- To analyse the chemistry of tribofilms, identifying similarities between results obtained using an aluminium-silicon alloy
- To correlate tribological performance to the tribochemistry of worn surfaces
- To devise mechanisms of film formation
- To identify which part(s) of the NOCH molecule are involved in film formation and hypothesise as to film generation

6.3. Tribology of Silicon Crystal

6.3.1. Materials

6.3.1.1. Silicon Crystal

In order to replicate the silicon grains found within an AluSil® substrate, a random orientation single crystal silicon substrate was obtained from Pi-KEM Ltd. The substrates were supplied with dimensions 7.0 mm x 7.0 mm x 3.5 mm (wxdxh). The samples possessed a very low surface roughness, with the R_a and R_q values for the substrates given in Table 24; these were obtained using a Taylor Hobson Form Talysurf 120L surface profilometer.

Parameter	Value
R_a	0.00904 µm
R_q	0.0139 µm

Table 24: Surface roughness of silicon crystal substrates

The mechanical properties of the silicon substrate were determined using nanoindentation, which was conducted using a Micro Materials Ltd NanoTest™ Platform One device. A maximum load and depth of 50 mN and 1000 nm obtained data from the substrate; the instrument would cease applying load if either parameter was attained. The loading / unloading rate was 0.5 mN / s. Data was collected from 100 indentation points, which were arranged in two columns, at a spacing 40 µm and 25 µm in the Y and Z axes per indentation point, respectively; the retraction distance for each indentation was 15 µm. The method used to determine the hardness and elastic modulus of the unworn silicon crystal substrate was that described in section 2.2.1.5, using the Poisson's ratio of silicon crystal given in Table 25.

The average data obtained for the substrate is shown in Table 25. For comparison, the equivalent average mechanical properties of the silicon grains within an unworn AluSil® substrate are listed. It is apparent that the hardness and elastic modulus values obtained for the single crystal substrate were very similar to those obtained for the silicon grains within AluSil®.

Parameter	Single Crystal Silicon	Silicon Grains within AluSil®
Poisson's Ratio	0.28 [260, 261]	0.28
Elastic Modulus (GPa)	149.0 ± 10.8	146.7 ± 10.7
Hardness (GPa)	11.0 ± 0.6	10.4 ± 1.9

Table 25: Mechanical properties of silicon crystal

6.3.1.2. Chromium Steel Pin

Replication of the material from which the piston ring was constructed was achieved using X17CrNi16-2 (EN 1.4057) martensitic stainless steel, manufactured into pin form. The rationale for this material selection was that this stainless steel contained a very similar chemical composition to that of the piston ring. As can be seen in Table 26, the two stainless steel substrates were identical in terms of their silicon, phosphorus and sulphur content.

The chromium and manganese content of the two substrates were also very similar. The main difference, however, was that the piston ring contained a greater amount of carbon and also molybdenum than the steel pin; in addition, the steel pin contained nickel.

	Chemical Composition (Wt. %)							
Substrate	**C**	**Si (Max.)**	**Mn**	**P (Max.)**	**S**	**Cr**	**Mo**	**Ni**
Piston Ring	0.95 - 1.20	1.00	≤1.00	0.04	≤0.015	16.0 - 18.0	0.40 - 0.80	0.00
Steel Pin	0.12 - 0.22	1.00	≤1.50	0.04	≤0.015	15.0 - 17.0	0.00	1.50 - 2.50

Table 26: Chemical composition of piston ring and steel pin substrates [221]

Steel pins were manufactured by Paterson Precision Ltd, each comprising 6.0 mm in length and 20.0 mm in diameter. The radius of curvature on the steel substrates was 90 mm ± 0.1 mm. Surface roughness of the steel pin substrates is given in Table 27, determined using a Taylor Hobson Form Talysurf 120L surface profilometer.

Parameter	Value
R_a	0.263 μm
R_q	0.353 μm

Table 27: Surface roughness of steel pin substrates

The steel pins were heat treated in order to increase their hardness to the greatest possible value, to facilitate replication of the very high surface hardness of the piston ring substrates (Table 28). As can be seen in Table 28, the hardness of the steel pins was 535 HV, which was greater than the bulk hardness of the piston rings, but less than that of the very hard surface layer. The elastic modulus and Poisson's ratio of the two stainless steels used for piston ring and steel pin substrates were identical (Table 28).

Parameter	Steel Pin	Piston Ring
Hardness (HV)	535	371 ± 0.5 (Bulk) 1051 ± 7.1 (Surface)
Elastic Modulus (GPa)	212 [221]	212 [221]
Poisson's Ratio	0.29 [222]	0.29 [222]

Table 28: Mechanical properties of steel pin

6.3.1.3. Lubricants

Six lubricants were evaluated using the steel pin and silicon crystal tribocouple (Table 29). The lubricating fluids used are those which were evaluated using the Al-Si tribosystem. However, because base oil and NOCH in base oil lubricants were determined to be poor lubricants of that tribocouple, these were not evaluated using the silicon crystal and steel pin tribosystem.

Lubricant		Mass % of Additive			Mass % of Base Oil	P.P.M. Phosphorus	Mass % Sulphated Ash
Name	Ref.	Secondary ZDDP	Calcium sulfonate	NOCH			
ZDDP	(Z)	0.50	0.00	0.00	99.50	500.00	0.08
ZDDP + NOCH	(ZN)	0.50	0.00	0.50	99.00	500.00	0.08
Calcium sulfonate	(C)	0.00	0.94	0.00	99.06	0.00	0.50
Calcium sulfonate + NOCH	(CN)	0.00	0.94	0.50	98.56	0.00	0.50
ZDDP + calcium sulfonate	(ZC)	0.50	0.94	0.00	98.56	500.00	0.50
ZDDP + calcium sulfonate + NOCH	(ZCN)	0.50	0.94	0.50	98.06	500.00	0.50

Table 29: Test lubricants for silicon crystal experiments

Calcium sulfonate was labelled using ^{13}C by Lubrizol® UK Ltd in order to determine which part of the detergent was responsible for the generation of a tribofilm on the silicon substrate. In this, the majority of the ^{12}C within the carbonate portion of the additive was replaced with the isotope ^{13}C. Due to problems with formulation, this labelling could only be completed with a 350 TBN version of the detergent. Therefore, experimentation was also completed using a conventional ^{12}C variant of the 350 TBN additive to allow for direct comparisons between labelled and non-labelled lubricants.

Similarly, to identify which parts of the NOCH molecule were involved in film formation, three labelled versions of triethyl citrate were prepared by Lubrizol® UK Ltd. The first two were labelled with ^{13}C in two different locations within the molecule, as shown in Figure 87. NOCH #1 was labelled at certain

CH_2 locations in the additive, whereas labelled NOCH #2 contained ^{13}C at the specific C=O positions (Figure 87).

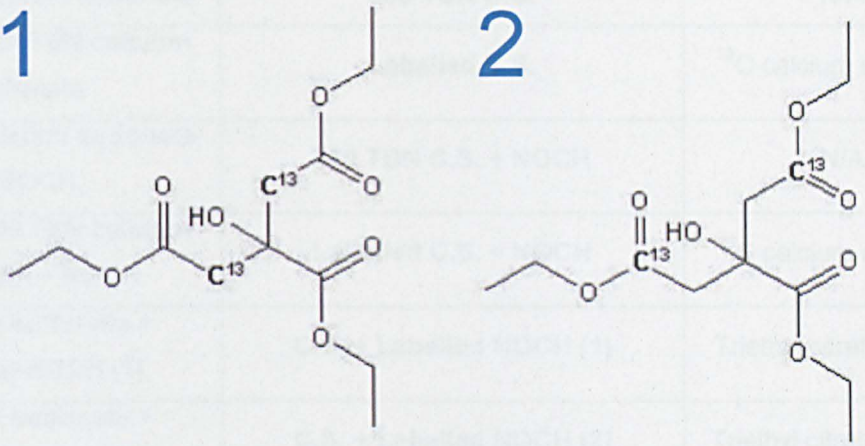

Figure 87: ^{13}C Labelled versions of triethyl citrate (NOCH)

The final labelled version of NOCH was that of which is shown in Figure 88. As can be seen in labelled triethyl citrate #3, hydrogen in the three ethyl sections of the molecule have been replaced with deuterium, which is an isotope of hydrogen [262].

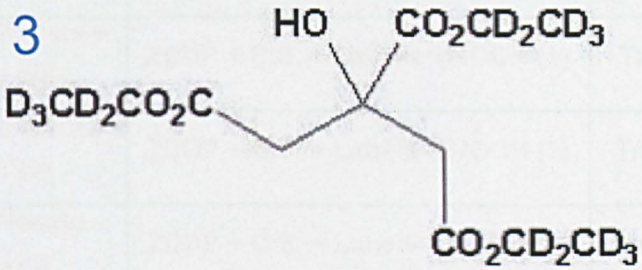

Figure 88: Deuterium labelled version of triethyl citrate (NOCH)

Therefore, in addition to the conventional test lubricants shown in Table 29, a further set of lubricating fluids were devised which incorporated 350 TBN calcium sulfonate, ^{13}C labelled calcium sulfonate and the three labelled versions of NOCH, respectively (Table 30). The interactions between ZDDP, calcium sulfonate and NOCH were seen as important in understanding the tribochemical mechanisms of the various additives. Therefore, lubricants were devised which contained labelled calcium sulfonate and labelled NOCH, respectively (Table 30).

Lubricant	Abbreviation	Labelled Section of Lubricant
350 TBN calcium sulfonate	350 TBN C.S.	N/A
Labelled 350 TBN calcium sulfonate	Labelled C.S.	^{13}C calcium sulfonate
350 TBN calcium sulfonate + NOCH	350 TBN C.S. + NOCH	N/A
Labelled 350 TBN calcium sulfonate + NOCH	Labelled C.S. + NOCH	^{13}C calcium sulfonate
Calcium sulfonate + Labelled NOCH (1)	C.S. + Labelled NOCH (1)	Triethyl citrate - $^{13}CH_2$
Calcium sulfonate + Labelled NOCH (2)	C.S. + Labelled NOCH (2)	Triethyl citrate - $^{13}C=O$
Calcium sulfonate + Labelled NOCH (3)	C.S. + Labelled NOCH (3)	Triethyl citrate - CD_2CD_3
ZDDP + 350 TBN calcium sulfonate + NOCH	ZDDP + 350 TBN C.S. + NOCH	N/A
ZDDP + Labelled 350 TBN calcium sulfonate + NOCH	ZDDP + Labelled C.S. + NOCH	^{13}C calcium sulfonate
ZDDP + calcium sulfonate + Labelled NOCH (1)	ZDDP + C.S. + Labelled NOCH (1)	Triethyl citrate - $^{13}CH_2$
ZDDP + calcium sulfonate + Labelled NOCH (2)	ZDDP + C.S. + Labelled NOCH (2)	Triethyl citrate - $^{13}C=O$
ZDDP + calcium sulfonate + Labelled NOCH (3)	ZDDP + C.S. + Labelled NOCH (3)	Triethyl citrate - CD_2CD_3

Table 30: Labelled test lubricants

6.3.2. Methods

6.3.2.1. Experimental

Tribological experiments were conducted using a Cameron Plint TE77 reciprocating tribometer. In order to replicate the documented contact conditions experienced by the silicon grains within the AluSil® substrate, a point contact was employed. Silicon crystal and steel pin substrates were submerged in acetone and placed in an ultrasonic bath for 10 minutes prior to experimentation.

The silicon crystal was placed into the non-reciprocating section of the tribometer and fastened into the bottom clamp within the heated oil bath. The steel pin was secured into the top clamp on the rig. Alignment of the two test substrates was paramount as to ensure the steel pin was directly incident on

the silicon crystal sample. The contact was also aligned vertically so that the pin was traversing a level section of the silicon substrate throughout one stroke of the reciprocating arm. As with the aluminium-silicon and steel piston ring contact, the stroke length of the tribometer was 5 mm and the frequency of oscillation was 20 Hz. The test oil volume was 10 ml, which was heated to 100 °C. The test duration was 2 hours and each oil was evaluated three times, in order to create an average set of results.

The equivalent elastic modulus for the tribosystem, E^*, was calculated for the contact by using Equation 8 and the values for both Poisson's ratio, ν, from the elastic modulus, E, of silicon crystal (Table 25) and steel pin (Table 28). Table 31 shows the calculated equivalent elastic modulus for the silicon crystal and steel pin tribocouple.

$$\frac{1}{E^*} = \left(\frac{1-(\upsilon_{Si}{}^2)}{E_{Si}}\right) + \left(\frac{1-(\upsilon_{Steel}{}^2)}{E_{Steel}}\right)$$

Equation 14: Equivalent elastic modulus of silicon tribosystem [233]

In order to calculate the maximum point contact pressure, P_0, applied to the silicon crystal, Equation 15 and Table 31 were used. Where W = applied load, E^* = equivalent elastic modulus and R^* = radius of curvature of steel pin. The mean point contact pressure, P_m, was deduced using Equation 16. Resultant contact pressures are given in Table 31.

$$P_0 = \sqrt[3]{\frac{6WE^{*2}}{R^{*2}\pi^3}}$$

Equation 15: Maximum Hertzian point contact pressure [233]

$$P_m = \frac{2}{3} \times P_0$$

Equation 16: Mean Hertzian line contact pressure [233]

Minimum film thickness (Table 31), h_{min}, for the silicon crystal and steel pin tribosystem was calculated using Equation 17 and Table 31. Where R^* = radius of curvature of steel pin, α = pressure - viscosity coefficient of lubricant (Table 20), η_0 = viscosity of lubricant at ambient temperature (Table 20), U = entrainment speed, E^* = equivalent elastic modulus, and W = applied load.

$$h_{min} = 1.79x\left(R^{*0.47}\right)\left(\alpha^{0.49}\right)\left(\eta_0{}^{0.68}\right)\left(U^{0.68}\right)\left(E^{*-0.12}\right)\left(W^{-0.07}\right)$$

Equation 17: Minimum Hertzian point contact film thickness [79]

In order to determine the lubrication regime occurring within the tribosystem, Equation 18 was utilised. This equation calculated the lambda ratio, λ, using the known minimum film thickness and R_q values of the two substrates (Table 24 and Table 27, respectively). As can be seen in Table 31, the lambda ratio predicts the boundary lubrication regime will dominate.

$$\lambda = \frac{h_{min}}{\sqrt{\left(\left(R_{q(Silicon)}\right)^2\right) + \left(\left(R_{q(Steel\ Pin)}\right)^2\right)}}$$

Equation 18: Lambda ratio of silicon tribosystem [14]

Variable	Value
Equivalent Elastic Modulus	95 GPa
Radius of Curvature	90 x 10^{-3} m
Applied Load	7 N
Maximum Contact Pressure	115 MPa
Mean Contact Pressure	77 MPa
Entrainment Speed	0.2 m / s
Film Thickness	2.41 x 10^{-2} μm
Lambda Ratio	6.8 x 10^{-2}

Table 31: Silicon crystal point contact conditions

Friction and electrical contact voltage data were collected using the setup described previously (section 4.3.3.1). 1000 samples per second were recorded, with the data interval every minute for the first five minutes and every five minutes thereafter. Average variability with regards to frictional response and ECV for the test lubricants was, on average, 3 % and 1 %, respectively.

6.3.2.2. Replication of Contact Conditions

As shown in literature [66, 77, 79, 98-100], the load placed upon an aluminium-silicon alloy is believed to be supported by silicon grains within the substrate. Indeed, it has been reported that values of ~ 700 MPa [79] or even ~ 1500 MPa [100] can be generated on silicon regions when a hypereutectic aluminium-silicon alloy is subject to wear testing.

The contact pressures shown in Table 31 compare well with those calculated for the AluSil® substrate, if silicon grains were to bear the load in the contact (Table 32). The contact conditions on silicon grains within the alloy were determined by measuring the volumetric coverage of protruding silicon grains in

AluSil® using a Veeco WYKO® NT3300S profiling system. Using VSI mode, ten areas within AluSil®, each measuring 0.9 mm x 1.2 mm, were analysed using 5.2 x magnification. Vison32® software subsequently determined that the silicon regions accounted for 30 % ± 6 % of the aluminium substrate surface. This resulted in a line contact length of approximately 2 mm on the aluminium alloy. Consequently, contact pressures were calculated using the line contact equations in section 4.3.3.1 and the elastic modulus and Poisson's ratio of the silicon grains (Table 25).

By comparing Table 31 with Table 32, it is possible to conclude that the maximum and mean applied contact pressures applied to the silicon crystal substrate were 30 MPa and 10 MPa greater, respectively, than those predicted on the silicon grains within the AluSil® material. This was ideal because the intention of the silicon crystal experiments was to identify whether tribofilm formation occurred on the non-ferrous substrate, whilst also providing an indication of the wear protection imparted by the lubricants.

Variable	Value
Maximum Contact Pressure	85 MPa
Mean Contact Pressure	67 MPa

Table 32: Calculated contact pressures for silicon grains in AluSil® supporting load

Comprehensive justification for the usage of silicon crystal as a replicate for silicon grains within an aluminium-silicon alloy is provided in section 7.6 of this thesis.

6.3.2.3. Labelled Additives

The lubricants shown in Table 30 were evaluated using the setup described in section 6.3.2.1. Experiments were conducted twice per lubricant; variability was identical to that reported in the abovementioned section. The intention of this work was to determine the film formation mechanisms of OBCS and triethyl citrate and thus, surface topography and wear rates were not sought.

6.3.2.4. Surface Analysis

6.3.2.4.1. SEM

Scanning electron microscopy was performed using a Philips XL30 environmental scanning electron microscope. Heptane was used to clean substrates prior to analysis.

Images of the silicon crystal substrate were obtained using a 15.0 kV acceleration voltage and a spot size of 8.0; these values were determined to be optimum for the semi conductor. SEM of the steel pins was carried out using an acceleration voltage of 20.0 kV and a 6.0 spot size. The working distance was maintained at 12.0 mm when analysing either substrate.

6.3.2.4.2. EDS

Energy dispersive x-ray spectroscopy was conducted on steel pins during SEM analysis. Data was obtained and analysed using the INCA microanalysis system connected to the scanning electron microscope. The working distance of the SEM was 12.0 mm, with a 20.0 kV acceleration voltage and a 5.0 spot size. Analysis was conducted using the Point and ID type of operation using a 1500 x magnification.

6.3.2.4.3. AFM

Atomic force microscopy data was obtained from silicon crystal substrates using a Veeco Explorer scanning probe microscope. The scan rate of the apparatus was 200.32 μm s^{-1}, with a 400 resolution; the scan range was 50 μm x 50 μm. Substrates were cleaned with Heptane prior to AFM analysis. Raw data was processed using the SPMLab software, in order to remove any noise from obtained images. Each image was levelled, to generate images of the silicon crystal substrate which would indicate height differences within the wear scar. Shading of these images allowed for a detailed depiction of the substrate surface.

Film thicknesses were obtained by applying a solution of ethylenediaminetetraacetic acid (EDTA) to the tribofilm on the silicon crystal samples. This process has been conducted previously on ferrous surfaces [177, 252]. EDTA is used because it is a chelating agent [252] and would easily remove the ZDDP [252] and also calcium [177] based tribofilms from the substrate surface. As with [177, 252], 0.05 M of EDTA within distilled water was prepared and applied to the tribofilm using a pipette. The solution was left on the substrate for one minute, with the excess removed using paper towel. AFM images were obtained across the newly exposed edge of the respective tribofilms within the wear scar on the substrate. A large scan area of 100 μm x 100 μm and a scan rate of 400.64 μm s^{-1} were used to obtain atomic force images. Using the software provided with the AFM, the step height between

substrate surface and tribofilm were measured in ten locations. This data was averaged and a standard deviation computed in order to calculate the thickness of each tribofilm.

6.3.2.4.4. Nanoindentation

The reduced elastic modulus of the tribofilms generated using the conventional test lubricants listed in Table 29 were determined using a Micro Materials Ltd NanoTest™ Platform One device.

One sample per lubricant was analysed using this instrument. Data was obtained from a setup of 25 columns comprising 4 rows of indentations with a spacing of 25 µm in the Y axis, and a 40 µm spacing in the Z axis; the retraction distance per indentation was 15 µm. In order to minimise the effects of the substrate mechanical properties on the results, a maximum load of 15 mN was employed. The maximum depth was set to 200 nm, which was determined after a series of experiments found that lower penetration depths did not produce repeatable load-displacement curves because of measurement limitations of the NanoTest™ Platform, which stopped appyling the load if the upper limit for either variable was obtained. The loading / unloading rate was 0.1 mN / s.

As the Poisson's ratio for the tribofilms were not known, the elastic modulus for each protective layer could not be calculated. Instead, Equation 19 was utilised, whereby the reduced elastic modulus for the various tribofilms, E^r_f, was determined.

$$\frac{1}{\left(2E^r_{app}a\right)} = \left[\frac{1}{1+\left(\frac{2t}{\pi a}\right)}\left(\frac{t}{\pi a^2 E^r_f} + \frac{1}{2aE^r_s}\right)\right]^{-1}$$

Equation 19: Indentation modulus of tribofilm [263]

This equation took into account the reduced elastic modulus at each indentation point for tribofilm and substrate, E^r_{app}, and the reduced elastic modulus of the silicon crystal substrate, E^r_s, which was determined to be 161.7 GPa ± 11.7 GPa using the data in section 6.3.1.1 and Equation 20.

$$\frac{E_s}{(1-\upsilon_s^2)} = \left[\frac{1}{E^r} - \frac{(1-\upsilon_i^2)}{E_i}\right] = E^r_s$$

Equation 20: Reduced elastic modulus of substrate [25, 152]

The radius of the *Berkovich* type indenter, a, was 100 nm [23, 66] and the average thickness of each tribofilm, t, in metres, was determined using the

AFM technique stated in section 6.3.2.4.3. Solving Equation 19 for E^r_f resulted in the calculation of a reduced modulus for each indentation point on a given substrate. The data was averaged and a standard deviation computed for the tribofilms generated from the six test lubricants in Table 29.

6.3.2.4.5. SIMS

Mini secondary ion mass spectrometry of the silicon crystal substrates was conducted using a Millbrook Mini SIMS MC 300 MKII device. The area of analysis on silicon crystal substrates was approximately 70 µm x 70 µm. Positive and negative ion static analysis scans were obtained using a range of 2 m / z - 200 m / z, with a step of 0.2 m / z and a dwell time of 0.01 seconds. For labelled NOCH containing lubricants, a scan range of 2 m / z - 300 m / z was employed. Three scans were conducted in each location of interest in both positive and negative ion modes, in order to reduce noise. A total of ten static scans in both polarities were obtained from each substrate. Three scans in both positive and negative modes of analysis were conducted outside the wear scar on each substrate. Static analysis data was averaged and placed in graphical form using Microsoft® Excel®.

Depth profiling was completed within the tribofilm on each substrate using an area measuring ~ 260 µm x 260 µm. Both positive and negative ion depth profiles were acquired from the tribofilm on each substrate. Separate areas of analysis were employed with each depth profile. The dwell time was 2.19 seconds per atomic mass unit analysed and 200 repeats were conducted. Data was entered into Microsoft® Excel® where it was analysed and placed in chart form.

Time-of-Flight SIMS analysis of tribofilms was conducted using a ToF-SIMS IV apparatus, in order to obtain high mass resolution data regarding the chemical nature of a tribofilm. The area of analysis was maintained at ~ 200 µm x 200 µm throughout static analysis and depth profiling, with a range of 0 m / z - 800 m / z employed. Data was obtained from the device using IONSPEC software, which was subsequently analysed and imported into Microsoft® Excel® for conversion into chart form.

6.3.2.5. Wear Measurement

Wear was measured on both the silicon crystal and steel pin using a Reichert Jung Polyvar MET™ light microscope employing a 4 x magnification. Motic®

Images Plus 2.0 software supplied with the apparatus obtained data using a Motic® MC V3 digital camera connected to the microscope. The software was calibrated in order to accurately measure areas of importance.

On the silicon crystal substrates, the wear scar width (WSW) in millimetres, was measured, as this is related to the antiwear ability of the lubricant [184]. Motic® Images Plus software was used to obtain three images of the wear scar per substrate, with the WSW measured in each location. All three repeats of the test lubricants listed in Table 29 were analysed, and the resulting WSW data averaged and a standard deviation computed.

To calculate the dimensional wear coefficient on the steel pins, an image was obtained from each of the three repeats of the six test lubricants in Table 29. Motic® Images Plus was used to measure the diameter of the wear scar on the steel pins, in mm^2. The volume loss per steel pin was determined using Equation 21, where V = volume loss (m^3), R^* = radius of curvature of the steel pin (m) (Table 33) and d = average diameter of the wear scar (m).

$$V = \frac{\pi(d)^4}{64R^*}$$

Equation 21: Volume loss on steel pin [264]

The dimensional wear coefficient for the steel pin was calculated using Equation 22, where K = dimensional wear coefficient, s = sliding distance and W = applied load. The data used to determine the dimensional wear coefficient is shown in Table 33.

$$K = \frac{V}{sW}$$

Equation 22: Dimensional wear coefficient [265]

Variable	Value
R^*	90×10^{-3} m
s	1440 m
W	7 N

Table 33: Data used to calculate dimensional wear coefficient for steel pins

The dimensional wear coefficients for all three steel pins per test lubricant were averaged and a standard deviation created using Microsoft® Excel®; results were subsequently placed into chart form.

7. Results and Discussion of Silicon Crystal as a Model to Assess Tribochemistry of a Novel Antiwear Additive

7.1. Introduction

This chapter presents and discusses the tribological, topographical and tribochemical results obtained from the lubrication of a silicon substrate using different test oils.

7.2. Friction Coefficients

7.2.1. Conventional Lubricants

The friction coefficients generated using the non-labelled lubricants are shown in Figure 89. All plots exhibited the same trend of decreasing from an initially high value of μ to a lower final reading. ZDDP had the greatest coefficient of friction in the tribosystem and the addition of NOCH reduced the frictional response. Lubricant ZC decreased the friction coefficient markedly compared to the sole use of the antiwear additive. Calcium sulfonate further reduced the frictional response of the silicon crystal and steel pin tribosystem, with the addition of NOCH to overbased calcium sulfonate not affecting the coefficient of friction. Lubricant ZCN behaved similarly to both OBCS and OBCS + NOCH throughout experimentation.

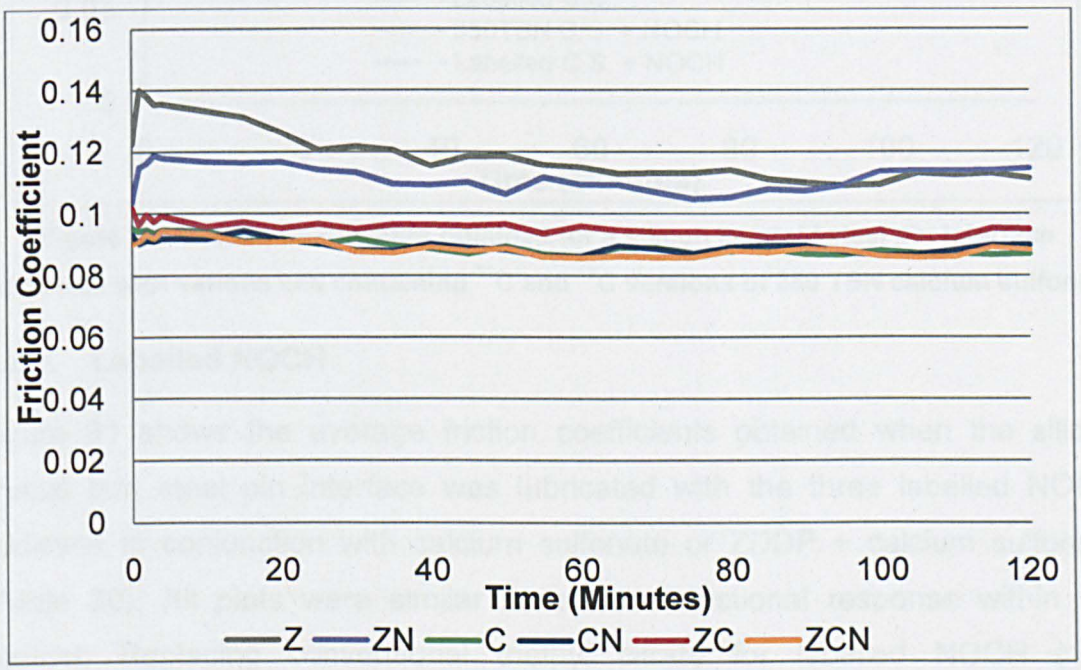

Figure 89: Friction coefficients obtained for a silicon crystal / steel pin interface lubricated with various oils

7.2.2. 350 TBN and ^{13}C Overbased Calcium Sulfonate

Figure 90 shows the frictional response of the tribosystem when the contact was lubricated with fluids containing 350 TBN calcium sulfonate and the ^{13}C type of this detergent. Of those lubricants shown, the lowest frictional response in the contact was imparted by 350 TBN calcium sulfonate. The addition of NOCH to the 350 TBN detergent increased the coefficient of friction in the tribosystem, which further enhanced with ZDDP + 350 TBN OBCS + NOCH. In comparison with conventional 400 TBN versions of OBCS (section 7.2.1), the 350 TBN variant decreased the coefficient of friction in the silicon crystal and steel pin interface. The substitution of the 350 TBN detergent for labelled calcium sulfonate increased the frictional response of the tribosystem.

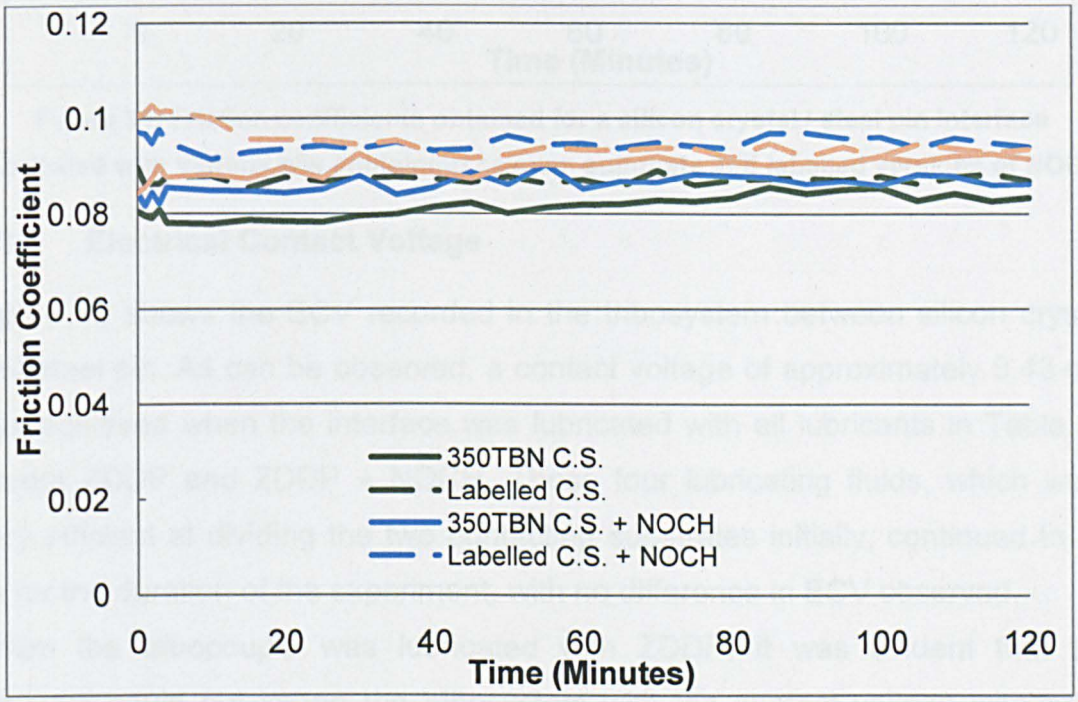

Figure 90: Friction coefficients obtained for a silicon crystal / steel pin interface lubricated with various oils containing ^{12}C and ^{13}C versions of 350 TBN calcium sulfonate

7.2.3. Labelled NOCH

Figure 91 shows the average friction coefficients obtained when the silicon crystal and steel pin interface was lubricated with the three labelled NOCH additives in conjunction with calcium sulfonate or ZDDP + calcium sulfonate (Table 30). All plots were similar in terms of frictional response within the contact. Replacing conventional triethyl citrate for labelled NOCH (1-3) increased the value of μ compared to calcium sulfonate + NOCH and ZDDP + calcium sulfonate + NOCH, respectively (section 7.2.1).

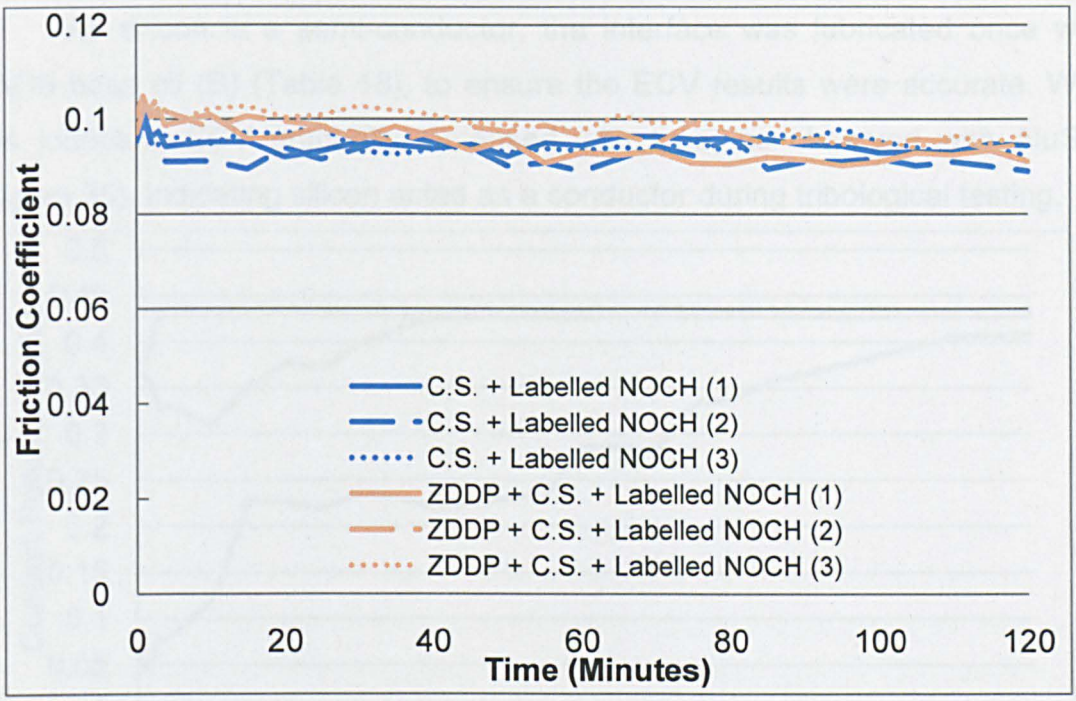

Figure 91: Friction coefficients obtained for a silicon crystal / steel pin interface lubricated with various oils containing calcium sulfonate and labelled versions of NOCH

7.3. Electrical Contact Voltage

Figure 92 shows the ECV recorded in the tribosystem between silicon crystal and steel pin. As can be observed, a contact voltage of approximately 0.43 mV was achieved when the interface was lubricated with all lubricants in Table 29 except ZDDP and ZDDP + NOCH. Those four lubricating fluids, which were very efficient at dividing the two contacting substrates initially, continued to do so for the duration of the experiment, with no difference in ECV observed.

When the tribocouple was lubricated with ZDDP, it was evident that the lubricant could not impart the tribosystem with the contact voltage witnessed when using calcium sulfonate-based lubricants. Indeed, an initial electrical contact voltage of 0.37 mV soon fell to a minimum value of 0.31 mV after 10 minutes of experimentation. Separation of the two substrates increased from this point, gradually increasing a maximum value of 0.43 mV after 65 minutes of testing; after which the contact voltage did not alter.

ZDDP + NOCH dramatically improved the ECV observed in the silicon crystal and steel pin tribosystem, compared to lubricating the interface with ZDDP. The starting electrical contact voltage recorded for ZDDP + NOCH was 0.38 mV, very similar to that obtained with ZDDP alone. Thereafter, however, the ECV value rapidly increased to 0.43 mV after 4 minutes of experimentation, where it remained for the entirety of the test.

As silicon is a semi-conductor, the interface was lubricated once with PAO6 base oil (B) (Table 18), to ensure the ECV results were accurate. With this lubricant, ECV gradually increased with time, as observed with AluSil® (Figure 35), indicating silicon acted as a conductor during tribological testing.

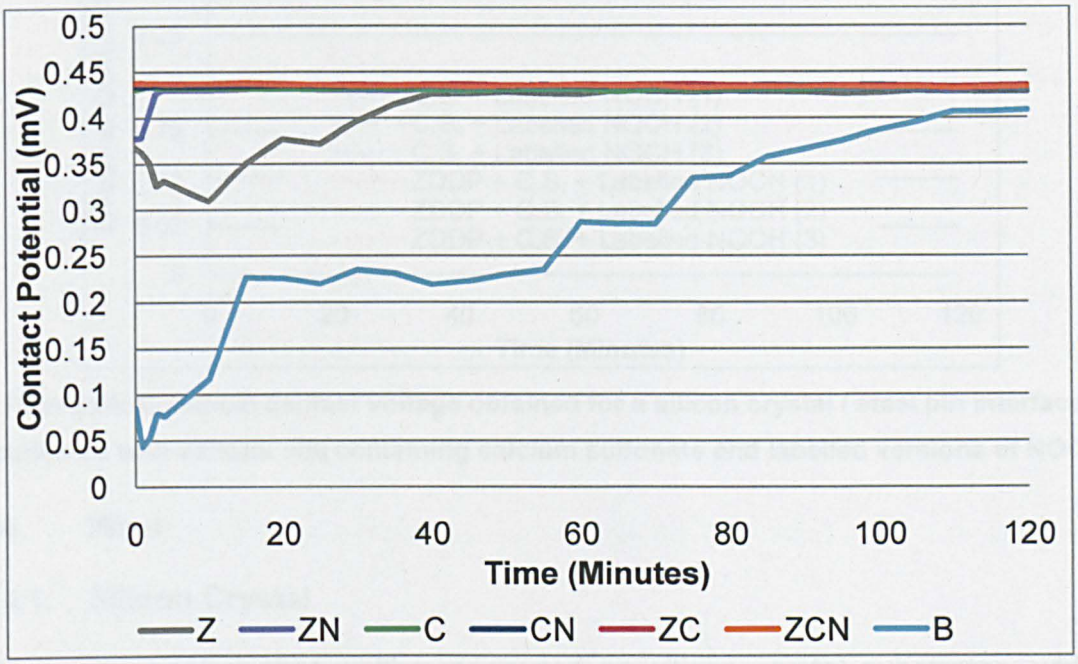

Figure 92: Electrical contact voltage obtained for a silicon crystal / steel pin interface lubricated with various oils

As shown in Figure 93 and Figure 94, electrical contact voltage was recorded for experiments conducted using lubricants comprised of either 350 TBN calcium sulfonate or labelled NOCH. Full separation of substrates was witnessed as soon as experimentation started, and remained here thereafter.

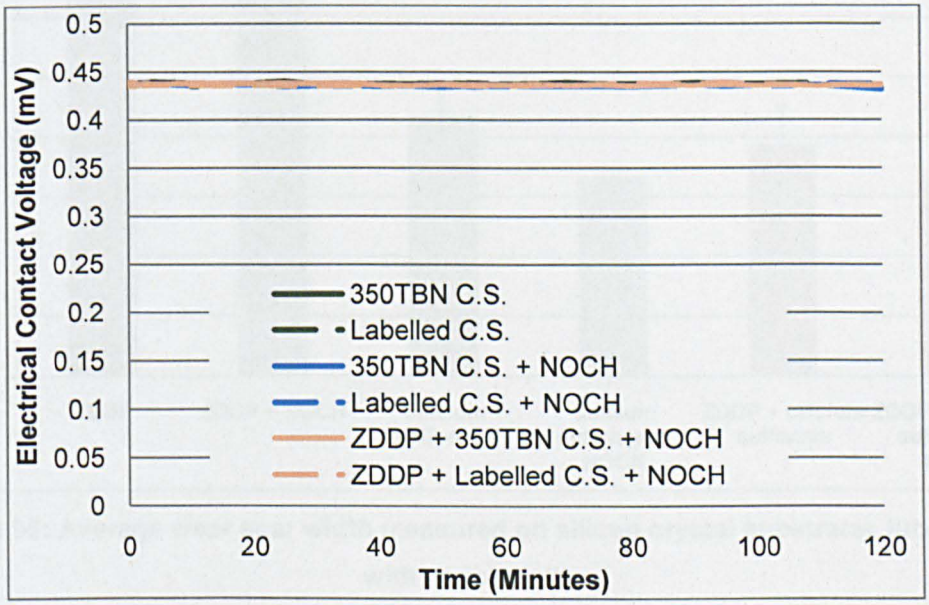

Figure 93: Electrical contact voltage obtained for a silicon crystal / steel pin interface lubricated with various oils containing ^{12}C and ^{13}C versions of 350 TBN calcium sulfonate

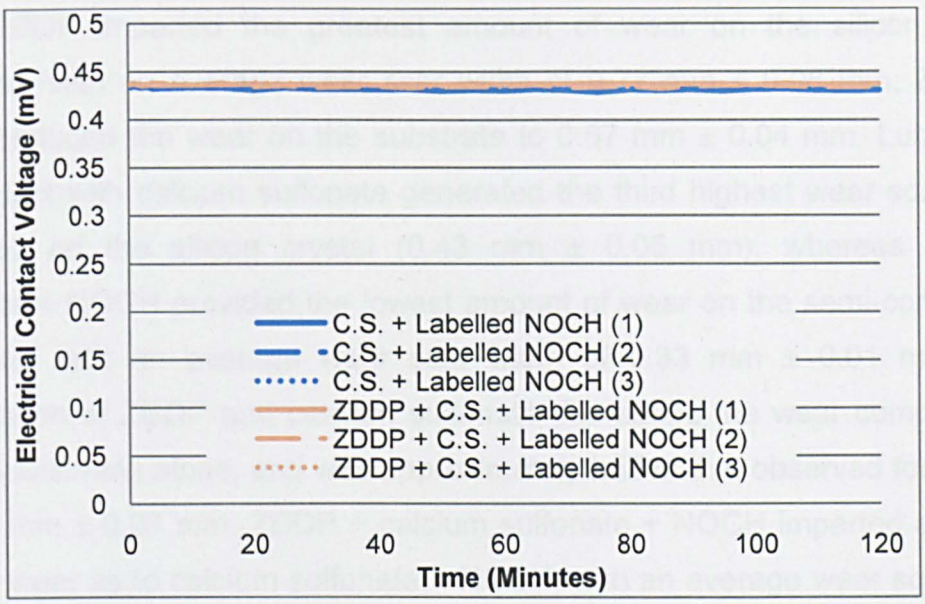

Figure 94: Electrical contact voltage obtained for a silicon crystal / steel pin interface lubricated with various oils containing calcium sulfonate and labelled versions of NOCH

7.4. Wear

7.4.1. Silicon Crystal

The average wear scar widths measured on silicon crystal substrates, which had been lubricated with those fluids given in Table 29, are shown in Figure 95.

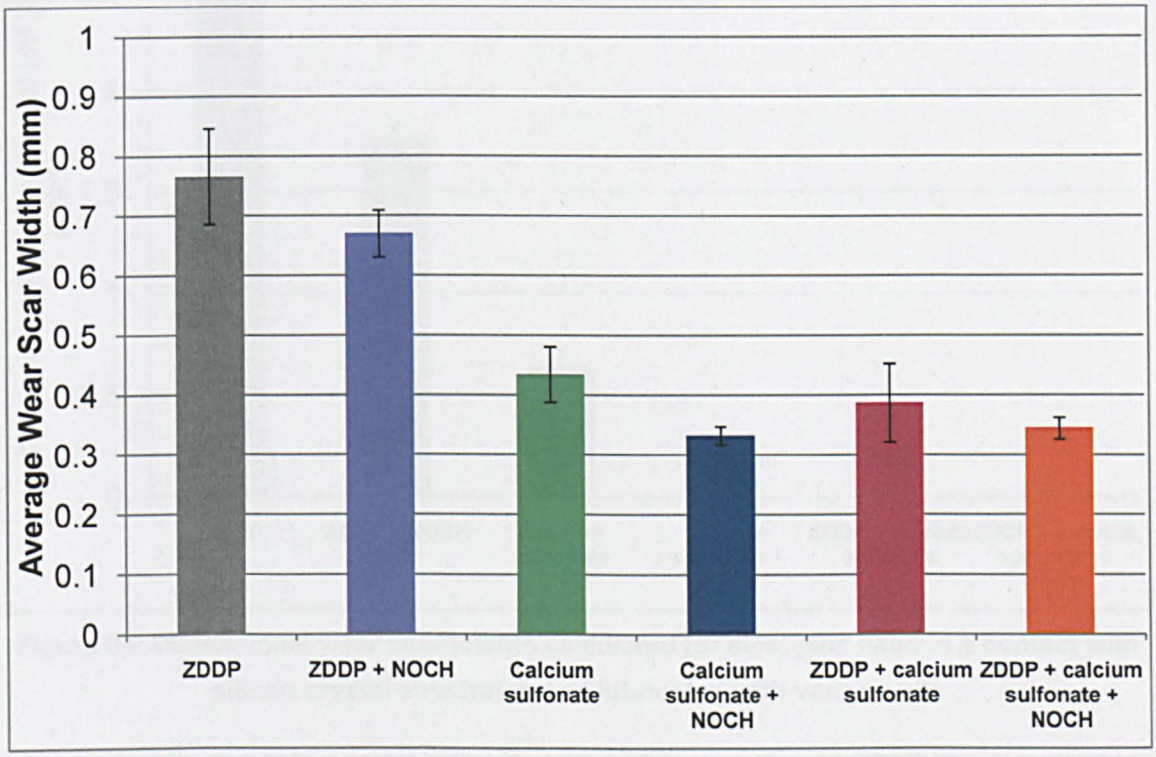

Figure 95: Average wear scar width measured on silicon crystal substrates lubricated with various oils

ZDDP imparted the greatest amount of wear on the silicon crystal substrate, with an average wear scar width of 0.77 mm ± 0.08 mm; ZDDP + NOCH reduced the wear on the substrate to 0.67 mm ± 0.04 mm. Lubricating the contact with calcium sulfonate generated the third highest wear scar width observed on the silicon crystal (0.43 mm ± 0.05 mm), whereas calcium sulfonate + NOCH provided the lowest amount of wear on the semi-conductive substrate, with an average wear scar width of 0.33 mm ± 0.01 mm. The combination of ZDDP and calcium sulfonate decreased the wear compared to calcium sulfonate alone, and was approximately half of that observed for ZDDP, at 0.39 mm ± 0.07 mm. ZDDP + calcium sulfonate + NOCH imparted a similar level of wear as to calcium sulfonate + NOCH, with an average wear scar width of 0.34 mm ± 0.02 mm.

7.4.2. Steel Pin

The dimensional wear coefficients calculated for the steel pins are shown in Figure 96.

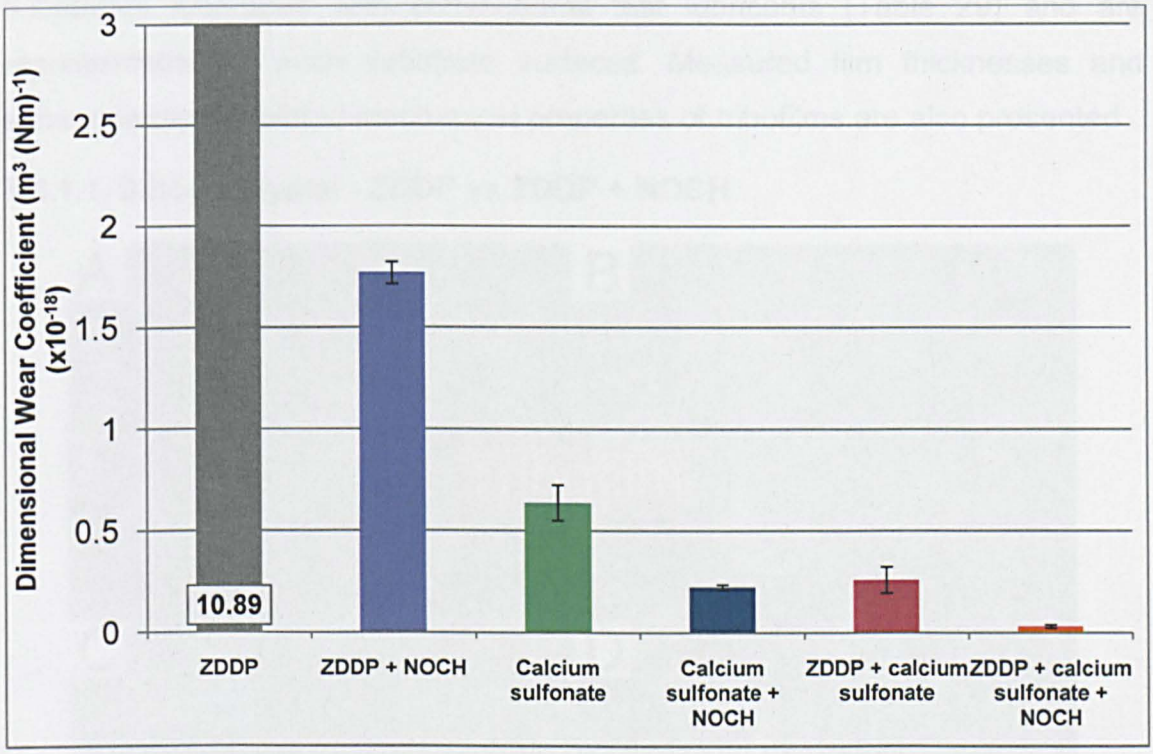

Figure 96: Dimensional wear coefficients calculated for steel pins used in a contact with silicon crystal substrates and lubricated with various oils

As can be observed, lubricating the tribosystem with ZDDP generated by far the greatest wear coefficient, with a value of 10.89 x 10^{-18} m^3 $(Nm)^{-1}$ ± 2.71 x 10^{-18} m^3 $(Nm)^{-1}$. The dimensional wear coefficient, on average, reduced by 84 % to 1.77 x 10^{-18} m^3 $(Nm)^{-1}$ ± 0.05 x 10^{-18} m^3 $(Nm)^{-1}$ when the contact was

lubricated with ZDDP + NOCH. Calcium sulfonate reduced the dimensional wear coefficient further, to 0.64 x 10^{-18} m^3 $(Nm)^{-1}$ ± 0.09 x 10^{-18} m^3 $(Nm)^{-1}$. When lubricating the contact with calcium sulfonate + NOCH, wear on the steel pin was reduced to the second lowest of any test lubricant to 0.23 x 10^{-18} m^3 $(Nm)^{-1}$ ± 0.01 x 10^{-18} m^3 $(Nm)^{-1}$. Lubricating the tribosystem with ZDDP + calcium sulfonate was, as seen on the silicon crystal, lower than both ZDDP and calcium sulfonate alone (0.26 x 10^{-18} m^3 $(Nm)^{-1}$ ± 0.06 x 10^{-18} m^3 $(Nm)^{-1}$). The lowest dimensional wear coefficient on the steel pin was obtained when the tribocouple was lubricated with ZDDP + calcium sulfonate + NOCH. Indeed, the value of the wear coefficient was 0.03 x 10^{-18} m^3 $(Nm)^{-1}$ ± 0.01 x 10^{-18} m^3 $(Nm)^{-1}$, considerably smaller than that obtained for the other lubricants.

7.5. Surface Analysis of Worn Silicon Crystal and Steel Pin

7.5.1. Surface Topography and Morphology

This section of the thesis presents images obtained from AFM and SEM of substrates lubricated with conventional test lubricants (Table 29) and are representative of worn substrate surfaces. Measured film thicknesses and subsequently calculated mechanical properties of tribofilms are also presented.

7.5.1.1. Silicon Crystal - ZDDP vs ZDDP + NOCH

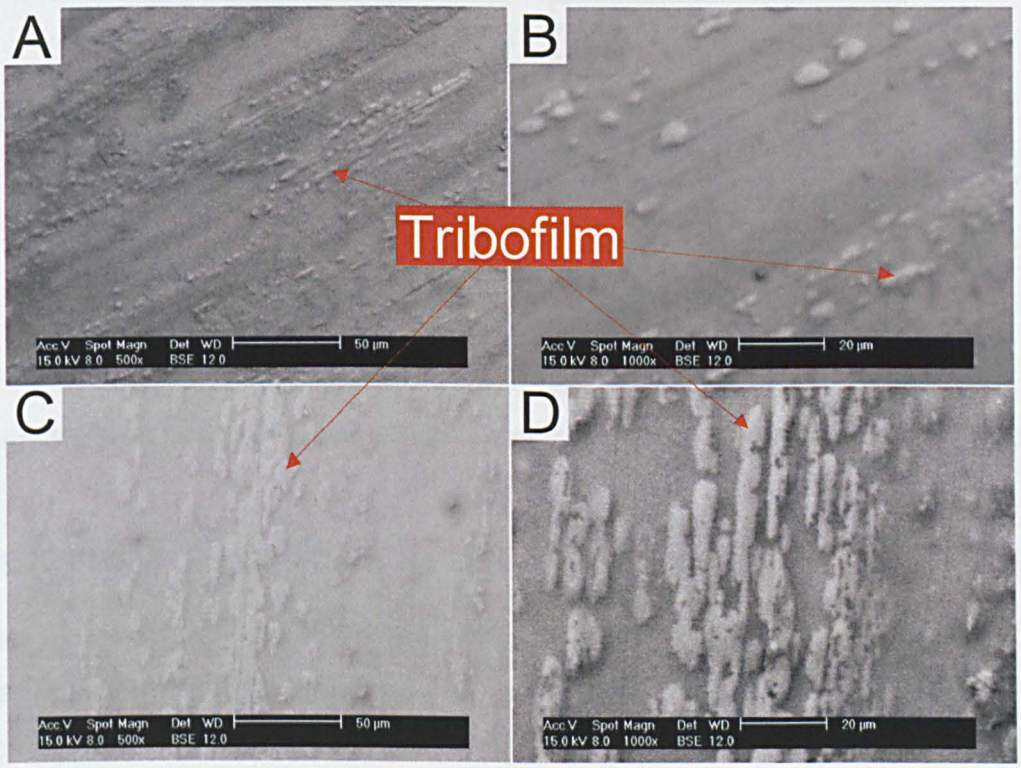

Figure 97: SEM image of silicon crystal lubricated with ZDDP (A&B) and ZDDP + NOCH (C&D)

As can be seen in Figure 97A&B, when the tribosystem was lubricated with ZDDP, a patchy tribofilm comprised of small pad-like structures was generated. This tribofilm was orientation in the direction of sliding and was sporadically located throughout the wear scar. Lubricating the interface with ZDDP + NOCH generated a tribofilm which comprised long lengths of pad-like regions (Figure 97C&D). These pads appeared to contain a number of pores, and were once again arranged in the sliding direction of the tribosystem.

Comparing AFM images for the two lubricants, it was clear that both surfaces contained wear debris (Figure 98). The ZDDP tribofilm was very patchy and difficult to identify (Figure 98A&B).Whereas that generated from ZDDP + NOCH was more evident on the surface of the substrate, and, as shown in the SEM images (Figure 97C&D), was constructed from long interlinked sections of pads (Figure 98C).

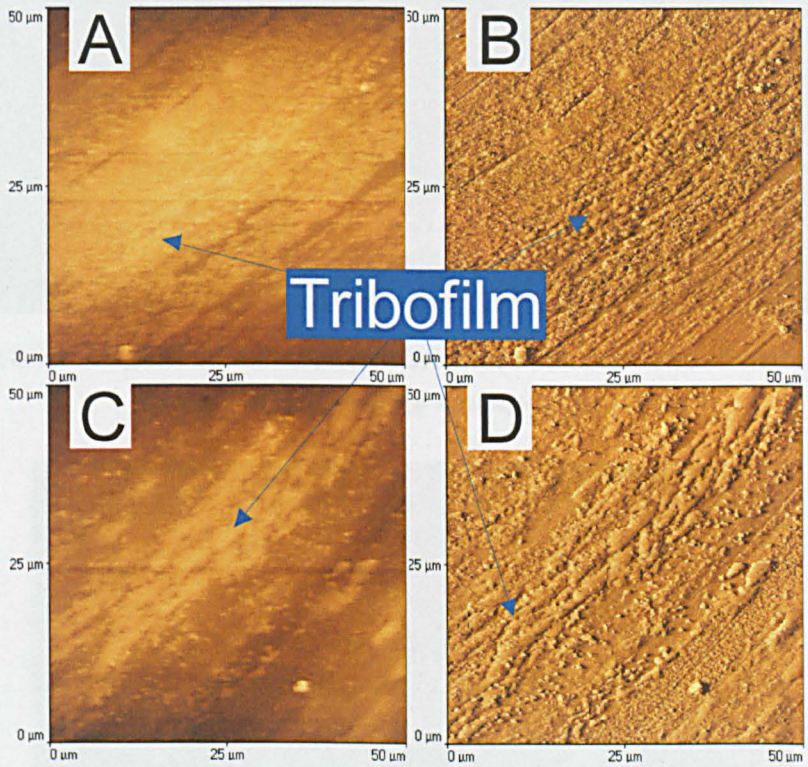

Figure 98: AFM image of silicon crystal lubricated with ZDDP (A&B) and ZDDP + NOCH (C&D)

7.5.1.2. Silicon Crystal - Calcium Sulfonate vs Calcium Sulfonate + NOCH

When the silicon crystal substrate was lubricated with calcium sulfonate, it was quite apparent that a tribofilm was generated (Figure 99A&B). Indeed, the tribofilm was orientated in the direction of sliding and comprised large pad-like structures, which were not linked together and covered the entire width of the

wear scar (Figure 99A&B). Lubricating the contact with calcium sulfonate + NOCH created a tribofilm upon the substrate which was constructed from much smaller pads that were now interlinked (Figure 99C&D). The increased magnification image of this tribofilm shown in Figure 100 identifies the structure of the protective layer more clearly.

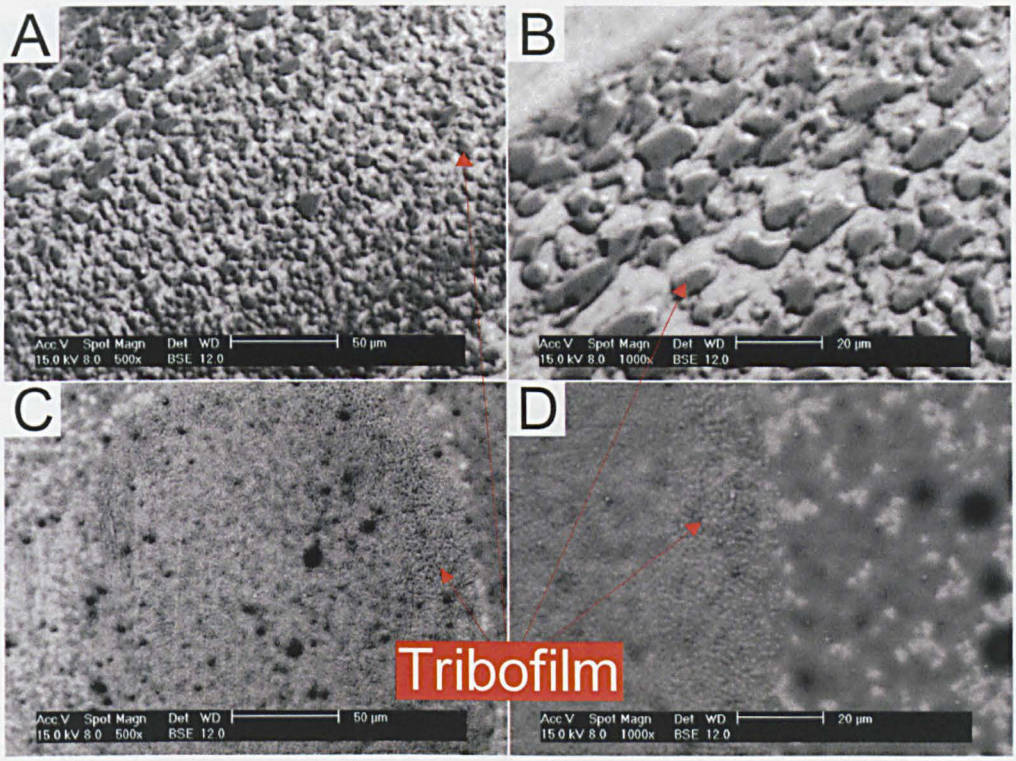

Figure 99: SEM image of silicon crystal lubricated with calcium sulfonate (A&B) and calcium sulfonate + NOCH (C&D)

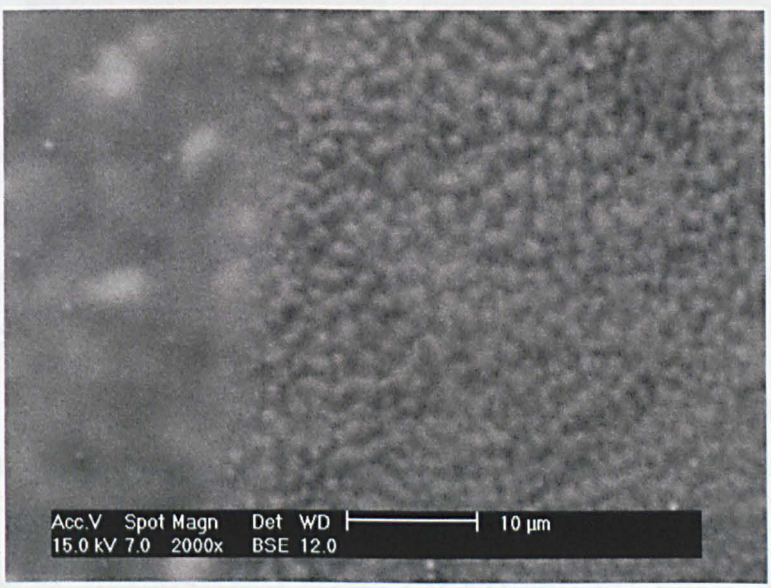

Figure 100: High magnification image of a silicon crystal which had been lubricated with calcium sulfonate + NOCH

As shown in Figure 101A&B, which reiterates the data obtained from SEM in Figure 99A&B, the calcium sulfonate-based tribofilm consisted of large pads around which the surface of the silicon substrate was clearly visible. Atomic force microscopy (Figure 101C&D) of the calcium sulfonate + NOCH tribofilm presented a clearer view of the protective layer than that obtained using SEM. Indeed, it was quite evident that the film comprised small pads which were joined together (Figure 101C&D). Sections of the film were orientated within the sliding direction. Both lubricant C and CN tribofilms were of a uniform height throughout the wear scar (Figure 101A&C).

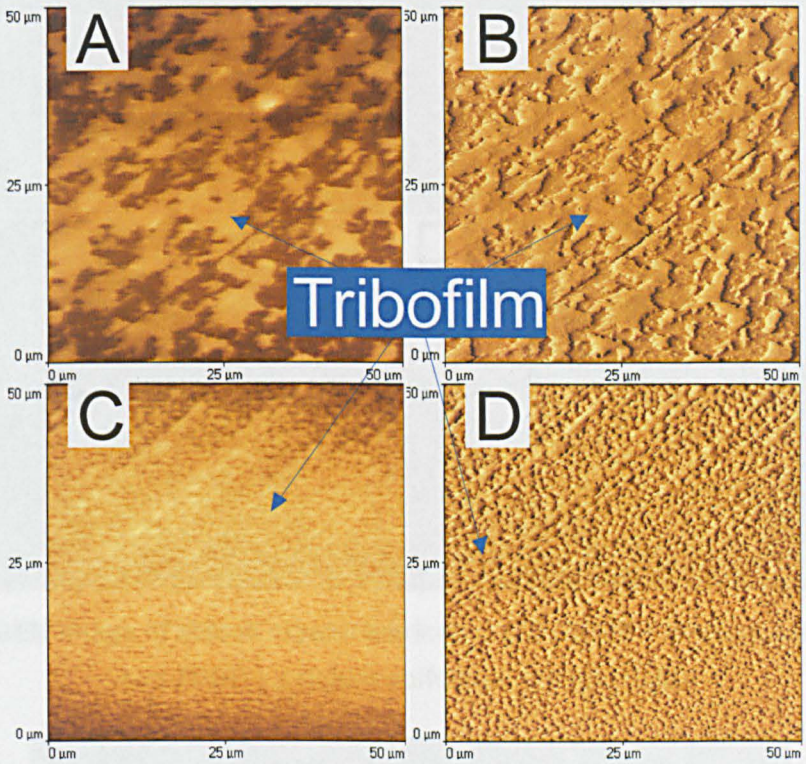

Figure 101: AFM image of silicon crystal lubricated with calcium sulfonate (A&B) and calcium sulfonate + NOCH (C&D)

7.5.1.3. Silicon Crystal - ZDDP + Calcium Sulfonate vs ZDDP + Calcium Sulfonate + NOCH

As observed in Figure 102A&B, the tribofilm generated upon the surface of the silicon crystal substrate when lubricated with ZDDP + calcium sulfonate comprised a mixture of unlinked calcium sulfonate pad-like structures, and a long glassy ZDDP type protective layer. Interestingly, the pads resembled that obtained with calcium sulfonate alone (Figure 99A&B) yet were much smaller in size. The phosphate section to the tribofilm was not as patchy as that obtained with ZDDP alone (Figure 97A&B). Both sections of the tribofilm were orientated

in the direction of sliding (Figure 102A&B). It is clear from Figure 102C&D that the lubricant C tribofilm extended the full width of the wear scar. Higher magnification imagery of the tribofilm on the non-ferrous substrate revealed a tribofilm which was pad-based, but contained a number of wear marks throughout the layer (Figure 103). The pads were of varying sizes and similar to those obtained when using calcium sulfonate + NOCH as lubricant (Figure 100).

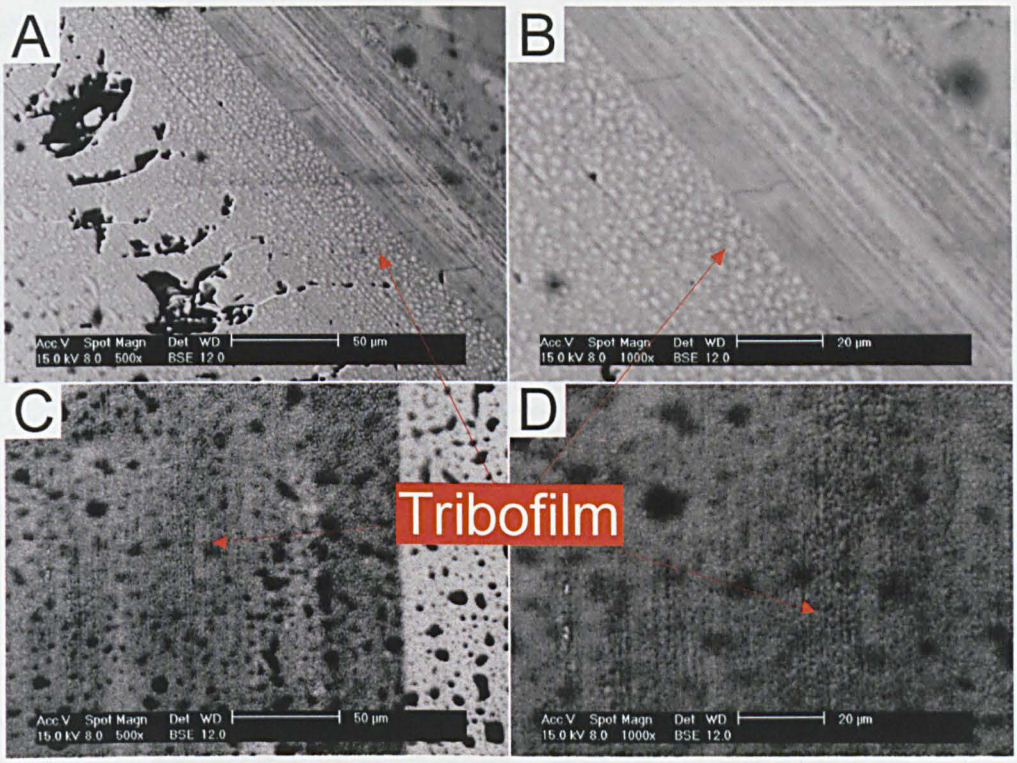

Figure 102: SEM image of silicon crystal lubricated with ZDDP + calcium sulfonate (A&B) and ZDDP + calcium sulfonate + NOCH (C&D)

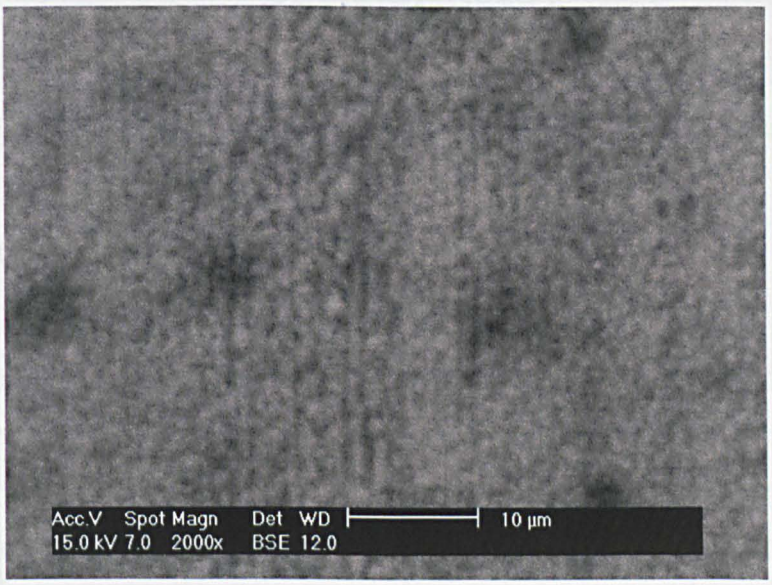

Figure 103: High magnification image of a silicon crystal which had been lubricated with ZDDP + calcium sulfonate + NOCH

Figure 104A&B highlights the two sections of tribofilm present within the ZDDP + calcium sulfonate protective layer, both of which extended from the surface of the substrate to a similar approximate height. The calcium sulfonate-derived pads were of a varying size, yet compared to calcium sulfonate alone, the surface density of the pads appeared to increase (Figure 101A&B). Long, interconnected sections of glassy tribofilm were orientated within the sliding direction (Figure 104A&B). The tribofilm created using ZDDP + calcium sulfonate + NOCH comprised small interlinked pads (Figure 104C&D). Wear marks in the direction of sliding were evident within the tribofilm; no glassy ZDDP type film was observed (Figure 104 C&D).

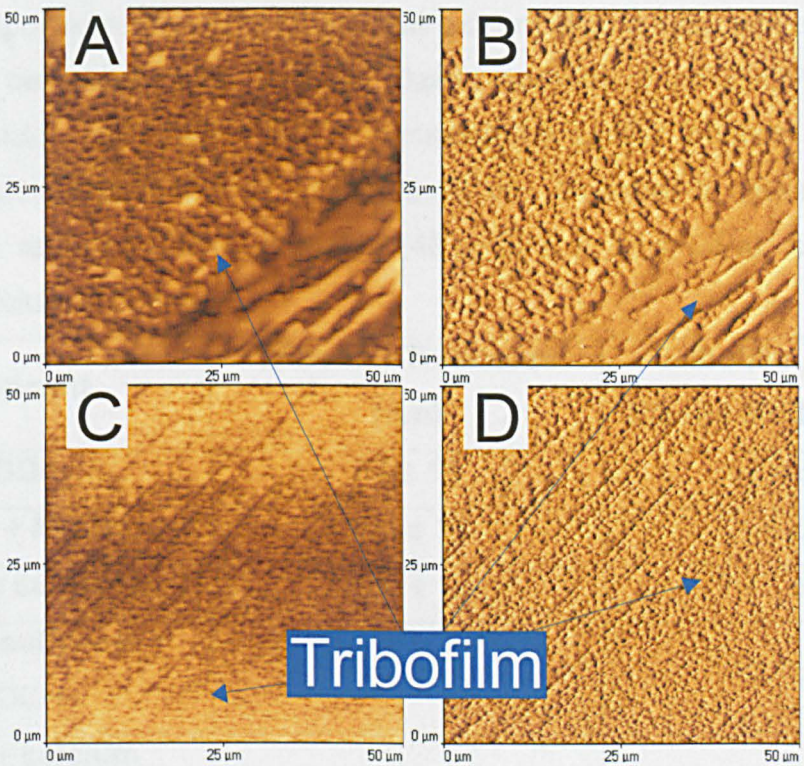

Figure 104: AFM image of silicon crystal lubricated with ZDDP + calcium sulfonate (A&B) and ZDDP + calcium sulfonate + NOCH (C&D)

7.5.1.4. Silicon Crystal - Tribofilm Properties

The thicknesses and reduced elastic modulus values determined for tribofilms generated on silicon crystal substrates from those lubricants listed in Table 29 are shown in Table 34. As it can be seen, when lubricating the contact with ZDDP, the tribofilm thickness was on average ~ 20 nm less than its ZDDP + NOCH counterpart. A comparison between the reduced elastic modulus values for the two lubricants also revealed an increase in the mechanical properties of the tribofilm derived from ZDDP + NOCH. Both calcium sulfonate and calcium

sulfonate + NOCH possessed similar tribofilm thicknesses of ~ 130 nm, which was ~ 50 nm and ~ 30 nm thicker than the equivalent protective films obtained from ZDDP and ZDDP + NOCH, respectively. The reduced elastic modulus for the tribofilm generated from calcium sulfonate was 70.7 GPa ± 14.1 GPa, but, interestingly, calcium sulfonate + NOCH saw a reduction in reduced elastic modulus to 60.1 GPa ± 7.2 GPa.

The tribofilm generated from ZDDP + calcium sulfonate had a thickness of 50 nm ± 12 nm; 60 % and 39 % of the average thickness recorded for ZDDP and calcium sulfonate alone, respectively. The reduced elastic modulus calculated for the ZDDP + calcium sulfonate-based tribofilm (37.5 GPa ± 10.2 GPa) was approximately half of that obtained for calcium sulfonate and had also decreased, compared to the reduced elastic modulus of the ZDDP-based film. ZDDP + calcium sulfonate + NOCH possessed a similar tribofilm thickness to ZDDP + calcium sulfonate at 47 nm ± 13 nm, however it featured a 20 % increase in reduced elastic modulus (48.8 GPa ± 15.1 GPa), compared to ZDDP + calcium sulfonate.

Lubricant	Tribofilm Thickness (nm)	Tribofilm Reduced Elastic Modulus (GPa)
ZDDP	84 ± 11	62.4 ± 6.4
ZDDP + NOCH	104 ± 14	71.4 ± 12.0
Calcium sulfonate	129 ± 18	70.7 ± 14.1
Calcium sulfonate + NOCH	132 ± 15	60.1 ± 7.2
ZDDP + calcium sulfonate	50 ± 12	37.5 ± 10.2
ZDDP + calcium sulfonate + NOCH	47 ± 13	48.8 ± 15.1

Table 34: Mechanical properties of tribofilms generated on silicon crystal substrates

7.5.1.5. Steel Pin - ZDDP vs ZDDP + NOCH

As observed in Figure 105A&B, the ZDDP-based tribofilm on the surface of the steel pin consisted of long pads. ZDDP + NOCH (Figure 105C&D) comprised a similar format, yet the density of these pads appeared to increase. Both tribofilms were orientated in the direction of sliding.

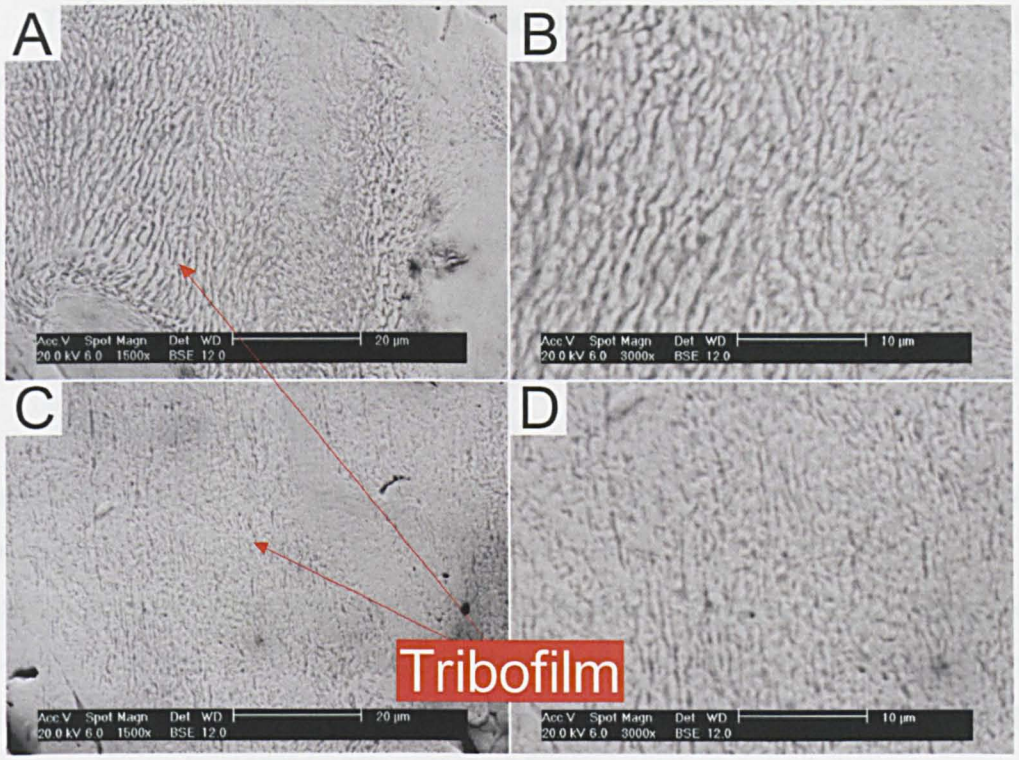

Figure 105: SEM image of a steel pin which has been in contact with a silicon crystal and lubricated with ZDDP (A&B) and ZDDP + NOCH (C&D)

7.5.1.6. Steel Pin - Calcium Sulfonate vs Calcium Sulfonate + NOCH

Figure 106 shows the wear scar region on lubricant C and CN steel pins.

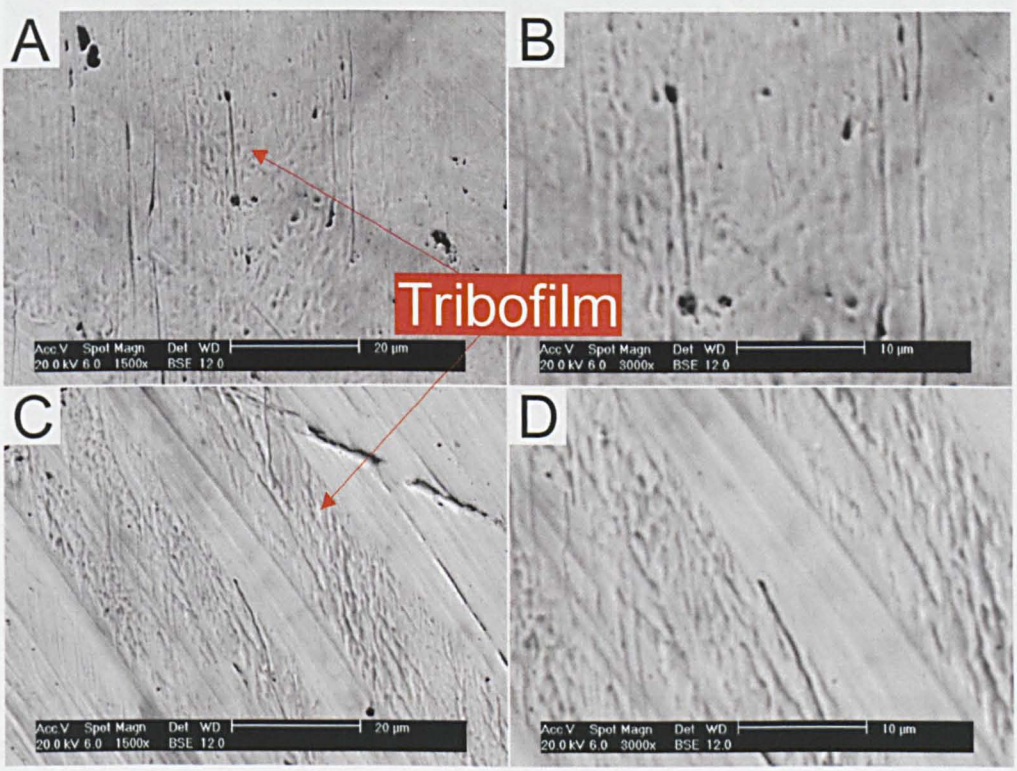

Figure 106: SEM image of a steel pin which has been in contact with a silicon crystal and lubricated with calcium sulfonate (A&B) and calcium sulfonate + NOCH (C&D)

The tribofilm generated from calcium sulfonate on the steel pin (Figure 106A&B) did not contain obvious pads, as was observed on silicon crystal substrates (Figure 99A&B). The protective layer contained a number of voids and was orientated in the direction of sliding. The film created using calcium sulfonate + NOCH contained a number of interlinked long pads (Figure 106C&D), which were arranged in the sliding direction.

7.5.1.7. Steel Pin - ZDDP + Calcium Sulfonate vs ZDDP + Calcium Sulfonate + NOCH

Lubricating the contact with ZDDP + calcium sulfonate (Figure 107A&B) generated a very different tribofilm to those witnessed with ZDDP (Figure 105) or OBCS (Figure 106). Indeed, the tribofilm was constructed from large pads of non-uniform shape and dimension, with a darkly shaded core. Wear marks were evident within this film, as shown in Figure 107B. The film formed from ZDDP + calcium sulfonate + NOCH (Figure 107C&D) was analogous to that obtained for calcium sulfonate alone (Figure 106A&B). A number of voids and wear marks were evident through the tribofilm (Figure 107D).

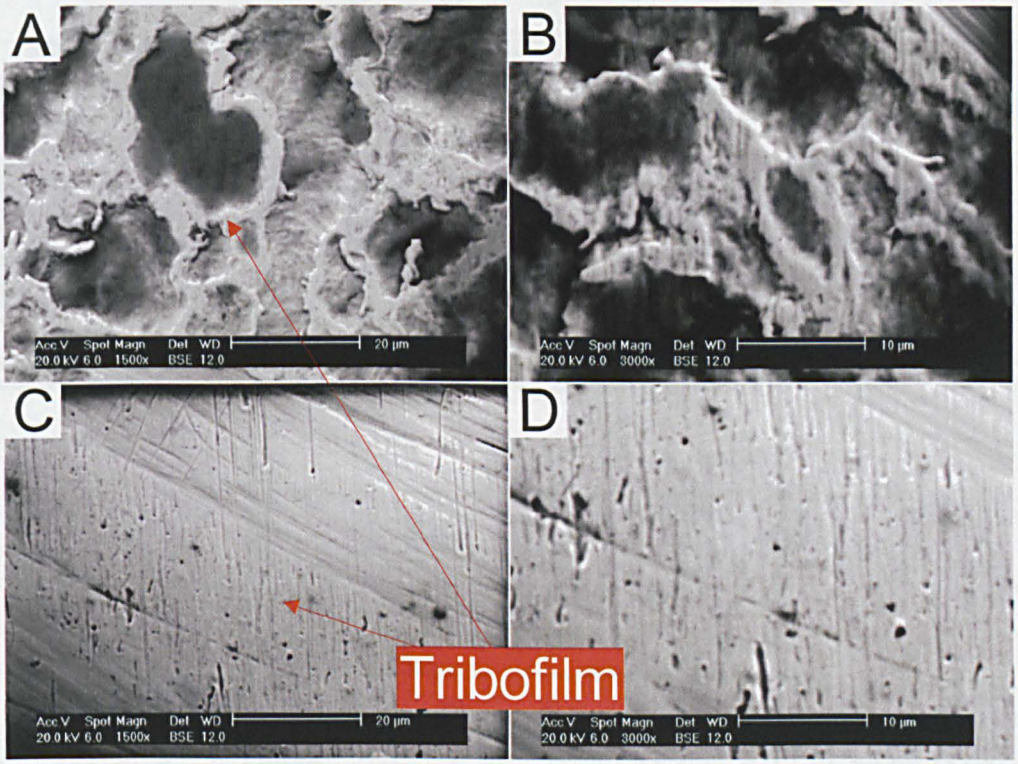

Figure 107: SEM image of a steel pin which has been in contact with a silicon crystal and lubricated with ZDDP + calcium sulfonate (A&B) and ZDDP calcium sulfonate + NOCH (C&D)

7.5.2. Mini SIMS

7.5.2.1. Silicon Crystal - ZDDP vs ZDDP + NOCH

Figure 108 displays the static mini SIMS data obtained from silicon crystal lubricated with ZDDP and ZDDP + NOCH, respectively.

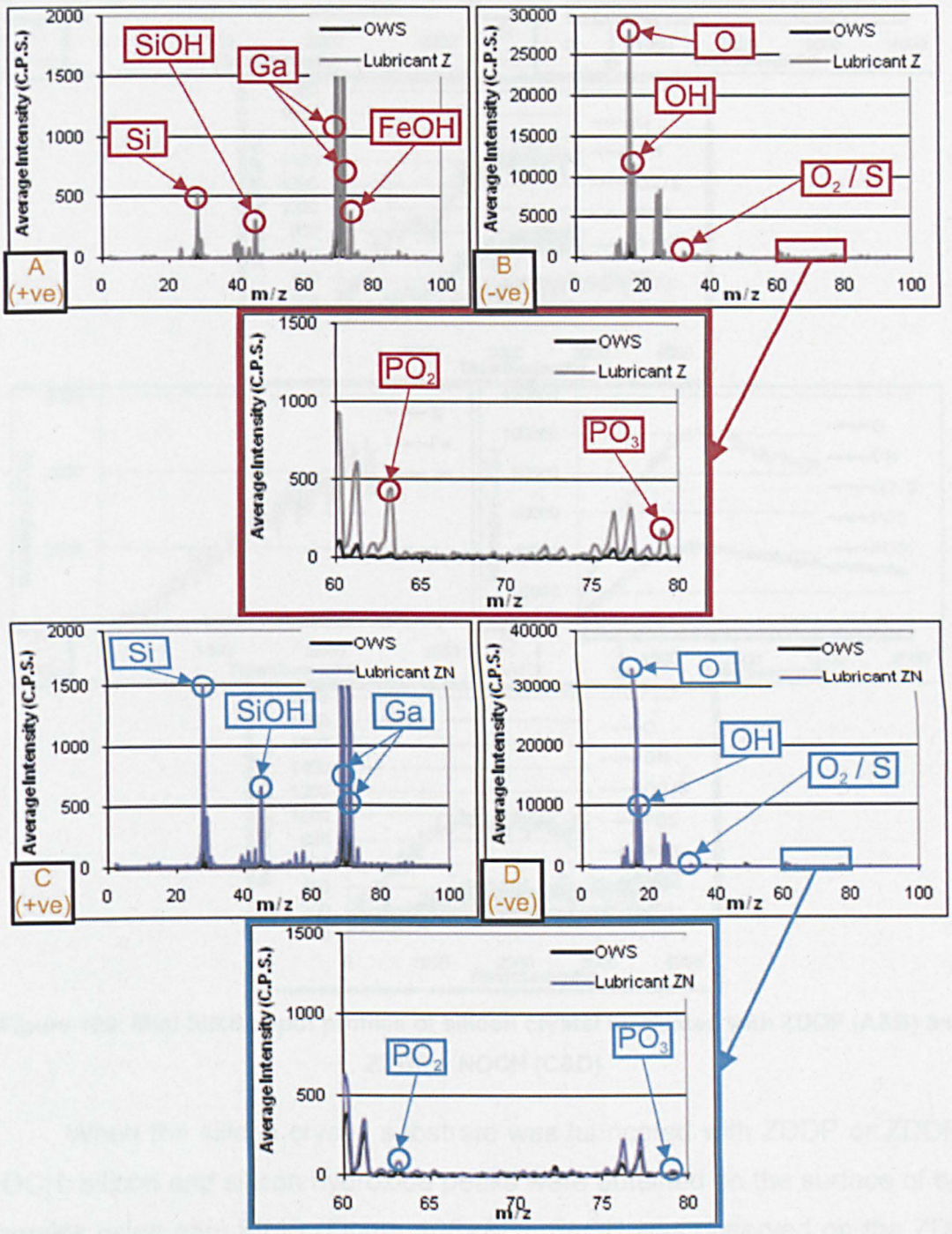

Figure 108: Static mini SIMS spectra of silicon crystal lubricated with ZDDP (A&B) and ZDDP + NOCH (C&D)

Figure 109 shows the depth profiles for Z and ZN lubricated silicon crystal.

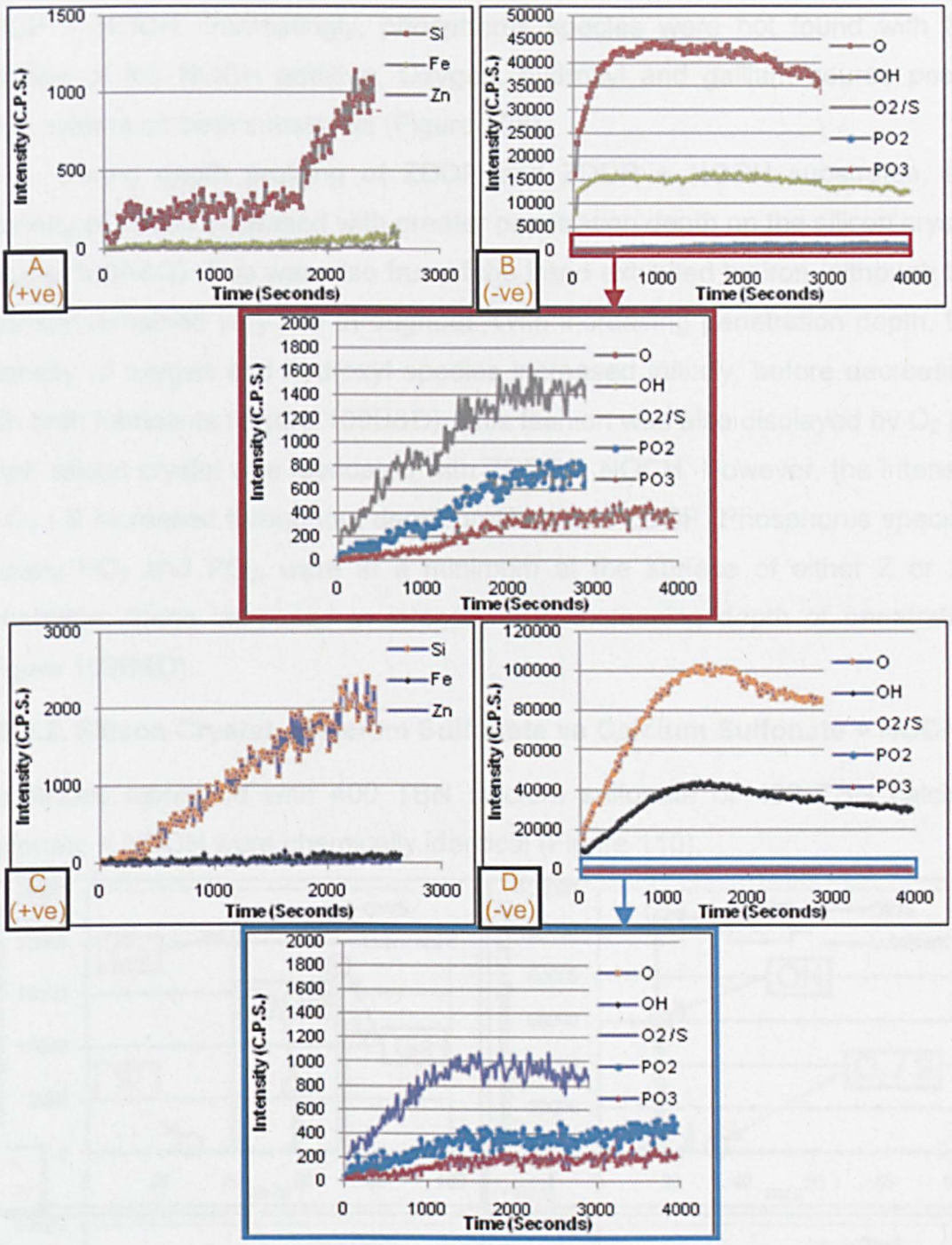

Figure 109: Mini SIMS depth profiles of silicon crystal lubricated with ZDDP (A&B) and ZDDP + NOCH (C&D)

When the silicon crystal substrate was lubricated with ZDDP or ZDDP + NOCH, silicon and silicon hydroxide peaks were obtained on the surface of both samples using mini SIMS (Figure 108A&C). FeOH was observed on the ZDDP substrate (Figure 108A). Zinc was not found on either substrate (Figure 108A&C) yet there were PO_2 and PO_3 peaks witnessed on silicon crystal lubricated with ZDDP (Figure 108B), along with an O_2 / S peak; these were not obtained OWS. The intensity of the O_2 / S peak had reduced considerably with

ZDDP + NOCH. Interestingly, phosphorus species were not found with the addition of the NOCH additive. Oxygen, hydroxyl and gallium source peaks were evident on both substrates (Figure 108).

During depth profiling of ZDDP and ZDDP + NOCH substrates, the intensity of silicon increased with greater penetration depth on the silicon crystal (Figure 109A&C). This was also true of the trend exhibited by iron, although the intensity remained very low throughout. With increasing penetration depth, the intensity of oxygen and hydroxyl species increased initially, before decreasing with both lubricants (Figure 109B&D). This fashion was also displayed by O_2 / S when silicon crystal was lubricated with ZDDP + NOCH. However, the intensity of O_2 / S increased throughout depth profiling with ZDDP. Phosphorus species, namely PO_2 and PO_3, were at a minimum at the surface of either Z or ZN substrates; these increased in intensity with increasing depth of penetration (Figure 109B&D).

7.5.2.2. Silicon Crystal - Calcium Sulfonate vs Calcium Sulfonate + NOCH

Substrates lubricated with 400 TBN calcium sulfonate or 400 TBN calcium sulfonate + NOCH were chemically identical (Figure 110).

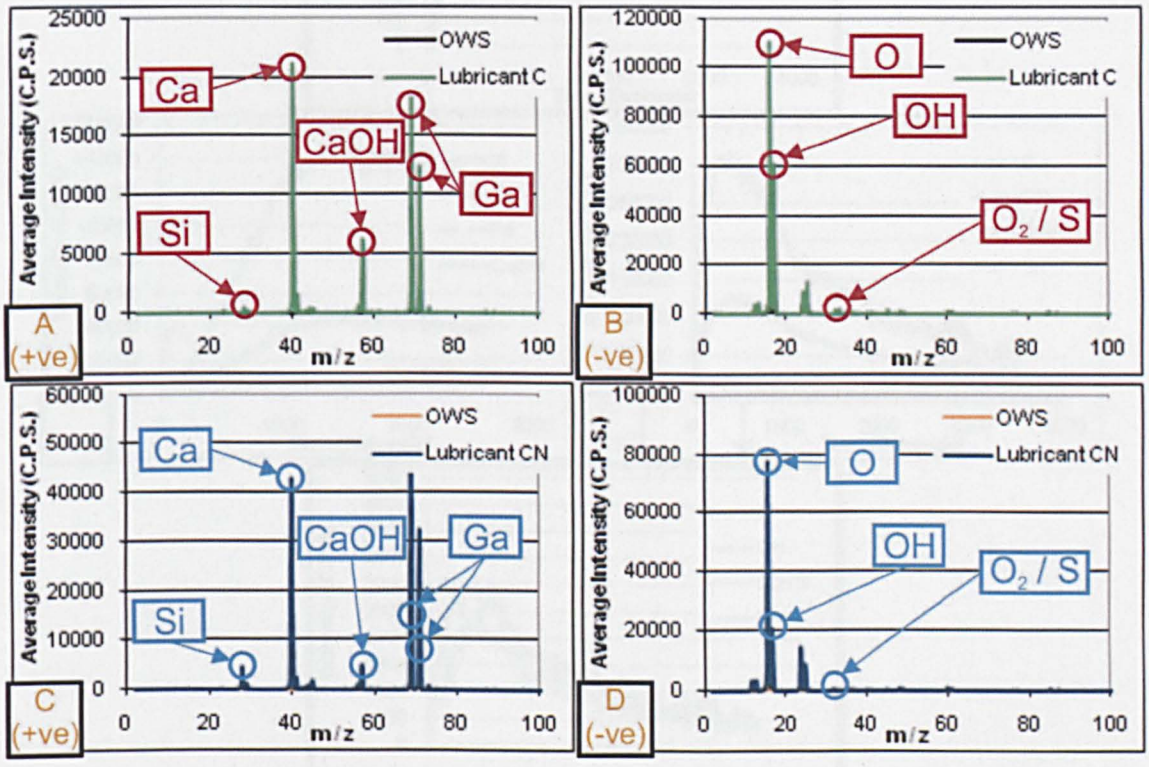

Figure 110: Static mini SIMS spectra of silicon crystal lubricated with calcium sulfonate (A&B) and calcium sulfonate + NOCH (C&D)

Indeed, both substrates contained large intensities of Ca and CaOH peaks on the positive ion mini SIMS spectra (Figure 110A&C). These peaks were not obtained OWS. Silicon was observed on both substrates in the positive polarity spectra also, with peaks originating from the gallium source clearly evident. As shown in Figure 110B&D, oxygen and hydroxyl were identified on the negative polarity spectra using either lubricant. Small intensities of O_2 / S were also observed on both substrates.

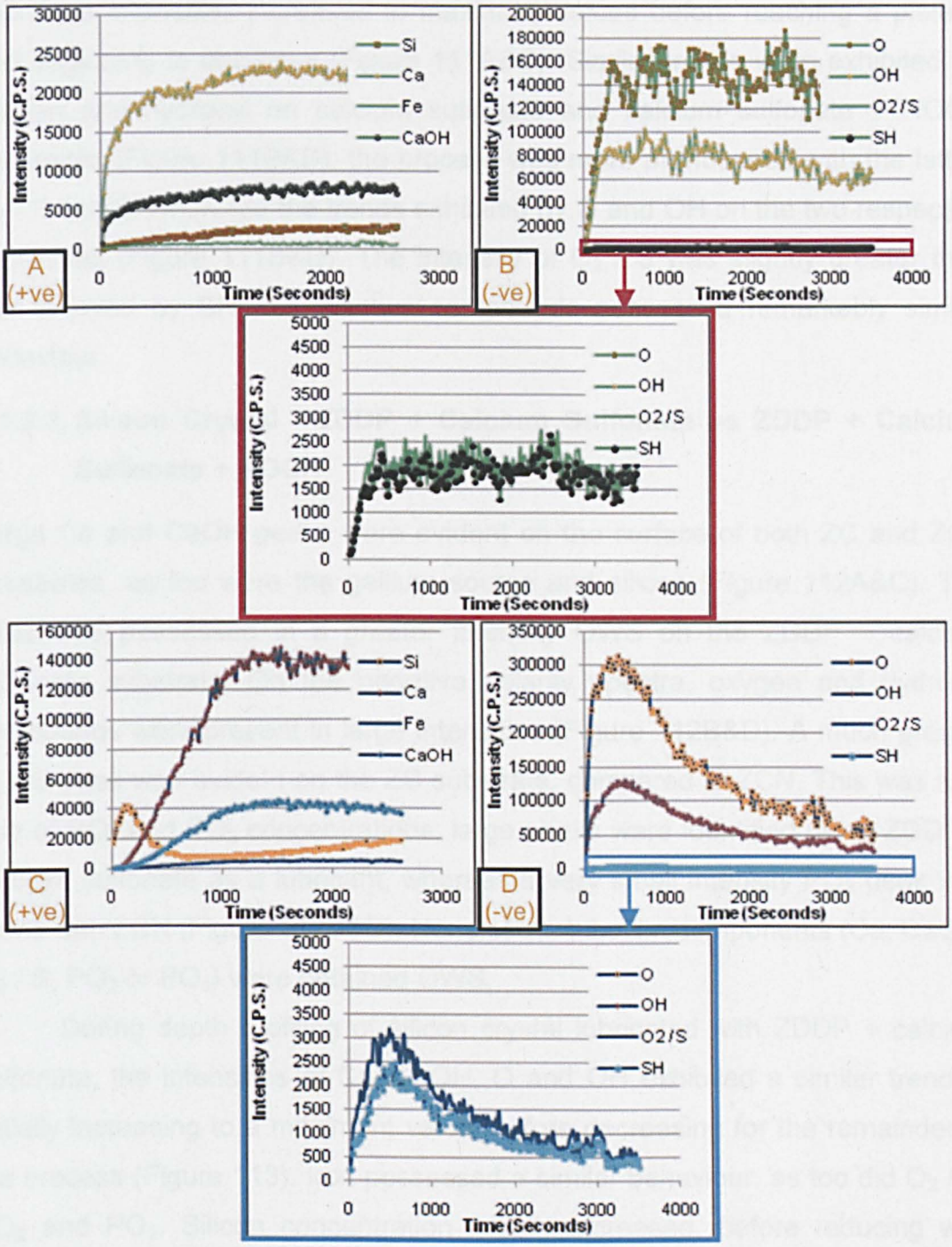

Figure 111: Mini SIMS depth profiles of silicon crystal lubricated with calcium sulfonate (A&B) and calcium sulfonate + NOCH (C&D)

With increasing penetration depth into the OBCS and OBCS + NOCH substrates, the intensities of iron and silicon increased (Figure 111A&C). However, on the calcium sulfonate + NOCH sample, the intensity of silicon initially increased to an overall maximum value and then decreased rapidly, before gradually increasing in concentration once more for the remainder of the process. This trend was not exhibited by calcium sulfonate, where the increase in silicon intensity was steady. With either lubricant, calcium and calcium hydroxide intensities increased to maximum values before reaching a plateau and beginning to decrease (Figure 111A&C). Similar trends were exhibited for oxygen and hydroxyl on calcium sulfonate and calcium sulfonate + NOCH substrates (Figure 111B&D); the process was more pronounced with the latter. O_2 / S and SH mirrored the trends exhibited by O and OH on the two respective substrates (Figure 111B&D). The intensity of O_2 / S was slightly greater than that enjoyed by SH, but the two compounds possessed remarkably similar behaviour.

7.5.2.3. Silicon Crystal - ZDDP + Calcium Sulfonate vs ZDDP + Calcium Sulfonate + NOCH

Large Ca and CaOH peaks were evident on the surface of both ZC and ZCN substrates, as too were the gallium source and silicon (Figure 112A&C). The latter was possessed in a greater intensity OWS on the ZDDP + calcium sulfonate substrate. On the negative polarity spectra, oxygen and hydroxyl compounds were present in large intensities (Figure 112B&D). A much greater O_2 / S peak was evident on the ZC substrate, compared to ZCN. This was also true of PO_2 and PO_3 concentrations; large peaks were identified using ZDDP + calcium sulfonate as a lubricant, whereas a very small intensity PO_2 peak was found with ZCN (Figure 112B&D). None of the tribofilm components (Ca, CaOH, O_2 / S, PO_2 or PO_3) were obtained OWS.

During depth profiling of silicon crystal lubricated with ZDDP + calcium sulfonate, the intensities of Ca, CaOH, O and OH exhibited a similar trend of initially increasing to a maximum value, before decreasing for the remainder of the process (Figure 113). Iron possessed a similar behaviour, as too did O_2 / S, PO_2 and PO_3. Silicon concentration initially increased, before reducing with increasing penetration depth (Figure 113A). A small intensity of zinc was observed near the surface of the substrate; this decreased during depth

profiling and was at a minimum value after approximately half way through the process (Figure 113A).

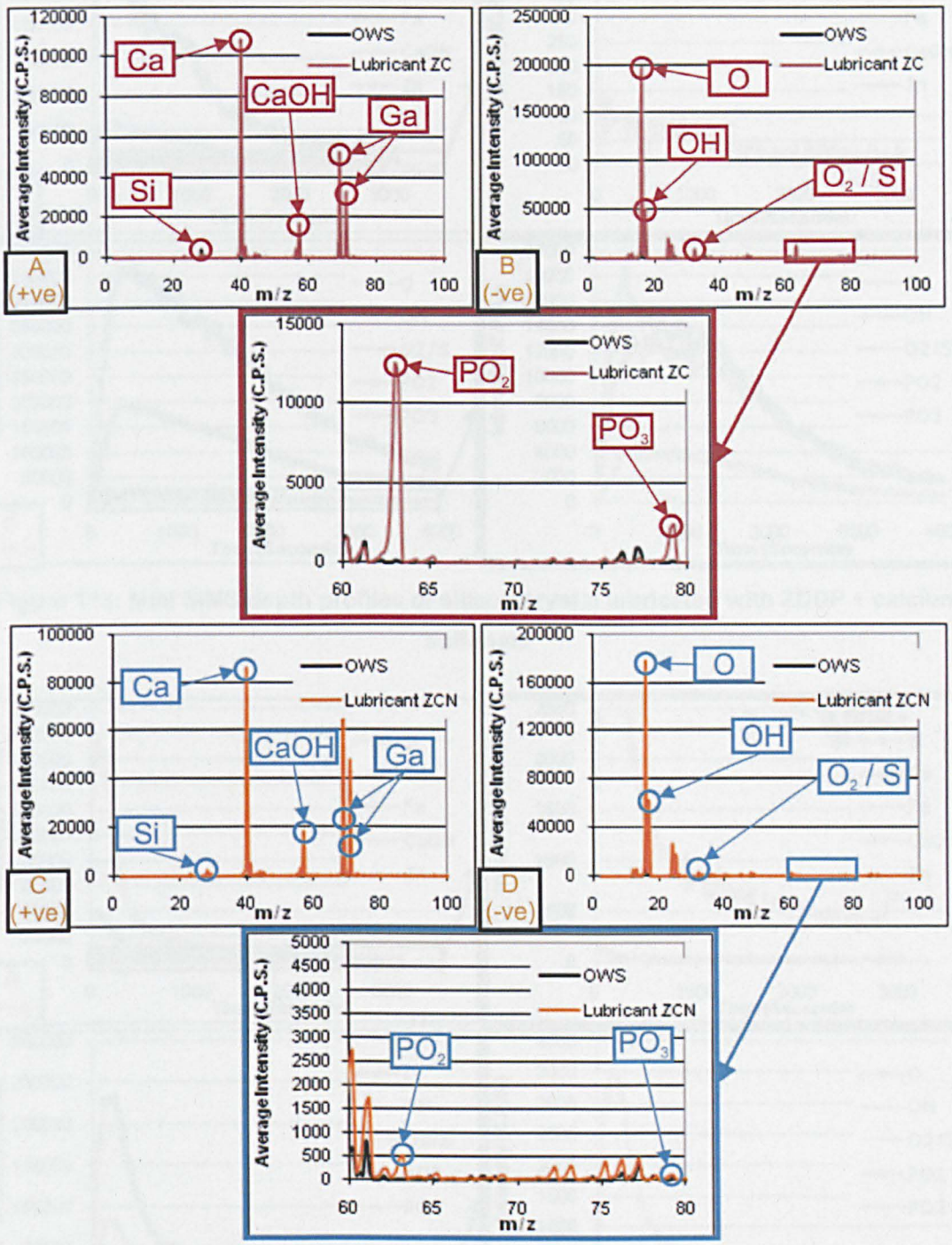

Figure 112: Static mini SIMS spectra of silicon crystal lubricated with ZDDP + calcium sulfonate (A&B) and ZDDP + calcium sulfonate + NOCH (C&D)

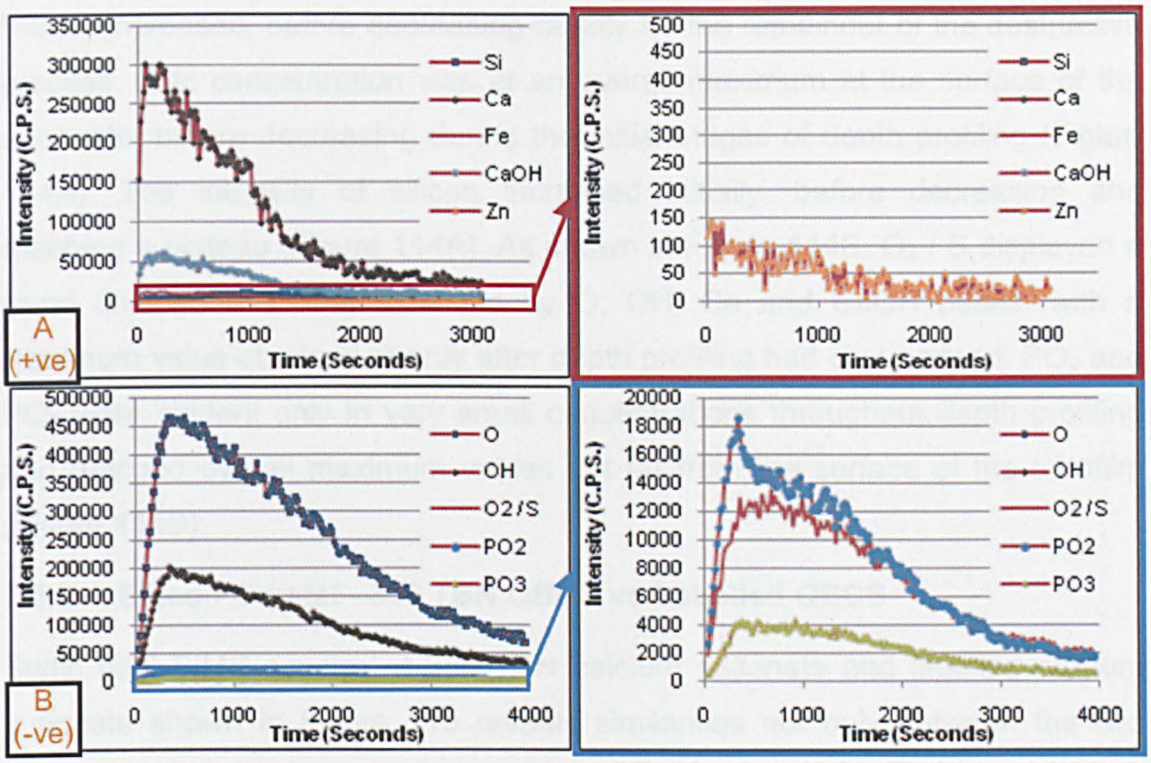

Figure 113: Mini SIMS depth profiles of silicon crystal lubricated with ZDDP + calcium sulfonate

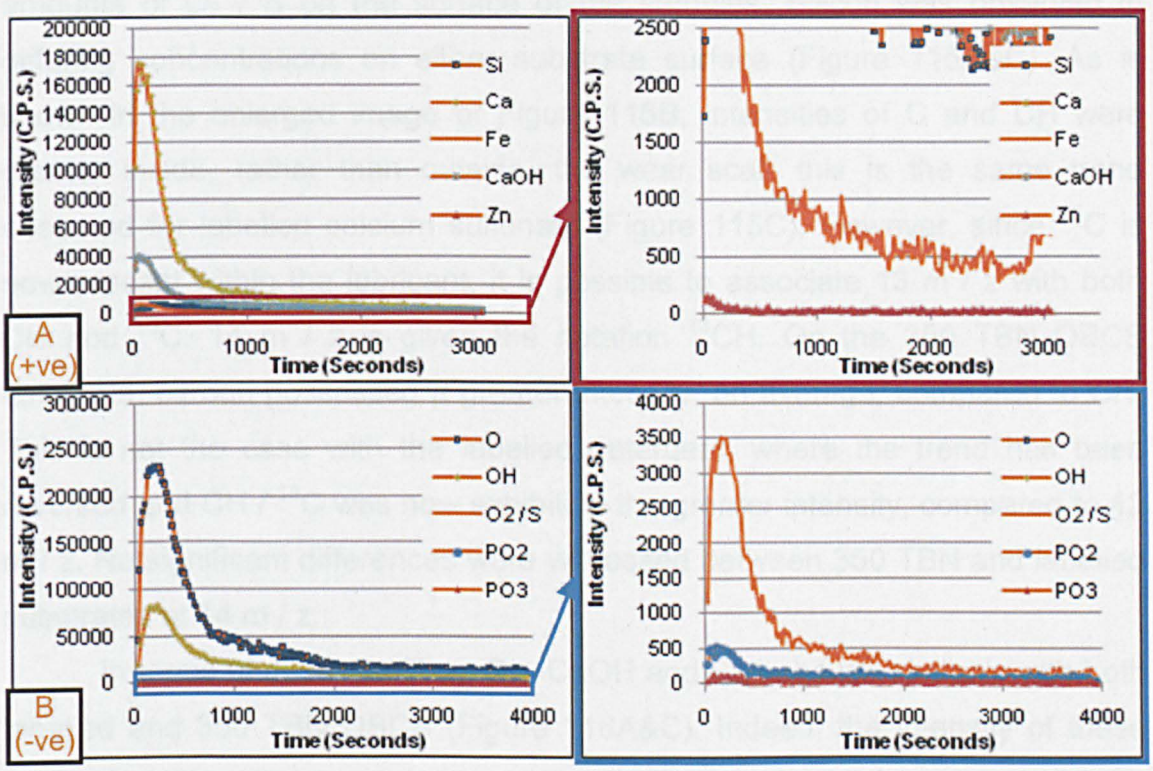

Figure 114: Mini SIMS depth profiles of silicon crystal lubricated with ZDDP + calcium sulfonate + NOCH

As with lubricant ZC, peaks assigned to Ca, CaOH, Fe, O and OH displayed similar behaviour during depth profiling of the ZDDP + calcium sulfonate + NOCH substrate (Figure 114). Indeed, the intensity of these peaks

initially increased, before decreasing rapidly for the remainder of the destructive process. Zinc concentration was at an overall maximum at the surface of the substrate, before decreasing during the initial stages of depth profiling (Figure 114A). The intensity of silicon increased initially, before decreasing and reaching a plateau (Figure 114A). As shown in Figure 114B, O_2 / S displayed a trend analogous to that exhibited by O, OH, Ca and CaOH peaks, with a maximum value obtained shortly after depth profiling had commenced. PO_2 and PO_3 were evident only in very small concentrations throughout depth profiling and reached overall maximum values not far from the surface of the tribofilm (Figure 114B).

7.5.2.4. Silicon Crystal - 350 TBN OBCS vs Labelled OBCS

Static mini SIMS spectra of 350 TBN calcium sulfonate and labelled calcium sulfonate shown in Figure 115 reveals similarities not only between the two substrates, but also the results obtained for 400 TBN calcium sulfonate (Figure 110A&B). Indeed, both substrates contained Ca and CaOH peaks, with minimal amounts of O_2 / S on the surface of the samples. Silicon was observed in differing concentrations on either substrate surface (Figure 115A&C). As is shown in the enlarged image of Figure 115B, intensities of C and CH were greater inside, rather than outside, the wear scar; this is the same trend observed for labelled calcium sulfonate (Figure 115C). However, since ^{13}C is now present within the lubricant, it is possible to associate 13 m / z with both CH and ^{13}C. 14 m / z is given the notation ^{13}CH. On the 350 TBN OBCS substrate, carbon possessed a greater intensity, on average, compared to CH. This is not the case with the labelled detergent, where the trend has been reversed and CH / ^{13}C was now exhibiting the greater intensity, compared to 12 m / z. No significant differences were witnessed between 350 TBN and labelled substrates at 14 m / z.

In terms of depth profiling, Ca, CaOH and Fe behaved similarly with both labelled and 350 TBN OBCS (Figure 116A&C). Indeed, the intensity of these peaks increased to a maximum value, before gradually decreasing. Silicon content decreased with increasing depth of penetration on the 350 TBN substrate, whereas silicon content gradually increased during depth profiling on the labelled sample. The behaviour of O_2 / S was mirrored by that of SH on both substrates, in which the intensity of the two compounds would enlarge to a

maximum overall value with increasing depth, before slowly decreasing in concentration. SH was always present in slightly smaller intensities than O_2 / S. Carbon and CH intensity decreased as the depth of penetration on both substrates increased. ^{12}C and ^{12}CH / ^{13}C intensities were very similar throughout the destructive process with 350 TBN OBCS, whereas ^{12}CH / ^{13}C (13 m / z) possessed greater intensities with labelled OBCS.

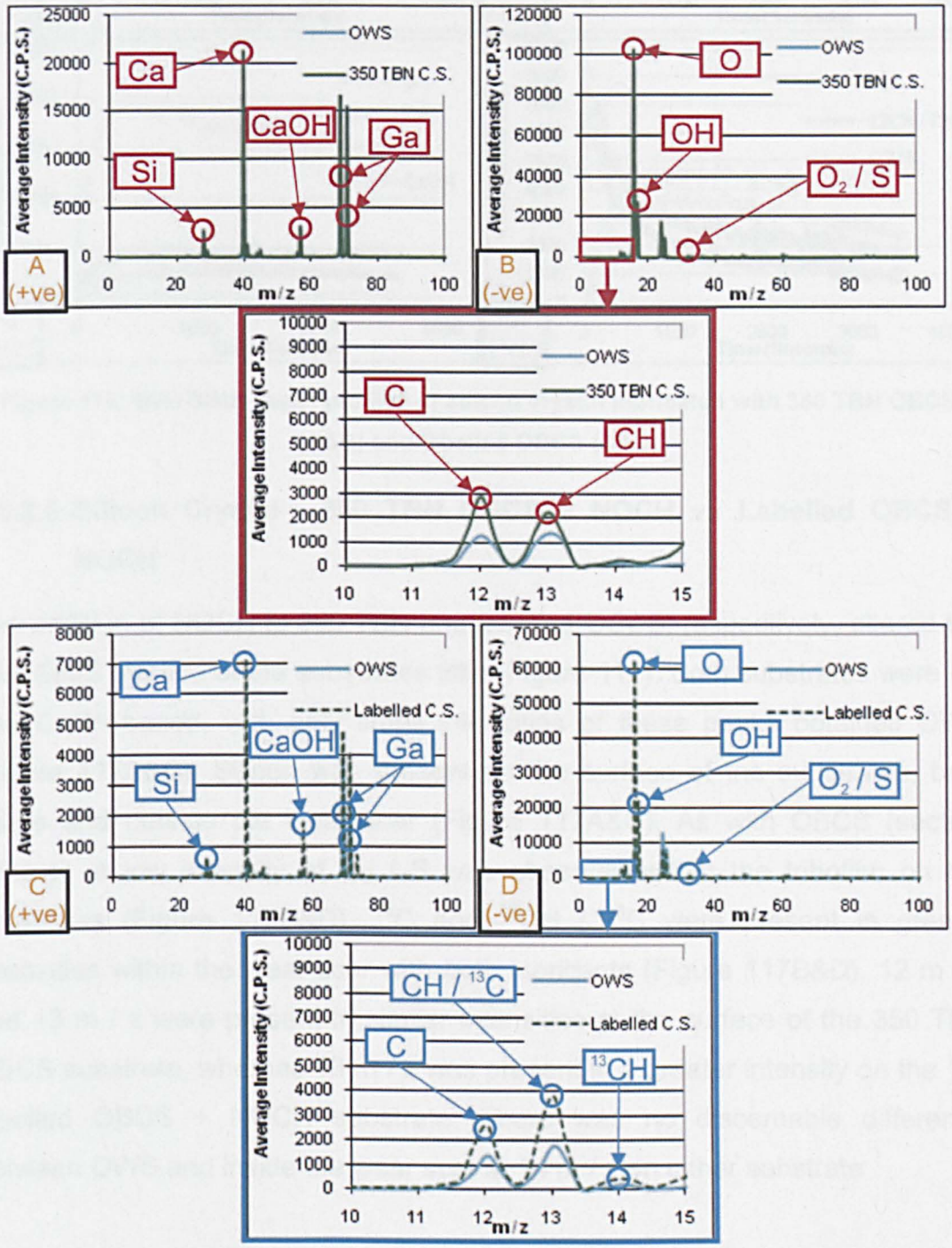

Figure 115: Static mini SIMS spectra of silicon crystal lubricated with 350 TBN OBCS (A&B) and labelled OBCS (C&D)

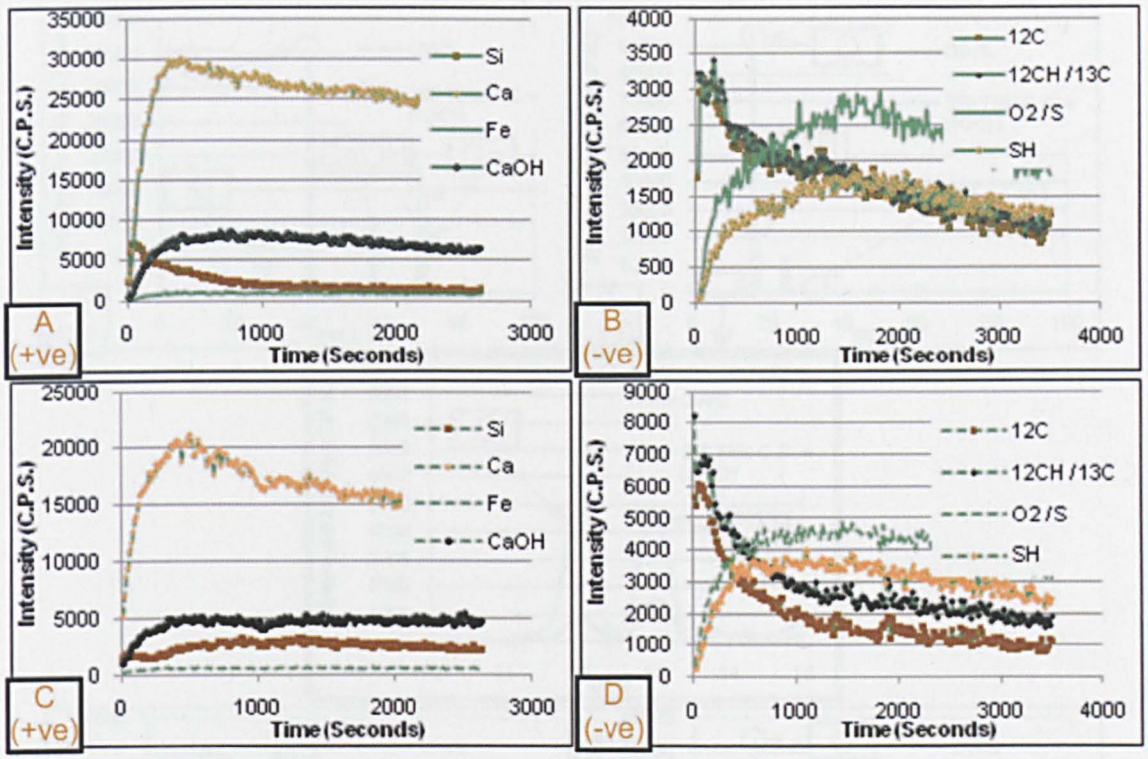

Figure 116: Mini SIMS depth profiles of silicon crystal lubricated with 350 TBN OBCS (A&B) and labelled OBCS (C&D)

7.5.2.5. Silicon Crystal - 350 TBN OBCS + NOCH vs Labelled OBCS + NOCH

The addition of NOCH to 350 TBN and labelled OBCS, respectively, altered the mini SIMS spectra of the substrates little (Figure 117). Both substrates were Ca and CaOH-based, with only small intensities of these peaks obtained OWS (Figure 117A&C). Silicon was present on the surface of the substrates, both inside and outside the wear scar (Figure 117A&C). As with OBCS (section 7.5.2.4), a low intensity of O_2 / S was observed within the tribofilm on the substrates (Figure 117B&D). ^{12}C and ^{12}CH / ^{13}C were present in greater intensities within the wear scar with both lubricants (Figure 117B&D). 12 m / z and 13 m / z were present in similar intensities at the surface of the 350 TBN OBCS substrate, whereas 13 m / z was present in a greater intensity on the ^{13}C labelled OBCS + NOCH substrate. There was no discernable difference between OWS and inside the wear scar at 14 m / z on either substrate.

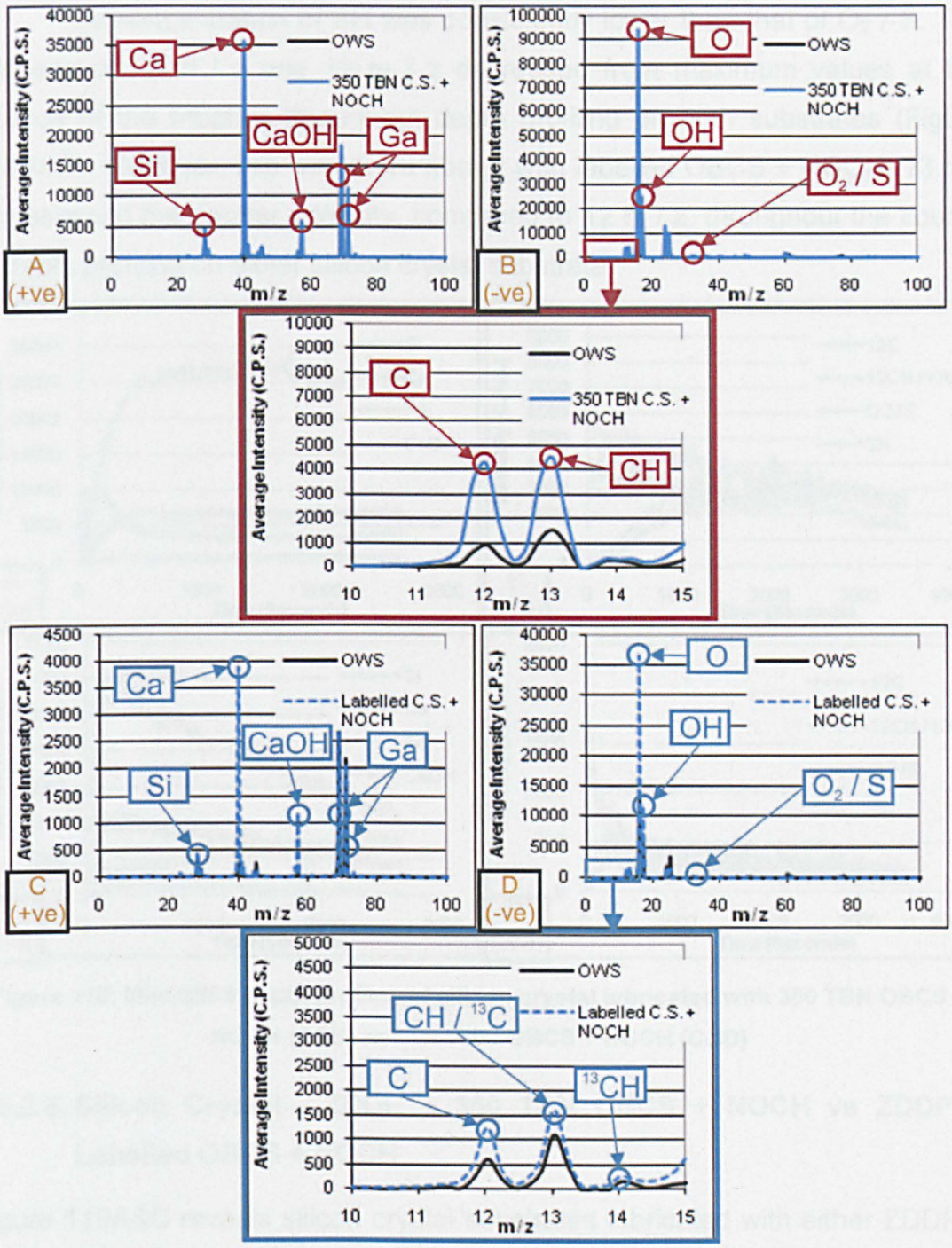

Figure 117: Static mini SIMS spectra of silicon crystal lubricated with 350 TBN OBCS + NOCH (A&B) and labelled OBCS + NOCH (C&D)

Ca, CaOH and Fe intensity increased initially, before decreasing during depth profiling of either substrate (Figure 118A&C). However, the decrease was more sudden with labelled OBCS + NOCH. Silicon content enhanced with increasing penetration depth, but a sharp rise and fall in concentration at the initial stages of depth profiling was witnessed with 350 TBN OBCS + NOCH. On both substrates, O_2 / S and SH increased to a maximum value with increasing penetration depth, before slowly decreasing in intensity (Figure 118B&D).

The concentration of SH was consistently lower than that of O_2 / S. The intensity of 12 m / z and 13 m / z decreased from maximum values at the surface of the tribofilm throughout depth profiling on both substrates (Figure 118B&D). However, this was more abrupt with labelled OBCS + NOCH. 13 m / z possessed the greater intensity, compared to 12 m / z, throughout the course of depth profiling on either silicon crystal substrate.

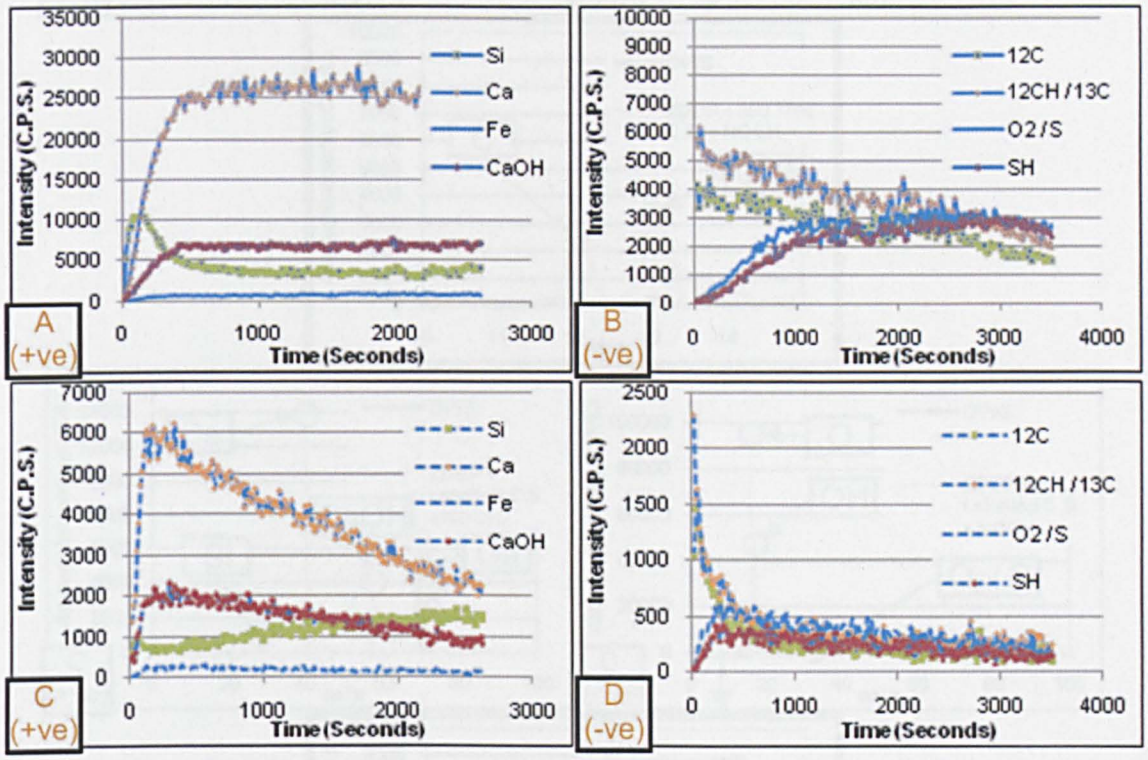

Figure 118: Mini SIMS depth profiles of silicon crystal lubricated with 350 TBN OBCS + NOCH (A&B) and labelled OBCS + NOCH (C&D)

7.5.2.6. Silicon Crystal - ZDDP + 350 TBN OBCS + NOCH vs ZDDP + Labelled OBCS + NOCH

Figure 119A&C reveals silicon crystal substrates lubricated with either ZDDP + 350 TBN OBCS + NOCH or ZDDP + labelled OBCS + NOCH contained Ca, CaOH and silicon. A silicon peak was observed OWS with both lubricants. Zinc was not witnessed on the surface of either substrate (Figure 119A&C) and PO_2 was only present in very small intensities inside the wear scar (Figure 119B&D). PO_3 was not obtained on either substrate. The concentration of C and ^{12}CH / ^{13}C was greater inside, rather than outside, the wear scar on both samples. 13 m / z was also present in greater intensity, compared to 12 m / z, on both 350 TBN and labelled versions of the ZCN lubricant. Little difference was observed at 14 m / z between the two lubricants.

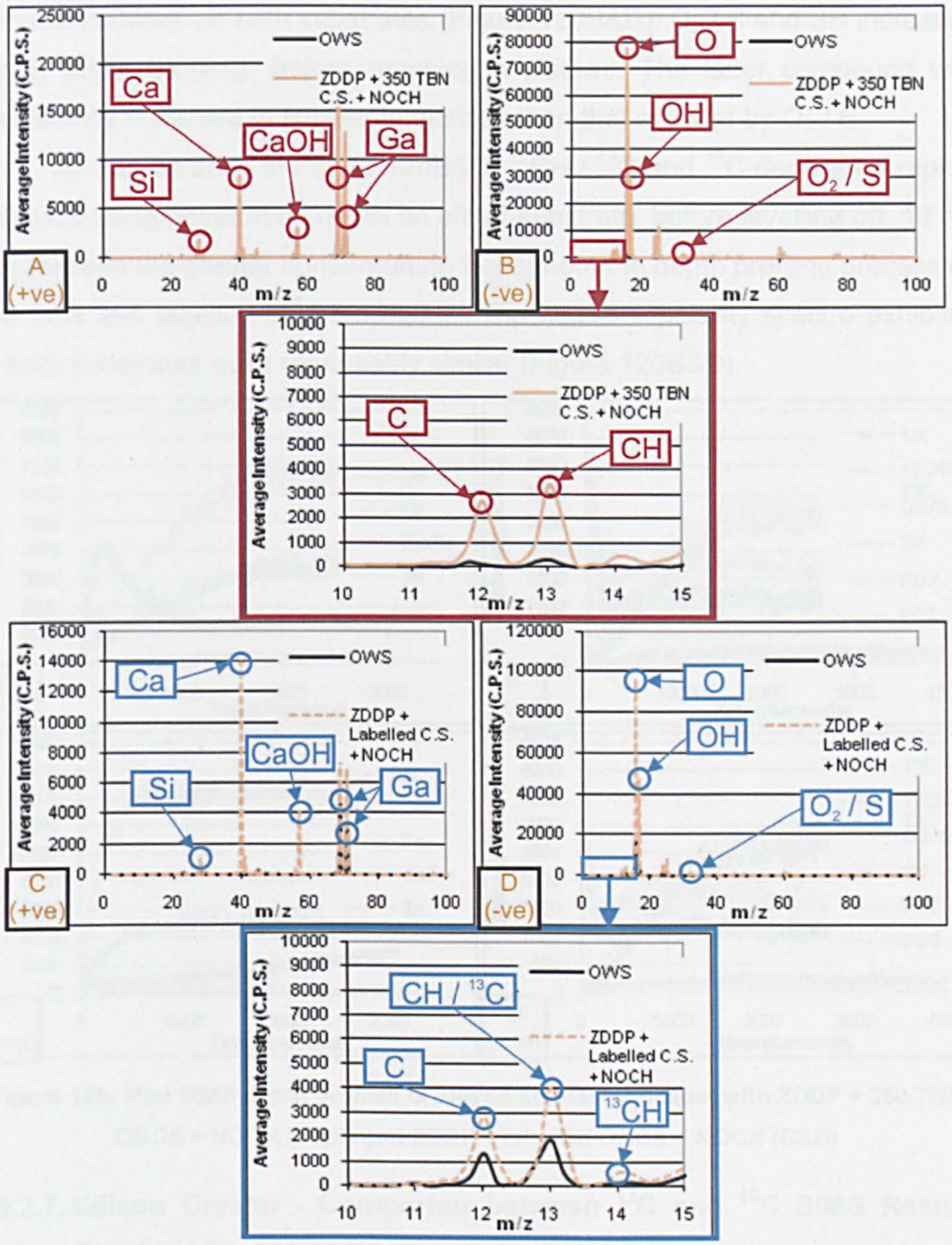

Figure 119: Static mini SIMS spectra of silicon crystal lubricated with ZDDP + 350 TBN OBCS + NOCH (A&B) and ZDDP + labelled OBCS + NOCH (C&D)

With increasing depth of penetration into either substrate, the intensity of Ca, CaOH and Fe peaks increased (Figure 120A&C). The zinc concentration on both samples remained at ~ zero throughout the destructive process. Silicon concentration increased during depth profiling with both lubricants, but a rapid increase and subsequent decrease in intensity was exhibited on the ZDDP + 350 TBN OBCS + NOCH substrate (Figure 120A&C). With increasing depth of penetration, PO_2 and PO_3 concentrations increased by small amounts in

identical fashions on both substrates (Figure 120B&D). O_2 / S and SH increased during depth profiling, before reaching a plateau. The latter compound was consistently observed in smaller intensities than that enjoyed by O_2 / S.

As can be seen in Figure 120B&D, ^{12}CH / ^{13}C and ^{12}C decreased rapidly with increasing penetration depth on either substrate, before levelling off. 13 m / z possessed the greater concentration throughout the depth profiling process on 350 TBN and labelled OBCS variants. The negative polarity spectra exhibited by both substrates were remarkably similar (Figure 120B&D).

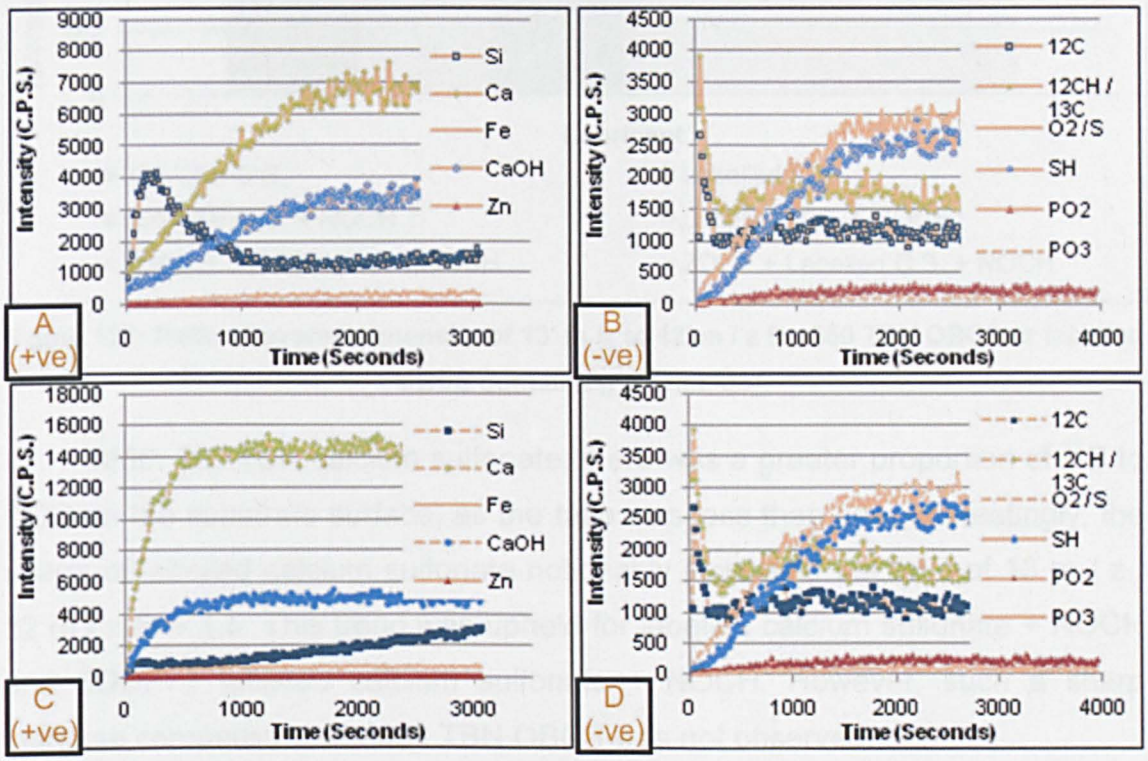

Figure 120: Mini SIMS depth profiles of silicon crystal lubricated with ZDDP + 350 TBN OBCS + NOCH (A&B) and ZDDP + labelled OBCS + NOCH (C&D)

7.5.2.7. Silicon Crystal - Comparion between ^{12}C and ^{13}C SIMS Results Obtained for 350 TBN and Labelled OBCS

The chart shown in Figure 121 highlights the ratio between the average intensity of 13 m / z and 12 m / z, obtained from static mini SIMS data, for lubricants which contained either 350 TBN OBCS or labelled OBCS. Data was acquired from inside the wear scar on substrates and is that shown in graphical format throughout this results section. This method of analysis has been employed in order to provide an indication as to the relative quantities of ^{12}C (12 m / z) and ^{12}CH / ^{13}C (13 m / z) on different substrates.

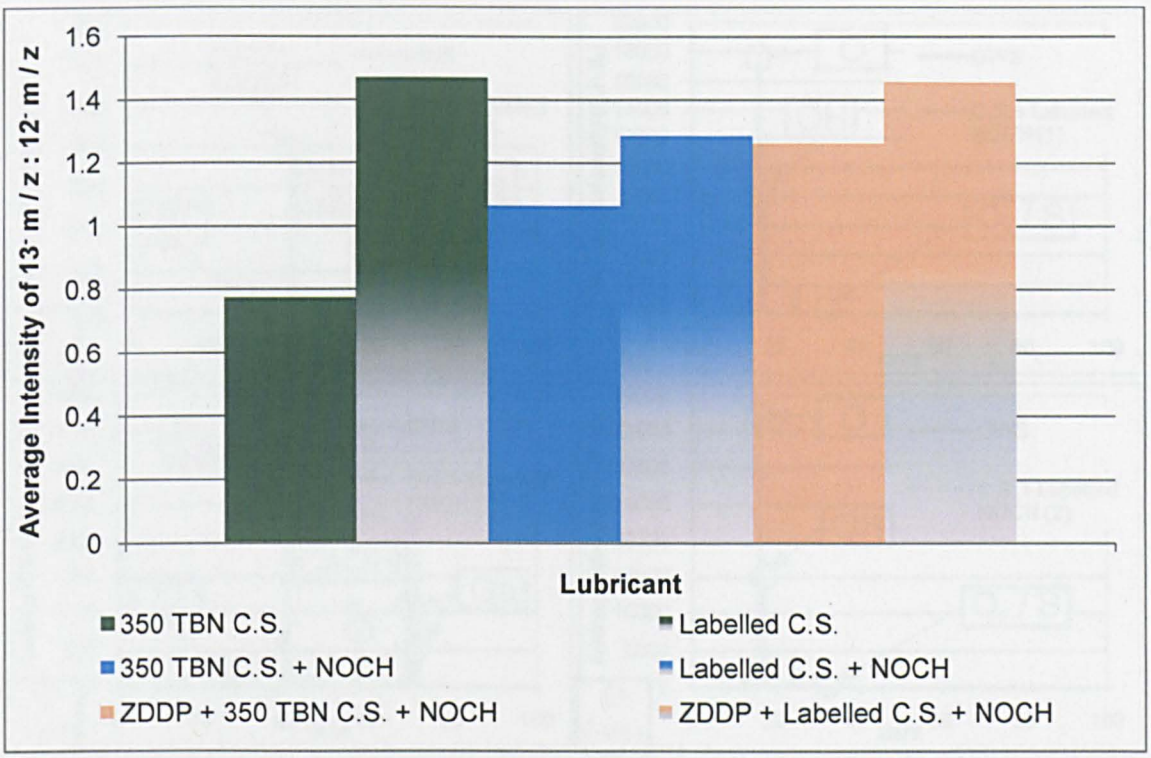

Figure 121: Ratio of average intensity of 13- m /z to 12- m / z for 350 TBN OBCS or labelled OBCS containing lubricants

With 350 TBN calcium sulfonate, there was a greater proportion of ^{12}C to ^{12}CH on the substrate surface, as the ratio was less than one. Interestingly, the usage of labelled calcium sulfonate noticeably increased the ratio of 13 m / z : 12 m / z to ~ 1.5. This trend was upheld for labelled calcium sulfonate + NOCH and ZDDP + labelled calcium sulfonate + NOCH. However, such a sharp increase compared to the 350 TBN OBCS was not observed.

7.5.2.8. Silicon Crystal - Calcium Sulfonate + Labelled NOCH

As can be observed in Figure 122, substrates lubricated with calcium sulfonate + labelled NOCH (1-3) were chemically analogous. Indeed, all three lubricants contained Ca, CaOH and Si peaks; the latter was also observed outside the wear scar. The Ca peak was obtained OWS with calcium sulfonate + labelled NOCH (2&3) (Figure 122C&E). Peaks associated with the gallium source were evident on all substrates, as too were oxygen and hydroxyl peaks (Figure 122). A low intensity O_2 / S peak was observed when silicon crystal was lubricated with calcium sulfonate + labelled NOCH (1-3).

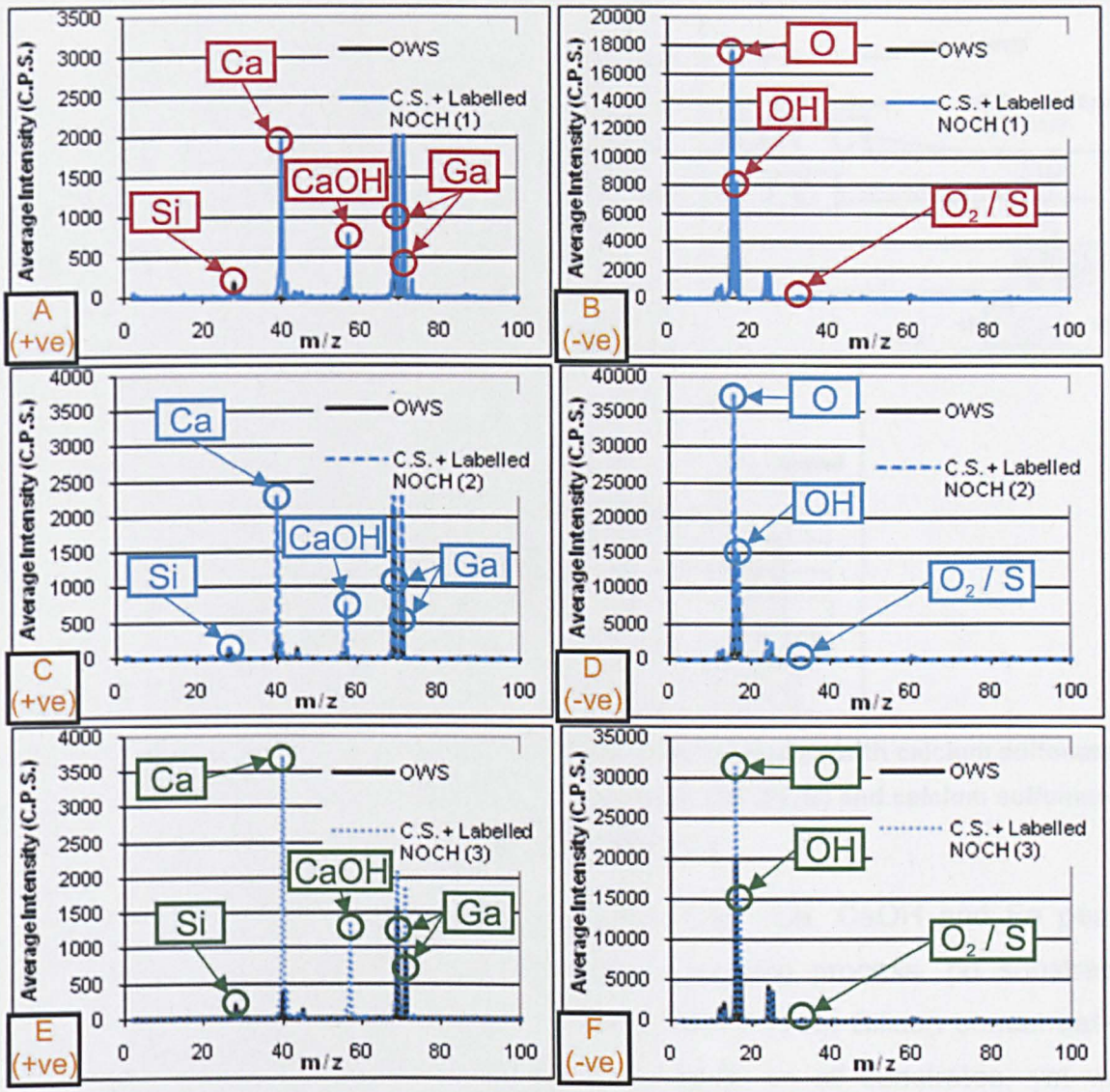

Figure 122: Static mini SIMS spectra of silicon crystal lubricated with calcium sulfonate + labelled NOCH (1) (A&B), calcium sulfonate + labelled NOCH (2) (C&D) and calcium sulfonate + labelled NOCH (3) (E&F)

Figure 123 shows the negative polarity data observed in Figure 122 with a modified x axis in order to reveal any differences between the lubricants between 0 m / z and 15 m / z. There were greater intensities of 12C and 12CH / 13C inside, rather than outside, the wear scar with labelled NOCH (1&2) (Figure 123A&B). The opposite was true in relation to calcium sulfonate + labelled NOCH (3) (Figure 123C). As with labelled calcium sulfonate, it is difficult to determine whether there were any significant differences in ^{13}CH intensity (14 m / z) on the respective substrates. The intensity of 13 m / z was greater on all substrates, compared to 12 m / z.

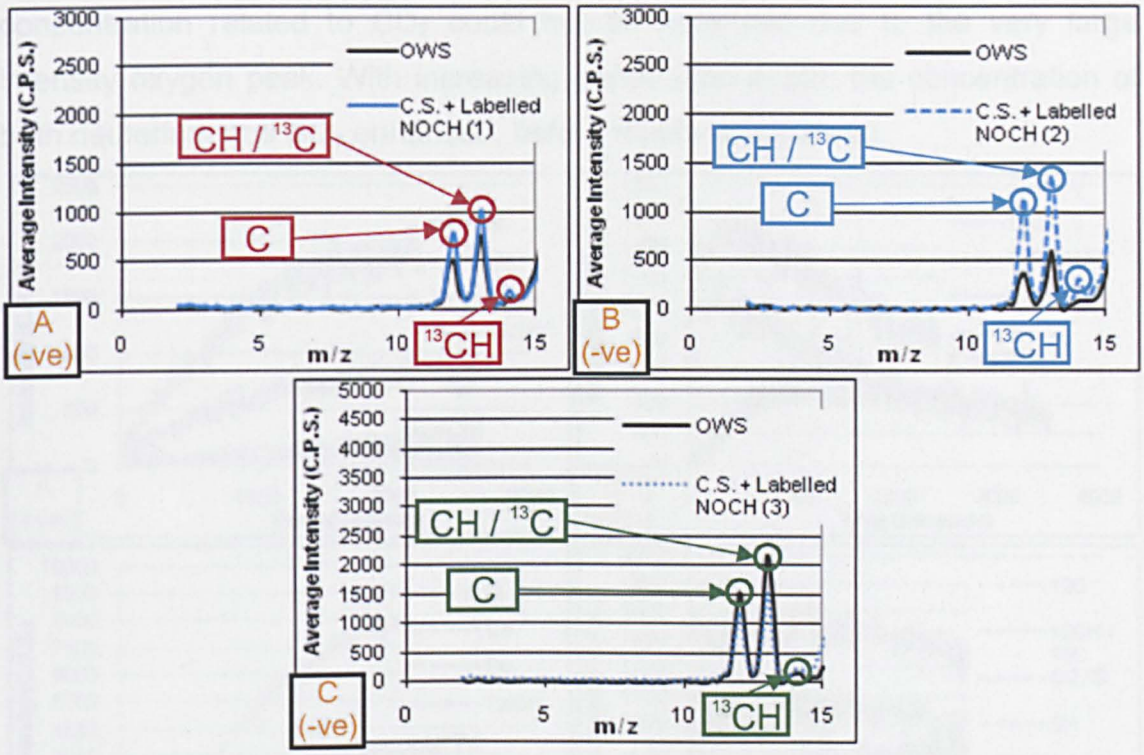

Figure 123: Static mini SIMS spectra of silicon crystal lubricated with calcium sulfonate + labelled NOCH (1) (A), calcium sulfonate + labelled NOCH (2) (B) and calcium sulfonate + labelled NOCH (3) (C)

As can be observed in Figure 124A, C&E, Ca, CaOH and Fe peaks increased in intensity throughout the depth profiling process, on substrates lubricated with calcium sulfonate + labelled NOCH (1-3). Silicon concentration also enhanced with increasing penetration depth on all substrates, yet with labelled NOCH (2) also increased and decreased rapidly at the beginning of the destructive analysis technique (Figure 124C). Intensities of O_2 / S and SH were analogous on all substrates and the compounds exhibited similar trends throughout depth profiling, where concentrations reached overall maximum values (Figure 124B, D&F). The intensities of the two compounds gradually decreased thereafter on calcium sulfonate + NOCH (1) (Figure 124B).

Concentrations of ^{12}C and ^{12}CH / ^{13}C initially increased, before decreasing with increasing penetration depth on calcium sulfonate + NOCH (1&2) substrates (Figure 124B&D). The intensity of ^{12}CH / ^{13}C was consistently greater than ^{12}C throughout depth profiling. In terms of calcium sulfonate + labelled NOCH (3), the intensity of deuterium (D) and CD_3 was plotted instead of carbon 12 and 13 during depth profiling (Figure 124F). This was because of the type of labelling used with NOCH (3) (section 6.3.2.3); mapping of CD_2 would be futile since this was also oxygen and small differences in

concentration related to CD_2 could not be observed due to the very large intensity oxygen peak. With increasing penetration depth, the concentration of both deuterium and CD_3 enhanced, before reaching a plateau.

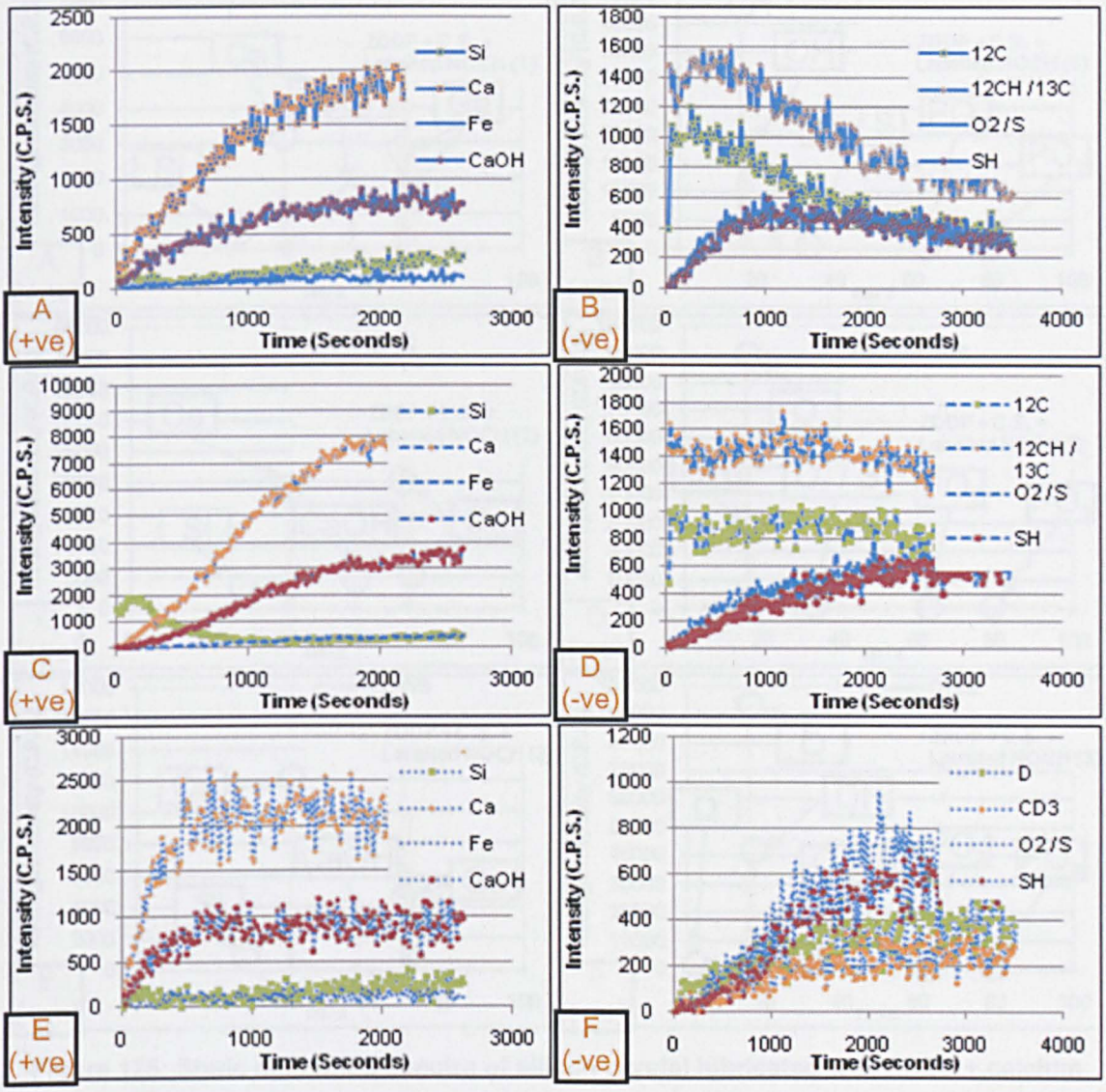

Figure 124: Mini SIMS depth profiles of silicon crystal lubricated with calcium sulfonate + labelled NOCH (1) (A&B), calcium sulfonate + labelled NOCH (2) (C&D) and calcium sulfonate + labelled NOCH (3) (E&F)

7.5.2.9. Silicon Crystal - ZDDP + Calcium Sulfonate + Labelled NOCH

There were many chemical similarities between ZDDP + calcium sulfonate + labelled NOCH (1-3) substrates, as shown in Figure 125. Indeed, the three respective substrates contained Ca, CaOH, Si, O and OH peaks. Ca and CaOH were obtained OWS also (Figure 125A, C&E). Small intensities of an O_2 / S peak were evident exclusively within the wear scar of all three substrates (Figure 125B, D&F). Phosphorus related peaks, namely PO_2 and PO_3, were not evident on the surface of the substrate (Figure 125B, D&F). A peak accredited

to deuterium at 2 m / z was obtained exclusively within the wear scar of the ZDDP + calcium sulfonate + labelled NOCH (3) substrate in Figure 125F.

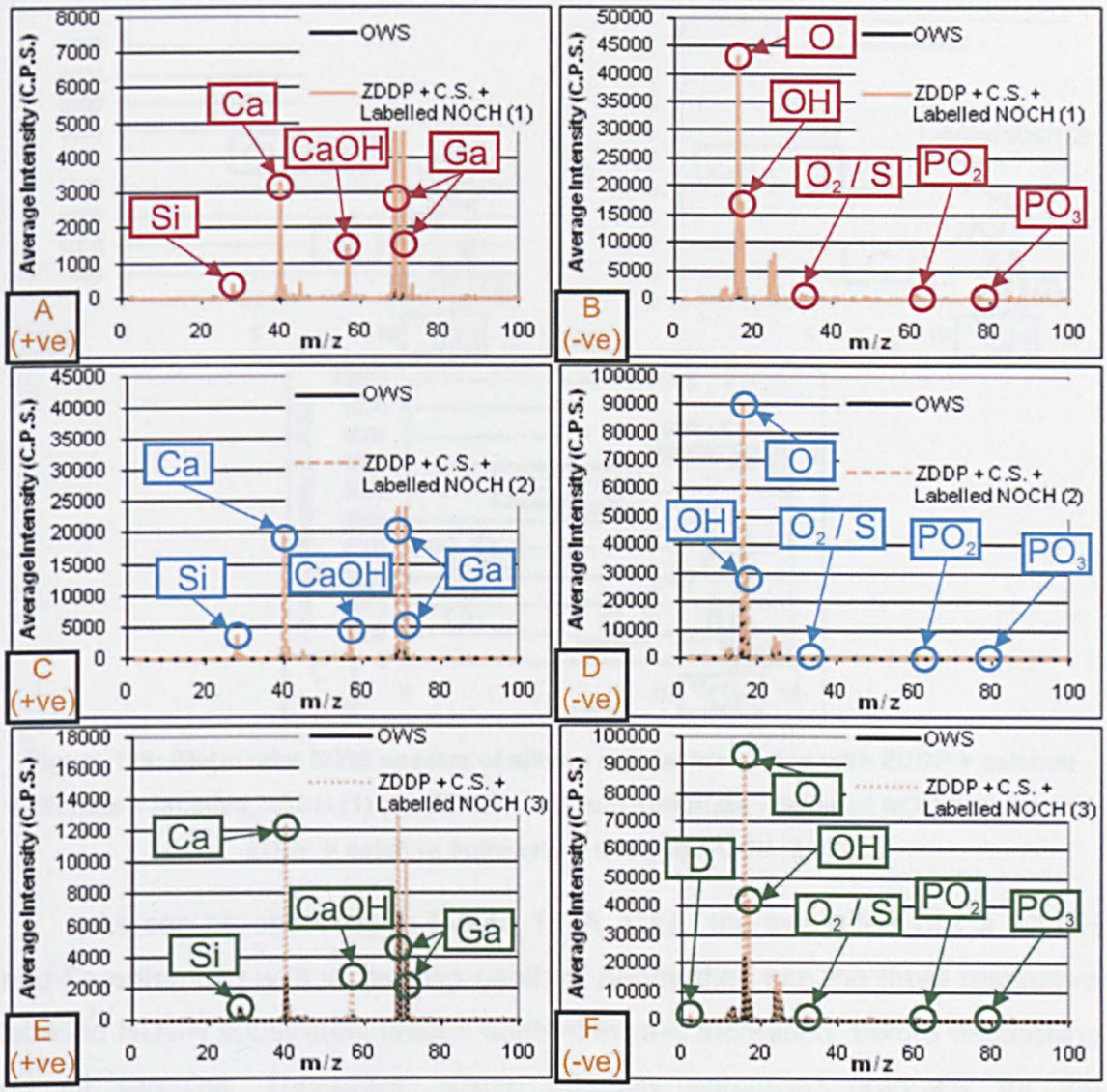

Figure 125: Static mini SIMS spectra of silicon crystal lubricated with ZDDP + calcium sulfonate + labelled NOCH (1) (A&B), ZDDP + calcium sulfonate + labelled NOCH (2) (C&D) and ZDDP + calcium sulfonate + labelled NOCH (3) (E&F)

The data shown in Figure 125B, D & F regarding carbon compounds is highlighted in Figure 126 more clearly using a reduced x axis scale of 0 m / z - 15 m / z. As can be observed, ^{12}C and ^{12}CH / ^{13}C intensities were greatest inside the wear scar using ZDDP + calcium sulfonate + labelled NOCH (1&2) (Figure 126A&B). The latter compound possessed the greater intensity on both substrates, compared to ^{12}C. The same is true regarding ZDDP + calcium sulfonate + labelled NOCH (3), however OWS intensities of the two peaks of interest were similar to those inside the wear scar (Figure 126C). No differences in intensity can be determined at 14 m / z between the three respective

substrates. The deuterium peak identified in Figure 125F is noticeable in Figure 126C.

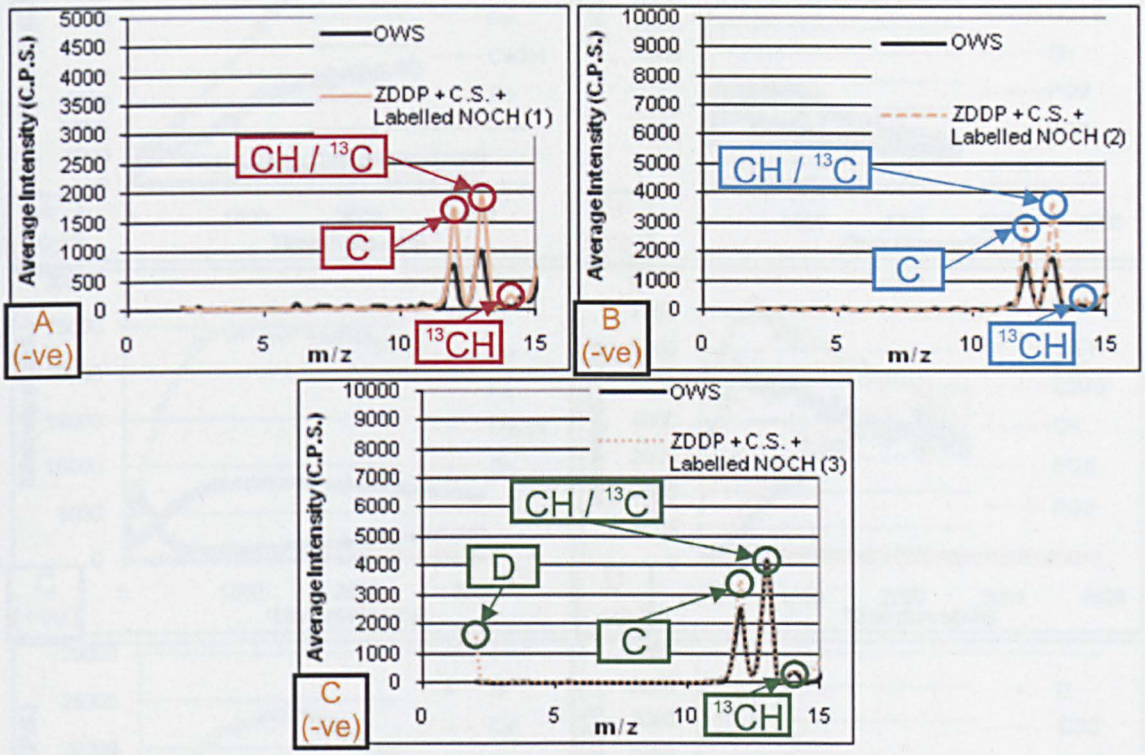

Figure 126: Static mini SIMS spectra of silicon crystal lubricated with ZDDP + calcium sulfonate + labelled NOCH (1) (A), ZDDP + calcium sulfonate + labelled NOCH (2) (B) and ZDDP + calcium sulfonate + labelled NOCH (3) (C)

As can be observed in Figure 127A, C&E, the intensities of Ca, CaOH and Fe enhanced with increasing depth of penetration into the three respective labelled NOCH substrates. Silicon content initially increased, before decreasing on all samples. Thereafter, silicon intensity enhanced gradually for the remainder of the depth profiling process. Phosphorus compounds, namely PO_2 and PO_3, increased from a minimum concentration at the surface of each substrate to an overall maximum intensity during depth profiling (Figure 127B, D&F). The concentration of the two compounds subsequently returned to their minimum values with increasing penetration depth. O_2 / S and SH intensities increased as the depth of analysis into the three respective tribofilms enhanced (Figure 127B, D&F), before subsequently decreasing. The two compounds possessed similar intensities throughout the depth profiling process when silicon crystal was lubricated with either labelled NOCH (1) or (2). However, the concentration of SH had reduced compared to O_2 / S when ZDDP + calcium sulfonate + labelled NOCH (3) was lubricant.

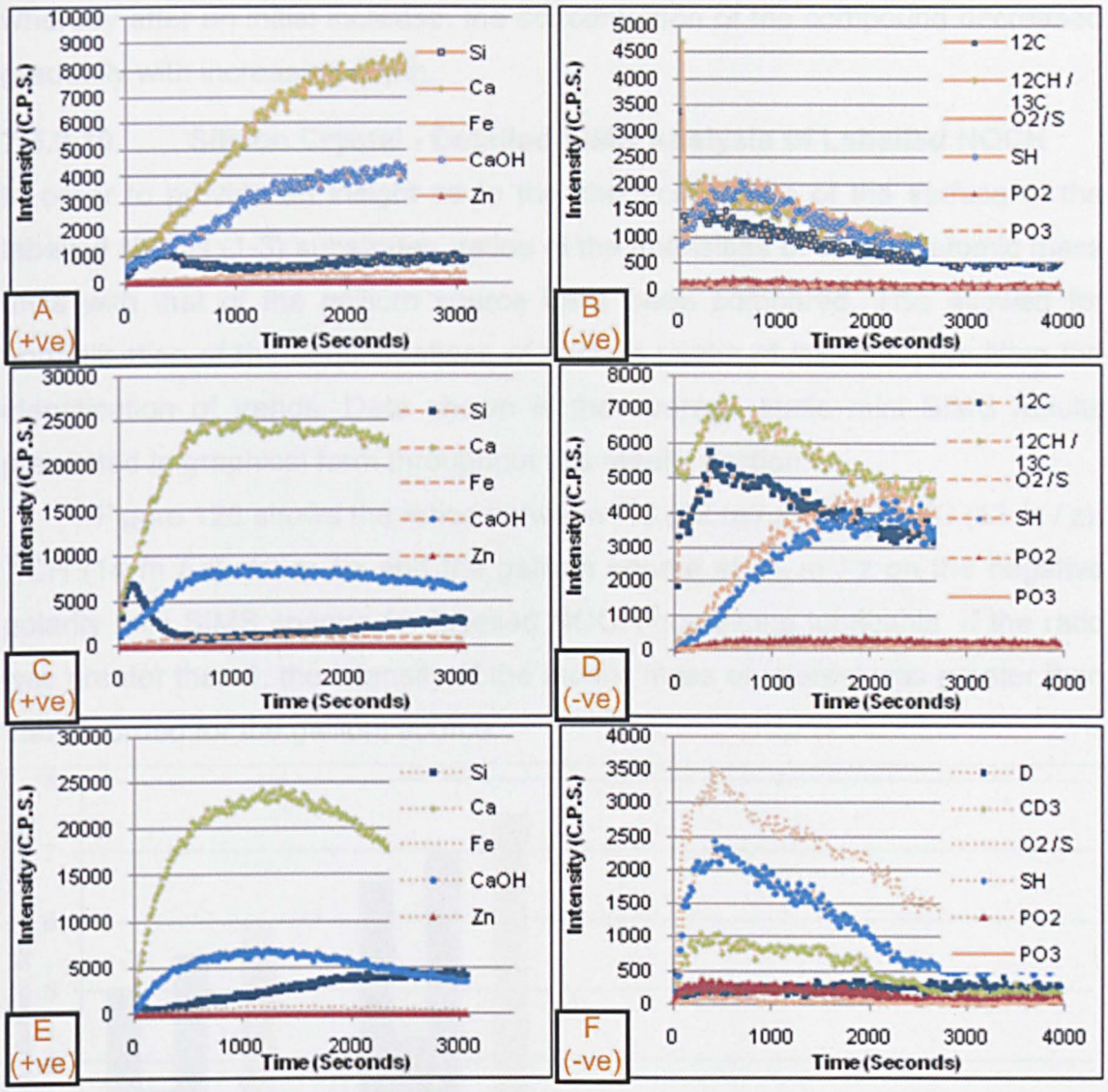

Figure 127: Mini SIMS depth profiles of silicon crystal lubricated with ZDDP calcium sulfonate + labelled NOCH (1) (A&B), ZDDP + calcium sulfonate + labelled NOCH (2) (C&D) and ZDDP + calcium sulfonate + labelled NOCH (3) (E&F)

For the ZDDP + calcium sulfonate + labelled NOCH (1) substrate, the intensity of ^{12}C and ^{12}CH / ^{13}C decreased from maximum values at the surface of the substrate to minimum concentrations at the final point of the depth profiling process (Figure 127B). In the case of ZDDP + calcium sulfonate + labelled NOCH (2), the intensity of ^{12}C and ^{12}CH / ^{13}C increased initially to an overall maximum, before decreasing for the remainder of the depth profile (Figure 127D). Throughout this destructive procedure, ^{12}CH / ^{13}C possessed the greater intensity on labelled NOCH (1&2) substrates. The concentration of deuterium within the ZDDP + calcium sulfonate + labelled NOCH (3) sample increased gradually with increasing penetration depth (Figure 127F). CD_3 displayed a similar trend to that observed with O_2 / S and SH on the substrate,

whereby after an initial increase, the concentration of the compound decreased gradually with increasing depth.

7.5.2.10. Silicon Crystal - Detailed SIMS Analysis of Labelled NOCH

In order to provide an insight as to the chemical nature of the surface of the labelled NOCH (1-3) substrates, ratios of the intensities of specific atomic mass units with that of the gallium source have been compared. This allowed for normalisation of the concentrations of various peaks of interest, permitting the identification of trends. Data shown is the average static mini SIMS results presented in graphical form throughout this results section.

Figure 128 shows the ratios between ^{12}C (12 m / z), ^{12}CH / ^{13}C (13 m / z), ^{13}CH (14 m / z), 19 m / z and the gallium source at 85 m / z on the negative polarity mini SIMS spectra for labelled NOCH containing lubricants. If the ratio was greater than 1, the intensity of the atomic mass of interest was greater than that recorded for the gallium source.

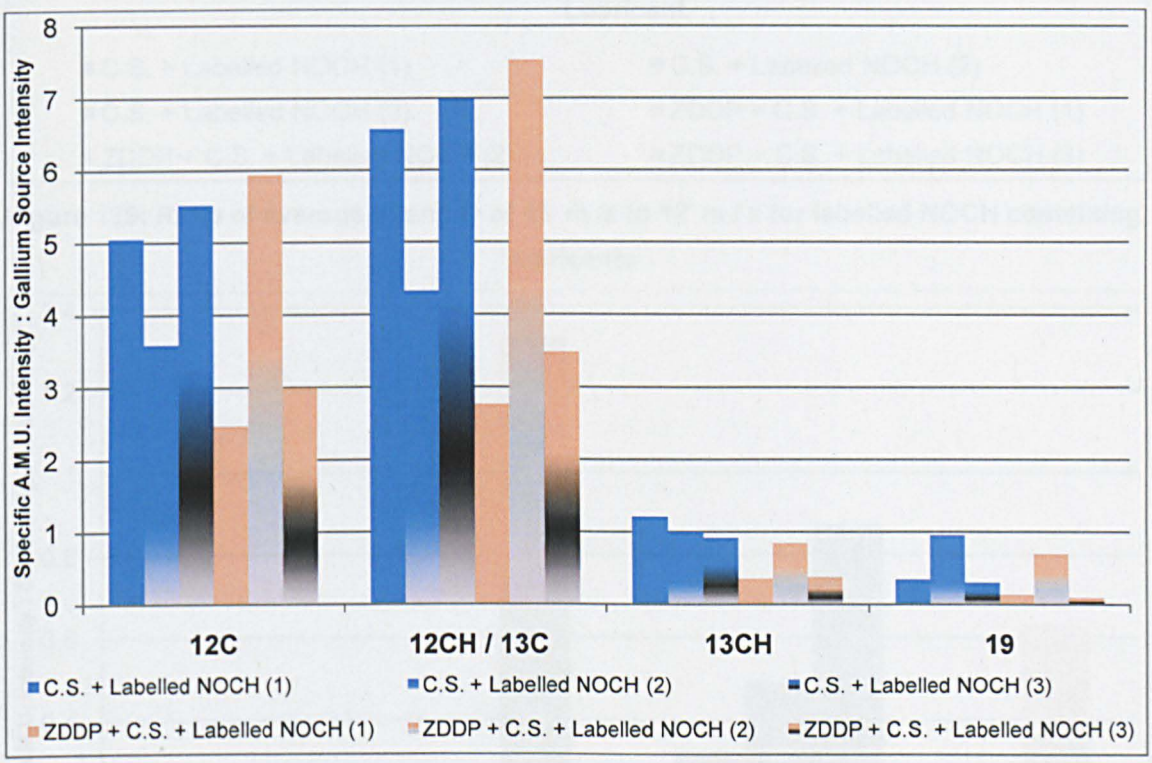

Figure 128: Ratios of specific atomic mass unit to gallium source for different lubricants

Ratios generated from ^{12}CH / ^{13}C were greater than those obtained for ^{12}C. However, no trend was identified which related the addition of ^{13}C to the lubricant (through labelled NOCH 1&2) with an increase in the quantity of ^{13}C observed at the surface of the substrate. This is shown more clearly in Figure 129 where the ratio between ^{13}C and ^{12}C on the six labelled NOCH lubricants

have been calculated. A discernable pattern was not determined for 14 m / z labelled as ^{13}CH in Figure 128. The ratio for 19 m / z against gallium source was displayed in Figure 128 because an increase in intensity of the former was observed exclusively in lubricants which contained labelled NOCH (2).

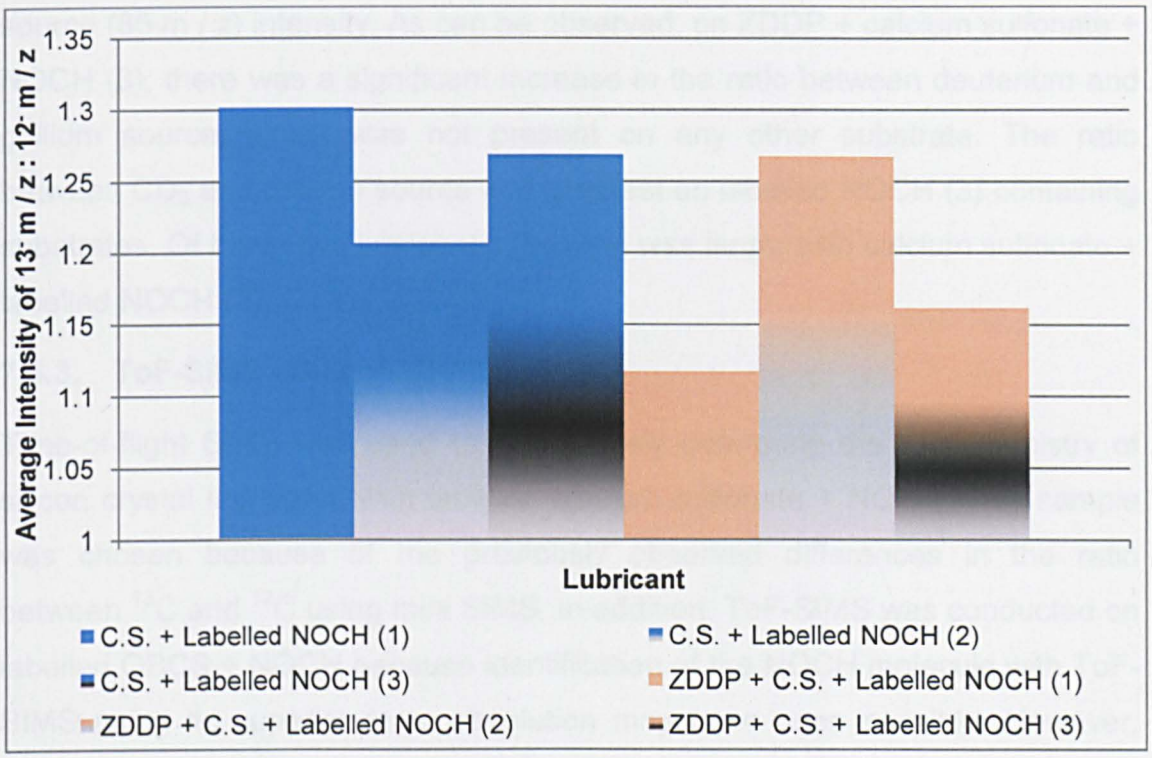

Figure 129: Ratio of average intensity of 13 m /z to 12 m / z for labelled NOCH containing lubricants

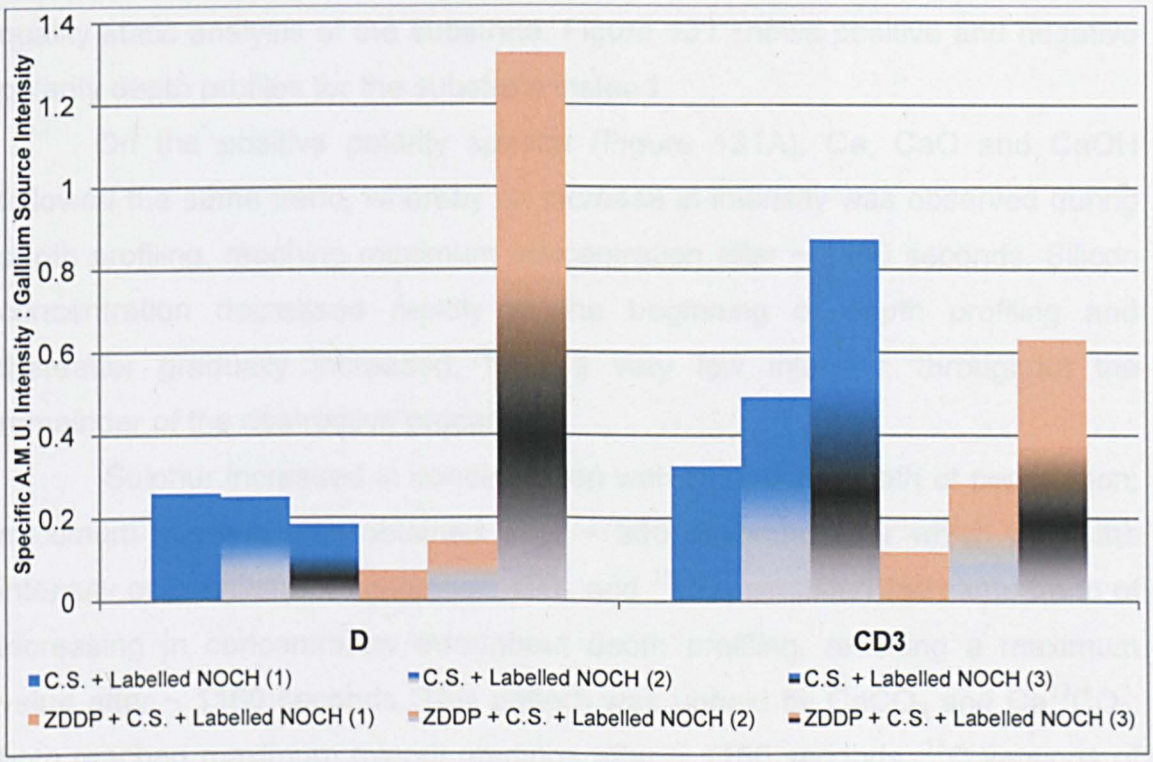

Figure 130: Ratios of deuterium and CD_3 to gallium source, respectively, for different lubricants

In order to determine whether the deuterium labelled NOCH molecule was evident within tribofilms generated on the surface of the silicon crystal substrates, Figure 130 was devised. In this, average intensities of deuterium (2 m / z) and CD_3 (18 m / z), respectively, were compared against the gallium source (85 m / z) intensity. As can be observed, on ZDDP + calcium sulfonate + NOCH (3), there was a significant increase in the ratio between deuterium and gallium source, which was not present on any other substrate. The ratio between CD_3 and gallium source was greatest on labelled NOCH (3) containing substrates. Of these two lubricants, the ratio was larger with calcium sulfonate + labelled NOCH (3).

7.5.3. ToF-SIMS - Silicon Crystal

Time-of-flight SIMS was used to conclusively determine the tribochemistry of silicon crystal lubricated with labelled calcium sulfonate + NOCH. This sample was chosen because of the previously observed differences in the ratio between ^{13}C and ^{12}C using mini SIMS. In addition, ToF-SIMS was conducted on labelled OBCS + NOCH because identification of the NOCH molecule with ToF-SIMS using its superior mass resolution may have been possible. However, triethyl citrate was not observed on the substrate, either as a whole molecule or broken down into smaller fragments. Contamination by PDMS resulted in poor quality static analysis of the substrate; Figure 131 shows positive and negative polarity depth profiles for the substrate instead.

On the positive polarity spectra (Figure 131A), Ca, CaO and CaOH followed the same trend, whereby an increase in intensity was observed during depth profiling, reaching maximum concentration after ~ 1160 seconds. Silicon concentration decreased rapidly at the beginning of depth profiling and thereafter gradually increased, from a very low intensity, throughout the remainder of the destructive process.

Sulphur increased in concentration with increasing depth of penetration; maximum intensity was obtained after ~ 900 seconds, after which point the intensity of the element decreased. CO_3 and $^{13}CO_3$ exhibited the same trend of increasing in concentration throughout depth profiling, reaching a maximum value after ~ 1160 seconds. This pattern was upheld by $CaCO_3$ and $Ca^{13}CO_3$; both reached maximum overall readings after ~ 1160 seconds. ^{13}C versions of both CO_3 and $CaCO_3$ were present in much reduced intensities compared to the

^{12}C form of the two compounds. O_3 increased in intensity during the depth profiling process but was present in the lowest concentration of those atomic masses of interest in the negative polarity spectra.

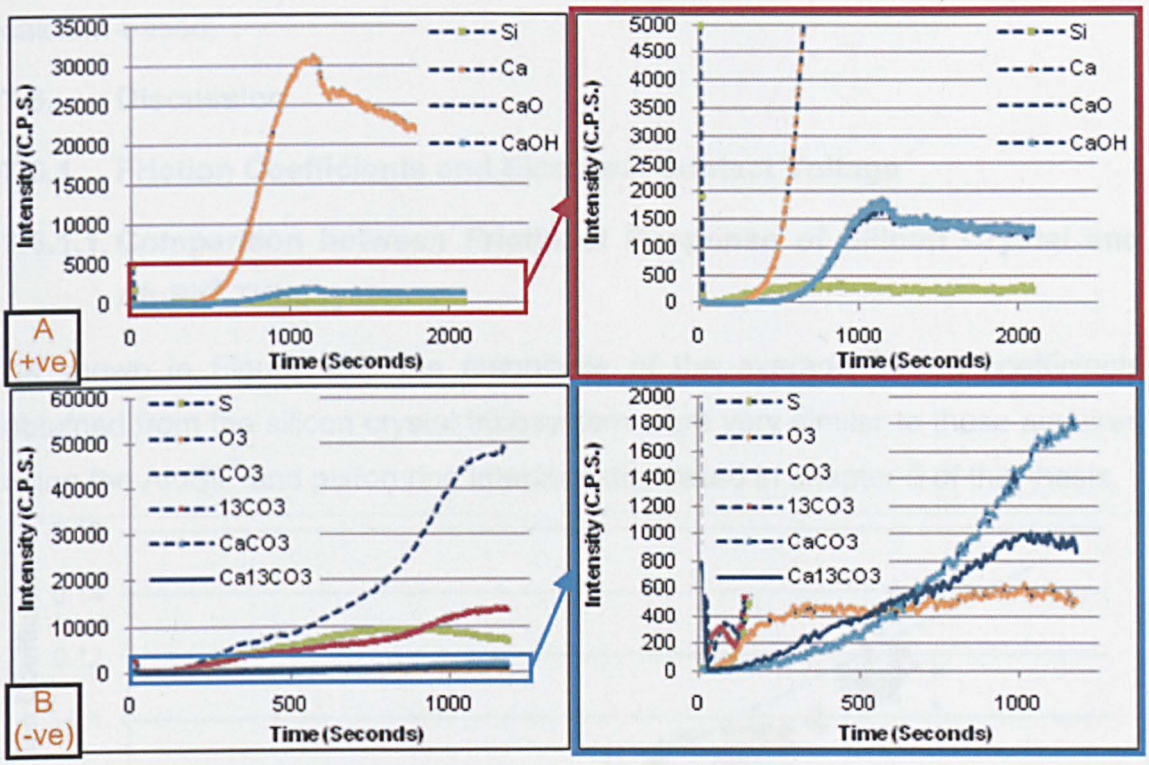

Figure 131: ToF SIMS depth profiles of silicon crystal lubricated with labelled calcium sulfonate + NOCH

7.5.4. EDS - Steel Pin

Table 35 shows the elemental composition of an unworn steel pin determined using energy dispersive x-ray spectroscopy.

Lubricant	Elements Observed
Unworn	C, O, Si, Cr, Mn, Fe, Ni
ZDDP	P, S, Zn
ZDDP + NOCH	P, S, Zn
Calcium sulfonate	S, Ca
Calcium sulfonate + NOCH	S, Ca
ZDDP + calcium sulfonate	P, S, Ca, Zn
ZDDP + calcium sulfonate + NOCH	P, S, Ca, Zn

Table 35: Elements observed during EDS analysis of tribofilms on steel pins used in the silicon crystal tribosystem

When the ferrous substrate was lubricated with ZDDP and ZDDP + NOCH, additional elements of phosphorus, sulphur and zinc were observed.

Lubricating the tribosystem with calcium sulfonate or calcium sulfonate + NOCH resulted in calcium and sulphur compounds being generated on the substrate. ZC or ZCN tribofilms were determined to be phosphorus, sulphur, zinc and calcium-based.

7.6. Discussion

7.6.1. Friction Coefficients and Electrical Contact Voltage

7.6.1.1. Comparison between Frictional Response of Silicon Crystal and AluSil® Tribosystems

As shown in Figure 132, the magnitude of the average friction coefficients obtained from the silicon crystal tribosystem were very similar to those acquired using the AluSil® and piston ring interface discussed in chapter 5 of this thesis.

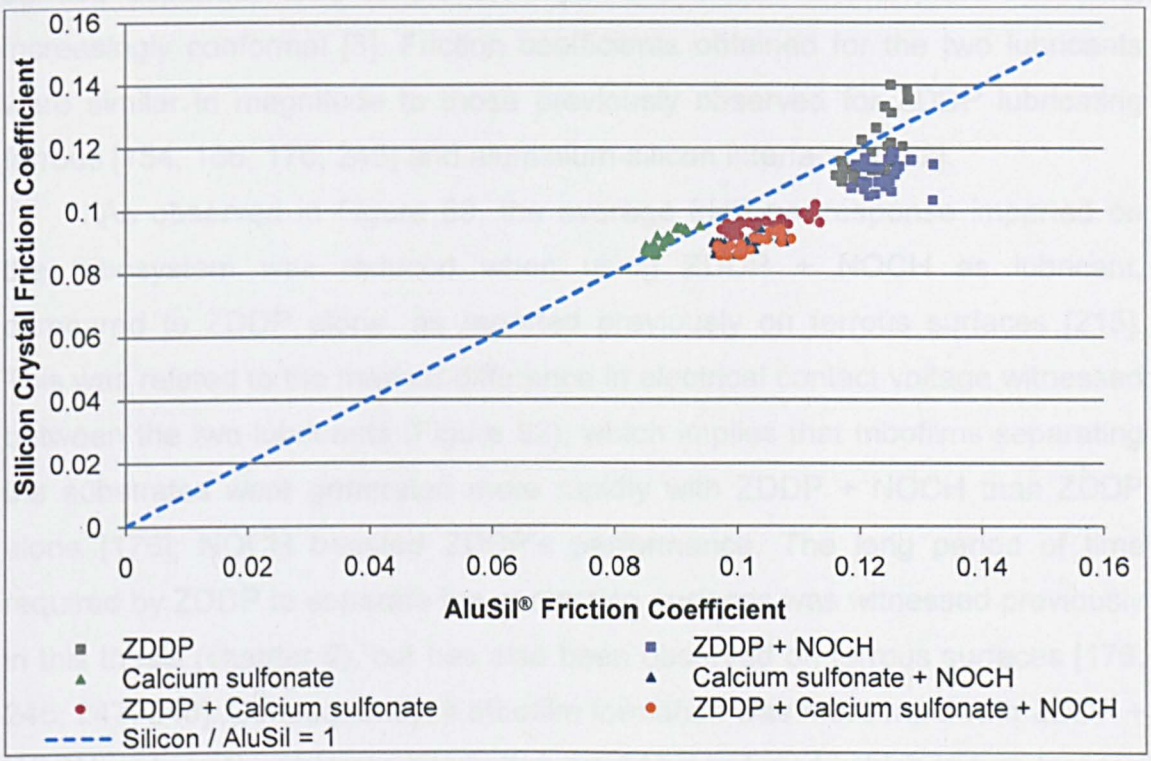

Figure 132: A comparison between average friction coefficients obtained from silicon crystal and AluSil® tribosystems

The frictional response imparted by the majority of test lubricants shown in Figure 132 was marginally greater on the aluminium-silicon tribosystem, compared to silicon crystal. This increase is due to the observed depression of silicon grains into [77, 79, 99, 100], and subsequent plastic deformation of [77, 79, 100], the soft matrix in the aluminium alloy, which act to increase the deformation component of friction [3]. The identical behaviour of calcium sulfonate on either interface suggests silicon depression was not the dominant

contributor to frictional response with this lubricant. Since fracture was observed on silicon grains (chapter 5) and silicon crystal substrate (Figure 102A), this must not contribute a great amount to the overall frictional response. However, the remarkable similarity on the two tribocouples indicates the replication of the contact conditions on silicon grains using silicon crystal was successful. Moreover, it follows that frictional response in either contact was derived from the interaction between tribofilms generated on steel and silicon surfaces.

7.6.1.2. ZDDP vs ZDDP + NOCH

Initial increases, followed by a gradual reduction in frictional response witnessed with both ZDDP and ZDDP + NOCH (Figure 89), can be accredited to the running in period of the two substrates, whereby interaction between surface asperities lead to the steel pin and silicon crystal plate becoming increasingly conformal [3]. Friction coefficients obtained for the two lubricants were similar in magnitude to those previously observed for ZDDP lubricating ferrous [154, 166, 176, 245] and aluminium-silicon interfaces [152].

As observed in Figure 89, the average frictional response imparted on the tribosystem was reduced when using ZDDP + NOCH as lubricant, compared to ZDDP alone, as reported previously on ferrous surfaces [215]. This was related to the marked difference in electrical contact voltage witnessed between the two lubricants (Figure 92), which implies that tribofilms separating the substrates were generated more rapidly with ZDDP + NOCH than ZDDP alone [176]; NOCH boosted ZDDP's performance. The long period of time required by ZDDP to separate the contacting surfaces was witnessed previously in this thesis (chapter 5), but has also been observed on ferrous surfaces [176, 245, 247, 248]. Consequently, if tribofilm formation was more rapid with ZDDP + NOCH, substrate-substrate interaction would be reduced, which in turn lessens both the deformation and adhesive components of friction and thus the frictional response of the tribosystem [3].

Since ZDDP-derived tribofilms are known to increase in size with duration of rubbing on silicon surfaces [66], the swift reduction in friction coefficient observed using either lubricant can be accredited to a progressive decline in substrate interaction through increased tribofilm surface coverage. Therefore, with extended periods of rubbing, the tribofilm's shear strength [160] would influence frictional response to a greater extent.

7.6.1.3. Calcium Sulfonate vs Calcium Sulfonate + NOCH

The frictional response (Figure 89) and electrical contact voltage (Figure 92) exhibited by calcium sulfonate and calcium sulfonate + NOCH were very similar. The magnitude of the frictional response [176] and the observed reduction in friction coefficient compared to ZDDP [166, 176] are analogous to that of which has been reported to occur on ferrous substrates lubricated with OBCS.

As documented in literature [176] and observed in chapter 5 of this thesis, overbased calcium sulfonate is known to separate contacting substrates rapidly. This was also observed for 350 TBN OBCS (Figure 93) and those lubricants containing 400 TBN OBCS + labelled NOCH (Figure 94). Since the wear scar on silicon crystal lubricated with OBCS and OBCS + NOCH was entirely covered with a tribofilm (Figure 99), it follows that the shear strength of the film must be dictating the frictional response in the tribosystem [160] and thus be the main contributor to the adhesive component of friction [3]. Therefore, this implies the reduction in friction coefficient compared to ZDDP and ZDDP + NOCH must be attributed to not only a decline in the interaction between substrates (reducing both adhesion and deformation [3]), but also through a lower shear strength possessed by OBCS tribofilms.

Since reductions in frictional response observed with the 350 TBN versions of calcium sulfonate and OBCS + NOCH (section 7.2) were not due to differences in electrical contact voltage (Figure 93), it follows that a decrease in μ must be derived from a slight reduction in shear strength and thus adhesive friction [3] proffered by the lower-TBN additive. This implies shear strength was related to the amount of $CaCO_3$ in the core of the detergent. Furthermore, given that the ^{13}C versions of both NOCH and overbased calcium sulfonate increased the frictional response compared to ^{12}C variants (section 7.2), it follows that the isotope of carbon also influenced the friction in the tribosystem.

7.6.1.4. ZDDP + Calcium Sulfonate vs ZDDP + Calcium Sulfonate + NOCH

Overbased calcium sulfonate was playing a major role in film formation when used in conjunction with ZDDP, since, as shown in Figure 92, separation of the substrates using ZDDP + calcium sulfonate was rapid and reminiscent of that obtained using calcium sulfonate alone. This behaviour was also mirrored in terms of ZDDP + calcium sulfonate + NOCH, and in addition, the variants of lubricant ZCN which contained 350 TBN OBCS, labelled OBCS or labelled

NOCH (section 7.2), respectively. Interestingly, even though the combination of OBCS and ZDDP is reported to hinder surface separation compared to the sole usage of either additive on ferrous substrates [176], the results acquired from this tribosystem and that in chapter 5 show emphatically that film formation was improved compared to ZDDP alone. This would explain the frictional response observed for lubricants ZC and ZCN compared to ZDDP (Figure 89), since the rapid separation of the substrates and thorough coverage of wear scars by generated tribofilms (Figure 102&Figure 104) minimised substrate-substrate interaction and thus the coefficient of friction [3].

Given that the frictional response (section 7.2) exhibited by lubricant ZCN was very similar to that displayed by lubricant CN, it follows that the two must have possessed a similar shear strength. However, the observed increase in frictional response of lubricant ZC compared to calcium sulfonate, and decrease compared to ZDDP, as has previously been reported on ferrous [176] and Al-Si (chapter 5) surfaces, implies ZDDP must be incorporated into the tribofilm and thus influencing μ. Furthermore, it follows that ZDDP must have influenced frictional response to a greater extent with lubricant ZC compared to ZCN, given that the coefficient of friction was higher with the former lubricant.

As with OBCS and OBCS + NOCH (section 7.6.1.3), frictional response decreased when the TBN of the detergent was reduced, yet increased when ^{13}C derivatives of OBCS and NOCH were employed. Therefore, since ECV results were identical (section 7.2), these frictional variations must be accredited to alterations in tribofilm shear strength [3].

7.6.1.5. Summary

Frictional responses obtained from the lubrication of silicon surfaces were slightly lower than those on AluSil®; this was accredited to the additional deformation force of friction originating from the depression of silicon grains and subsequent plastic deformation of the aluminium matrix within the aluminium-silicon alloy.

On the silicon crystal substrate, due to superior film formation and surface coverage, ZDDP + NOCH reduced friction in the contact compared to ZDDP alone. Lubricants C & CN reduced frictional response compared to ZDDP and ZDDP + NOCH, because of the minimisation of substrate-substrate interaction, together with a reduction in shear strength of the detergent

tribofilms. Lubricant ZCN imparted similar frictional response as to that obtained with lubricant CN, whereas an increase in frictional response witnessed by lubricant ZC was attributed to a greater incorporation of ZDDP into the tribofilm. Lower TBN detergents imparted reduced frictional responses, whilst the incorporation of ^{13}C $CaCO_3$ or NOCH increased the coefficient of friction.

7.6.2. Surface Topography, Wear and Tribofilm Mechanical Properties

7.6.2.1. ZDDP vs ZDDP + NOCH

As shown in Figure 97 and Figure 98, tribofilms were generated on silicon crystal when lubricated with ZDDP or ZDDP + NOCH. Both possessed a structure which was remarkably similar to that observed on ferrous [122, 145-147, 149, 252-255] and aluminium-silicon surfaces [66], respectively, but did not cover large areas of the wear scar. However, the film formed from ZDDP + NOCH was far less patchy and comprised larger pad sizes compared to ZDDP; identical behaviour was observed on silicon grains within AluSil® (chapter 5). Similarly, although tribofilms generated on the counterpart steel pins consisted of a structure resembling that obtained from ZDDP on other ferrous substrates [122, 145-147, 149, 252-255] (Figure 105) and covered the wear scar on the pin, the surface density of the pads appeared to increase with the usage of ZDDP + NOCH. Therefore, two conclusions can drawn from these results; the first is that film formation on both ferrous and silicon surfaces was improved when ZDDP + NOCH was used as lubricant, and the second, is that it can be implied that ZDDP film formation is far superior on ferrous, rather than silicon surfaces.

The reduction in wear witnessed with ZDDP + NOCH, compared to ZDDP, has been observed previously on ferrous surfaces [215] and on AluSil® in chapter 5. The more distinct decrease in wear levels on the ferrous (Figure 96), rather than silicon substrate (Figure 95) with ZDDP + NOCH, implies that the tribofilm has a greater influence on the wear of ferrous surfaces. Since ECV can be related to wear [176], it follows that due to the inferior surface separation afforded to the contact by ZDDP (Figure 92), substrate-substrate interaction [234] and thus wear in the tribosystem amplified. Indeed, referring to Figure 97 and Figure 98, it is apparent that a large quantity of wear debris was present on the silicon crystal substrate when lubricated with ZDDP; this reduced with ZDDP + NOCH. Due to the inherent hardness of the silicon crystal substrate (Table

25), it follows that wear debris will primarily originate from abrasive wear of the softer steel pin [7] (Table 28). The origin of this material could also be from asperities which have been removed through adhesion and entrained into the tribosystem [7].

As shown in Table 36, the thickness and reduced elastic modulus of the tribofilms generated from ZDDP + NOCH were greater than those fashioned from ZDDP on silicon crystal. Nonetheless, the mechanical properties of lubricant Z and ZN tribofilms were within the range of those obtained on silicon grains within aluminium-silicon alloys (Table 36), yet declined in magnitude compared to films generated on ferrous substrates (Table 36).

Substrate	Thickness (nm)	Reduced Elastic Modulus (GPa)
Ferrous Surface	150 [120, 148] 120 [143]	82 ± 18 [122] 96.7 ± 25.7 [145] 87 ± 23 [146] 74 ± 20 [146] 117 ± 16 [149]
Silicon Grain within Aluminium-Silicon Alloy	42 ± 4 [152] 40 - 225 [25] 150 - 250 [66]	30.3 ± 7.8 [153] 84 ± 10 [152] 77 ± 11 [25]
Silicon Surface	84 ± 11 (ZDDP) 104 ± 14 (ZDDP + NOCH)	62.4 ± 6.4 (ZDDP) 71.4 ± 12.0 (ZDDP + NOCH)

Table 36: Comparison between mechanical properties of ZDDP-based tribofilms from literature and current work

Tribofilms generated on silicon surfaces must impart wear protection onto the tribosystem through the reported qualities of ZDDP-based layers formed on ferrous surfaces, namely preferential wear [145] and load carrying [120, 146]. Since the reduced elastic modulus of the tribofilms was much less than that of the silicon substrate (section 6.3.1.1), tribofilms would undergo plastic deformation in preference to the silicon crystal [145]. Differences in reduced elastic modulus between tribofilms may therefore affect wear performance. However, it is concluded that the reduction in wear by ZDDP + NOCH can be accredited to the increased surface coverage and thickness of

the tribofilms compared to ZDDP; the load placed upon the tribosystem was therefore supported to a greater extent by the tribofilm [146].

7.6.2.2. Calcium Sulfonate vs Calcium Sulfonate + NOCH

The observed reduction in wear on both pin and plate (Figure 95&Figure 96) compared to ZDDP when using calcium sulfonate as lubricant, has been reported previously on ferrous surfaces [165, 166, 169, 176]. As with ZDDP + NOCH, lubricant CN imparted a further reduction in wear on both ferrous and silicon substrates compared to calcium sulfonate; this has been observed previously [215]. Unlike lubricants Z or ZN, however, the electrical contact voltage results (Figure 92) obtained for OBCS and OBCS + NOCH were identical; differences in wear levels due to poor film formation [176] can be discarded.

Tribofilms were generated across the entire wear scar on the silicon substrates with lubricants C and CN (Figure 99&Figure 101). Such a large surface coverage is most probably the reason for the dramatic reduction in wear compared to ZDDP and ZDDP + NOCH; this increase in tribofilm coverage was also witnessed on silicon grains within AluSil® substrates (chapter 5). Films fashioned from OBCS very much resembled those observed on ferrous surfaces [177]. The non-connected pads were identical to those identified on silicon grains within AluSil® (section 5.5.1.3).

The measured thicknesses of the tribofilms on silicon crystal generated from OBCS and OBCS + NOCH (Table 34) were analogous to one another and were within the range reported for overbased calcium sulfonate films formed on ferrous substrates [177]; differences in wear performance between the detergents cannot be accredited to film thickness. Indeed, the antiwear properties of overbased calcium sulfonates are thought to originate from the tribofilm minimising interaction between contacting substrates [160] and enduring wear in preference to substrate surfaces [165]. Therefore, it follows that since the film formed from OBCS + NOCH on either substrate was free of voids and more dense, the pores located within the OBCS tribofilms must have facilitated a degree of substrate-substrate interaction [160], which resulted in the observed moderate increase in wear levels. In addition, since the calcium sulfonate + NOCH tribofilm was more susceptible to plastic deformation than OBCS (Table 34), it is logical to suggest that this may lead to lower wear levels

through an increase in the tendency to undergo plastic deformation relative to the silicon crystal substrate [145].

7.6.2.3. ZDDP + Calcium Sulfonate vs ZDDP + Calcium Sulfonate + NOCH

Marked differences in structure were observed between tribofilms generated on substrates lubricated with ZDDP + calcium sulfonate, compared to lubricant ZCN (Figure 102&Figure 104). Indeed, referring to section 7.5.1, triethyl citrate removed the ZDDP-derived phosphate glass section from lubricant ZCN films generated on ferrous and silicon surfaces.

An increase in wear has been reported on ferrous surfaces lubricated with ZDDP + overbased calcium sulfonate, compared to ZDDP or OBCS, respectively [166, 184, 185]. However, this is not the case herein, since lubricant ZC was superior in antiwear performance compared to the sole use of either additive on ferrous and silicon substrate (Figure 95&Figure 96). Furthermore, the addition of NOCH to lubricant ZC imparted lower wear levels on the interface, but this was not achieved through a variation in film thickness (Table 34), which was double that obtained using XANES analysis of a ZDDP + OBCS tribofilm on a ferrous substrate [185].

Perhaps the marked reduction in voids within the ZCN tribofilm (Figure 102&Figure 104) resulted in the observed lower wear levels; surface interaction [160] was minimised. Additionally, since differences in the reduced elastic modulus of tribofilms affect wear, the lubricant ZCN film may have provided an optimum elasticity for the tribosystem, being sufficiently low to preferentially wear [145], but great enough to retain its structure under tribological conditions [120]. As shown by the significant decline in wear on the steel pin (Figure 96) the ZCN tribofilm appeared to be more beneficial to ferrous, rather than silicon substrates.

7.6.2.4. Summary

The formation of tribofilms on both silicon and steel surfaces was improved with lubricant ZN compared to ZDDP, with both films similar to those obtained on ferrous substrates. ZDDP + NOCH reduced the wear in the tribosystem compared to lubricant Z; this was accredited to an increased surface coverage of the tribofilm and a greater film thickness.

OBCS and OBCS + NOCH further reduced the wear in the interface due to a marked increase in tribofilm surface coverage. Lubricant CN provided

additional lower wear levels due to a denser tribofilm, which was more prone to plastic deformation. As with OBCS and OBCS + NOCH, lubricant ZCN reduced wear compared to ZC not through film thickness, but instead through an increase in surface coverage and variation in the reduced elastic modulus of generated tribofilms. An overview of the benefits of NOCH in terms of tribological performance and surface topography are shown in Table 37.

Lubricant	Effect of the Addition of NOCH
ZDDP	Decreased friction; improved surface separation and film formation; reduced wear; improved film thickness
Calcium sulfonate	Reduced wear; improved film surface coverage and density
ZDDP + calcium sulfonate	Decreased friction coefficient; reduced wear; improved film surface coverage

Table 37: Overview of the effect of the addition of NOCH on test oils used to lubricate an silicon crystal and steel pin tribosystem

7.6.3. Tribochemical Analysis and Film Formation

7.6.3.1. ZDDP vs ZDDP + NOCH

7.6.3.1.1. Tribochemistry

The observation of Si, SiOH and FeOH within the wear scar of ZDDP and ZDDP + NOCH silicon crystal samples (7.5.2) indicated both the possible contamination by PDMS [258] and also the presence of the underlying substrate, since generated tribofilms did not cover large areas (section 7.6.2.1). Silicon intensity increased noticeably throughout depth profiling, indicating greater volumes of the silicon crystal surface were being analysed with increasing depth of analysis, as expected. The observed increase in iron intensity throughout depth profiling, albeit greatly reduced compared to that obtained for Si, suggests material transfer from steel pin to hard silicon substrate occurred; as discussed in section 7.6.2.1.

Analysis of silicon crystal lubricated with ZDDP identified the main zinc diakyldithiophosphate tribofilm SIMS related peaks of O_2 / S, PO_2 and PO_3 [118, 266], which were not obtained OWS; identical to that obtained on AluSil® (section 5.6.3.2) previously. The tribofilm therefore appears to be polyphosphate-based [118]. Sulphur was likely to be in the form of sulphide, as

this is known to be present within ZDDP-based tribofilms [118, 120, 125, 126, 132, 139]. Interestingly, however, these compounds were not obtained at the tribofilm surface of the ZDDP + NOCH substrate. These findings correlate well with the results obtained using AluSil® (chapter 5), since the intensity of these compounds on the surface the alloy lubricated with ZDDP + NOCH were reduced markedly compared to ZDDP alone. The explanation for this could be that the addition of NOCH lead to a greater carbon concentration on the surface of the tribofilm, which reduced the signal intensity for phosphorus and sulphur species during static analysis.

However, during the depth profiling process, it was quite evident that unlike the results found on the aluminium-silicon substrate (chapter 5), the maximum intensity, and indicatively, one could assume volume, of O_2 / S, PO_2 and PO_3 were obtained when using ZDDP as lubricant. Although, due to the SIMS process being non-quantitative, this cannot be verified. Two possibilities arise for the explanation of this finding; the first is that since there was a greater volume of wear debris on silicon crystal lubricated with ZDDP (section 7.6.2.1), it follows that this may have housed tribofilm species which subsequently contributed to the recorded concentration of phosphorus and sulphur compounds. Alternatively, given that the differences in intensity between lubricant Z and ZN were only slight, and nowhere near as marked as on AluSil® samples, it follows that these semi-conductive samples were difficult to analyse using mini SIMS.

With increasing penetration depth, the concentration of oxygen and hydroxyl increased on the substrates, as previously observed on AluSil® (chapter 5) lubricated with ZDDP or ZDDP + NOCH. However, whereas on those substrates phosphorus and sulphur intensities decreased with increasing penetration depth, the opposite is true here. Indeed, it appears that intensities of the tribofilm species were at a maximum near the surface of the silicon crystal substrate. Due to the lack of zinc observed throughout both static and depth analyses, it follows that the polyphosphate-based tribofilm must be iron related. Given that results from EDS analysis showed evidence for phosphorous, sulphur and zinc within the tribofilm on the steel pin, it must follow that the tribofilm was of a relatively similar structure to those generated on the silicon surface, with the addition of associated zinc tribofilm species.

7.6.3.1.2. Film Formation

As discussed in section 5.6.3.2, an amalgamation of two well known ZDDP film formation processes has been used to explain tribofilm generation on substrates. Since it was apparent that iron polyphosphates were the sole type of phosphate species throughout tribofilms on the silicon surfaces, it is logical to assume that the ferrous pin was involved in film formation. Hence, as discussed in section 7.6.2.1, under the initial stages of rubbing, the steel pin was worn by the harder silicon surface, creating iron oxide which was transferred to the silicon substrate. Iron was also identified previously on silicon grains within worn AluSil® (section 5.5.3.2). The oxide layer, which is known to react with zinc polyphosphates [267], permitted the adsorption of a linkage isomer and or ZDDP onto both ferrous and silicon surfaces [98, 131]. Incorporating the mechanism described by Martin et al. using the chemical hardness approach [126], iron phosphates subsequently formed as a result of the substitution of Zn^{2+} for Fe^{3+}, via interaction with iron oxide. Since ZnO is predicted to form here also [126], it must be present in very small volumes, given that zinc was not observed on the silicon crystal. In addition, iron / zinc phosphorus compounds were also generated on the steel pin [126, 139]. Simultaneously, the NOCH molecule generated metal complexes (Figure 79) with both steel and silicon surfaces, as previously predicted (chapter 5), where M = Cr, Fe or Si.

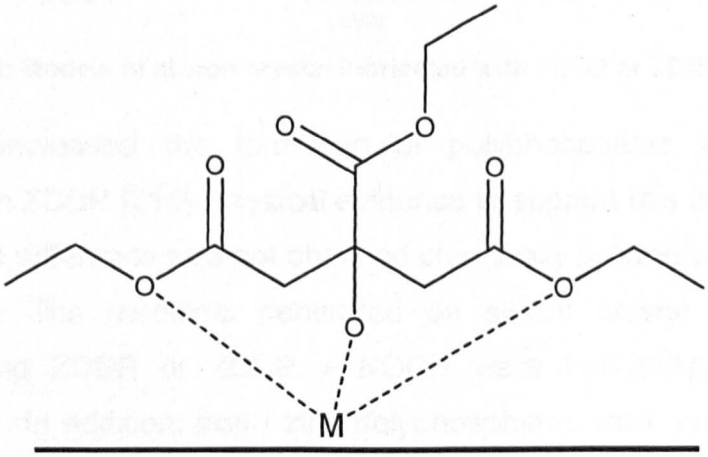

Figure 79: Metal complex formed using triethyl citrate

Oxygen then initiated the thermo-oxidative decomposition of the adsorbed compounds on either substrate, creating both associated iron and zinc polyphosphate and sulphur compounds using the process described by Fuller et al. [131]. Since NOCH supplied the tribosystem with a greater concentration of oxygen, it follows that ZDDP decomposition increased; oxygen

enhancement is known to improve wear [141]. This resulted in enhanced phosphate and sulphur intensities compared to ZDDP alone, as previously reported on AluSil® and steel piston ring surfaces (section 5.6.3.2) and in literature [215]. Although this was not identified chemically on the silicon crystal surfaces, it was clear from microscopy results that the generated polyphosphate tribofilms were in a greater abundance and of larger dimensions on silicon crystal lubricated with ZDDP + NOCH, compared to ZDDP (section 7.6.2.1).

7.6.3.1.3. Summary

Models of the respective tribofilms generated on silicon crystal substrates are shown in Figure 133.

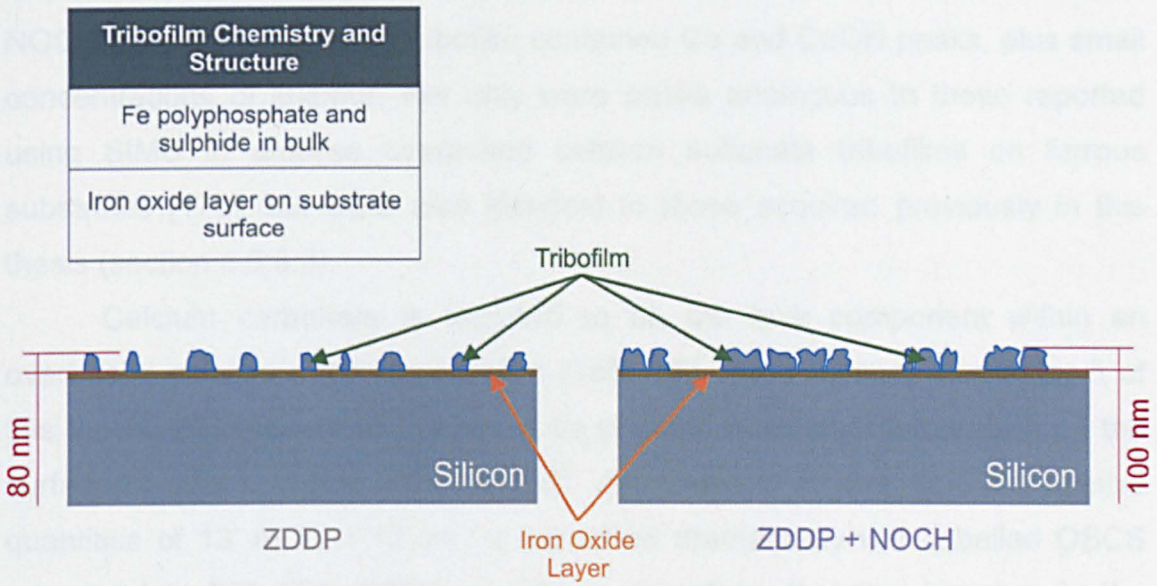

Figure 133: Models of silicon crystal lubricated with ZDDP or ZDDP + NOCH

NOCH increased the formation of polyphosphates when used in conjunction with ZDDP [215]; physical evidence to support this theory has been produced, but a difference was not obtained chemically between lubricant Z and ZN substrates. The tribofilms generated on silicon crystal and steel pin substrates using ZDDP or ZDDP + NOCH were iron polyphosphate and sulphide-based. In addition, iron / zinc polyphosphates were predicted to form on the ferrous substrate. As observed in literature [267], iron oxide facilitated tribofilm formation and was seen as an early step in film generation. The main difference observed herein on the silicon crystal substrates compared to that on AluSil® (section 5.6.3.2) was the formation of zinc related polyphosphate and sulphide species on the latter surface. It must follow that greater volumes of iron oxide were transferred to the silicon crystal, rather than silicon grain surface,

which lead to iron phosphate creation, rather than a mixed iron / zinc polyphosphate [126]. The reduction in wear imparted by ZDDP + NOCH compared to ZDDP was due to an enhancement in the oxygen concentration resulting in the greater decomposition of ZDDP. This, in turn, generated a tribofilm which covered the substrate surface to a larger degree and reduced interaction between pin and plate.

7.6.3.2. Calcium Sulfonate vs Calcium Sulfonate + NOCH

7.6.3.2.1. Tribochemistry

As shown in section 7.5.2, the chemistry of films formed on silicon crystal lubricated with the many variants of calcium sulfonate and calcium sulfonate + NOCH were identical; each tribofilm contained Ca and CaOH peaks, plus small concentrations of sulphur. Not only were peaks analogous to those reported using SIMS to analyse overbased calcium sulfonate tribofilms on ferrous substrates [178], but were also identical to those acquired previously in this thesis (section 5.6.3.3).

Calcium carbonate is reported to be the bulk component within an overbased calcium sulfonate tribofilm [165, 167, 168]. Indeed, in chapter 5 of this thesis, FTIR identified $CaCO_3$ to be present in an amorphous form on the surface of silicon grains within AluSil®. As shown in Figure 121, the relative quantities of 13^- m / z : 12^- m / z increased dramatically with labelled OBCS compared to 350 TBN OBCS. It follows, therefore, that this increase in the relative amount of 13 m / z could only derive from the ^{13}C labelled carbonate core of the overbased micelle; this proves that $CaCO_3$ was present within generated tribofilms. Unlike that reported in literature, it was not possible using the mini SIMS technique to state whether NOCH enhanced calcium carbonate formation [215].

During depth profiling of each of the three variants of calcium sulfonate and calcium sulfonate + NOCH evaluated, the observed behaviour of calcium hydroxide and the calcium peak found at 40^+ m / z suggests these were the bulk component of the film. The peak associated with iron mirrored the trend of CaOH, and it is most likely that this is CaO, having been previously observed on ferrous surfaces [166, 178, 180]. PDMS contamination [258] was evident on the majority of substrates as the Si peak rapidly declined in intensity at the beginning of the depth profiling process. Since the trend observed for O_2 / S

was mirrored by SH during depth profiling, it follows that this must be indicating the presence of sulfonate chains within the tribofilm, given that this was the only source of sulphur in the lubricant. This has been reported on ferrous surfaces [178] and therefore is most probably the form of sulphur witnessed on the steel pin via EDS analysis (Table 35).

Conclusive evidence for the structure of the generated film from overbased calcium sulfonate tribofilms was obtained using ToF-SIMS. The depth profiles shown in Figure 131 reiterate that of which has been observed using mini SIMS hitherto. However, it can now be stated irrefutably that the Fe peak observed on silicon crystal substrates using mini SIMS was CaO, since this compound and CaOH share the same trends during ToF-SIMS analysis. The observation of $CaCO_3$ is in accordance with literature [178].

By assuming a constant rate of penetration using ToF-SIMS, the structure of an OBCS tribofilm can be defined as containing a bulk section constructed from $CaCO_3$. Presumably, if CaOH was maintaining the carbonate's amorphous nature [168], then $CaCO_3$ is non-crystalline, as observed on AluSil® (section 5.6.3.3) and within the OBCS micelle prior to test [163]. Since the intensity of sulphur reached a maximum prior to that of the calcium compounds, it follows that sulfonate chains must be located at the outer edge of the tribofilm, as reported in literature [178]. This is most probably due to an entrainment process which has mixed separated sulfonate chains into the outer regions of the film.

7.6.3.2.2. Film Formation

Since the chemistry of overbased calcium sulfonate tribofilms did not vary from that witnessed on silicon grains within AluSil®, nor indeed from the surface of the counterpart piston rings (section 5.6.3.3), it follows that film formation by OBCS is a generic process. Therefore, referring to an overbased calcium sulfonate micelle, and as described in section 5.6.3.3, sulfonate chains were removed mechanistically [165, 168] in order to allow for the consequent calcium carbonate build up on contacting surfaces [165, 167, 169]. The sulfonate chains were mixed into the top section of the calcium carbonate layer through entrainment. Hence, films generated on both steel pin and silicon crystal are presumed to bear the same chemical structure. The addition of NOCH to a

lubricant would result in chemical complexes be generated (Figure 79), where M = Cr, Fe, Si or indeed, Ca from the detergent tribofilm.

7.6.3.2.3. Summary

Overbased calcium sulfonate tribofilms are remarkable since they are chemically identical on a range of surfaces and at different degrees of overbasing. The films comprised calcium carbonate, onto which an outer region of sulfonate chains were located. These were most probably situated in this position due to a mixing process which entrained previously removed sulfonate chains into the tribofilm. The reported hypothesis that NOCH enhances calcium carbonate formation [215] cannot be verified, however. Superior wear protection afforded by the OBCS + NOCH tribofilm on both ferrous and silicon surfaces was not accredited to alterations in tribochemistry, but instead related to the structure of the film. A representative model of the tribofilms formed using OBCS and OBCS + NOCH on silicon crystal substrates are shown in Figure 134.

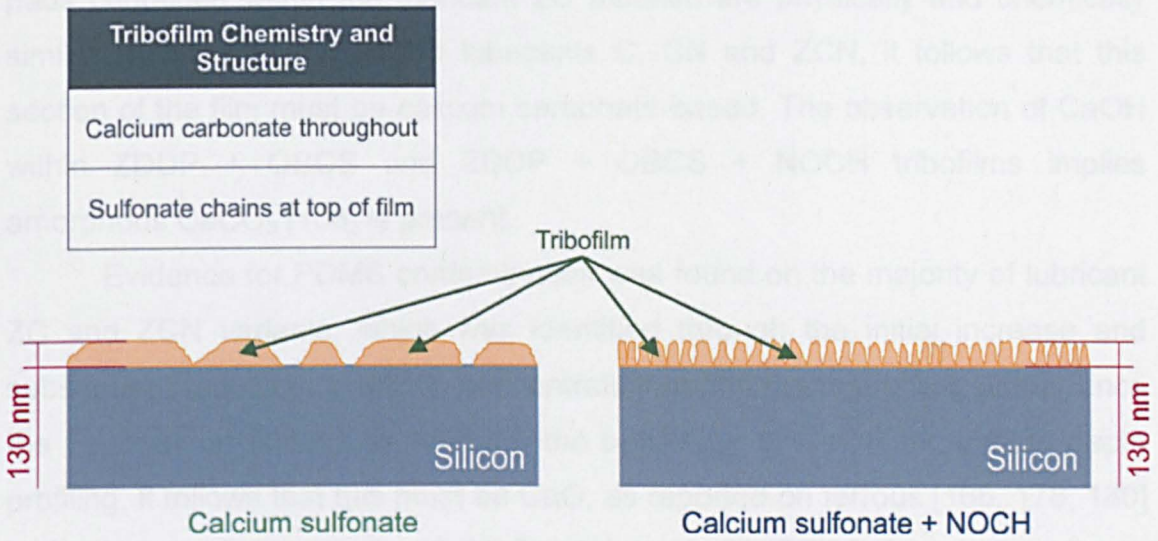

Figure 134: Models of silicon crystal lubricated with calcium sulfonate or calcium sulfonate + NOCH

7.6.3.3. ZDDP + Calcium Sulfonate vs ZDDP + Calcium Sulfonate + NOCH

7.6.3.3.1. Tribochemistry

As scanning electron and atomic force microscopy (section 7.5.1.3) have previously eluded, there are key differences in the structure and tribochemistry of ZDDP + calcium sulfonate and ZDDP + calcium sulfonate + NOCH tribofilms (section 7.5.2.3). Indeed, although both films contained Ca and CaOH peaks, there were large concentrations of PO_2, PO_3 and O_2 / S within the wear scar of

ZDDP + OBCS, indicative of a polyphosphate structure to the tribofilm [118]. However, only a small PO_2 intensity was determined to reside within the lubricant ZCN tribofilm; this was consistent across 350 TBN and labelled OBCS versions of the lubricant (section 7.5.2.6). The findings are consistent with those obtained from the steel piston ring observed in section 5.6.3.4 of this thesis. Presumably, similar behaviour would also be occurring on silicon grains within AluSil®, however, constraints in the spatial resolution of the mini SIMS cannot verify this. Small concentrations of Ca were obtained occasionally OWS on ZC and ZCN substrates; this was accredited to residual lubricant not removed using Heptane.

Since an increase in the ratio between 13^- m / z and 12^- m / z was observed via SIMS static analysis of silicon surfaces lubricated with ZDDP + labelled OBCS + NOCH compared to the non-labelled 350 TBN OBCS alternative (Figure 121), it follows that $CaCO_3$ was present with the film, as with overbased calcium sulfonate alone (section 7.6.3.2). Therefore, given that the pads contained within the lubricant ZC tribofilm are physically and chemically similar to those obtained with lubricants C, CN and ZCN, it follows that this section of the film must be calcium carbonate-based. The observation of CaOH within ZDDP + OBCS and ZDDP + OBCS + NOCH tribofilms implies amorphous $CaCO_3$ [168] is present.

Evidence for PDMS contamination was found on the majority of lubricant ZC and ZCN variants, which was identified through the initial increase and subsequent reduction in silicon concentration during depth profiling [258]. Since the Fe peak on substrates mirrored the behaviour of CaOH throughout depth profiling, it follows that this must be CaO, as reported on ferrous [166, 178, 180] and silicon surfaces (section 7.6.3.2) lubricated with OBCS. Large phosphorus and sulphur concentrations were observed during depth analysis of lubricant ZC tribofilms; an initial enhancement followed by a gradual decline in intensity suggests that these were contained within the bulk section of the film, as observed previously (section 7.5.1.3). Conversely, the observation that O_2 / S, PO_2 and PO_3 reached maximum values shortly after the onset of depth profiling with lubricant ZCN variants indicates that these were contained at the outer region of the film. Since PO_2 and PO_3 mirrored the behaviour of both Ca and Zn during depth profiling on 400 TBN ZC and ZCN lubricants, it follows that the observed phosphate species must be calcium and zinc-based. The generation

of calcium phosphate has been observed previously on ferrous surfaces [184, 185, 187]. Sulphur is probably in two forms; first, as sulfonate at the outer edge of $CaCO_3$ regions of tribofilm [178] and as sulphide [118, 126, 132, 139] within the phosphate sections of the tribofilms.

It is presumed that tribofilms on the steel pin will mirror the chemical composition of those formed on silicon crystal, since phosphorus, sulphur, calcium and zinc were observed on both ZC and ZCN substrates (Table 35). Interestingly, phosphate formation with ZDDP + OBCS seems to have improved on the silicon crystal substrate compared to ZDDP; this is in contrast to that reported on ferrous substrates [176]. Perhaps the inherent stability of calcium phosphate [185] is linked to film formation. The lack of zinc on 350 TBN and labelled OBCS variants of lubricant ZCN suggests zinc phosphate formation is influenced by calcium content.

7.6.3.3.2. Film Formation

Calcium carbonate will be generated upon ZDDP + OBCS and ZDDP + OBCS + NOCH substrates using the method described previously (section 7.6.3.2). This rapid process explains the reasoning behind the ECV output discussed in section 7.6.1.4; the $CaCO_3$-based tribofilm separated the contacting substrates quickly. Sulfonate chains were intermixed into the outer region of the tribofilm [178] by an entrainment process. In combination with this, adsorption of a linkage isomer and or ZDDP onto both ferrous and silicon surfaces ensued [131]; through decomposition mechanisms, zinc polyphosphates and sulphide species were generated [131]. At this point, according to Kasrai et al. [185], chemical reaction lead to calcium phosphate formation. The reduced film thickness compared to ZDDP (Table 34) may be accredited to a decrease in phosphate chain length, provoked by the aforementioned reaction with calcium [186, 189].

However, since the phosphate and sulphide generation was heavily reduced when using lubricant ZCN, it follows that ZDDP was being out-competed by the NOCH molecule in order to associate with the substrate surfaces and thus generate the metal complex given in Figure 79. The presence of phosphorus species toward the outer edge of the tribofilm with the variants of ZDDP + calcium sulfonate + NOCH suggests a small amount of adsorption and decomposition of ZDDP occurred, however.

7.6.3.3.3. Summary

Both lubricant ZC and ZCN tribofilms were calcium carbonate-based. However, of all the lubricants studied herein, NOCH had the most profound effect on the structure of the ZDDP + calcium sulfonate tribofilm. Indeed, referring to the model silicon substrates shown in Figure 135, in addition to $CaCO_3$, the ZDDP + OBCS film contained zinc polyphosphates and sulphide species, together with calcium phosphate within the bulk section of the film. The addition of NOCH to the lubricant heavily reduced the polyphosphate and sulphide concentration within the aforementioned film, as witnessed in the AluSil® and piston ring contact (section 5.6.3.4), resulting in a bulk tribofilm of calcium carbonate only, with phosphorus and sulphur species residing at the outer regions of the protective layer. Since the wear protection afforded by ZDDP + calcium sulfonate + NOCH was not only superior to that provided by ZDDP + OBCS, but also improved compared to calcium sulfonate + NOCH, it follows that a bulk section of calcium carbonate with an overlying layer of mixed calcium and zinc phosphates, together with zinc sulphide and sulfonate chains, generates excellent wear performance.

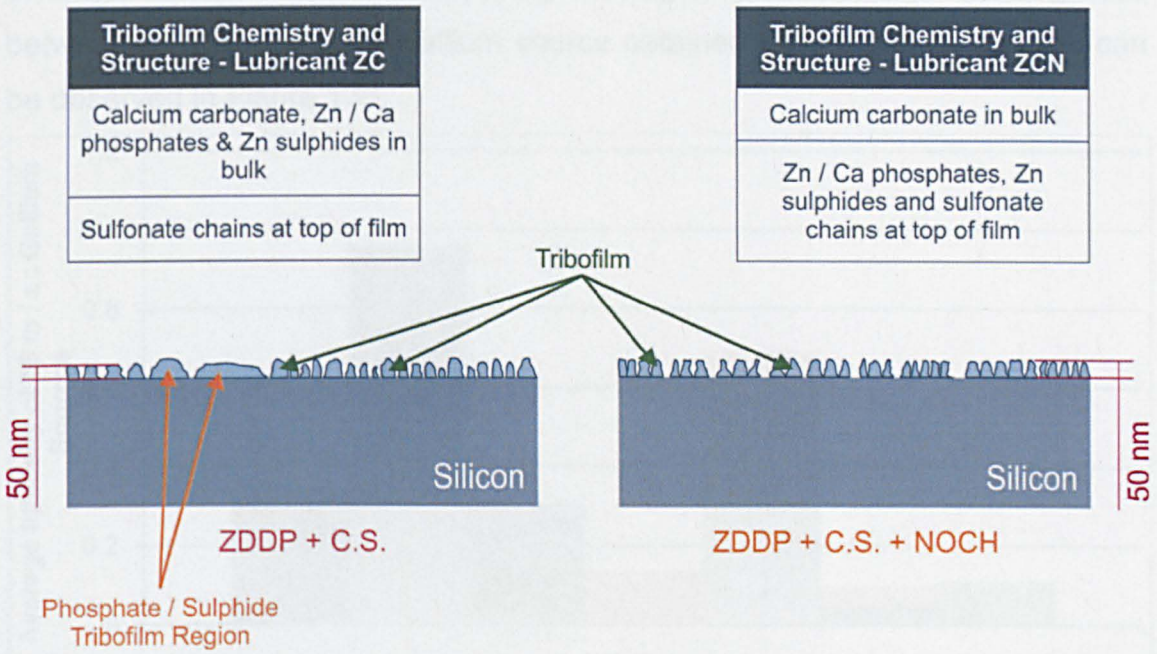

Figure 135: Models of silicon crystal lubricated with ZDDP + calcium sulfonate or ZDDP + calcium sulfonate + NOCH

7.6.3.4. Triethyl Citrate

7.6.3.4.1. Tribochemistry

Calcium sulfonate + labelled NOCH (1-3) and ZDDP + calcium sulfonate + labelled NOCH (1-3) were chemically identical to lubricants CN and ZCN in terms of containing a bulk tribofilm composition of Ca, CaOH and Fe (CaO) (section 7.5.2). The outer region of these tribofilms were identical to non-labelled variants, containing sulfonate chains in the case of lubricant CN and in addition, small concentrations of phosphate and sulphide species with lubricant ZCN.

However, three main differences were determined between the lubricants, the first of which was the identification of a peak at 19^- m / z; only obtained with fluids which contained labelled NOCH (2) (Figure 128). Given that ^{13}C was present within labelled NOCH (2), 19^- m / z could have been $^{13}CH_6$, or indeed, contamination by fluorine, since both share same similar atomic masses. Therefore, for clarification, labelled NOCH (2) was purified by Lubrizol® UK Ltd to remove any possible contaminants, blended into ZDDP + calcium sulfonate + NOCH and subsequently tribologically tested. The resulting ratio between 19^- m / z and the gallium source obtained for the purified sample can be observed in Figure 136.

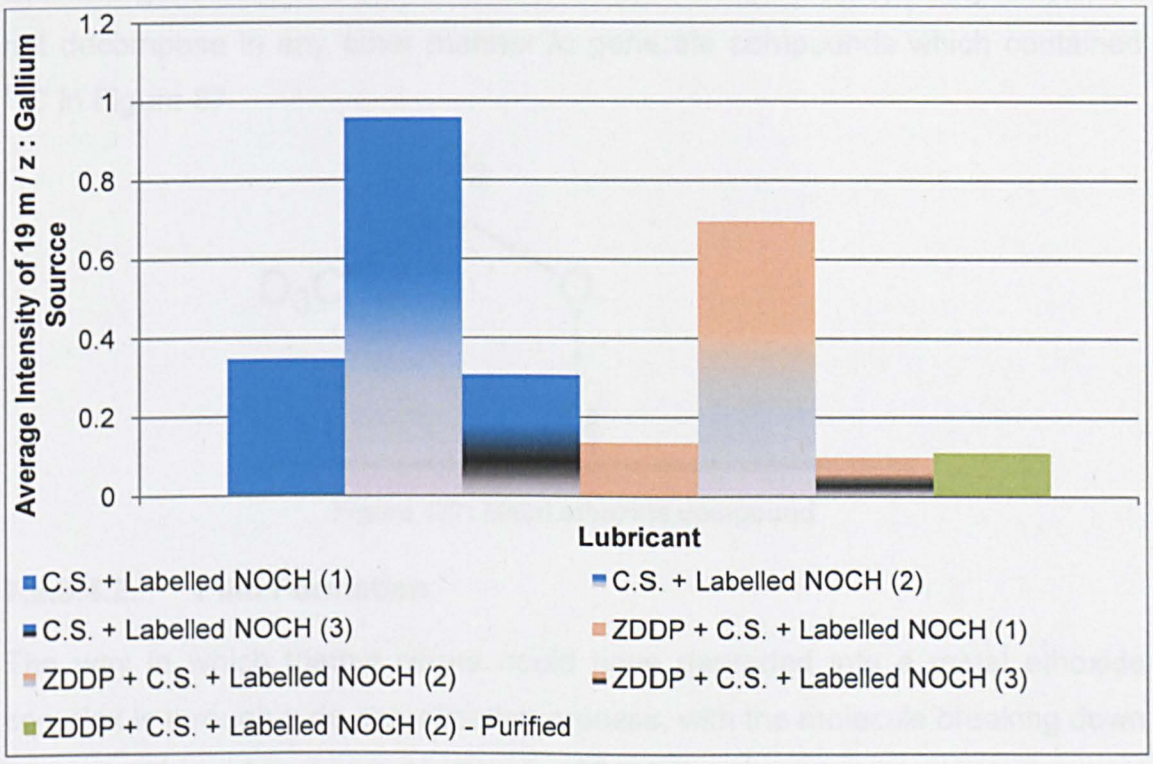

Figure 136: Ratio of average intensity of 19^- m /z to gallium source for labelled NOCH containing lubricants

Referring to ZDDP + calcium sulfonate + labelled NOCH (2) - Purified, the aforementioned ratio was similar to that obtained with labelled NOCH (1&3) variants of lubricant ZCN, and reduced markedly compared to un-purified labelled NOCH (2). Therefore, this is conclusive evidence that the peaks previously observed at 19^- m / z (Figure 128) were due to contamination by fluorine within the additive and not a compound which contained ^{13}C. Indeed, ^{13}C was not observed with any lubricant which contained labelled NOCH (1&2) (Figure 128&Figure 129).

The two other chemical differences were identified solely with the use of labelled NOCH (3). Indeed, CD_3 was obtained with both lubricants CN and ZCN which contained this variant of NOCH, whilst deuterium was also obtained with calcium sulfonate + labelled NOCH (3) (Figure 130). Due to the way in which the SIMS technique operates (section 2.2.2.3), it is logical to assume that D and CD_3 were fragments of a larger portion of the NOCH molecule. Combining this information with the fact that labelled NOCH (1&2) were not observed during SIMS analysis, it follows that triethyl citrate must not be present as a whole molecule on the CN and ZCN substrates, as previously hypothesised (Figure 79). Thus, the only portion of the molecule which could have been detected with the sole use of labelled NOCH (3) (Figure 88) is an ethoxide (OCH_2CH_3), which will have generated a metal complex as shown in Figure 137. Triethyl citrate did not decompose in any other manner to generate compounds which contained ^{13}C in Figure 87.

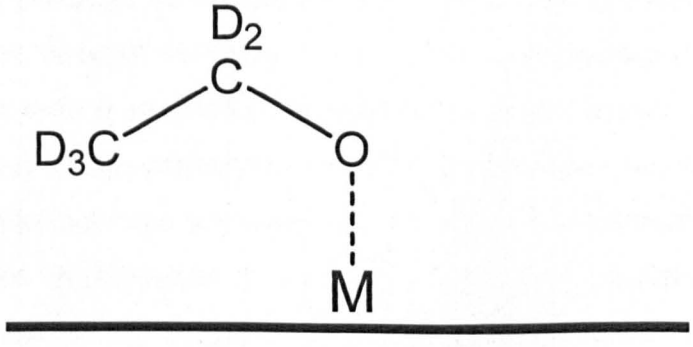

Figure 137: Metal ethoxide compound

7.6.3.4.2. Film Formation

The way in which triethyl citrate could have degraded into a metal ethoxide complex is through a de-esterification process, with the molecule breaking down at the positions shown in red in Figure 138 [268].

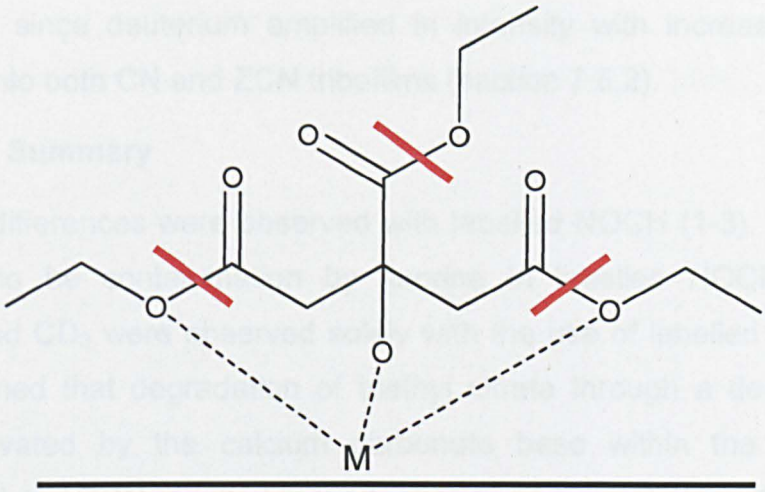

Figure 138: De-esterification of triethyl citrate

As discussed previously, during film formation of lubricants CN and ZCN, calcium carbonate was deposited on substrate surfaces (sections 7.6.3.2 & 7.6.3.3). Simultaneously, NOCH would be forming complexes with metal cations, such as Cr or Fe (Figure 79). However, triethyl citrate would also be binding to calcium within the carbonate contained in the aforementioned tribofilm.

Since de-esterification can be activated by a base [269, 270], which in this case, was calcium carbonate, initiation of the degradation of NOCH ensued, resulting in the metal ethoxide given in Figure 137. The fact that the metal ethoxide was not observed when ZDDP + labelled NOCH (3) was used to lubricate ferrous surfaces [251] only helps to underline the theory that calcium carbonate must therefore be involved in the degradation of triethyl citrate.

Therefore, through its basic nature, $CaCO_3$ encouraged the breakdown of NOCH, which in turn, promoted deposition of further calcium carbonate [268]. This would explain the difference in structure between lubricant C and CN tribofilms, whereby perhaps a greater surface density of calcium carbonate was generated, which is indicative of enhanced calcium carbonate deposition, as reported previously [215]. It also follows that calcium preferentially coordinated with the ethoxide, rather than phosphate compounds in the lubricant ZCN tribofilm, since phosphate formation was reduced compared to lubricant ZC (section 7.6.3.3). The fashioned ethoxide would be able to move from one metal cation to another, which suggests the compound could be present on the surface of the substrates, as well as within the tribofilm. This seems to be the

case herein, since deuterium amplified in intensity with increasing depth of penetration into both CN and ZCN tribofilms (section 7.5.2).

7.6.3.4.3. Summary

Three main differences were observed with labelled NOCH (1-3). The first was determined to be contamination by fluorine in labelled NOCH (2), whilst deuterium and CD_3 were observed solely with the use of labelled NOCH (3). It was determined that degradation of triethyl citrate through a de-esterification process activated by the calcium carbonate base within the tribofilms of lubricants CN and ZCN resulted in the formation of a metal ethoxide compound. Reduced phosphorus concentration compared to lubricant ZC with lubricant ZCN could be explained, in addition to competition, by the fact that calcium carbonate preferentially coordinated with the ethoxide, rather than phosphorus compounds.

7.7. Conclusions

Replication of contact conditions on silicon grains within AluSil® using silicon crystal was successful. This permitted a greater range of surface analysis techniques to be employed in order to understand tribofilm topography, chemistry and film formation on silicon surfaces. The following sub-sections conclude the findings from the lubrication of the silicon crystal and steel pin tribosystem using ZDDP, OBCS or ZDDP + OBCS. The benefits obtained from the addition of NOCH to these lubricants are also presented, together with an overview of the decomposition and functionality of triethyl citrate.

ZDDP vs ZDDP + NOCH

- The addition of NOCH to ZDDP reduced the frictional response of the interface
- Film formation was improved with lubricant ZN, compared to ZDDP. This originated from an increase in phosphate formation through enhanced decomposition of ZDDP by NOCH, although both lubricant Z and ZN films appeared chemically analogous
- Enhanced wear protection was imparted by the addition of triethyl citrate to ZDDP. This was due to an increase in the resultant surface coverage and thickness of the tribofilm

Calcium Sulfonate vs Calcium Sulfonate + NOCH

- Lubricant C and CN tribofilms were generated on substrates through a mechanistic process
- Tribofilm coverage was vastly superior to that observed with ZDDP or ZDDP + NOCH, resulting in a marked reduction in wear
- The thicknesses of lubricant C and CN tribofilms were identical
- All variants of lubricants C and CN were chemically identical. Calcium carbonate was contained as a bulk section, with sulfonate chains mixed into the top region of the film
- Compared to OBCS, lubricant CN reduced the wear in the tribosystem due to an increase in the surface density of calcium carbonate-based pads

ZDDP + Calcium Sulfonate vs ZDDP + Calcium Sulfonate + NOCH

- Lubricant ZCN imparted a lower frictional response compared to ZDDP + calcium sulfonate
- Lubricant ZC and ZCN tribofilms were calcium carbonate-based and housed sulfonate chains toward the outer edge of the tribofilm
- Lubricant ZC also contained large concentrations of O_2 / S, PO_2 and PO_3. These were present in the bulk section of the film and were associated with zinc and calcium phosphates, plus zinc sulphides
- The addition of triethyl citrate to lubricant ZC markedly reduced phosphate and sulphide formation. Furthermore, this region was subsequently located at the periphery of the lubricant ZCN tribofilm
- Since lubricant ZC and ZCN tribofilm thicknesses were similar, yet wear protection was vastly superior with the addition of NOCH, it followed that the structure and reduced elastic modulus of the ZCN tribofilm imparted lower wear in the tribosystem

Triethyl Citrate

- When used in conjunction with calcium sulfonate or ZDDP + calcium sulfonate, triethyl citrate degraded to form a metal ethoxide
- Decomposition was achieved through a process of de-esterification activated by calcium carbonate

- The observed increase in surface density of $CaCO_3$ pads on lubricant CN tribofilms was accredited to the NOCH molecule encouraging carbonate deposition
- The observed reduction in phosphorus concentration with lubricant ZCN compared to ZC was attributed to two areas. The first was competition with ZDDP and the second, via calcium carbonate preferentially coordinating with the ethoxide, rather than phosphorus compounds

The following two chapters of this thesis will address the relative merits of the aluminium matrix within an aluminium-silicon alloy in terms of wear protection, tribofilm formation and the role the base material plays during ultra-mild wear of an Al-Si substrate.

8. An Aluminium Alloy Replicating the Aluminium Matrix within an Al-Si Alloy

8.1. Introduction

It has been shown thus far in this thesis that silicon grains within aluminium-silicon alloys support the load in the contact and facilitate tribofilm formation (chapters 5&7). Therefore, it follows that if the silicon regions can maintain a height extension from the soft aluminium matrix, the wear in the tribosystem will originate from the interaction between silicon grains and counterpart material. However, under extended sliding conditions, the aluminium matrix undergoes wear [77, 99, 100], due to excessive depression of the silicon areas [77, 100] into the 3D structure that is an aluminium-silicon alloy.

In order to fully understanding the mechanisms of wear in boundary lubricated aluminium-silicon alloys, it is therefore important to identify the interactions between the various engine oil additives studied herein and the aluminium base material of an Al-Si alloy. Film formation reported previously [25, 66, 153] (chapter 5) on aluminium regions of the alloy when using ZDDP as lubricant were accredited to film transfer [25, 66, 153] or ZDDP thermal decomposition [25]. It is the intention of this work to address this topic and provide conclusive evidence to state whether ZDDP generates a film on the aluminium matrix through frictional processes, or indeed that the tribofilm must have transferred from silicon regions or thermally decomposed. It is also interesting to observe whether the interactions witnessed previously (chapter 7) between the NOCH additive and OBCS or ZDDP occur on these soft substrates.

In this chapter, the boundary lubricated interface between an aluminium alloy and a chromium steel pin lubricated with the conventional test oils (Table 29) is evaluated both tribologically and tribochemically. AFM and SEM are used to evaluate the worn substrates, whilst FTIR and SIMS provided chemical analysis of the aluminium alloy after experimentation. The steel pins were analysed using EDS. The interaction between aluminium alloy, steel pin and the engine oil additives employed herein are discussed with reference to literature and the work conducted thus far in this thesis.

8.2. Aim and Objectives

8.2.1. Aims

- Tribologically and tribochemically analyse an aluminium alloy undergoing boundary lubricated wear

8.2.2. Objectives

- To evaluate the tribological performance of a range of test lubricants
- To evaluate the morphology of substrates after experimentation and identify whether tribofilms generate on the aluminium alloys
- To analyse the chemistry of worn aluminium surfaces
- To correlate observed topography and tribochemistry to frictional response and wear
- To identify similar behaviour to that reported previously between triethyl citrate and OBCS or ZDDP

8.3. Tribology of an Aluminium Alloy

8.3.1. Materials

8.3.2. Aluminium Alloy

The chemical composition of the aluminium-silicon alloy used in chapter 4 of this work is shown in Table 38.

	Chemical Composition (Wt. %)									
Substrate	**Si**	**Fe**	**Cu**	**Mn**	**Mg**	**Cr**	**Ni**	**Zn**	**Ti**	**Al**
AluSil®	16.0-18.0	0.5	4.0-5.0	0.1	0.45-0.65	0.0	0.0	0.1	0.2	Balance
EN AW 2014A	0.85	0.28	4.6	0.8	0.63	0.02	0.0	0.05	0.03	Balance

Table 38: Comparison between chemical compositions of AluSil® [84] and EN AW 2014A

In order to accurately replicate the aluminium matrix of the substrate, it was important that the substitute alloy contained Fe, Cu, Mn and Mg, since these are known to be important alloying elements within an aluminium-silicon substrate (section 3.3.2). Furthermore, given that copper and magnesium are

added to an aluminium-silicon alloy in order to improve its strength [63, 71], it was vital that the wt. % of these elements were maintained in the replicate substrate. Since silicon is contained in small concentrations throughout the matrix of a hypereutectic Al-Si alloy, for accurate representation, this should also hold true regarding the replicate aluminium alloy. Therefore, in order to meet these criteria, EN AW 2014A was selected as suitable alternative for the aluminium matrix; its chemical composition is shown in Table 38.

The aluminium alloy was supplied by Paterson Precision Ltd with dimensions 7.0 mm x 7.0 mm x 3.5 mm (wxdxh). An unworn substrate is shown in Figure 139, with surface polishing marks evident.

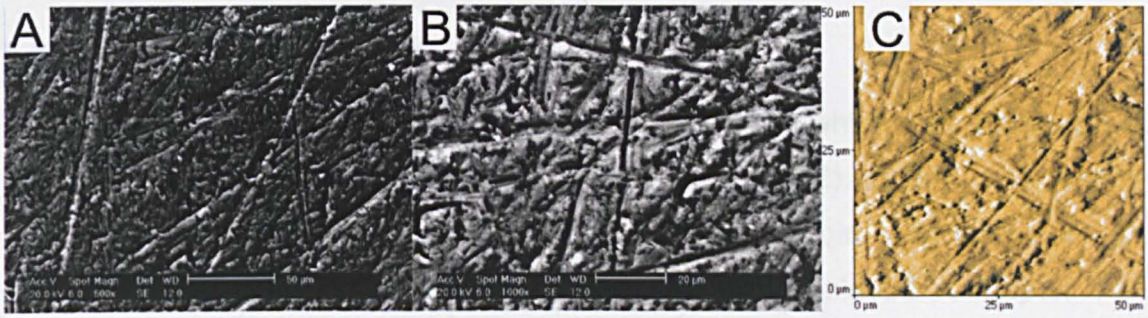

Figure 139: Unworn EN AW 2014A. A&B = SEM images of substrate, C = Shaded AFM image of unworn material highlighting polishing marks

The surface roughness of the aluminium alloy was determined by a Taylor Hobson Form Talysurf 120L surface profilometer and is given in Table 39.

Parameter	Value
R_a	0.122 µm
R_q	0.157 µm

Table 39: Surface roughness of EN AW 2014A substrates

Nanoindentation was performed on the aluminium substrates using a Micro Materials Ltd NanoTest™ Platform One device. The method described in the general techniques section of this work was employed in order to obtain the mechanical properties of the substrate (section 2.2.1.5). A maximum load and depth of 50 mN and 1000 nm accurately and repeatedly determined the mechanical properties of the aluminium alloy; the loading / unloading rate was 0.50 mN / s. One hundred indentations were performed, which were arranged in 25 columns comprising 4 indentation points; the spacing between these was 40 µm in the Y axis and 25 µm in the Z axis. A retraction distance of 15 µm per

indentation was employed. Obtained data was converted from reduced elastic modulus using the Poisson's ratio of the EN AW 2014A given in Table 40 and Equation 4. Results were averaged and a standard deviation computed using Microsoft® Excel®; the ensuing elastic modulus and hardness of the aluminium alloy are shown in Table 40.

Parameter	Value
Poisson's Ratio	0.33 [271]
Elastic Modulus (GPa)	64.0 ± 8.3
Hardness (GPa)	1.7 ± 0.3

Table 40: Mechanical properties of EN AW 2014A

8.3.3. Chromium Steel Pin

The counterpart substrate used in this work was that of which was employed in the silicon crystal chapter of this work (section 6.3.1.2). Briefly, this was a X17CrNi16-2 (EN 1.4057) martensitic chromium steel pin, and was used to replicate the chemical composition of the piston ring employed in chapter 4 of this thesis. The radius of curvature was 90 mm and the hardness 535 HV.

8.3.4. Lubricants

Six lubricants were under evaluation in this chapter and are listed in Table 29. These lubricating fluids are the same as those evaluated using the silicon crystal and steel pin setup described previously (section 6.3.1.3) and comprised ZDDP, 400 TBN overbased calcium sulfonate and NOCH, respectively.

8.3.5. Method

8.3.5.1. Experimental

The objective of these aluminium alloy experiments was to understand the tribological performance of the aluminium matrix within an aluminium-silicon alloy, whilst also identifying whether tribofilms form on these non-ferrous substrates.

The method used to tribologically evaluate the EN AW 2014A and steel pin tribosystem was analogous to that employed in section 6.3.2.1 of this thesis. Briefly, substrates were loaded into a Cameron Plint TE77 reciprocating tribometer after being submerged in acetone and placed in an ultrasonic water bath. The contact was flooded with 10 ml of test oil, which was heated to 100 °C. An applied load of 7 N was placed onto the contact. The frequency of

oscillation was 20 Hz and the stroke length 5.0 mm. Tests were conducted for 2 hours and each oil evaluated three times using virgin substrates, to generate an average set of results. The variability of the frictional response and ECV determined for all lubricants, on average, was 6 % and 1%, respectively. The contact conditions shown in Table 41 were calculated using Equation 14-18 stated in section 6.3.2.1.

Variable	Value
Equivalent Elastic Modulus	55 GPa
Radius of Curvature	90×10^{-3} m
Applied Load	7 N
Maximum Contact Pressure	80 MPa
Mean Contact Pressure	53 MPa
Entrainment Speed	0.2 m / s
Film Thickness	2.57×10^{-2} µm
Lambda Ratio	6.6×10^{-2}

Table 41: Aluminium alloy point contact conditions

8.3.5.2. Surface Analysis

8.3.5.2.1. SEM

Scanning electron microscopy was conducted using a Philips XL30 environmental scanning electron microscope. Data was obtained from representative areas on worn aluminium and steel substrates, respectively. Samples were rinsed with Heptane prior to analysis. The acceleration voltage of the electron beam was 20.0 kV, with a 6.0 spot size; the working distance of the microscope was 12.0 mm.

8.3.5.2.2. EDS

Energy dispersive x-ray spectroscopy was completed on the steel pins whilst SEM analysis was conducted. As with silicon crystal (chapter 6), chemical data was obtained and analysed using the INCA microanalysis system connected to the Philips XL30 environmental scanning electron microscope. The operating conditions of the microscope were those stated in section 8.3.5.2.1, except the spot size of the electron beam was reduced to 5.0. EDS analysis was carried out at 1500 x magnification, using the Point and ID mode of operation.

8.3.5.2.3. AFM

Atomic force microscopy was conducted on aluminium substrates using a Veeco Explorer SPM. The scan range and resolution employed were 50 µm x 50 µm and 400, respectively, whilst the scan rate was 200.32 µm s^{-1}. Substrates were cleaned with Heptane prior to analysis. Data was collected and analysed using the SPMLab software supplied with the device. Both levelled and shaded images of worn substrates are shown herein, since the former affords an indication as to variations in height on a substrate, whilst shaded images provide detailed information regarding surface topography.

8.3.5.2.4. FTIR

Fourier transform infrared analysis of worn aluminium substrates was carried out using a PerkinElmer® Spotlight 400 Imaging system at wavenumbers between 4000 cm^{-1} and 600 cm^{-1}. The aperture size on the apparatus was 100 µm x 100 µm, with ten scans performed in each location of interest in order to minimise noise.

8.3.5.2.5. Mini SIMS

Secondary ion mass spectrometry was used to further analyse the tribochemistry of worn aluminium substrates. SIMS was conducted using a Millbrook Mini SIMS MC 300 MKII instrument, which, when in static mode of operation, analysed areas ~ 70 µm x 70 µm on worn substrates. Samples were cleaned prior to analysis using Heptane. Analysis was completed in both positive and negative polarity modes, using a scan range of 2 m / z - 200 m / z. The dwell time was set at 0.01 seconds, with a step of 0.2 m / z employed. At each location of interest, be it inside or outside the wear scar, three scans were completed in both negative and positive polarities of operation, in order to minimise noise. Ten areas of analysis were identified within the wear scar, whilst three were evaluated outside the wear region on the aluminium substrates. Static data was averaged and converted into chart form.

Regions of analysis within the wear scar on substrates with dimensions ~ 260 µm x 260 µm were the subject of depth profiling. Positive and negative ion modes of operation were used to attain data from separate regions of the tribofilm on substrates. A total number of 200 repeats were completed in each location of interest; the dwell time was 2.19 seconds per atomic mass unit. Microsoft® Excel® converted the resultant data into graphical format.

8.3.5.3. Wear Measurement

The wear on both ferrous and aluminium substrates was measured using a Reichert Jung Polyvar MET™ light microscope, operating at 4x magnification. Data was obtained in digital format from the microscope using a Motic® MC V3 digital camera and Motic® Images Plus 2.0 software supplied with the apparatus. The method of data acquisition and subsequent analysis in order to determine average values for both aluminium alloy plate and steel pin substrates was the same as that described in section 6.3.2.5 of this thesis.

9. Results and Discussion of An Aluminium Alloy Replicating the Aluminium Matrix within an Al-Si Alloy

9.1. Introduction

In this chapter, the results obtained from the lubrication of an aluminium alloy and steel pin interface are presented and discussed.

9.2. Friction Coefficients

The average coefficients of friction generated by the test lubricants shown in Table 29 are displayed in Figure 140. As can be observed, ZDDP showed the highest friction throughout the experiment. The addition of NOCH to lubricant Z reduced the frictional response of the aluminium alloy and steel pin tribocouple.

The frictional response imparted by calcium sulfonate reduced rapidly from its initial value to the lowest observed, after which frictional response remained steady state. Calcium sulfonate + NOCH imparted the second lowest coefficient of friction on the tribosystem. Lubricants ZC and ZCN had analogous frictional responses, which were only lower than that observed for ZDDP.

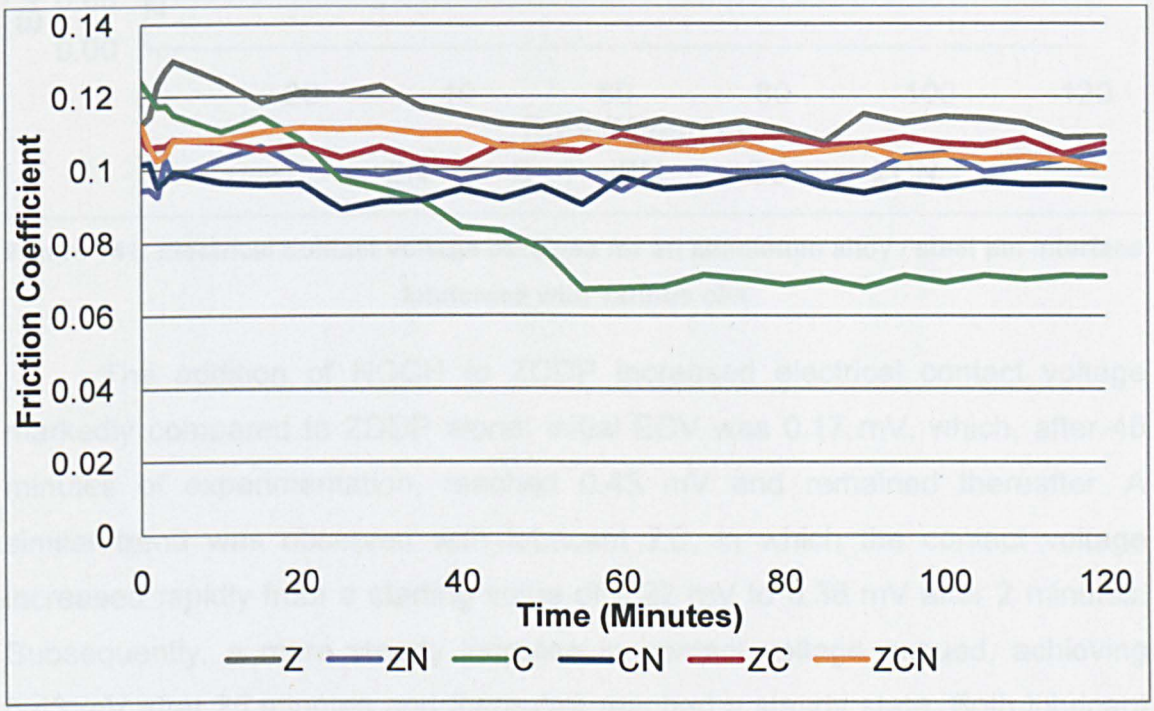

Figure 140: Friction coefficients obtained for an aluminium alloy / steel pin interface lubricated with various oils

9.3. Electrical Contact Voltage

Noticeable variations in electrical contact voltage were observed for the six respective lubricants, as shown in Figure 141. Indeed, both calcium sulfonate

and ZDDP possessed initial ECV values of 0.04 mV and 0.05 mV, respectively. In terms of lubricant C, the contact voltage gradually and erratically increased with time to 0.43 mV after 55 minutes of experimentation. Whereas a more rapid increase in electrical contact voltage over the first 35 minutes of experimentation was experienced by the tribosystem when lubricated with ZDDP. However, after this point, a slow increase in contact voltage ensued and the maximum contact voltage of 0.43 mV was not achieved until the end of experimentation.

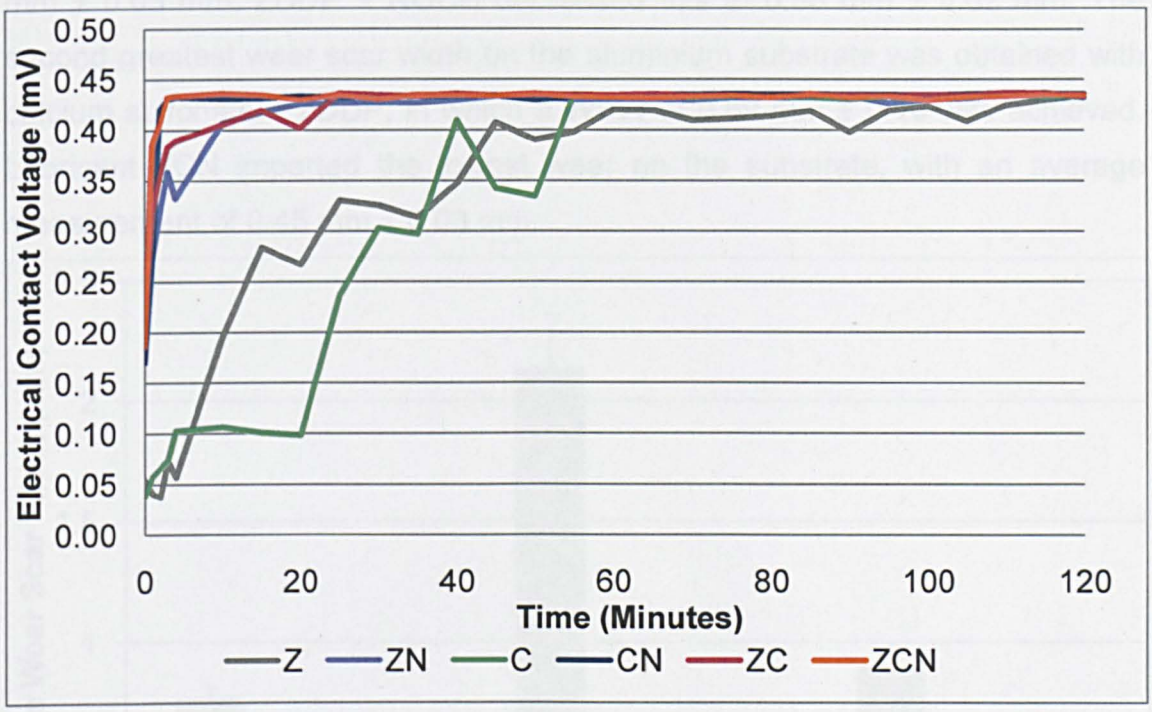

Figure 141: Electrical contact voltage obtained for an aluminium alloy / steel pin interface lubricated with various oils

The addition of NOCH to ZDDP increased electrical contact voltage markedly compared to ZDDP alone; initial ECV was 0.17 mV, which, after 45 minutes of experimentation, reached 0.43 mV and remained thereafter. A similar trend was observed with lubricant ZC, in which the contact voltage increased rapidly from a starting value of 0.22 mV to 0.36 mV after 2 minutes. Subsequently, a more steady increase in contact voltage ensued, achieving 0.43 mV after 25 minutes and thereafter reached a steady state. Both lubricant CN and ZCN were identical in terms of electrical contact voltage. Indeed, initial values of ~ 0.18 mV increased very rapidly to 0.42 mV after 2 minutes; a steady state value of 0.43 mV was achieved shortly thereafter.

9.4. Wear

9.4.1. Aluminium Alloy

Figure 142 shows the average wear scar widths measured on aluminium substrates. Calcium sulfonate imparted the greatest wear scar width on the aluminium substrate, which measured 2.14 mm ± 0.22 mm on average. The addition of NOCH to calcium sulfonate reduced the wear to 0.63 mm ± 0.05 mm. When lubricated with ZDDP, the WSW on the aluminium alloy was 0.77 mm ± 0.05 mm; ZDDP + NOCH decreased this to 0.56 mm ± 0.02 mm. The second greatest wear scar width on the aluminium substrate was obtained with calcium sulfonate + ZDDP, in which a WSW of 0.89 mm ± 0.10 was achieved. Lubricant ZCN imparted the lowest wear on the substrate, with an average measurement of 0.45 mm ± 0.03 mm.

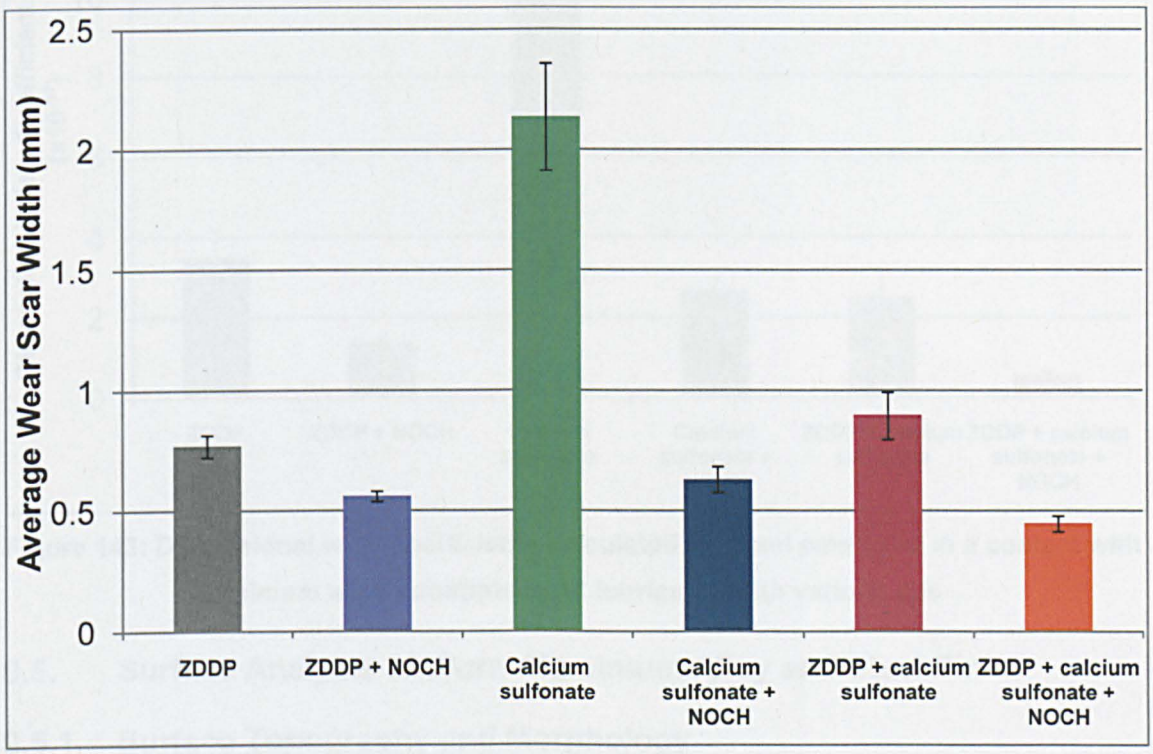

Figure 142: Average wear scar width measured on aluminium alloy substrates lubricated with various oils

9.4.2. Steel Pin

Figure 143 shows the dimensional wear coefficients calculated for the steel pins which were in contact with EN AW 2014A and lubricated with the oils listed in Table 29. Calcium sulfonate imparted the greatest wear on the ferrous substrate, achieving a value of 11.32×10^{-17} m^3 $(Nm)^{-1}$ ± 0.62×10^{-17} m^3 $(Nm)^{-1}$. The addition of NOCH to overbased calcium sulfonate resulted in a marked

reduction in wear, such that the wear coefficient equalled 2.64 x 10^{-17} m^3 $(Nm)^{-1}$ ± 0.35 x 10^{-17} m^3 $(Nm)^{-1}$. ZDDP imparted greater wear on the ferrous substrate than with lubricant CN; a coefficient of 3.50 x 10^{-17} m^3 $(Nm)^{-1}$ ± 0.67 x 10^{-17} m^3 $(Nm)^{-1}$ was obtained. ZDDP + NOCH reduced the wear on the steel pin to 1.33 x 10^{-17} m^3 $(Nm)^{-1}$ ± 0.17 x 10^{-17} m^3 $(Nm)^{-1}$. Lubricant ZC afforded a similar wear coefficient to that observed with lubricant CN, with a value of 2.50 x 10^{-17} m^3 $(Nm)^{-1}$ ± 0.71 x 10^{-17} m^3 $(Nm)^{-1}$. ZDDP + calcium sulfonate + NOCH imparted the lowest dimensional wear coefficient on the ferrous substrate; this was determined to be 0.53 x 10^{-17} m^3 $(Nm)^{-1}$ ± 0.09 x 10^{-17} m^3 $(Nm)^{-1}$.

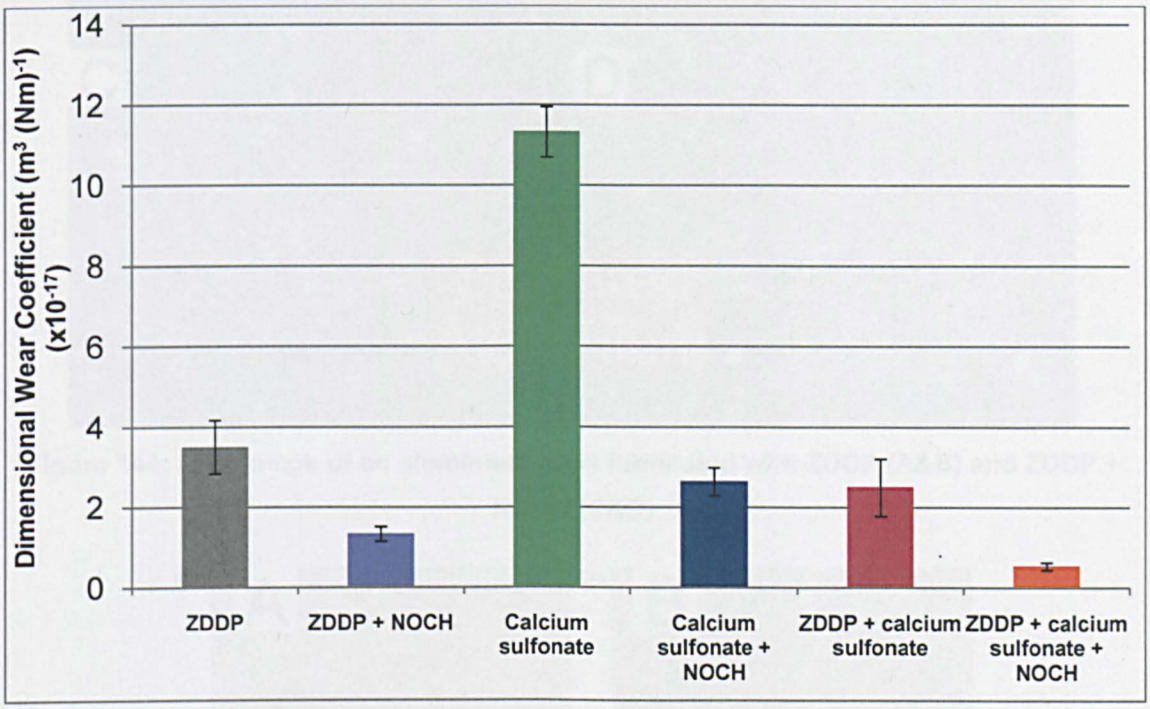

Figure 143: Dimensional wear coefficients calculated for steel pins used in a contact with aluminium alloy substrates and lubricated with various oils

9.5. Surface Analysis of Worn Aluminium Alloy and Steel Pin

9.5.1. Surface Topography and Morphology

This section of the thesis introduces the surface topography of worn aluminium and steel substrates, which have been analysed using AFM and SEM.

9.5.1.1. Aluminium Alloy - ZDDP vs ZDDP + NOCH

As can be observed in Figure 144A&B, the surface of the aluminium alloy was damaged when lubricated with ZDDP. The alloy appears to have been worn in such a manner as to produce long, smeared areas of aluminium orientated in the direction of sliding, within which a number of pores were located. When the contact was lubricated with ZDDP + NOCH (Figure 144C&D), smearing had

reduced and machining marks were evident within the wear scar (Figure 144C). Long tracks orientated in the sliding direction were still observed with lubricant ZN, however. A tribofilm was not observed on either aluminium alloy.

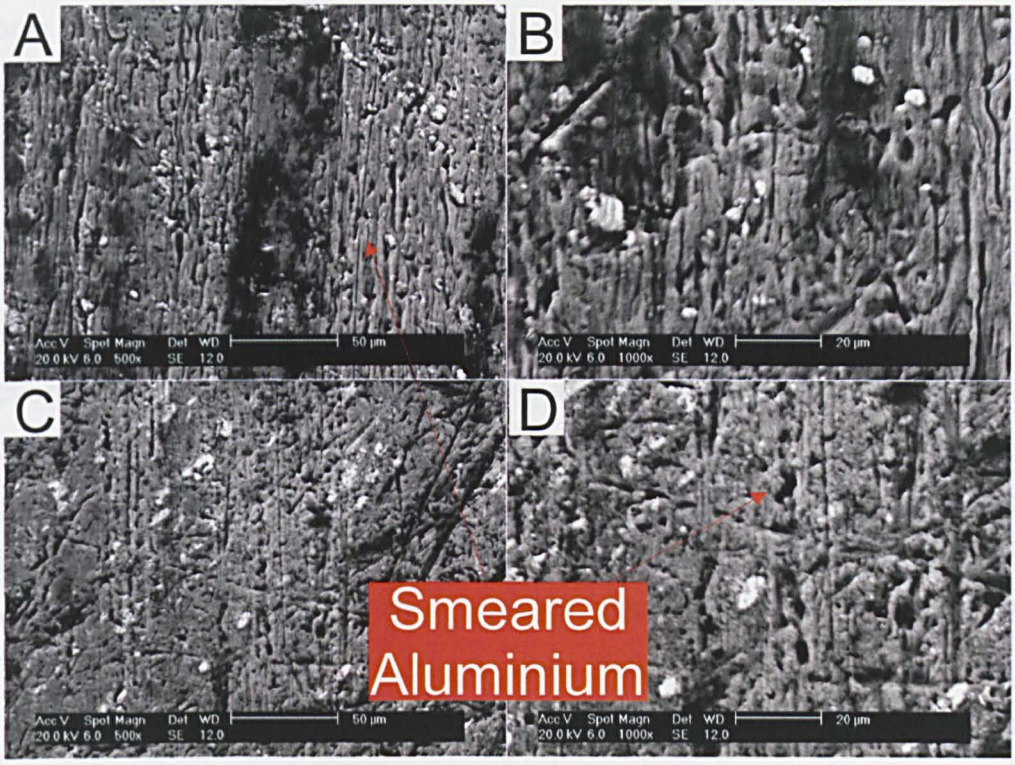

Figure 144: SEM image of an aluminium alloy lubricated with ZDDP (A&B) and ZDDP + NOCH (C&D)

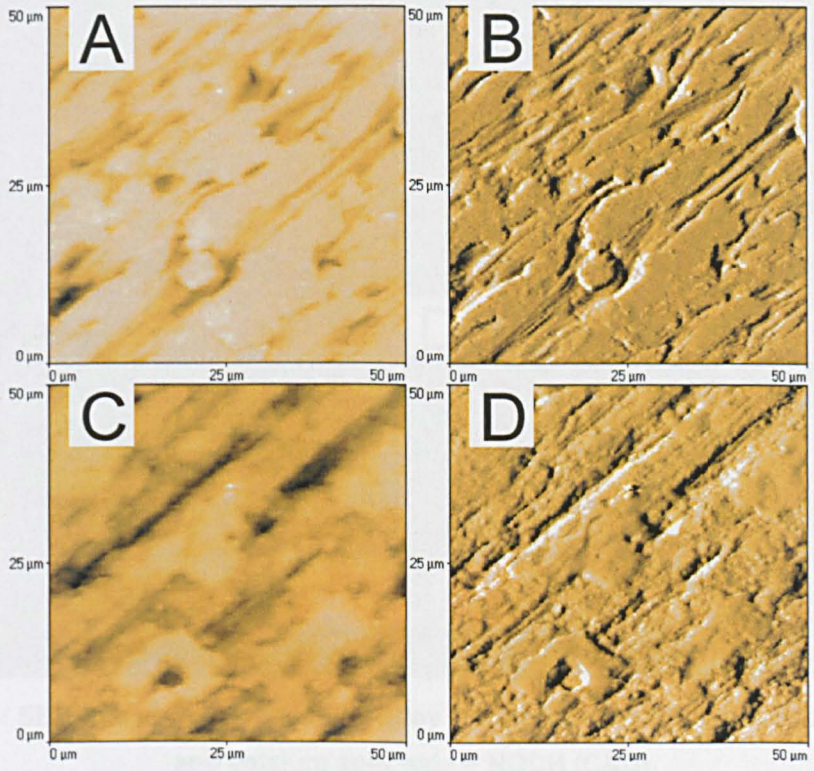

Figure 145: AFM image of an aluminium alloy lubricated with ZDDP (A&B) and ZDDP + NOCH (C&D)

The images shown in Figure 145 reiterates that observed using SEM, with smearing evident on both substrates, but reduced markedly with ZDDP + NOCH (Figure 145). The surface of the alloy lubricated with ZDDP was of a uniform height distribution (Figure 145A), whilst the roughness of EN AW 2014A lubricated with ZDDP + NOCH increased, as shown in Figure 145C.

9.5.1.2. Aluminium Alloy - Calcium Sulfonate vs Calcium Sulfonate + NOCH

Figure 146 shows the surface of EN AW 2014A when lubricated with calcium sulfonate or calcium sulfonate + NOCH. Wear marks orientated in the sliding direction were evident on the aluminium substrate when lubricated with calcium sulfonate (Figure 146A&B). Additionally, a tribofilm was observed on the substrate adjacent to the wear tracks. Calcium sulfonate + NOCH protected the substrate to a greater extent that lubricant C, since machining marks were evident after experimentation within the wear scar of the aluminium alloy (Figure 146C&D) and only a small number of wear marks were observed. A tribofilm was identified within the wear scar of the aluminium substrate when lubricated with calcium sulfonate + NOCH.

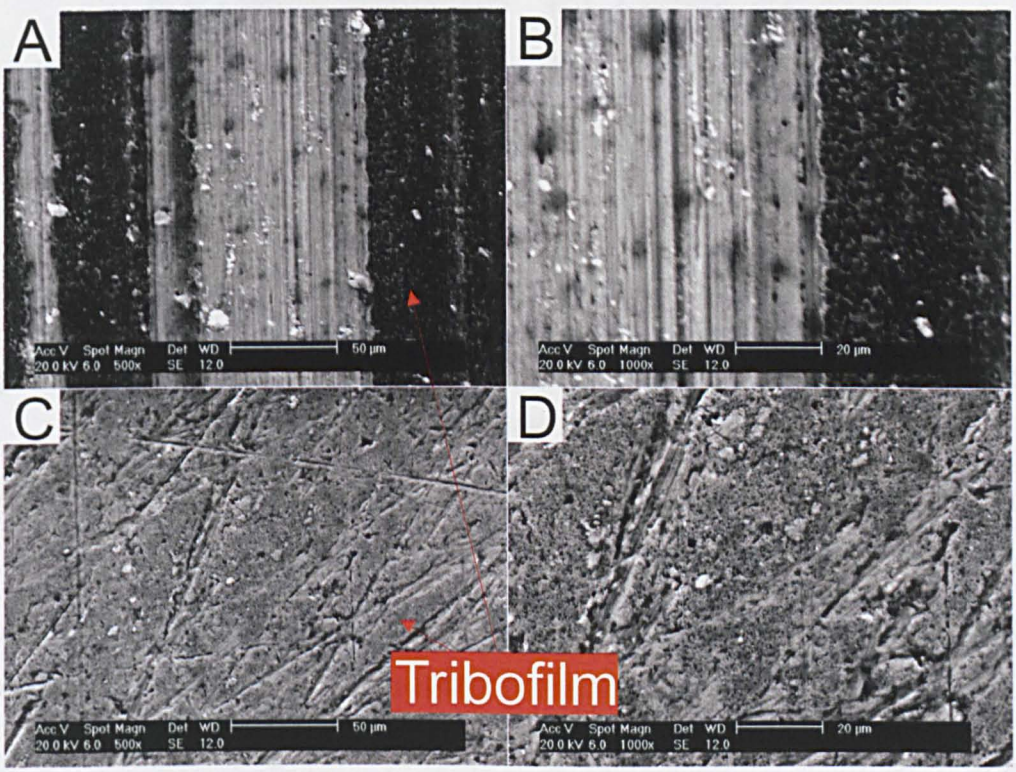

Figure 146: SEM image of an aluminium alloy lubricated with calcium sulfonate (A&B) and calcium sulfonate + NOCH (C&D)

The surface of the aluminium alloy lubricated with calcium sulfonate was non-uniform in height distribution (Figure 147A). A number of pores were contained within the substrate (Figure 147B), presumably derived from the tribofilm region previously identified in Figure 146A&B. When lubricated with calcium sulfonate + NOCH, a tribofilm comprised of small pads was observed on the surface of EN AW 2014A (Figure 147D). These varied in dimension and were not orientated in a particular direction, appearing to be of a uniform height across the substrate (Figure 147C). Machining marks and pores, present on unworn EN AW 2014A (Figure 139), were also apparent within the wear scar of the lubricant CN substrate, as shown in Figure 147C&D.

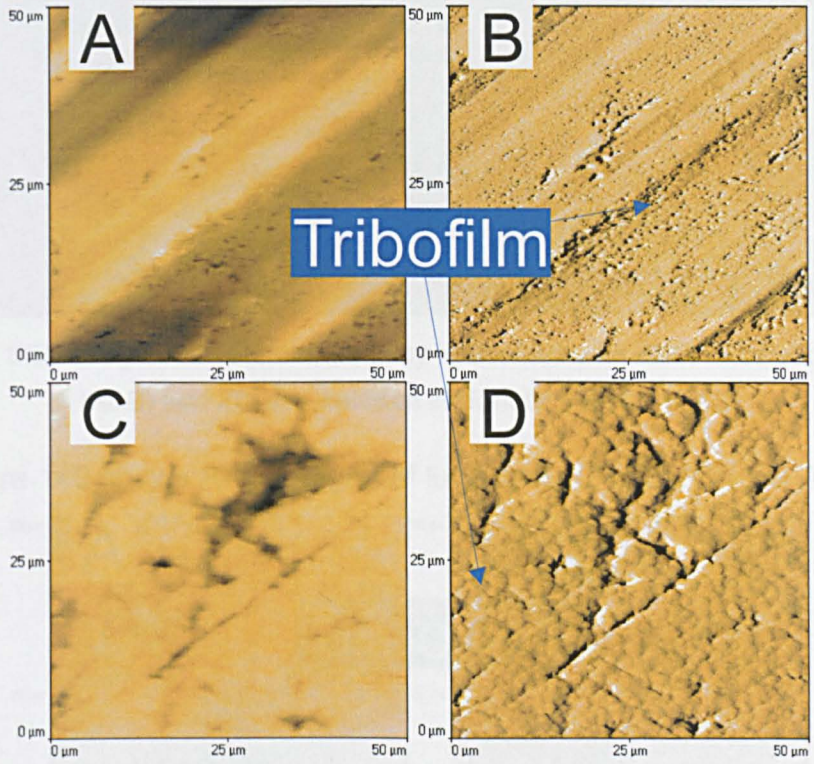

Figure 147: AFM image of an aluminium alloy lubricated with calcium sulfonate (A&B) and calcium sulfonate + NOCH (C&D)

9.5.1.3. Aluminium Alloy - ZDDP + Calcium Sulfonate vs ZDDP + Calcium Sulfonate + NOCH

When the aluminium alloy was lubricated with ZDDP + calcium sulfonate, a tribofilm was generated on the substrate (Figure 148A&B). Indeed, this tribofilm was non-homogenous, comprised of areas which resembled the tribofilm formed with calcium sulfonate (Figure 146A&B), but in addition also contained regions which housed large-interconnected pads. The aluminium alloy lubricated with ZDDP + calcium sulfonate + NOCH (Figure 148C&D) very much

resembled that of calcium sulfonate + NOCH (Figure 146C&D), containing a tribofilm and machining marks within the wear scar of the substrate.

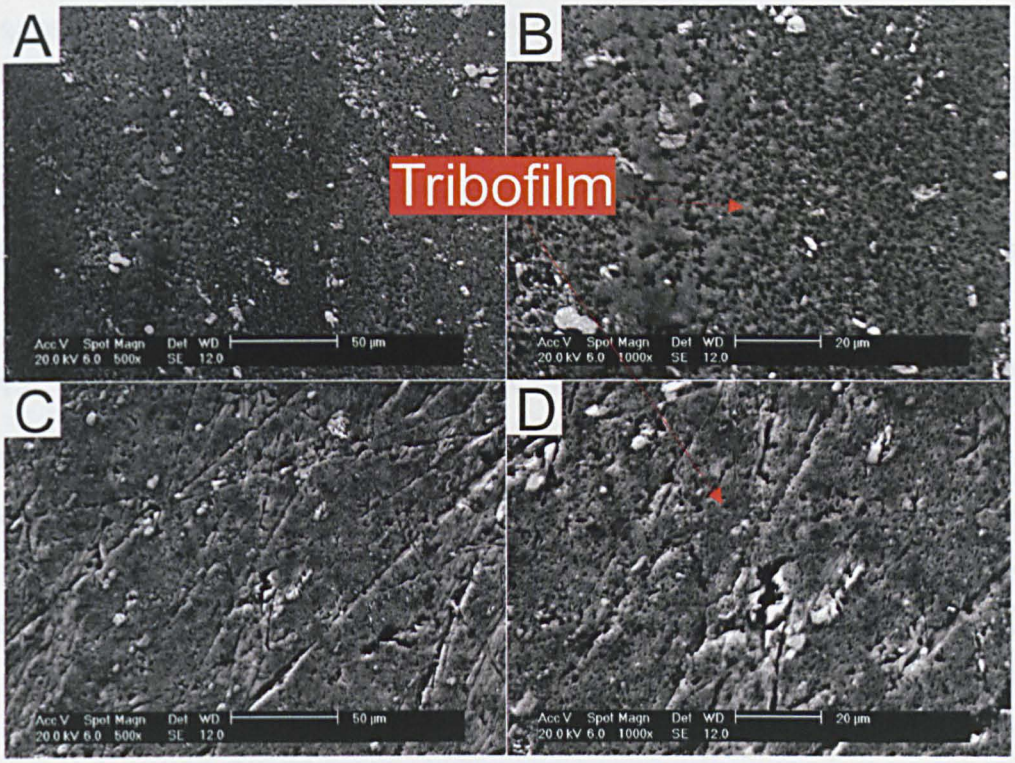

Figure 148: SEM image of an aluminium alloy lubricated with ZDDP + calcium sulfonate (A&B) and ZDDP + calcium sulfonate + NOCH (C&D)

Figure 149 shows AFM images of lubricant ZC and ZCN EN AW 2014A.

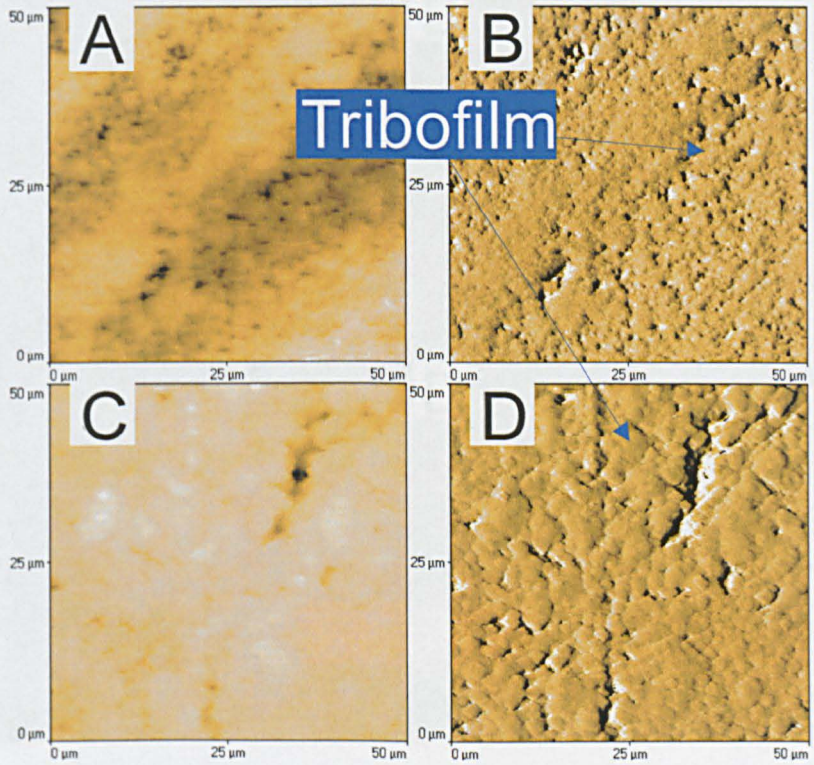

Figure 149: AFM image of an aluminium alloy lubricated with ZDDP + calcium sulfonate (A&B) and ZDDP + calcium sulfonate + NOCH (C&D)

The tribofilm generated on the aluminium alloy when lubricated with ZDDP + calcium sulfonate was non-uniform in height across the wear scar of the substrate (Figure 149A&B) and was orientated in the sliding direction. The varying dimensions of the pads from which the tribofilm was comprised are shown in detail in Figure 149A&B. The lubricant ZCN tribofilm contained small pads, which were not orientated in the sliding direction (Figure 149C&D). The surface of the substrate was level, yet pores were observed within the wear scar of the alloy, such as that displayed in Figure 149D.

9.5.1.4. Steel Pin - ZDDP vs ZDDP + NOCH

When the steel pin was lubricated with ZDDP, a tribofilm was generated, as shown in Figure 150A&B. The film comprised long narrow pads, orientated in the sliding direction. These pads were of varying dimensions, and were non-uniformly distributed throughout the wear scar on the substrate (Figure 150B). The protective layer generated from ZDDP + NOCH (Figure 150C&D) appeared similar in format to that fashioned from ZDDP alone. However, as shown in Figure 150D, the tribofilm possessed a more homogeneous structure, comprised of uniformly sized pads. A reduction in the voids observed between these pads was evident with ZDDP + NOCH, compared to ZDDP.

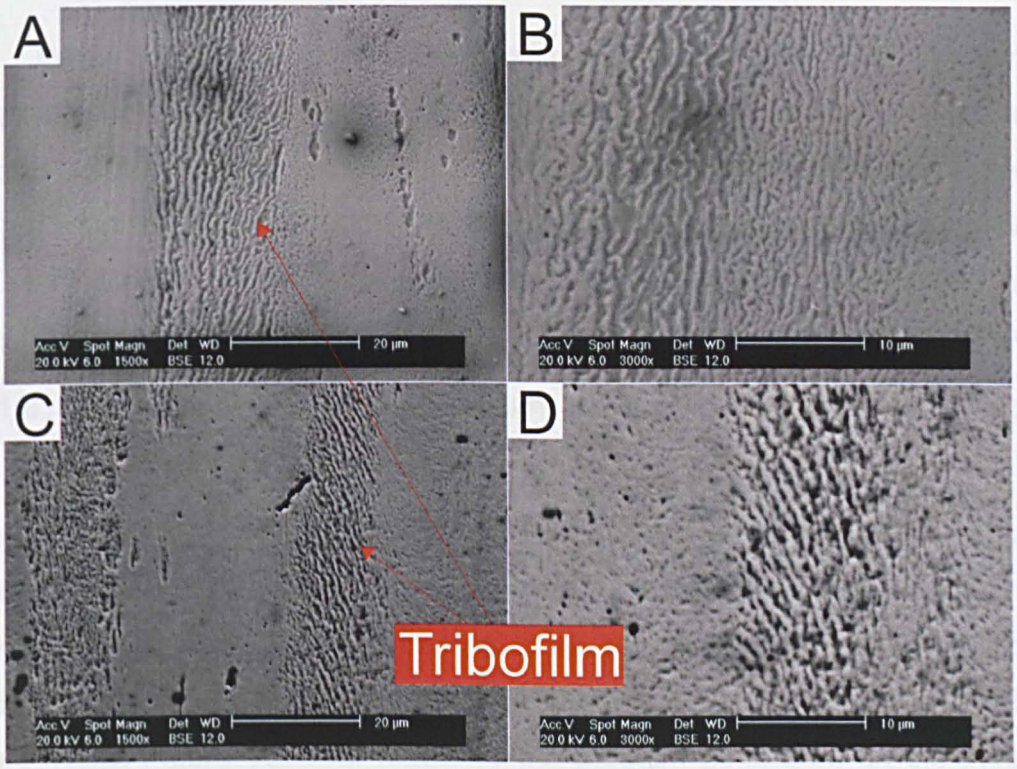

Figure 150: SEM image of a steel pin which has been in contact with an aluminium alloy and lubricated with ZDDP (A&B) and ZDDP (C&D)

9.5.1.5. Steel Pin - Calcium Sulfonate vs Calcium Sulfonate + NOCH

Figure 151 shows the wear scar on steel pins lubricated with calcium sulfonate or calcium sulfonate + NOCH.

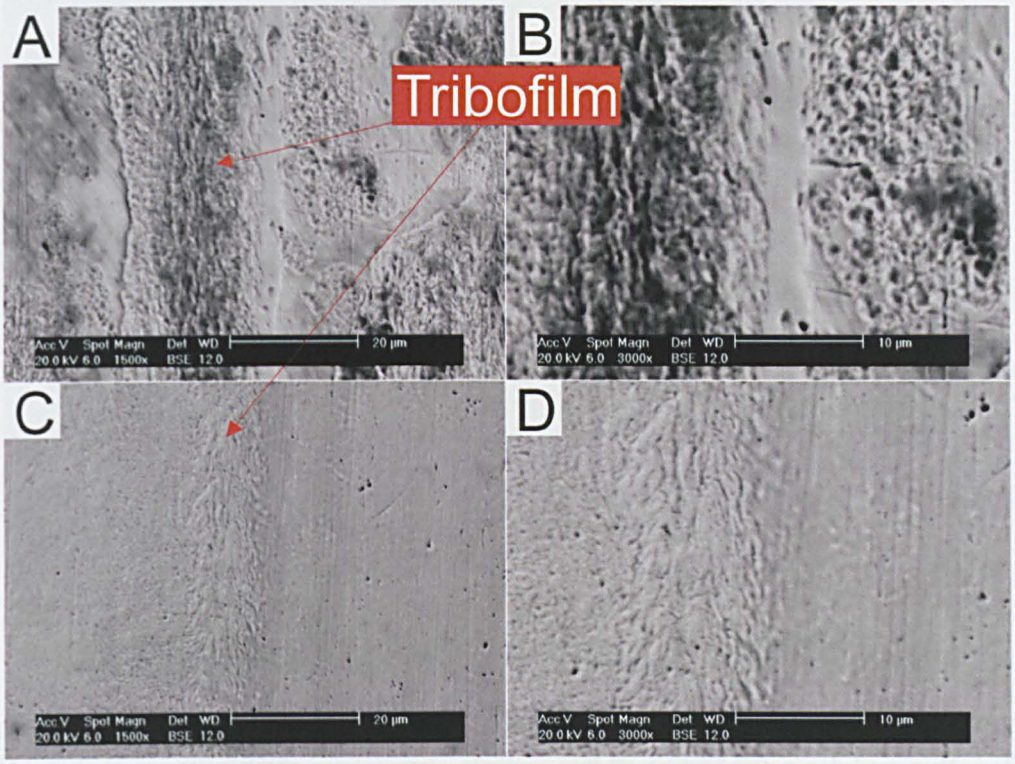

Figure 151: SEM image of a steel pin which has been in contact with an aluminium alloy and lubricated with calcium sulfonate (A&B) and calcium sulfonate + NOCH (C&D)

When the tribosystem was lubricated with calcium sulfonate, the ferrous-based pin housed a tribofilm (Figure 151A&B), which was orientated in the direction of sliding and comprised pad-like regions of varying sizes. A clearly defined tribofilm was evident on the steel pin lubricated with calcium sulfonate + NOCH (Figure 151C&D). This layer was constructed from large pads, which were orientated in the direction of sliding, interlinked and of varying dimensions.

9.5.1.6. Steel Pin - ZDDP + Calcium Sulfonate vs ZDDP + Calcium Sulfonate + NOCH

Lubricating the contact with ZDDP + calcium sulfonate resulted in the formation of a tribofilm on the steel pin, as shown in Figure 152A&B. The tribofilm comprised long pads, which appeared to be orientated in the sliding direction. Voids were evident between the long pad-like sections of film, as displayed in Figure 152B. Figure 152C&D identifies the tribofilm generated on the steel pin when lubricated with ZDDP + calcium sulfonate + NOCH. This protective layer

possessed a greater density than that observed with lubricant ZC and was not orientated in a particular direction (Figure 152D).

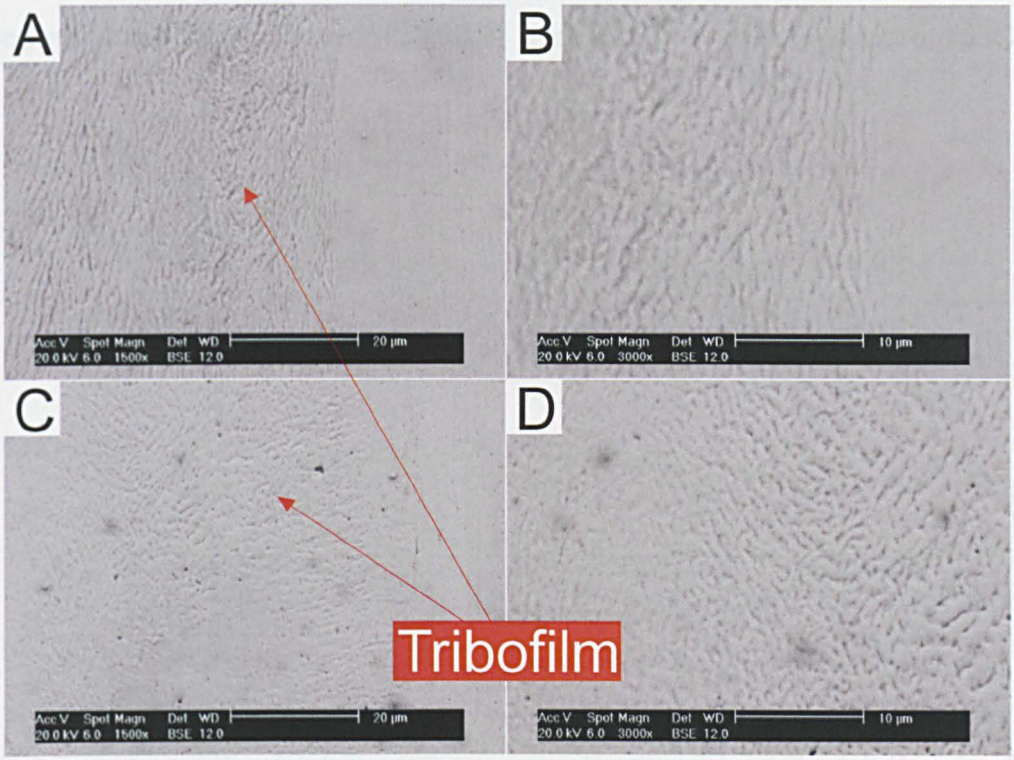

Figure 152: SEM image of a steel pin which has been in contact with an aluminium alloy and lubricated with ZDDP + calcium sulfonate (A&B) and ZDDP + calcium sulfonate + NOCH (C&D)

9.5.2. FTIR

The FTIR spectra displayed in this section are representative of the worn EN AW 2014A aluminium alloy substrates. Differences were identified between the lubricating oils (Figure 29&Figure 30) and the worn surfaces.

As with AluSil® substrates (section 5.5.2), all spectra contain bands between ~ 1485 cm^{-1} and ~ 1320 cm^{-1}, which were assigned to the C-H deformation vibration [224] of the alkane groups within the oil. The stretching vibration of C-H was observed between ~ 3000 cm^{-1} and ~ 2860 cm^{-1} [224]. Additionally, peaks at 670 cm^{-1}, 720 cm^{-1} and 890 cm^{-1} were observed on all samples; these were derived from the PAO6 base oil (Figure 29).

9.5.2.1. ZDDP vs ZDDP + NOCH

Figure 153 shows the spectra obtained from infrared analysis of EN AW 2014A lubricated with ZDDP (Figure 153A&B) and ZDDP + NOCH (Figure 153C&D).

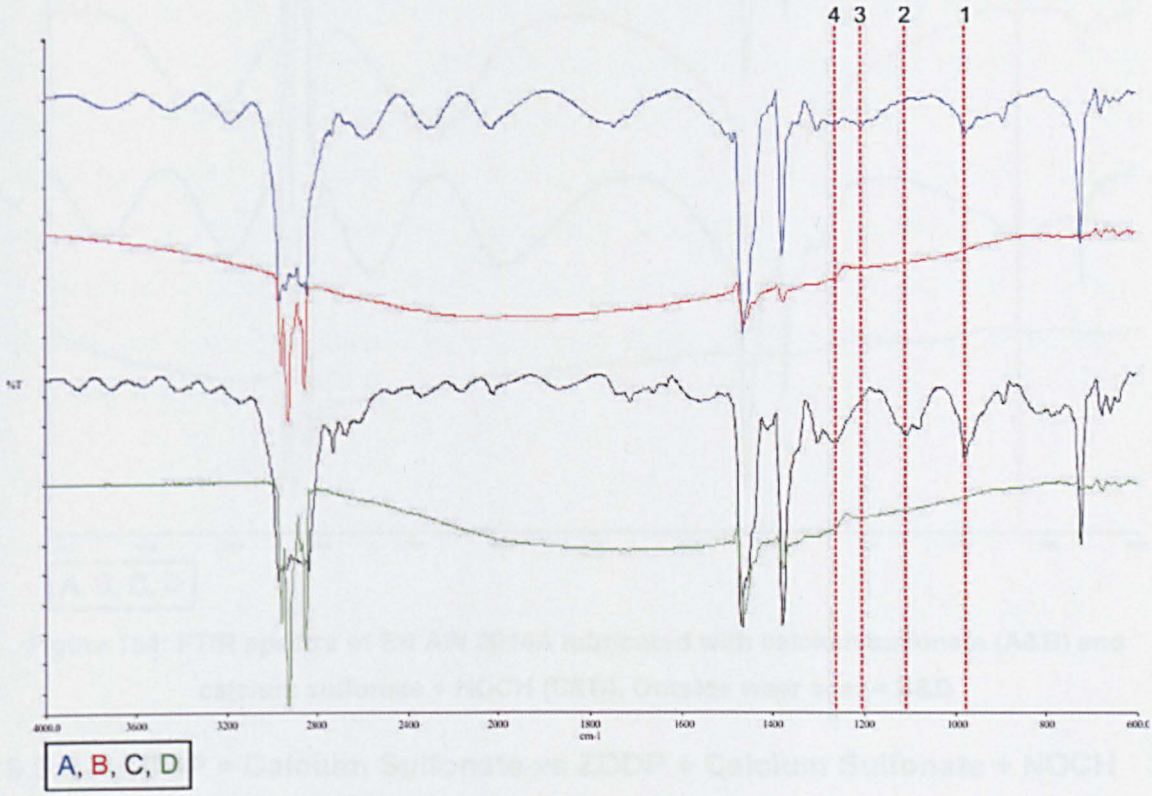

Figure 153: FTIR spectra of EN AW 2014A lubricated with ZDDP (A&B) and ZDDP + NOCH (C&D). Outside wear scar = B&D

As can be observed, peak #1 at 975 cm^{-1}, present in both lubricants prior to test (Figure 30), was obtained on lubricant Z and ZN substrates; this was attributed to the stretching of the P-O-C group within the ZDDP molecule [127, 229, 230]. Peaks #2 and #4, with wavenumbers of 1107 cm^{-1} and 1263 cm^{-1}, respectively, were accredited to the stretching vibrations of PO_2 [127]. Peak #3 at 1205 cm^{-1} was attributable to PO_3 (metaphosphate) [272]. Peaks #1 - #4 were indentified exclusively within the wear scar of the substrates (Figure 153A&C). Wavenumbers of interest were witnessed in greater intensities on lubricant ZN substrates, compared to ZDDP alone (Figure 153).

9.5.2.2. Calcium Sulfonate vs Calcium Sulfonate + NOCH

As with AluSil® (section 5.5.2.3), when the aluminium alloy was lubricated with either calcium sulfonate or calcium sulfonate + NOCH, one peak was identified solely within the wear scar of the worn substrates (Figure 154). This peak, labelled #1 in Figure 154, had a wavenumber of ~ 860 cm^{-1} and was attributed to calcium carbonate [227, 228, 244].

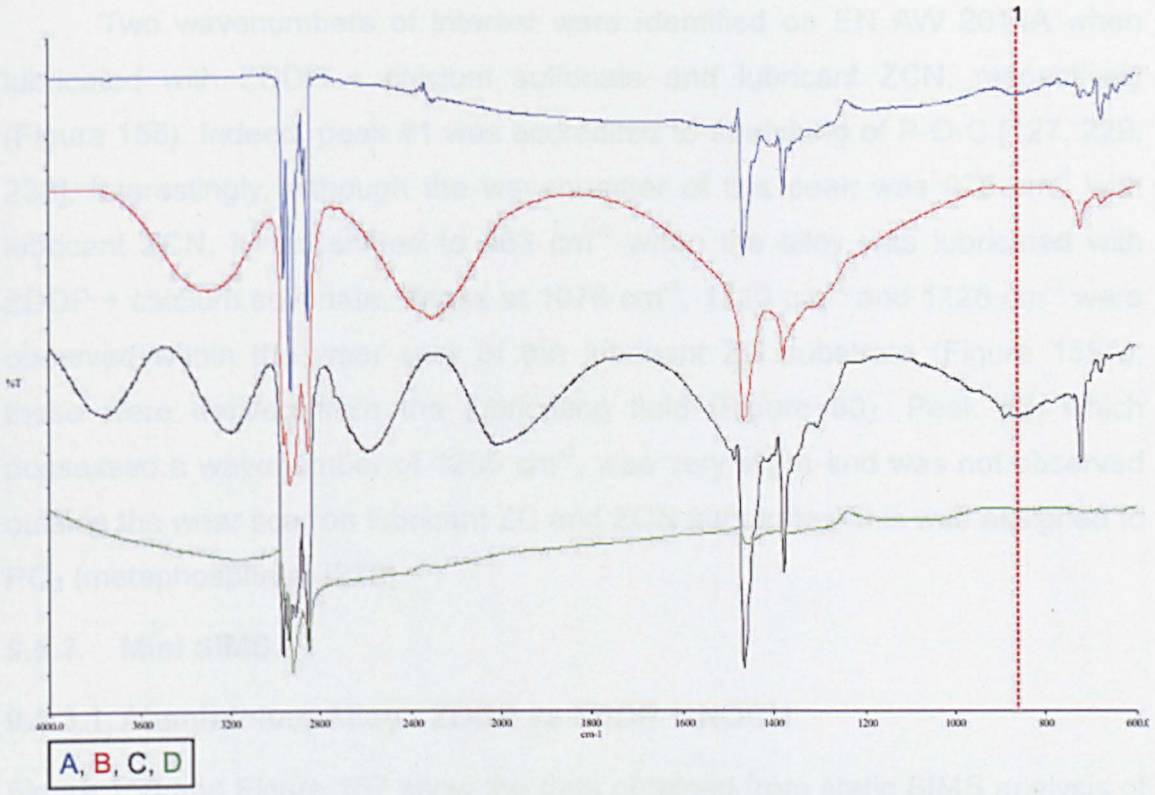

Figure 154: FTIR spectra of EN AW 2014A lubricated with calcium sulfonate (A&B) and calcium sulfonate + NOCH (C&D). Outside wear scar = B&D

9.5.2.3. ZDDP + Calcium Sulfonate vs ZDDP + Calcium Sulfonate + NOCH

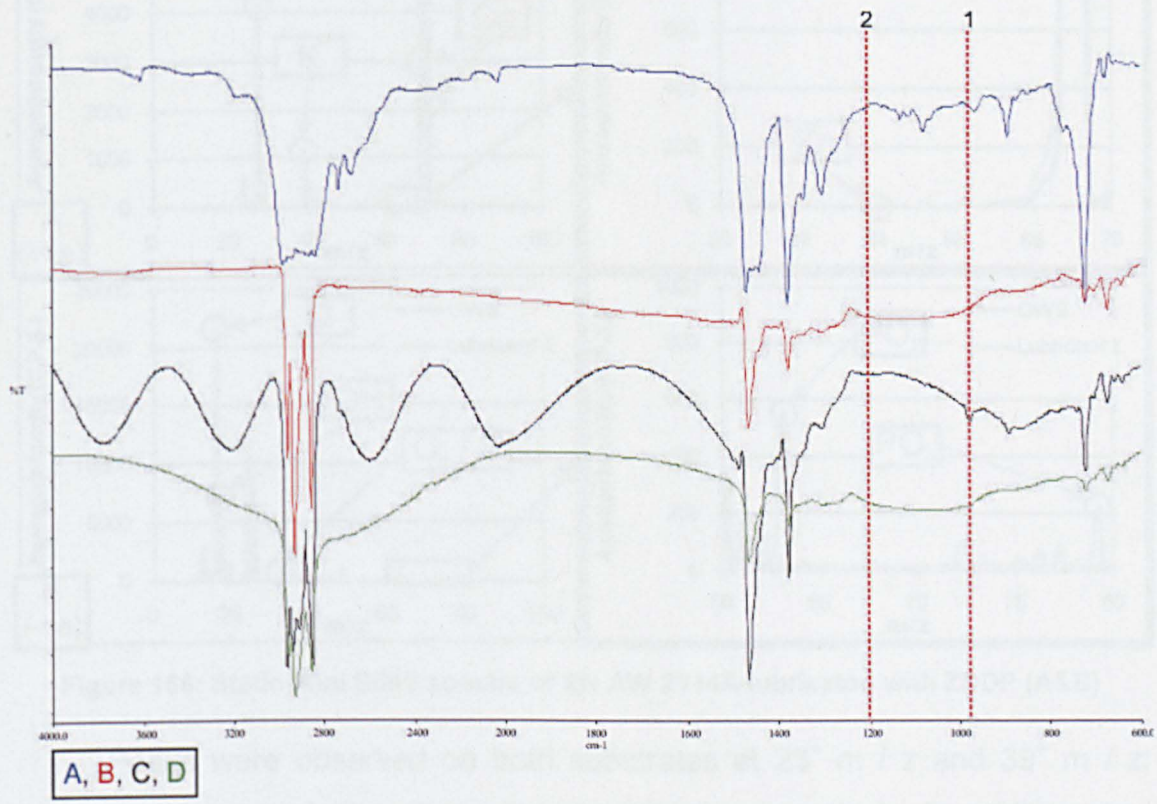

Figure 155: FTIR spectra of EN AW 2014A lubricated with ZDDP + calcium sulfonate (A&B) and ZDDP + calcium sulfonate + NOCH (C&D). Outside wear scar = B&D

Two wavenumbers of interest were identified on EN AW 2014A when lubricated with ZDDP + calcium sulfonate and lubricant ZCN, respectively (Figure 155). Indeed, peak #1 was accredited to stretching of P-O-C [127, 229, 230]. Interestingly, although the wavenumber of this peak was 975 cm^{-1} with lubricant ZCN, it had shifted to 963 cm^{-1} when the alloy was lubricated with ZDDP + calcium sulfonate. Peaks at 1076 cm^{-1}, 1110 cm^{-1} and 1128 cm^{-1} were observed within the wear scar of the lubricant ZC substrate (Figure 155A); these were derived from the lubricating fluid (Figure 30). Peak #2, which possessed a wavenumber of 1205 cm^{-1}, was very slight and was not observed outside the wear scar on lubricant ZC and ZCN substrates; this was assigned to PO_3 (metaphosphate) [272].

9.5.3. Mini SIMS

9.5.3.1. Alumininium Alloy - ZDDP vs ZDDP + NOCH

Figure 156 and Figure 157 show the data obtained from static SIMS analysis of EN AW 2014A lubricated with ZDDP and ZDDP + NOCH.

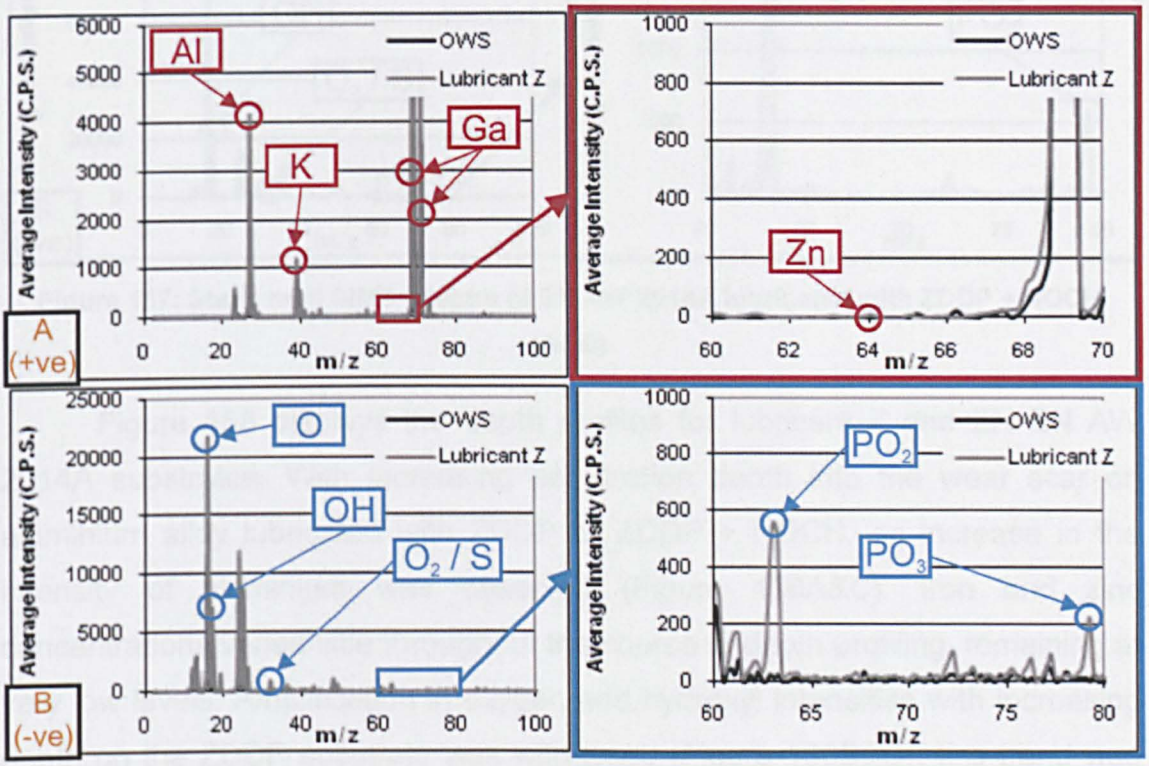

Figure 156: Static mini SIMS spectra of EN AW 2014A lubricated with ZDDP (A&B)

Peaks were observed on both substrates at 23^+ m / z and 39^+ m / z; these were assigned to sodium and potassium, respectively. In addition, two strong intensity peaks, attributed to the gallium source, were located at 69^+ m / z and 71^+ m / z on either sample. The aluminium base material was present at

27^+ m / z. Zinc was not evident on the surface of the wear scars, as indicated by the enlarged positive polarity spectra displayed in Figure 156 and Figure 157. In terms of the negative ion spectra, oxygen and hydroxyl were present in large intensities both inside and outside the wear scar with either lubricant. O_2 / S, PO_2 and PO_3 were witnessed with ZDDP and ZDDP + NOCH substrates (Figure 156B&Figure 157B); these compounds were not observed outside the wear scar.

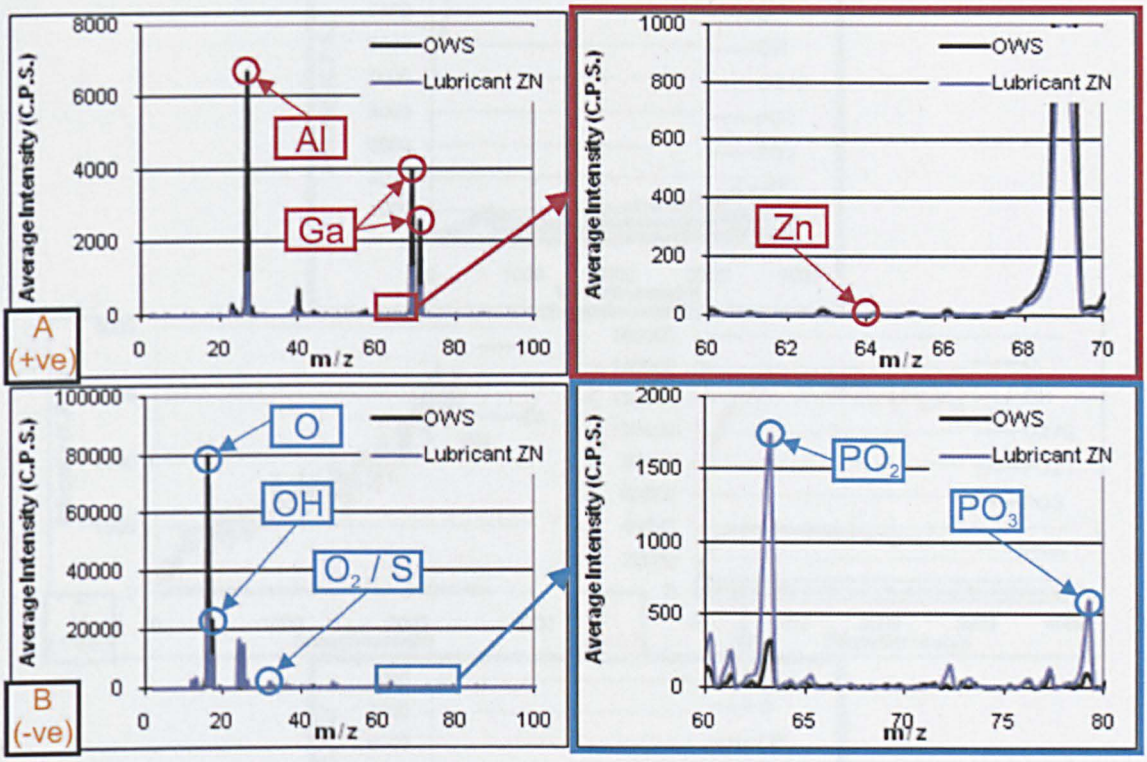

Figure 157: Static mini SIMS spectra of EN AW 2014A lubricated with ZDDP + NOCH (A&B)

Figure 158 displays the depth profiles for lubricant Z and ZN EN AW 2014A substrates. With increasing penetration depth into the wear scar on aluminium alloy lubricated with ZDDP or ZDDP + NOCH, an increase in the intensity of aluminium was observed (Figure 158A&C). Iron and zinc concentrations varied little throughout the course of depth profiling, remaining at very low levels. Amplification in oxygen and hydroxyl intensities with increasing depth on the ZDDP substrate was witnessed (Figure 158B&D); this trend was mirrored by O_2 / S, PO_2 and PO_3. However, when EN AW 2014A was lubricated with ZDDP + NOCH, maximum intensity of O, OH, O_2 / S, PO_2 and PO_3 were observed shortly after the start of the depth profiling process, after which point the concentrations of each decreased.

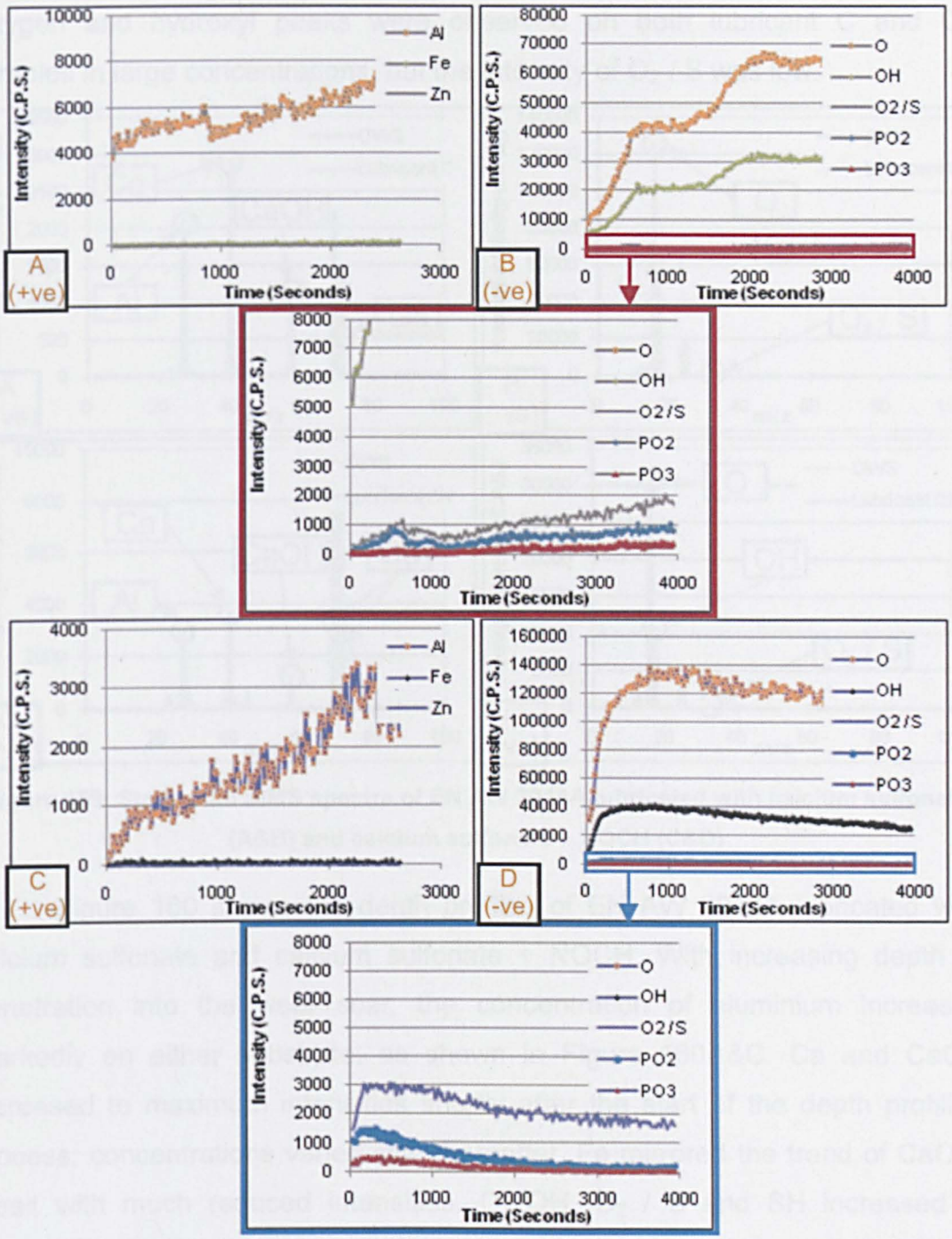

Figure 158: Mini SIMS depth profiles of EN AW 2014A lubricated with ZDDP (A&B) and ZDDP + NOCH (C&D)

9.5.3.2. Aluminium Alloy - Calcium Sulfonate vs Calcium Sulfonate + NOCH

As shown in Figure 159A&C, when the aluminium alloy was lubricated with calcium sulfonate or calcium sulfonate + NOCH, the wear scar on either substrate housed Ca and CaOH peaks. The gallium source was evident in the static analysis of either substrate, as too was an aluminium peak at 27^{+} m / z.

Oxygen and hydroxyl peaks were observed on both lubricant C and CN samples in large concentrations, but the intensity of O_2 / S was low.

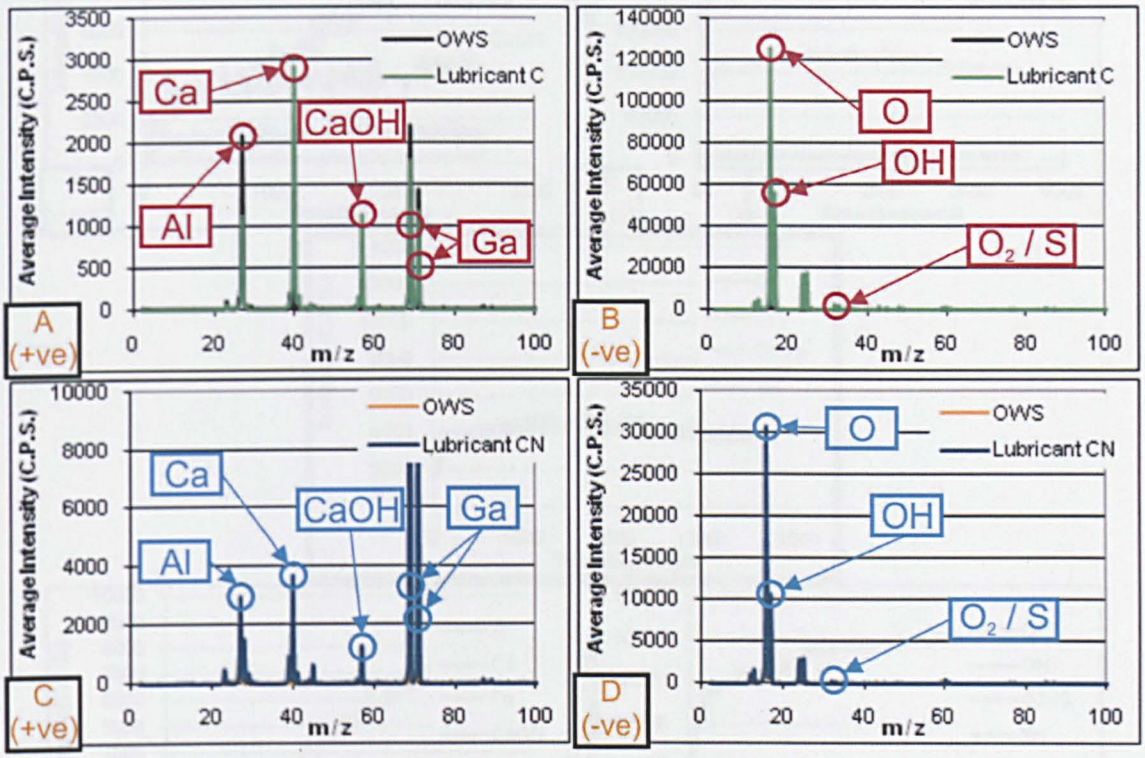

Figure 159: Static mini SIMS spectra of EN AW 2014A lubricated with calcium sulfonate (A&B) and calcium sulfonate + NOCH (C&D)

Figure 160 shows the depth profiles of EN AW 2014A lubricated with calcium sulfonate and calcium sulfonate + NOCH. With increasing depth of penetration into the wear scar, the concentration of aluminium increased markedly on either substrate, as shown in Figure 160A&C. Ca and CaOH increased to maximum intensities shortly after the start of the depth profiling process; concentrations varied little thereafter. Fe mirrored the trend of CaOH, albeit with much reduced intensities. O, OH, O_2 / S and SH increased in concentration with increasing penetration depth on either substrate (Figure 160B&D). Toward the end of the surface destructive process, the intensities of these peaks reached a plateau and began to decrease. Concentrations of O_2 / S and SH were very similar during the entirety of the depth profiling process.

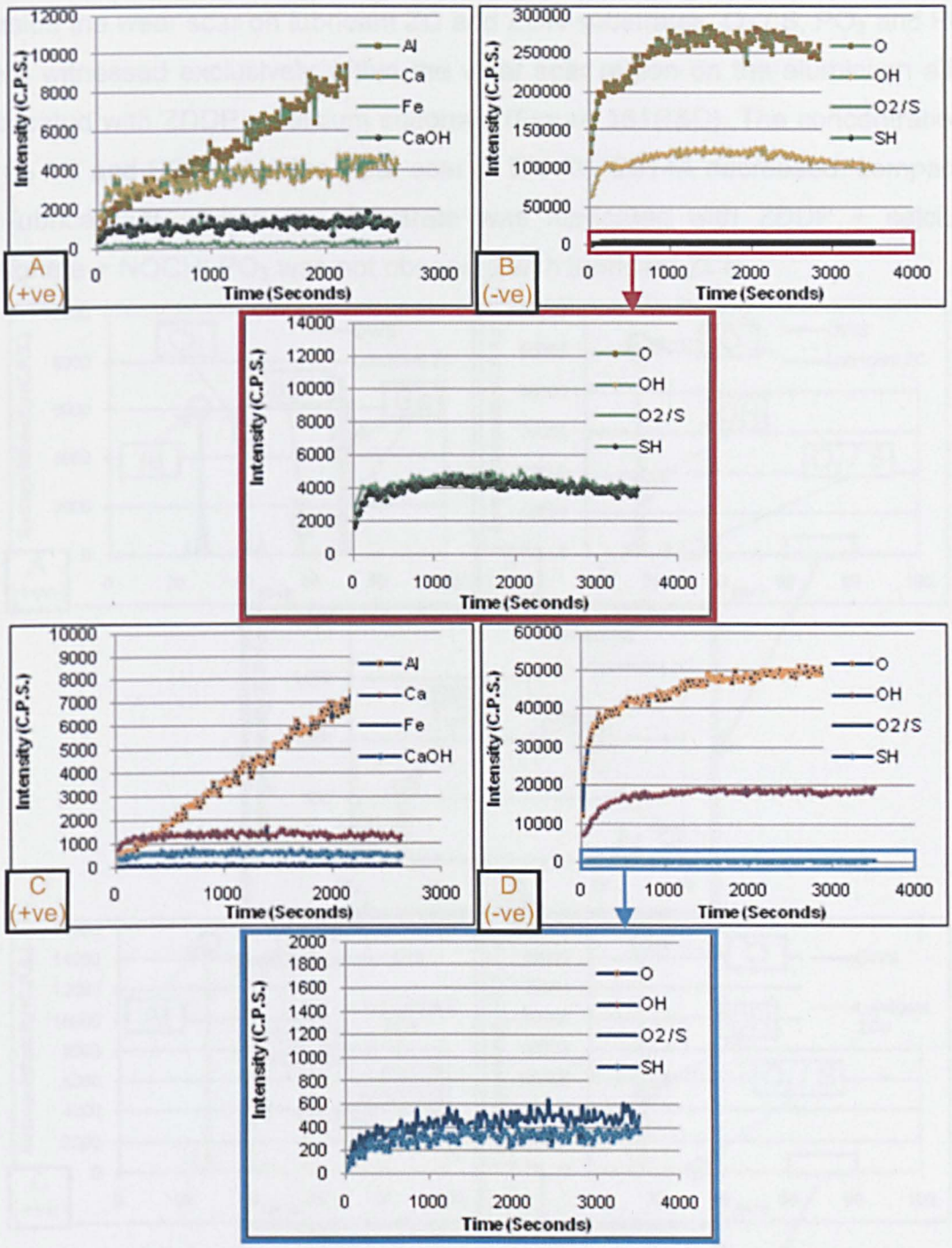

Figure 160: Mini SIMS depth profiles of EN AW 2014A lubricated with calcium sulfonate (A&B) and calcium sulfonate + NOCH (C&D)

9.5.3.3. Aluminium Alloy - ZDDP + Calcium Sulfonate vs ZDDP + Calcium Sulfonate + NOCH

In addition to the aluminium base material observed within the wear scar of EN AW 2014A lubricated with ZDDP + calcium sulfonate or ZDDP + calcium sulfonate + NOCH, Ca and CaOH peaks were witnessed (Figure 161A&C). Zinc was not present on the surface of either substrate, but peaks attributed to the gallium source were. Oxygen and hydroxyl were observed both inside and

outside the wear scar on lubricant ZC and ZCN substrates. O_2 / S, PO_2 and PO_3 were witnessed exclusively within the wear scar region on the aluminium alloy lubricated with ZDDP + calcium sulfonate (Figure 161B&D). The concentrations of O_2 / S and PO_2 within the wear scar of EN AW 2014A decreased, compared to lubricant ZC, when the substrate was lubricated with ZDDP + calcium sulfonate + NOCH; PO_3 was not observed with lubricant ZCN.

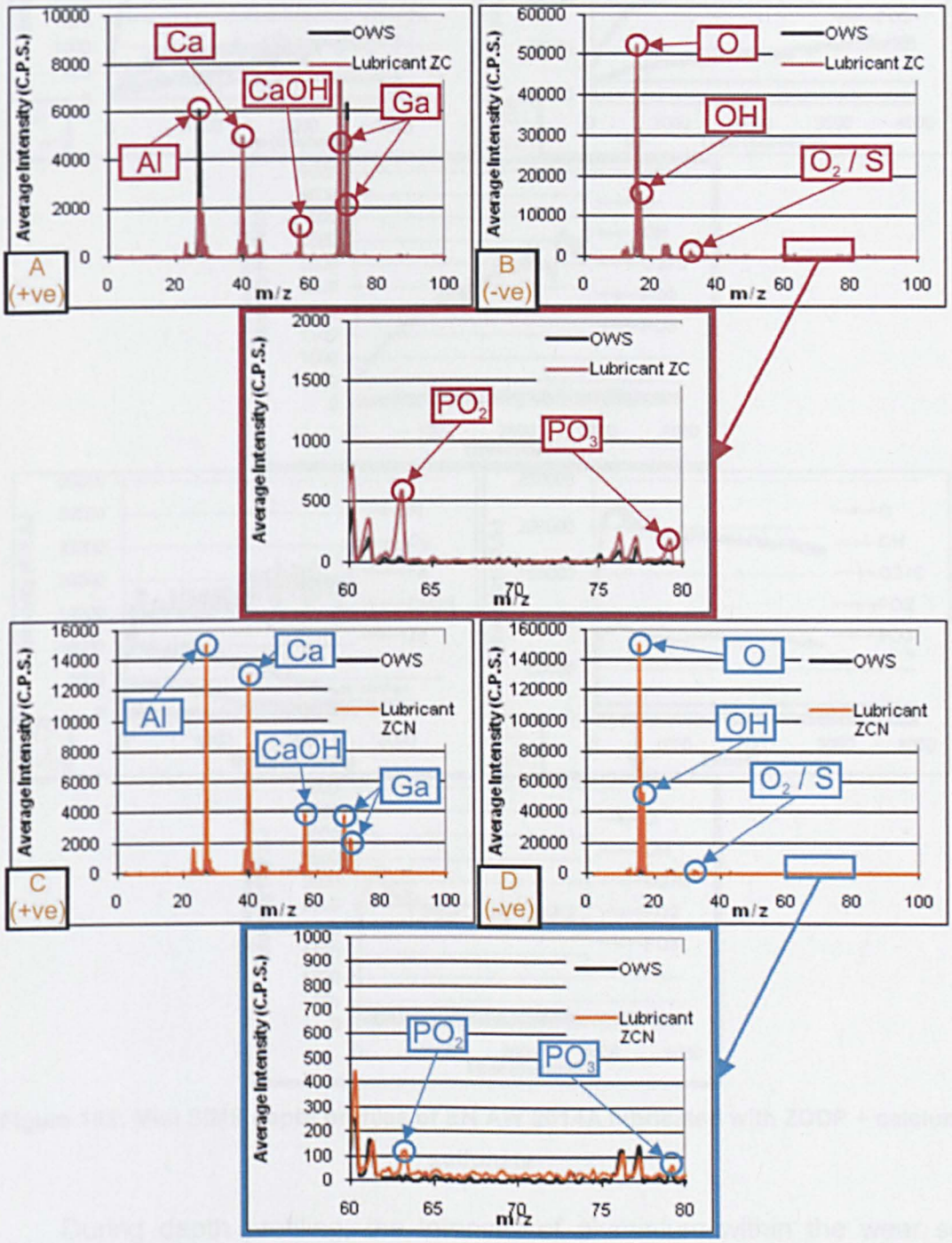

Figure 161: Static mini SIMS spectra of EN AW 2014A lubricated with ZDDP + calcium sulfonate (A&B) and ZDDP + calcium sulfonate + NOCH (C&D)

Figure 162 shows the depth profiles obtained from mini SIMS analysis of EN AW 2014A lubricated with ZDDP + calcium sulfonate or ZDDP + calcium sulfonate + NOCH.

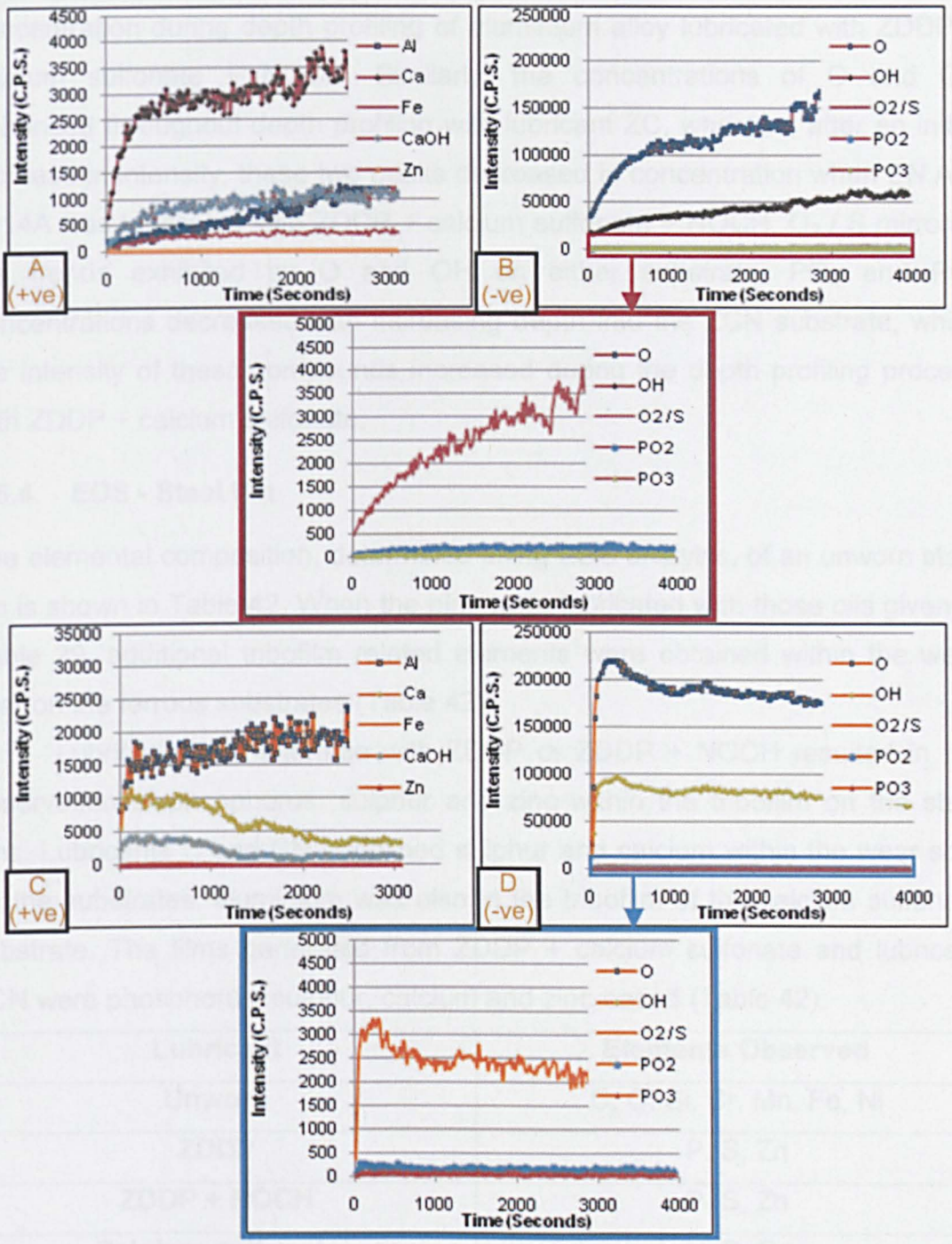

Figure 162: Mini SIMS depth profiles of EN AW 2014A lubricated with ZDDP + calcium sulfonate

During depth profiling, the intensity of aluminium within the wear scar region of lubricant ZC and ZCN substrates increased (Figure 162A&B). Zinc content did not vary throughout the destructive process, remaining at approximately zero intensity. The behaviour of the Ca peak throughout depth

profiling on either substrate was mirrored by CaOH and Fe. With lubricant ZC, the intensity of Ca, CaOH and Fe amplified with increasing penetration depth. Whereas, after an initial increase in intensity, these three peaks decreased in concentration during depth profiling of aluminium alloy lubricated with ZDDP + calcium sulfonate + NOCH. Similarly, the concentrations of O and OH enhanced throughout depth profiling with lubricant ZC, whereas, after an initial increase in intensity, these two peaks decreased in concentration when EN AW 2014A was lubricated with ZDDP + calcium sulfonate + NOCH. O_2 / S mirrored the trends exhibited by O and OH on either substrate. PO_2 and PO_3 concentrations decreased with increasing depth into the ZCN substrate, whilst the intensity of these compounds increased during the depth profiling process with ZDDP + calcium sulfonate.

9.5.4. EDS - Steel Pin

The elemental composition, determined using EDS analysis, of an unworn steel pin is shown in Table 42. When the pins were lubricated with those oils given in Table 29, additional tribofilm related elements were obtained within the wear scar on the ferrous substrates (Table 42).

Lubricating the interface with ZDDP or ZDDP + NOCH resulted in the observation of phosphorus, sulphur and zinc within the tribofilm on the steel pins. Lubricants C and CN contained sulphur and calcium within the wear scar on the substrates; aluminium was also in the tribofilm of the calcium sulfonate substrate. The films generated from ZDDP + calcium sulfonate and lubricant ZCN were phosphorus, sulphur, calcium and zinc-based (Table 42).

Lubricant	Elements Observed
Unworn	C, O, Si, Cr, Mn, Fe, Ni
ZDDP	P, S, Zn
ZDDP + NOCH	P, S, Zn
Calcium sulfonate	Al, S, Ca
Calcium sulfonate + NOCH	S, Ca
ZDDP + calcium sulfonate	P, S, Ca, Zn
ZDDP + calcium sulfonate + NOCH	P, S, Ca, Zn

Table 42: Elements observed during EDS analysis of tribofilms on steel pins used in the aluminium alloy tribosystem

9.6. Discussion

9.6.1. Friction Coefficients and Electrical Contact Voltage

9.6.1.1. ZDDP vs ZDDP + NOCH

The lubrication of EN AW 2014A was more successful with ZDDP + NOCH compared to ZDDP alone, as shown in Figure 140 and Figure 141. Indeed, given that full surface separation was not achieved until toward the end of experimentation with ZDDP, it follows that the aluminium alloy and steel pin were interacting with one another [234]; slow enhancement in contact voltage by ZDDP has been reported previously on ferrous substrates [176, 245, 247, 248]. Therefore, as a result of the poor separation, referring to Figure 144, the main contributor to frictional response was adhesion [3], since, through interaction with the steel pin, smearing of the aluminium alloy had occurred. Surface separation, and thus film formation, improved with the addition of NOCH [176].

The frictional response exhibited by ZDDP was slightly greater than reported in literature on steel-on-aluminium tribocouples [273, 274], similar to that on ferrous substrates [154, 176, 245], yet lower than on aluminium-silicon [152] and silicon crystal (chapter 7) surfaces. As observed on ferrous [215] and silicon surfaces (chapter 7), NOCH decreased the coefficient of friction in the tribosystem. This was derived from a reduction in adhesion [3] of the aluminium substrate with lubricant ZN, compared to ZDDP (Figure 144), due to the aforementioned superior substrate separation. Therefore, as film formation improved with ZDDP + NOCH, frictional response must have been derived primarily from the shear of the generated lubricant ZN tribofilm [160].

9.6.1.2. Calcium Sulfonate vs Calcium Sulfonate + NOCH

Calcium sulfonate did not generate a tribofilm effectively on aluminium substrates (Figure 141), in contrast to that reported on aluminium-silicon (chapter 5), silicon (chapter 7) and ferrous surfaces [176]. Indeed, this resulted in a high degree of plastic deformation in the form of ploughing on the aluminium alloy (Figure 146A&B). The amount of ploughing, and thus frictional energy consumed by deformation [3], reduced gradually during the first 60 minutes of experimentation (Figure 140). This was probably due to a combination of increasing surface separation due to film formation (Figure 141),

together with enhanced conformity between the surfaces due to running-in [3]; minimum frictional response coincided with the full separation of the substrates. Therefore, it follows that the final steady-state frictional response was derived from the shear of the films generated on either ferrous or aluminium substrate [160] and thus adhesion [3] was the sole contributor to the friction coefficient.

The addition of NOCH to overbased calcium sulfonate dramatically improved film formation in the tribosystem (Figure 141) [176]. However, surface separation was slightly slower than that witnessed on aluminium-silicon (chapter 5) and silicon (chapter 7) surfaces. Given that the aluminium substrate did not experience ploughing or smearing (Figure 146C&D), it follows that the frictional response in the contact was imparted primarily by the shear of the lubricant CN tribofilm [160], which was lower than that of ZDDP + NOCH (Figure 140). The observed coefficient of friction was similar to that reported with OBCS on ferrous [176] and steel-on-aluminium tribocouples [273]. A comparison between the shear strengths of the two detergent tribofilms could not be afforded due to the markedly different wear levels on the aluminium samples.

9.6.1.3. ZDDP + Calcium Sulfonate vs ZDDP + Calcium Sulfonate + NOCH

Calcium sulfonate and NOCH must influence film formation with lubricant ZCN since the electrical contact voltage exhibited by ZDDP + calcium sulfonate + NOCH was analogous to that observed with lubricant CN (Figure 141). Surface separation was slightly impaired with lubricant ZC, indicating a greater amount of time was required to generate tribofilms on the rubbing surfaces [176], compared to lubricant ZCN. However, the combination of ZDDP + OBCS improved surface separation relative to the sole use of either additive, implying synergistic behaviour had occurred. This is in contrast to that reported on ferrous surfaces, where the combination of antiwear and detergent additive is known to hinder film formation [176].

However, the observed differences in electrical contact voltage between lubricants ZC and ZCN did not result in marked variations in frictional response (Figure 140). As reported on ferrous substrates [176], the friction coefficient reduced with ZDDP + calcium sulfonate, compared to ZDDP alone; similar behaviour was observed on silicon and Al-Si substrates in this thesis (chapters 5&7). With either lubricant, deformation must have not played a major role in frictional response, since ploughing or smearing of the aluminium alloy was not

observed (Figure 148) [3]. However, as tribofilms were clearly generated on EN AW 2014A with lubricants ZC and ZCN (Figure 148), it follows that the friction coefficients in the two tribocouples were principally derived from the shear of the films [160] on the steel and aluminium surfaces. The shear strengths, therefore, of the two tribofilms must have been analogous if frictional response was comparable.

9.6.1.4. Summary

ZDDP generated the greatest frictional response in the tribosystem due to inadequate separation of the aluminium and steel surfaces, resulting in smearing of the aluminium alloy. The addition of NOCH to ZDDP improved film formation and thus the friction coefficient due to a reduction in substrate-substrate interaction. Therefore, the shear of the tribofilm was the primary source of the frictional response in the lubricant ZN tribocouple.

Calcium sulfonate did not separate the two substrates effectively and this resulted in a marked variation in frictional response compared to any other lubricant. During the running-in period, the frictional response declined gradually until full separation of the substrates was afforded; the frictional response then derived from the shear of the tribofilm. The addition of NOCH dramatically improved film formation and imparted a low coefficient of friction on the tribosystem, implying the lubricant CN tribofilm possessed a low shear strength.

Frictional response was comparable with lubricants ZC and ZCN. The combination of detergent and antiwear additive improved film formation compared to the sole use of either engine oil additive. Calcium sulfonate and NOCH were influencing the film formation of ZDDP + calcium sulfonate + NOCH.

9.6.2. Surface Topography and Wear

An attempt was made to determine the thickness and mechanical properties of tribofilms generated on aluminium substrates using the methods described in chapter 6 of this thesis. However, these two parameters could not be measured, which is indicative of the very thin films generated on aluminium substrates.

9.6.2.1. ZDDP vs ZDDP + NOCH

As shown in section 9.5.1.1, and reported previously [208], adhesive wear [7] was witnessed on aluminium lubricated with ZDDP. However, since abrasive

wear [7] nor a tribofilm was not observed on the alloy, it is natural to suggest that the film generated on the steel pin (section 9.5.1.4) reduced the wear on the non-ferrous substrate. This tribofilm also protected the steel surface and resembled that previously reported on ferrous substrates using zinc dialkyldithiophosphate [122, 145-147, 149, 252-255]. Wear was lower on the aluminium alloy than that reported previously using ZDDP [274].

As shown in Figure 163, the ratio between the average WSW on aluminium and silicon substrates (chapter 7) lubricated with ZDDP was approximately equal to one. Therefore, since ZDDP was a poor lubricator of silicon surfaces (chapter 7), it must follow that zinc dialkyldithiophosphate also imparted insufficient lubrication to the aluminium alloy, as reported in literature [274]. Hence, the film observed on the matrix of ZDDP and ZDDP + NOCH lubricated-AluSil® (chapter 5) must originate from film transfer from silicon grains and not be generated on the aluminium matrix.

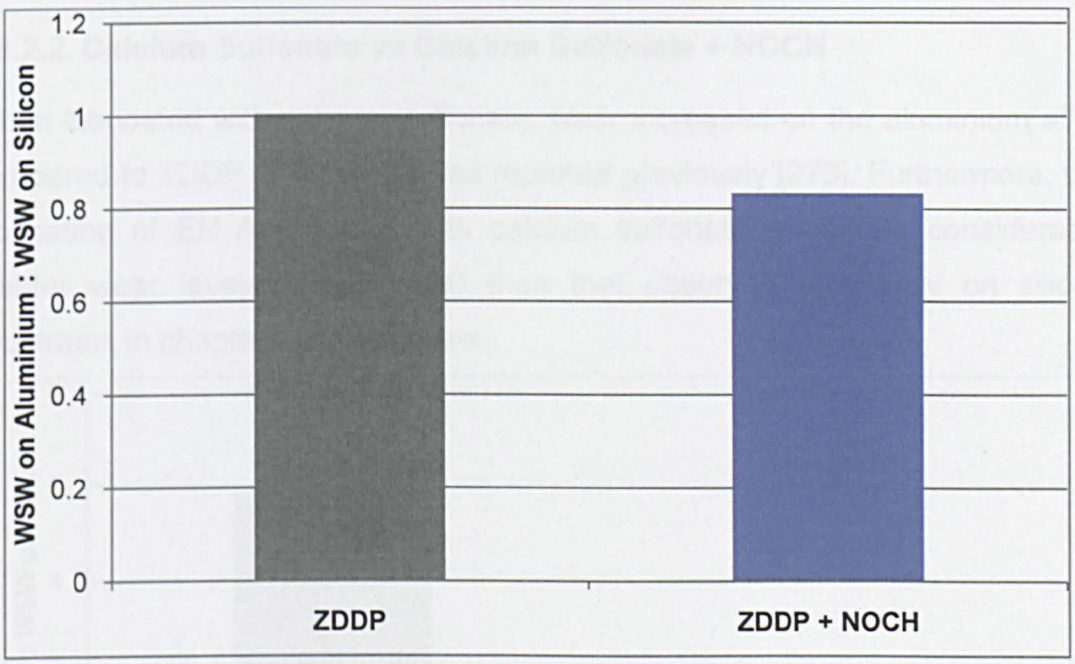

Figure 163: Ratio between the average wear scar widths on aluminium and silicon substrates, when lubricated with ZDDP or ZDDP + NOCH

As Figure 163 displays, wear protection afforded by lubricant ZN on EN AW 2014A was approximately similar to that on silicon substrates. The addition of NOCH to ZDDP reduced wear on the aluminium alloy and steel pin (Figure 142&Figure 143), as previously reported on ferrous [215], silicon (chapter 7) and aluminium-silicon (chapter 5) surfaces. However, wear reduction was more noticeable on the steel pin, rather than aluminium alloy (Figure 143), highlighting a greater efficiency on the steel substrate. Since a physical tribofilm

was not observed on EN AW 2014A, yet adhesive wear had reduced (section 9.5.1.1), it follows that the increased wear protection must be derived from the steel pin. Indeed, referring to section 9.5.1.4, the reduction in wear can be accredited to an enhanced surface density of the tribofilm generated on the ferrous substrate, compared to ZDDP alone. Consequently, a reduction in substrate-substrate interaction and thus adhesion [7] of the soft aluminium substrate ensued; identical behaviour was observed previously on silicon tribosystems (chapter 7). Since abrasive wear was witnessed on the aluminium alloy with ZDDP + NOCH (section 9.5.1.1), this is indicative of the lubricant ZN tribofilm generated on the steel pin possessing a greater hardness than the aluminium substrate [7]. Wear protection imparted by the ZDDP-based tribofilms was due to mechanisms previously proposed in literature, namely preferential wear [145] and load carrying [120, 146]. It follows, therefore, that ZDDP + NOCH was the more successful of the two lubricants in these respects.

9.6.2.2. Calcium Sulfonate vs Calcium Sulfonate + NOCH

When lubricated with calcium sulfonate, wear increased on the aluminium alloy compared to ZDDP (Figure 142), as reported previously [273]. Furthermore, the lubrication of EN AW 2014A with calcium sulfonate generated considerably greater wear levels (Figure 164) than that observed previously on silicon substrates in chapter 7 of this thesis.

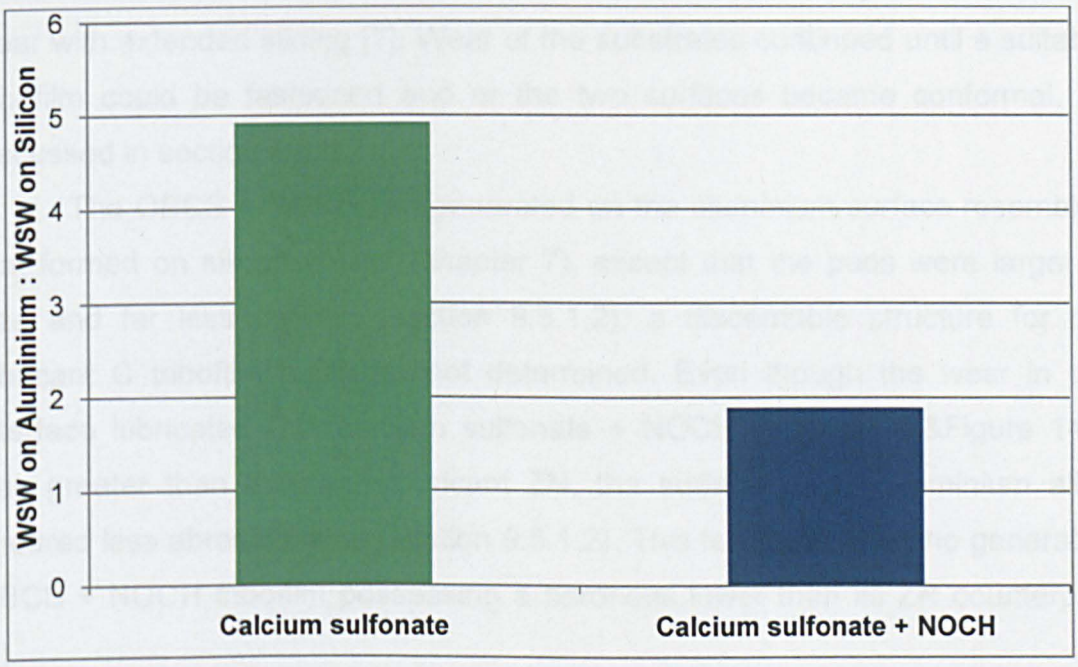

Figure 164: Ratio between the average wear scar widths on aluminium and silicon substrates, when lubricated with calcium sulfonate or calcium sulfonate + NOCH

Indeed, as shown in section 9.5.1.2, the surface of the alloy had been badly worn primarily through abrasive wear [7], which has been observed on lubricated aluminium alloys previously [274, 275]. Subsequently generated wear debris was transferred to the ferrous pin, resulting in the formation of a non-homogeneous layer (section 9.5.1). The reduction in wear by lubricant CN, compared to calcium sulfonate, on both steel pin (Figure 143) and aluminium alloy (Figure 142) has been reported previously [215] (chapter 7). The formation of effective lubricant CN-based tribofilms on either surface (section 9.5.1) are accredited with the observed decline in wear.

Antiwear protection was imparted by the tribofilms minimising interaction between contacting substrates [160] and enduring wear in preference to substrate surfaces [165]. Therefore, if similar behaviour was being observed as on silicon substrates, wear protection partly derived from the calcium sulfonate + NOCH tribofilm having an increased tendency to plastically deform (chapter 7). The variation in wear levels between calcium sulfonate and lubricant CN could also be related to electrical contact voltage [176]. The ECV results for OBCS (section 9.6.1.2) indicate that any generated tribofilms did not impart sufficient reduction in substrate-substrate interaction [234] during experimentation. Indeed, this must derive from the increase in density of the lubricant CN tribofilm (section 9.5.1), as reported previously (chapter 7). Thus, initial adhesive wear of the OBCS-lubricated aluminium alloy led to abrasive wear with extended sliding [7]. Wear of the substrates continued until a suitable tribofilm could be fashioned and or the two surfaces became conformal, as discussed in section 9.6.1.2.

The OBCS + NOCH film generated on the aluminium surface resembled that formed on silicon crystal (chapter 7), except that the pads were larger in size and far less defined (section 9.5.1.2); a discernable structure for the lubricant C tribofilm could be not determined. Even though the wear in the interface lubricated with calcium sulfonate + NOCH (Figure 142&Figure 143) was greater than that with lubricant ZN, the surface of the aluminium alloy endured less abrasive wear (section 9.5.1.2). This is indicative of the generated OBCS + NOCH tribofilm possessing a hardness lower than its ZN counterpart [7].

Referring to Figure 164, the increase in wear on aluminium, compared to silicon substrates, when lubricated with OBCS or OBCS + NOCH implies that

the detergent was far less effective in terms of wear protection on aluminium, compared to silicon-based tribosystems. This was most likely due to the high hardness of the silicon crystal, which was less susceptible to abrasive and adhesive wear and could support film formation.

9.6.2.3. ZDDP + Calcium Sulfonate vs ZDDP + Calcium Sulfonate + NOCH

Tribofilms were generated on aluminium and steel substrates (section 9.5.1) when lubricated with ZDDP + calcium sulfonate or lubricant ZCN. Furthermore, the tribofilms formed on the aluminium alloy loosely resembled those generated with these lubricants on silicon crystal (chapter 7).

The combination of ZDDP + calcium sulfonate reduced wear on both steel and aluminium substrates compared to calcium sulfonate alone (Figure 142&Figure 143); identical behaviour was reported in chapter 7 of this thesis. Since an additional reduction in wear was observed compared to ZDDP with lubricant ZC on the steel substrate, this is indicative of synergistic behaviour between the two engine oil additives. Furthermore, it follows that superior antiwear performance was afforded to the ferrous, rather than aluminium substrate. Indeed, lubricant ZC's effectiveness on aluminium was limited, since the recorded WSW was the 2nd greatest, and surface machining marks had been removed (section 9.5.1.3). As shown in Figure 165, lubricant ZC was more efficient at reducing wear on silicon substrates, compared to aluminium.

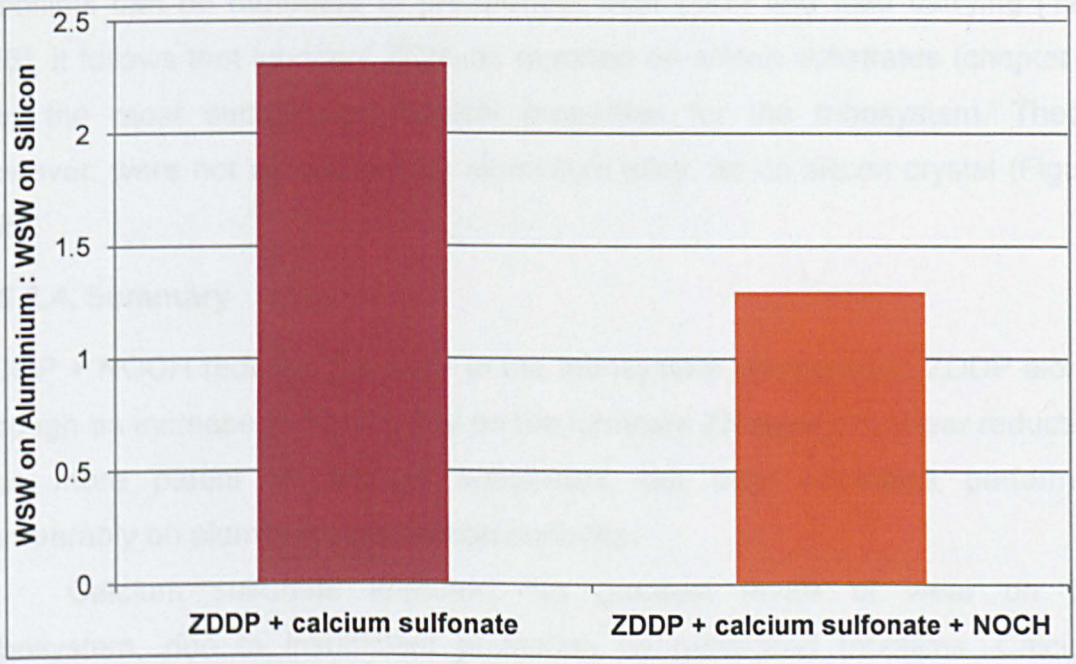

Figure 165: Ratio between the average wear scar widths on aluminium and silicon substrates, when lubricated with ZDDP + calcium sulfonate or ZDDP + calcium sulfonate + NOCH

With either lubricant, adhesion [7] was the dominant wear mechanism on aluminium substrates, since grooves in the alloy were not observed (section 9.5.1.3) and localised areas of material removal were evident (Figure 148D). However, given that calcium phosphate is physically very hard (H = 5) [190] and is known to be present within a tribofilm generated from ZDDP + calcium sulfonate [184, 185, 187], it follows that EN AW 2014A lubricated with ZDDP + OBCS must have been subject to abrasive wear [7] also. An enhancement in tribofilm hardness would also explain the observed wear increase compared to ZDDP.

As reported in the silicon-based tribosystem (chapter 7), lubricant ZCN imparted the lowest wear levels in the interface; this is accredited to two main areas. Firstly, as reported on silicon (chapter 7) and steel piston ring (chapter 5) substrates, the addition of NOCH to lubricant ZC promotes the formation of calcium carbonate, which is considerably softer than calcium phosphate (H = 3) [182], resulting in less abrasive wear compared to ZDDP + calcium sulfonate. Secondly, the enhanced surface density of the tribofilm afforded by lubricant ZCN on the steel pin (section 9.5.1.6) reduced substrate-substrate interaction, thereby minimising adhesion; this was identified previously on the silicon tribosystem (chapter 7).

Since the antiwear protection imparted by lubricant ZC and ZCN tribofilms can be attributed to preferential wear [145] and load carrying [120, 146], it follows that lubricant ZCN, as reported on silicon substrates (chapter 7) had the most suitable mechanical properties for the tribosystem. These, however, were not as efficient on aluminium alloy, as on silicon crystal (Figure 165).

9.6.2.4. Summary

ZDDP + NOCH reduced the wear in the tribosystem compared to ZDDP alone, through an increase in film density on the lubricant ZN steel pin. Wear reduction was more patent on ferrous substrates, but both lubricants performed comparably on aluminium and silicon surfaces.

Calcium sulfonate imparted the greatest levels of wear on the tribosystem, due to insufficient protection by generated tribofilms. Calcium sulfonate + NOCH improved the wear performance compared to ZDDP and OBCS because of the formation of tribofilms on both aluminium and steel

surfaces. Furthermore, lubricant CN reduced abrasive wear on the aluminium alloy compared to ZDDP + NOCH, due to a decline in tribofilm hardness. Calcium sulfonate and OBCS + NOCH were more effective in terms of wear performance on silicon substrates compared to EN AW 2014A.

Protective films were observed on both components of the tribosystem when lubricated with ZC and ZCN. ZDDP + calcium sulfonate performed synergistically in terms of antiwear protection on ferrous substrates, whereas the wear reduction imparted on the aluminium alloy was only lower than that observed with calcium sulfonate. Lubricant ZCN imparted the lowest wear on either substrate, as the result of an enhanced surface density and reduction in hardness of the generated tribofilms. Silicon surfaces were more compatible with the antiwear performance afforded by lubricant ZC and ZCN, compared to the aluminium alloy. An overview of the benefits of NOCH in terms of tribological performance and surface topography are shown in Table 43.

Lubricant	Effect of the Addition of NOCH
ZDDP	Decreased friction; improved surface separation and film formation; reduced wear
Calcium sulfonate	Improved surface separation; reduced wear; improved film surface coverage
ZDDP + calcium sulfonate	Improved surface separation; reduced wear; improved film density

Table 43: Overview of the effect of the addition of NOCH on test oils used to lubricate an aluminium alloy and steel pin tribosystem

9.6.3. Tribochemical Analysis and Film Formation

9.6.3.1. ZDDP vs ZDDP + NOCH

9.6.3.1.1. Tribochemistry

As reported previously [276] (chapter 5), non-decomposed ZDDP was evident on the surface of the aluminium alloy when lubricated with ZDDP-containing fluids (Figure 153). The presence of PO_2 [127] and PO_3 [272] (chapter 5) within the wear scar of Z and ZN lubricated EN AW 2014A agrees with reported findings on AluSil® (chapter 5). Given that NOCH related peaks (Figure 29) were not observed on the aluminium alloy, this is indicative of either decomposition of triethyl citrate, or it is not present in large concentrations on

the substrate surface; identical results were obtained on AluSil® (chapter 5). Contaminants identified using mini SIMS of EN AW 2014A have been previously reported on worn Al-Si substrates (chapter 5).

Given that PO_2, PO_3 and O_2 / S were identified exclusively within the wear scar of Z and ZN aluminium substrates using SIMS (section 9.5.3.1), this is indicative of polyphosphate formation in the interface [118]. However, since a tribofilm was not observed on the alloy (section 9.6.2.1), and, in addition, Zn or Fe were not present within the wear scar of the substrate, this implies tribofilm formation did not occur on EN AW 2014A. Instead, it follows that zinc and iron polyphosphates [118, 129, 131, 132, 139] were generated on the steel pin (Table 42) and film transfer to the aluminium alloy occurred. Sulphur was most probably in the form of zinc or iron sulphide [118, 125, 126, 132, 139] or contained within phosphate regions, as sulphide in solid solution [187] on the aluminium substrate.

Therefore, it is possible to suggest that the tribofilm species on the aluminium alloy (section 9.5.3.1) were related to the chemical composition of the films formed on the steel surfaces. Hence, it follows that greater concentrations of phosphorus and sulphur species were generated on the steel pin with ZDDP + NOCH, which resulted in a reduction in wear in the tribosystem (section 9.6.2.1); this has been reported previously [215] (chapter 5). The results obtained also conclude that tribofilms identified previously on the aluminium matrix of an Al-Si substrate [25, 66, 153] (chapter 5) must originate from either film transfer [25, 66, 153] or ZDDP thermal decomposition [25], not through in-situ film formation.

9.6.3.1.2. Film Formation

Tribofilm formation occurred on the steel substrates using the multi-stage process described previously (sections 5.6.3.2&7.6.3.1). Therefore, using the method developed by Fuller et al. [131], ZDDP and its linkage isomer were adsorbed onto the ferrous substrate. Subsequently, through a reaction with iron oxide, iron phosphate was generated, along with mixed Fe / Zn phosphorus compounds; ZnO formation was induced by both reactions [126]. When lubricated with ZDDP + NOCH, triethyl citrate was simultaneously generating metal complexes, as predicted previously (Figure 79) (chapter 5), where M = Cr, Fe or Al.

By further incorporating the processes suggested by Fuller et al. [131], polyphosphates and sulphur compounds were generated through thermo-oxidative decomposition of the mixed phosphorus compounds, adsorbed ZDDP and its linkage isomer [131]. Given that FTIR and SIMS results were indicative as to the concentration of tribofilm species being greater on ZDDP + NOCH substrates (section 9.5.3.1&Figure 153), it follows that, as reported previously (chapters 5&7), NOCH enhanced the decomposition of ZDDP. This resulted in a greater concentration of tribofilm species within the protective layer on the steel surface, which were subsequently transferred to the aluminium alloy. In addition, aluminium phosphide formation may have occurred in small concentrations on EN AW 2014A according to the processes proposed by Nicholls et al. [98].

9.6.3.1.3. Summary

Representative models of aluminium substrates lubricated with ZDDP or ZDDP + NOCH are shown in Figure 166. Tribofilm formation occurred exclusively on the steel pin using ZDDP or ZDDP + NOCH, with which iron and zinc polyphosphates and sulphur species were generated. The addition of NOCH to lubricant Z enhanced the decomposition of ZDDP. Phosphorus and sulphur species were transferred from steel substrate to aluminium alloy under tribological conditions, and mixed into the substrate through wear processes.

Tribofilm Chemistry and Structure
Phosphate and sulphur species transferred from steel pin and contained within worn aluminium alloy

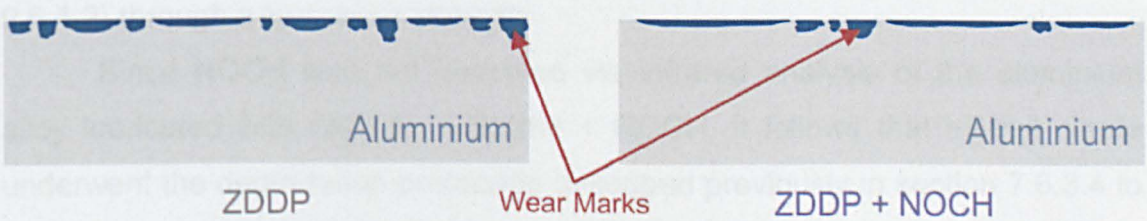

Figure 166: Models of EN AW 2014A lubricated with ZDDP or ZDDP + NOCH

9.6.3.2. Calcium Sulfonate vs Calcium Sulfonate + NOCH

9.6.3.2.1. Tribochemistry

The chemical compositions of the tribofilms generated on aluminium substrates lubricated with calcium sulfonate or calcium sulfonate + NOCH were analogous to those formed on ferrous [178], silicon (chapter 7) and aluminium-silicon surfaces (chapter 5). Indeed, the films contained Ca and CaOH peaks (section 9.5.3.2), which, together with the FTIR results (Figure 154), are indicative of $CaCO_3$ formation [34, 178]. The observation of CaOH [168] and the wavenumber of the FTIR peak observed (~ 860 cm^{-1} [244, 259]), implies amorphous calcium carbonate was generated; identical to that witnessed on silicon and aluminium-silicon substrates in this thesis (chapters 5&7).

Depth profiling of either substrate revealed analogous results to those obtained with silicon crystal (chapter 5), in which calcium and calcium hydroxide concentrations, along with O_2 / S and SH, increased as the depth into the film enhanced (section 9.5.3.2). Therefore, it is natural to suggest, that the tribofilms generated from lubricants C and CN on EN AW 2014A possessed an identical structure to those on silicon crystal. This would consist of a calcium carbonate bulk section [165, 167, 168], with sulfonate chains toward the outer region of the film [178]. The peak identified as Fe during depth profiling (Figure 160) was most likely CaO, since it mirrored CaOH throughout the process; this has been observed previously [178, 180].

As tribofilm structure on the steel pin is thought to be identical to that on the counterpart substrate (chapter 7), it follows the same must be true herein, given the identification of calcium and sulphur species on steel pins lubricated with calcium sulfonate or calcium sulfonate + NOCH (Table 42). However, in addition to the tribofilm on the OBCS steel pin, aluminium transfer material was evident; the combination of which presumably afforded low friction (section 9.6.1.2) through a low shear strength.

Since NOCH was not observed via infrared analysis of the aluminium alloy lubricated with calcium sulfonate + NOCH, it follows that triethyl citrate underwent the degradation processes described previously in section 7.6.3.4 to afford a metal ethoxide (Figure 137). This explains the observed increase in surface density of the $CaCO_3$-based tribofilm on both aluminium and ferrous substrates (section 9.5.1) and is therefore indicative of enhanced carbonate

deposition (chapter 7), as previously predicted [215]. Hence, referring to section 9.6.2.2, it is natural to suggest wear reduction was achieved through an increase in calcium carbonate formation, rather than variations in chemical composition.

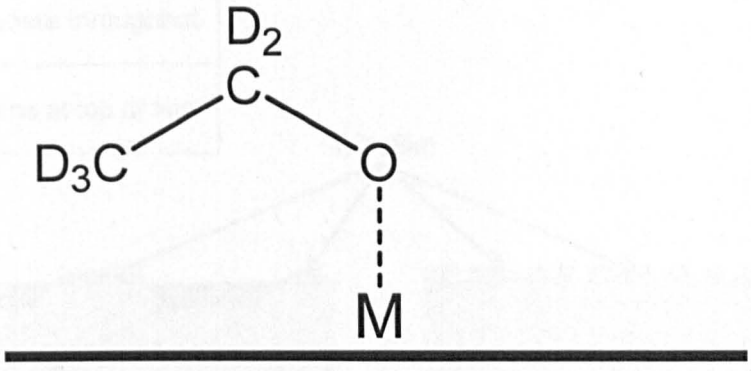

Figure 137: Metal ethoxide compound

9.6.3.2.2. Film Formation

As film formation by overbased calcium sulfonate has been proven to be generic (section 7.6.3.2), through a mechanistic process, sulfonate chains were removed from calcium sulfonate micelles during tribological rubbing [165, 168]. Thereafter, calcium carbonate built up on aluminium and steel substrates [165, 167, 169] and the removed chains were mixed into the $CaCO_3$ film. Simultaneously, NOCH generated metal complexes with aluminium, chromium, iron and calcium (Figure 79). Ensuing de-esterification induced by the calcium carbonate base [269, 270] afforded a metal ethoxide (Figure 137), which, subsequently, promoted further calcium carbonate deposition [268].

9.6.3.2.3. Summary

Models of aluminium substrates lubricated with calcium sulfonate or calcium sulfonate + NOCH are shown in Figure 167. Tribofilms generated on both steel and aluminium alloy substrates with lubricants C and CN were comprised a bulk section of amorphous calcium carbonate, with sulfonate chains located at the outer regions of this film. The tribofilms were chemically identical to that generated previously on silicon, Al-Si and ferrous substrates, which indicates a generic film formation process employed by the lubricants on a range of substrates. The marked wear improvement with calcium sulfonate + NOCH was attributed to an increase in the deposition of calcium carbonate on substrate

surfaces as a result of the decomposition of triethyl citrate to form a metal ethoxide compound.

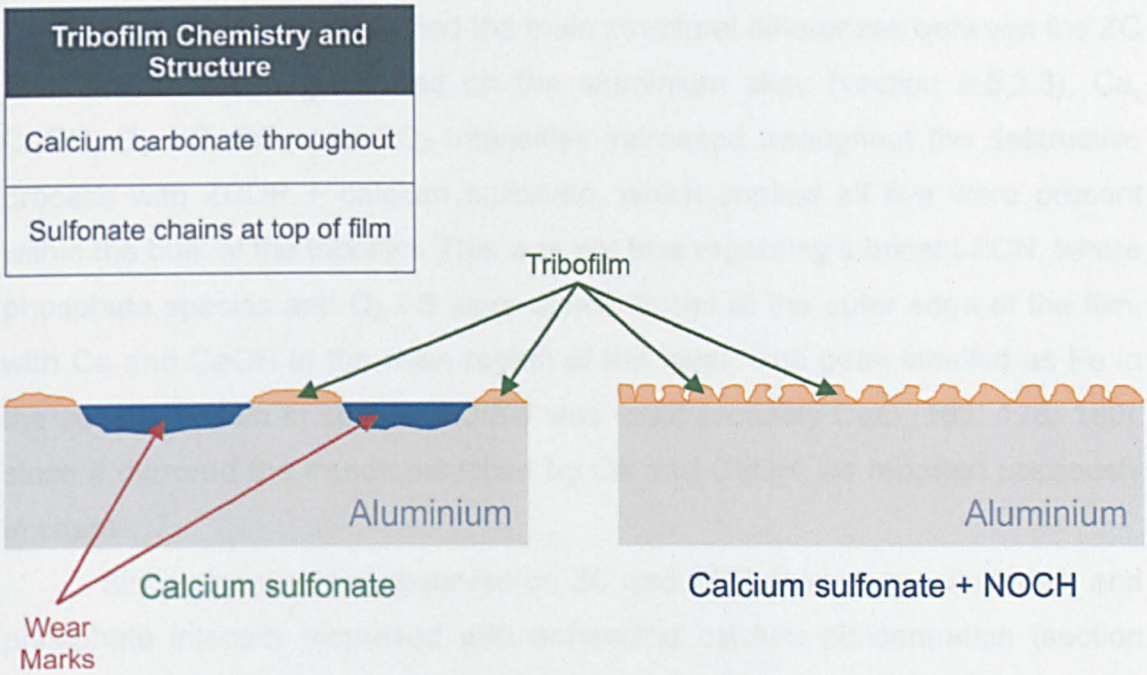

Figure 167: Models of EN AW 2014A lubricated with calcium sulfonate or calcium sulfonate + NOCH

9.6.3.3. ZDDP + Calcium Sulfonate vs ZDDP + Calcium Sulfonate + NOCH

9.6.3.3.1. Tribochemistry

As previously reported on AluSil® (chapter 5), non-decomposed ZDDP was observed within the wear scar of EN AW 2014A when lubricated with ZDDP + calcium sulfonate or ZDDP + calcium sulfonate + NOCH (Figure 155). In addition, P-O-C shifted to a lower wavenumber with lubricant ZC; similar behaviour has been reported previously [276]. This may be due to the erratic optical behaviour of aluminium [277] when subject to the wavelengths employed by FTIR analysis herein. The identification of PO_3 within the wear scar of the substrates relates well with the data obtained in chapter 5 of this thesis.

Tribofilms generated on aluminium alloy using either lubricant (section 9.5.3.3) were chemically identical to those formed on steel piston ring (chapter 5) and silicon crystal (chapter 7). Indeed, it was apparent that both films contained polyphosphates [118], which were formed exclusively within the wear scar of either aluminium substrate. However, phosphate generation was far more successful with ZDDP + calcium sulfonate, as witnessed previously (chapters 5&7). Even though $CaCO_3$ was not observed using FTIR (Figure 155), the Ca and CaOH peaks identified on lubricant ZC and ZCN tribofilms are

indicative of calcium carbonate formation [34, 178]. Furthermore, the observation of CaOH implies $CaCO_3$ is in an amorphous form [168].

Depth profiling indentified the main structural differences between the ZC and ZCN tribofilms generated on the aluminium alloy (section 9.5.3.3); Ca, CaOH, O_2 / S, PO_2 and PO_3 intensities increased throughout the destructive process with ZDDP + calcium sulfonate, which implied all five were present within the bulk of the tribofilm. This was not true regarding lubricant ZCN, where phosphate species and O_2 / S were concentrated at the outer edge of the film, with Ca and CaOH in the main region of the layer. The peak labelled as Fe in the spectra shown in section 9.5.3.3 was most probably CaO [166, 178, 180], since it mirrored the trends exhibited by Ca and CaOH, as reported previously in chapter 7.

Since zinc was not observed on ZC and ZCN aluminium substrates, and phosphate intensity increased with enhancing calcium concentration (section 9.5.3.3), it follows that calcium phosphate formation occurred; this has been reported previously on ferrous [184, 185, 187] and silicon surfaces (chapter 7). However, given the wear on the ZC substrate was high (section 9.6.2.3), and PO_2 and PO_3 intensity also enlarged with increasing aluminium content, aluminium phosphide formation [98] cannot be discredited.

Therefore, these results are indicative as to suggest the lubricant ZC tribofilm was constructed from a bulk mixture of phosphorus species and calcium carbonate, as reported previously (chapter 7). The ZDDP + calcium sulfonate + NOCH film on aluminium substrates appeared to be identical to that fashioned on silicon crystal (chapter 7) in so far as being comprised of a bulk section of calcium carbonate and sulfonate chains, with a phosphate outer region. This would therefore explain the remarkably similar physical structure to the ZCN film as that possessed by lubricant CN (Figure 146&Figure 148).

Therefore, it follows sulphur was present in two forms within the tribofilms, namely as sulphide [118, 126, 132, 139] in the polyphosphate regions and as sulfonate at the outer edges of the calcium carbonate sections [178]. It can be assumed that this was also the structure of the films on the steel pins; the observation of zinc on both ferrous substrates implies zinc polyphosphate formation occurred herein, however (Table 42).

9.6.3.3.2. Film Formation

Calcium carbonate was formed rapidly on either substrate using the generic process described previously (section 9.6.3.2), resulting in sulfonate chains mixed into the outer region of this film [178]. The addition of NOCH to lubricant ZC imparted enhanced calcium carbonate deposition through the breakdown of triethyl citrate into the metal ethoxide shown in Figure 137, which subsequently imparted a similar topography to the tribofilm as that possessed by calcium sulfonate + NOCH (Figure 146&Figure 148). Hence, this explains the identical electrical contact voltage results observed between lubricants CN and ZCN in Figure 141.

The reason why the ZC interface did not endure wear levels similar to those of calcium sulfonate alone (section 9.6.3.2) during calcium carbonate deposition, was due to the simultaneous adsorption of ZDDP and its linkage isomer onto the steel substrate [131]. Subsequent generation of zinc polyphosphate and sulphide [131] and chemical reaction resulting in additional calcium phosphate formation [185], protected the interface from greater wear levels. Consequently, ZDDP and its linkage isomer were adsorbed onto aluminium oxide [98], with calcium phosphate [185] and sulphur species subsequently generated [98]. In addition, through reaction with aluminium, generated as a result of initial abrasive and adhesive wear of the soft substrate (section 9.6.2.3), aluminium phosphide [98] was formed.

Due to the NOCH molecule out-competing ZDDP with lubricant ZCN, together with the enhanced surface coverage of the calcium carbonate tribofilm (section 9.6.2.3), the quantity of surface active sites available on either substrate were reduced, which minimised phosphate formation. Furthermore, as discussed in (section 7.6.3.4), calcium must have possessed a greater affinity to coordinate with the metal ethoxide fashioned from triethyl citrate, compared to ZDDP. It follows, however, that this limited polyphosphate formation, in combination with the calcium carbonate tribofilms, imparted the superlative wear performance in the tribosystem (Figure 142&Figure 143). Indeed, this rationale is the same as that used to explain the performance of ZDDP + calcium sulfonate + NOCH when lubricating silicon tribosystems (chapter 7).

9.6.3.3.3. Summary

Tribofilms generated on ferrous and aluminium substrates from ZDDP + calcium sulfonate and ZDDP + calcium sulfonate + NOCH were calcium carbonate-based. However, films formed using lubricant ZC also contained large concentrations of calcium phosphate on both ferrous and aluminium surfaces, with zinc polyphosphate observed exclusively on the steel pin. Generation of aluminium phosphide on EN AW 2014A was predicted. With lubricant ZCN, calcium carbonate deposition was enhanced, resulting in a reduction in phosphate formation. Sulphur was present in the forms of sulphide and sulfonate in either ZC or ZCN tribofilms. A combination of calcium carbonate and limited phosphate formation afforded superior wear performance to the lubricant ZCN tribosystem. Representative models of worn aluminium surfaces when lubricated with ZDDP + calcium sulfonate or ZDDP + calcium sulfonate + NOCH are shown in Figure 168.

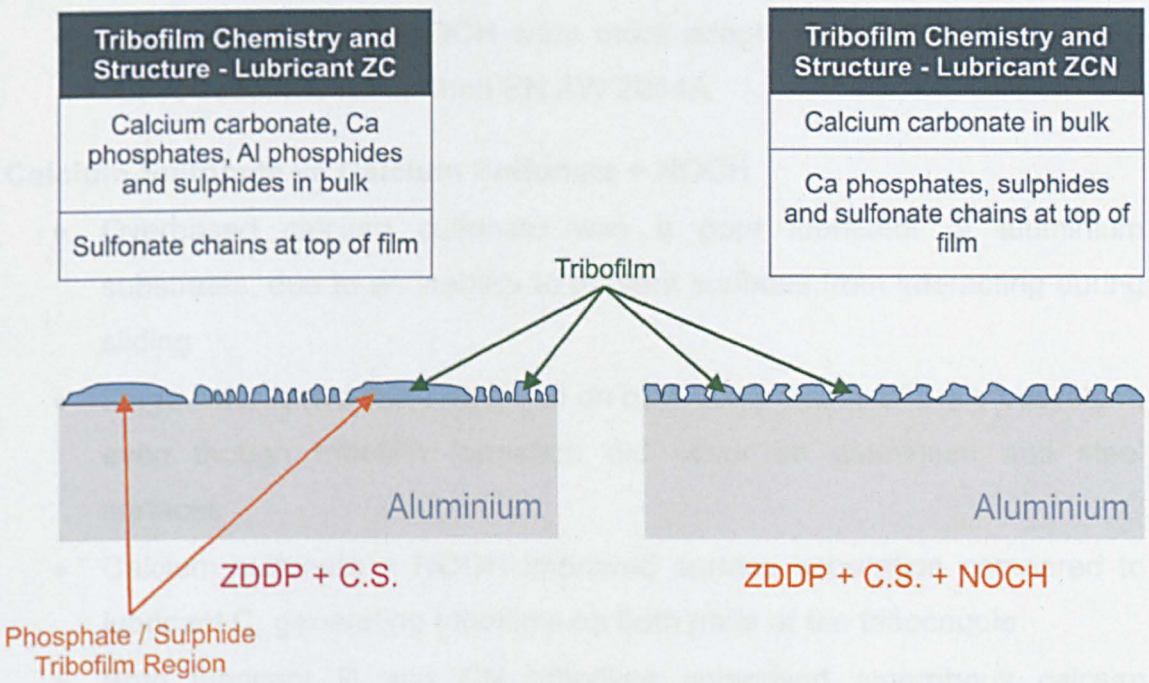

Figure 168: Models of EN AW 2014A lubricated with ZDDP + calcium sulfonate or ZDDP + calcium sulfonate + NOCH

9.7. Conclusions

The tribological performance and tribochemistry of a replicate aluminium matrix lubricated with various test oils has been determined. The following sub-sections conclude the findings from the aluminium alloy and steel pin tribosystem, when lubricated with ZDDP, OBCS or ZDDP + OBCS. The benefits obtained from the addition of NOCH to these lubricants are also presented.

ZDDP vs ZDDP + NOCH

- ZDDP generated the greatest frictional response in the tribosystem
- The addition of NOCH to zinc diakyldithiophosphate improved both the coefficient of friction and also surface separation
- Lubricant ZN reduced the wear of both aluminium and ferrous substrates, compared to ZDDP, due to an enhanced surface density of the tribofilm on the steel pin
- Polyphosphate and sulphide-based tribofilms were generated exclusively on ferrous substrates with either lubricant
- Subsequently, phosphate and sulphur species were transferred to the aluminium alloy through rubbing processes
- Results indicate ZDDP film formation does not occur on the matrix of an aluminium-silicon substrate, with observed tribofilms originating from transfer or thermal decomposition
- ZDDP and ZDDP + NOCH were more adept at protecting the ferrous-based substrate rather than EN AW 2014A

Calcium Sulfonate vs Calcium Sulfonate + NOCH

- Overbased calcium sulfonate was a poor lubricator of aluminium substrates, due to an inability to prevent surfaces from interacting during sliding
- Large wear levels were obtained on both components of the tribosystem, even though tribofilm formation did occur on aluminium and steel surfaces
- Calcium sulfonate + NOCH improved surface separation compared to lubricant C, generating tribofilms on both parts of the tribocouple
- Both lubricant C and CN tribofilms comprised amorphous calcium carbonate, with sulfonate chains located at the tribofilm outer region
- Wear was reduced markedly with lubricant CN compared to calcium sulfonate, due to an enhanced surface density of calcium carbonate as a result of the decomposition of triethyl citrate
- Either detergent was more successful at reducing wear on silicon, compared to aluminium substrates

ZDDP + Calcium Sulfonate vs ZDDP + Calcium Sulfonate + NOCH

- Lubricant ZCN provided the lowest wear on either surface
- Frictional response imparted by lubricant ZC and ZCN were similar, but film formation was improved with the addition of NOCH
- Tribofilms were generated on ferrous and aluminium surfaces with either lubricant, and resembled those formed on silicon crystal
- Both ZC and ZCN films comprised calcium carbonate bulk sections, with sulfonate chains contained at the outer regions of this layer. Calcium phosphate and sulphide species were generated in both tribocouples, with zinc polyphosphates obtained solely on the steel pins
- With lubricant ZC, the phosphate and sulphur species were contained within the bulk section of the film, with aluminium phosphide predicted to also form
- The addition of NOCH enhanced the deposition of $CaCO_3$ and out-competed ZDDP for substrate surfaces. This resulted in inferior phosphate and sulphide formation compared to lubricant ZC, with these regions located at the periphery of the tribofilm
- The differences in chemical composition and structure between the two lubricant tribofilms were accredited with the marked wear reduction afforded by ZDDP + calcium sulfonate + NOCH
- Lubricants ZC and ZCN were more effective at providing antiwear protection to silicon substrates, rather than aluminium surfaces

Replication of the aluminium matrix within an aluminium-silicon alloy has revealed that the base material of the composite substrate must not play a major role in the wear of an Al-Si alloy. The results obtained from this section of the thesis have been combined with the findings from the lubrication of both aluminium-silicon and silicon crystal substrates, to generate an advanced hypothesis of the lubrication of aluminium-silicon alloys; the resultant mechanism is described in the following chapter.

10. Final Conclusions and Future Work

10.1. Advanced Hypothesis of the Lubrication of Aluminium-Silicon Alloys

It is extremely important that a conclusive model for the lubrication of aluminium-silicon alloys is devised in order to extend the life of these substrates. Manufacturers of cylinder liners and engine oils could subsequently create products that conform to the aforementioned model. Such a mechanism is introduced here, which correlates the results obtained from the lubrication of aluminium-silicon, silicon and aluminium surfaces to the methods by which aluminium-silicon alloys endure wear.

Under boundary lubrications conditions, the wear mechanism of an aluminium-silicon alloy is complicated and varies depending on the antiwear properties of the lubricating fluid. Indeed, as shown in chapter 5, it was apparent that base oil or NOCH in base oil were ineffective lubricants for the tribosystem, resulting in catastrophic wear of both silicon and aluminium regions of the alloy. Mild wear performance was afforded to the Al-Si substrates by ZDDP, with the remaining lubricants providing ultra-mild wear. The silicon regions of the alloy were seen to be vital as to the effective lubrication of the Al-Si substrate, since these physically hard regions supported the load in the contact and facilitated film formation. Hence, the ability of a fluid to lubricate these non-conductive surfaces effectively dictates the overall wear on an aluminium-silicon substrate.

So as to evaluate the antiwear performance of the lubricating fluids on silicon surfaces, contact conditions on silicon grains were replicated using silicon crystal substrates (chapter 7). Results indicated that both ZDDP and ZDDP + NOCH were poor lubricants of silicon surfaces, whilst fluids that contained overbased calcium sulfonate improved wear performance markedly through the generation of a surface-covering tribofilm. Excellent antiwear behaviour was imparted by both calcium sulfonate + NOCH and ZDDP + calcium sulfonate + NOCH. Thus, if the wear of the silicon regions is minimised, it follows the life expectancy of the alloy will increase, since the wear of the soft aluminium matrix will occur at a faster rate if the silicon regions are worn more rapidly. In addition, the depression of silicon grains into the 3D structure that is an aluminium-silicon substrate will also result in wear of the aluminium matrix. Hence, to afford a conclusive lubrication hypothesis for an aluminium-silicon

substrate, the lubrication of the aluminium matrix was evaluated using a representative aluminium alloy and the aforementioned test oils. It was observed that calcium sulfonate was a poor lubricator of aluminium substrates; the antiwear performance of oils containing overbased calcium sulfonate were reduced compared to silicon surfaces. Both ZDDP and ZDDP + NOCH were ineffective lubricants of the aluminium alloy; consummate antiwear performance was afforded by ZDDP + calcium sulfonate + NOCH through effectual film formation.

Thus, the results obtained imply that in order to effectively lubricate an aluminium-silicon substrate, the silicon regions within the tribosystem must be protected from excessive wear through the formation of tribofilms that cover the surface of the silicon regions and also the counterpart substrate. Furthermore, with extended rubbing, when the aluminium matrix interacts with the incident substrate, protection must be afforded to the soft substrate through the generation of an effective film on the aluminium alloy. Analysing the results obtained in this work, two lubricants consistently provided excellent antiwear performance to silicon, aluminium and steel surfaces, namely, calcium sulfonate + NOCH and ZDDP + calcium sulfonate + NOCH.

The results presented in this thesis were used to generate an advanced hypothesis of the lubrication of aluminium-silicon alloys, which is a development of the hypotheses generated in section 5.7. According to which, the following steps describe the lubrication of an aluminium-silicon alloy, with the accompanying model being shown in Figure 169.

1. Some silicon grains fracture, reducing their size [99, 100]. If silicon grain size can be preserved, wear levels will not increase [99]

2. Fragments of silicon are created via wear and lead to abrasive wear of matrix and also silicon grains [99, 104]

3. Tribofilm forms on exposed silicon grains; calcium sulfonate-based tribofilm is well adhered and covers the majority of silicon grain surface. Oil residue only evident if ZDDP is contained within lubricant

4. Load carrying silicon grains depress into matrix [77, 79, 99, 100]

5. Aluminium matrix plastically deforms under applied load and becomes amassed around depressed silicon grains [77, 79, 100].

6. Wear of the silicon grains is dictated by the antiwear properties of the generated tribofilm. Wear of the aluminium matrix ensues [77, 99, 100] once the silicon regions have been further depressed [77, 100] or worn [99].

7. Formation of an effective tribofilm on the matrix regulates wear levels and extends the life of the alloy

8. The soft aluminium substrate is particularly susceptible to wear; catastrophic failure of the alloy will occur if insufficient antiwear protection to the matrix is provided.

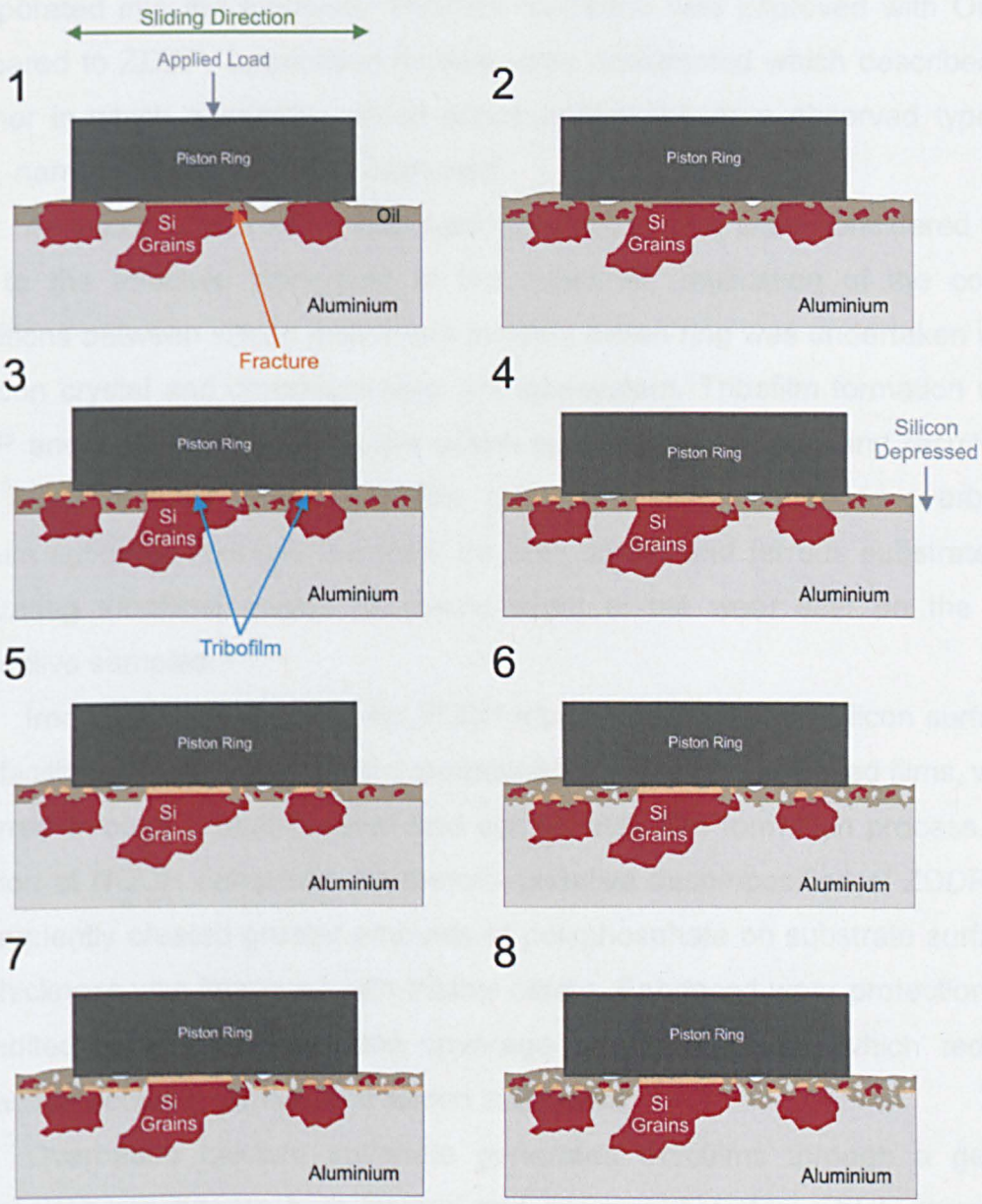

Figure 169: Advanced hypothesis of the lubrication of an aluminium-silicon substrate

10.2. Final Conclusions

The lubrication of a hypereutectic aluminium-silicon cylinder liner in contact with a chromium steel top compression piston ring was investigated using a range of test oils. This work constitutes the first study of the lubrication of an aluminium-silicon substrate using overbased calcium sulfonate. A wide range of physical and chemical surface analysis techniques were employed to evaluate worn substrates.

Both base oil and NOCH in base oil lubricants were deemed to provide insufficient antiwear protection to the aluminium substrates. Although tribofilms were generated on silicon grains using all lubricants, film transfer was additionally observed on the aluminium matrix of the alloy when ZDDP was incorporated into the lubricant. Tribofilm formation was improved with OBCS, compared to ZDDP. Lubrication models were constructed which described the manner in which aluminium-silicon alloys underwent three observed types of wear, namely *Heavy*, *Mild* and *Ultra mild*.

As silicon grains within the aluminium-silicon alloy were considered to be vital to the effective lubrication of the substrate, replication of the contact conditions between silicon grains and incident piston ring was undertaken using a silicon crystal and chromium steel pin tribosystem. Tribofilm formation using ZDDP and ZDDP + NOCH on the silicon surfaces was limited and resulted in high levels of wear in the interface. Lubricants which contained overbased calcium sulfonate reduced the wear on both silicon and ferrous substrates by generating tribofilms across the entire width of the wear scar on the non-conductive samples.

Iron oxide was required for ZDDP tribofilm formation on silicon surfaces. This facilitated the generation of polyphosphate and sulphide-based films, which occurred through a multi-faceted and complicated film formation process. The addition of NOCH enhanced the thermo-oxidative decomposition of ZDDP and subsequently created greater amounts of polyphosphate on substrate surfaces; film thickness was improved with triethyl citrate. Enhanced wear protection was accredited to a greater surface coverage of the tribofilms, which reduced interaction between ferrous and silicon substrates.

Overbased calcium sulfonate generated tribofilms through a generic mechanistic process on both ferrous and silicon substrates, which comprised

amorphous calcium carbonate, with sulfonate chains located at the outer edges of the film. ^{13}C labelled derivatives of OBCS conclusively revealed the structure of the tribofilm generated on silicon and ferrous substrates. The addition of NOCH to the detergent enhanced the surface density of the resultant tribofilm. Through labelling triethyl citrate with deuterium, it was demonstrated that the basic nature of OBCS initiated the breakdown of the organic molecule into metal ethoxide compounds, which subsequently facilitated further deposition of $CaCO_3$. Improved wear protection afforded by OBCS + NOCH was attributed to both improved surface coverage of the tribofilm and an increased propensity to undergo plastic deformation; triethyl citrate did not alter film thickness, however.

Tribofilms formed from ZDDP + calcium sulfonate and ZDDP + calcium sulfonate + NOCH were calcium carbonate-based, with sulfonate chains contained at peripheral regions of this film. In addition, a polyphosphate and sulphide-based region was present within the bulk section of the tribofilm on lubricant ZC substrates. The concentration of this ZDDP-derived section was reduced with lubricant ZCN, due to triethyl citrate out-competing ZDDP; the polyphosphate and sulphide-based regions were limited to the outer layer of the carbonate-based film with the addition of NOCH. Calcium phosphate was observed within the polyphosphate regions in both ZC and ZCN tribofilms. Triethyl citrate enhanced the deposition of $CaCO_3$ in the ZDDP + calcium sulfonate + NOCH tribofilm, the structure of which was analogous to that of calcium sulfonate + NOCH. The addition of triethyl citrate improved the elastic modulus of the ZDDP + calcium sulfonate film, but did not alter film thickness. Lubricant ZCN imparted the most effective antiwear characteristics of any test oil to the tribosystem, this being attributed to the chemical composition of the film and its optimum mechanical properties.

Due to the effective replication of the silicon grains within the aluminium-silicon alloy, the observed behaviour exhibited by the test lubricants in terms of antiwear ability, film formation and tribofilm structure on the silicon crystal substrates would be identical to that occurring on the silicon regions within AluSil®. However, in order to understand the wear on aluminium-silicon alloys which were undergoing extended sliding distances, the lubrication of an aluminium alloy was additionally investigated, which replicated the aluminium matrix within the Al-Si substrate.

Whilst tribofilms were not generated on the alloy when lubricated with either ZDDP or ZDDP + NOCH, antiwear protection was nevertheless imparted by the polyphosphate and sulphide-based films generated on the steel pin. Film formation was accredited to the same processes as in the aluminium-silicon and silicon tribosystems, which resulted in lower wear levels being obtained with the addition of NOCH. It was determined that film formation did not occur on the aluminium matrix of an Al-Si substrate and the presence of such films were due to transfer or thermal decomposition of ZDDP.

Calcium sulfonate was a poor lubricator of the aluminium alloy substrates, resulting in large quantities of abrasive wear on the soft substrate. However, the addition of NOCH to the detergent dramatically improved the wear protection on both ferrous and aluminium substrates. With either lubricant, tribofilms were observed on the aluminium alloy, which were of identical chemical composition to those fashioned on both silicon and ferrous surfaces and which had been generated through analogous film formation processes. Triethyl citrate enhanced antiwear performance by means of improved surface deposition of $CaCO_3$, and thereby minimised substrate-substrate interaction.

The addition of NOCH to ZDDP + calcium sulfonate had the same effect on the aluminium alloy as seen in the case of silicon surfaces. Indeed, although films generated on the aluminium substrate were $CaCO_3$-based, triethyl citrate improved wear performance by enhancing calcium carbonate deposition by out-competing ZDDP for surface active sites. Polyphosphate and sulphide-based films were observed in the bulk of the ZDDP + calcium sulfonate layer, but were only present in small volumes on the outer edges of lubricant ZCN tribofilms. As with the silicon tribosystem, lubricant ZCN was the most effective antiwear agent in the aluminium alloy and steel pin tribocouple.

Overall, superior frictional behaviour in all tribosystems was imparted by overbased calcium sulfonate, with ZDDP generating the greatest frictional response, excluding base oil or NOCH in base oil. Tribofilms comprising overbased calcium sulfonate were more effective on silicon, compared to aluminium substrates, presumably due to the resistance to deformation afforded by the hard silicon surfaces. ZDDP and ZDDP + NOCH were equally poor lubricants on either surface.

The investigation into the lubrication of an aluminium-silicon alloy with an overbased calcium sulfonate detergent revealed that the additive was a very

effective lubricator of silicon surfaces, owing to the lack of surface reaction required to initiate rapid film formation. Conversely, ZDDP was a poor lubricator of silicon surfaces as both its adsorption and complicated decomposition mechanism were required prior to film formation. Triethyl citrate was a very effective antiwear additive on silicon, aluminium and ferrous surfaces, when used in conjunction with overbased calcium sulfonate. The organic additive enhanced the performance of ZDDP, but this was inferior to that of the combination of metallic detergent and NOCH or ZDDP + OBCS + NOCH.

An advanced hypothesis as to the lubrication of aluminium-silicon alloys undergoing low wear levels was generated, which incorporated tribofilm formation onto load-bearing silicon grains, with subsequent depression of these regions into the aluminium matrix, which plastically deformed. The antiwear properties of the generated tribofilm dictated the rate of wear of silicon grains. Wear of the aluminium matrix would occur once the silicon regions had been either further depressed or worn away. Consequently, the alloy would either be protected by the lubricant through effective film formation or the aluminium matrix would undergo catastrophic wear, which, in turn, would result in the failure of the aluminium-silicon alloy.

10.3. Future Work

Several areas of further research may well prove of interest, namely:

- The development of a more effective version of the NOCH molecule, by evaluating the performance of a metal ethoxide compound with the overbased calcium sulfonate detergent employed in this work;
- An investigation into the effects the variation of metallic base and or chemistry of the detergent additive has on the lubrication of Al-Si alloys;
- To determine whether the NOCH molecule degrades in conjunction with the above mentioned alternative detergents in an analogous manner to that reported in this work;
- To investigate the film formation mechanism(s) of triethyl citrate when used in conjunction with ZDDP on Al-Si surfaces using labelling techniques;
- To substitute the AluSil® substrate employed herein with alternative production aluminium-silicon cylinder liners and to identify whether the lubrication hypothesis proposed in this work relates to these substrates;

References

1 **Rabinowicz, E.** Friction. *Friction and Wear of Materials*, pp. 65-123 (Wiley, New York; Chichester, 1995).

2 **Teer, D.G. and Arnell, R.D.** Friction Theories. In Halling, J., ed. *Principles of Tribology*, pp. 72-93 (Macmillan, London, 1975).

3 **Bhushan, B.** Friction. *Introduction to Tribology*, pp. 207-286 (Wiley, New York; Chichester, 2002).

4 **Rabinowicz, E.** Friction. *Friction and Wear of Materials*, p. 68 (Wiley, New York; Chichester, 1995).

5 **Rabinowicz, E.** Friction. *Friction and Wear of Materials*, p. 69 (Wiley, New York; Chichester, 1995).

6 **Rabinowicz, E.** Types of Wear. *Friction and Wear of Materials*, pp. 124-142 (Wiley, New York; Chichester, 1995).

7 **Bhushan, B.** Wear. *Introduction to Tribology*, pp. 331-422 (Wiley, New York; Chichester, 2002).

8 **Sarkar, A.D.** Adhesive Wear. *Friction and Wear*, pp. 33-63 (Academic Press, London, 1980).

9 **Teer, D.G. and Arnell, R.D.** Wear. In Halling, J., ed. *Principles of Tribology*, pp. 94-127 (Macmillan, London, 1975).

10 **OUP**. tribology. In Simpson, J.A. and Weiner, E.S.C., eds. *The Oxford English Dictionary* (Clarendon Press, Oxford, 1989).

11 **Bhushan, B.** Introduction. *Introduction to Tribology*, pp. 1-8 (Wiley, New York; Chichester, 2002).

12 **Bhushan, B.** Fluid Film Lubrication. *Introduction to Tribology*, pp. 423-532 (Wiley, New York; Chichester, 2002).

13 **Hutchings, I.M.** Lubricants and Lubrication. *Tribology: Friction and Wear of Engineering Materials*, pp. 58-76 (Edward Arnold, London, 1992).

14 **Williams, J.A.** Boundary Lubrication and Friction. *Engineering Tribology*, pp. 348-380 (Oxford University Press, Oxford, 1994).

15 **Reimer, L.** Introduction. *Scanning Electron Microscopy: Physics of Image Formation and Microanalysis*, pp. 1-12 (Springer, Berlin, 1998).

16 **Reimer, L.** Image Contrast and Signal Processing. *Scanning Electron Microscopy: Physics of Image Formation and Microanalysis*, pp. 207-252 (Springer, Berlin, 1998).

17 **Johnson, D., Hilal, N. and Bowen, W.R.** Basic Principles of Atomic Force Microscopy. In Bowen, W.R. and Hilal, N., eds. *Atomic Force Microscopy in Process Engineering: An Introduction to AFM for Improved Processes and Products*, pp. 1-30 (Butterworth-Heinemann, Oxford; Burlington, 2009).

18 **Kaupp, G.** Atomic Force Microscopy. *Atomic Force Microscopy, Scanning Nearfield Optical Microscopy and Nanoscratching: Application to Rough and Natural Surfaces*, pp. 1-86 (Springer, Berlin, 2006).

19 **Veeco**. Scanning Probe / Atomic Force Microscopy: Technology Overview and Update (http://www.veeco.com/pdfs/appnotes/AN48r2_SPM_AFM_278.pdf). (Accessed 11th June 2010).

20 **Hwa Li, S., Chhatpar, T. and Robert, F.** Stylus Profilometry. In Hwa Li, S., Miller, R.M., Willardson, R.K. and Weber, E.R., eds. *Chemical Mechanical Polishing in Silicon Processing*, p. 236 (Elsevier Science and Technology, Oxford, 2000).

21 **Hariharan, P.** Introduction. *Basics of Interferometry*, pp. 1-2 (Elsevier / Academic Press, Amsterdam: London, 2007).

22 Fischer-Cripps, A.C. Introduction. *Nanoindentation*, pp. xxi-xxii (Springer, New York; London, 2004).
23 Fischer-Cripps, A.C. Nanoindentation Testing. *Nanoindentation*, pp. 21-38 (Springer, New York; London, 2004).
24 Oliver, W.C. and Pharr, G.M. An improved technique for determining hardness and elastic modulus using load and displacement sensing indentation experiments. *Journal of Materials Research*, 1992, **7**(6), 1564-1583.
25 Pereira, G., Lachenwitzer, A., Nicholls, M.A., Kasrai, M., Norton, P.R. and De Stasio, G. Chemical characterization and nanomechanical properties of antiwear films fabricated from ZDDP on a near hypereutectic Al–Si alloy. *Tribology Letters*, 2005, **18**(4), 411-427.
26 Reimer, L. Elemental Analysis and Imaging with X-Rays. *Scanning Electron Microscopy: Physics of Image Formation and Microanalysis*, pp. 379-448 (Springer, Berlin, 1998).
27 Brugel, W. Introduction. *An Introduction to Infrared Spectroscopy*, pp. 1-8 (Methuen, London, 1962).
28 Nakamoto, K. Theory of Normal Vibrations. *Infrared and Raman spectra of inorganic and coordination compounds. Part A, Theory and applications in inorganic chemistry* pp. 1-148 (Wiley, Hoboken, N.J., 2009).
29 Günzler, H. and Gremlich, H.-U. Absorption and Molecular Design. *IR Spectroscopy: An Introduction*, pp. 9-36 (Wiley-VCH, Weinheim; Cambridge, 2002).
30 Günzler, H. and Gremlich, H.-U. Spectrometers. *IR Spectroscopy: An Introduction*, pp. 37-94 (Wiley-VCH, Weinheim; Cambridge, 2002).
31 Sundararajan, D. Introduction. *The discrete fourier transform: theory, algorithms and applications*, pp. 1-6 (World Scientific, Singapore, 2001).
32 Briggs, D. Static SIMS (SSIMS). *Surface Analysis of Polymer by XPS and Static SIMS*, pp. 88-118 (Cambridge University Press, Cambridge, 1998).
33 Vaeck, L.V., Adriaens, A. and Gijbels, R. Static secondary ion mass spectrometry (S-SIMS) Part 1: methodology and structural interpretation. *Mass Spectrometry Reviews*, 1999, **18**(1), 1-47.
34 Cizaire, L., Martin, J.M., Le Mogne, T. and Gresser, E. Chemical analysis of overbased calcium sulfonate detergents by coupling XPS, ToF-SIMS, XANES, and EFTEM. *Colloids and Surfaces A: Physicochemical and Engineering Aspects*, 2004, **238**(1-3), 151-158.
35 ACEA. ACEA Euopean Oil Sequences. http://www.acea.be/index.php/news/news_detail/acea_european_oil_sequences_2008. (ACEA, Brussels, 2008).
36 EU. Commission Regulation (EC) No 692/2008. *Official Journal of the European Union*, 2008, **L199**, 1-136.
37 ILSAC. ILSAC GF-5 Standard for Passenger Car Engine Oils. http://www.gf-5.com/uploads/File/ILSAC_GF-5_Dec-22-09_final.pdf. (ILSAC, 2009).
38 Caines, A.J., Haycock, R.F. and Hiller, J.E. Safety, Health, and the Environment (SHE). *Automotive Lubricants Reference Book*, pp. 373-392 (Professional Engineering Publishing, London, 2004).
39 Rexeis, M. and Hausberger, S. Trend of vehicle emission levels until 2020 - Prognosis based on current vehicle measurements and future emission legislation. *Atmospheric Environment*, 2009, **43**(31), 4689-4698.
40 LUBRIZOL and ILSAC. Main GF-5 Site Home http://www.gf-5.com/. 2010).

41 ACEA. ACEA - European Automobile Manufacturers' Association http://www.acea.be/. 2010).
42 Spikes, H. The History and Mechanisms of ZDDP. *Tribology Letters*, 2004, **17**(3), 469-489.
43 Taylor, C.M. Automobile engine tribology--design considerations for efficiency and durability. *Wear*, 1998, **221**(1), 1-8.
44 Andersson, B.S. Company Perspectives in Vehicle Tribology - Volvo. In Dowson, D., Taylor, C.M. and Godet, M., eds. *Vehicle Tribology: Proceedings of the 17th Leeds-Lyon Symposium on Tribology*, pp. 503-506 (Elsevier, New York, 1991).
45 Tung, S.C. and McMillan, M.L. Automotive tribology overview of current advances and challenges for the future. *Tribology International*, 2004, **37**(7), 517-536.
46 Jakobs, R. Engine Components: Piston Rings. In Van Basshuysen, R. and Schafer, F., eds. *Internal Combustion Engine*, pp. 100-107 (SAE International, Warrandale, 2002).
47 Taylor, B.J. and Eyre, T.S. A review of piston ring and cylinder liner materials. *Tribology International*, 1979, **12**(2), 79-89.
48 Pawlus, P. Change of cylinder surface topography in the initial stage of engine life. *Wear*, 1997, **209**(1-2), 69-83.
49 Priest, M. and Taylor, C.M. Automobile engine tribology -- approaching the surface. *Wear*, 2000, **241**(2), 193-203.
50 Dowson, D., Ruddy, B.L. and Economou, P.N. The Elastohydrodynamic Lubrication of Piston Rings. *Proceedings of the Royal Society of London. Series A, Mathematical and Physical Sciences*, 1983, **386**(1791), 409-430.
51 Dowson, D. Piston Assemblies; Background and Lubrication Analysis. In TAYLOR, C.M., ed. *Engine Tribology*, p. 220 (Elsevier, Amsterdam; New York, 1993).
52 Barrell, D.J.W., Priest, M. and Taylor, C.M. Bench Test Study of Piston Ring Flank and Piston Groove Interaction. In Dowson, D., ed. *Lubrication at the Frontier: The Role of the Interface and Surface Layers in the Thin Film and Boundary Regime*, pp. 343-351New York, 1998).
53 Zwein, F. and Müller, M. Engine Components: Cylinders. In Van Basshuysen, R. and Schafer, F., eds. *Internal Combustion Engine*, pp. 118-124 (SAE International, Warrandale, 2002).
54 Bolander, N.W., Steenwyk, B.D., Sadeghi, F. and Gerber, G.R. Lubrication regime transitions at the piston ring-cylinder liner interface. *Proceedings of the Institution of Mechanical Engineers, Part J (Journal of Engineering Tribology)*, 2005, **219**(J1), 19-31.
55 Brown, S.R. and Hamilton, G.M. The partially lubricated piston ring. *ARCHIVE: Journal of Mechanical Engineering Science 1959-1982 (vols 1-23)*, 1977, **19**(2), 81-89.
56 Eilon, S. and Saunders, O.A. A Study of Piston-Ring Lubrication. *Proceedings of the Institution of Mechanical Engineers*, 1957, **171**, 427-462.
57 Lloyd, T. The Hydrodynamic Lubrication of Piston Rings. *Proceedings of the Institution of Mechanical Engineers*, 1968, **183**(3P), 28-34.
58 Dienwiebel, M., Pöhlmann, K. and Scherge, M. Origins of the wear resistance of AlSi cylinder bore surfaces studies by surface analytical tools. *Tribology International*, 2007, **40**(10-12), 1597-1602.

59 Tomastik, C., Jech, M., Wopelka, T. and Franek, F. Surface analysis of cylinder liners from tribological model experiments and internal combustion engines. *Surface and Interface Analysis*, 2010, **42**(6-7), 1357-1360.

60 So, H., Lin, Y.C., Huang, G.G.S. and Chang, T.S.T. Antiwear mechanism of zinc dialkyl dithiophosphates added to a paraffinic oil in the boundary lubrication condition. *Wear*, 1993, **166**(1), 17-26.

61 Tomsic, J.L. and Hodder, R.S. Eutectic Mixtures. In Tomsic, J.L., ed. *Dictionary of Materials and Testing, 2nd Edition*, pp. 212-213 (SAE, Warrandale, 2000).

62 Murray, J. and McAlister, A. The Al-Si (Aluminum-Silicon) system. *Journal of Phase Equilibria*, 1984, **5**(1), 74-84.

63 ASM. Friction and Wear of Aluminium-Silicon Alloys. In Shabel, B.S., Granger, D.A. and Truckner, W.G., eds. *ASM Handbook, Volume 18*, pp. 785-794 (ASM International, Materials Park: Ohio, 1998).

64 Rhines, F.N. Binary Eutectic Systems. *Phase Diagrams in Metallurgy : Their Development and Application*, pp. 34-56 (McGraw-Hill, New York, London, 1956).

65 Clegg, A.J. and Das, A.A. Wear of a hypereutectic aluminium-silicon alloy. *Wear*, 1977, **43**(3), 367-373.

66 Nicholls, M.A., Norton, P.R., Bancroft, G.M., Kasrai, M., De Stasio, G. and Wiese, L.M. Spatially resolved nanoscale chemical and mechanical characterization of ZDDP antiwear films on aluminum–silicon alloys under cylinder/bore wear conditions. *Tribology Letters*, 2005, **18**(3), 261-278.

67 Reddy, A.S., Bai, B.N.P., Murthy, K.S.S. and Biswas, S.K. Wear and seizure of binary Al---Si alloys. *Wear*, 1994, **171**(1-2), 115-127.

68 Clarke, J. and Sarkar, A.D. Wear characteristics of as-cast binary aluminium-silicon alloys. *Wear*, 1979, **54**(1), 7-16.

69 Sarkar, A.D. and Clarke, J. Friction and wear of aluminium-silicon alloys. *Wear*, 1980, **61**(1), 157-167.

70 Torabian, H., Pathak, J.P. and Tiwari, S.N. Wear characteristics of Al-Si alloys. *Wear*, 1994, **172**(1), 49-58.

71 Mondolfo, L.F. Aluminium-Silicon, Aluminium-Magnesium Silicide Alloys. *Aluminium Alloys : Structures and Properties*, pp. 759-841 (Butterworth, London, 1976).

72 Pramila Bai, B.N. and Biswas, S.K. Effect of magnesium addition and heat treatment on mild wear of hypoeutectic aluminium-silicon alloys. *Acta Metallurgica et Materialia*, 1991, **39**(5), 833-840.

73 García-Infanta, J.M., Swaminathan, S., Zhilyaev, A.P., Carreño, F., Ruano, O.A. and McNelley, T.R. Microstructural development during equal channel angular pressing of hypo-eutectic Al-Si casting alloy by different processing routes. *Materials Science and Engineering: A*, 2008, **485**(1-2), 160-175.

74 Merlin, M., Timelli, G., Bonollo, F. and Garagnani, G.L. Impact behaviour of A356 alloy for low-pressure die casting automotive wheels. *Journal of Materials Processing Technology*, 2009, **209**(2), 1060-1073.

75 Ferrarini, C.F., Bolfarini, C., Kiminami, C.S. and Botta F, W.J. Microstructure and mechanical properties of spray deposited hypoeutectic Al-Si alloy. *Materials Science and Engineering A*, 2004, **375-377**, 577-580.

76 Petty, E.R. Hot Hardness and Other Properties of Some Binary Intermetallic Compounds of Aluminium. *Jounal of the Institute of Metals*, 1960-1961, **89**, 343-349.

77 Chen, M., Perry, T. and Alpas, A.T. Ultra-mild wear in eutectic Al-Si alloys. *Wear*, 2007, **263**(1-6), 552-561.

78 Madelaine-Dupuich, O. and Storlarz, J. Fatigue of Eutectic Al-Si Alloys. In Driver, J.H., Dubost, B., Durand, F., Fougeres, R., Guyot, P., Sainfort, P. and Suery, M., eds. *5th International Conference ICAA5*, pp. 1343-1348 (Transtec, Grenoble, France, 1996).

79 Chen, M. and Alpas, A.T. Ultra-mild wear of a hypereutectic Al-18.5 wt.% Si alloy. *Wear*, 2008, **265**(1-2), 186-195.

80 Dwivedi, D.K. Wear behaviour of cast hypereutectic aluminium silicon alloys. *Materials & Design*, 2006, **27**(7), 610-616.

81 ASM. Properties of Cast Aluminium Alloys. In Kearney, A.L. and Kearney, A., eds. *ASM Handbook, Volume 2*, pp. 152-177 (ASM International, Materials Park: Ohio, 1992).

82 ASM. Properties of Pure Metals : Aluminium (Al). In Hunsicker, H.Y., Mondolfo, L.F. and Tomblin, P.A., eds. *ASM Handbook, Volume 2*, pp. 1099-1100 (ASM International, Materials Park: Ohio, 1992).

83 Stone, R. Mechanical Design Considerations. *Introduction to Internal Combustion Engines*, pp. 397-424 (MacMillan Press, Hong Kong, 1992).

84 SAE. Non-Ferrous Materials. *2000 SAE Handbook, Volume One*, pp. 10.01-10.25 (SAE, Warrandale, 2000).

85 Angus, H.T. Mechanical, Physical and Electrical Properties of Cast Iron. *Cast Iron: Physical and Engineering Properties*, pp. 34-160 (Butterworth, London, 1976).

86 Bertado, R. Grey cast irons for thermal stress analysis. *Journal of Strain Analysis*, 1970, **5**(2), 98-109.

87 Neville, A., Morina, A., Haque, T. and Voong, M. Compatibility between tribological surfaces and lubricant additives--How friction and wear reduction can be controlled by surface/lube synergies. *Tribology International*, 2007, **40**(10-12), 1680-1695.

88 BSI. Founding. *Grey Cast Irons* (BSI, 1997).

89 Becker, E.P. Trends in tribological materials and engine technology. *Tribology International*, 2004, **37**(7), 569-575.

90 Enomoto, Y. and Yamamoto, T. New materials in automotive tribology. *Tribology Letters*, 1998, **5**(1), 13-24.

91 Taylor, C.F. Engine Materials. *The Internal-Combustion Engine in Theory and Practice : Combustion, Fuels, Materials and Design*, pp. 306-351 (M. I. T. Press, Cambridge; Massachusetts
London, 1968).

92 Hu, L., Chen, J., Liu, W., Xue, Q. and Kajdas, C. Investigation of tribochemical behavior of Al-Si alloy against itself lubricated by amines. *Wear*, 2000, **243**(1-2), 60-67.

93 Konishi, T., Klaus, E.E. and Duda, J.L. Wear Characteristics of Aluminum-Silicon Alloy under Lubricated Sliding Conditions. *Tribology Transactions*, 1996, **39**(4), 811-818.

94 Timmermans, G. and Froyen, L. Fretting wear behaviour of hypereutectic P/M Al-Si in oil environment. *Wear*, 1999, **230**(2), 105-117.

95 Wang, Y. and Tung, S.C. Scuffing and wear behavior of aluminum piston skirt coatings against aluminum cylinder bore. *Wear*, 1999, **225-229**(Part 2), 1100-1108.

96 Wilson, R. Putting the "W" in VW and Audi(Awdi?). *Automotive Industries*, 2003, **183**(10), 12-13.

97 Yoon, H., Sheiretov, T. and Cusano, C. Tribological evaluation of some aluminum-based materials in lubricant/refrigerant mixtures. *Wear*, 1998, **218**(1), 54-65.
98 Nicholls, M.A., Norton, P.R., Bancroft, G.M. and Kasrai, M. X-ray absorption spectroscopy of tribofilms produced from zinc dialkyl dithiophosphates on Al-Si alloys. *Wear*, 2004, **257**(3-4), 311-328.
99 Dey, S.K., Perry, T.A. and Alpas, A.T. Micromechanisms of low load wear in an Al-18.5% Si alloy. *Wear*, 2009, **267**(1-4), 515-524.
100 Chen, M., Meng-Burany, X., Perry, T.A. and Alpas, A.T. Micromechanisms and mechanics of ultra-mild wear in Al-Si alloys. *Acta Materialia*, 2008, **56**(19), 5605-5616.
101 Greenwood, J.A. and Williamson, J.B.P. Contact of Nominally Flat Surfaces. *Proceedings of the Royal Society of London. Series A. Mathematical and Physical Sciences*, 1966, **295**(1442), 300-319.
102 Greenwood, J.A. and Tripp, J.H. The elastic contact of rough spheres. *Journal of Applied Mechanics*, 1967, **34**, 153-159.
103 Elmadagli, M. and Alpas, A.T. Progression of wear in the mild wear regime of an Al-18.5% Si (A390) alloy. *Wear*, 2006, **261**(3-4), 367-381.
104 Slattery, B.E., Perry, T. and Edrisy, A. Microstructural evolution of a eutectic Al-Si engine subjected to severe running conditions. *Materials Science and Engineering: A*, 2009, **512**(1-2), 76-81.
105 OUP. "oil" A Dictionary of Chemistry. In Daintith, J., ed (Oxford University Press, 2008).
106 Siedel, G.H. Operating Fluids. In van Basshuysen, R. and Schäfer, F., eds. *Internal Combustion Engine Handbook*, pp. 627-688 (SAE International, Warrandale, 2004).
107 Caines, A.J., Haycock, R.F. and Hiller, J.E. Constituents of Modern Lubricants. *Automotive Lubricants Reference Book*, pp. 45-88 (Professional Engineering Publishing, London, 2004).
108 Nicholls, M.A., Do, T., Norton, P.R., Kasrai, M. and Bancroft, G.M. Review of the lubrication of metallic surfaces by zinc dialkyl-dithiophosphates. *Tribology International*, 2005, **38**(1), 15-39.
109 Mills, A.J., Lindsay, C.M. and Atkinson, D.J. The Formulation of Automotive Lubricants. In Orszulik, R.M. and Mortier, S.T., eds. *Chemistry and Technology of Lubricants*, pp. 203-227 (Blackie Academic and Professional, London, 1997).
110 Asseff, P.A. Lubricant. In Office, U.S.P.a.T., ed1941).
111 Bovington, C.H. Friction, Wear and the Role of Additives in their Control. In Orszulik, R.M. and Mortier, S.T., eds. *Chemistry and Technology of Lubricants*, pp. 320-348 (Blackie Academic and Professional, London, 1997).
112 Cook, E.W. and Thomas Jr., W.D. Crankcase Lubricant and Chemical Compound Therefor. In Office, U.S.P.a.T., ed1944).
113 Freuler, H.C. Modified Lubricating Oil. In Office, U.S.P.a.T., ed1944).
114 Freuler, H.C. Modified Lubricating Oil. In Office, U.S.P.a.T., ed1944).
115 Bidwell, J.B. and Williams, R.K. The New Look in Lubricating Oils. *SAE Transactions*, 1955, **63**, 349-361.
116 Coy, R.C. and Jones, R.B. The Thermal Degradation and EP Performance of Zinc Dialkyldithiophosphate Additives in White Oil. *ASLE Transactions*, 1979, **24**(1), 77-90.
117 Gellman, A.J. and SPENCER, N.D. Surface Chemistry in Tribology. *Proceedings of the Institute of Mechanical Engineers, Part J*, 2002, **216**(6), 443-461.

118 Minfray, C., Martin, J.M., De Barros, M.I., Mogne, T.L., Kersting, R. and Hagenhoff, B. Chemistry of ZDDP Tribofilm by ToF-SIMS. *Tribology Letters*, 2004, **17**(3), 351-357.

119 Kapadia, R., Glyde, R. and Wu, Y. In situ observation of phosphorous and non-phosphorous antiwear films using a mini traction machine with spacer layer image mapping. *Tribology International*, **40**(10-12), 1667-1679.

120 Bec, S., Tonck, A., Georges, J.M., Coy, R.C., Bell, J.C. and Roper, G.W. Relationship between mechanical properties and structures of zinc dithiophosphate anti-wear films. *Proceedings of the Royal Society of London, Series A (Mathematical, Physical and Engineering Sciences)*, 1999, **455**(1992), 4181-4203.

121 Fuller, M., Yin, Z., Kasrai, M., Bancroft, G.M., Yamaguchi, E.S., Ryason, P.R., Willermet, P.A. and Tan, K.H. Chemical characterization of tribochemical and thermal films generated from neutral and basic ZDDPs using X-ray absorption spectroscopy. *Tribology International*, 1997, **30**(4), 305-315.

122 Pereira, G., Lachenwitzer, A., Munoz-Paniagua, D., Kasrai, M., Norton, P., Abrecht, M. and Gilbert, P.U.P.A. The role of the cation in antiwear films formed from ZDDP on 52100 steel. *Tribology Letters*, 2006, **23**(2), 109-119.

123 Pereira, G., Munoz-Paniagua, D., Lachenwitzer, A., Kasrai, M., Norton, P.R., Capehart, T.W., Perry, T.A. and Cheng, Y.-T. A variable temperature mechanical analysis of ZDDP-derived antiwear films formed on 52100 steel. *Wear*, 2007, **262**(3-4), 461-470.

124 Spedding, H. and Watkins, R.C. The antiwear mechanism of zddp's. Part I. *Tribology International*, 1982, **15**(1), 9-12.

125 Watkins, R.C. The antiwear mechanism of zddp's. Part II. *Tribology International*, 1982, **15**(1), 13-15.

126 Martin, J.M. Antiwear mechanisms of zinc dithiophosphate: a chemical hardness approach. *Tribology Letters*, 1999, **6**(1), 1-8.

127 Willermet, P.A., Carter Iii, R.O. and Boulos, E.N. Lubricant-derived tribochemical films--An infra-red spectroscopic study. *Tribology International*, 1992, **25**(6), 371-380.

128 Willermet, P.A., Dailey, D.P., Carter, R.O., Schmitz, P.J. and Zhu, W. Mechanism of formation of antiwear films from zinc dialkyldithiophosphates. *Tribology International*, 1995, **28**(3), 177-187.

129 Bancroft, G.M., Kasrai, M., Fuller, M., Yin, Z., Fyfe, K. and Tan, K.H. Mechanisms of tribochemical film formation: stability of tribo- and thermally-generated ZDDP films. *Tribology Letters*, 1997, **3**(1), 47-51.

130 Ferrari, E.S., Roberts, K.J., Sansone, M. and Adams, D. A multi-edge X-ray absorption spectroscopy study of the reactivity of zinc di-alkyl-di-thiophosphates anti-wear additives: 2. In situ studies of steel/oil interfaces. *Wear*, 1999, **236**(1-2), 259-275.

131 Fuller, M., Kasrai, M., Bancroft, G.M., Fyfe, K. and Tan, K.H. Solution decomposition of zinc dialkyl dithiophosphate and its effect on antiwear and thermal film formation studied by X-ray absorption spectroscopy. *Tribology International*, 1998, **31**(10), 627-644.

132 Yin, Z., Kasrai, M., Fuller, M., Bancroft, G.M., Fyfe, K. and Tan, K.H. Application of soft X-ray absorption spectroscopy in chemical characterization of antiwear films generated by ZDDP Part I: the effects of physical parameters. *Wear*, 1997, **202**(2), 172-191.

133 Fujita, H. and Spikes, H. The formation of zinc dithiophosphate antiwear films. *Proceedings of the Institution of Mechanical Engineers, Part J: Journal of Engineering Tribology*, 2004, **218**(4), 265-278.

134 Gallopoulos, N.E. Thermal decomposition of metal dialkyldithiophosphate oil blends. *ASLE Transactions*, 1964, **7**, 55-63.

135 Dickert, J.J. and Rowe, C.N. Thermal decomposition of metal O,O-dialkyl phosphorodithioates. *The Journal of Organic Chemistry*, 1967, **32**(3), 647-653.

136 Ashford, J.S., Bretherick, L. and Gould, P. The thermal decomposition of zinc di-(4-methylpentyl-2) dithiophosphate. *Journal of Applied Chemistry*, 1965, **15**, 170-178.

137 Brazier, A.D. and Elliott, J.S. The thermal stability of zinc dithiophosphates. *Journal of the Institute of Petroleum*, 1967, **53**(518), 63-76.

138 Jones, R.B. and Coy, R.C. The chemistry of the thermal degradation of zinc dialkyldithiophosphate additives. *ASLE Transactions*, 1979, **24**(1), 91-97.

139 Martin, J.M., Grossiord, C., Le Mogne, T., Bec, S. and Tonck, A. The two-layer structure of Zndtp tribofilms: Part I: AES, XPS and XANES analyses. *Tribology International*, 2001, **34**(8), 523-530.

140 Pearson, R.G. *Chemical Hardness*. (Wiley-VCH, Weinheim; New York, 1997).

141 Willermet, P.A., Kandah, S.K., Siegl, W.O. and Chase, R.E. The influence of molecular oxygen on wear protection by surface-active compounds. *ASLE Transactions*, 1982, **26**(4), 523-531.

142 Willermet, P.A. and Kandah, S.K. Some observations on the role of oxygen in lubricated wear. *Lubrication Science*, 1993, **5**(2), 129-147.

143 Taylor, L., Dratva, A. and Spikes, H.A. Friction and Wear Behavior of Zinc Dialkyldithiophosphate Additive. *Tribology Transactions*, 2000, **43**(3), 469 - 479.

144 Spikes, H. The History and Mechanisms of ZDDP. *Tribology Letters*, 2004, **17**(3), 483.

145 Aktary, M., McDermott, M.T. and McAlpine, G.A. Morphology and Nanomechanical Properties of ZDDP Antiwear Films as a Function of Tribological Contact Time. *Tribology Letters*, 2002, **12**(3), 155-162.

146 Graham, J.F., McCague, C. and Norton, P.R. Topography and nanomechanical properties of tribochemical films derived from zinc dialkyl and diaryl dithiophosphates. *Tribology Letters*, 1999, **6**(3), 149-157.

147 Zhang, Z., Yamaguchi, E.S., Kasrai, M. and Bancroft, G.M. Tribofilms generated from ZDDP and DDP on steel surfaces: Part 1, growth, wear and morphology. *Tribology Letters*, 2005, **19**(3), 211-220.

148 Taylor, L.J. and Spikes, H.A. Friction-Enhancing Properties of ZDDP Antiwear Additive: Part I Friction and Morphology of ZDDP Reaction Films. *Tribology Transactions*, 2003, **46**(3), 303-309.

149 Li, Y.-R., Pereira, G., Lachenwitzer, A., Kasrai, M. and Norton, P. X-Ray Absorption Spectroscopy and Morphology Study on Antiwear Films Derived from ZDDP Under Different Sliding Frequencies. *Tribology Letters*, 2007, **27**(3), 245-253.

150 Fuller, M., Fernandez, R.L., Massoumi, G.R., Lennard, W.N., Kasrai, M. and Bancroft, G.M. The use of X-ray absorption spectroscopy for monitoring the thickness of antiwear films from ZDDP. *Tribology Letters*, 2000, **8**(4), 187-192.

151 Fuller, M., Kasraia, M., Sheasby, J.S., Bancroft, G.M., Fyfe, K. and Tan, K.H. X-ray absorption spectroscopy of antiwear films on aluminum alloys

generated from zinc dialkyldithiophosphate. *Tribology Letters*, 1995, **1**(4), 367-378.

152 Pereira, G., Lachenwitzer, A., Kasrai, M., Norton, P.R., Capehart, T.W., Perry, T.A., Cheng, Y.T., Frazer, B. and Gilbert, P.U.P.A. A multi-technique characterization of ZDDP antiwear films formed on Al (Si) alloy (A383) under various conditions. *Tribology Letters*, 2007, **26**(2), 103-117.

153 Jiménez, A.E., Morina, A., Neville, A. and Bermúdez, M.D. Surface interactions and tribochemistry in boundary lubrication of hypereutectic aluminium–silicon alloys. *Proceedings of the Institution of Mechanical Engineers, Part J: Journal of Engineering Tribology*, 2009, **223**(3), 593-601.

154 Xia, X., Morina, A., Neville, A., Priest, M., Roshan, R., Warrens, C.P. and Payne, M.J. Tribological performance of an Al–Si alloy lubricated in the boundary regime with zinc dialkyldithiophosphate and molybdenum dithiocarbamate additives. *Proceedings of the Institution of Mechanical Engineers, Part J: Journal of Engineering Tribology*, 2008, **222**(3), 305-314.

155 Rounds, F. Effects of Hydroperoxides on Wear as Measured in Four-Ball Wear Tests. *Tribology Transactions*, 1993, **36**(2), 297-303.

156 Habeeb, J.J. and Stover, W.H. The role of hydroperoxides in engine wear and the effect of zinc dialkyldithiophosphates. *ASLE Transactions*, 1987, **30**(4), 419-426.

157 Aktary, M., McDermott, M.T. and Torkelson, J. Morphological evolution of films formed from thermooxidative decomposition of ZDDP. *Wear*, 2001, **247**(2), 172-179.

158 Minfray, C., Mogne, T., Lubrecht, A.A. and Martin, J.M. Experimental simulation of chemical reactions between ZDDP tribofilms and steel surfaces during friction processes. *Tribology Letters*, 2006, **21**(1), 65-76.

159 Najman, M., Kasrai, M., Michael Bancroft, G. and Davidson, R. Combination of ashless antiwear additives with metallic detergents: interactions with neutral and overbased calcium sulfonates. *Tribology International*, 2006, **39**(4), 342-355.

160 Chinas-Castillo, F. and Spikes, H.A. Film Formation by Colloidal Overbased Detergents in Lubricated Contacts. *Tribology Transactions*, 2000, **43**(3), 357-366.

161 Ven, A.M.C.v.d., Johal, P.S. and Jansen, L. The characterisation of synthetic sulphonate and phenate detergents by nuclear magnetic resonance and infrared spectroscopy. *Lubrication Science*, 1993, **6**(1), 1-19.

162 Tavacoli, J.W., Dowding, P.J., Steytler, D.C., Barnes, D.J. and Routh, A.F. Effect of Water on Overbased Sulfonate Engine Oil Additives. *Langmuir*, 2008, **24**(8), 3807-3813.

163 Galsworthy, J., Hammond, S. and Hone, D. Oil-soluble colloidal additives. *Current Opinion in Colloid & Interface Science*, 2000, **5**(5-6), 274-279.

164 Giasson, S., Espinat, D., Palermo, T., Ober, R., Pessah, M. and Morizur, M.F. Small angle X-Ray scattering (SAXS) on calcium sulfonate dispersions: effects of friction on microstructure. *Journal of Colloid and Interface Science*, 1992, **153**(2), 355-367.

165 Mansot, J.L., Hallouis, M. and Martin, J.M. Colloidal antiwear additives 2. Tribological behaviour of colloidal additives in mild wear regime. *Colloids and Surfaces A: Physicochemical and Engineering Aspects*, 1993, **75**, 25-31.

166 Minami, I., Ichihashi, T., Kubo, T., Nanao, H. and Mori, S. Tribochemical approach toward mechanism for synergism of lubricant additives on antiwear and friction reducing properties. In Dowson, D., Priest, M., Dalmaz,

G. and Lubrecht, A.A., eds. *Life Cycle Tribology: Tribology and Interface Engineering Series*, pp. 259-268 (Elsevier, 2005).

167 Giasson, S., Palermo, T., Buffeteau, T., Desbat, B. and Turlet, J.M. Study of boundary film formation with overbased calcium sulfonate by PM-IRRAS spectroscopy. *Thin Solid Films*, 1994, **252**(2), 111-119.

168 Cizaire, L., Martin, J.M., Gresser, E., Dinh, N.T. and Heau, C. Tribochemistry of Overbased Calcium Detergents Studied by ToF-SIMS and Other Surface Analyses. *Tribology Letters*, 2004, **17**(4), 715-721.

169 Shirahama, S. and Hirata, M. The effects of engine oil additives on valve train wear. *Lubrication Science*, 1989, **1**(4), 365-384.

170 Xu, X.-R., Cai, A.-H., Liu, R., Pan, H.-H., Tang, R.-K. and Cho, K. The roles of water and polyelectrolytes in the phase transformation of amorphous calcium carbonate. *Journal of Crystal Growth*, 2008, **310**(16), 3779-3787.

171 Tang, H., Yu, J. and Zhao, X. Controlled synthesis of crystalline calcium carbonate aggregates with unusual morphologies involving the phase transformation from amorphous calcium carbonate. *Materials Research Bulletin*, 2009, **44**(4), 831-835.

172 Mullin, J.W. The Crystalline State. *Crystallization*, pp. 1-31 (Butterworth-Heinemann, Oxford, 2001).

173 Ulrich, J. Crystallization. In KIRK, R.E. and OTHMER, D.F., eds. *Kirk-Othmer Encylopedia of Chemical Technology*, pp. 95-147 (Wiley, New York, 2002).

174 Koga, N., Nakagoe, Y. and Tanaka, H. Crystallization of amorphous calcium carbonate. *Thermochimica Acta*, 1998, **318**(1-2), 239-244.

175 Chinas-Castillo, F. and Spikes, H.A. Film Formation by Colloidal Overbased Detergents in Lubricated Contacts. *Tribology Transactions*, 2000, **43**(3), 365.

176 Yamaguchi, E.S., Ryason, P.R., Yeh, S.W. and Hansen, T.P. Boundary Film Formation by ZnDTPs and Detergents Using ECR. *Tribology Transactions*, 1998, **41**(2), 262-272.

177 Topolovec-Miklozic, K., Forbus, T. and Spikes, H. Film Forming and Friction Properties of Overbased Calcium Sulphonate Detergents. *Tribology Letters*, 2008, **29**(1), 33-44.

178 Kubo, T., Fujiwara, S., Nanao, H., Minami, I. and Mori, S. TOF-SIMS analysis of boundary films derived from calcium sulfonates. *Tribology Letters*, 2006, **23**(2), 171-176.

179 Giasson, S., Espinat, D. and Palermo, T. Study of microstructural transformation of overbased calcium sulphonates during friction. *Lubrication Science*, 1993, **5**(2), 91-111.

180 Kubo, T., Fujiwara, S., Nanao, H., Minami, I. and Mori, S. Boundary film formation from overbased calcium sulfonate additives during running-in process of steel-DLC contact. *Wear*, 2008, **265**(3-4), 461-467.

181 Dana, J.D., Dana, E.S. and Gaines, R.V. Simple Oxides. *Dana's New Mineralogy: The System of Mineralogy of James Dwight Dana and Edward Salisbury Dana*, pp. 204-254 (Wiley, New York, Chichester, 1997).

182 Dana, J.D., Dana, E.S. and Gaines, R.V. Anhydrous Carbonates. *Dana's New Mineralogy: The System of Mineralogy of James Dwight Dana and Edward Salisbury Dana*, pp. 426-461 (Wiley, New York, Chichester, 1997).

183 Dana, J.D., Dana, E.S. and Gaines, R.V. Hydroxides and Oxides Containing Hydroxyl. *Dana's New Mineralogy: The System of Mineralogy of James Dwight Dana and Edward Salisbury Dana*, pp. 266-291 (Wiley, New York, Chichester, 1997).

184 Kasrai, M., Vasiga, M., Fuller, M.S., Bancroft, G.M. and Fyfe, K. Study of the effects of Ca sulfonate on antiwear film formation by X-ray absorption spectroscopy using synchrotron radiation. *Journal of Synchrotron Radiation*, 1999, **6**(3), 719-721.

185 Kasrai, M., Fuller, M.S., Bancroft, G.M. and Ryason, P.R. X-Ray Absorption Study of the Effect of Calcium Sulfonate on Antiwear Film Formation Generated From Neutral and Basic ZDDPs: Part 1 - Phosphorus Species. *Tribology Transactions*, 2003, **46**(4), 534-542.

186 Wan, Y., Fuller, M.S., Kasrai, M., Bancroft, G.M., Fyfe, K., Torkelson, J.R., Hu, Y.F. and Tan, K.H. Effects of detergent on the chemistry of tribofilms from ZDDP: studied by X-ray absorption spectroscopy and XPS. In Dowson, D., Priest, M., Dalmaz, G. and Lubrecht, A.A., eds. *Boundary and Mixed Lubrication: Science and Applications*, pp. 155-166 (Elsevier, 2002).

187 Kasrai, M., Fuller, M.S., Bancroft, G.M., Yamaguchi, E.S. and Ryason, P.R. X-Ray Absorption Study of the Effect of Calcium Sulfonate on Antiwear Film Formation Generated From Neutral and Basic ZDDPs: Part 2 - Sulfur Species. *Tribology Transactions*, 2003, **46**(4), 543-549.

188 Pereira, G., Lachenwitzer, A., Kasrai, M., Bancroft, G.M., Norton, P.R., Abrecht, M., Gilbert, P.U.P.A., Regier, T., Blyth, R.I.R. and Thompson, J. Chemical and mechanical analysis of tribofilms from fully formulated oils Part 1 Films on 52100 steel. *Tribology - Materials, Surfaces & Interfaces*, 2007, **1**, 48-61.

189 Willermet, P.A., Dailey, D.P., Carter, R.O., Schmitz, P.J., Zhu, W., Bell, J.C. and Park, D. The composition of lubricant-derived surface layers formed in a lubricated cam/tappet contact II. Effects of adding overbased detergent and dispersant to a simple ZDTP solution. *Tribology International*, 1995, **28**(3), 163-175.

190 Dana, J.D., Dana, E.S. and Gaines, R.V. Anhydrous Normal Phosphates, Arsenates, and Vanadates. *Dana's New Mineralogy: The System of Mineralogy of James Dwight Dana and Edward Salisbury Dana*, pp. 700-734 (Wiley, New York, Chichester, 1997).

191 Pereira, G., Lachenwitzer, A., Li, Y.R., Kasrai, M., Bancroft, G.M., Norton, P.R., Abrecht, M., Gilbert, P.U.P.A., Regier, T., Hu, Y.F. and Zuin, L. Chemical and mechanical analysis of tribofilms formed from fully formulated oils Part 2 Films on AlSi alloy (A383). *Tribology - Materials, Surfaces & Interfaces*, 2007, **1**, 105-112.

192 Pereira, G., Lachenwitzer, A., Munoz-Paniagua, D., Kasrai, M., Norton, P.R., Capehart, T.W., Perry, T.A. and Cheng, Y.T. Nanoscale chemistry and mechanical properties of tribofilms on AlSi alloy (A383): interaction of ZDDP, calcium detergent and molybdenum friction modifier. *Tribology - Materials, Surfaces & Interfaces*, 2007, **1**, 4-17.

193 Hironaka, S. and Sikurai, T. The effect of pentaerythritol partial ester on the wear of aluminum. *Wear*, 1978, **50**(1), 105-114.

194 Hotten, B.W. Bidentate Organic Oxygen Compounds as Boundary Lubricants for Aluminium. *Lubrication Engineering*, 1974, **30**(8), 398-403.

195 Hu, Y. and Liu, W. Tribological properties of alcohols as lubricating additives for aluminum-on-steel contact. *Wear*, 1998, **218**(2), 244-249.

196 Hu, Y. and Liu, W. Effect of chemical structure of organo-chlorine compounds on the lubricity of A12024 against steel. *Wear*, 1998, **218**(1), 78-83.

197 Igari, S., Mori, S. and Takikawa, Y. Effects of molecular structure of aliphatic diols and polyalkylene glycol as lubricants on the wear of aluminum. *Wear*, 2000, **244**(1-2), 180-184.

198 Kajdas, C. About an anionic-radical concept of the lubrication mechanism of alcohols. *Wear*, 1987, **116**(2), 167-180.
199 Kawamura, M. and Fujita, K. Antiwear property of lubricant additives for high Silicon Aluminium alloy under boundary lubricating conditions. *Wear*, 1983, **89**(99-105), 99.
200 Konishi, T. and Perez, J.M. Properties of Polyol Esters-Lubrication of an Aluminum Silicon Alloy. *Tribology Transactions*, 1997, **40**(3), 500-506.
201 Montgomery, R.S. The effect of alcohols and ethers on the wear behavior of aluminum. *Wear*, 1965, **8**(6), 466-473.
202 Montgomery, R.S. Chemical effects on wear in the lubrication of aluminum. *Wear*, 1965, **8**(4), 289-302.
203 Montgomery, R.S. The lubrication of aluminum by phthalic acid esters. *Wear*, 1966, **9**(4), 297-299.
204 Montgomery, R.S. Lubrication of bearing aluminum with polyphenyl ethers. *Wear*, 1969, **14**(3), 213-217.
205 Montgomery, R.S. and Garrett, H.L. An electron-microscopic study of aluminum wear particles formed during sliding in the presence of polyglycols. *Wear*, 1967, **10**(4), 310-312.
206 St Pierre, L.E., Owens, R.S. and Klint, R.V. Chemical effects in the boundary lubrication of aluminum. *Wear*, 1966, **9**(2), 160-168.
207 Wan, Y., Liu, W. and Xue, Q. Effects of diol compounds on the friction and wear of aluminum alloy in a lubricated aluminum-on-steel contact. *Wear*, 1996, **193**(1), 99-104.
208 Wan, Y. and Xue, Q. Effect of antiwear and extreme pressure additives on the wear of aluminium alloy in lubricated aluminium-on-steel contact. *Tribology International*, 1995, **28**(8), 553-557.
209 Hotten, B.W. Bidentate Organic Oxygen Compounds as Boundary Lubricants for Aluminium. *Lubrication Engineering*, 1974, **30**(8), 399.
210 Liu, W., Hu, Y., He, Z., Zhang, P. and Xue, Q. Friction and Wear Behaviour of an Al-Si Alloy against Steel Lubricated with N- and O-containing Organic Compounds. *Lubrication Science*, 1998, **11**(1), 37-49.
211 Kolah, A.K., Asthana, N.S., Vu, D.T., Lira, C.T. and Miller, D.J. Triethyl Citrate Synthesis by Reactive Distillation. *Industrial & Engineering Chemistry Research*, 2008, **47**(4), 1017-1025.
212 Smith, J. and Hong-Shum, L. Part I. Acidulants. *Food additives data book*, pp. 1-74 (Blackwell Science, 2003).
213 Smith, J. and Hong-Shum, L. Part II. Antioxidants. *Food additives data book*, pp. 75-120 (Blackwell Science, 2003).
214 Migdal, C.A. and Rowland, R.G. Lubricant and fuel compositions containing hydroxy polcarboxylic acid esters. In Organisation, W.I.P., edUS, 2005).
215 Jayne, D., Gieselman, M.D. and Qureshi, F.S. Understanding the Mechanism of Ashless Anti-Wear Components. *Additives 2009* York, UK, 2009).
216 Kolbenschmidt Pierburg, A. Kolbenschmidt Pierburg AG - Low-Pressure Die Cast Cylinder Blocks. 2010).
217 Pawlus, P., Cieslak, T. and Mathia, T. The study of cylinder liner plateau honing process. *Journal of Materials Processing Technology*, 2009, **209**(20), 6078-6086.
218 GmbH, M.M.S.I. Reconditioning of Aluminium Engine Blocks. 2010).

219 Kaufman, J.G. Table 6b - Typical Mechanical Properties of Cast Aluminium Alloys (Metric Units). *Aluminium Alloy Database* (Knovel, Norwich, N. Y., 2004).
220 Kaufman, J.G. Table 5b - Typical Physical Properties of Cast Aluminium Alloys (Metric Units). *Aluminium Alloy Database* (Knovel, Norwich, N. Y., 2004).
221 BSI. Stainless Steels. *Part 1: List of Stainless Steels*, p. 18 (BSI, 2005).
222 Weston, D.P., Shipway, P.H., Harris, S.J. and Cheng, M.K. Friction and sliding wear behaviour of electrodeposited cobalt and cobalt-tungsten alloy coatings for replacement of electrodeposited chromium. *Wear*, 2009, **267**(5-8), 934-943.
223 Ball, D. The Spectrum. *The basics of spectroscopy*, pp. 53-64 (SPIE-The International Society for Optical Engineering, Bellingham, 2001).
224 Socrates, G. Alkane Group Residues: C-H Group. *Infrared and Raman Characteristic Group Frequencies: Tables and Charts*, pp. 50-67 (Wiley, Chichester, 2001).
225 Socrates, G. Hydroxyl Group Compounds: O-H Group. *Infrared and Raman Characteristic Group Frequencies : Tables and Charts* pp. 94-100 (Wiley, Chichester, 2001).
226 Bellamy, L.J. and Pace, R.J. The origins of group frequency shifts--Part III: Carbonyl frequencies. *Spectrochimica Acta*, 1963, **19**(11), 1831-1839.
227 Socrates, G. Polymers - Macromolecules. *Infrared and Raman Characteristic Group Frequencies: Tables and Charts*, pp. 259-282 (Wiley, Chichester, 2001).
228 Günzler, H. and Gremlich, H.-U. Qualitative Spectral Interpretation. *IR Spectroscopy: An Introduction*, pp. 171-278 (Wiley-VCH, Weinheim; Cambridge, 2002).
229 Rockett, J. The Infrared Spectra of Metal Dialkylphosphorodithioates. *Appl. Spectrosc.*, 1962, **16**(2), 39-40.
230 Kapur, G.S., Chopra, A., Ramakumar, S.S.V. and Sarpal, A.S. Molecular spectroscopic studies of ZDDP - PIBS interactions. *Lubrication Science*, 1998, **10**(4), 309-321.
231 Socrates, G. Organic Phosphorus Compounds. *Infrared and Raman Characteristic Group Frequencies: Tables and Charts*, pp. 229-240 (Wiley, Chichester, 2001).
232 Haque, T., Morina, A., Neville, A., Kapadia, R. and Arrowsmith, S. Non-ferrous coating/lubricant interactions in tribological contacts: Assessment of tribofilms. *Tribology International*, 2007, **40**(10-12), 1603-1612.
233 Williams, J.A. Appendix 5. *Engineering Tribology* (Oxford University Press, Oxford, 1994).
234 Gao, H., McQueen, J.S., Black, E.D., Gangopadhyay, A.K. and Jensen, R.K. Reduced Phosphorus Concentration Effects on Tribological Performance of Passenger Car Engine Oils. *Tribology Transactions*, 2004, **47**(2), 200-207.
235 Wan, Y., Kasrai, M., Bancroft, G.M. and Zhang, J. Characterization of tribofilms derived from zinc dialkyldithiophosphate and salicylate detergents by X-ray absorbance near edge structure spectroscopy. *Tribology International*, 2010, **43**(1-2), 283-288.
236 Schneider, E.W. and Blossfeld, D.H. Radiotracer method for measuring real-time piston-ring and cylinder-bore wear in spark-ignition engines. *Nuclear Instruments and Methods in Physics Research Section A: Accelerators, Spectrometers, Detectors and Associated Equipment*, 2003, **505**(1-2), 559-563.

237 Gara, L., Zou, Q., Sangeorzan, B.P., Barber, G.C., McCormick, H.E. and Mekari, M.H. Wear measurement of the cylinder liner of a single cylinder diesel engine using a replication method. *Wear*, 2010, **268**(3-4), 558-564.

238 Donghui, H., Pingsheng, W., Weizhi, T., Dequan, Z., Guangzhou, C., Bangfa, N., Xiuhua, Z., Lin, L., Guiying, Z., Cunxiong, L. and Dehong, L. Study on real-time wear measurement of piston-ring and cylinder-bore in an engine using thin layer activation method. *Applied Radiation and Isotopes*, 2008, **66**(8), 1073-1078.

239 Eyre, T.S., Dutta, K.K. and Davis, F.A. Characterization and simulation of wear occurring in the cylinder bore of the internal combustion engine. *Tribology International*, 1990, **23**(1), 11-16.

240 Johansson, S., Nilsson, P.H., Ohlsson, R., Anderberg, C. and Rosén, B.-G. New cylinder liner surfaces for low oil consumption. *Tribology International*, 2008, **41**(9-10), 854-859.

241 Weidner, A. and et al. 3D roughness evaluation of cylinder liner surfaces based on structure-oriented parameters. *Measurement Science and Technology*, 2006, **17**(3), 477.

242 Papadopoulos, P., Priest, M. and Rainforth, W. Investigation of fundamental wear mechanisms at the piston ring and cylinder wall interface in internal combustion engines. *Proceedings of the Institution of Mechanical Engineers, Part J: Journal of Engineering Tribology*, 2007, **221**(3), 333-343.

243 Socrates, G. Organic Silicon Compounds. *Infrared and Raman Characteristic Group Frequencies: Tables and Charts*, pp. 241-246 (Wiley, Chichester, 2001).

244 Andersen, F.A. and Brecevic, L. Infrared Spectra of Amorphous and Crystalline Calcium Carbonate. *Acta Chemica Scandinavica*, 1991, **45**, 1018-1024.

245 Yamaguchi, E.S., Ryason, P.R. and Hansen, T.P. Electrical contact resistance studies on zinc dithiophosphates. *Tribology Letters*, 1997, **3**(1), 27-33.

246 Taylor, L.J. and Spikes, H.A. Friction-Enhancing Properties of ZDDP Antiwear Additive: Part II Influence of ZDDP Reaction Films on EHD Lubrication. *Tribology Transactions*, 2003, **46**(3), 310-314.

247 So, H. and Lin, R.C. The combined effects of ZDDP, surface texture and hardness on the running-in of ferrous metals. *Tribology International*, 1999, **32**(5), 243-253.

248 Yamaguchi, E.S., Roby, S.H. and Yeh, S.W. Time-Dependent Film Formation from ZnDTPs and Nonphosphorus Antiwear Agents. *Tribology Transactions*, 2005, **48**(1), 57-68.

249 Timmermans, G. and Froyen, L. Tribological performance of hypereutectic P/M Al-Si during sliding in oil. *Wear*, 1999, **231**(1), 77-88.

250 Das, S., Varalakshmi, K., Jayaram, V. and Biswas, S.K. Ultra Mild Wear in Lubricated Tribology of an Aluminium Alloy. *Journal of Tribology*, 2007, **129**(4), 942-951.

251 Greenall, A. Investigation of the Tribological Performance and Tribochemical Interactions of a Novel, Organic Antiwear Additive in Ferrous Contacts. *Thesis; Mechanical Engineering* (The University of Leeds, Leeds, 2010).

252 Topolovec-Miklozic, K., Forbus, T. and Spikes, H. Film thickness and roughness of ZDDP antiwear films. *Tribology Letters*, 2007, **26**(2), 161-171.

253 Warren, O.L., Graham, J.F., Norton, P.R., Houston, J.E. and Michalske, T.A. Nanomechanical properties of films derived from zinc dialkyldithiophosphate. *Tribology Letters*, 1998, **4**(2), 189-198.

254 Nicholls, M.A., Norton, P.R., Bancroft, G.M., Kasrai, M., Do, T., Frazer, B.H. and De Stasio, G. Nanometer Scale Chemomechanical Characterization of Antiwear Films. *Tribology Letters*, 2004, **17**(2), 205-216.

255 Li, Y.-R., Pereira, G., Kasrai, M. and Norton, P. Studies on ZDDP Anti-Wear Films Formed Under Different Conditions by XANES Spectroscopy, Atomic Force Microscopy and 31P NMR. *Tribology Letters*, 2007, **28**(3), 319-328.

256 Grobelny, J.P., Celichowski, G., Cichomski, M., Kulik, A.J., Piwoński, I.J. and Plaza, S. Comparison of Two Methods of Methyl Group Grafting to the Silica Thin Film Surface and Its Tribological Properties Measured by Atomic Force Microscopy. *Tribology Letters*, 2004, **16**(3), 181-185.

257 Davis, F.A. and Eyre, T.S. The effect of silicon content and morphology on the wear of aluminium-silicon alloys under dry and lubricated sliding conditions. *Tribology International*, 1994, **27**(3), 171-181.

258 Mahoney, C.M., Yu, J., Fahey, A. and Gardella, J.J.A. SIMS depth profiling of polymer blends with protein based drugs. *Applied Surface Science*, 2006, **252**(19), 6609-6614.

259 Brecevic, L. and Nielsen, A.E. Solubility of amorphous calcium carbonate. *Journal of Crystal Growth*, 1989, **98**(3), 504-510.

260 Brantley, W.A. Calculated elastic constants for stress problems associated with semiconductor devices. *Journal of Applied Physics*, 1973, **44**(1), 534-535.

261 Lu, C.-J. and Bogy, D.B. The effect of tip radius on nano-indentation hardness tests. *International Journal of Solids and Structures*, 1995, **32**(12), 1759-1770.

262 OUP. deuterium. In Simpson, J.A. and Weiner, E.S.C., eds. *The Oxford English Dictionary* (Clarendon Press, Oxford, 1989).

263 Bec, S., Tonck, A., Georges, J.M., Georges, E. and Loubet, J.L. Improvements in the indentation method with a surface force apparatus. *Philosophical Magazine*, 1996, **74**(5), 1061-1072.

264 Trezona, R.I. and Hutchings, I.M. Three-body abrasive wear testing of soft materials. *Wear*, 1999, **233-235**, 209-221.

265 Hutchings, I.M. Sliding Wear. *Tribology: Friction and Wear of Engineering Materials*, pp. 77-132 (Edward Arnold, London, 1992).

266 Smith, G.C. and Bell, J.C. Multi-technique surface analytical studies of automotive anti-wear films. *Applied Surface Science*, 1999, **144-145**, 222-227.

267 Minfray, C., Le Mogne, T., Martin, J.-M., Onodera, T., Nara, S., Takahashi, S., Tsuboi, H., Koyama, M., Endou, A., Takaba, H., Kubo, M., Del Carpio, C.A. and Miyamoto, A. Experimental and Molecular Dynamics Simulations of Tribochemical Reactions with ZDDP: Zinc Phosphate–Iron Oxide Reaction. *Tribology Transactions*, 2008, **51**(5), 589-601.

268 Cook, S. Personal Communication with Michael Burkinshaw: Discussion with Chemists at Lubrizol UK Ltd. 2010).

269 Incledon, B.J. and Hall, J.C. Enzymatic De-Esterification of Xenobiotics in Plants. In Hatzios, K.K., ed. *Regulation of enzymatic systems detoxifying xenobiotics in plants*, pp. 67-82 (Springer, 1997).

270 Stefanidis, D. and Jencks, W.P. General base catalysis of ester hydrolysis. *Journal of the American Chemical Society*, 1993, **115**(14), 6045-6050.

271 Kaufman, J.G. Table 4b - Typical Physical Properties of Wrought Aluminium Alloys (Metric Units). *Aluminium Alloy Database* (Knovel, Norwich, N. Y., 2004).

272 Socrates, G. Inorganic Compounds and Coordination Complexes. *Infrared and Raman Characteristic Group Frequencies: Tables and Charts*, pp. 283-327 (Wiley, Chichester, 2001).

273 Wan, Y., Xue, Q. and Liu, W. Tribological behavior of lubricating oil additives in lubricated aluminum-on-steel contact. *Wear*, 1996, **196**(1-2), 87-91.

274 Wan, Y.e.a. Friction and wear characteristics of ZDDP in the sliding of steel against Aluminium alloy. *Tribology International*, 1997, **30**(10), 767-772.

275 Chen, C., Bosse, H. and Deters, L. Effects of various base oils and additives on the tribological behaviour of lubricated aluminium- on-aluminium and steel-on-aluminium contacts. *Proceedings of the Institution of Mechanical Engineers, Part J: Journal of Engineering Tribology*, 2009, **223**(3), 571-580.

276 Piras, F.M., Rossi, A. and Spencer, N.D. Growth of Tribological Films: In Situ Characterization Based on Attenuated Total Reflection Infrared Spectroscopy. *Langmuir*, 2002, **18**(17), 6606-6613.

277 Ordal, M.A., Bell, R.J., Alexander, J.R.W., Newquist, L.A. and Querry, M.R. Optical properties of Al, Fe, Ti, Ta, W, and Mo at submillimeter wavelengths. *Appl. Opt.*, 1988, **27**(6), 1203-1209.